POSTCRANIAL VARIATION IN PLIO-PLEISTOCENE HOMININS OF AFRICA

by

MELISSA TALLMAN

A dissertation submitted to the Graduate Faculty in Anthropology in partial fulfillment of the requirements for the degree of Doctor of Philosophy,
The City University of New York.

2010

This manuscript has been read and accepted for the
Graduate Faculty in Anthropology in satisfaction of the
dissertation requirement for the degree of Doctor of Philosophy.

Date	Chair of Examining Committee: Eric Delson
Date	Executive Officer: Gerald Creed

William E. H. Harcourt-Smith

F. James Rohlf

William L. Jungers

Supervision Committee

THE CITY UNIVERSITY OF NEW YORK

Abstract

POSTCRANIAL VARIATION IN PLIO-PLEISTOCENE HOMININS OF AFRICA

by

MELISSA TALLMAN

Adviser: Professor Eric Delson

Postcrania are a key component of functional analyses of Plio-Pleistocene hominin behavior, but many specimens are unassociated or fragmentary and have thus been largely ignored by researchers. This dissertation examined all relevant Plio-Pleistocene postcranial material to examine whether there are consistent patterns of morphology that characterize Plio-Pleistocene taxa and whether there are different locomotor types represented.

Data on all available Plio-Pleistocene hominin humeri, radii, ulnae, femora and tibiae were collected with a microscribe 3-D digitizer and compared to a modern sample of four populations of *Homo sapiens*, two subspecies of *Pan troglodytes*, two subspecies of *Gorilla gorilla*, *Pongo pygmaeus* and *Pan paniscus* in order to make taxonomic and functional conclusion about overall patterns of postcranial variation in the appendicular skeleton of hominins.

The most informative areas were the distal femur, tibia, radius, and humerus, and the proximal femur and ulna. In the distal humerus, individuals from Koobi Fora had a more pleisomorphic morphology than all of the other fossils, including those with much earlier dates. The variation present in the proximal femur of *A. afarensis* was greater than most single modern species. The pattern of variation in the distal femur was tested against an ontogenetic sample of modern humans and chimpanzees in order to assess whether the differences present were caused by heterochronic change; this hypothesis was not supported.

There are few postcranial characters that can be tied to specific groups. Among hominins, *Paranthropus robustus* and *Homo habilis sensu lato* had the most distinctive patterns of morphology. There was a temporal pattern in the distal tibia with individuals the least like modern humans occurring the earliest in time and those most like them occurring latest, but there were no temporal patterns to any other segment sampled. There was a clear difference in the way that humans and apes covary in the fore- and hindlimb. There was no evidence of developmental shape integration between serial homologues. As a group, Plio-Pleistocene hominins had patterns of covariance that were most similar to modern humans, with the exception of pairings involving the distal femur.

This is dedicated to my parents.

ACKNOWLEDGMENTS

While a dissertation has only a single author, it is not completed in isolation. My thanks must go first and foremost to my advisor, Dr. Eric Delson. His critiques of my work are always honest and helpful, and he pushes me to make things better and more interesting. My graduate career has certainly been shaped by being his student. My sincere thanks also go to Dr. Will Harcourt-Smith for assisting me in my first-ever independent research project and being a ready and willing ear for ideas for all subsequent projects. I also thank my other two committee members, Dr. F. James Rohlf for his helpful critique of my statistical work and Bill Jungers, for his helpful comments and critiques.

I used many museum collections for my research, and my thanks go out to all of those who allowed me access to material: Malcolm Harmon at the Powell-Cotton Museum, Birchington-on-Sea, England; Louise Humphrey, Rob Kryzynsky, and Paula Jenkins at the Natural History Museum, London, England; W. Wendelen at the Royal Museum of Central Africa in Tervuren, Belgium; Martin Freiss and Philippe Mennecier at the Musée de L'Homme in Paris, France; Mamitu Yilma and Menkir at the National Museum of Ethiopia, Addis Ababa, Ethiopia; Amandus Kwekason at the National Museum of Tanzania, Dar es Salaam, Tanzania; Emma Mbua and Sam Ngui at the Kenya National Museum, Nairobi, Kenya; Bernard Zipfel at the University of Witswatersrand, Johannesburg, South Africa; and Alan Morris at the University of Cape Town, Cape Town, South Africa.

A special thanks goes to Stephany Potze and Dr. Francis Thackery at the Transvaal Museum in Preoria, South Africa. They could not have been kinder, more accommodating hosts. Stephany was so thoughtful in helping me plan for my visit and even left some food in the fridge at the cottage, anticipating my mood after the long flight from New York. Francis insisted that I

take a day off so he could take me to see Kromdraai, Sterkfontein and Swartkrans. They made accessing the fossil material easy and my stay extremely comfortable.

For access to unpublished fossil material, I thank Dr. Terry Harrison who allowed me access to a tibia from Laetoli and Dr. Tim White who allowed me to see much of the material from the Middle Awash. Terry Harrison also gave me invaluable advice on navigating the administrative process for getting permits in Tanzania

The American Museum of Natural History has been my home base for the bulk of my dissertation research. Eileen Westwig, Ken Mowbray, Ian Tattersall and Gisselle Garcia have all been so helpful in allowing me access to the museum collections in Anthropology and Mammalogy.

I traveled all over the world collecting data, and I met many people along the way who smoothed my path and went out of their way to help me. My sincere thanks go to Jill Greenburg, the then-proprietess of the Greenview Inn, who joined me for dinners and movies, gave me invaluable advice, and generally made the bleak Kent winter more bearable; and Carla Meertens in Tervuren who, when I was very ill, helped me find a doctor who spoke fluent English and opened up her home to me. Such generosity is not expected from a relative stranger, but it is certainly is appreciated. Michelle Gross found me a place to stay at the last minute in Paris, allowed me into her circle of friends, and generally made my stay more fun than it should have been. Finally, in Nairobi, I must thank Ari Grossman for assisting me during my difficulties with my American bank.

Many other people gave me advice and encouragement along the way. Thanks to: Drs. Stephen Frost and Kieran McNulty for helping me love statistics and answering my endless stream of questions; Siobhán Cooke, Lauren Halenar and Jessica Brinkworth for being good

sounding boards for ideas and sympathetic ears for tales of woe; Toby Greenfield, Eileen Larsson, Jenna Lawrence, and David Sasse for being good friends to me throughout this process; and Brett Bingman for his unending patience. There is no possible way I can ever thank my parents enough for all of their love and support for me. They sent me to college, fully supported me in my pursuit of a graduate education, and even wired me money to two different African countries, all without ever really understanding what it is I actually do.

Finally, I must acknowledge my sources of funding, without which I would not have been able to complete this project. Thank you to all of the anonymous reviewers who reviewed this research idea favorably. My dissertation research was supported by the Sigma Xi Foundation, The City University of New York, the Wenner-Gren Foundation (WG 7515) and the National Science Foundation (NSF DDI 0550901 and partial funding from NSF 0333415 to NYCEP and NSF 0513360 to Eric Delson and others).

TABLE OF CONTENTS

LIST OF TABLES

LIST OF FIGURES

CHAPTER 1: INTRODUCTION

Postcrania are a key component of taxonomic analyses and behavioral reconstructions in the human fossil record. Many studies have focused on searching for variation in the internal and external morphology of early hominins in order to make inferences about the differences in their locomotor repertoires, (*e.g.,* Napier, 1964), body size dimorphism (*e.g.,* McHenry, 1991), and activity patterns (*e.g.,* Ruff, 2002). In turn, these differences have been used to draw taxonomic conclusions about early hominins (*e.g.,* Wood and Collard, 1999).

This dissertation proposes an investigation into the postcranial variation in Plio-Pleistocene hominins (i.e., those dating roughly between 3.5-1.5 Ma). Postcranial elements of early human fossils provide the best clues to interpreting their mode of locomotion, but the isolated nature of many specimens means that they have not been securely allocated to taxa that have been defined mainly by craniodental morphology. Using a three-dimensional geometric morphometric approach (see Chapter 2), anatomical differences between specimens will be quantified. Unassociated postcranial remains will be classified (as far as possible) based on consistent anatomical differences and comparisons to the few postcranial elements that have strong associations with cranial remains. Researchers such as Harrison (1987 *et seq*.) have argued that genera (at least) can be separated using postcranial features at the same time that these features are used to infer locomotor adaptation. I will extend this discussion to a consideration of species-specific differences in morphology by using three-dimensional geometric morphometrics to capture precise details of such differences on single elements and across functional complexes. These findings will then be reviewed to seek their implications for functional anatomy and palaeoecology of Plio-Pleistocene hominins.

This project has two broad research questions:

1. Are there postcranial traits that are characteristic of specific Plio-Pleistocene hominin groups?

Previous studies indicate quantifiable gross differences in postcranial morphology, at least between early specimens (i.e., *A. afarensis*) and late specimens (i.e., *H. erectus sensu lato*). The majority of these studies have been carried out using traditional linear methods to quantify morphology. This study will investigate the resolution at which differences can be detected within the fossil record by using three-dimensional geometric morphometrics to quantify overall shape.

2. What do postcranial remains imply about the locomotor repertoires of Plio-Pleistocene hominins? Are there different locomotor types?

Many previous studies have concentrated on a careful analysis of single postcranial elements. The next step is to incorporate these data into analyses that take into account the ways that the bones of the postcranium work together during locomotion. The proposed project will examine patterns of covariation in fore- and hind-limb morphology and within joint complexes to evaluate the degree of mosaicism present in the human fossil record. This will then be analyzed in the context of functional implications as well as environmental differences across different Plio-Pleistocene sites.

Background

Craniodental Hominin Phylogenies

Cladistic and phylogenetic analyses of Plio-Pleistocene hominins are typically constructed using craniodental remains to estimate the evolutionary relationships among taxa

(*i.e.* Wood, 1991; Strait and Grine, 2004). While there is much argument as to the ulimate shape of the hominin tree**,** all of these craniodental phylogenies are similar in that they track the evolution of derived, human-like characteristics through time. Thus, all of the species that occur later in time have the highest number of synapomorphies with modern humans and those that occur earlier in time have the least. These synapomorphies include such traits as the enlargement of the brain, reduction in the size of the dentition, and reduction in facial prognathism (Wood, 1991)**.**

Often postcrania are dismissed as being prone to homoplasy. In general, cranial elements (particularly basicranial elements) are assumed to be more conservative, and are often weighted more heavily than postcranial ones. However, in ignoring information from the postcrania, valuable information about the way Plio-Pleistocene evolution occurred could be lost. Several recent papers have suggested that the information from the postcranial record contradicts the view that as time progressed, hominins became more and more human-like. Studies of both limb proportions and postcranial shape have concluded that in some instances, very ape-like morphologies occur later in time and more modern morphologies occur earlier in time (Hartwig-Scherer and Martin, 1991; McHenry and Berger, 1998; Richmond *et al.* 2002; Hauesler and McHenry, 2007; Green *et al.* 2007; McHenry and Brown, 2008).

The postcrania is assumed to be homoplastic because of the influence of locomotion on postcranial evolution. However, Sánchez-Villagra and Williams (1998) compared levels of homoplasy in cranial, dental and postcranial characters for individuals in 41 different data sets from various mammalian groups (including Primates), and found no significant differences at any taxonomic level and Young (2003) was able to accurately reproduce phylogeny in Primates using cladistic characters derived from the forelimb. He determined that homoplasy in his dataset

was low, with convergence of *Ateles* on the great apes accounting for the majority of the homoplasy present.

Postcranial morphology has been successfully used in cladistic analyses over multiple taxa. Horovitz and Sánchez-Villagra (2003) used postcranial characters for a cladistic analysis of marsupial mammals, recovering all family groups of extant marsupials, and correctly placing the outgroups. Postcranial remains have also been used to try to resolve the phylogeny of early primates (Harrison, 1987; Szalay**,** 1976). Sargis (2002) used twenty-seven postcranial characters to evaluate the "Primatomopha" and "Volitantia" hypothesis for ordinal level relationships among tree shrews, primates, and bats. Beard *et al.* (1988) used carpal and tarsal morphology to test the monophyly of the Adapiformes, as well as to discern their position within the primate clade. Gebo *et al.* (2001) used only tarsal morphology to divide up an assemblage of middle Eocene haplorhine primates into twelve to sixteen species.

For Plio-Pleistocene hominins, one of the best known examples of the use of postcranial remains to make taxonomic conclusions is the work of Wood and Collard (1999). These authors redefined the criterion for genus attribution to include all individuals that occupy a similar adaptive niche. For fossil hominins, this "adaptive niche" was determined for each taxon using such criteria as body size and shape (including intermembral index) and locomotor behavior. It was (in part) on the basis of these kinds of characters that Wood and Collard advocated the placement of *H. habilis* and *H. rudolfensis* in the genus *Australopithecus.*

Anatomy of a Biped

The pre-human body has gone through a series of adaptive changes for obligate bipedal posture. When a quadruped walks, its center of mass is somewhere between all four limbs, which makes balancing relatively easy, so it generates horizontal ground reaction forces between

its limbs and the ground. Bipeds have their center of mass between only the two lower limbs, which makes balancing a greater challenge. When a biped walks, the ground reaction forces are directed upwards and are of a lesser magnitude. Most of the changes in the bipedal skeleton are related to maintaining balance and being energetically efficient when walking on only two supports (Lovejoy, 1988; Aiello and Dean, 1990).

The lumbar region of the spine is elongated by the inclusion of an additional lumbar vertebra as on average, *Homo* has five lumbar vertebrae; in *Pongo* and *Gorilla,* the average is only four. There is also an increase in the height of the vertebrae in *Homo*, and the lower spine is characterized by a lordosis which functions to keep the center of mass above the hips (Robinson, 1972). The overall lengthening of the trunk helps to stabilize a longer and heavier hindlimb (Preuschoft, 2004).

Modern human pelves are rounder and have a longer anterior-posterior dimension for giving birth to large brained babies. The ilium in modern humans is shorter than in quadrupeds, putting less stress on the gluteus maximus by shortening its lever arm. The sacrum is wider in bipeds, and the bowl shaped pelvis stabilizes the viscera. Increasing the lateral flare of the ilia and increasing the length of the femoral neck in bipeds serves to increase the mechanical advantage of the hip abductors (Lovejoy 1988).

The femora of humans have a series of changes that fundamentally separate them from quadrupedal apes. Humans have a bicondylar, or valgus, angle. This angulation of the femur is an epigenetic trait and occurs because the force of walking bipedally stimulates faster bone growth on the lateral side during ontogeny (Shefelbine *et al.,* 2002). Functionally, it both keeps the knee directly in line with the center of gravity for balance, and allows for an energetically efficient swing and transfer of weight (see the gait cycle below) (Lovejoy, 1988). The large,

globular femoral head in *Homo* functions to support the greater amount of weight passing vertically during bipedal locomotion compared to quadrupedal apes (Ruff, 1988), while the low and laterally projecting greater trochanter helps to put the gluteus minimus and medius in their most mechanically advantageous position while allowing for maximal mobility at the hip joint (Aiello and Dean, 1990).

There are many changes in the distal femur as well. In humans, the lateral and medial condyles are of similar size because they equally important in transmitting downward forces during bipedal locomotion. In apes, the medial condyle is larger and is used more in load transmission. Also, humans have condyles that are more elliptical (particularly the lateral condyle) and more symmetrical in order to provide a larger surface for articulation with the tibia. The condyles also increase the lever arm for the quadriceps femoris (which is the main flexor of the knee) by making a flatter anterior surface; this then orients the patella more anteriorly than is seen in the apes (Aiello and Dean, 1990). The deep, asymmetrical patellar groove in *Homo* is likely to prevent the patella from being laterally dislocated during flexion of the knee. In *Homo,* the quadriceps femoris pulls up along the human bicondylar angle, pulling the patella in the lateral direction, whereas in a quadruped, it is pulled proximally in a straight line (Heiple and Lovejoy, 1971; Stern and Susman, 1983).

Finally, the shape of the foot in humans is drastically different than that of the quadrupedal apes. Rather than having a grasping foot, the human foot is built more for balance and shock absorption. The hallux is abducted and in line with the rest of the pedal phalanges which allows for greater balance and a forceful toe-off during the gait cycle and the presence of a transverse arch acts as a shock absorber for the downward forces during locomotion (Napier, 1964).

The Gait Cycle

The gait cycle is composed of a stance phase and a swing phase. Beginning from a standing position where the center of mass is between the two feet, the gait cycle begins when the muscles in the lower segments of the leg relax and the body tips forward with gravity, resulting in the center of mass shifting forward. One leg then swings forward and the heel is placed on the ground, once again placing the center of mass between the two feet. At the same time, the pelvis rotates, and the gluteus minimus and medius contract to hold it stable above the stance leg. The degree of pelvic rotation determines the length of the stride; the greater the rotation, the longer the stride length. The stance leg then propels the person forward by engaging the muscles of the lower leg to push against the ground with the ball of the foot first and finally the big toe (called the "toe off"). Peroneus brevis and peroneus longus are active during this portion of the stance phase by dorsiflexing and everting the foot during heel rise of the support leg (Jungers *et al.,* 1993; Otis *et al* 2004). This completes the stance phase of the gait cycle.

During the swing phase, the back leg swings forward, bent at both the hip and the knee such so that it does not drag on the ground. The iliopsoas functions to swing the leg forward, and the hamstrings exert an opposing force to slow down the forward swing of the leg. Then the leg straightens at the ankle so that the heel strikes the ground (Napier, 1967; Lovejoy, 1988). Extensor digitorum longus, tibialis anterior and peronius tertius are all active during the swing phase. Peronius tertius exerts an everting force on the foot to counteract the inverting force of tibialis anterior in order to level and stabilize the foot during heel-strike (Jungers *et al.,* 1993). A complete walking cycle, or stride, is marked from the heel strike of one leg through the heel strike of the other (Napier, 1967).

In humans, gluteus maximus is the extensor of the trunk. Gluteus maximus functions most strongly during running or climbing/walking up an incline, and its main function is to keep the trunk from "jackknife[ing]" on the legs (Napier, 1967). Napier (1967) suggested that due to the gluteus maximus' role in running, the evolution of a human-like gluteus maximus occurred fairly late, while the evolution of a human-like arrangement of the gluteus medius and minimus would have occurred extremely early.

During the gait cycle, the human body is displaced in both the horizontal and vertical planes. During the stance phase while the supporting leg is extending, the human body reaches the highest point of vertical displacement. The lowest point occurs between the stance phase and the swing phase when both feet are on the ground. The body also sways horizontally as the center of gravity is moved back and forth over the supporting legs in each stride. The bony morphology of the lower limb reduces these displacements to make the bipedal gait more efficient. The distance of vertical displacement is minimized by the movements of the pelvis. The pelvis pivots laterally around the stance leg, as opposed to superiorly, and the gluteal muscles do not hold the pelvis parallel to the ground but at a slight downward angle. The bicondylar angle keeps the knee joints close together, thereby minimizing the distance of horizontal displacement (Lovejoy, 1988; Aiello and Dean, 1990).

A running gait differs from a walking gait in three major ways: first, each foot has a shorter period of contact time with the ground per stride; second, the amount of force that each foot generates as it hits the ground fluctuates less than in a walking gait; and third, the overall vertical ground reaction forces are higher during running (Aiello and Dean, 1990). During a running gait, the greatest vertical displacement occurs during the aerial phase, and the lowest point is during midstance when a flexed knee, hip and ankle act as a spring. While it is difficult

to distinguish between skeletal adaptations for walking and running, there do seem to be some traits that are more indicative of the capacity for endurance running. The presence of a transverse groove on the calcaneus for the Achilles tendon, a well developed plantar arch, and the presence of a projecting medial flange on the proximal cuboid are traits that have been linked to effective endurance running (Bramble and Lieberman, 2004).

While humans are not particularly good sprinters, human endurance running capabilities are comparable to those of social carnivores, like dogs, and migratory cursors, like wildebeests and horses. Unlike other mammals, humans increase running speed by increasing stride length as opposed to increasing stride rate. Humans should switch to a running gait when the cost of running is less than the cost of walking at increased speeds. It is possible that the capacity for endurance running was specifically selected for in the human lineage as a way to increase and maintain home range sizes and as a method of hunting and/or scavenging animal prey (Bramble and Lieberman, 2004; Lieberman *et al.,* 2007), although others have questioned this assertion based on evidence from the modern ethnographic record (Pickering and Bunn, 2007).

A chimpanzee's bipedal gait is biomechanically different from that of a human. When chimpanzees walk bipedally, they do so with a "bent-hip, bent-knee" (BHBK) gait, where both the hip and a knee joint are flexed. When a chimpanzee walks, the knee and the ankle joint both stay in front of the hip joint during the entire gait cycle, and the lack of a bicondylar angle in the chimpanzee femur results in a greater degree of horizontal displacement. Finally, when a chimpanzee walks, the pelvis is rotated over the supporting leg, moving the entire center of gravity over that leg, resulting in greater vertical displacement as well (Aiello and Dean, 1990).

A chimpanzee must walk with a BHBK gait because of the positions of the hip and thigh musculature. In quadrupedal animals, the gluteus medius and minimus are both extensors of the

trunk whereas in humans, they are functionally abductors of the trunk. A BHBK gait places the gluteus minimus and medius in their most functionally advantageous positions for efficient bipedal movement. Also, nonhuman primates walking bipedally often recruit peronius longus or peronius brevis during the swing phase of the gait cycle. Jungers *et al.,* (1993) hypothesized that as these muscles are plantar flexors (as well as everters) of the foot, primates use them to counteract the force of tibialis anterior, as humans do with peroneus tertius. Originally, peroneus tertius was thought to be unique to humans, but anatomical studies have found it in low frequencies in other primates. Peroneus tertius is more efficient than peroneus brevis and peroneus longus at counteracting tibialis anterior; because the genetic underpinning for them is present in modern apes, one could assume that natural selection would have selected for this trait in early hominins, making it more frequent in the human lineage (Jungers *et al.,* 1993).

Bone Plasticity and Activity Patterning

Morphological changes in the postcranial skeleton can indicate functional changes in activity at the individual level. Studies have concentrated on gross morphology of the upper and lower limbs (including the plasticity of proximal and distal ends in comparison to the midshaft), as well as on changes in the internal bone structure. Ruff (2002) completed the most comprehensive study on the effects of locomotion on long bone morphology. For this study, he sampled thirteen species of catarrhines, including both fore and hindlimb measurements for the purposes of correlating cross-sectional geometry at the midshaft and at the articular ends with locomotor mode. He found that locomotion affects the midshaft and the proximal and distal ends of bones differently. Primates with a more varied locomotor repertoire or with a repertoire that emphasizes slow, cautious movements had larger joint surfaces in comparison to diaphyseal size.

This is because the bending pressures on the diaphyses of primates that practice a more varied locomotor repertoire are less than those that practice some sort of habitual movement. In this study, Ruff concentrated on variation in size, as opposed to looking at shape differences.

This finding is supported by similar studies. Stock and Pfeiffer (2001) surveyed structural variability in two different modern human hunter-gatherer populations that practiced different subsistence modes. They noted that diaphyseal shape changed depending on the activity pattern (land-based subsistence versus water-based subsistence), but that the proximal and distal ends responded differently to the loadings. Similarly, Holt (2003) found more circular mid-shaft femoral cross sections in more sedentary human populations. Flattening of the femur at the midshaft in more mobile populations is a result of the increased bending loads from hunter-gather lifestyle.

Lieberman *et al.,* (2001) used different age classes of sheep to model the ways that an increase in exercise affects long bone morphology. These authors found that increase in exercise most greatly affected the hindlimb diaphyses, but did not affect the joint articular surface area at all. They found that the articular surfaces are phenotypically constrained, although these authors hypothesized that the increase in exercise did not lead to sufficient stress to cause changes in the proximal and distal ends. They further hypothesized that if they had increased the applied stress, there would have been changes in the articular surface area, and that those changes would have been greatest in the distal ends, as they receive the most force. An earlier study by Ruff (1994) corroborates this hypothesis. He found that in young tennis players, the distal radius of their "racket hand" is enlarged, in comparison to the opposite hand. It's also important to note that an increase in articular surface area will have different effects depending on where that surface area is added (Ruff, 2002). Ruff (2002) also found that in species where the emphasis is on forelimb

locomotor behaviors, the forelimbs are enlarged, whereas in species where the emphasis in on leaping and hindlimb locomotor behavior, the hindlimbs are enlarged.

Using a micro-CT scanner, it is possible to examine the trabecular structure of bone to make inferences about locomotion. Fajardo and Muller (2001) did an analysis using micro-CT of the proximal femora and humeri in four nonhuman primates and found that the degree of anisotropy in the trabecular structure is correlated with locomotor repertoire, with the greatest degree of anisotropy being found in primates that are habitual terrestrial bipeds.

There are a number of epigenetic traits that are associated with obligate bipedalism. In modern humans, the angle of the femoral neck to the femoral diaphysis is correlated with the degree of mobility. The more mobile a person is during the period of growth, the more acute his or her femoral neck angle will be (Anderson and Trinkaus, 1998). The formation of the bicondylar angle is another epigenetic trait. As a child grows and begins to walk, the medial side of the distal metaphysis grows faster than the lateral side. This results in the formation of the bicondylar angle, and this growth reaches a stable point by the age of eight. In children unable to walk during this stage of growth, the bicondylar angle never forms (Shefelbine *et al.*, 2002). Tardieu (1999) examined three features of the human distal femoral epiphysis: the prominence of the external lip or the trochlea; the profile of the external condyle; and the anteroposterior lengthening of the epiphysis. These traits are generally linked with the development of a bicondylar angle later in life, and increased stability of the knee joint. She also found that the bicondylar angle in humans is an epigenetic functional feature that develops during early childhood growth. The fact that all australopiths have a bicondylar angle indicates an early shift in activity patterning during the Pliocene. She also determined that there was a genetic shift between *Australopithecus* and *Homo* that changed the muscle insertion of the lateral meniscus

from a single insertion (in *Australopithecus*) to a double insertion. This would have caused increased knee stability in early *Homo*. However, Dugan and Holliday (2009) noted that this feature is variable in modern humans and should be used cautiously in interpreting the fossil record.

Evolution of Bipedalism

Modern humans are the only extant ape that does not have a mosaic locomotor pattern. The extant apes, particularly chimpanzees, possess a compromise morphology, meaning that they do not perform any form of locomotion at peak efficiency, but they are capable of performing a broader spectrum of movement. The quadrupedal gait used by *Pan* is less energetically efficient than bipedalism in humans and quadrupedalism in *Papio.* The evolution of obligate bipedalism could have happened slowly by changing the compromise morphology of the last common ancestor to a more committed morphology (Rose, 1991).

Before considering the potential selective advantage of being bipedal, it is instructive to consider the costs of bipedalism. The morphological changes required in the postcranial skeleton mean the loss of agility in the trees. Trees provide food sources, sleeping spots and potential escape routes (Lovejoy, 1988). The changes to the pelvis would also have made giving birth more difficult, possibly necessitating assistance during birth. In monkey and apes, the infant exits the birth canal facing the mother, allowing her to assist its exit. In *Homo sapiens,* the infant exits the birth canal facing backwards due to the modifications in the pelvis, making it difficult for the mother to assist the baby's exit without damaging it (Rosenberg and Trevathan, 1996). The selective advantages for bipedalism must have been greater than those costs in order for bipedalism to have evolved.

Theories for why bipedalism evolved can be loosely grouped into four categories: forelimb use, social behavior, feeding, and a catch-all category for everything else (after Rose, 1991).

Group One: Forelimb Use

Forelimb use is a broad category and covers the use of forelimbs for carrying tools, food, weapons and infants. Darwin (1871) suggested that bipedalism evolved in response to having the hands free to carry stone tools. In Darwin's model, bipedalism evolved in concert with the behavioral shift towards a greater percentage of diet being made of animal proteins. Having the hands free would have allowed for the use of stone tools in hunting and carcass processing. He also suggested that having the hands free would indirectly have led to a reduction in canine size as earlier hominins relied more and more upon handheld weapons for aggressive interactions. However, in the last hundred fifty years, there have been many more fossil discoveries, and we now know that bipedalism well pre-dated the manufacture of stone tools (Richmond and Jungers, 2008; Lovejoy *et al.,* 2009a,b).

Lovejoy (1988, 2009) has also suggested that having the hands free was the major selective advantage for bipedal posture. In Lovejoy's model, having the hands free would have allowed males to carry food and provision females and bipedalism would have evolved in concert with a pair-bonded social system and male philopatry. This system would have also resulted in low degrees of sexual dimorphism, reduced canine size, the elimination of the sectorial canine complex, a decrease in testes size and sperm production, and a cryptic estrus. While Lovejoy's model is persuasive on the surface, it is impossible to conclusively link changes in soft tissue anatomy to any particular time in human evolutionary history; doing so is purely speculative as there is no soft tissue evidence from the hominin fossil record. Additionally,

while *Ardipithecus ramidus* may be somewhat monomorphic (Lovejoy, 2009; Lovejoy *et al.,* 2009; White, 2009), most researchers have found that later australopiths were not (Kimbel and White, 1988; Lague and Jungers, 1996; Lague, 2002; Plavcan *et al.,* 2005; Harmon, 2006; Harmon 2009). Finally, monomorphism and reduced canine size are not irrefutably connected to pairbonding; as Lovejoy himself pointed out, gibbons are pair-bonded yet possess very large canines (Lovejoy, 2009). Bonobos and chimpanzees both have relatively low levels of dimorphism (particularly in comparison to the highly dimorphic *Gorilla, Pongo* or *Papio*) but live in a multi-male, multi-female social system where mating is promiscuous (Leutenegger and Kelly, 1977; Strier, 2000).

Another suggestion is that bipedalism evolved so that early hominins could use their hands for defense. Bipedalism could have evolved in response to the need to throw stones powerfully and accurately. Throwing behaviors have been witnessed in many modern human groups and have documented lethal results (Isaac, 1987). The bipedal body plan is ideally adapted to stone throwing due to its low center of gravity and strong launching platform (Fifer, 1987). If stone throwing is considered to be the selective advantage, then it resolves some seemingly contradictory evidence such as the retention of longer arms in the already partially bipedal australopiths, as throwing distance is positively correlated with arm length (Dunsworth *et al.,* 2003). Capuchin monkeys use throwing in a number of situations, including throwing food items between groups and throwing stones at small prey items and they are able to throw accurately at both moving and stationary targets. In a study using captive bred capuchin monkeys, preference for a bipedal throwing posture increased as target distance increased (Westergaard *et al.,* 2000).

Historically, stone throwing has been discussed within the context of hunting from a distance (*e.g.* Darwin, 1971), although more recently it has been proposed that stone throwing could have evolved as a way to punish "cheaters" in social systems where there is reciprocal altruism. This form of punishment would do maximal harm to the cheater with minimal cost to the non-cheating partner (Bingham, 1999). While it is interesting to speculate about this, thus far there is no direct evidence in the fossil record to support the throwing hypotheses, and there is a lack of rigorous kinematic studies to explore this theory (Preuschoft, 2004).

Kortlandt (1980) also postulated that bipedalism arose as a defense mechanism. He believed that carnivore predation would have been the main selective pressure for the acquisition of bipedal posture. Early hominins could have fended off large carnivores by wielding thorny branches as weapons. Kortlandt experimentally tested this theory using captive lions and found that lions were unlikely to approach bait that was covered with thorn branches. He thought that this behavior might have started with the Dryopithecinae in Europe and was adapted by the entire hominin clade. While this idea is interesting, it would be difficult to test using the fossil record. Further observation of wild carnivores and primates could lend support or discredit this hypothesis.

It is also possible that bipedalism was selected for as a way to carry increasingly heavy infants. Amaral (1989) has said that hairlessness evolved in the human lineage while hominins were still living in forested environments. Hairlessness is at the greatest thermoregulatory advantage for dissipating heat generated by activity in environments where ambient temperatures are below normal body temperatures. This is contra Wheeler (1992) who has argued that hairlessness would not have evolved until hominins moved into more open habitats. Amaral (2008) has further suggested that infant carrying could be considered either a cost or an

advantage of bipedal gait, depending on when hairlessness evolved. Bipedal posture exceeds the maximum angle for safe infant carrying using the typical primate dorsal clinging method; therefore females would have been forced to carry dependent infants in their arms, limiting their forelimb use. However, if hairlessness evolved early as Amaral (1989) previously postulated, then infant carrying could been seen as the selective advantage for bipedalism as hominin hair would no longer have had enough tensile strength to bear the weight of an infant. Genetic differences between chimpanzees and humans relating to hairlessness have been discovered, but gene trees estimating the divergence of these genes would be needed in order to support or reject this hypothesis (Amaral, 2008).

Group Two: Social Behavior

Jablonski and Chaplin (1993) argued that the last common ancestor of hominoids and cercopithecoids would have had the ability to walk bipedally for short periods of time during various activities, including carrying and display. These authors discussed how the extant apes avoid harmful aggressive interactions as a model for the behavior of early hominins. In *Gorilla,* size dimorphism prevents most aggressive interactions; in *Hylobates* and *Pongo,* solitary/monogamous social organizations prevent aggressive interactions; in *Pan* aggressive interactions are managed through violence and more importantly, through displays - many of which include bipedal stands and charges as components of the display.

The drying climates in the Late Miocene would have resulted in a lack of resource availability and an increase in both intra- and intergroup competition. This in turn would have increased the use of mock bipedal fights and bipedal runs, such as those seen in *Pan,* and using these ritualized displays would have made injuries less frequent in times of aggression. This

behavior would have been spread by females when immigrating to new groups (Jablonski and Chaplin, 1993). This theory relies on the idea that there was a shift in the environment in the Miocene, but that has been questioned by some researchers. DeMenocal (2004) has suggested that in Africa the main period of drying occurred in the Pliocene, well after the emergence of bipedalism.

Parker (1987) suggested that bipedalism could have been selected for due to sexual selection. This argument posits that females would have selected males bearing "nuptial gifts" of favored food resources and this would have been especially important in dry, seasonal habitats. Females would have differentially mated with those males best able to acquire these resources, such as scavenged animals, nuts, or other high quality foods. Parker (1987) thought that males might have even have brought small samples of their food resources to females to entice them. Unfortunately, Parker (1987) has no actual data from extant primate populations to support this hypothesis.

Group Three: Feeding

The feeding category covers several different types of food sources, including terrestrial gathering, seed eating, arboreal gathering, and aquatic vegetation. When extant primates use bipedal postures, it is generally in the context of feeding. Bipedalism composes less than two percent of the baboon locomotor repertoire, but when used it is always in a feeding context. Gibbons also use bipedal postures in feeding contexts, as well as for travel. Evidence from these and other primates could indicate that feeding is the greatest selective advantage for bipedalism. Once bipedalism arose in the hominin lineage, it could have been further reinforced by other benefits, such as carrying objects (Rose, 1991).

Isbell and Young (1996) have suggested that there was a trio of correlated events in the Late Miocene: a cooling and drying trend, the evolution of bipedalism and the divergence of *Pan* and *Homo.* These authors hypothesized that the fission-fusion grouping pattern seen in *Pan* and the adoption of bipedal locomotion in *Homo* are two possible solutions to a decrease in the density of resources caused by the cooling climate and the adoption of these two strategies is a form of niche partitioning. Fission-fusion grouping patterns are beneficial when resources are dispersed because it decreases intragroup feeding competition. According to these authors, bipedal locomotion would do the same by increasing home range size. Having a large home range would allow early hominins to get the same number of calories in a patchier environment (Rodman and McHenry, 1980). This theory assumes that the bipedalism of early australopiths was as efficient as that of *Homo erectus*.

It is also possible that bipedalism evolved as an adaptation for feeding on seeds. Using *Theropithecus* as a model, Jolly (1970) suggested that early hominins could have been living in edaphic grasslands, where nutritious, high-calorie seeds are abundant. Early hominins would have started by squatting, as *Theropithecus* does, holding their torso directly over the pelvis. They would have used a shuffling form of bipedalism to move to new foraging locations and obligate bipedalism would have arisen from there.

There are several lines of evidence to support theories of arboreal foraging for the evolution of bipedalism. Most observed bipedal events by wild chimpanzees in Tanzania were in the context of feeding in short, understory fruit trees. Bipedal posture allowed the chimps to reach further into the trees and increased their rate of food collection. The terrestrial bipedal shuffle was used most frequently over the short distances between these trees (Hunt, 1994). In the Bwindi Impenetrable Forest, all bouts of bipedalism were in an arboreal context and were

related to reaching to pick fruit from higher limbs. Mostly the chimpanzees used bipedal posture and not bipedal locomotion (Stanford, 2006).

Vidian and McGrew (2001) attempted to test various hypotheses for the evolution of bipedalism using captive chimpanzee and bonobos. They found that when they gave the chimpanzees piles of food or elevated platforms with food on them, it increased their rate of bipedal locomotion. Giving them branches (to test the display hypothesis) or erecting barriers (to test the vigilance hypotheses) yielded no result.

The last feeding hypothesis is that bipedalism evolved in a context of aquatic gathering, a hypothesis more commonly known as the "aquatic ape" hypothesis. Traditionally, this hypothesis has been largely ignored by the scientific community as being invalid; however Langdon (1996) made the point that while this hypothesis might be invalid, it should still be addressed in a scientifically rigorous manner. The aquatic ape hypothesis was first proposed by Hardy (1960) and popularized by Elaine Morgan (1972); it postulates that hominins would have moved to foraging in the sea or on coastlines in order to avoid competition from other apes for fruits in the trees and that the buoyancy of the water would have allowed for bipedal posture to evolve in a semi-gravity-free environment. Hardy also used the aquatic environment as the trigger to the evolution of many other unique human traits, such as relative hairlessness and voluntary breath control.

Verhaegen *et al.* (2002) more recently added to this theory. These authors discarded the idea that bipedalism would have evolved in a non-aquatic environment, because the need for bipedal posture would have been temporary and no other primate that lives in a primarily terrestrial setting has anything like obligate bipedalism. Bipedalism would have evolved in the context of wading and foraging for aquatic vegetation, and having the arms free would have

allowed primates to grasp overhanging trees for balance when wading into water. While these hypotheses that seek to explain many aspects of human evolution with a single contained theory are attractive, they rarely hold up under intense scrutiny. The reliance of this hypothesis on soft tissue morphology makes it impossible to corroborate with the fossil record. Additionally, the idea that bipedalism evolved in coastal environments is inconsistent with what we know about the human fossil record (Langdon, 1996).

Group 4: Others (Variability selection, thermoregulation)

There are some theories for the selective pressure for the evolution of bipedalism that do not fall into any of the previous groupings. Wheeler (1991, 1993) hypothesized that bipedalism was selected for as a mechanism to keep core temperatures low in hot climates. He used several lines of evidence for this: first, hominoids lack adaptations such as carotid rete and large evaporative surfaces in the nasal passages; second, standing bipedally exposes less of the body to direct solar radiation during the warmest part of the day; and third, standing upright exposes more of the body to greater winds which will facilitate evaporative cooling. The long, linear limbs and increase in height increases surface area for heat loss. Wheeler's model (1993) indicated that an individual with *H. erectus* like proportions would need to sweat 21-29% less than those with *A. afarensis* like proportions and consequently, they would need to drink approximately 13-15% less water than an individual with *A. afarensis* proportions. Needing less to drink would have been beneficial in open environments where drinking water was scarce or required significant travel times. Wheeler's model relies on the idea that bipedalism evolved in concert with a move to savanna, a fact that has been called into question in light of the discovery

of bipedally adapted primates in more closed environments (White *et al.,* 2006; Richmond and Jungers, 2008; Lovejoy *et al.,* 2009)

Variability selection is the idea that a feature would have been selected for because it gave individuals an advantage in a climate that was subject to both short term and long term fluctuations. It predicts that over time, hominins occupied a wider and wider variety of environments as each successive generation adapted to the current environmental extreme. Bipedalism would have arisen within the context of drying habitats where hominins would have had to be able to be adept both in dense forests and more open environments (Potts, 1998).

Finally, Pickford (2006) dismissed many of the previous theories as simply advantages once an organism has become bipedal, but not sufficient to be the cause of the adoption of bipedal posture. He suggested that bipedal posture arose because it is energetically efficient and allowed hominins to invade areas of Africa with a shorter growing season and be more "eurytopic" (= able to adapt to a variety of environmental conditions). Although Pickford never cited Potts' variability hypothesis (1998), his conclusions do most closely mirror those of Potts. The efficiency of bipedal gait is discussed in greater detail in the following section.

Locomotor energetics in humans, chimpanzees and early hominins

There have been many studies comparing the locomotor efficiency of human bipedalism, chimpanzee bipedalism and quadrupedalism to the presumptive form of bipedalism practiced by *Australopithecus afarensis* (using AL 288) and *Homo erectus* (using WT 15000). In general, bipedalism has been found to be more efficient than quadrupedalism. Leonard and Robertson (1997) examined the question of energy efficiency of bipedalism by comparing the effects of bipedal gait on maintenance energy expenditure (*i.e.,* feeding, BMR) and productive energy

expenditure (*i.e.,* growth and reproduction). They found that the benefits for energetically efficient movement are greater in organisms that have large day ranges and that bipedalism was more energetically efficient than quadrupedalism in many mammals. Even if *A. afarensis* did not have a complete modern gait, there would still have been a substantial gain in energetic efficiency with the shift to bipedalism. Pontzer *et al.,* (2009) used a combination of variables that represent the length of stride, the effective mechanical advantage of the limb, and the fascile length (the length of the muscle fiber bundles) of the joint in order to estimate locomotor efficiency. They found that the metabolic cost of the form of bipedalism practiced by *A. afarensis* would have been less than for *Pan* and that locomotor efficiency might have contributed to the evolution of bipedality. It should be noted that their calculations are based on a knuckle-walking last common ancestor of *Pan* and *Homo.*

Australopithecus afarensis, as represented by AL 288, does not have a fully modern human body plan. Her short stature is due to a having a shorter hind-limb than modern humans; her humerus in the same size as that seen in modern humans of similar size and mass (Jungers,1982). It has been suggested that having a shortened hindlimb would have resulted in a less efficient gait (although it would have been beneficial for vertical climbing) (Jungers and Stern, 1983). However, Kramer (1999) argued that shorter legs are not inherently less efficient than a longer stride. Using anatomical data, Kramer concluded that *Australopithecus afarensis* would have used less energy to move than a modern human and found no evidence in the skeleton which would have precluded a modern form of bipedal locomotion (as opposed to a BHBK gait). The pelvis of AL 288 is very broad mediolaterally in comparison to the anteroposterior direction, unlike that of modern humans. Rak (1991) hypothesized that the long, narrow pelvic dimensions of AL 288 were a novel adaptation particular to early hominins to

reduce the vertical displacement of the torso and thereby reduce ground reaction forces. In modern humans, the lengthening of the legs functions similarly; therefore AL 288 would not have needed longer legs for a relatively efficient gait.

Additionally, Kramer and Eck (2000) found that the shorter legs of *Australopithecus afarensis* were optimal for slow-speed foraging. In a comparison between Lucy and a modern human female, Lucy's slow speed walking was more efficient. However, the transition speed from a walk to a run was lower in *A. afarensis* and Lucy's running gait was less efficient. This has led these authors to postulate that bipedalism as it is expressed in *A. afarensis* was an adaptation to foraging in an area where food resources were dense whereas the long-legged modern human body would have evolved once early hominins had to range over a larger area. In a study that evaluated the necessary muscle power in AL 288 and WT 15000, Wang *et al.,* (2004) found that these individuals WT 15000 and AL 288 would have expended an equal amount of power per pound of body mass. However, when distance was figured into the equation, WT 15000 would have used less overall muscle power. This led these authors to conclude that long distance foraging or the need for speed and endurance over longer distances may have been the selective factor for the modern human body plan.

Berge (1994) tested whether a *Homo*-like or ape-like musculature better suited the pelvis of AL 288. She found that osteology of AL 288 corresponded better with that of the ape-like muscle pattern. Thus, this author concluded that AL 288 could not have moved like a modern human. She postulated that the hip would have lacked stability and bipedalism would have consisted of an inefficient "waddling gait". However, the greater mobility in the lower limb could be interpreted as the retention of arboreal adaptations.

The bent-hip/bent-knee gait used by chimpanzees while bipedal is far less efficient than a human bipedal gait. Individuals walking with a BHBK gait do not have efficient energy conservation mechanisms during the gait cycle (Wang, 2003). Crompton *et al.* (1998) tested the mechanical efficiency of *Australopithecus afarensis* walking with a BHBK gait versus a fully upright posture and found that the energetic cost of the BHBK gait would have precluded any advantage gained by bipedal posture. These authors also determined that Lucy's limb portions had exceeded the point where she could have walked with a chimpanzee-like bent hip/bent knee gait. These results were further supported by Wang (2004) who also found that for *A. afarensis,* a BHBK gait would have been extremely inefficient, and the limb proportions of *Australopithecus afarensis* could have resulted in reasonably efficient upright postures. Wang further suggested that the modern human body plan could have been selected for by an increased need for tool and raw material transport, as opposed to an increase in day ranges. He found that the BHBK gait is especially inefficient for carrying and that an individual with the proportions of Nariokotome would have been able to efficiently transports loads of up to 15% of his body weight.

The Earliest Bipeds

Although this study concentrates on hindlimb morphology in hominins during the period between roughly 3.8 and 1.0 Ma in Africa, the origins of bipedalism pre-date this time period. Three different taxa from the Late Miocene/Early Pliocene have also been reconstructed to have a bipedal component to their locomotor repertoires. This striking evidence has come from *Oreopithecus bambolii, Orrorin tugenensis* and *Ardipithecus ramidus*.

The hypodigm of *Orrorin tugenensis* consists of some isolated teeth, two mandibular fragments and a small collection of postcranial remains, including two proximal femora, all of which were found in Kenya. Of the two femora, BAR 1002'00 is the most complete although neither femur has the greater trochanter preserved. Both femora have characteristics of bipeds, including: an anteriorly rotated, spherical femoral head; a fovea capitis that is somewhat wide; a somewhat deep trochanteric fossa that leads to an intertrochanteric groove that ends above the lesser trochanter; and a neck shaft angle between 120° and 130° (Pickford *et al.,* 2001; Senut *et al.,* 2001). Later metric analyses found that the *Orrorin* remains were most similar to *Australopithecus* and *Paranthropus* proximal femora and were therefore at least habitually bipedal (Richmond and Jungers, 2008).

Ardipithecus ramidus is dated to 4.4 Ma and includes the oldest relatively complete hominin skeleton that has been discovered to date (White *et al.* 2008). While *Ardipithecus ramidus* is too young to be the last common ancestor between chimpanzees and humans, its discoverers have placed it as one of the oldest fossils in the human lineage (White *et al.* 2008). The *Ardipithecus* skeleton is characterized by: forelimbs and hindlimbs of similar lengths; a relatively short metacarpus paired with long manual phalanges and a robust hallux; a foot adapted more for quadrupedal walking than for grasping; a flexible lumbar region; and, an expanded iliac region. Lovejoy *et al.,* (2009) have used this information to reconstruct the locomotor pattern of *Ardipithecus ramidus* to be similar to *Proconsul* or a cercopithecoid, consisting mainly of careful, above branch quadrupedalism and a small amount of facultative bipedalism. If *Ardipithecus ramidus* is assumed to be a direct hominin ancestor (as these authors postulate), then adaptations for suspension evolved independently in *Hylobates, Pongo, Pan* and *Gorilla* (Lovejoy *et al.,* 2009). It should be noted, however, that it is more parsimonious to

assume that the adaptive suite related to suspension did derive from a common ancestor, and thus that the modifications of the skeleton towards bipedalization could have evolved twice. This alternate scenario is particularly interesting when looked at in concert with *Oreopithecus,* a Miocene ape with a mosaic of postcranial features.

Oreopithecus bambolii is a Late Miocene ape from Tuscany, Italy, and its postcranium has been interpreted to have some convergent morphology with that of bipedal hominins. In the vertebral column, *Oreopithecus* has a marked lumbar lordosis and increased caudal surface area of the vertebral laminae, both characteristics of bipeds (Köhler and Moyà-Solà, 1997). The femur of *Oreopithecus* has a valgus angle, indicative of habitual bipedal posture. The external pelvis of *Oreopithecus* is convergent with *Homo* in that it has a well-developed anteroinferior iliac spine (Köhler and Moyà-Solà, 1997) and the internal trabecular morphology has an organized pattern similar to that seen in *Homo.* This well-organized, well-supported pattern starts developing in humans at a young age due to the downward stresses of bipedal locomotion (Rook *et al.,* 1999). The foot of *Oreopithecus* is unlike that of any extant primate in that it has a mosaic of traits that would have sacrificed both speed and agility for having a rigid platform to support the body in bipedal postures and slow bipedal shuffles (Köhler and Moyà-Solà, 1997). It should be noted that the locomotor pattern of *Oreopithecus* is still debated, and some authors (*e.g.* Susman, 2004) have concluded that these seemingly bipedal traits were actually adaptations to vertical climbing.

Considering the case of *Oreopithecus* is instructive when thinking about the evolution of hominin bipedalism. It is possible that the selective pressure for bipedal posture in *Oreopithecus* was for efficiency; because *Oreopithecus* inhabited an island devoid of predators, it was able to sacrifice the more energetically expensive arboreal locomotor activities for more efficient

terrestrial bipedal foraging. It is possible that walking bipedally would also have made *Oreopithecus* a more efficient forager, (Köhler and Moyà-Solà, 1997), not unlike the chimpanzee models that have been used for *Australopithecus* (*e.g.,* Hunt, 1994; Stanford, 2006). In addition to the taxa discussed, it is even possible that apes as old as *Proconsul africanus* may have used a rudimentary form of bipedalism in conjunction with quadrupedal climbing (Rose, 1991). Thus, the ideas that there could have been a great amount of bipedal locomotor diversity in Africa and that bipedalism could have evolved multiple times is not as far-fetched as some authors would make it seem (Lovejoy, 1981 *et seq.*).

Overview of the Text

In order to accomplish the goals of the project, the data have been broken up into sections. First, Chapter 2 gives a general overview of Plio-Pleistocene postcranial material and paleontological sites. It also details the extant comparative sample and the statistical methods used for the analytical chapters. Chapters 3 through 5 are the analytical chapters. Chapter 3 examines the forelimb, including the humerus, radius and ulna, while chapters 4 examines the hindlimb, including the femur and tibia. These chapters examine the variation present in single limb elements as well as patterns of co-variation across joints. Chapter 5 tests hypotheses about developmental and evolutionary integration between the forelimb and the hindlimb and examines patterns of fore-/hindlimb co-variation in associated Plio-Pleiostcene skeletons. Finally, Chapter 6 reviews the results of all the analytical chapters in order to consider the broader implications of the results of these analyses.

Abbreviations and Taxonomy

Throughout the text, various museum abbreviations are used. These abbreviations are:

- **AMNH-A –** American Museum of Natural History, Department of Anthropology, New York, NY;
- **AMNH-M –** American Museum of Natural History, Department of Mammology, New York, NY;
- **KNM –**Kenya National Museum, Department of Palaeontology, Nairobi, Kenya;
- **NHM-A –** Natural History Museum London, Department of Anthropology, London, UK;
- **NME –** National Museum of Ethiopia, Addis Ababa, Ethiopia;
- **NMT –** National Museum of Tanzania, Dar es Salaam, Tanzania;
- **PCM –** Powell Cotton Museum, Birchington-on-Sea, UK;
- **RMCA –** Royal Museum of Central Africa, Tervuren, Belguim;
- **TMP –** Transvaal Museum, Pretoria, South Africa;
- **UCT-A –** University of Cape Town, Department of Anthropology Cape Town, South Africa; and
- **UWMA –** University of the Witwatersrand, Department of Anatomy, Johannesburg, South Africa.

There is a series of statistical abbreviations that will also be used frequently. These are:

- **2BPLS** – Two-block partial least squares analysis, a multivariate statistical analysis that is used to find the way that two data sets covary symmetrically;
- **3DGM –** Three-dimensional geometric morphometrics, the quantification of shape in three dimensional spaces;

- **GPA –** Generalized Procrustes Analysis, the process of size scaling, rotating and transposing *x,y,z,* coordinate data by minimizing the least squares distance between specimens; and
- **PCA –** Principal components analysis, a multivariate ordination analysis that maximizes the difference in a sample via a singular value decomposition and projection into two-dimensional space.

In addition, all taxonomic references follow these attributions:

- **Hominidae**, hominid: A family level group containing *Homo, Pan, Gorilla,* and *Pongo* as well as direct fossil ancestors of these taxa (Gray, 1825);
- **Homininae,** hominine: A subfamily level group containing *Homo, Pan, Gorilla* and direct fossil ancestors of these taxa (Gray, 1825);
- **Hominini**, hominin: A tribe containing *Homo* and all fossil ancestors of *Homo* (Gray, 1825) plus australopiths; and
- **australopith**: A non-taxonomic term used to reference all members of the genus *Australopithecus*.

CHAPTER 2: MATERIALS

This chapter will describe the specimens collected for this project and methodology used to collect the data. This will include a discussion of three dimensional geometric morphometrics, the collection process and its applications to biology and paleoanthropology in particular. An account of the fossils examined will be given, as well as a discussion and justification for the extant individuals used.

Modern Comparative Sample

The modern comparative sample consists of 237 extant individuals from the following groups: *Gorilla gorilla gorilla, Gorilla gorilla graueri, Gorilla gorilla beringei, Pan troglodytes troglodytes, Pan trogolodytes schweinfurthii, Pan pansicus*, *Pongo pygmaeus,* and *Homo sapiens* from four different populations – Late Stone Age South Africans, Andaman Islanders, Australian Aborigines and Point Hope Ipiutak (see Table 2.1). All individuals sampled were adults and displayed full epiphyseal closure at all joints. The elements and data collected are described below. Where sex was not indicated on the specimen, it was determined using the pelvis in *Homo sapiens* and using size for *Pongo* and *Gorilla*. If the sex was not given for *Pan,* or if the pelvis was missing for *Homo sapiens*, specimens were listed as unknown. No zoo specimens were sampled. The target sample size for each group was fifty individuals, split evenly between males and females. In almost all cases this was impossible due to the relative scarcity of postcranial skeletons in comparison with crania and because of collection and cataloguing practices at museums earlier in the last century (in some collections, skeletons have been broken up and catalogued by element as opposed to by individual).

As the closest evolutionary relatives of early hominin taxa, *Homo* will provide an appropriate measure for the amount of variation we should expect in a single hominin species, and *Pan* species will provide an appropriate measure for the amount of variation we should expect in a single hominin genus. *Pan* and *Homo* are also appropriate functional analogs, as much of the functional debate surrounding hominin postcranial remains centers around the degree of bipedalism practiced by each taxon (see Napier, 1964; Leakey *et al.* 1964; Clarke and Tobias, 1995; Kidd *et al*., 1996; McHenry and Berger, 1998).

The *H. sapiens* sample was chosen from maximally different populations in order to encompass the full range of modern human variability. No modern morphological collections were sampled for modern humans as they presumably exhibit a high degree of genetic admixture; instead archaeological and more isolated populations were sampled**.** In order to have a comparison to generic level differences, both *Pan troglodytes and Pan pansicus* were sampled. Finally, by sampling two subspecies within *Pan troglodytes* (*P. t. troglodytes* and *P. t. schweinfurthi*) and within *Gorilla gorilla* (*G. g. graueri* and *G. g. gorilla*) I have an analog for the type of variation that would be expected in subspecies.

Pongo and *Gorilla* are good examples where a large amount of size dimorphism and postcranial shape variation are contained in a single genus. *Gorilla,* as well as being highly sexually dimorphic, presents subspecifically consistent differences in the morphology of the elbow and shoulder joints, as well as in the length of the metacarpals (Inouye, 1992; Taylor, 1997). Therefore, information from these taxa gives a good estimate of the maximum amount of both size and shape variation that can be accommodated in a single taxon.

Table 2.1 List of extant specimens used for this study by species, subspecies and sex.

	Males	Females	Unknown	Total
***Gorilla* (n = 77)**				
Gorilla gorilla beringei[1]	2	3	0	5
Gorilla gorilla gorilla [2]	24	26	0	50
Gorilla gorilla graueri[3]	13	9	0	22
***Homo sapiens* (n = 76)**				
Andaman Islanders	11	10	8	29
Australian aborigines	3	3	8	14
Late Stone Age South Africans	8	4	1	13
Point Hope Ipiutak	15	15	0	30
***Pan* (n = 88)**				
Pan paniscus [3]	7	9	0	16
Pan troglodytes schweinfurthii [3]	7	7	14	28
Pan troglodytes troglodytes [2]	19	25	0	44
***Pongo* (n = 16)**				
Pongo pygmaeus	9	6	1	16

[1] Virunga isolates; RMCA, [2] Cameroon (and some gorilla males from R o Congo); PCM, [3] DRC; RMCA, AMNH-M, [4]Borneo, Sumatra; AMNH-M, NHM-M

Homo

Data were collected on four populations of modern humans, two of archaeological origin. All of the Andaman Island skeletons that were sampled in the NHM Anthropology Department were collected from individuals who died within 50 years of the first British occupation in 1858. The Andaman Islands are a series of almost 200 small islands off the coast of India in the Indian Ocean, and their inhabitants represent an isolated population that was probably colonized quite early in human history (Late Pleistocene). They had very little contact with individuals from other nearby islands and almost no contact with Western countries. They have a very distinct

phenotype, being smaller and more gracile than most modern human populations (Endicott, 2003).

The Australian skeletons studied at the NHM are presumed to be Australian Aborigines collected from mainland Australia (not part of the recently repatriated Tasmanian collection), however there is no precise data on the origins of the collection, or where the individuals were originally located.

Data were collected on Late Stone Age South Africans from pre-pastoralist groups dated to before 2000 BP, prior to the emergence of the more modern Khoikhoi populations. All individuals were recovered from the south-western coast of South Africa, either in shallow dune burials or in rough rock shelters; they are housed at UCT-A. Most of the specimens are from two clusters of individuals – a group found near Faraoskop in the Vrendendal District (dated to approximately 2100 BC) and a group found in the Oakhurst Rock shelter near the town of George (dated to approximately 6000 BC). Although their dates are quite far apart, these individuals were all likely part of one continuous population that had a similar lifestyle centered around gathering and coastal fishing (Morris, 1992).

The Point Hope Ipiutak sample studied at AMNH-A is an archaeological population excavated from Point Hope, Alaska during the Rainey-Larson Point Hope Expeditions between 1939 and 1941. They represent a cold-adapted group practicing typical subsistence foraging. Radiocarbon dates indicate that the area was settled around 2000 BC and was under continuous settlement up to the present. There were at least three cultural shifts in the Point Hope area – pre-Ipiutak, Ipiutak and Tigara (Rainey, 1941; Mason, 1998). Only indvidiuals from the Ipiutak population were sampled in order to limit the effects of genetic introgression.

Fossil Sample

The time frame of interest is roughly demarcated by 4.1 Ma-1.5 Ma. Data were collected on 149 fossil individuals from localities in both East and South Africa, attributed to 9 different species, including: *A. anamensis, A. afarensis, A. africanus, A. garhi, H. habilis sensu lato* (including putative *H. rudolfensis* of which there are currently no associated postcranial remains) , *H. erectus, P. boisei,* and *P. robustus.* Several of these may have lived sympatrically at sites in both East Africa (e.g., *P. boisei, H. habilis sensu lato* and *H. erectus* at Koobi Fora) and South Africa (e.g., *A. africanus* and *H. habilis* at Sterkfontein). All data were collected on the actual specimens; no casts were utilized for this study. The following section briefly describes the fossils by site, with a summary in Table 2.2.

ETHIOPIA

Hadar

The fossil-bearing region of Hadar is located in the west-central region of Ethiopia. The three upper members of the Hadar Formation (Sidi Hakoma, Denen Dora and Kada Hadar) are the important fossiliferous sediments. The oldest fossils are dated to approximately 3.4 Ma and the youngest to approximately 3.1 Ma (Kimbel and Walter, 2000). All of the fossil hominins have generally been assigned to the taxon *Australopithecus afarensis* (Johanson *et al.* 1978 *et seq*.) although some researchers have argued that these individuals should be divided into two separate taxa on the basis of size (Zihlman, 1985; Senut, 1992). Data were collected on 20 individuals from the Hadar region at NME, including: AL 128-1, 129-1, 137-48, 288, 322-1, 333-107, 333-12, 333-123, 333-29, 333-3, 333-4, 333-42, 333-6, 333-7, 333-95, 333w-33, 333w-36, 333w-56, 333x-26 and 333x-5.

There are three individuals with associated elements from the Hadar material. AL 129-1 consists of a distal femur and proximal tibia; Johanson and Taieb (1976) suggested in their original description that AL 128 (a proximal femur) belonged to the same individual, based on size and proximity. AL 137-48 consists of a distal humerus and distal ulna. Of AL 288 ("Lucy"), I examined only a partial humerus, radius, ulna, femur and tibia. The rest of the assemblage consists of individuals represented by a single element. There are two distal humeri (AL 322-1, 333-29), one proximal humerus (AL 333-107), one proximal radius (AL 333w-33), two proximal ulnae (AL 333w-36, 333x-5), one distal ulna (AL 333-12), four proximal femora (AL 128-1, 333-123, 333-3, 333-95) two distal femora (AL 333-4, AL 333x-56), two proximal tibiae (AL 333-42, 333x-26) and two distal tibiae (AL 333-6, 333-7). All of the AL 333 material is part of a single assemblage and is dated to 3.2 Ma, while Lucy is dated to 3.18 Ma (Walter, 1994)

Middle Awash

The Middle Awash is located south of Hadar, along the Awash river. This geologically complex region has a stratigraphic sequence that spans that last 6 million years. The region is broken up into distinct areas based on the Afar tribal designations. (White, 2000a). The specimens studied here derive from the later sediments of the Bouri area on the west side of the Awash River and the Maka and Matabaietu areas on the east side of the Awash River.

Seven specimens are from Bouri, with three from the Hata Member (BOU-VP 11/1, 12/1, 35/1, and four from the Daka Member (BOU-VP 1/17, 1/109, 19/63, 35/1). The specimens from the Hata Member have been dated to approximately 2.5 Ma and have not been attributed to any specific taxon, although there is speculation that they could belong to *A. garhi* (Asfaw *et al.,* 1999). BOU-VP-12/1 is an associated skeleton including a partial humerus, proximal radius, an

extremely fragmentary ulna and a femoral shaft. BOU-VP-11/1 is a proximal ulna, and BOU-VP-35/1 is a femoral shaft. The specimens from the Daka Member have been attributed to the taxon *Homo erectus* and are dated to ca. 1 Ma (Asfaw *et al.* 2002). They consist of two femoral shafts (BOU-VP 1/17, 2/15), one partial distal femur (BOU-VP-19/63) and one proximal tibia (BOU-VP-1/109).

Data were also collected on one specimen from Matabaietu (MAT-VP-1/1, a distal humerus) and one specimen from Maka (MAK-VP-1/1, a proximal femur). The Maka femur has been dated to 3.5 Ma and attributed to *Australopithecus afarensis* (Lovejoy *et al.*, 2002) while the Matabaietu humerus has been dated to 2.5 Ma and has not been attributed to any particular taxon (Asfaw *et al.,* 1999).

Melka Kontouré

Melka Kontouré is located in Central Ethiopia along the Awash River and is composed largely of fluvial deposits, with interspersed with volcanic layers. The archaeological sequence spans the time from the Oldowan through the Middle Stone Age (White, 2000b). Data on one distal humerus from the Melka Kontouré region (Gomboré I-B 7594) were collected at NME. The specimen is dated to 1.6 Ma and has been attributed to early *Homo* (Senut and Tardieu, 1985) and *Homo erectus* (Coppens, 2004).

Omo Valley

The Omo River Valley represents the northern-most extension of the East African Rift. Data were collected from five specimens at NME. Omo Kibish 1 is an associated skeleton including (for the purposes of this study) right and left distal humeri, proximal ulna, distal femur

and distal tibia. It is considered to be one of the earliest modern *Homo sapiens,* now dated to approximately 200 Ka (McDougall *et al.,* 2005). Four specimens derive from the Shungura Formation and were placed in stratigraphic context by Feibel *et al.*, 1989. Omo 119-1973-2710 is a proximal humerus dated to 2.43 Ma, and L40-19 is a nearly complete ulna which been attributed to *Paranthropus boisei* (McHenry *et al*., 1976) and dated to 2.37 Ma. Omo 75s-1970-1317 is a proximal radius and Omo 141-1972-23 is a proximal ulna dated to 2.2 Ma, both from Lower Member G (Feibel *et al.* 1989).

KENYA

Turkana Basin

The Turkana Basin refers to the potion of the east African rift with Lake Turkana in northern Kenya and the Omo Valley in Ethiopia (see previous section). The Turkana Basin has sediments dating from the Late Oligocene through the Late Pleistocene. The hominin bearing regions are West Turkana, Koobi Fora, Kanapoi and Allia Bay, and they date from 4.17 Ma through 0.05 Ma (Brown, 2000).

Data on 40 specimens from the Turkana Basin, Kenya were collected at KNM. Three specimens (KP 271, 29285, ER 20419) come from deposits at Kanapoi dated between 4.17 and 4.07 Ma (Leakey *et al.* 1988). These include a distal humerus, proximal and distal tibia and proximal and distal radius; all specimens are attributed to *Australopithecus anamensis* (Leakey, 1995; Ward, 2001). Two specimens from West Turkana were sampled: WT 15000 and WT 19700. The humerus, ulna, femur and tibia were sampled from WT 15000 ("Nariokotome Boy"), an associated skeleton of a juvenile *H. erectus* dated to 1.6 Ma (Brown *et al.,* 1985;

Feibel *et al.* 1989; Walker, 1994)**.** WT 19700 is a complete proximal tibia from the Nachukui Formation (Walker, 1994).

There are several sets of associated postcranial remains from East Turkana whose ages have been assessed by Feibel *et al.* (1989): ER 803, 1481, 1500, 1808 and 3735. ER 803 and 1808 both consist of associated femoral and tibial shafts. ER 803 is dated to approximately 1.57 Ma and has been attributed to *Homo* sp. indet (Leakey and Day, 1973) while ER 1808 is dated between 1.53 -0.05 Ma and is considered to be *Homo erectus* (Leakey and Leakey, 1978). ER 1481 consists of an associated proximal and distal femur and tibia. It has been dated between 1.89-0.05 Ma and attributed to the genus *Homo* (Leakey, 1973; Senut and Tardieu, 1985). ER 1500 is dated to 1.90 -1.88 Ma and is composed of a proximal radius, proximal ulna, distal femur and proximal and distal tibia. It has been considered by most researchers to be *Paranthropus boisei* (Leakey, 1973; Senut and Tardieu, 1985; Grausz *et al.*1988). ER 3735 has been attributed to the genus *Australopithecus (Paranthropus)* (Senut and Tardieu, 1985) and is composed of a distal humerus and proximal radius. This specimen is dated to 1.88 – 1.90 Ma

All other individuals sampled were represented by a single element. KNM-ER 1473 (1.89-0.05 Ma) is the only proximal humerus. ER 739 (1.53 -0.05 Ma), 1504 (1.89-0.05 Ma), 1591, 1824 and 6020 (1.7 Ma) are all distal humeri. ER 3736 (1.89-0.05 Ma Ma), 3888 (1.57-0.05 Ma), and 3956A (1.89-0.05 Ma) are proximal radii. Seven individuals were represented by proximal femora – ER 738 (1.88 Ma), 815 (1.77-0.10 Ma), 999 (0.5 – 0.1 Ma), 1503, 1505A, 3728, and 5880 (1.89-0.05 Ma). ER 1472 is composed of a nearly complete proximal and distal femur (1.89-0.05 Ma). Three other distal femora were sampled – ER 993 (1.53-0.05 Ma), 1592 (1.85 Ma) and 3951 (1.89-0.05 Ma). ER 736 (1.7 Ma), 737 (1.6 Ma), 1463 (1.53 -0.05 Ma), 1807 (1.53 -0.05 Ma), and 1809 (1.77-0.05 Ma) are represented by femoral shafts only. ER 741 (1.53

-0.05 Ma), 1471 (1.89-0.05 Ma), 1476B (1.88 Ma), 1810 (1.89-0.05 Ma) and 2594A (1.53 -0.05 Ma) are all proximal tibiae (all dates from Feibel *et al.* 1989).

Baringo Basin

The Baringo Basin is located in Western Kenya and is notable for its long primate bearing stratigraphic sequence. The oldest sediments in the Baringo Basin sequence are approximately 15 Ma and have yielded many individuals attributed to *Kenyapithecus*, a Middle Miocene ape. The Lukeino, Chemeron and Kapthurin formations are all hominin bearing, with the Lukeino molar perhaps being the earliest hominin found at 6 Ma (Delson *et al.,* 2000).

Data on two specimens from the Baringo Basin were collected at the KNM. The first is a proximal humerus from the Chemeron Formation, dated to approximately 5.07 Ma and assumed to be a very early member of the genus *Australopithecus,* or even *Ardipithecus*, considering the early date. The second specimen is an ulna from the Kapthurin Formation, dated to less than 0.66 Ma, which has been attributed to *Homo erectus* or "archaic" *Homo sapiens* (Wood, 1999).

TANZANIA

Laetoli

Laetoli is located in northern Tanzania and is the type site for *Australopithecus afarensis.* There are two relevant fossiliferous deposits at Laetoli: the Upper Laetolil beds, spanning the time period between 3.63-3.85 Ma and the Upper Ndolanya Beds which are dates to 2.66 Ma (Harrison, in press). Data on one proximal tibia (field number EP 1000/98) was collected from Laetoli at NMT. This proximal tibia was recovered from the Upper Ndolanya Beds and has been

cautiously attributed to *P. aethiopicus* as the sole hominin taxon deriving from these beds (Harrison, in press).

Olduvai Gorge

Olduvai Gorge is also located in Northern Tanzania and is a dry, y-shaped valley with multiple branches that have strata starting in the Upper Pliocene and ending in the late Pleistocene (White, 2000c). Data were collected on seven postcranial specimens from Olduvai Gorge at the National Museum of Tanzania in Dar es Salaam and at the Kenya National Museum in Nairobi (OH 20, 28, 34, 35, 36, 53, 62). OH 62 is an extremely fragmentary partial skeleton consisting of a fragmentary humerus, proximal ulna and femoral shaft. It is associated with cranial remains that have been attributed to both *H. habilis* (Johanson *et al.*, 1987; Lieberman *et al.,* 1996) and *Homo* sp. indet (neither *H. habilis* or *H. rudolfensis*) (Blumenschine *et al.,* 2003). It comes from Lower Bed I and is dated between 1.85 and 1.75 Ma (Johanson *et al.,* 1987). OH 36 is a proximal ulna from Upper Bed II dated 1.52- 1.33 Ma (Aiello *et al.*, 1999). This specimen has been attributed to *H. erectus* (Leakey, 1973), *P. boisei* (Walker and Leakey, 1993) and to an indeterminate hominin (Aiello *et al.,* 1999). OH 20 and 34 are partial proximal femora. OH 20 was found on the surface of Lower Bed II and was attributed to *P. boisei* in the original description of the fossil (Day, 1969)**.** OH 34 was found at site JK2 West during the 1962 excavations at Olduvai. Its exact provenance is unknown, although it is said to come from Bed III (Kleindeinst, 1973), dated 1.15-0.8 Ma (Hay, 1976). OH 28 and 53 are femoral shafts from Bed IV and Upper Bed II respectively. OH 35 is a proximal tibia from the FLK floor dated to approximately 1.66 Ma (Walter *et al.* 1992). In the original description, it was classified as "Indet" (Davis, 1965) but has since been suggested to be *H. habilis* (Susman and Stern, 1982).

SOUTH AFRICA

Kromdraai

Kromdraai is a small site in the Transvaal province of South Africa, composed of dolomitic limestone deposits. Data were collected on TM 1517, a distal humerus that is part of the type specimen of *Paranthropus robustus* (Broom, 1938), found in Kromdraai B. Because Kromdraai is a cave site, dating this fossil precisely has been difficult. New paleomagnetic dates of a matrix similar to that found on the TM 1517 skull dates this fossil (and the sediments at Kromdraai B) to 1.9 Ma (Thackeray *et al.,* 2002).

Makapansgat

The site of Makapangsgat is located in the northern Transvaal and consists of a series of karst caves and solution chambers. The exact dating and provenance of the Makapansgat fossils is difficult as many of the fossils were found in the debris from the limeworks, although most authors accept an age close to 3 Ma. Data were collected on one proximal femur (MLD 46) from Makapansgat at UW, attributed to *A. africanus*. MLD 46 was found in Member 4 whereas most other hominin fossils were found in Member 3, the "grey breccia" (Reed *et al.* 1993).

Swartkrans

Swartkrans is located just west of Sterkfontein in the Transvaal area of South Africa and are composed of a series of karst cave breccia deposits. The dating of Swartkrans is unclear, although most current estimates put all of the fossil bearing members between 1.5 and 1.8 Ma (following Delson, 1988). Data were collected on 16 specimens from Swartkrans at TMP. SK 860, SKX 10924, SKX 3774 and SKX 24600 are distal humeri. SKX is from Member 3 and has

been attributed to *Homo* cf. *erectus* (Susman *et al.* 2001). SKX 3774 and 24600 are from Member 1 and are attributed to *P. robustus.* SK 18b, SK 2045, SKX 3699, and SKX 24601 are proximal radii. SK 18b and 2045 are attributed to *H.* cf *erectus* and are from Member 2 (Broom and Robinson, 1949; Susman *et al.* 2001). SKX 3699 and 24601 are attributed to *P. robustus* with the former from Member 1 and the latter from Member 2. SKX 3682 is a distal radius from Member 2 attributed to *P. robustus*. SK 8761 is a proximal ulna attributed to *P. robustus* from Member 1 (Susman, 1989). SK 82, 97, 3121, 14024 and SKW 19 are proximal femora attributed to *P. robustus.* SK 3121 is from the Member 2, but the other four are from the Hanging Remnant (Napier 1964; Susman *et al.,* 2001). SK 1896 is a distal femur from Member 2 attributed to *H.* cf *erectus* (Susman *et al.* 2001).

Sterkfontein

Sterkfontein is another karst-cave breccia site, located near the town of Krugersdotp. This site was originally a limestone quarry in the late 1890s. Due to the nature of the deposits, the dating of the layers is unclear. Most of the hominin fossils derive from Members 4 and 5. Member 4 is dated to somewhere between 2.8 and 2.2 Ma and Member 5 to 2 - 1.5 Ma. (Grine, 2000).

Data were collected on 41 specimens from Sterkfontein at UW and TMP. There is only one individual with associated postcranial elements. The distal humerus, proximal radius and proximal ulna were sampled from Stw 431. It was found in Member 4 and attributed to *A. africanus* (McHenry and Berger, 1997). The partial skeleton STS 14 is probably associated with the Sts 5 cranium ("Mrs. Ples") (Thackeray, *et al.* 2001) and therefore also attributed to *Australopithecus africanus; only* the proximal femur was sampled for this project.

All other individuals are represented by a single element. There are two proximal humeri (Stw 328 and Stw 517) and one humeral shaft (Stw 348). There are three proximal radii (Stw 105, 139 and 516) and one distal radius (Stw 46). Stw 113, 349, 380, 390, 398, and 571 are proximal ulnae and Stw 326 and 399 are distal ulnae. Most of the proximal femora are represented by the femoral head only (Stw 25, 30a, 65, 311, 392, 403, 479, 501, 522, and 527); Stw 99 is the only complete proximal femur. Sts 34, Stw 129 and 318, and TM 1513 and 3601 are distal femora while Stw 121 is a femoral shaft. Stw 396 and 514 are proximal tibiae while Stw 181, 358, 389, 515 and 567 are distal tibiae. Table 2.2 indicates the stratigraphic position of these fossils.

Table 2.2 A list of the fossils that were sampled, including their ages and stratigraphic position

Accession No.	Element	Site/Region	Stratigraphic Position/Locality	Age
AL 128-1	Prox. Femur	Hadar	Sidi Hakoma Member[2]	3.4 Ma[1]
AL 129-1	Prox. Femur	Hadar	Sidi Hakoma Member[2]	3.4 Ma[1]
AL 137-48	Dist. Humerus & Dist. Ulna	Hadar	Sidi Hakoma Member[2]	3.4 Ma[1]
AL 288	Assoc. Skeleton	Hadar	Kada Hadar Member[2]	3.18 Ma[1]
AL 322-1	Dist. humerus	Hadar	Denen Dora Member[2]	3.2 Ma[1]
AL 333-107	Prox. Humerus	Hadar	Denen Dora Member[2]	3.2 Ma[1]
AL 333-12	Dist. Ulna	Hadar	Denen Dora Member[2]	3.2 Ma[1]
AL 333-123	Prox. Femur	Hadar	Denen Dora Member[2]	3.2 Ma[1]
AL 333-29	Dist. Ulna	Hadar	Denen Dora Member[2]	3.2 Ma[1]
AL 333-3	Prox. Femur	Hadar	Denen Dora Member[2]	3.2 Ma[1]
AL 333-4	Dist. Femur	Hadar	Denen Dora Member[2]	3.2 Ma[1]
AL 333-42	Prox. Tibia	Hadar	Denen Dora Member[2]	3.2 Ma[1]
AL 333-6	Dist. Tibia	Hadar	Denen Dora Member[2]	3.2 Ma[1]
AL 333-7	Dist. Tibia	Hadar	Denen Dora Member[2]	3.2 Ma[1]
AL 333-95	Prox. femur	Hadar	Denen Dora Member[2]	3.2 Ma[1]
AL 333w-33	Prox. radius	Hadar	Denen Dora Member[2]	3.2 Ma[1]
AL 333w-36	Prox. Ulna	Hadar	Denen Dora Member[2]	3.2 Ma[1]
AL 333w-56	Dist. Femur	Hadar	Denen Dora Member[2]	3.2 Ma[1]
AL 333x-26	Prox. Tibia	Hadar	Denen Dora Member[2]	3.2 Ma[1]
AL 333x-5	Prox. Ulna	Hadar	Denen Dora Member[2]	3.2 Ma[1]
BC 1745	Prox. Humerus	Baringo	Chemeron Formation[3]	5.07 Ma[3]
BK 66	Prox. Ulna	Baringo	Kapthurin Formation[3]	< 0.66 Ma[3]
BOU-VP-1/109	Prox. Tibia	Middle Awash	Bouri, Daka Member[4]	1 Ma[4]
BOU-VP-1/17	Femoral Shaft	Middle Awash	Bouri, Daka Member[4]	1 Ma[4]
BOU-VP-11/1	Prox. Ulna	Middle Awash	Bouri, Hata Member[5]	2.5 Ma[5]
BOU-VP-12/1	Prox. Radius	Middle Awash	Bouri, Hata Member[5]	2.5 Ma[5]
BOU-VP-19/63	Dist. Femur	Middle Awash	Bouri, Daka Member[4]	1 Ma[4]
BOU-VP-2/15	Femoral Shaft	Middle Awash	Bouri, Daka Member[4]	1 Ma[4]
BOU-VP-35/1	Humeral Shaft	Middle Awash	Bouri, Hata Member[5]	2.5 Ma[5]
EP 1000/98	Prox. Tibia	Laetoli	Upper Ndolanya Beds[6]	2.66 Ma[6]
Gomboré IB 7594	Dist. Humerus	Melka Kontouré	Gomboré, site IB[7]	1.6 Ma[7]
ER 736	Femoral Shaft	Koobi Fora	Upper KBS Member[9]	1.7 Ma[9]
ER 737	Femoral Shaft	Koobi Fora	Lower Okote Member[9]	1.6 Ma[9]
ER 738	Prox. Femur	Koobi Fora	KBS Channel Complex[9]	1.88 Ma[9]
ER 739	Dist. Humerus	Koobi Fora	Upper Okote Member[9]	1.53 -0.05 Ma[9]
ER 741	Prox. Tibia	Koobi Fora	Upper Okote Member[9]	1.53 – 0.05 Ma[9]
ER 803	Femoral and Tibial Shafts	Koobi Fora	Upper Okote Member[9]	1.53-0.05 Ma[9]
ER 815	Prox. Femur	Koobi Fora	KBS Member [9]	1.77 -0.10 Ma[9]
ER 993	Dist. Femur	Koobi Fora	Upper Okote Member [9]	1.53 – 0.05 Ma[9]

Table 2.2 cont. A list of the fossils that were sampled, including their ages and stratigraphic position

Accession	Element	Site	Stratigraphic Position/Locality	Age
ER 999	Prox. Femur	Koobi Fora	Chari Member ("Guomde Fmn")[8,9]	0.5 – 0.1 Ma[9]
ER 1463	Femoral Shaft	Koobi Fora	Upper Okote Member[9]	1.53 – 0.05 Ma[9]
ER 1471	Prox. Tibia	Koobi Fora	Upper Burgi Member[9]	1.89-0.05 Ma[9]
ER 1472	Prox. and Dist. Femur	Koobi Fora	Upper Burgi Member[9]	1.89-0.05 Ma[9]
ER 1473	Prox. Humerus	Koobi Fora	Upper Burgi Member[9]	1.89-0.05 Ma[9]
ER 1476B	Prox. Tibia	Koobi Fora	KBS Channel Complex[9]	1.88 Ma[9]
ER 1481	Prox. and Dist. Femur and Tibia	Koobi Fora	Upper Burgi Member[9]	1.89-0.05 Ma[9]
ER 1500	Assoc. Skeleton	Koobi Fora	Upper Burgi Member[9]	1.88-1.90 Ma[9]
ER 1503	Prox. Femur	Koobi Fora	Upper Burgi Member[9]	1.89-0.05 Ma[9]
ER 1504	Dist. Humerus	Koobi Fora	Upper Burgi Member[9]	1.89-0.05 Ma[9]
ER 1505A	Femoral head	Koobi Fora	Upper Burgi Member[9]	1.89-0.05 Ma[9]
ER 1591	Dist. Humerus	Koobi Fora	KBS Member[9]	1.7 Ma[9]
ER 1592	Dist. Femur	Koobi Fora	Lower KBS Member[9]	1.85 Ma[9]
ER 1807	Femoral Shaft	Koobi Fora	Upper Okote Member[9]	1.53 – 0.05 Ma[9]
ER 1808	Femoral and Tibial Shafts	Koobi Fora	KBS Member[9]	1.7 Ma[9]
ER 1809	Femoral Shaft	Koobi Fora	KBS Member[9]	1.77 -0.10 Ma[9]
ER 1810	Prox. Tibia	Koobi Fora	Upper Burgi Member[9]	1.89-0.05 Ma[9]
ER 1824	Dist. Humerus	Koobi Fora	Upper KBS Member[9]	1.7 Ma[9]
ER 2594A	Prox. Tibia	Koobi Fora	Upper Okote Member[9]	1.53 -0.05 Ma[9]
ER 3728	Prox. Femur	Koobi Fora	Upper Burgi Member[9]	1.89-0.05 Ma
ER 3735	Dist. Humuers and Prox. Radius	Koobi Fora	Upper Burgi Member[9]	1.88-1.90 Ma[9]
ER 3736	Prox. Radius	Koobi Fora	Upper Burgi Member[9]	1.89-0.05 Ma[9]
ER 3888	Prox. Radius	Koobi Fora	Okote Member[9]	1.57-0.08 Ma[9]
ER 3951	Dist. Femur	Koobi Fora	Upper Burgi Member[9]	1.89-0.05 Ma[9]
ER 3956A	Prox. Raidus	Koobi Fora	Upper Burgi Member[9]	1.89-0.05 Ma[9]
ER 5880	Prox. Femur	Koobi Fora	Upper Burgi Member[9]	1.89-0.05 Ma[9]
ER 6020	Dist. Humerus	Koobi Fora	KBS Member[9]	1.77-0.10 Ma[9]
ER 20419	Prox. and Dist. Radius	Allia Bay	Sibilot Hill[12]	4.17-4.07 Ma[11]
KP 271	Dist. Humerus	Kanapoi	Naringangoro Hill, surface find[12]	4.17-4.07 Ma[11]
KP 29285	Dist. Tibia	Kanapoi	surface find[12]	4.17-4.07 Ma[11]
WT 15000	Assoc. Skeleton	West Turkana	NK3, Natoo Member[13]	1.6 Ma[9]
WT 19700	Prox. Tibia	West Turkana	Nachukui Fmn	
MAK-VP-1/1	Prox. Femur	Middle Awash	Maka Beds[14]	3.4 Ma[14]
MAT-VP-1/1	Dist. Humerus	Middle Awash	Matabiaetu[14]	2.5 Ma[14]
MLD 46	Prox. Femur	Makapansgat	Member 4[15]	3 Ma[15]
OH 20	Prox. Femur	Olduvai Gorge	HWK, Lower Bed II/Upper Bed I[16]	1.8 Ma[16]
OH 28	Femoral Shaft	Olduvai Gorge	WK, Bed IV[16]	1.2-1.07 Ma[16]
OH 34	Prox. Femur	Olduvai Gorge	JK2, Bed III[17]	1.33-1.2 Ma[17]
OH 35	Dist. Tibia	Olduvai Gorge	FLKNN, Upper Bed I[18]	1.8-1.76 Ma[18]
OH 36	Prox. Ulna	Olduvai Gorge	SC, Upper Bed II[19]	1.33-1.48 Ma[19]
OH 53	Femoral Shaft	Olduvai Gorge	SHK, Middle Bed II[20]	1.65-1.52 Ma[20]
OH 62	Assoc. Skeleton	Olduvai Gorge	DDH, Bed I[21]	1.85-1.75 Ma[21]

Table 2.2 cont. A list of the fossils that were sampled, including their ages and stratigraphic position

Accession	Element	Site	Stratigraphic Position/Locality	Age
Omo Kibish 1	Assoc. Skeleton	Omo	Kibish Formation[22]	200-150 Ka[22]
Omo 119-1973-2710	Prox. Humerus	Omo	Shunguru Fmn [9]	2.43 Ma[9]
Omo 141-72-23	Prox. Ulna	Omo	Lower Member G[9]	2.2 -0.1Ma[9]
Omo 75 S70-1317	Prox. Radius	Omo	Lower Member G [9]	2.2 -0.1Ma[9]
Omo L40-19	Ulna	Omo	Shunguru Fmn [9]	2.37 Ma[9]
SK 18	Prox. Radius	Swartkrans	Member 2[24]	1.8-1.5 Ma[23]
SK 19	Prox. Femur	Swartkrans	Member 1 Hanging Remnant[24]	1.8-1.5 Ma[23]
SK 82	Prox. Femur	Swartkrans	Member 1 Hanging Remnant[24]	1.8-1.5 Ma[23]
SK 97	Prox. Femur	Swartkrans	Member 1 Hanging Remnant[24]	1.8-1.5 Ma[23]
SK 860	Dist. Humerus	Swartkrans	Member 1 Hanging Remnant[24]	1.8-1.5 Ma[23]
SK 1896	Dist. Femur	Swartkrans	Member 1 Hanging Remnant[24]	1.8-1.5 Ma[23]
SK 2045	Prox. Radius	Swartkrans	Member 2[24]	1.8-1.5 Ma[23]
SK 3121	Prox. Femur	Swartkrans	Member 2[24]	1.8-1.5 Ma[23]
SK 14024	Prox. Femur	Swartkrans	Undescribed	
SKX 3602	Dist. Radius	Swartkrans	Member 1[24]	1.8-1.5 Ma[23]
SKX 3699	Prox. Radius	Swartkrans	Member 2[24]	1.8-1.5 Ma[23]
SKX 3774	Dist. Humerus	Swartkrans	Member 1[24]	1.8-1.5 Ma[23]
SKX 8761	Prox. Ulna	Swartkrans	Member 1[25]	1.8-1.5 Ma[23]
SKX 10924	Dist. Humerus	Swartkrans	Member 3[24]	1.8-1.5 Ma[23]
SKX 12814	Radial Shaft	Swartkrans	Member 1?	1.8-1.5 Ma[23]
SKX 24600	Dist. Humerus	Swartkrans	Member 1 Lower Bank[24]	1.8-1.5 Ma[23]
SKX 24601	Prox. Radius	Swartkrans	Member 1 Lower Bank[24]	1.8-1.5 Ma[23]
Sts 14	Prox. Femur	Sterkfontein	Member 4[26]	2.8-2.5 Ma[23]
Sts 34	Dist. Femur	Sterkfontein	Member 4[26]	2.8-2.5 Ma[23]
Sts 65	Prox. Femur	Sterkfontein	Member 4[26]	2.8-2.5 Ma[23]
Stw 25	Prox. Femur	Sterkfontein	Member 4[26]	2.8-2.5 Ma[23]
Stw 30a	Prox. Femur	Sterkfontein	Member 4[26]	2.8-2.5 Ma[23]
Stw 46	Dist. Radius	Sterkfontein	Member 4[26]	2.8-2.5 Ma[23]
Stw 105	Prox. Radius	Sterkfontein	Member 4[26]	2.8-2.5 Ma[23]
Stw 113	Prox. Ulna	Sterkfontein	Member 5[26]	2-1.5 Ma[23]
Stw 121	Femoral Shaft	Sterkfontein	Member 4[26]	2.8-2.5 Ma[23]
Stw 129	Dist. Femur	Sterkfontein	Member 5[26]	2-1.5 Ma[23]
Stw 139	Prox. Femur	Sterkfontein	Member 5[26]	2-1.5 Ma[23]
Stw 181	Dist. Tibia	Sterkfontein	Member 4[26]	2.8-2.5 Ma[23]
Stw 311	Prox. Femur	Sterkfontein	Member 5[26]	2-1.5 Ma[23]
Stw 318	Dist. Femur	Sterkfontein	Member 4[26]	2.8-2.5 Ma[23]
Stw 326	Dist. Ulna	Sterkfontein	Member 4[26]	2.8-2.5 Ma[23]
Stw 328	Prox. Humerus	Sterkfontein	Member 4[26]	2.8-2.5 Ma[23]
Stw 348	Humeral Shaft	Sterkfontein	Member 4[26]	2.8-2.5 Ma[23]
Stw 349	Prox. Ulna	Sterkfontein	Member 4[26]	2.8-2.5 Ma[23]
Stw 358	Dist. Tibia	Sterkfontein	Member 4[26]	2.8-2.5 Ma[23]
Stw 380	Prox. Ulna	Sterkfontein	Member 4[26]	2.8-2.5 Ma[23]
Stw 389	Dist. Tibia	Sterkfontein	Member 4[26]	2.8-2.5 Ma[23]
Stw 390	Prox. Ulna	Sterkfontein	Member 4[26]	2.8-2.5 Ma[23]
Stw 392	Prox. Femur	Sterkfontein	Member 4[26]	2.8-2.5 Ma[23]
Stw 396	Prox. Tibia	Sterkfontein	Member 4[26]	2.8-2.5 Ma[23]

Table 2.2 cont. A list of the fossils that were sampled, including their ages and stratigraphic position

Accession	Element	Site	Stratigraphic Position/Locality	Age
Stw 398	Prox. Ulna	Sterkfontein	Member 4[26]	2.8-2.5 Ma[23]
Stw 399	Dist. Ulna	Sterkfontein	Member 4[26]	2.8-2.5 Ma[23]
Stw 403	Prox. Femur	Sterkfontein	Member 4[26]	2.8-2.5 Ma[23]
Stw 431	Assoc. Skeleton	Sterkfontein	Member 4[26]	2.8-2.5 Ma[23]
Stw 479	Prox. Femur	Sterkfontein	Member 4[27]	2.8-2.5 Ma[23]
Stw 501	Prox. Femur	Sterkfontein	Member 4[27]	2.8-2.5 Ma[23]
Stw 514	Prox. Tibia	Sterkfontein	Member 4[27]	2.8-2.5 Ma[23]
Stw 515	Dist. Tibia	Sterkfontein	Member 4[27]	2.8-2.5 Ma[23]
Stw 516	Prox. Radius	Sterkfontein	Member 4[27]	2.8-2.5 Ma[23]
Stw 517	Prox. Humerus	Sterkfontein	Member 4[27]	2.8-2.5 Ma[23]
Stw 522	Prox. Femur	Sterkfontein	Member 4[27]	2.8-2.5 Ma[23]
Stw 527	Prox. Femur	Sterkfontein	Member 4[27]	2.8-2.5 Ma[23]
Stw 567	Dist. Tibia	Sterkfontein	Member 4[27]	2.8-2.5 Ma[23]
Stw 571	Prox. Ulna	Sterkfontein	Member 5[27]	2-1.5 Ma[23]
TM 1513	Dist. Femur	Sterkfontein	Member 4[27]	2.8-2.5 Ma[23]
TM 1517	Dist. Humerus & Prox. Ulna	Kromdraai	B	1.9 Ma[28]
TM 3601	Dist. Femur	Sterkfontein?	Undescribed	

[1] Walter, 1994 ; [2] Kimbel and Walter, 2000; [3] Wood, 1999; [4] Asfaw *et al.,* 2002; [5] Asfaw *et al.,* 1999; [6] Harrison, in press; [7]Coppens, 2004; [8]Leakey *et al.* ; [9] Feibel *et al.* 1989; [11]Leakey *et al.* 1988; [13]Brown *et al.,* 1985; [12]Ward *et al.* 2001; [14] Lovejoy *et al.,* 2002; [15] Reed *et al.* 1993; [16]White, 2000c; [17]Day and Molleson, 1976; [18]Walter *et l.* 1992; [19]Aiello *et al.* 1999; [20]Wood *et al.,* 1998; [21]Johansen *et al.* 1987; [22]Brown and Fuller, 2008; [23]Delson, 1988; [24]Susman *et al.* 2001 ; [25]Susman, 1989; [26]McHenry, 1994; [27]Pickering *et al.* 2004; [28]Thackeray *et al.* 2002

Methods

Morphometrics is the statistical study of shape variation and its covariation with other variables in biology. Traditionally, morphometrics has relied on linear measures of distance, angles, and various indices using those measures in order to quantify shape differences between specimens. These measures, although useful, cannot accurately reproduce the original shape of a specimen, as they contain no information about the ways that the different linear measures relate spatially to one another (Rohlf and Marcus, 1993; Adams *et al*., 2004).

Geometric morphometrics (GM) is a morphometric approach that allows the retention of shape information. The shape information is preserved in most statistical analyses which allows for the visualization of shape changes in the original specimens. In GM, homologous points

(landmarks) are selected on each specimen. There are four major landmark types: Type I, Type II, Type III, and semi-landmarks. Type I landmarks represent the juxtaposition of three or more bones at a single point, and are generally seen to be the most homologous and biologically meaningful. Type II landmarks refer to points that are chosen using geometric evidence, as opposed to histological evidence; e.g., a point of maximum curvature. Type III landmarks are defined in reference to other landmarks, and not any biological structure; e.g., the end point of a diameter. Semi-landmarks are sets of points along a space curve that are mathematically derived using two Type I, II or III landmarks as endpoints, to describe some form of curvature in its entirety (Bookstein, 1991).

I recorded *x*,*y*,*z* coordinates of landmarks on the humerus, radius, ulna, femur and tibia using a Microscribe 3DX digitizer. I recorded 25 landmarks on the humerus, 16 landmarks on the radius, 23 landmarks on the ulna, 32 landmarks on the femur and 20 landmarks on the tibia (Tables 2.3-2.7; figures located throughout the text in various chapters). These landmarks were designed to capture articular surfaces and other areas of functional interest on the postcranium. Additionally, these landmarks have been selected to encompass some standard osteological measurements, thus rendering them comparable to previous studies done on this topic. Reduced landmarks sets were used in analyses including fossils that were incomplete.

All specimens were stabilized with modeling clay in a position such that all landmark points were able to be recorded in a single view. Where possible, the left side of each element was digitized in order to minimize random differences due to slight bilateral asymmetry. Data on all fossil specimens were collected three times and the average coordinate points were used in analyses to minimize the effects of random error. Modern specimens were used only if at least four out of the five elements were present.

Table 2.3 Description of landmarks taken on the humerus

Number	Type	Description
Humeral Head		
1	II	Proximal tip of greater tubercle, regardless of position
2	II	Proximal tip of lesser tubercle, regardless of position
3	II	Proximal extreme of the edge of the articular surface where it meets the bicipital groove.
4	II	Most medial point of head
5	III	Distal most point of the head on edge of articular surface opposite point 3.
6	III	Medial point on head on edge of articular surface, line with point 7 perpendicular to axis of points 3 and 5.
7	III	Lateral point on head opposite to point 6 on edge of articular surface, line with point 6 perpendicular to axis of points 3 and 5.
Medial Epicondyle		
8	II	Most lateral point on the epicondyle
9	II	Most medial point on the epicondyle
10	II	Most posterior point on the epicondyle
Trochlea		
11	II	Proximo-medial extreme of trochlea (emphasizing proximal)
12	II	Proximal extreme on the anterior surface of the medial facet margin.
13	II	Proximate extreme on the posterior surface medial facet margin.
14	II	Distal extreme of the medial facet margin.
15	II	Proximal extreme on the anterior surface of the trochlear groove
16	II	Proximal extreme on the posterior surface of the trochlear groove
17	II	Distal extreme of the trochlear groove
18	II	Most posterior point on the lateral side of the distal end of the trochlear groove
Capitulum		
19	III	Most proximal point on the distal capiulum between the capitulum and zona conoidea
20	II	Most anterior point of the capitulum
21	III	Most proximal point in line with the most anterior point of the capitulum
22	III	Most distal point in line with the most anteior point of the capitulum
23	III	Most lateral-anterior point in line with the most anterior point of the capitulum
24	II	Most proximolateral point of the capitulum
Olecranon Fossa		
25	II	Most proximate point on olecranon fossa

Table 2.4 Description of the landmarks taken on the radius

Number	Type	Description
Radial Head		
1	II	Deepest point on the radial head
2	II	Most medial point on radial head
3	II	Most lateral point on the radial head
4	II	Most anterior point on the radial head
5	II	Most posterior point on the radial head
Radial Tuberosity		
6	II	Center of radial tuberosity
7	II	Most distal point of the tuberosity
Styloid Process		
8	II	Tip of the styloid process
Ulnar Notch		
9	II	Most proximoanterior point on the margin of the ulnar notch
10	II	Most proximoposterior point on the margin of the ulnar notch
11	II	Most anterior point on the facet margin of the ulnar notch
12	II	Most posterior point on the facet margin of the ulnar notch
13	II	Deepest point inside the ulnar notch
Facet margin		
14	II	Facet margin between lunate and scaphoid articular surfaces - most anterior point
15	II	Facet margin between lunate and scaphoid articular surfaces - most posterior point
16	II	Facet margin between lunate and scaphoid articular surfaces - deepest point along that line

Table 2.5 Description of landmarks taken on the ulna

Number	Type	Description
Olecranon		
1	II	Proximal-most point on the olecranon process.
2	II	Posterior-most point on the olecranon process.
3	II	Medial-most point on maximum constriction of the olecranon.
4	II	Lateral-most point of maximum constriction of the olecranon.
Trochlear Facet		
5	II	Proximolateral extreme of margin of the trochlear facet
6	II	Anterior-most point on proximal margin of trochlear facet, in middle of proximal trochlear facet
7	II	Proximomedial-most point on the margin of the trochlear facet
8	II	Deepest point in the trochlear notch, in midline of articular facet.
9	II	Medial most point on distal part of trochlear facet.
Coronoid Process		
10	II	Anterior tip of the coronoid process.
Radial Facet		
11	II	Posterior-most point on the radial facet.
12	II	Deepest point of radial facet
13	II	Most proximal and distal point of the radial facet
14	II	most anterior point on the radial facet
Ulnar Head		
15	II	Distal-most point on ulnar head.
16	II	Lateral-most point on ulnar head
17	II	Posterior-most point on the ulnar head
18	II	Anterior-most point on the ulnar head
Styloid Process		
19	II	Distal-most point on styloid process.

Table 2.6 Description of landmarks taken on the femur

Number	Type	Description
Femoral Head		
1	II	Middle of fovea capitus
2	II	Most proximal point on the femoral head
3	II	Most proximal point on the facet margin
4	II	Most distal point of the facet margin
5	II	Most anterior point of the facet margin
6	II	Most posterior point of the facet margin
Greater Trochanter		
7	II	Maximum point of constriction on ridge running from lesser trochanter to the femoral head
8	II	Deepest point of the proximal neck
9	II	middle of the trochenteric fossa
10	II	Tip of greater trochanter
11	II	Most lateral point of greater trochanter
12	II	Most proximoanterior point of the greater tubercle
Lesser Trochanter		
13	II	Tip of lesser trochanter
14	II	origin of pectineal line
Epicondyles		
15	II	most medial point on epicondyle
16	II	most lateral point on epicondyle
17	II	most proximomedial point of the facet margin on the anterior aspect of the distal articular surface of lateral condyle
18	II	most proximolateral point of the facet margin on the anterior aspect of the distal articular surface of lateral condyle
19	II	Most proximal point where the groove ends on the anterior aspect of the articular surface of lateral condyle
20	II	Most distal point of groove
21	II	Most distal point of the medial facet margin
22	II	Most distal point of the lateral facet margin
23	II	Most posterior point of the medial facet margin
24	II	Most posterior point of the lateral facet margin
25	II	Most proximomedial point of lateral condylar surface of the posterior aspect of the articular surface of lateral condyle
26	II	Most proximolateral point of lateral condylar surface of the posterior aspect of the articular surface of lateral condyle
27	II	most proximomedial point of the facet margin on the anterior aspect of the distal articular surface of medial condyle
28	II	most proximolateral point of the facet margin on the anterior aspect of the distal articular surface of medial condyle
29	II	Most proximomedial point of lateral condylar surface of the posterior aspect of the articular surface of medial condyle
30	II	Most proximolateral point of lateral condylar surface of the posterior aspect of the articular surface of medial condyle
31	II	Most posterio-medial point of the groove (notch)
32	II	Most posterior point of the groove (notch)

Table 2.7 Description of landmarks taken on the tibia

Number	Type	Description
Tibial Condyles		
1	II	Anterior-most point on medial tibial condyle on outer edge of articular surface
2	II	Medial-most point on the medial tidial condyle.
3	II	Posterior-most point on medial tibial condyle.
4	II	Lateral -most point on the medial tibial condyle
5	II	Anterior-most point on lateral tibial condyle.
6	II	Medial-most point on the lateral tidial condyle.
7	II	posterior-most point on lateral tibial condyle.
8	II	Lateral-most point on the lateral tidial condyle.
Tuberosity		
9	II	Anterior-most point on tibial tuberosity.
Talar Facet		
10	II	Anterior-most point on talar facet.
11	II	Medial point on the talar facet.
12	II	Posterior-most point on talar facet.
13	II	Lateral edge of facet in mid anteriorposterior plane.
14	II	Deepest point in mid anteriorposterior plane of the talar facet where it meets the medial malleolar facet.
15	II	Most anterior point in mid anteriorposterior plane of the talar facet where it meets the medial malleolar facet.
16	II	Most posterior point in mid anteriorposterior plane of the talar facet where it meets the medial malleolar facet.
17	II	Most medial point of the medial malleolus
18	II	Distal tip of medial malleolus
19	II	Most lateral point of talar facet
20	II	Most lateral point on the fibular facet

By collecting data as a series of *x,y,z* coordinates, I was able to use these landmarks to visualize the three-dimensional shape of a specimen using Morpheus (Slice, 1998) and *morphologika* (O'Higgins & Jones, 1998, 2006). Specimens were registered with respect to one another using a Generalized Procrustes Analysis (GPA). A GPA minimizes the sums of squared distances between the landmark configurations of each specimen by centering all landmark configurations on a common origin (the centroid), rotating them about this point, and adjusting them for size (Rohlf and Slice, 1990). Once the landmarks were registered, then the landmark configurations could be visualized. Changes in shape from one individual to another are

visualized as deformations from a reference to a target specimen, and differences between individuals can be pinpointed with more accuracy than with traditional, linear morphometrics (Bookstein, 1991; Adams *et al.* 2004).

PRECISION TEST

All data for this study were collected by the author. In order to determine whether intra-observer error would be the cause of any significant findings, a precision test was untaken. In this test, ten replicate landmark sets were collected for each bone on an adult, white male from the anatomy collection at the American Museum of Natural History (New York, USA). The replicates were not taken on each bone in sequential order; rather, each bone was mounted, the data were collected, and that bone was unmounted and set aside. Data on these specimens were then subjected to a Generalized Procrustes Analysis (GPA) and the Procrustes distance between each replicate and the consensus landmark configuration was calculated. Ten adult white males from the same morphology collection were then subjected to a GPA, and procrustes distances from each individual to the consensus landmark configuration were calculated. These results are presented in Table 2.8. The results of t-tests show that for all elements, the mean procrustes distances for the replicates of the same specimen are significantly smaller than the distances between ten individuals of the same sex, from the same populations.

In order to assess the error at each individual landmark, the mean, minimum and maximum procrustes distances from each individual landmark to the consensus landmark were calculated. The mean percentage error for each landmark was calculated as each mean landmark error divided by the mean distance between the consensus landmark coordinates and its centroid,

multiplied by 100 (Singleton, 2002). In all cases, the percent error was below 0.4%, which was considered acceptable. These results are presented in Table 2.9.

Table 2.8 Procrustes distances (*d*) between each replicate (rep.) and the consensus configuration, and each individual (x) and the consensus configuration.

Humerus

Rep.	*d*	x	*d*
1	0.0188838	1	0.04025
2	0.0121221	2	0.02887
3	0.0217167	3	0.02307
4	0.0123922	4	0.03094
5	0.0104748	5	0.08228
6	0.0090207	6	0.02954
7	0.008324	7	0.02164
8	0.0104983	8	0.02707
9	0.0091885	9	0.03514
10	0.012214	10	0.02214
AVERAGE	**0.0124835**		**0.03409**
***p* = 0.0008**			

Radius

Rep.	*d*	x	*d*
1	0.014909	1	0.065787
2	0.01425	2	0.058867
3	0.015576	3	0.060158
4	0.020141	4	0.084484
5	0.024709	5	0.073876
6	0.017283	6	0.067624
7	0.019649	7	0.054736
8	0.00951	8	0.083871
9	0.012225	9	0.085287
10	0.017532	10	0.075051
AVERAGE	**0.016578**		**0.070974**
***p* = < 0.0001**			

Ulna

Rep.	*d*	x	*d*
1	0.0124520	1	0.0350460
2	0.0105499	2	0.0270610
3	0.0114089	3	0.1395306
4	0.0112572	4	0.0375275
5	0.0133149	5	0.0321153
6	0.010849	6	0.0323940
7	0.0113057	7	0.0270336
8	0.0160494	8	0.0274352
9	0.0138255	9	0.0309272
10	0.0138125	10	0.0302884
AVERAGE	**0.0124826**		**0.0419368**
***p* = 0.007**			

Femur

Rep.	*d*	x	*d*
1	0.0105839	1	0.027592
2	0.0097056	2	0.020099
3	0.0080857	3	0.02265
4	0.0111851	4	0.022731
5	0.0087269	5	0.019499
6	0.0078037	6	0.026027
7	0.0127367	7	0.029197
8	0.0102955	8	0.021333
9	0.0100383	9	0.027688
10	0.0093378	10	0.022137
AVERAGE	**0.00985**		**0.0239**
***p* = < 0.0001**			

Tibia

Rep.	*d*	x	*d*
1	0.0103357	1	0.02103
2	0.0035923	2	0.01647
3	0.0043507	3	0.01974
4	0.0046981	4	0.01983
5	0.0061045	5	0.01488
6	0.0060346	6	0.02555
7	0.0047411	7	0.01764
8	0.0038013	8	0.01303
9	0.0043288	9	0.0184
10	0.0057601	10	0.02038
AVERAGE	**0.00537**		**0.0187**
***p* = < 0.0001**			

Table 2.9 The average, maximum and minimum procrustes distance from each replicate to the consensus configuration. Percent error was calculated as the average error divided by the distance between each consensus landmark and its centroid, multiplied by 100.

LANDMARK	AVERAGE	MIN	MAX	% ERROR
Humerus				
1	0.0022	0.0010	0.0034	0.14
2	0.0020	0.0010	0.0040	0.13
3	0.0019	0.0008	0.0031	0.12
4	0.0025	0.0010	0.0053	0.17
5	0.0038	0.0008	0.0099	0.25
6	0.0045	0.0016	0.0103	0.29
7	0.0059	0.0012	0.0163	0.39
8	0.0033	0.0012	0.0059	0.18
9	0.0012	0.0007	0.0021	0.06
10	0.0011	0.0006	0.0019	0.06
11	0.0010	0.0004	0.0016	0.06
12	0.0009	0.0003	0.0021	0.05
13	0.0031	0.0017	0.0050	0.17
14	0.0007	0.0001	0.0013	0.04
15	0.0011	0.0005	0.0018	0.06
16	0.0015	0.0004	0.0037	0.09
17	0.0006	0.0003	0.0010	0.03
18	0.0010	0.0002	0.0025	0.06
19	0.0010	0.0002	0.0019	0.06
20	0.0017	0.0008	0.0031	0.09
21	0.0011	0.0005	0.0021	0.06
22	0.0011	0.0003	0.0027	0.06
23	0.0018	0.0004	0.0031	0.10
24	0.0008	0.0003	0.0019	0.05
25	0.0010	0.0003	0.0017	0.06
Radius	0.0019	0.0005	0.0047	0.09
1	0.0023	0.0005	0.0054	0.11
2	0.0030	0.0015	0.0061	0.15
3	0.0035	0.0012	0.0061	0.18
4	0.0050	0.0028	0.0096	0.25
5	0.0029	0.0012	0.0077	0.15
6	0.0020	0.0010	0.0036	0.10
7	0.0020	0.0009	0.0034	0.13
8	0.0019	0.0007	0.0038	0.12
9	0.0019	0.0011	0.0034	0.12
10	0.0022	0.0011	0.0035	0.14
11	0.0017	0.0004	0.0030	0.11
12	0.0015	0.0011	0.0025	0.09
13	0.0023	0.0011	0.0049	0.15
14	0.0015	0.0005	0.0043	0.10
15	0.0018	0.0014	0.0024	0.12
16	0.0019	0.0005	0.0047	0.09

Table 2.9 continued

LANDMARK	AVERAGE	MIN	MAX	% ERROR
Ulna				
1	0.0019	0.0007	0.0025	0.12
2	0.0036	0.0013	0.0053	0.22
3	0.0013	0.0006	0.0024	0.08
4	0.0028	0.0006	0.0061	0.17
5	0.0023	0.0010	0.0043	0.14
6	0.0018	0.0006	0.0025	0.11
7	0.0019	0.0007	0.0038	0.12
8	0.0024	0.0010	0.0042	0.15
9	0.0026	0.0009	0.0053	0.16
10	0.0023	0.0012	0.0036	0.14
11	0.0028	0.0014	0.0045	0.17
12	0.0020	0.0012	0.0045	0.12
13	0.0038	0.0012	0.0097	0.23
14	0.0026	0.0011	0.0039	0.16
15	0.0023	0.0011	0.0036	0.14
16	0.0025	0.0012	0.0034	0.15
17	0.0020	0.0005	0.0043	0.12
18	0.0016	0.0004	0.0026	0.09
19	0.0019	0.0010	0.0026	0.09
20	0.0023	0.0007	0.0051	0.11
21	0.0030	0.0012	0.0058	0.15
22	0.0015	0.0010	0.0022	0.07
23	0.0014	0.0005	0.0024	0.07
Femur				
1	0.0012	0.0006	0.0018	0.08
2	0.0019	0.0006	0.0037	0.12
3	0.0013	0.0004	0.0021	0.08
4	0.0013	0.0003	0.0021	0.08
5	0.0022	0.0005	0.0054	0.14
6	0.0027	0.0008	0.0052	0.17
7	0.0013	0.0005	0.0023	0.08
8	0.0013	0.0003	0.0020	0.08
9	0.0012	0.0007	0.0028	0.08
10	0.0011	0.0006	0.0018	0.07
11	0.0021	0.0005	0.0041	0.13
12	0.0017	0.0002	0.0035	0.10
13	0.0012	0.0003	0.0024	0.07
14	0.0014	0.0002	0.0026	0.09
15	0.0020	0.0009	0.0039	0.11
16	0.0028	0.0011	0.0040	0.15
17	0.0007	0.0003	0.0012	0.04
18	0.0012	0.0005	0.0020	0.06
19	0.0017	0.0004	0.0030	0.09
20	0.0017	0.0005	0.0026	0.09

Table 2.9 continued

LANDMARK	AVERAGE	MIN	MAX	% ERROR
21	0.0011	0.0003	0.0023	0.06
22	0.0025	0.0002	0.0051	0.13
23	0.0007	0.0003	0.0012	0.04
24	0.0008	0.0002	0.0014	0.05
25	0.0007	0.0004	0.0011	0.04
26	0.0010	0.0003	0.0021	0.05
27	0.0015	0.0005	0.0028	0.08
28	0.0013	0.0005	0.0025	0.07
29	0.0025	0.0013	0.0054	0.14
30	0.0008	0.0003	0.0019	0.05
31	0.0009	0.0003	0.0015	0.05
32	0.0008	0.0001	0.0015	0.04
Tibia				
1	0.0021	0.0009	0.0074	0.14
2	0.0012	0.0003	0.0033	0.08
3	0.0015	0.0002	0.0037	0.10
4	0.0007	0.0003	0.0011	0.04
5	0.0010	0.0001	0.0023	0.06
6	0.0008	0.0004	0.0021	0.05
7	0.0009	0.0003	0.0018	0.06
8	0.0014	0.0002	0.0026	0.09
9	0.0014	0.0008	0.0030	0.09
10	0.0007	0.0002	0.0014	0.04
11	0.0007	0.0002	0.0013	0.04
12	0.0008	0.0004	0.0013	0.04
13	0.0007	0.0002	0.0013	0.04
14	0.0008	0.0004	0.0023	0.04
15	0.0007	0.0001	0.0014	0.04
16	0.0008	0.0004	0.0014	0.04
17	0.0007	0.0002	0.0013	0.04
18	0.0007	0.0003	0.0015	0.04
19	0.0006	0.0001	0.0012	0.03
20	0.0007	0.0004	0.0016	0.04

CHAPTER 3: HOMININ FORELIMB MORPHOLOGY

Introduction

In general (with some exceptions), studies looking at the originals of bipedalism of hominins have concentrated on looking at the hindlimb, as the hindlimb is extremely derived in modern humans. However, when looking at overall patterns of locomotor diversity and trying to assess the locomotor patterns of fossil individuals, it is important to consider the forelimb as well. The forelimb certainly has many clues to offer researchers when thinking about the evolution of bipedalism.

This chapter aims to answer four basic research questions:

- Does each Plio-Pleistocene hominin have a unique morphological pattern for the shoulder, elbow and wrist joints or do all hominins have the same basic morphology?
    - If there is more variation in the fossil sample for a limb segment than seen in any of the extant species, then it could be reasonably concluded that there are multiple morphological patterns in various species of hominins. However, if there is less than or equal variation in the fossil sample as compared to the extant sample, then it could be concluded that there is no specific pattern that characterizes any of the different hominin species for the bones of the forelimb. This does assume that levels of intraspecific variation extinct taxa are equivalent to that of extant taxa.
- Do the changes in each of these joints follow a linear progression from an ape-like pattern to a human-like pattern?
    - If changes in postcranial morphology follow a linear progression, then changes towards a human-like condition should roughly correlate with the age of the fossil, with the most ape-like individuals occurring the earliest in time and the

most human-like individuals occurring the latest in time. If there is no temporal pattern to the postcranial affiliation, then it could be concluded that changes towards a human-like pattern occur randomly, as opposed to linearly.

- For individuals that are either associated or have secure taxonomic attributions, is the taxonomic and functional signal the same across all bones?
    - If a particular fossil taxon is always affiliated with the same extant taxon regardless of what segment is sampled, then it could be concluded that the functional and taxonomic signal is consistent across all the bones of the forelimb. If a fossil taxon is affiliated with different extant taxa depending on the segment, then it would have a more mosaic morphological pattern.
- Are there any solid clues in the forelimb that indicate a particular mode of locomotion as the precursor to bipedalism?
    - If there are structures in the forelimb that are firmly linked to either knuckle-walking or suspensory locomotion, then it could possibly be concluded that those are the result of phylogenetic lag (Vrba, 1980; Vrba and Gould, 1986) and are the remnants of locomotor past. It would be more likely to find these traits in taxa such as *Australopithecus anamensis* that occur earliest in time. If there are no traits that can be definitively linked to a non-bipedal mode of locomotion, then no conclusions can be drawn on this subject.

Precursors to Bipedalism

One of the biggest arguments surrounding the evolution of bipedalism centers around the locomotor pattern that was the direct precursor to bipedal posture. This discussion was begun at the dawn of the 20th century by Keith (1903), who suggested that bipedalism was ultimately

rooted in a hylobatid-like, brachiating ancestor. The argument is still ongoing and has been fueled by a greater biomechanical understanding of different locomotor patterns as well as a greater understanding of the phylogeny and divergence dates in the hominoid cluster.

Morton (1927), like Keith, argued for an immediate suspensory ancestor. He believed that the positions of the internal organs of the thoracic and abdominal cavity in humans and the way that they rest on perineal structures points towards an upright, suspensory ancestor. He also pointed to supposedly bipedal characteristics in the Dryopithecinae that indicate that bipedalism arose out of a suspensory "proanthropoid" group. Tuttle (1969 *et seq.*) supported this based on the retention of suspensory traits in the shoulder joint. Washburn (1967) suggested that the lack of hair on the mid-phalangeal joint in modern humans was indicative of knuckle-walking ancestory, but Tuttle refuted that in two ways. He showed that that there is a similar hairless pattern seen on the toes and that there is no histological evidence to link hairlessness to knuckle-walking. Tuttle proposed that knuckle-walking and bipedalism were two separate strategies employed by members of the hominoid cluster to adapt to more open environments.

Washburn (1967) was the first to propose the idea that bipedalism evolved from a knuckle-walking stage in hominin evolution. He suggested that the move to terrestriality was not an adaptation for open environments but a mechanism to avoid competition with other arboreal species. He recognized that humans had a close genetic relationship with chimpanzees, and for him the fact that chimps were able to walk bipedally for short distances and possess good manipulative ability pointed towards a knuckle-walking stage. More recently, Richmond and Strait (2000) argued strongly in favor of a knuckle-walking ancestor. Based on four dimensions of the distal radius, these authors determined that the wrists of *A. anamensis* and *A. afarensis* possessed many traits in common with *Pan* and *Gorilla* that represent retentions from a knuckle-

walking ancestor, including a distally projecting and medially oriented dorsal ridge and intermediate scaphoid notch size. According to them these traits would function to stabilize the wrist during extension during knuckle-walking. In response to this article, Corruccini and McHenry (2001) also advocated a knuckle-walking ancestor based on their own independent dataset.

Kelley (2001) lent support to this theory based on human anatomy. He suggested that the interosseus membrane between the radius and ulna helps to transmit forces from the radiocarpal joint to the humeroulnar joint and up to the humerus. Tensile forces from suspensory positions acting on these joints would stress the interosseus membrane and lead to pain and possible tearing. Additionally, in modern humans and the extant great apes, the contrahentes muscles in the hands and feet have been reduced to fascia which could lend support and stability to the hands during dorsiflexion. The fatty pads on the proximal phalangeal joints might be useful for shock absorption during knuckle-walking postures.

Begun (2003) also supported the knuckle-walking hypothesis. Aside from reiterating some of the morphological characters that Richmond and Strait (2001) pointed towards, he showed that a knuckle-walking ancestor is most parsimonious. In this view, knuckle-walking has to evolve only one time, in the common ancestor leading to the hominid cluster. If bipedalism did not arise from a knuckle-walking ancestor, then knuckle-walking must have evolved twice; once along the branch leading to *Gorilla* and once along the branch leading to *Pan* (and *Homo*). While Begun suggested this second option to be less parsimonious, Dainton and Macho (1999) had found that this view is more likely. They analyzed the development of knuckle-walking in chimpanzees and gorillas and found that they knuckle-walk slightly differently. Gorillas stress the ulnar side of the arm more and chimps stress the radial side more.

The shapes of the carpals on the ulnar side are significantly different in *Gorilla* and *Pan,* and these differences could not be accounted for by differences in locomotor patterns during ontogeny.

Stern (1975) was the first to propose an "antipronograde"**,** or vertical climbing/clambering stage in the evolution of bipedalism. He suggested this based on musculature similarities between the hip and thigh of *Homo sapiens* and ateline primates as well as some osteological similarities between humans and orangutans. Prost (1980) showed, using diagrams of fore- and hind-limb movements, that both gibbon and chimpanzee bipedalism are very different from human bipedality. However, the movement of chimpanzee vertical climbing could easily be transformed into human bipedalism. Based on this evidence, Prost concluded that bipedalism arose from a strong hindlimb vertical climbing pattern. Thorpe *et al*. (2007) suggested that human bipedalism arose as a response to foraging on thin, flexible branches. Based on approximately 3,000 observations of orangutans, these authors concluded that antipronograde postures are "pre-adaptive" to bipedalism, particularly postures used to navigate smaller, flexible branches. The knee and hip extension seen in orangutans on these small flexible branches is similar to the way that humans extend the hip and the knee during bipedalism, as opposed to the more flexed limb positions in the knuckle-walkers. They also argued that an antiprograde ancestor is more kinematically parsimonious as there is evidence for an orthograde posture in crown hominoids such as *Pierolapithecus* (Crompton and Thorpe, 2007). These authors did not examine any fossils to support their observational data, but if this hypothesis was correct, we would expect to see the retention of suspensory, orangutan-like morphology in the forelimb of early fossil hominins.

Begun *et al.* (2007) questioned the results of Thorpe *et al.* based on the degree of support that the hindlimbs play in orangutan locomotion. These authors asserted that the suspensory positional behaviors on small terminal branches are supported largely by the forelimbs and not the hindlimbs. The orangutan hindlimbs completely lack any of the human bipedal characteristics that are consistent with load bearing joints.

Lending further support to the antipronograde hypothesis is work done by Cartmill and Milton (1977). They examined the wrists of lorises and galagos and found that lorises have a suite of adaptations for slow climbing that are convergent on adaptations for brachiating in the hominoids. These adaptations include: a high intermembral index, several features of the scapula, a shorter styloid process, and a radioulnar joint that is deeper and functions like a ball and socket joint. These adaptations allow for an increase in both ulnar deviation and the ability to pronate and supinate the hand. These are useful in a slow climber as they need need to have flexible limbs to manipulate overhead supports. These same adaptions are not present in the phylogentically similar galagos that have a different locomotor repertoire. Following this, it is possible that the traits cited in modern humans as being remnants of a brachiating ancestor were actually adaptions for slow climbing in a pre-bipedal ancestor.

Kelley (2001) refuted all suspensory hypotheses based on differences in the musculature between non-human apes and *Homo sapiens.* All extant great apes possess the dorso-epitrochlearis muscle, which fires strongly during the support phase of vertical climbing. In *Homo sapiens* this muscle is reduced to fascia. He also suggested that the orientation of the supraspinatus muscle precludes the regular use of the upper arm in fully abducted postures as this muscle rubs the acromion process and has a tendency to become inflamed.

Gebo (1996) also refuted the vertical climbing hypothesis. While argued that while the ancestral catarrhine probably used vertical scrambling and climbing as a major component of its locomotor repertoire, this then shifted to forelimb suspension in hominoids. According to Gebo's hypothesis, from there the protohominid went through some kind of terrestrial phase. He used human wrist anatomy - which he interprets as being adapted for weight-bearing - as well as the fact that humans and the extant great apes share a similar heel-strike mode of plantigrady to support his theory. Therefore, any shared morphology between oranguatans and modern humans would be evidence for a shared brachiating ancestor prior to a terrestrial phase.

Deloison (2003) has suggested that there is no need to look for a recent precursor to hominin bipedalism. Instead, she suggested that the "protohominoid" locomotor mode was a flexible form of plantigrade bipedalism that arose approximately 15 million years ago. Such a protohominoid would have been able to take refuge in the trees as well as be an effective biped during terrestrial locomotion. She pointed to a lack of specialization in the carpals of modern humans and fossil hominins for any weight bearing locomotor pattern.

One of the goals of this chapter is to consider the morphology of the hominid forelimb in order to make inferences about the locomotor pattern immediately preceding bipedalism. Selective pressures were likely strongest on the hindlimb during the shift to bipedalism while selection on the forelimb would have been lessened. Therefore, it should be possible to detect a locomotor signal from the forelimb in the earliest hominins. Once hominins became fully bipedal, selection would have acted again more strongly on the forearm to favor adaptations for increased manipulative ability (Begun, 2003).

Functional Morphology of the Extant Hominoid Forelimb

In order to identify features in the fossil record that are indicative of positional behavior, it is important to understand the morphology of the extant hominoids. Traits that are adaptive for a particular locomotor repertoire for extant species might have been adaptive for similar reasons for individuals in the fossil record. Much of the literature on hominoids has focused on looking for traits that are indicative of knuckle-walking or suspensory behaviors. The knuckle-walking forearm is built to stabilize the wrist during hyperextension and resist compressive forces during quadrupedal locomotion (Begun, 2003).

The elbow joint has many modifications in *Pan* and *Gorilla* that are advantageous for knuckle-walking. The lateral ridge of the trochlea is very prominent and helps to stabilize the ulna during flexion and extension. The trochlea is relatively wider in *Gorilla,* possibly for weight support (Knussman, 1967) or possibly as a compromise between the necessity of weight support and the necessity for manual dexterity. The olecranon fossa is deep and has a steep lateral margin to stabilize the joint during hyperextension. In the ulna, the coronoid process is robust and the trochlear notch has a stronger anterior extension to support the weight of the humerus in during extension of the forearm (Knussman, 1967; Aiello and Dean, 1990). The trochlear notch is expanded distolaterally also for support during full extension in the gait cycle (Drapeau, 2008).

At the elbow joint, there are also adaptions for strong pronation and supination while the forearm is extended. The capitulum is oriented distally and has a large area for radial articulation (Patterson and Howells, 1967). The radial neck is long which increases the moment arm of the biceps brachii muscle (Aiello and Dean, 1990). *Pan* and *Pongo* are similar in their trochlear notch morphology. Both of these taxa have keeled notches, possibly as an adaptation

to resist the transverse forces generated by the flexors of the fingers, as opposed to *Gorilla* and *Homo* which have flatter notches (Drapeau, 2008).

The wrist joint in knuckle-walkers is also highly modified. As with all hominoids, the styloid process of the ulna does not articulate directly with the carpal bones. Instead, it articulates with a fibrocartilaginous disc which allows for a greater range of movement. The disc is well developed for effective transmission of compressive forces (Lewis, 1969; Begun, 2003). The distal articulation of the radius has a smaller articulation area for the lunate and an enlarged area for the scaphoid in comparison to *Pongo,* most likely for stabilization purposes (Cartmill, 1981). The dorsal ridge of the radius projects distally which would limit dorsiflexion of the wrist during knuckle-walking (Aiello and Dean, 1990).

The forelimb of *Pongo* is adapted for mobility during slow, quadrumanous climbing. The proximal humerus is modified for rotational ability and postures where the arm is in an elevated position. They have narrow bicipital grooves, and the most proximal point on the humeral head extends above the proximal border of the greater and lesser tuberosities. The elbow and wrist joints are more mobile than that of knucklewalkers. The olecranon process is short and can fit entirely into the olecranon fossa during extension (Morbeck and Zihlman, 1988; Tuttle and Cortright, 1988). The trochlea is broad and the trochlear notch has a well defined ridge (Morbeck and Zihlman, 1988). They have a less well developed trochlear keel and a shallow zona conoidea since there is less need for stability at the elbow joint (Begun, 2003). *Pongo* has a tightly curved trochlear notch with a strong sigmoid keel as a mechanism to stabilize the elbow while having more mobile radial joints (Drapeau, 2008). Orangutans have a shorter radial neck and as the radial neck is the lever arm for the biceps brachii muscle, this

would indicate that they possess less power supinating abilities than those with longer radial necks (Aiello and Dean, 1990).

In the wrist, *Pongo* has an extremely short styloid process and a larger articulation for the lunate (Morbeck and Zihlman, 1988; Begun, 2003). *Pongo* also retains the os centrale which is fused to the scaphoid in African apes and humans. In African apes and humans, the wrist bones form a double arched structure that can be close-packed during dorsiflexion for stability at the wrist joint. In the Asian apes, the os centrale disrupts this arched pattern and prevents the close-packed position. In fist-walking, *Pongo* abducts the wrist which positions the carpal bones such that the carpal arch cannot collapse. However, the retention of the os centrale and the more flexible wrist joint allows Asian apes greater flexibility in the wrist during suspensory locomotion (Kelley, 2001).

Materials and Methods

Table 3.1 List of fossil specimens included in the analyses of the humerus.

Distal Humerus	**Proximal Humerus**
MK-76-OMIB-7594	AL 288
AL 137-48a	AL 333-107
AL 288	BC 1745
AL 322	Omo 119-73-271b
ER 1504	Stw 328
ER 3735	Stw 517
ER 6020	
ER 739	
KP 271	
MAT -VP-1/1	
SKX 10924	
SKX 24600	
Stw 431	
TM 1517	

For the humerus, two anatomical areas were analyzed: the complete proximal humerus (without landmarks 9 and 20), and the complete distal humerus. The humerus was not analyzed as a whole because there are no Plio-Pleistocene individuals with complete fossil humeri. Table 3.1 lists the specimens that were used in each analysis of the humerus.

The radius was also split into two anatomical areas: the proximal and the distal. The majority of fossil individuals retained all landmarks on either the proximal or distal radius. In the instances where there was no complete

proximal radius (as in SKX 24601, Stw 431 and Stw 516), the remaining morphology was not sufficient to yield a good signal. See table 3.2 for a complete list of fossils included in this analysis.

Table 3.2 List of specimens included in analyses of the radius.

Distal Radius	**Proximal Radius**
AL 288	AL 288
ER 20419	AL333x-33
SKX 3602	BOU-VP-12/1
Stx 46	Omo 75S-1317
	ER 1500
	ER 3735
	ER 3736
	ER 3888
	ER 3956
	ER 20419
	SK 18
	SKX 2045
	SKX 24601
	Stw 431

Table 3.3 List of specimens included in analyses of the ulna.

Distal Ulna	**Proximal Ulna**
AL 288	AL 288
AL 137-48	BK 66
AL 333-12	BOU-VP-1/11
Stw 326	OH 36
Stw 399	OH 62
	Omo 141-72-23
	L40-19
	SKX 8761
	Stw 113
	Stw 380
	Stw 398
	Stw 571

The ulna was similarly separated into two anatomical areas: the proximal end and the distal end. Landmarks 1 and 2 were omitted for analyses on the proximal end to allow for the inclusion of OH 62. See table 3.3 for a list of fossils used in these analyses.

Data were subjected to principal components analyses and regression analyses using *PAST* (Hammer *et al.* 2001) and shape changes were visualized using *morphologika*^{2} (O'Higgins, 2008) and *Morpheus* (Slice, 1998). Shape changes were visualized as deformations between extant genera and fossil taxa along the major principal axes. A two-block partial least squares analysis (2B-PLS) was conducted using *PAST* ver.1.89 (Hammer *et al.*, 2009) on the elements comprising the elbow joint. 2B-PLS is a way of assessing the covariance between two independent sets of data (Rohlf and Corti, 2000), and has been used successfully to look for covariance between shape data and geographical coordinates (Frost *et al.* 2003), patterns of

covariance between dorsal and ventral views of mouse skulls (Corti and Fadda, 1996), and hominoid distal tibial and proximal astragalar surfaces (Harcourt-Smith *et al.* 2008).

Humerus

Full humerus results

Figure 3.1 shows the results of a principal components analysis (PCA) of the Procrustes aligned data of the full landmark set for the humerus of the extant hominoids (see Chapter 2 for details about GPA). On principal component 1 (PC 1), there is a lot of overlap between the extant groups. It is driven largely by the degree of humeral torsion and the relative sizes of the joints in comparison to its diaphyseal length. Principal component 2 (PC 2) partially separates *Pongo* from the rest of the extant hominoids and is driven by the orientation and proximal projection of the humeral head. The proximal humerus in *Pongo* is oriented more proximally and has shorter greater and lesser tuberosities than the other extant hominoids (see fig. 3.2). PC 1 is significantly correlated with centroid size.

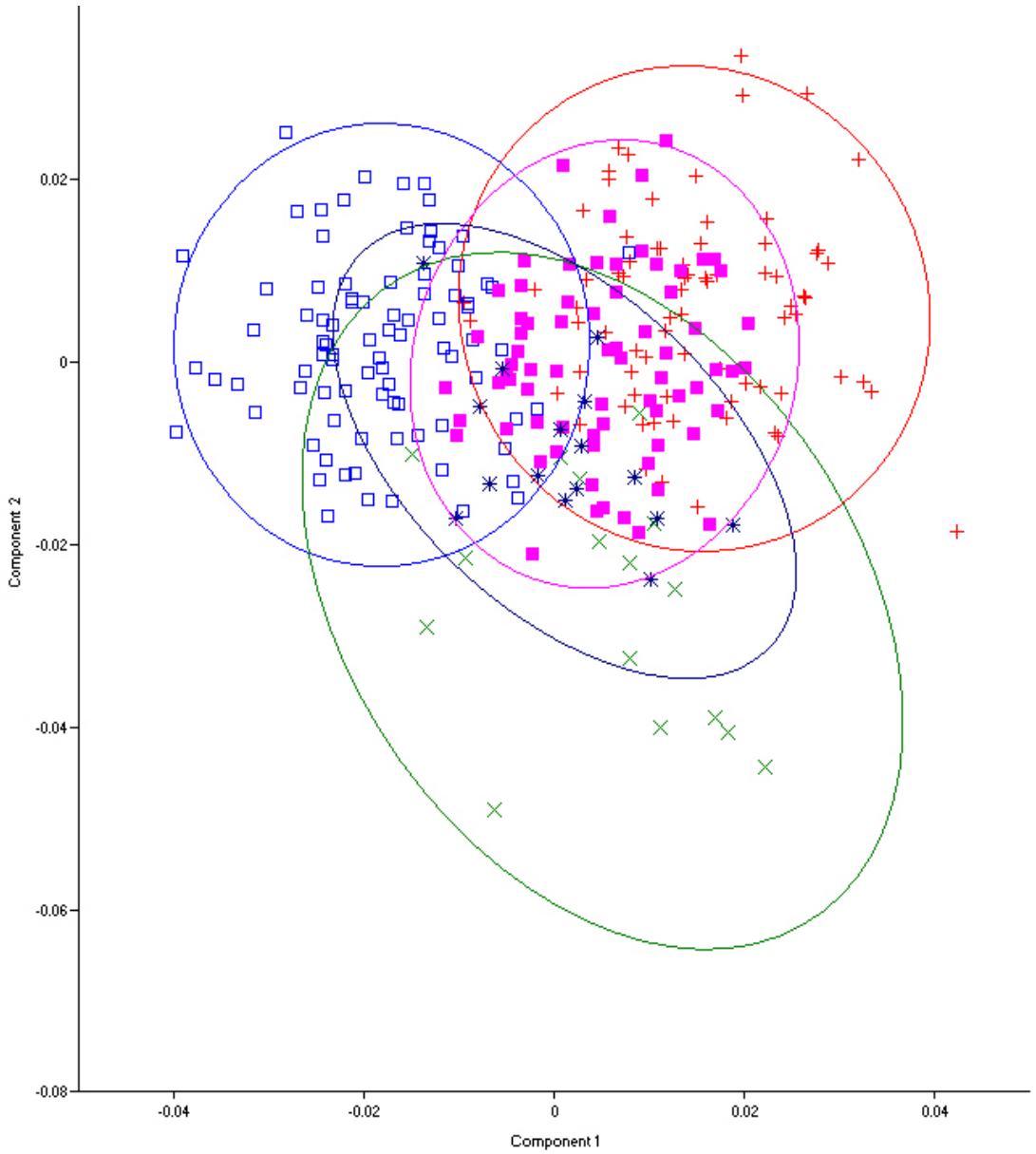

Fig 3.1 Principal components analysis of the full humerus. *Homo* is represented by blue open squares, *Pongo* by green Xes, *Gorilla* by red crosses, *Pan troglodytes* by purple squares and *Pan paniscus* by dark blue stars. PC1 explains 24% of the total variance and PC2 explains 15% of the overall variance. Each closed curve represents a 95% equal frequency ellipse.

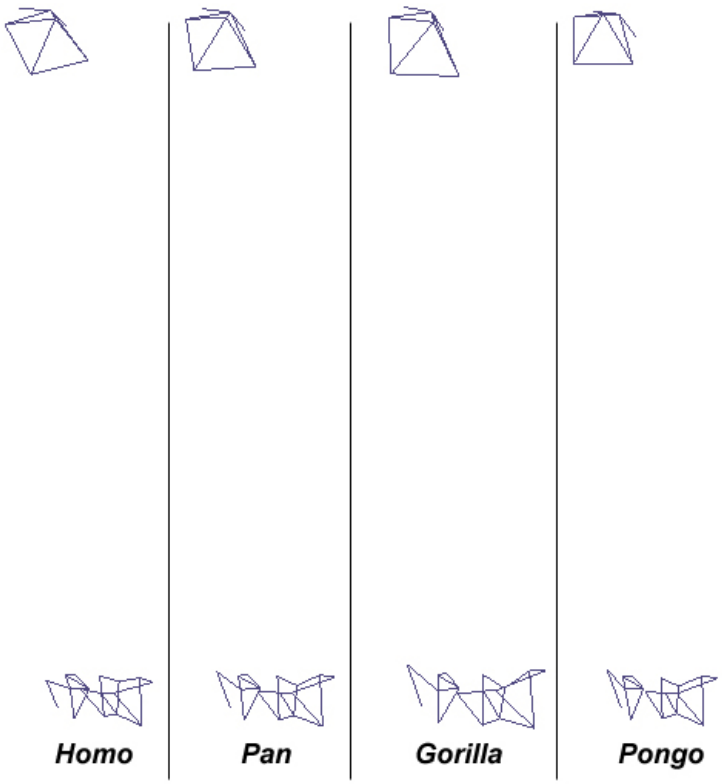

Fig 3.2 Wireframe deformations for the full humerus of the extant hominoids, looking from an anterior view. Diagrams of the landmarks on a photo of the bone are located in the distal and proximal humerus portions of the chapter.

Fig. 3.3 Side-by-side comparison of a gorilla, orangutan, chimpanzee and human humerus. The orangutan has been mirrored using Adobe CS 5.

Full humerus discussion and analysis

The amount of overlap is somewhat surprising, considering the obvious anatomical differences in the bony morphology of these taxa. It is possible that the similarities among all the extant taxa in the proximal humerus are somewhat balancing and swamping out the differences present in the distal portion of the humerus. The change along principal component 1 in the relative joint size in comparison to length is consistent with Aiello and Dean's (1990) hypothesis that the larger joint surfaces in gorillas are adapted to provide greater stability during terrestrial locomotion. While that explanation makes a certain amount of intuitive sense, the prediction does not work when other primates are studied. *Papio hamadryas* and *Macaca nemstrina* are both highly terrestrial catarrhines, but their distal humeri are narrower than those of their smaller, more arboreal counterparts, particularly in the trochlea (Richmond *et al.* 1998). It is more likely that the larger overall joint sizes in *Gorilla* and *Pan* represent a functional compromise between the need for stability during terrestrial and arboreal locomotion and the need for manual manipulative ability (Rose, 1993)**.** The change in humeral head orientation along principal component 2 is consistent with what is known about the arboreal positional behavior of orangutans. Orangutans have a more proximally oriented humeral head and lower greater and lesser tubercles to allow for the greatest possible range of motion while the arms are extended over the head (Morbeck and Zihlman, 1988; Tuttle and Cortright, 1988).

Distal Humerus

Results

The humerus was segmented into proximal and distal regions. The distal humerus consists of 13 landmarks over the entire distal articular surface. A PCA of the Procrustes aligned data for the distal humerus is presented in figure 3.4. There is reasonably good separation among all extant genera. In fact, with the exception of *Pongo,* the separation among the extant

hominoids is better than for the entire humerus. This is likely because the differences between taxa in the distal end are greater than the differences in the proximal end of the humerus, and the similarity in humeral head shape was swamping the distal data. Most of the fossils fall within the range of modern humans with the exception of ER 739, ER 1504, ER 3735, ER 6020 and TM 1517. ER 739 and ER 1504 fall within the range of modern gorillas, and ER 3735, ER 6020 and TM 1517 fall within the range of modern chimpanzees and bonobos, although ER 3735 is very close to the 95% equal frequency ellipse for modern humans. With the exception of IB 7594, all of the fossils fall within the range of *Pongo,* although that is most likely an artifact of having a small sample enough sample size that the equal frequency ellipse encloses all data points with no outliers.

PC 1 is driven mainly by the depth and width of the trochlea, where trochlea is wider and deeper in apes and it is higher, narrower and more assymetrical in humans. The capitulum is also oriented more anteriorly in humans as compared to the apes (figs 3.5 and 3.6). PC 2 separates *Pan* and female *Gorilla* from the rest of the sample based on the most posterior point of the lateral epicondyle, which is more distal in *Pan* and female *Gorilla.* PC 1 (fig 3.7) has a minimal relationship to centroid size, with a weak r value. Considering the shape of the ellipses, it is most likely that any relationship with size lies at a 45 degree angle to the first two PC axes.

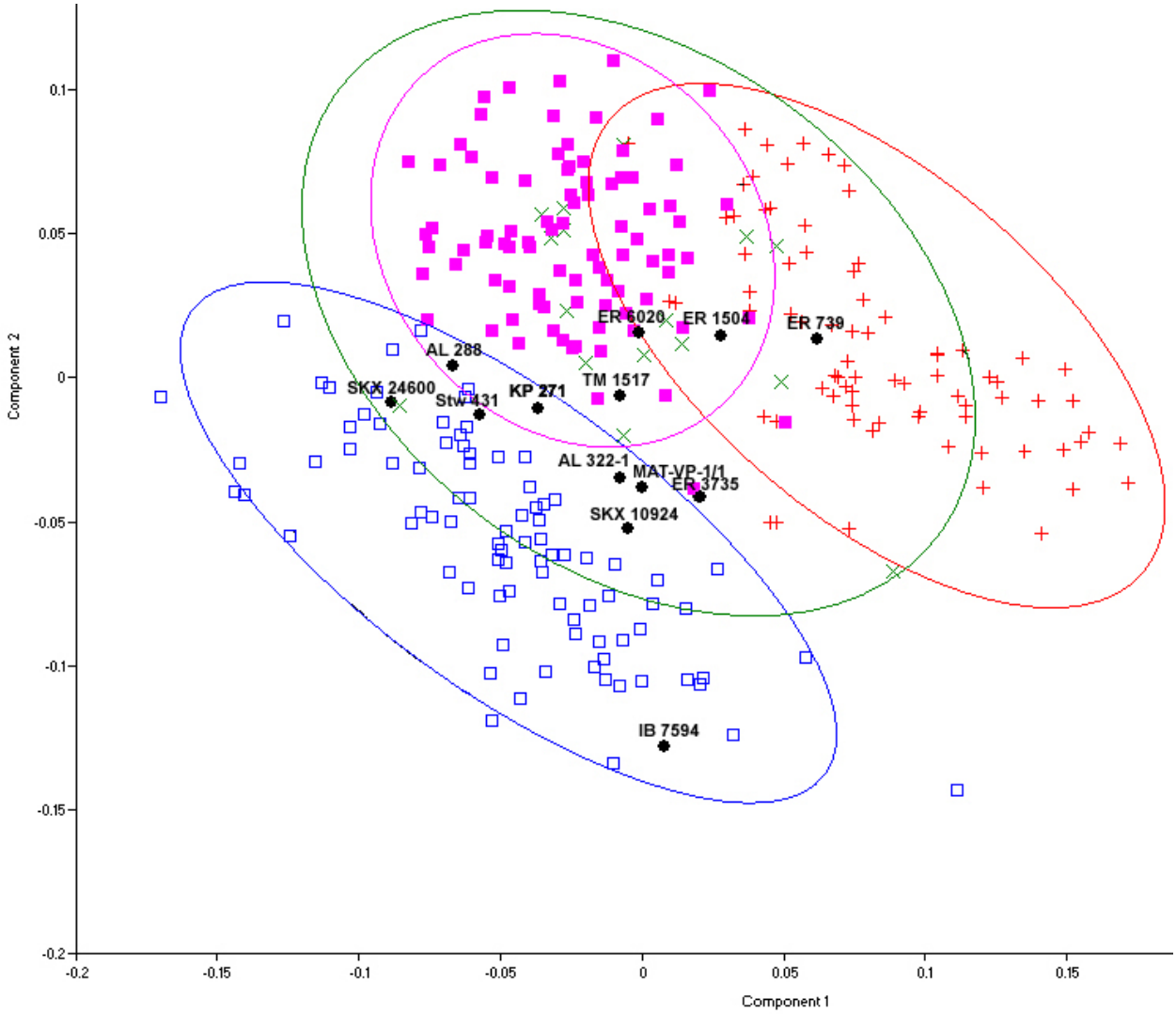

Fig 3.4 PCA of the distal humerus utilizing landmarks 8, 10-19 and 21-25. *Homo* is represented by blue open squares, *Pongo* by green Xes, *Gorilla* by red crosses, and *Pan troglodytes* by purple squares. The fossils are represented by black dots and are labeled in the graph. Closed curves are 95% equal frequency ellipses. Removing points 9 and 20 allowed for the inclusion of two additional fossil specimens – ER 6020 and ER 3735. Removing those points did not significantly change the shape space and the positions of the various complete fossils. PC 1 represents 19% of the total variance and PC 2 represents 13% of the overall variance.

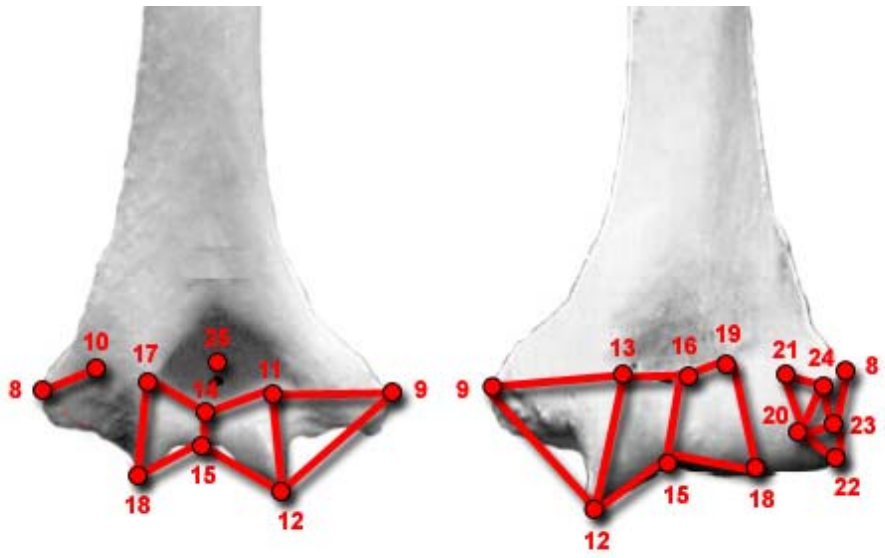

Fig. 3.5 Diagram of illustrating the landmark and wireframe configuration on an extant *Homo* humerus in posterior (L) and anterior (R) view.

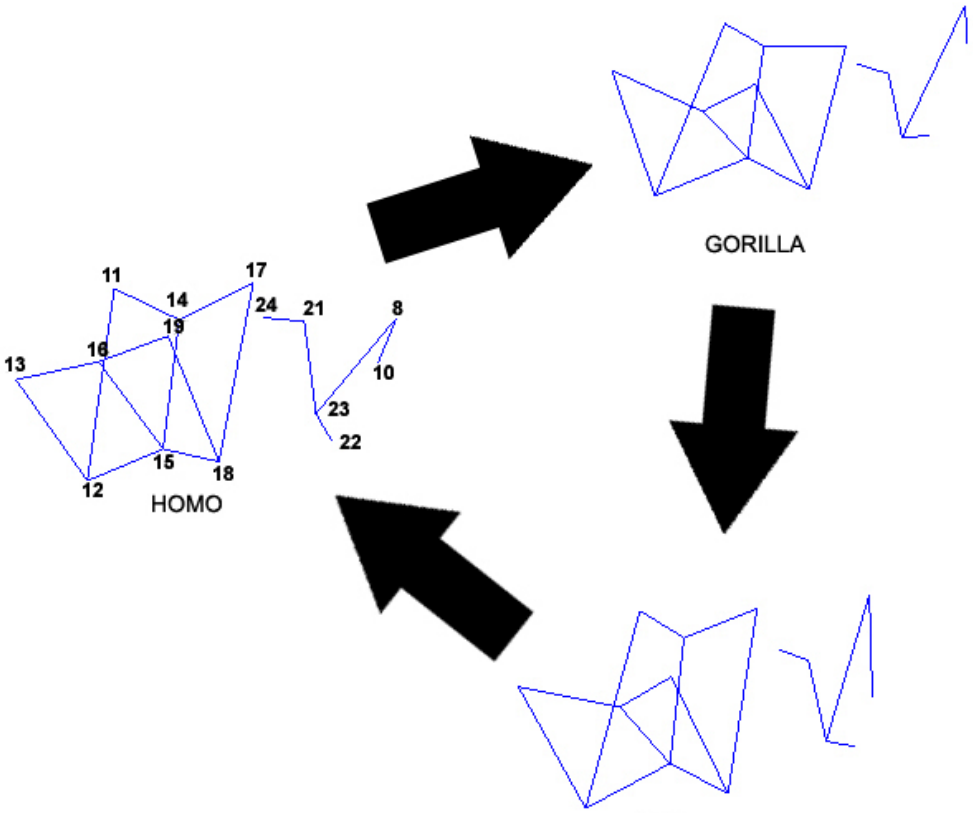

Fig 3.6 This figure shows the shape deformation between the *Homo, Pan* and *Gorilla* distributions for the distal humerus *Pongo* was not included its distribution completely overlaps the distribution of *Pan.* This is an anterior view. The points are labeled on the *Homo* wireframe for the purposes of aiding in visualization and orientation.

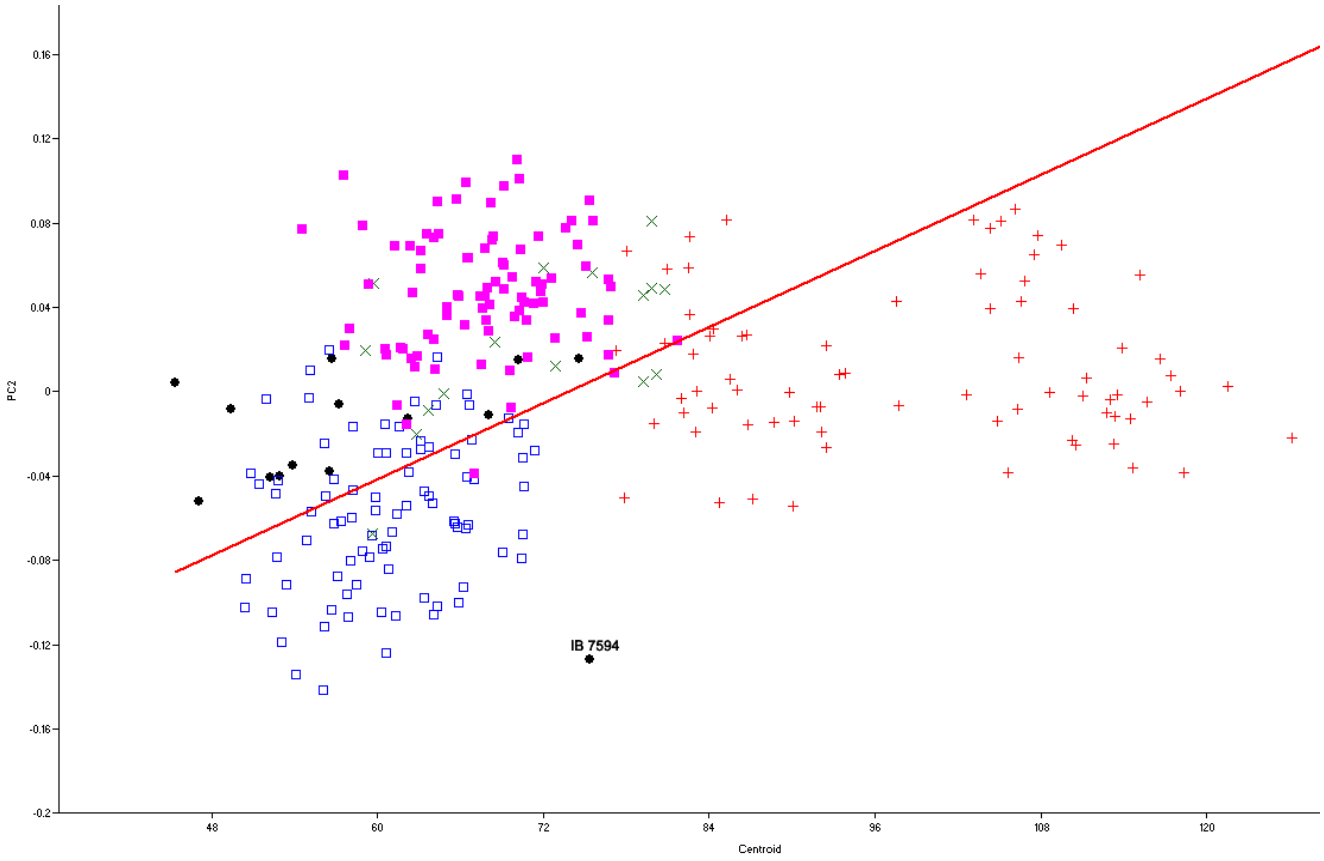

Fig 3.7 Regression of PC 1 for the distal humerus on centroid size. There is a significant correlation and r =0.250. IB 7594 falls well off of the regression line; further than all other fossils. It is labeled in the graph and has PC values of a much smaller specimen. Homo is represented by blue open squares, Pongo by green Xes, Gorilla by red crosses, and Pan troglodytes by purple squares. PC 2 was also correlated with centroid size, but that graph is not shown

Means were calculated for each species and additional analyses were performed using these means and the fossil individuals. The results of a PCA with a minimum spanning tree (MST) are presented in Fig. 3.8. These results further confirm the results from the entire sample. Most of the fossils fall nearest to modern *Homo sapiens.* Exceptions to this include ER 739, ER 1504, ER 3735 which form their own group along PC 1, although are connected directly to *Homo* through IB 7594. ER 6020 and TM 1517 (the type for *P. robustus*) are most similar to *Pongo* and MAT-VP-1/1 and AL 137-48a are closest to *P. pansicus.* There is no correlation between PC 1 and size. PC 1 is driven largely by the shape of the capitulum, and the position of landmark 10, the most posterior point on the later epicondyle. In the Koobi Fora group,

landmark 10 occurs more medially than in the other specimens and the capitulum projects more distally. Additionally along PC 1, in the Koobi Fora individuals the trochlea is more symmetrical than in the other group (see the wireframes in figure 3.8).

A neighbor-joining tree (Fig. 3.9) was also generated. Some of the clusters are still well-supported (ER 739, ER 1504 and ER 3735 form a group) but some groups are different, although bootstrap values are very low through the middle of the tree. All of the extant non-human apes form a cluster separate from all of the fossils and *Homo.* Transformations from AL 288 to ER 739 and AL 288 to TM 1517 are shown in figure 3.10. These fossils were chosen because they represent distant clusters of individuals and the species attributions for AL 288 (*A. afarensis* – "Lucy") and TM 1517 (*P. robustus* type specimen) are not disputed.

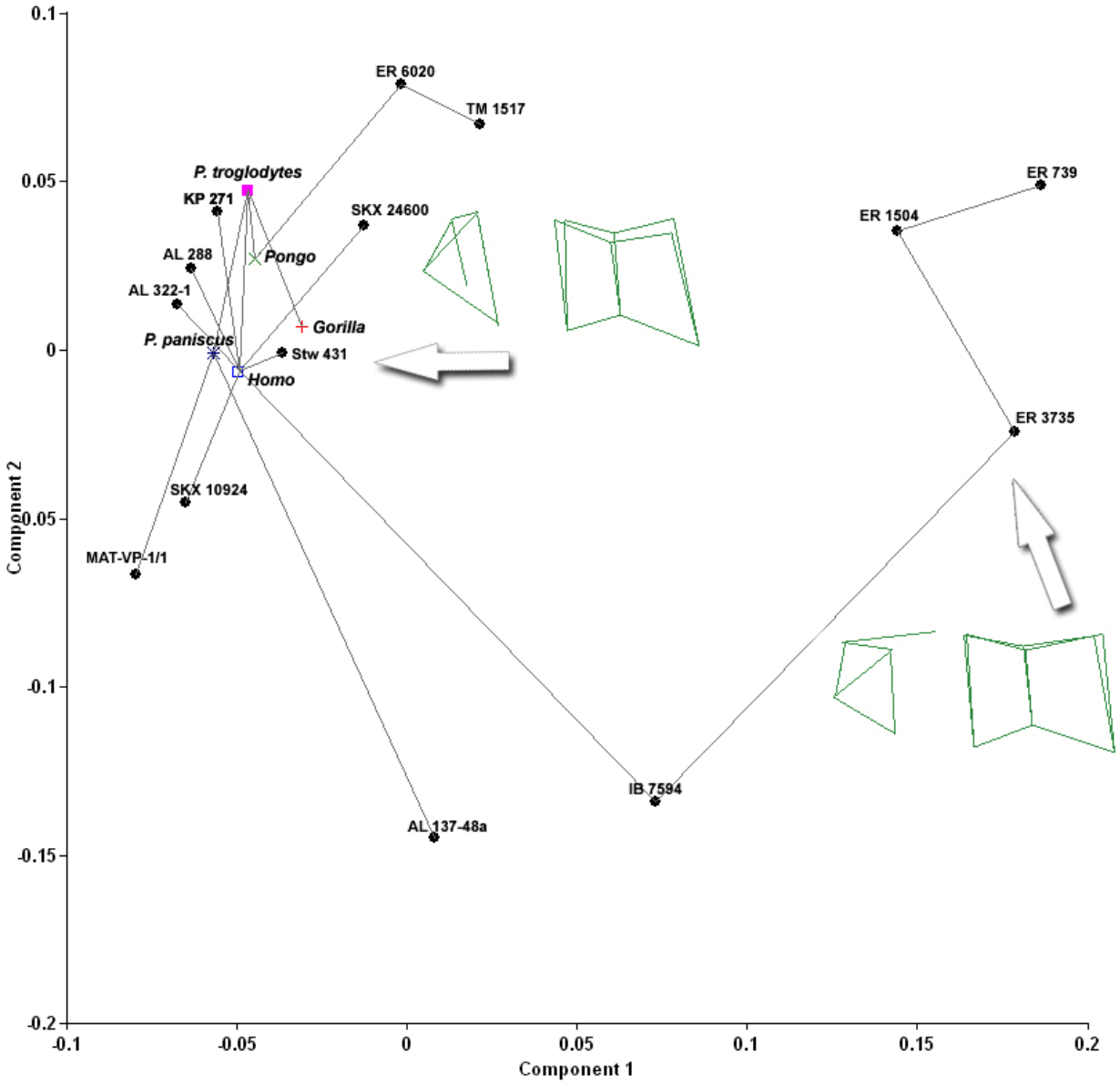

Fig 3.8 Principal components analysis for the distal humerus using the means of each extant species and a minimum spanning tree plotted on top. Wireframes are from an anterior view. The wireframe on the left describes the ER 3735, 104 and 739 cluster. The wireframe on the right describes the major cluster of the other fossils + extant means.

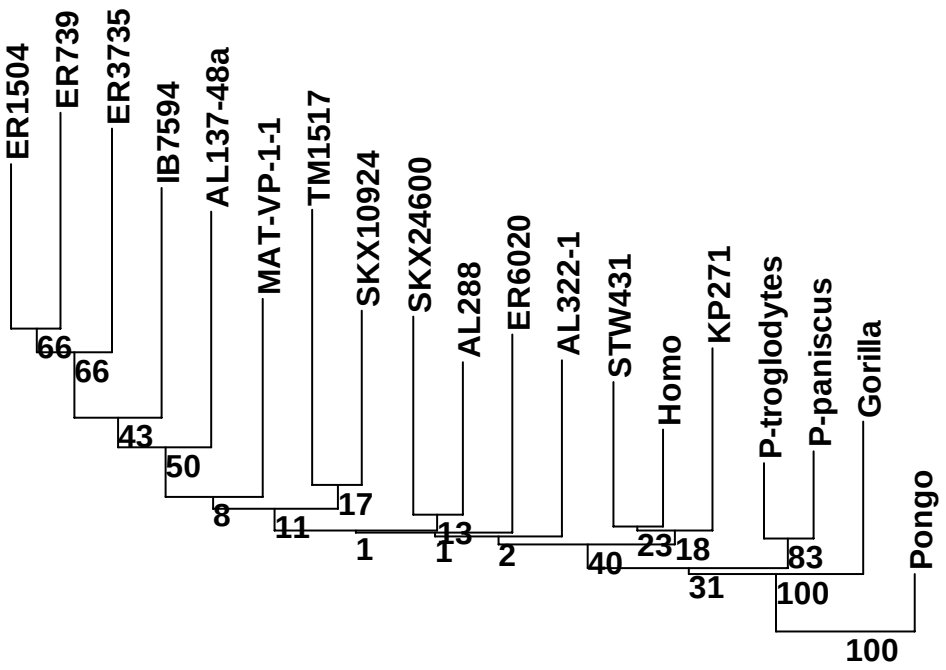

Fig 3.9 Neighbor joining tree based on procrustes chord distances for the coordinate data on the distal humerus. Means for each extant species were used. The tree is rooted with *Pongo*. Bootstrap values after 5000 replicates.

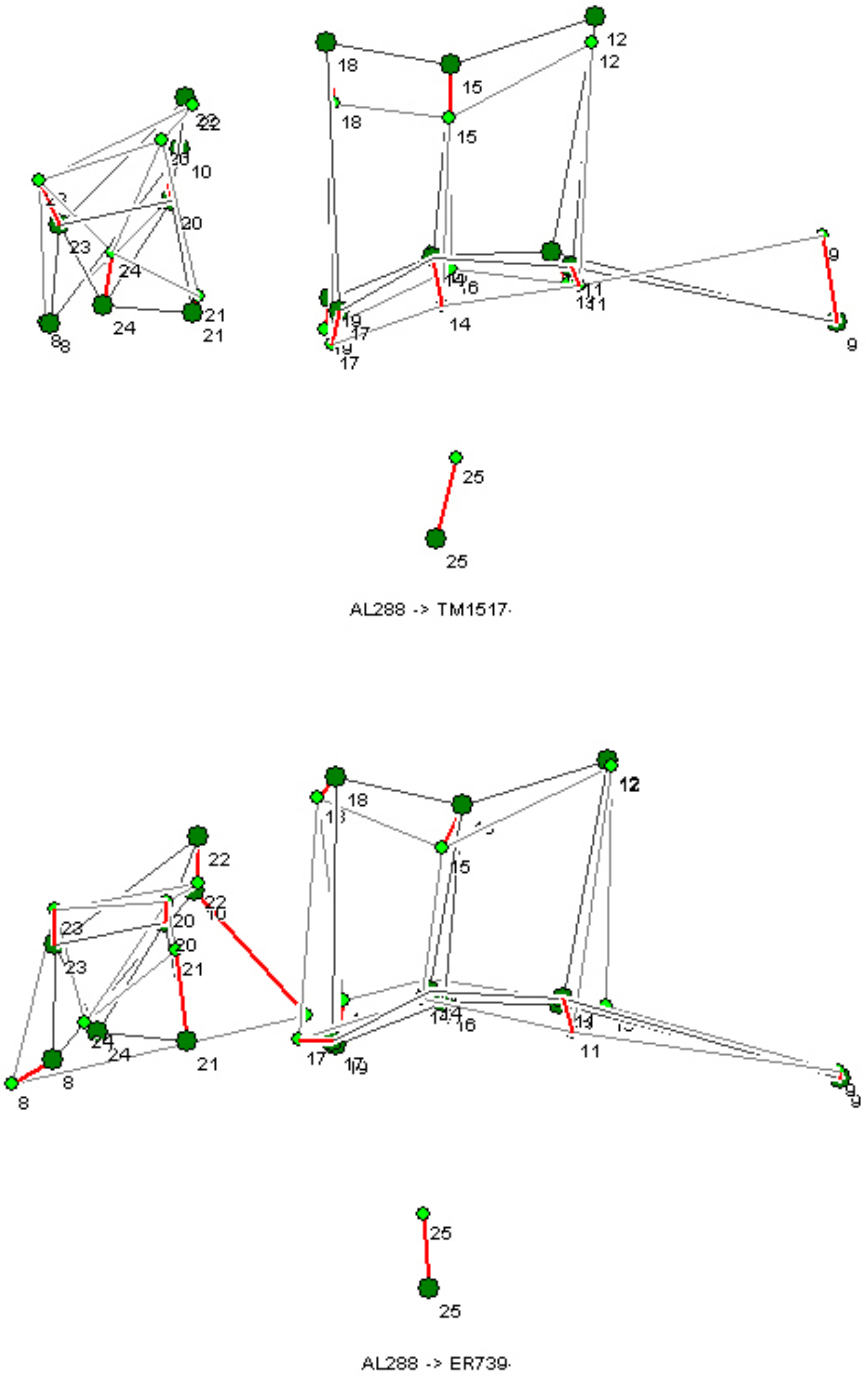

Fig 3.10 Wireframe transformations for the distal humerus between AL 288 (*A. afarensis*) and TM 1517 *(P. robustus*) on top and between AL 288 and ER 739 (possible *P. boisei*) below. The red lines represent vectors of change from one individual to the other. The longer red lines represent greater change between individuals. Point 10, the most distal point on the medial epicondyle, is driving the differences between the *Homo*-like group represented by AL 288 and the group of 3 from Koobi Fora, represented by ER 739 (the longest red line on the posterior surface is the bottom picture). AL 288 is represented by the larger, dark green circles in both diagrams.

Distal humerus analysis and discussion

Senut and Tardieu (1985) analyzed the distal humerus in a study that built on Senut's earlier work using distal humeral outlines (1981). They found three distinct fossil groups: the "human-like" first group contained IB 7594, KP 271 and AL 333w-39 and was distinguished by a low lateral crest of the trochlea, a less projecting lateral epicondyle and a more proximally oriented capitulum; the second, "more ape-like" group contained ER 739, ER 1504 and ER 3735 and was distinguished by a shallow olecranon fossa, a low lateral trochlea crest and a strongly proximo-laterally oriented lateral epicondyle; the third group contained AL 288, AL 322-1 and AL 137-48a and had a strongly developed lateral trochlea crest and a less laterally projecting lateral epicondyle. Taxonomically, they concluded that there are two species present at Hadar: *Homo,* represented by AL 333w-29 and *A. afarensis* represented by the other humeri in their sample. Functionally, these authors rejected the idea that the elbow was stabilized for knuckle-walking and suggested that if these individuals were adapted for arboreal life, it would be some form of vertical climbing.

Lague and Jungers (1996) analyzed a similar sample of Plio-Pleistocene distal humeri. They took a series of linear measurements on: AL 137-48a, AL 288, AL 322, IB 7594, ER 739, ER 1504, KP 271 and TM 1517. The data collected through their linear measurements is easily encompassed by the landmark coordinates collected for this study. Lague and Jungers also found that ER 1504 and ER 739 were morphologically distinct, but found that all the other fossils fell into a single group that could not be easily distinguished from one another. Regardless of this finding, they assigned IB 7594 to *P. boisei.* They rejected Senut and Tardieu's assertion that there are two species at Hadar based on the abraded condition of the AL333w-29 distal humerus. These authors came to no real functional conclusions, but they

suggested that their data would support a more arboreal form of locomotion for all fossil individuals than is seen in modern *Homo*.

Most recently, McHenry and Brown (2008) analyzed a larger sample of distal humeri from *Australopithecus anamensis* to *Homo erectus* using standard linear measurements for the purpose of looking at patterns of variation through time for the distal humerus. In reference to specific fossils, these authors found that KP 271 (*A. anamensis*) and AL 288 (*A. afarensis*) looked most like modern humans. Stw 431 (*A. africanus*) was distinct from all of the other fossils in their analysis, and closest to the *Gorilla* centroid in their discriminant function analyses. They found the distal humeri from Koobi Fora to be a heterogeneous group with WT 15000 most similar to *Homo* and the other distal humeri (ER 739, 1504, 3735 and 6020) most similar to *Gorilla*.

Table 3.4 A list of fossil distal humeri broken into groups based on morphological affinity.

Group 1	Group 2	Group 3
ER 739	TM 1517	AL 137-48a
ER 1504		AL 288
ER 1591		AL 322
ER 3735		IB 7594
ER 6020		KP 271
		MAT-VP-1/1
		SKX 10924
		SKX 24600
		Stw 431

The data presented in this chapter agree with some of the findings of these previous authors. These data suggest that fossil distal humeri can be placed in three different groups (presented in Table 3.4, and referred to throughout the rest of this text). When analyzed in the context of the extant individuals, the fossils have a higher average within-group procrustes distance than any of the extant intraspecific pairings, indicating that there are at least two taxa represented in the sample (fig. 3.11). The first group proposed here contains ER 739, ER 1504, ER 3735, and, tentatively, ER 1591 and 6020; the second group contains only TM 1517; while the third group contains all of the rest of the fossils.

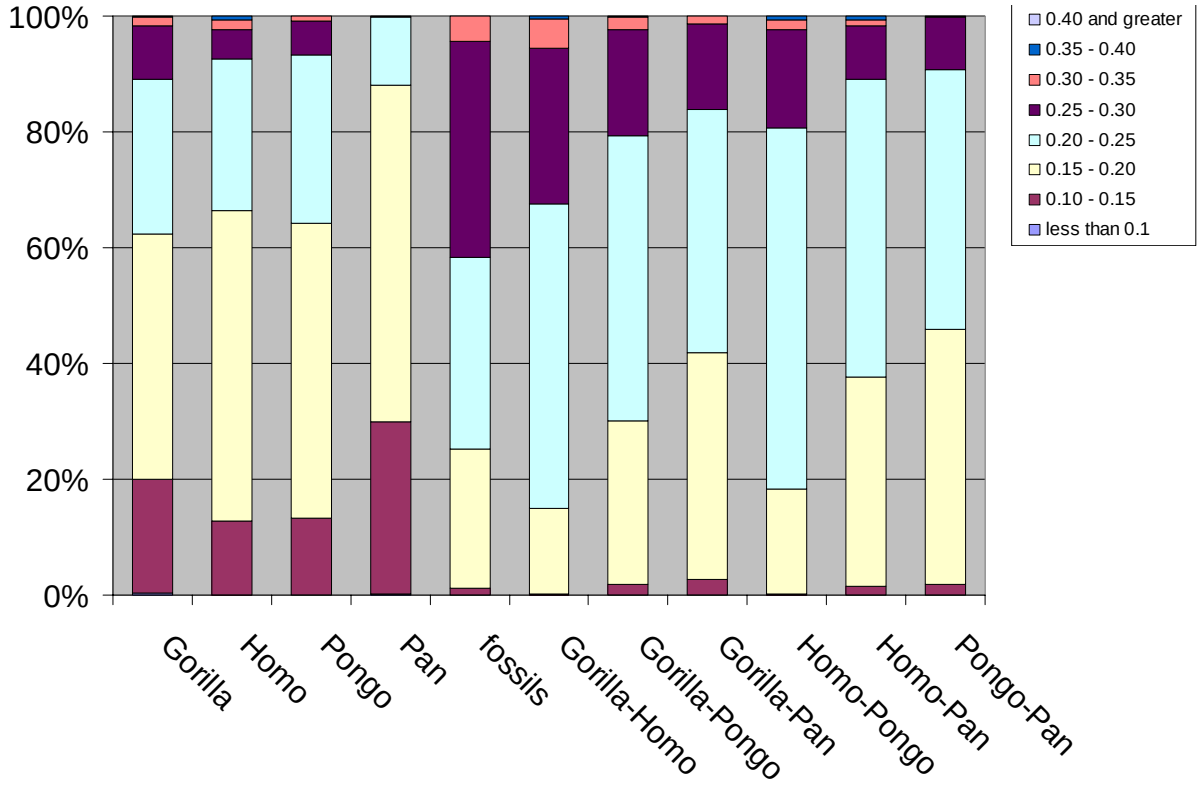

Fig 3.11 This bar graph is a representation of the distribution of procrustes chord distances within and between the different genera in the sample for the distal humerus. The array of procrustes distances were segmented into arbitrary units of 0.05. The group of fossils has the highest average procrustes distance of all of categories.

Functional Overview

As stated in the results portion of this chapter, PC 1 for the PCA of the entire sample of distal humeri is driven mainly by the depth and width of the trochlea and the position of the capitulum (fig 3.4 and fig 3.6). This corresponds to the known functional differences in the ways that apes use their elbow joints, as opposed to humans. Humans have a less developed trochlear keel, particularly on the posterolateral aspect as well as a shallow, poorly developed zona conoidea. The more anteriorly facing capitulum is correlated with a reduced ability to hyperextend the forearm (in comparison to non-human hominoids) and a reduction in the weight-bearing capability of the radius. This has the effect of reducing the stabilizing aspects of the elbow joint and maximizing muscular control of the forearm muscles while the forearm is in a

flexed position (Aiello and Dean, 1990; Rose, 1993). The most posterior point on the lateral epicondyle separates female *Gorilla* and *Pan* from part of the human sample along PC 2 in the same analysis: in *Pan* and female *Gorilla,* this point is more distal. This point is an indicator of the way that compression forces run through the humerus. In *Homo*, the higher position of the 10th landmark is indicative of the more square shaped cross section of the lateral humerus whereas in *Pan* it is more triangular. This represents a shift in the maximum strength of the humerus towards the lateral side in *Homo* (Aiello and Dean, 1990).

Group 1

The divergent morphology of ER 739, 1504 and 3735 is in line with the previous findings by Senut and Tardieu (1985) and Lague and Jungers (1996). Lague and Jungers did not include ER 3735 in their study, they noted that upon visual inspection it seemed similar to ER 739 and ER 1504. ER 739 was originally attributed *Paranthropus (Australopithecus) boisei* (Howell, 1978) but that attribution has been called into question many times due to presence of multiple hominin species. McHenry (1991) hypothesized that the ER 739 humerus was too large to be *P. boisei* based on the relatively small postcrania from more securely attributed *Paranthropus* skeletons. Lague and Jungers (1996) tentatively assigned ER 739 to *H. rudolfensis* and ER 1504 and ER 3735 to *H. habilis* based on extreme differences in size and a higher stratigraphic position for ER 739. However, the fact that these specimens are so similar in morphology despite the difference in size could argue for a single, sexually dimorphic taxon despite the differences in the ages of the three specimens. As ER 3735 is part of a partial skeleton attributed to *H.* cf. *habilis,* all three of these specimens could be tentatively assigned to that species. This would lend support to the idea that *H. habilis* is a sexually dimorphic species and specimens that some

researchers attribute to *H. rudolfensis* are simply large bodied *H. habilis* individuals. Alternatively, it could indicate that the morphology of *Homo habilis* and *Homo rudolfensis* are quite similar and that the only real postcranial difference between them is size.

ER 6020's position changes in the various analyses, but it looks most similar to ER 739 in both size and shape. The major differences between ER 6020 and the fossils in this group are the position of the most posterior point on the lateral epicondyle (point 10) and the most posterior point on the articular surface of the capitulum (point 22). In ER 6020, this most posterior point on the lateral epicondyle is located more distally and the articular surface of the capitulum extends more posteriorly than in the other three fossils (see fig. 3.12).

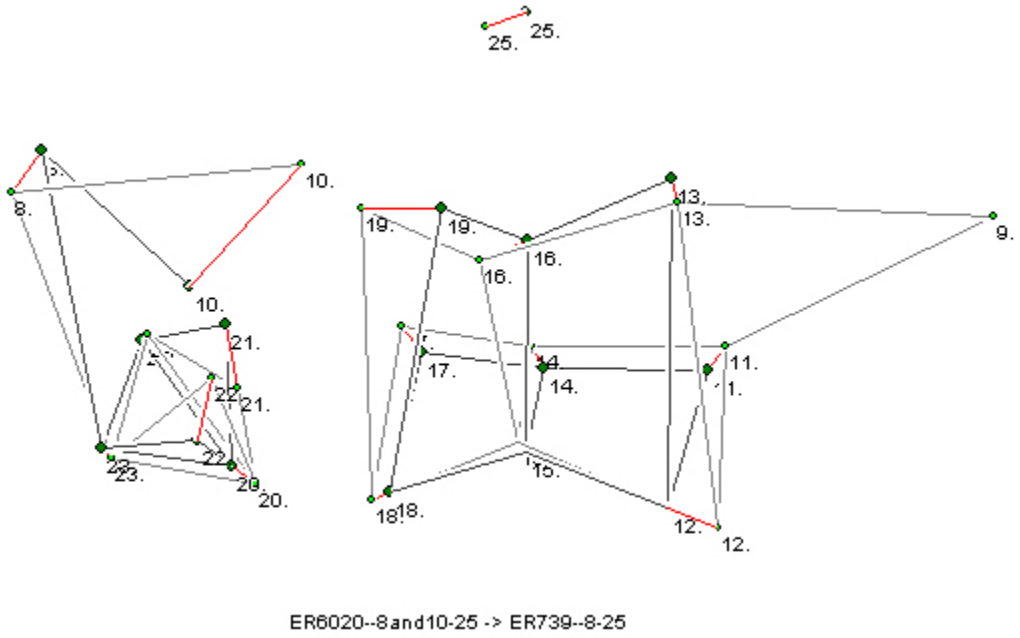

Fig. 3.12. Posterior view of the distal humerus showing the wireframe for ER 6020 (in black) superimposed over ER 739 (in gray). The figure is angled such that the extreme difference in point 10 – the most posterior point on the later epicondyle – can be seen.

Data were collected on ER 1591, and while it is not included in any of the previous analyses as it is only a trochlea, its shape is quite similar to this group (fig 3.13). When neighbor-joining trees were generated for this sample including only the trochlea, ER 1591

clustered most closely with ER 739 and ER 1504 (fig. 3.14). Analyses on the trochlea alone still discriminate between extant taxa, although not as strongly as in the entire distal humerus (fig 3.15).

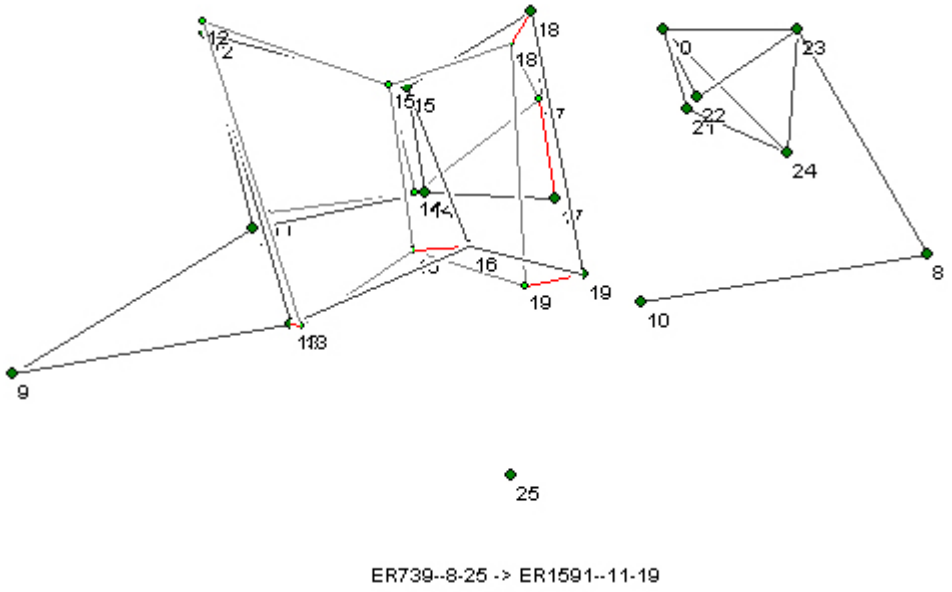

Fig. 3.13 Anterior view of the trochlea of ER 1591 (in grey) superimposed on the distal humerus of ER 739 (in black). While the two specimens are not identical, the variation between them is not extreme.

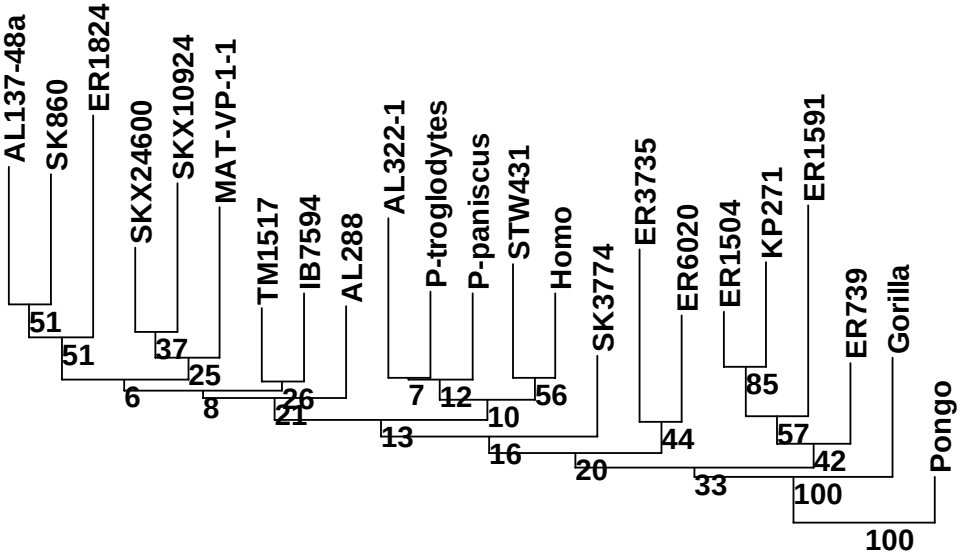

Fig 3.14 Neighbor joining tree based on Procrustes chord distances for the coordinate data on the trochlea. Means for each extant species were used. The position of ER 1591 falls within the cluster that also contains the individuals that form the putative *Homo habilis/rudolfensis* group. KP 271 also falls within this cluster for the trochlea region which indicates that its trochlea might be more like these other specimens, even if its overall morphology is most similar to the *Australopithecus* group. This tree is rooted with *Pongo* and bootstrap values are after 5000 replicates.

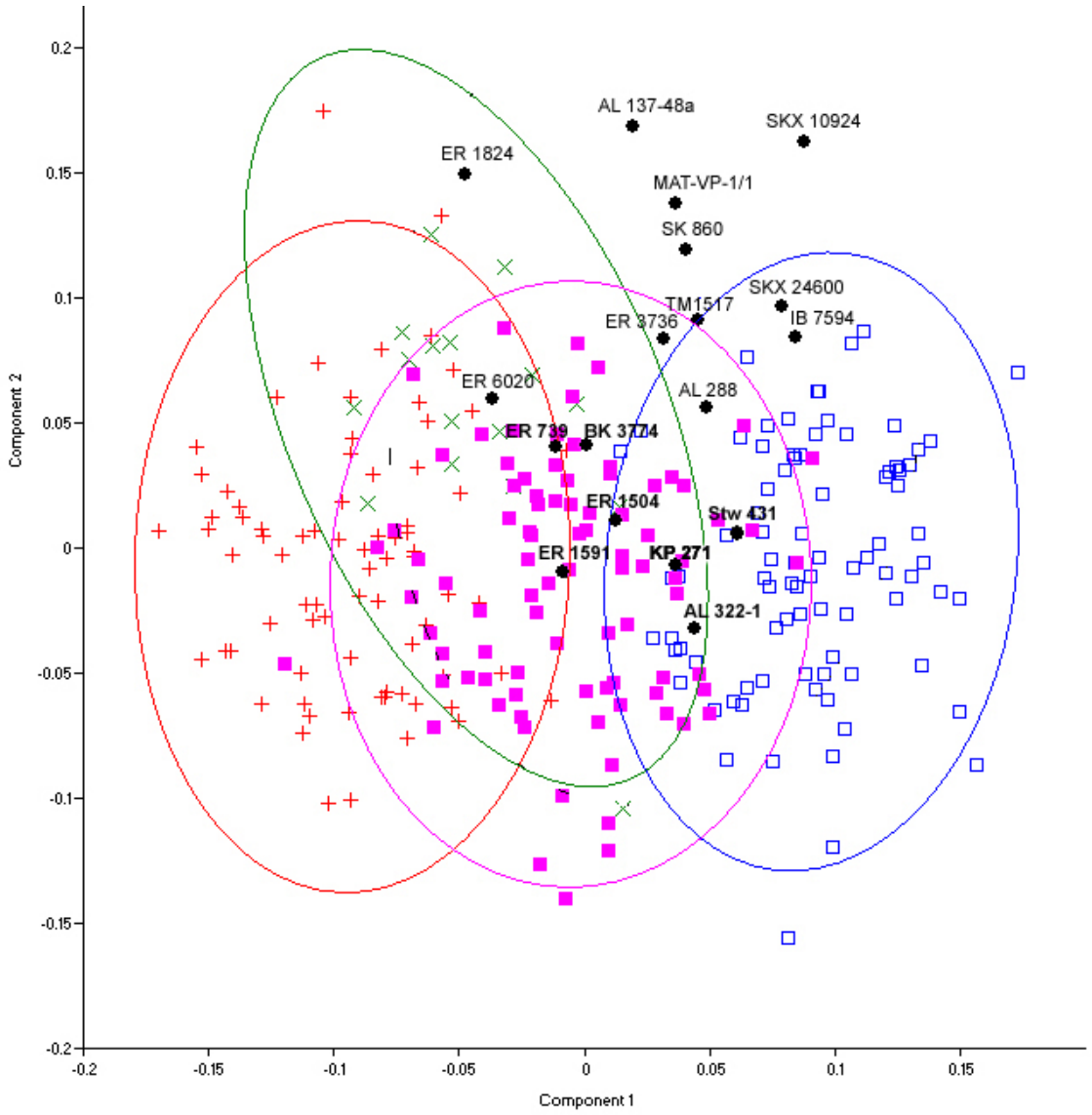

Fig 3.15 PCA of the procrustes aligned landmarks for the trochlea (11-18; see Ch. 2). Fossils are labeled in the graph and represented by black dots. PC 1 represents 22% and PC2 represents 11% of the total variance. *Homo* is represented by blue open squares, *Pongo* by green Xes, *Gorilla* by red crosses, and *Pan troglodytes* by purple squares Each group is surrounded by a 95% equal frequency ellipse.

The fossils in Group 1 fall squarely within the ape distribution and are dated between 1.9 and 1.53 Ma (Feibel *at al*, 1989). Thus, for the distal humerus, a more conservative condition occurs later in time than a more derived condition. This indicates that: 1) there was a reversal in the specimens from Koobi Fora back to a more ape-like condition; 2) that there are multiple

evolutionary trajectories for locomotor repertoire during the Plio-Pleistocene; or 3) we are only seeing part of the picture. Kay (1973) suggested that the large forearm of ER 739 in comparison to estimates for body size indicates that it would have still been used for locomotion in this individual. The shape data from these analyses supports this idea. The more symmetrical trochlea and distally oriented capitulum indicate weight-bearing capacity and the overall robusticity of the individual and the heavy muscle markings on the distal humerus indicate powerful ability to both pronate and supinate. This morphology is generally shared by all of the members of this group. ER 3735 even has the appearance of a perforation in the olecranon fossa. If this is not a taphonomic effect, it would indicate continual contact between the ulna and humerus deep in the olecranon fossa, a condition seen in many *Pongo* specimens (Rose, 1993).

Group 2

The second group contains TM 1517, the type of *Paranthropus robustus.* It seems to have a slightly different pattern than all of the other fossils in this analysis. In the first principal components analysis (fig. 3.4), it falls outside the range of modern human variation, closer to the extant apes and the fossils in the putative *Homo habilis* group from Koobi Fora. In the PCA/MST of the means, its nearest neighbor in both the PCA and the cluster analysis is ER 6020, part of the same putative *Homo habilis* grouping (fig 3.8). However, the similarity between TM 1517 and ER 6020 is based mostly on the extreme position of point 10, the most posterior point on the lateral epicondyle. An analysis of all of the complete fossil distal humeri *without* that landmark illustrates the unique morphology of TM 1517 (fig. 3.16). A non-metric MDS analysis with landmark 10 also confirms these results (fig 3.17).

While TM 1517 also falls within the ape distribution in a PCA of all extants and fossils (fig. 3.4 and 3.5), there are differences between it and those of Group 3 when the fossils are examined individually. TM 1517 is different from all of the other fossils in that the medial epicondyle is flexed and points distally. It also has a very flat capitulum, especially in the anterior aspect, and a narrow and very asymmetrical trochlea due to a pronounced medial trochlear keel. Specifically in comparison to ER 739, TM 1517 has a trochlea that is extended more in the posterolateral direction and the lateral epicondyle in TM 1517 is oriented more posteriorly and proximally than in ER 739. Like ER 739 (although unlike AL 288), is has the more distal position for the most posterior point on the lateral epicondyle, which is the same as the extant apes.

The suite of traits in TM 1517 is not seen in any extant hominoid. The medially developed trochlear keel could lead to increased stability in quadrupedal locomotion, as seen in terrestrial cercopithecoids (Rose, 1993), except that the lateral trochlear keel is not equally well developed and the capitulum is flat. The flat capitulum would not be beneficial in any kind of weight bearing locomotor postures, although the flat articulation could lead to a greater range of motion in the articulation with the radius. The pronator teres originates at the medial epicondyle, inserts into the radial shaft and is a pronator of the forearm. The strongly projecting and slightly distally flexed medial epicondyle in TM 1517 might indicate some modification and/or reliance on strong pronating ability. While this is purely conjecture, such a suite of traits might be adaptive in some kind of trunk based, vertical climbing activity.

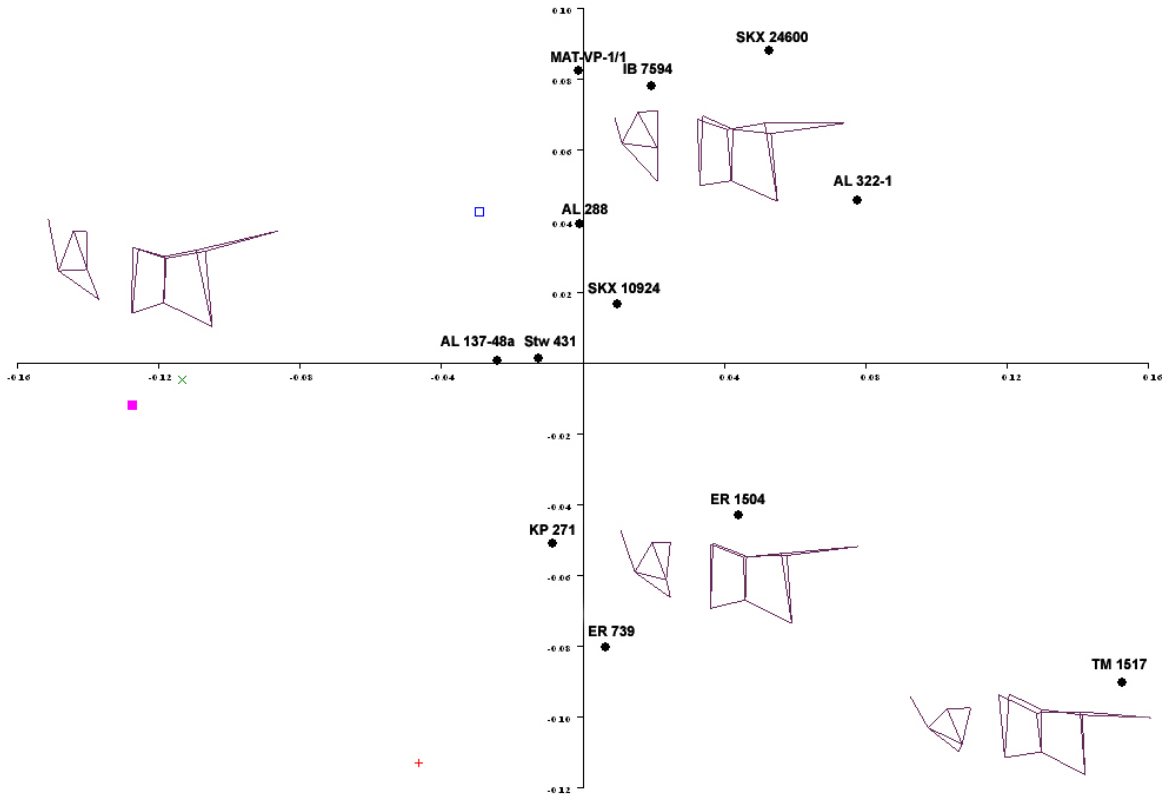

Fig. 3.16 PCA of all complete fossil distal humeri without landmark 10. All fossils are labeled in the graph. PC 1 contains 23% of the variation present in the sample. PC 2 contains 16% of the variation. The wireframes are in an anterior view and are place on the graph in approximately the place that they represent. *Pan* is represented by a purple square, *Pongo* by a green X, *Homo* by a blue open square and *Gorilla* by a red cross. Fossils are in black and labeled in the graph.

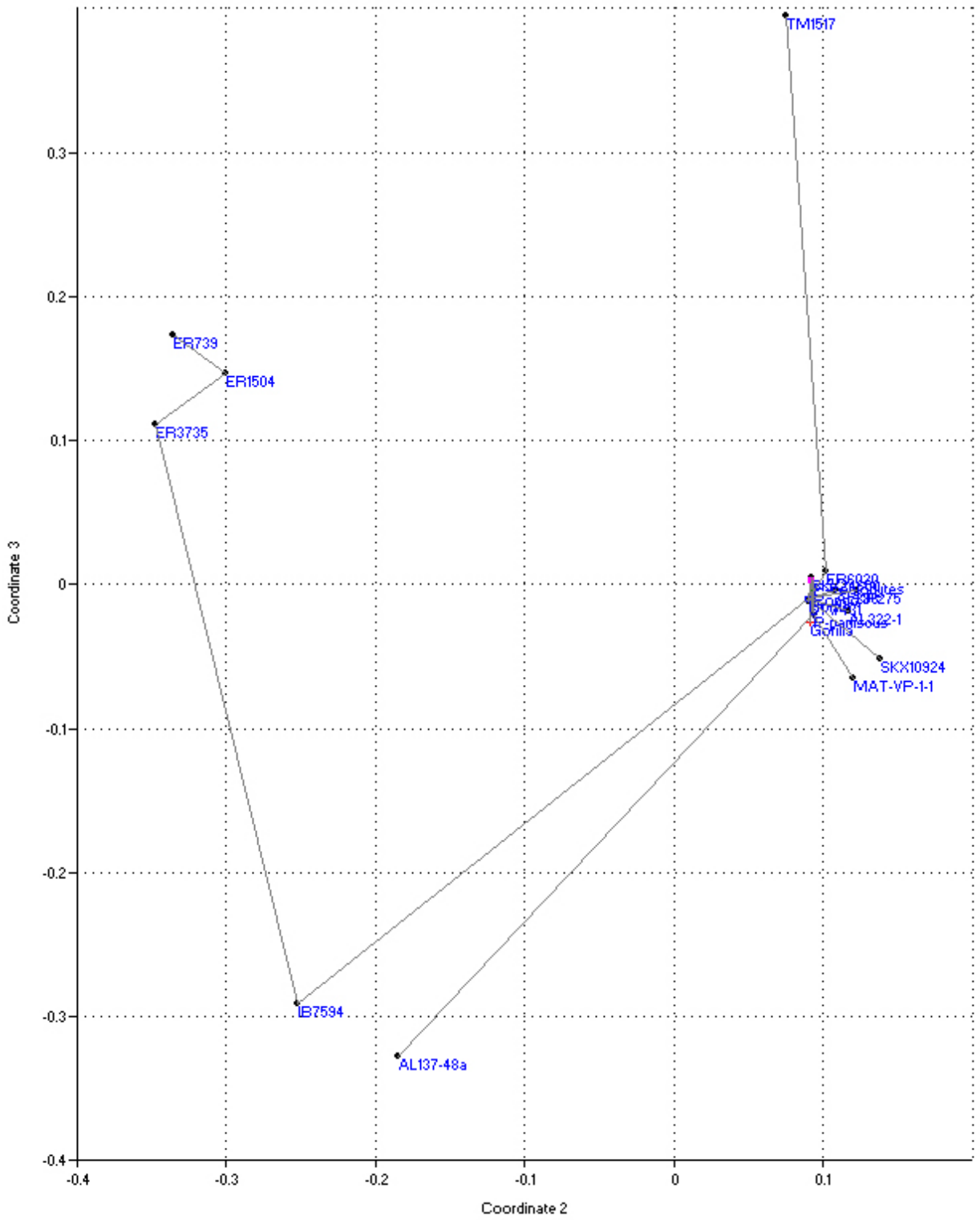

Fig 3.17 A non-metric MDS analysis of the distal humerus using the means for the extant species with the fossils. Euclidean distances were used as the similarity measure. An MST was plotted on top of these results. All of the extant individuals form single cluster on the right side of the graph. Stress = 0.40

Group 3

The third group is *Homo*-like and contains all of the remaining fossils including: Gombore IB 7594, all Hadar specimens, KP 271, Stw 431, SKX 10924, SKX 24600, and MAT-VP-1/1. The specimens from Hadar, KP 271, MAT-VP-1/1 and Stw 431 have all been attributed to the genus *Australopithecus* (Johansen *et al.* 1978; Asfaw *et al.* 1999; Ward *et al.* 2001; Partridge *et al.* 2003) All of the fossils from Hadar are within this group which contradicts Senut and Tardieu's (1985) idea that there are two different species present. AL333-29w was not used for this study as its condition was too poor for accurate data collection. The inclusion of Stw 431 in this group is contra McHenry and Brown (2008) who placed it with *Gorilla.* SKX 10924 and SKX 24600 have been attributed to *H. erectus* and *P. robustus* respectively (Susman *et al.* 2001). However, the fact that SKX 24600 does not cluster with TM 1517 sheds some doubt on that attribution. KP 271 is attributed to *Australopithecus anamensis* and is the oldest fossil in this sample. Ward *et al* (2001) suggest that this fossil is indistinguishable from *Australopithecus afarensis*, and this study supports that conclusion. These authors also note that the cortical bone mass in KP 271 is greater than all of the extant African apes, and most like the condition seen in *Pongo.*

The distal humerus from Gombore is substantially younger in time than the other specimens in this group at 1.6 Ma (Coppens, 2004). It has been attributed to *Paranthropus boisei* by Lague and Jungers (1996), *Homo habilis* by Senut and Tardieu (1985) and *Homo erectus* by Coppens (2004). The position of this fossil changes fairly radically in the various analyses, falling with only *Homo* in the PCA of the entire sample, with the ER 739, 1504, 3735 grouping in the neighbor-joining tree, and by itself in the MST and PCA of the means. This may be due to its large size, as Gombore IB has the largest centroid size of any of the fossils. It is

most similar to the individuals from Hadar, and specifically AL 288 (see fig. 3.18), which is why it falls off the regression line (fig 3.7). Its similarity to AL 288 clearly puts it within the "*Homo*-like" fossil grouping.

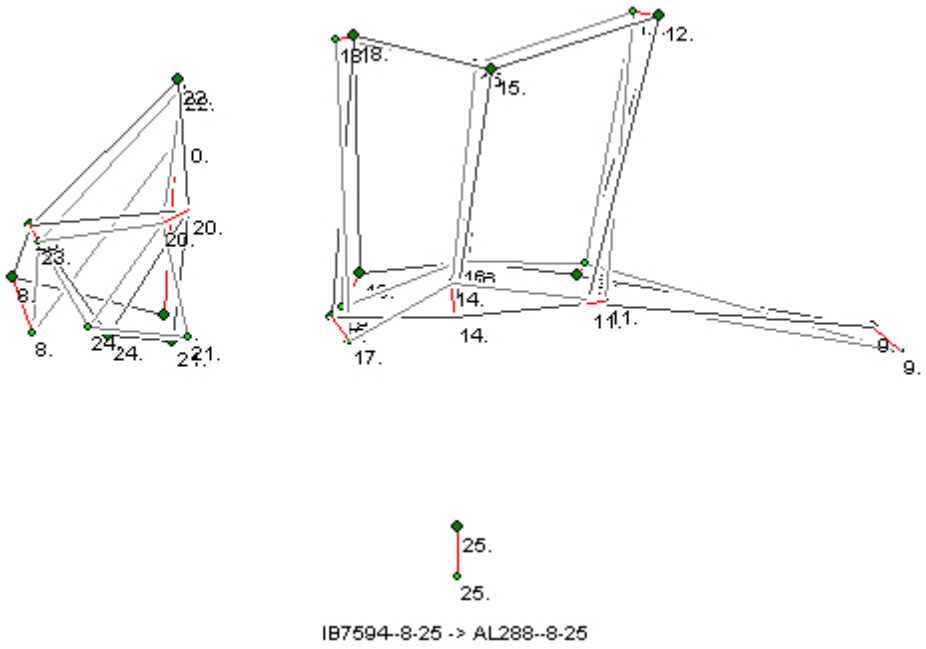

Fig. 3.18 An anterior view of IB7594 superimposed on AL 288 – *A. afarensis.* With the exception of the lateral epicondyle (point 8), the shapes of these two individuals are remarkably similar.

Oxnard (1975) suggested that the evidence from multiple postcranial elements, including the distal humerus, indicated that *Australopithecus* is most similar to *Pongo.* These data do not agree with that intepretation. In this analysis, the fossils in Group 3 fall squarely within the 95% confidence ellipse for modern *Homo sapiens.* While there is some overlap between *Pongo* and *Homo,* this is mostly due to a single individual in the *Pongo* sample; the majority of *Pongo* individuals fall outside the 95% confidence ellipse of modern humans. This would indicate that these individuals represent species which had already made the anatomical shift away from using the forearms in a weight-bearing capacity. Included in group three is KP 271, *Australopithecus*

anamensis, dated between 4.17 and 4.07 Ma (Leakey *et al.* 1988) as well as all of the individuals from Hadar attributed to *Australopithecus afarensis* and dated to 3.5-3.2 Ma (Walters, 1994). This indicates that a very human-like pattern in the forelimb was already developed early in the human fossil record and if these individuals were not obligate bipeds, they likely relied very heavily on bipedal postures and lightly on weight-bearing quadrupedal stances. These findings support those of McHenry and Brown (2008) who also found what appear to be very human-like distal humeri early in the record and ape-like humeri very late.

Summary

In summary, there are distinct differences between Plio-Pleistocene humeri that do not seem to correlate with time (*i.e.* group 1 occur more recently than most of the fossils in group 3). Functionally, the more conservative traits present in groups 1 and 2 (represented by TM 1517 and ER 739 in fig 3.19) could indicate a greater reliance on the forelimb for various positional behaviors than that seen in modern human populations.

Taxonomically, little can be said about group 3 as they all appear to be similar to modern humans although KP 271 (*Australopithecus anamensis*) does seem to share some affinities with group 1, particularly in the shape of the trochlea (see fig. 3.14). It is unlikely that the Gombore humerus belongs in *Paranthropus boisei*, considering its similarity to AL 288 and distance from TM 1517; if anything, this data supports Coppens' (2004) attribution of *Homo erectus.* In terms of group 1, due to the affinity of ER 739 and ER 1504 with ER 3735 (*H. habilis),* those fossils could tentatively be assigned to that species. Alternatively, they could be assigned to *H. rudolfensis* as Lague and Jungers (1996) recommended if *H. habilis* is not a sexually dimorphic taxon.

Fig 3.19 Side by side comparison of AL 288, TM 1517 and ER 739 to scale. Note that ER 739 has been reflected left to right using Adobe Photoshop in order to compare it more easily to the other two fossils. In comparing the morphology between the three fossil groups, ER 739, AL 288 and TM 1517 were used. AL 288 and TM 1517 were selected because their taxonomic status is not disputed and ER 739 was selected as the most complete and best preserved fossil from that group.

Proximal humerus

Results

The proximal humerus consists of 7 landmarks describing the humeral head and greater and lesser tubercles. The landmarks for the proximal humerus fail to discriminate between extant taxa particularly well (see fig 3.20). PC 1 and 2 are presented, although there is no discrimination between the extant taxa on any principal axis. This is likely for two reasons: first, the proximal humerus is simply not very different across extant apes when the information relating to the distal portion is removed; and second, there are no type I landmarks and few type II landmarks to collect on the proximal humerus. Any real biological signal present might be obscured because of slight variation in data collection. Indeed, PC 1 was driven largely by the placement of the most anterior landmark along the articular surface of the humeral head and it drifts up and down across the axis. PC 2 may be more biologically meaningful as it is driven by

the tilt of the humeral head with reference to the points defining the border of the articular surface of the humeral head. PC 1 is correlated with centroid size (fig. 3.21) but many of the fossils fall off of the regression line.

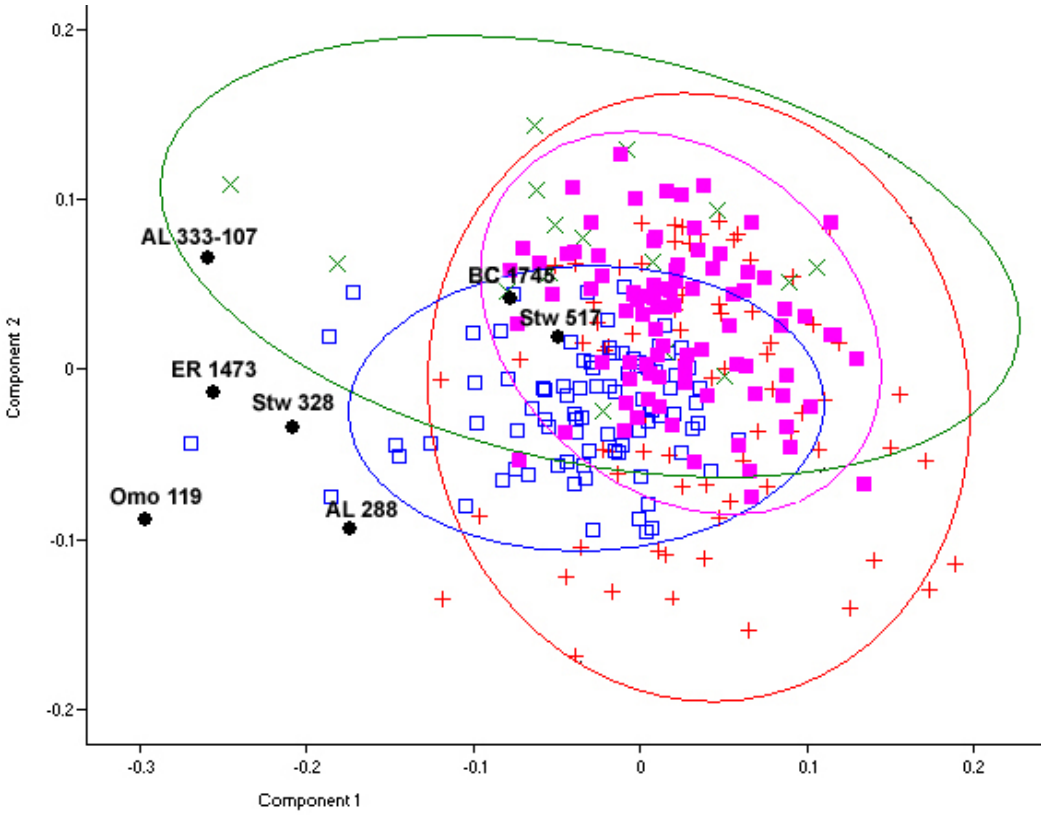

Fig 3.20 Principal components analysis of the proximal humerus utilizing landmarks 2 through 7. PC1 represents 28% of the overall variation and PC2 represents 17%. *Homo* is in blue open squares, *Pongo* is in green Xes, *Gorilla* is in red crosses, *Pan troglodytes* is in purple squares Each group is surrounded by a 95% equal frequency ellipse. Fossil specimens are labeled in the graph

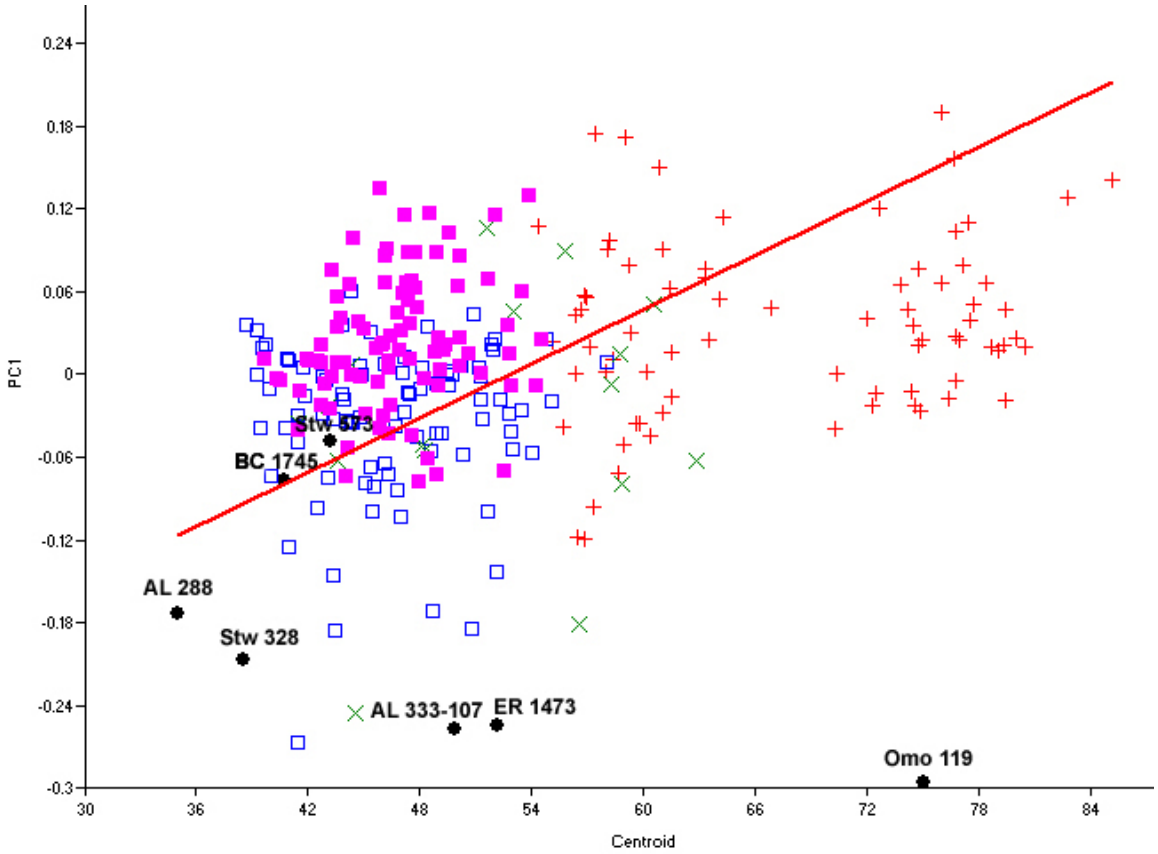

Fig 3.21 Centroid size regressed on principal component one for the proximal humerus. For this analysis, r = 0.27659.

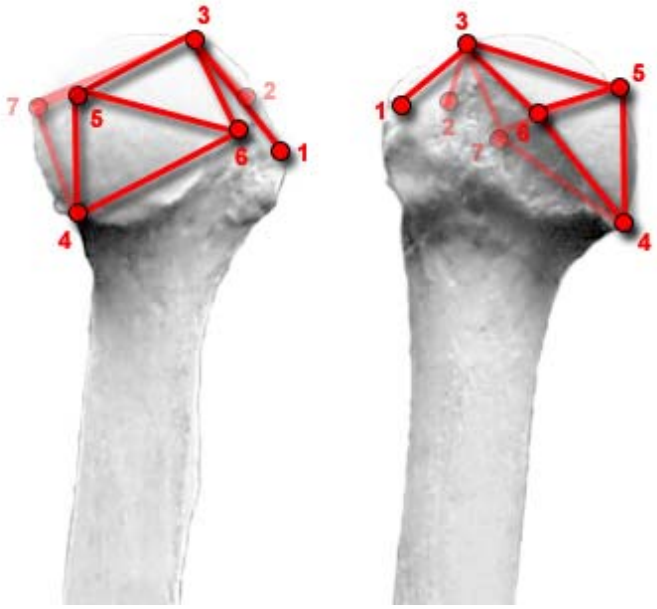

Fig. 3.22 Landmark configuration and wireframe for the proximal humerus. Transparent lines indicate points on the opposite side of the bone.

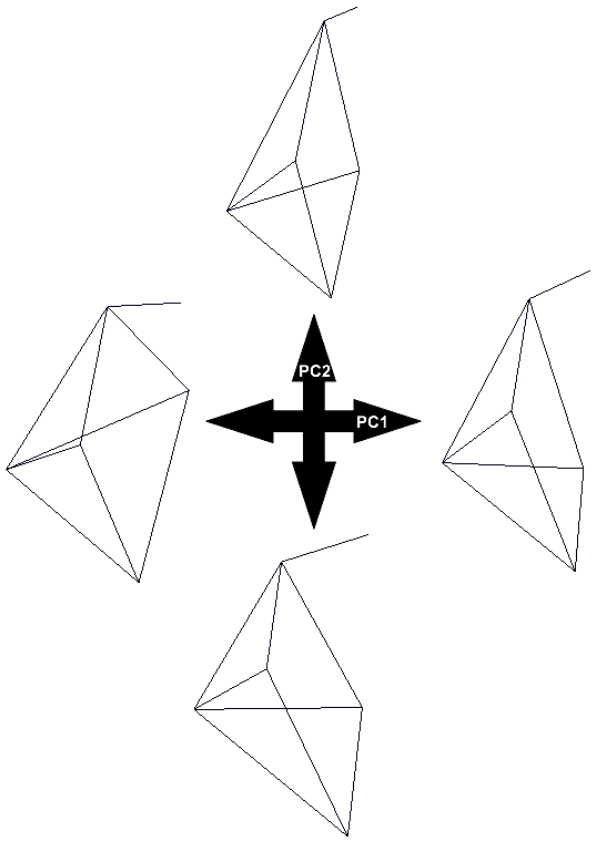

Fig 3.23 Wireframe transformation between individuals along PC1 and PC2 for the proximal humerus.

Means were calculated for each extant species and analyzed with the fossil individuals. A PCA with MST is shown in fig. 3.24 and neither PC is correlated with centroid size. PC 1 is driven by the distance between the edge of the articular surface of the humeral head and the most proximal point on the greater tubercle. Most of the fossils have a very short distance between these two points. PC 2 is driven by the height of the greater tubercle; in both BC 1745 and Stw 517, it is high in comparison to point 3, the place where the bicipital groove meets the articular surface of the humeral head.

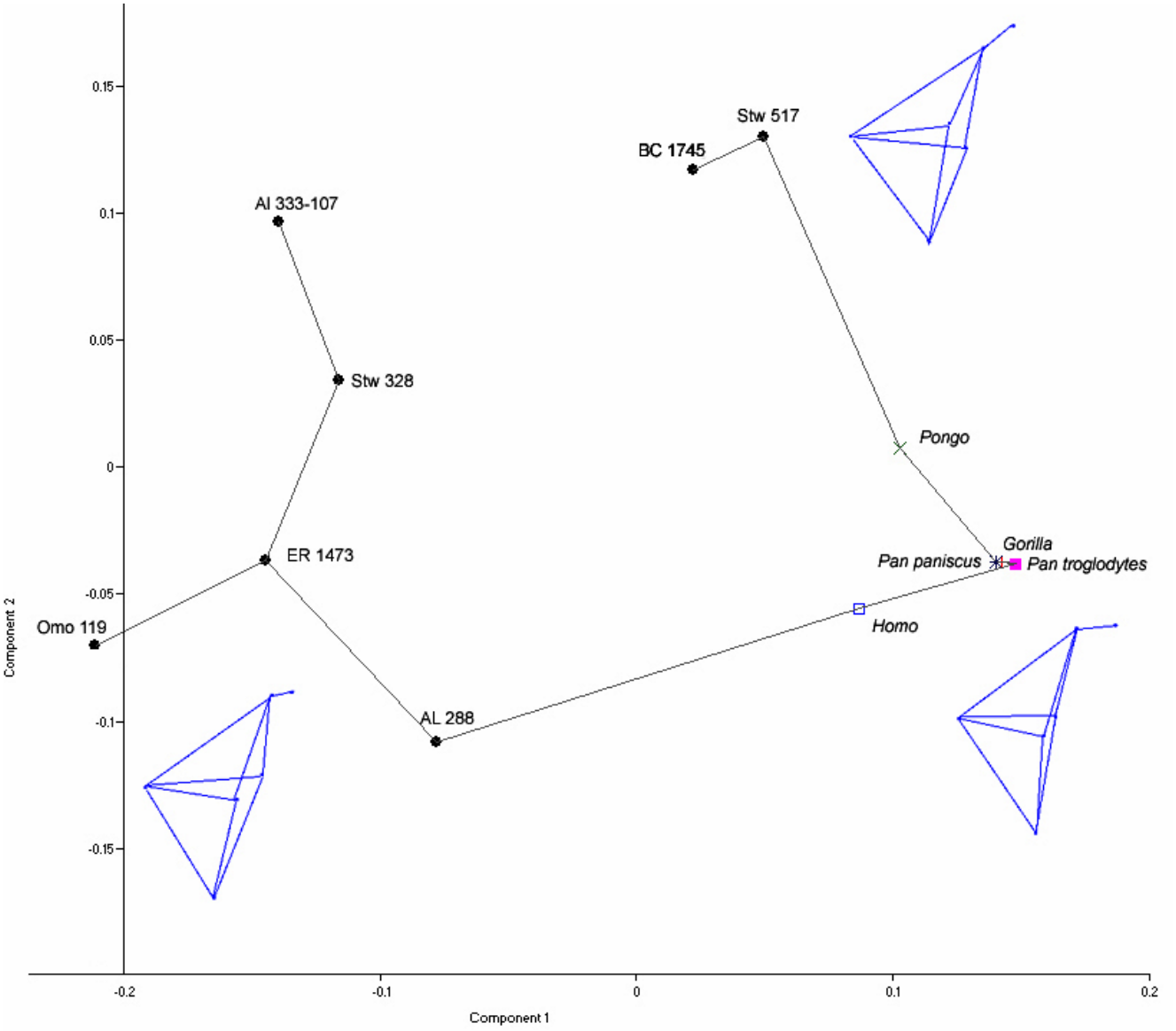

Fig 3.24 PCA using the means for the extant taxa and a MST plotted on top for the proximal humerus. PC 1 represents 55% and PC 2 represents 20% of the overall variance. The wireframes are from a posterior view.

A neighbor joining tree is shown in fig 3.25. Both the cluster analysis and the PCA indicate a cluster of the extant species and a cluster with most of the fossils. Among the fossils, BC 1745 and Stw 517 are more similar to each other than they are to the other fossils in this sample and the division between these two fossils and the rest of fossils is well supported. However, as *Pan troglodytes* and *Pan paniscus* are not sister taxa in this analysis, these results can not be interpreted conclusively.

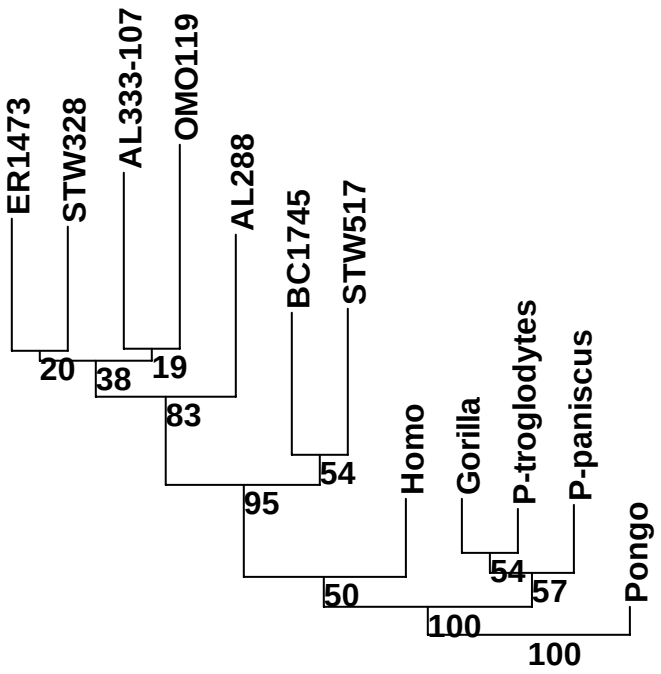

Fig 3.25 Neighbor joining tree based on Procrustes chord distances for the coordinate data on the proximal humerus. Means for each extant species were used. *Pongo* was specified as the outgroup. Bootstrap values are after 5000 replicates.

Proximal Humerus Analysis

In general, the functional and/or phylogenetic signals in this data set seem to be at least partially obscured by intraobserver error in landmark collection. Certainly the PCA in fig. 3.20 is uninformative and driven by slight variation in the placement of the landmarks around the humeral head. There are likely real differences between these specimens, but there are not enough points reliably taken to capture those differences. In the future, perhaps laser surface scanning and using denser patches of points might yield better and more consistent results.

The results of the PCA/MST and neighbor-joining tree are slightly more positive (figs. 3.24-3.25). The strongest result is the affinity between BC 1735 (possible *A. anamensis;* Wood, 1999) and Stw 573. They are similar in that they have a high greater tubercle in relation to the height of the humeral head. A high greater tubercle would limit motion in overhead positions

and is unique in comparison to the extant hominoids and is more like the cercopithecids (Aiello and Dean, 1999). The functional benefit of such a change is unclear.

Radius

Complete Radius Results

Figure 3.26 shows the results of a principal components analysis of the entire radius for the extant sample. There is good separation between all extant species. PC 1 is driven mostly by the position of the radial tuberosity on the radial shaft, as well as the size of the joints in comparison to the length of the shaft. *Homo* and *Pongo* have small joints in comparison to the length of the radial shafts, whereas *Gorilla* has large joints. *Pan* is intermediate. *Homo* and *Pongo* have radial tuberosities that are very close to the radial head, whereas *Gorilla* has the most distally located radial tuberosities. PC 1 is correlated with centroid size, though *Pongo* plots away from the regression line (see Fig. 3.27). PC 2 is driven by the angulation of the distal articular surface with respect to the long axis of the bone. In *Pongo,* it is tilted at more than a 90 degree angle, whereas in *Homo* the angle is closest to 90 degrees. Figure 3.28 shows a wireframe transformation between the extant taxa.

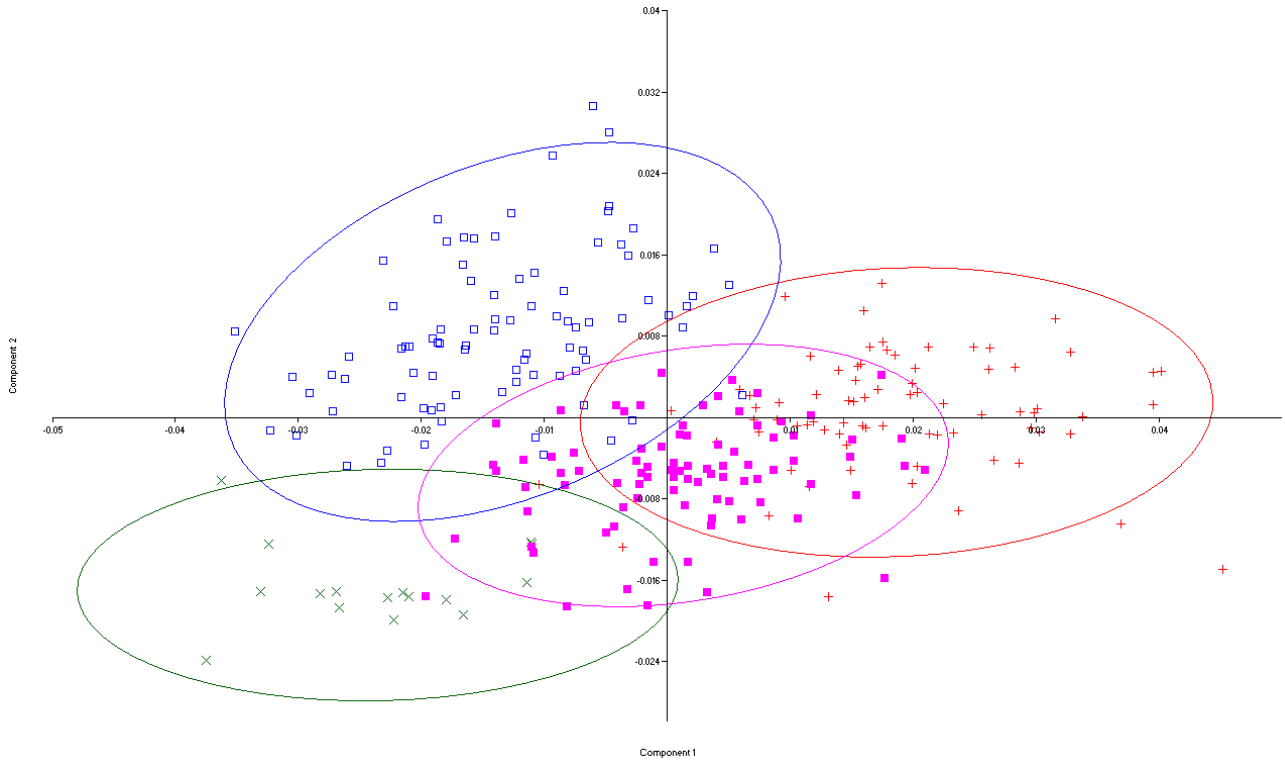

Fig. 3.26 PCA of the extant sample for the full radius. PC1 represents 40.3% of the variance and PC 2 represents 12.6% of the variance. *Homo* is represented by blue open squares, *Pongo* by green Xes, *Gorilla* by red crosses, and *Pan troglodytes* by purple squares. Each group is surrounded by a 95% equal frequency ellipse.

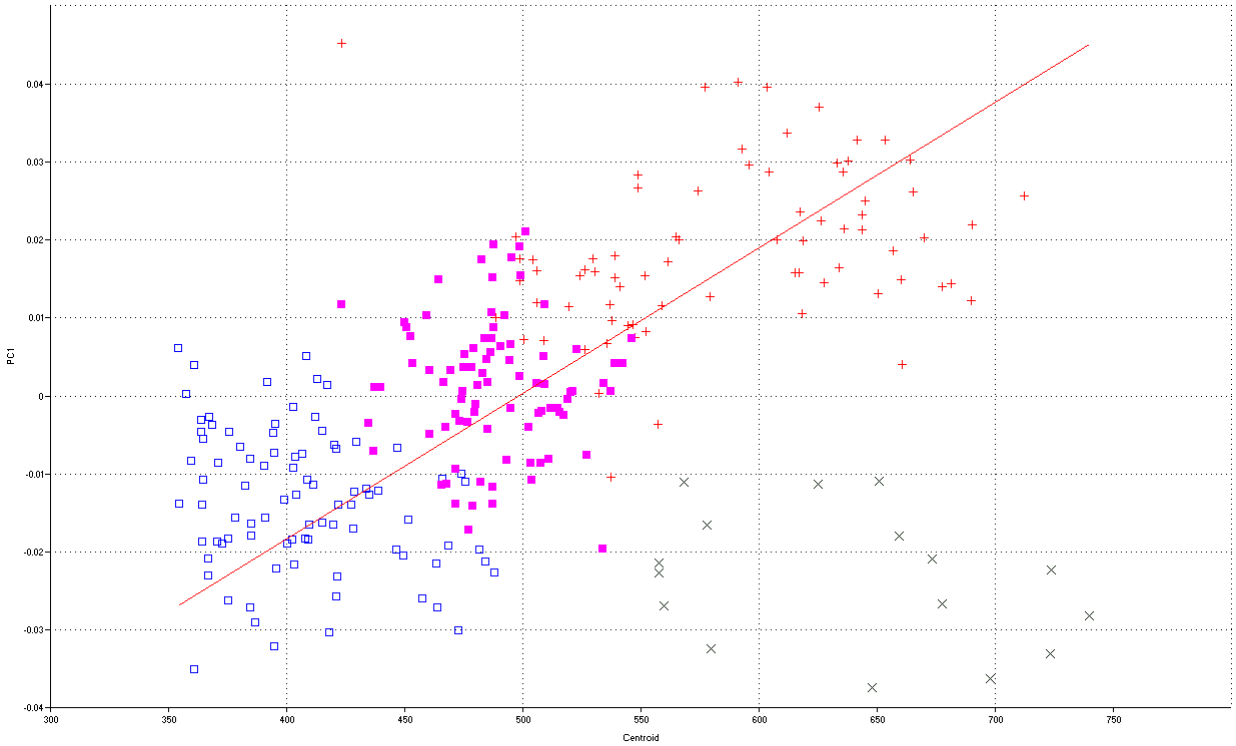

Fig 3.27 Centroid size regressed on PC 1 for the complete radius with all extant individuals. *Homo* is shown blue, *Pongo* in green, *Gorilla* in red and *Pan* in purple. In this analysis r=0.448.

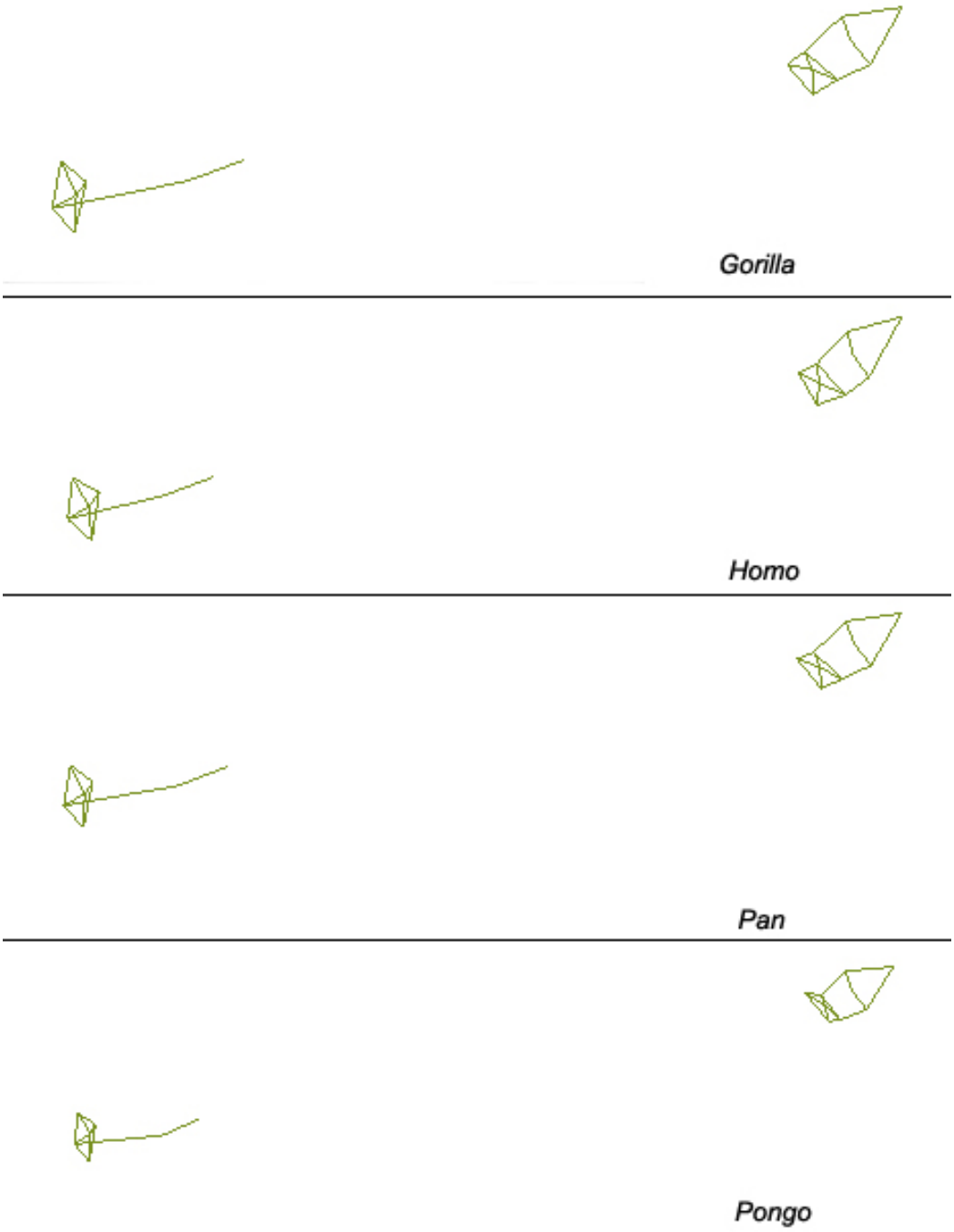

Fig 3.28 This lateral/posterior view of a wireframe transformation between the hominoid taxa from the complete radius, landmarks 1 through 18.

Complete radius discussion and analysis

The joint size and position of the radial tuberosity seem to simply scale with body size, except in the case of *Pongo*. For *Gorilla, Pan* and *Homo,* the larger the body size, the larger the joint. This pattern is distorted in *Pongo*, due to the elongated nature of their forearms for use in more suspensory behaviors. The radial tuberosity is the insertion point of the biceps brachii and the more distally placed it is, the longer the lever arm (Rose, 1993). *Pongo* has a shorter radial neck and more proximally placed radial tuberosity in comparison to body size because of the way that the biceps brachii works during supination of the forearm (Aiello and Dean, 1990).

Proximal Radius Results

The proximal radius consists of 7 landmarks covering the radial head and tuberosity. Figure 3.29 is a PCA of the proximal radius. There is no clear separation between any of the extant taxa. The modern humans tend to fall further to the right on PC 1 and *Pan* falls more to the left, but the area of overlap is enormous. The fossils fall almost randomly. AL 333x-33 plots on the human side of the graph just outside of the 95% equal frequency ellipse. AL 288 plots more toward the *Pan* side just inside the 95% equal frequency ellipse. ER 3736 and SKX 2045 are outside of the range of human variation, but within the range of ape variation. ER 3735, Omo 75-S75-1317, ER 1500 and Omo 75-S70-1317 all fall outside the range of any modern variation. All of the other fossils plot within the area of overlap of all extant taxa. PC 1 is driven by the size of the radial head in comparison to the length of the neck. Individuals that fall on the left side of the graph have smaller heads and longer necks with radial tuberosities that are less robust. PC 2 is driven by the size of the radial tuberosity. Individuals at the bottom of the graph have long tuberosities and those at the top of the graph have short tuberosities. PC 1 is correlated with centroid size.

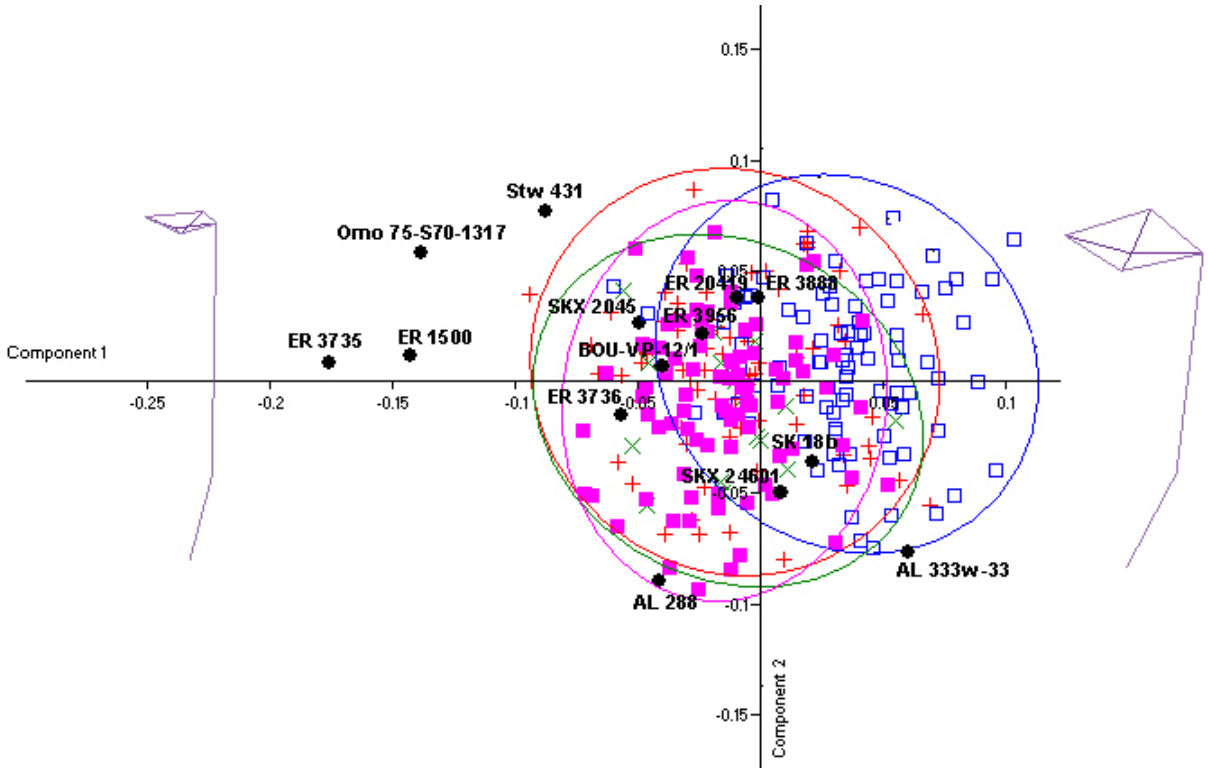

3.29 PCA of the proximal radius, landmarks 1-8. PC1 is 28% of the total variance and PC2 is 20%. *Homo* is represented by blue open squares, *Pongo* by green Xes, *Gorilla* by red crosses, and *Pan troglodytes* by purple squares Each group is surrounded by a 95% equal frequency ellipse. Fossils are in black and labeled.

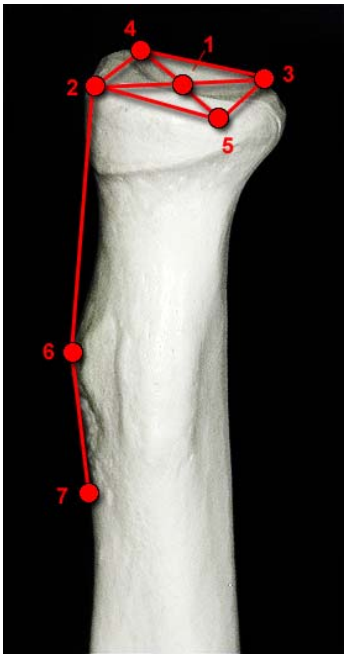

3.30 Landmarks and wireframe of the complete proximal radius.

Means were calculated for each of the extant species and a PCA was run with those means and the fossil individuals. A MST was plotted on some of the principal components results and the results of that analysis are presented in figure 3.31. The pattern is similar to what is seen with the analysis of the entire sample. PC 1 separates ER 1500, Omo 75-S75-1317 and ER 3735 from the rest of the sample and the cluster analysis indicates that these individuals are also nearest to each other in

shape space. PC 2 separates SKX 2045 and AL 333w-33 from the rest of the sample. PC 1 is driven by size of the radial head and the radial tuberosity, with Omo 75-S75-1317, ER 1500 and ER 3735 having the smallest radial heads and the smallest, most distally located radial tuberosities. PC 2 is driven by the depth of the radial head, with SKX 2045 having the deepest head and AL 333w-33 having the shallowest. PC 1 is not correlated with centroid size.

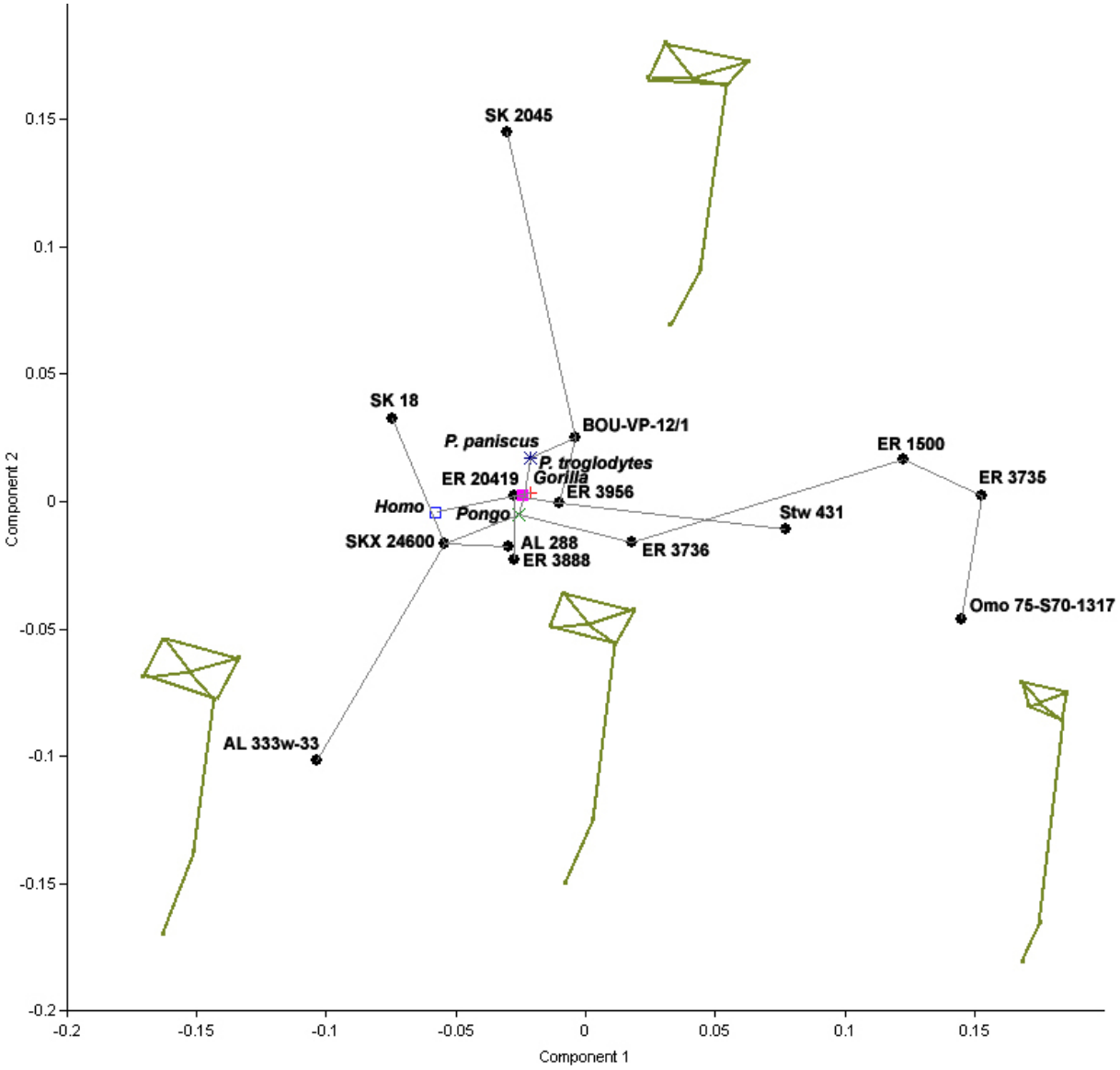

Fig. 3.31 MST and PCA for the means for the proximal radius. PC1 accounts for 45% of the variance and PC2 accounts for 21% of the total variance. All individuals are labeled in the graph. Wireframe transformations are oriented in a superiomedial view.

Finally, a neighbor-joining tree was generated using procrustes chord distances. (fig 3.32). The first relatively well supported cluster consists of: Omo 75-S70-1317, ER 3735, ER 1500, Stw 431 and ER 3736, most of which were also linked together in the previous MST/PCA analysis. ER 20419, ER 3888 and ER 3956 also form a cluster with ER 20419 and ER 3888 as well supported sister taxa. BOU-VP-12/1 is the outgroup to both of these cluster, although that is not well supported. The cluster containing *Homo* also contained SK 18, SK 2045, AL 288, AL 333w-33 and SKX 24601, although there are no really strong bootstrap values in that group. The apes fall outside all of the fossil containing clusters.

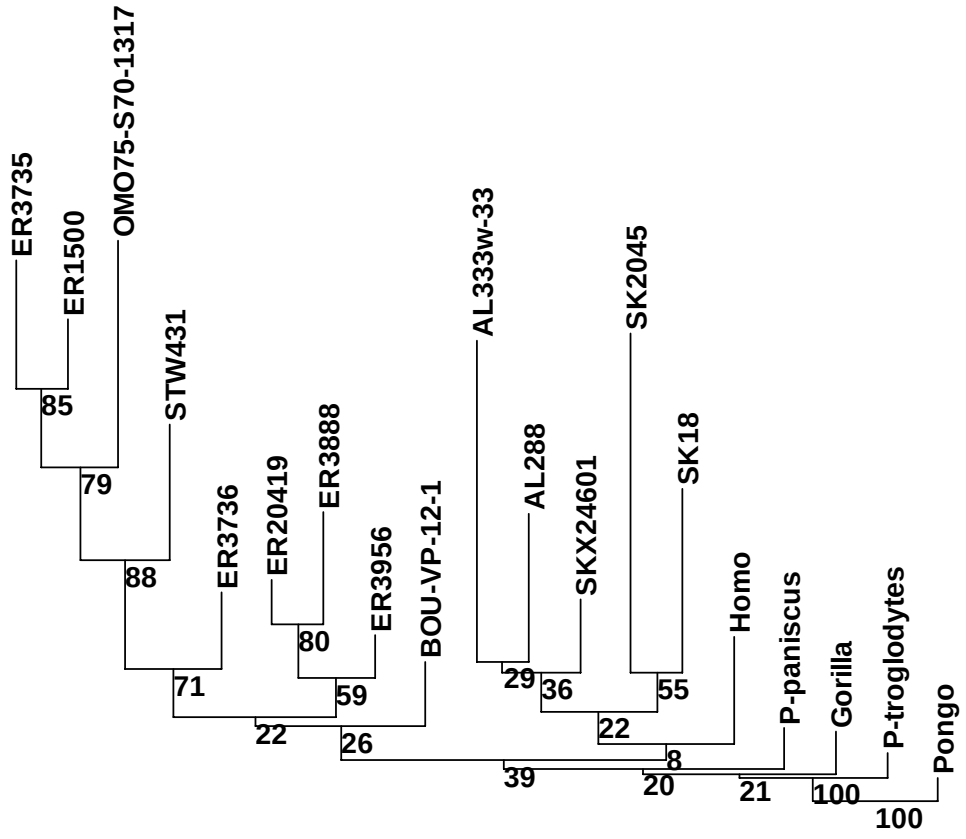

Fig. 3.32 Neighbor-joining tree for the proximal radius using the fossil data with the means for the extant individuals. Procrustes chord distances were used to form this tree and it was rooted with *Pongo* as the outgroup as indicated by the molecular data. Bootstrap values are after 5000 replicates.

Proximal Radius Discussion and Analysis

With the exception of fossil descriptions, proximal radii have been largely ignored in studies of fossil postcrania. However, the proximal radius is important in thinking about the functional complex of the elbow, particularly in terms of stability. The proximal radius is beveled in all hominoids in order to contact with the zona conoidea of the humerus for stability. Specifically in *Gorilla* and *Pan,* the proximal head is somewhat asymmetrical with the fovea being placed off to the side which also serves to increase stability (Rose, 1993).

In the following studies, decisions about morphological affinities were made based on phenetic similarity with few measurements and few fossils for comparison. In the description of ER 20419, Heinrich *et al (*1993) suggested that *A. anamensis* had a human-like radial neck thickness combined with a long radial neck for powerful flexion, which gives the lever advantage to the biceps brachii (Rose, 1993). Susman *et al.* (2001) attributed SKX 2045 to *Homo* cf. *erectus* and suggest that SKX 2045 has a human-like radial tuberosity and radial neck size, and its morphology is divergent from Stw 431 and SKX 3699. Grine and Susman (1991) placed Sk 18b as *Homo erectus* based on a lack of an articular surface for the zona conoidea. In their comparative analysis, they suggested that ER 3735 and 3736 are modern human-like. That idea was supported by Leakey *et al.* (1989), who attributed both ER 3735 and ER 3736 to *Homo habilis.* Leakey and Walker (1985) placed ER 3888 as a hominid and Howells and Coppens (1974) placed Omo 75s-1317 as a hominid, but Senut (1981) excluded ER 3888 and Omo 75S-1317 from her analyses based on her belief that those specimens are monkeys.

Patel (2005) conducted a thorough comparative analysis of the proximal radius including all extant hominoids, including *Hylobates,* using a series of linear measurements. He included casts of ER 20419, AL 288-1p, Stw 139, Stw 431, ER 1500e, SKX 3699 and SK 18b. In his

analysis, the morphology of the African apes was indistinguishable from the morphology of Hylobatids; thus, he concluded that the proximal radius was of limited functional and phylogenetic use.

The results of this study on the proximal radius are weakly significant. In general, there is less variation in the proximal radius within and between groups; however, the fossils still have the greatest variation in procrustes chord distances, far outstripping the variation between pairs of extant genera (fig 3.33). The separation of the extant genera in the PCA was poor and this is likely due to intraobserver error in collecting landmarks around the radial head. The proximal radius has only type II and type III landmarks, which are more difficult to collect accurately (Bookstein, 1991). However, the cluster analysis shows a more interesting result.

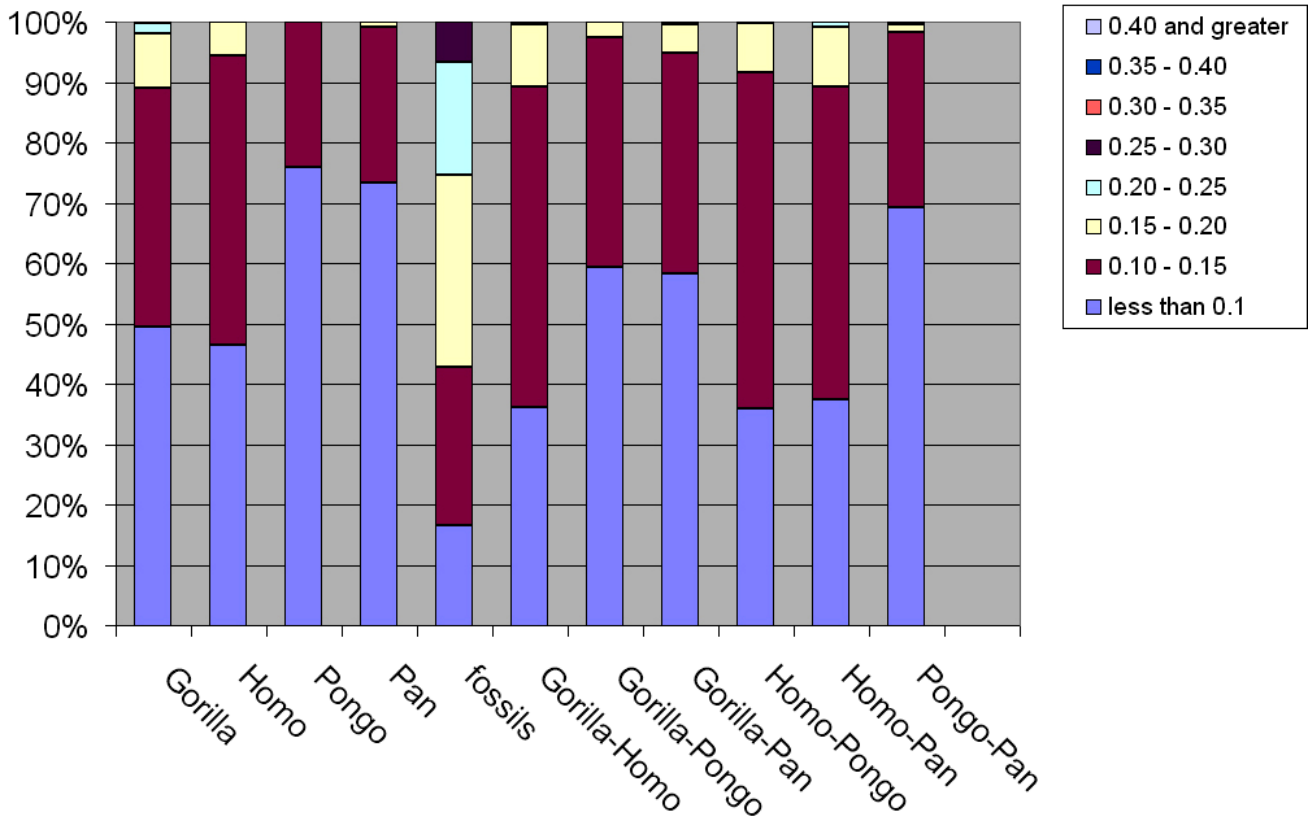

Fig 3.33 This bar graph is a representation of the distribution of procrustes chord distances within and between the different genera in the sample of proximal radii. The array of procrustes distances were segmented into units of 0.05. The group of fossils has the highest average procrustes distance (0.16).

Based on the cluster analysis, the fossils can be split into two groups. The first group has *Homo* as a sister taxon and contains: AL 288, AL 333w-33, SK 18b, SKX 2045, and SKX 24601. The inclusion of SKX 24601 in this group that is closer to modern humans further supports the idea that it belongs in the genus *Homo* and not *Paranthropus,* as suggested by Susman *et al* (2001). SKX 2045 and SK18b are both attributed to *Homo erectus* and AL 288 and AL 333w-33 are attributed to *Australopithecus afarensis.*

The second group contains: BOU-VP-12/1, ER 1500e (*P. boisei)*, ER 3735 *(H. habilis sensu lato)*, ER 3956, ER 3888, ER 3736, ER 20419 *(A. anamensis)*, Omo 75S-1317, and Stw 431 *(A. africanus)*. The fact that ER 3888 and Omo 75S-1317 cluster with the rest of the specimens argues against the idea that they are monkeys. Within this group ER 3735, ER 1500 and Omo 75S-1317 form a cohesive cluster characterized by a relatively smaller radial head and a more distally located radial tuberosity. This would indicate that this group had a longer lever arm for the biceps brachii and would have had stronger ability for flexion coupled with a less stable humero-radial joint (Rose, 1993). In some ways, this pattern is quite *Pongo*-like (although *Pongo* has a relatively larger radial head than these fossils) and may have been beneficial in activities requiring pulling up the body weight such as climbing. However, the significance of all of this should not be overstated as a canonical variates analysis fails to discriminate well between any of the extant groups or the fossils (fig 3.34).

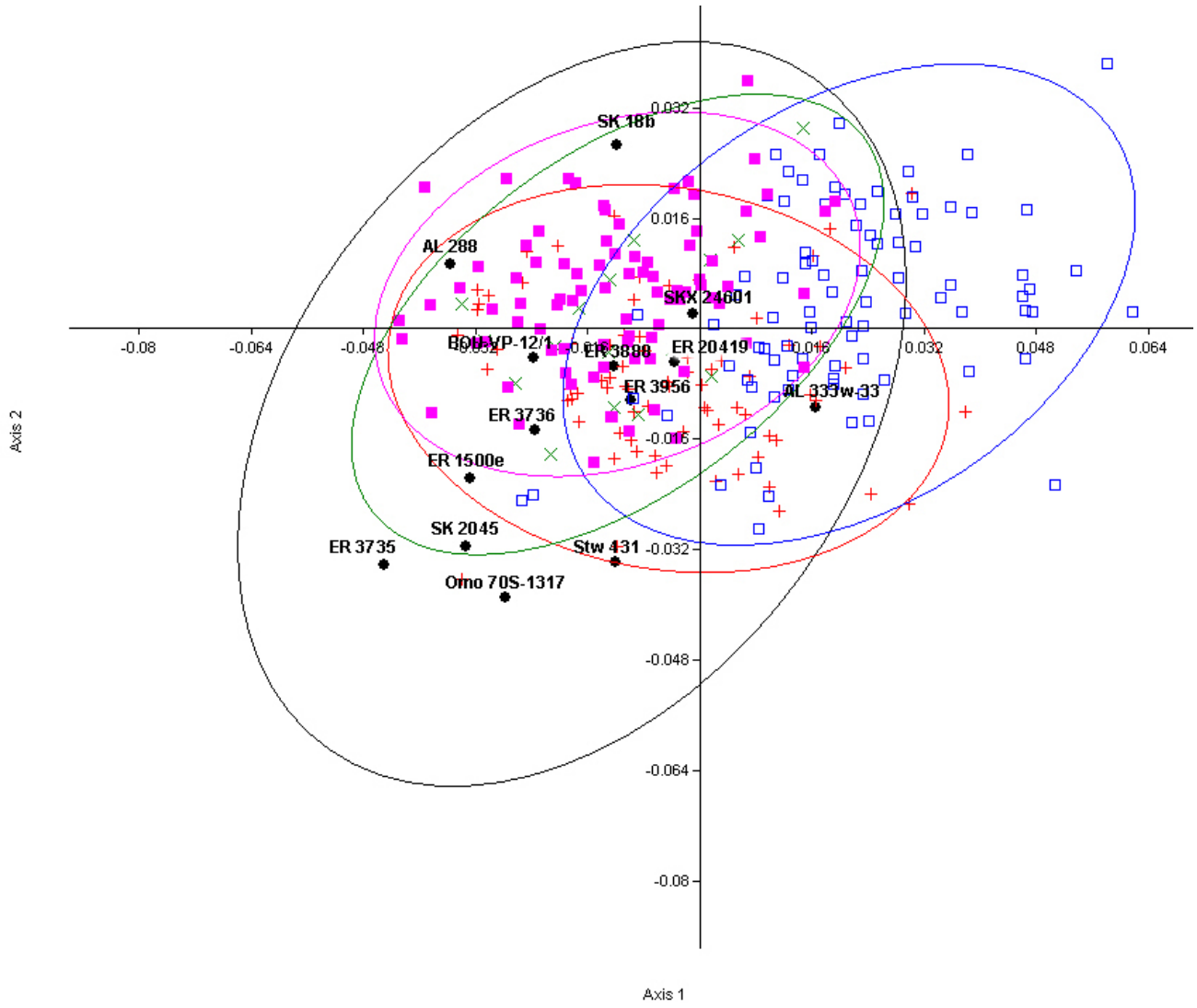

Fig. 3.34 Canonical variates analysis of the extant taxa and fossils for the proximal radius. It fails to separate the extant groups well. Axis 1 is 67.95% of the total variance and axis 2 is 17.5% of the total variance. Fossils were designated as a separate group, and are labeled in the group. *Homo* is represented by blue open squares, *Pongo* by green Xes, *Gorilla* by red crosses, and *Pan troglodytes* by purple squares. Each group is surrounded by a 95% equal frequency ellipse.

Distal Radius Results

The distal radius consists of 9 points covering the distal articular surface and the ulnar notch. Figure 3.35 illustrates a PCA of the distal radius for all extant individuals and fossils where the distal articular surface is preserved. All landmarks on the distal radius (points 8 through 16; see fig. 3.36) were used. PC 1 is driven by the width of the proximal border of the

radioulnar articulation, as well as the overall size of that articulation. Individuals with negative values on PC1 have a wide proximal border and a short articulation and individuals with positive values have a narrow proximal border and long articulations. PC1 is not correlated with centroid size, and does not divide the sample in any meaningful way. PC 2 differentiates modern humans from extant apes although the extant apes are not differentiated in any further meaningful way. PC2 is mainly driven by the depth of the scapho-lunate facet – it is wider and deeper in chimpanzees, gorillas and orangutans (fig. 3.37). The ulnar notch is also relatively larger in the extant apes. There are four fossil distal radii in this sample: AL 288, ER 20419, SKX 3602 and Stw 46. ER 20419 (*A. anamensis*) and AL 288 ("Lucy", *A. afarensis*) fall within the ape distribution. Stw 46 (*A. africanus*) and SKX 3602 (*P. robustus*) fall within the modern human distribution. Unlike PC 1, PC 2 is correlated with centroid size, although ER 20419 plots far off of the regression line indicating that it has human-like centroid size with a more chimpanzee-like shape (fig. 3.38).

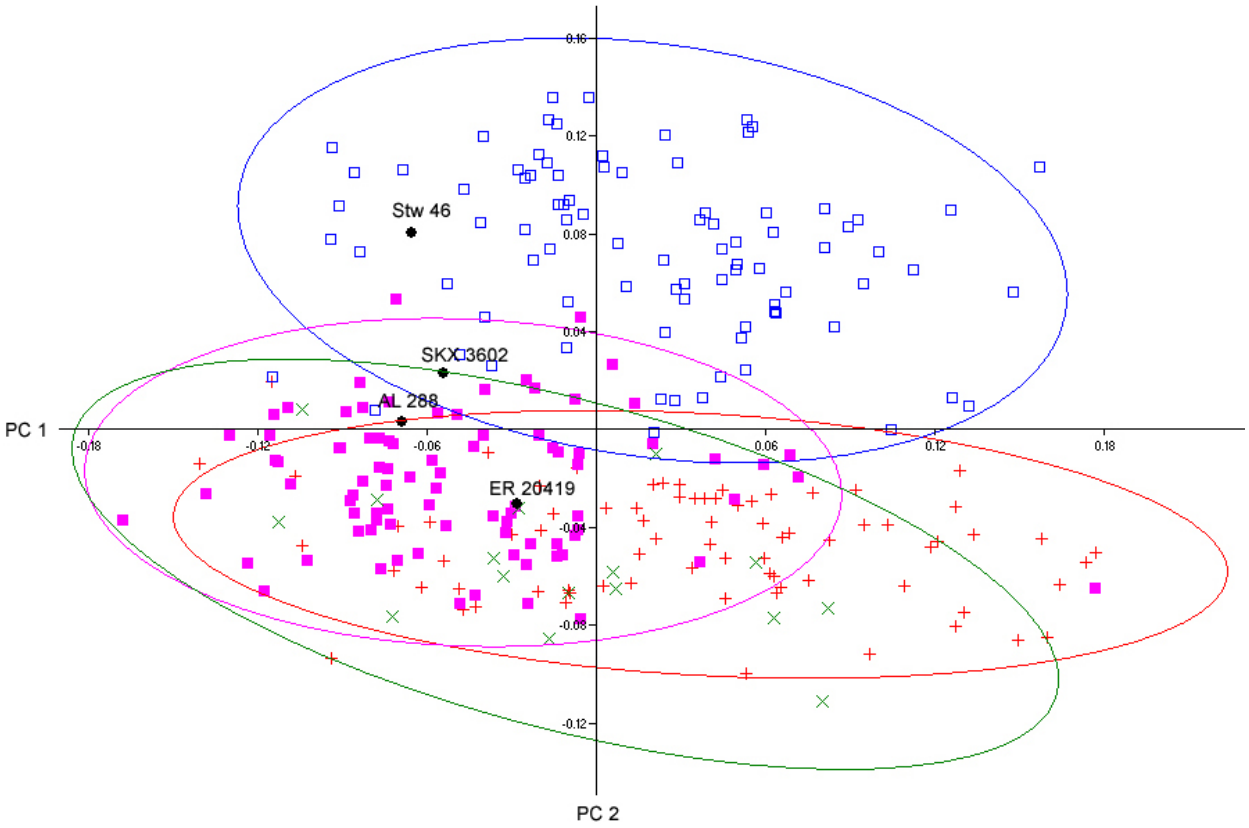

Fig 3.35 PCA of the distal radius (landmarks 8-16) including fossil specimens. PC1 is 21.9% and PC2 is 15.2% of the total variance. *Homo* is represented by blue open squares, *Pongo* by green Xes, *Gorilla* by red crosses, and *Pan troglodytes* by purple squares. Each group is surrounded by a 95% equal frequency ellipse. Fossils are labeled in the graph.

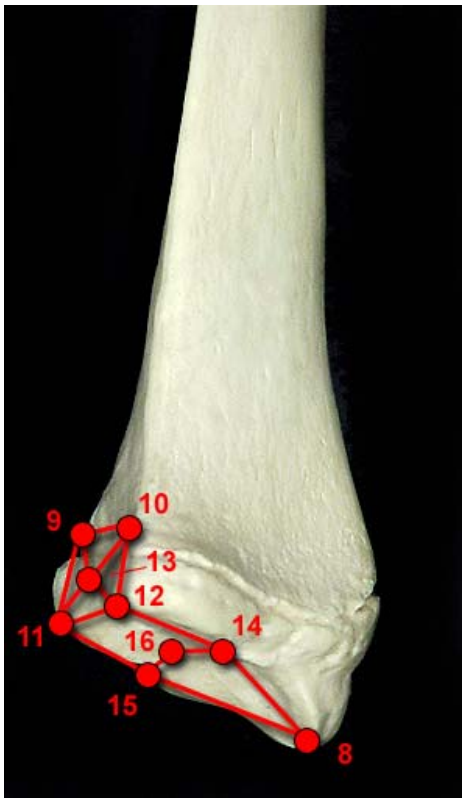

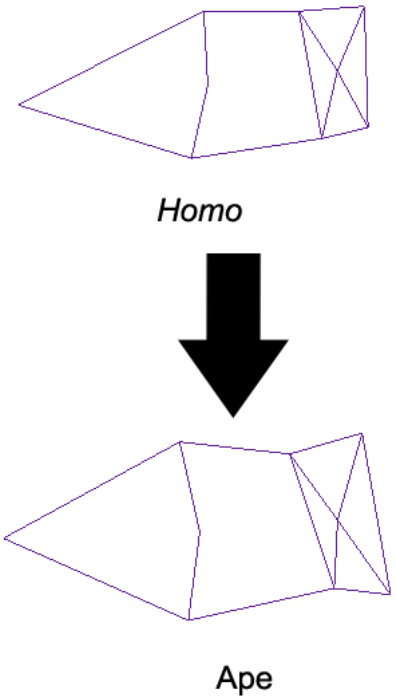

Fig. 3.36 (left) Landmarks and wireframe on the distal radius.

Fig. 3.37 (right) Wireframe transition between *Homo* and the extant apes along PC 2 for the distal radius. The view is looking down into the distal articulation of the radius.

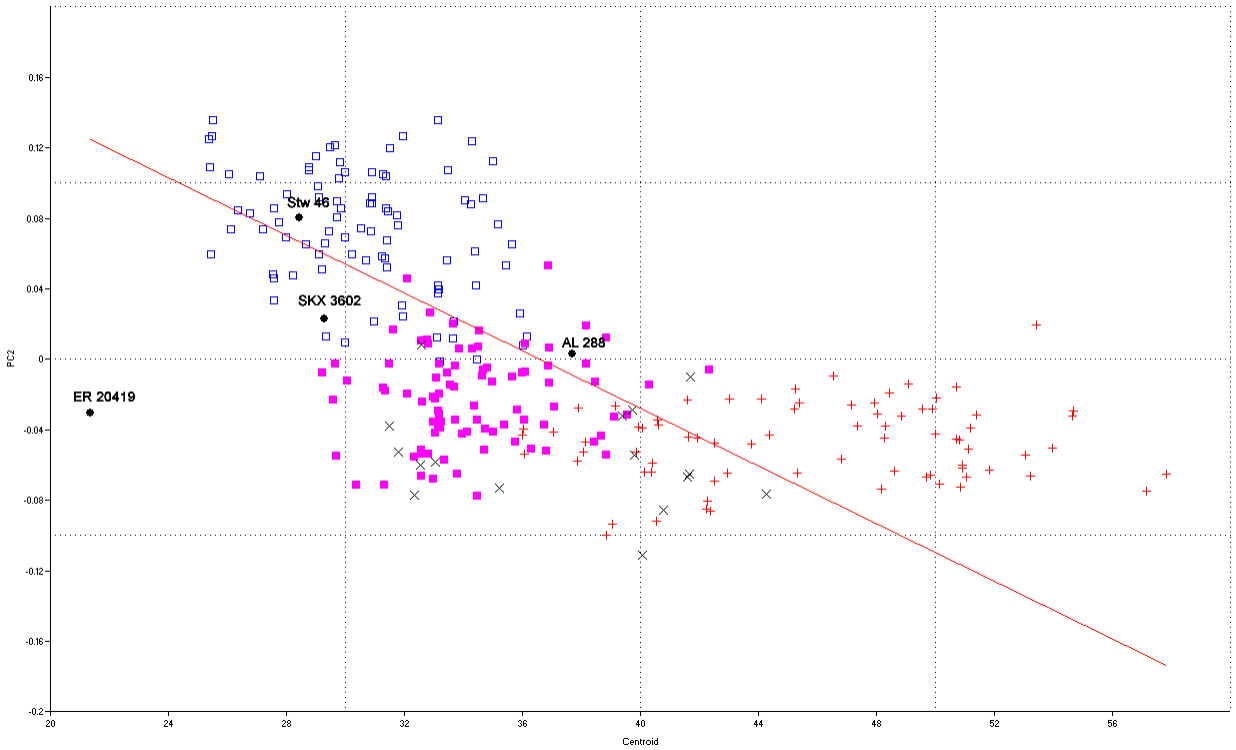

Fig 3.38 Linear regression of principal component 2 on centroid size for the distal radius. In this analysis, r = -0.600. *Homo* is represented by blue open squares, *Pongo* by green Xes, *Gorilla* by red crosses, and *Pan troglodytes* by purple squares.

Means were calculated for each species and additional analyses were run using these means and the fossil individuals. The results of a principal components analysis and minimum spanning tree are presented in Fig. 3.39. This analysis further supports the analysis of the entire sample previously presented. PC 1 separates *Pongo, Gorilla* and *Pan troglodytes* at one extreme from Stw 46 at the other extreme. PC 2 separates ER 20419 and AL 288 at one extreme from the rest of the sample. The MST shows that three of the four fossils are nearest in shape space to *Pan paniscus* and only Stw 46 is nearest to *Homo.* Overall, this pattern is consistent with the one seen in the previous analysis. Neither component is correlated with centroid size.

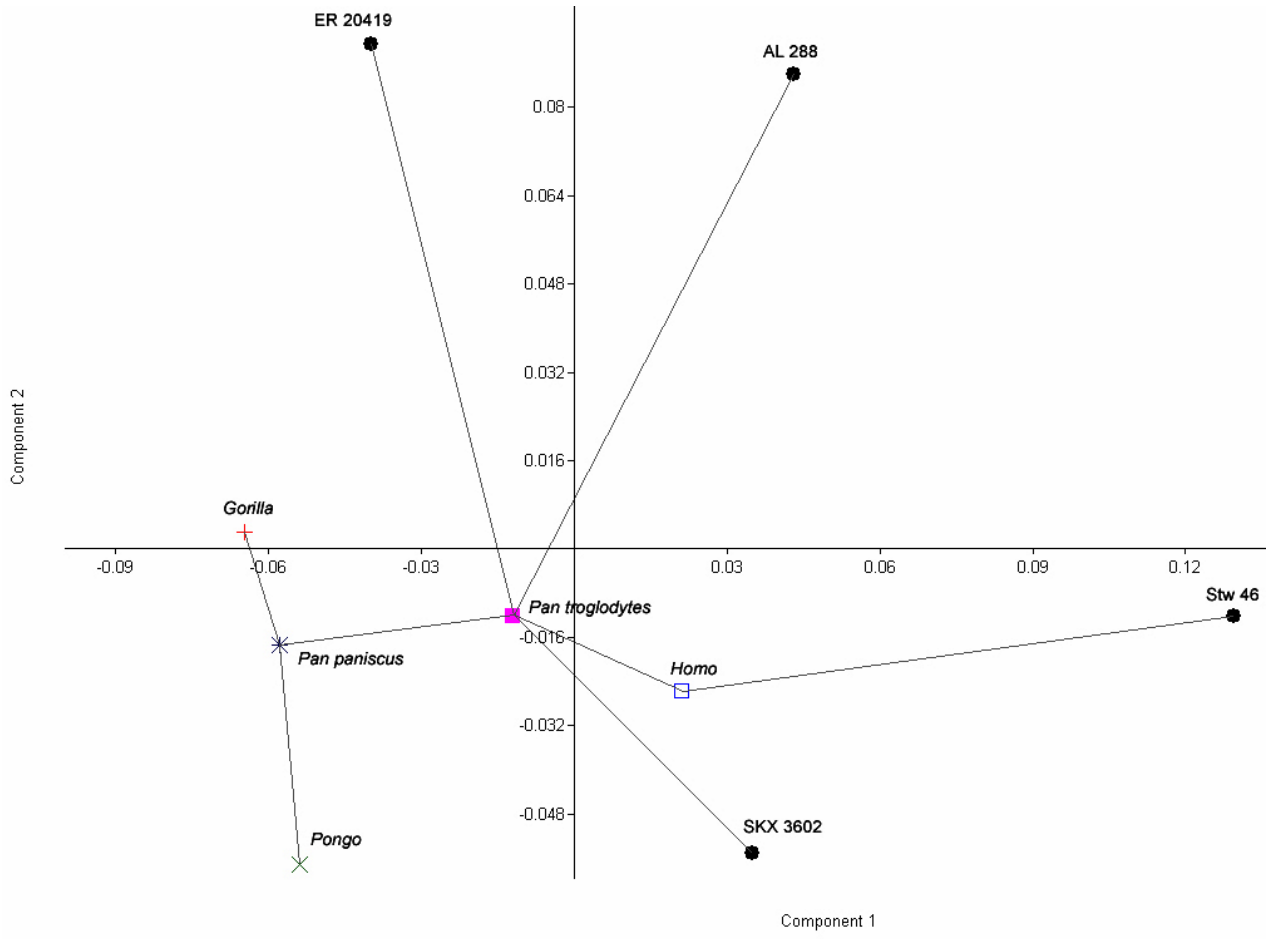

Fig 3.39 Means were calculated for each species and a minimum spanning tree was plotted on top of the principal component graph for the distal radius. PC 1 represents 38.3% of the total variance and PC 2 represents 23.1% of the total variance.

A neighbor-joining tree was also generated (fig. 3.40). None of the clusters are well supported, but in general SKX 3602, Stw 46 and AL 288 are nearer to *Homo* whereas ER 20419 is nearer to the apes. The position of ER 20419 has better support than most of the other branch positions.

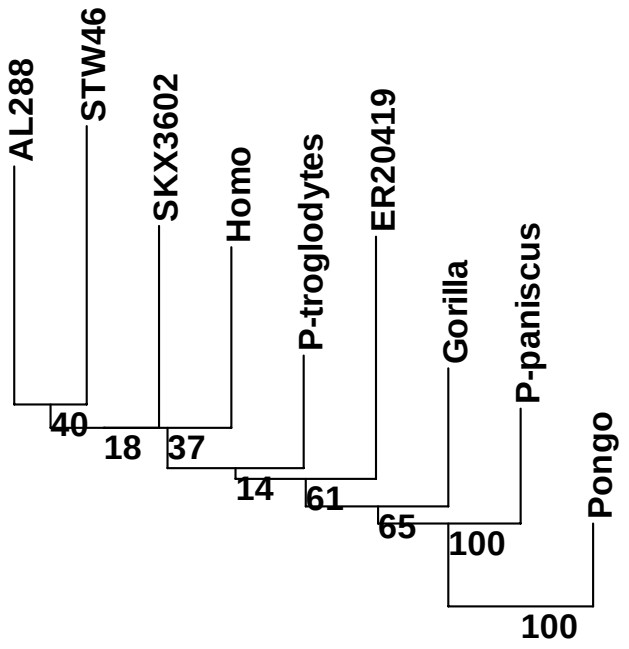

Fig. 3.40 Neighbor-joining tree for the distal radius, using the fossil data with the means for the extant individuals. Procrustes chord distances were used to form this tree and it was rooted with *Pongo* as the outgroup. Bootstrap values are after 5000 replicates.

A CVA was also performed in order to maximize the difference between the extant groups in order to see if any of the fossils were particularly similar to one of the extant apes (fig. 3.42) Stw 46 again fell within the range of modern humans, whereas ER 20419 fell within the range of overlap between chimpanzees and gorillas. AL 288 and SKX 3602 fell in a similar place, with SKX 3602 just within the range of human and chimpanzee variation and AL 288 just outside the range of human variation, but within the chimpanzee distribution.

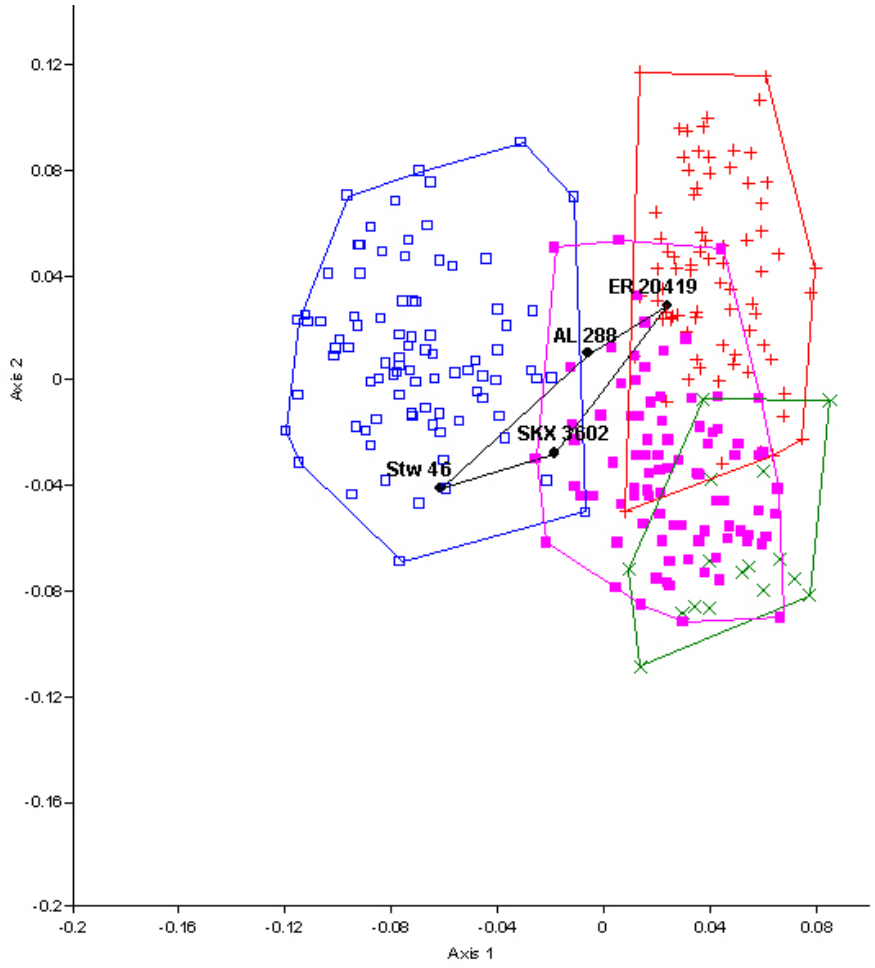

Fig 3.41 A CVA of the distal radius. The fossils were designated as a group *a priori*. *Homo* are represented by blue squares, *Pan* by purple squares, *Pongo* by green Xs, and *Gorilla* by red pluses. Axis 1 is 75% of the variation and Axis 2 is 16% of the total variation in the sample. Solid lines represent convex hulls drawn around each group.

Finally, wireframes were generated for all of the fossils and the pairwise comparisons between them are illustrated in figure 3.41. AL 288 and SKX 3602 (middle, left) are the most similar, with the major shape difference between them being that SKX 3602 has a higher proximal margin for the ulnar notch. Stw 46 and ER 20419 (top right) are the most different fossils with ER 20419 being narrower, having a more flexed distal articular surface and posteriorly rotated ulnar notch (see later text for a more complete discussions of these wireframes).

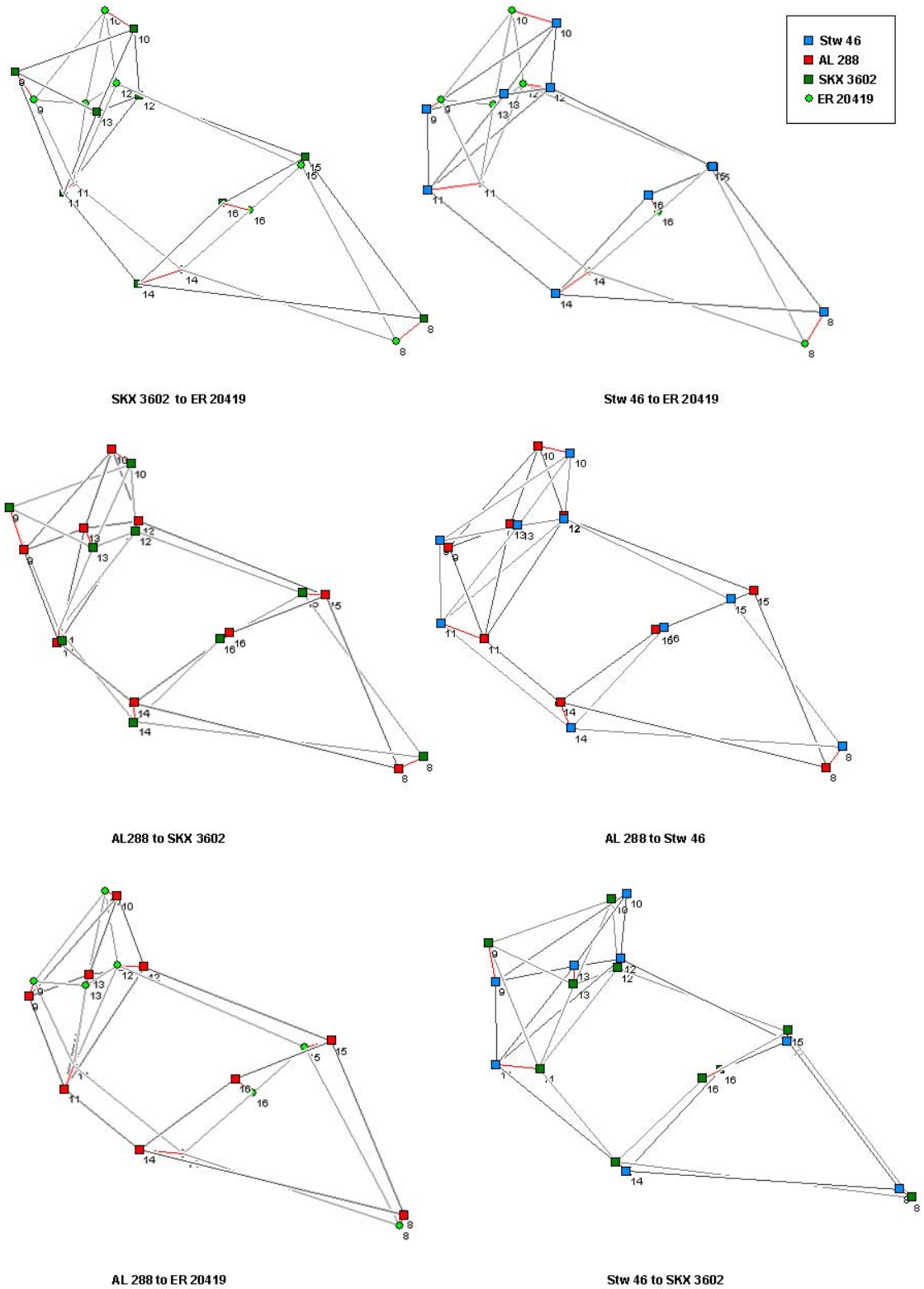

Fig 3.42 Wireframe transformations between all pairs of fossil distal radii Transformations were generated using *Morpheus* (Slice, 1998) and are in the same orientation in all images. The angle is looking into the distal articular facet with the ulnar facet on the left. The red lines are vectors indicating the direction of change for each landmark.

Distal radius discussion and analysis

There are only a few distal radii from the Plio-Pleistocene, but fortunately some have relatively secure taxonomic attributions. For this fossil sample, ER 20419 (*Australopithecus anamensis)* clearly has the most ape like distal radius. In every analysis, it falls closest to either *Pan* or *Gorilla.* This result is not at all based on the size of the specimen, as it is the only fossil that falls off of the regression line (fig 3.38); based on size, it should be consistently falling within the range of modern human variation. When ER 20419 is compared with the other three fossil radii in this sample (see fig 3.42), the ulnar notch is rotated slightly more posteriorly in comparison to the more *Homo*-like SKX 3602 and Stw 46. The distal articulation is flatter and narrower than all of the other fossils in this sample and is also more flexed than Stw 46 and SKX 3602. The lunate facet is larger in comparison to the scaphoid facet, whereas the other fossils have lunate and scaphoid facets of approximately the same size. Richmond *et al* (2001) associated a flexed distal articulation with knuckle-walking in that a tilted distal articulation would help to close-pack the carpals and increase stability. However, Heinrich *et al. (*1993) noted the large lunate facet present and suggested that this individual might have been a good quadrumanous climber, like *Pongo.* As an alternative hypothesis, the presence of both of these traits might indicate a wrist that has been adapted for a wide range of functional uses.

AL 288 (*Australopithecus afarensis,* "Lucy") also consistently falls within the distribution of the extant African apes in every analysis but the neighbor joining tree (fig. 3.40). It is most similar in shape to ER 20419, and differs from that fossil only in that it is wider and slightly flatter. The distal articulation is more flexed than SKX 3602 and Stw 46 and the ulnar notch is rotated posteriorly in comparison to those fossils (as also seen in ER 20419.) Again,

functionally this seems to indicate a wrist that was capable of a wide range of functional uses, including ones that would require greater stability (Richmond *et al.*, 2001).

SKX 3602 seems to be intermediate among all of the fossils. SKX 3602 was found in the Member 1, Lower Bank and has been attributed to *Paranthropus robustus* (Grine and Susman, 1991). In both analyses using the entire sample (fig. 3.33, fig 3.47), SKX 3602 falls in the area of overlap between *Homo* and the extant African apes. In the cluster analyses, SKX 3602 sometimes appears more like *Homo* (fig. 3.40) and sometimes appears more like *Pan* (fig. 3.39). Susman (2004) described SKX 3602 as human-like, although he made no taxonomic assertions at that time. These data support the idea that it is quite human-like. The only appreciable difference between it and the extremely *Homo*-like Stw 46 is the ulnar notch in that in SKX 3602, it is rotated more anteriorly than Stw 46.

Stw 46 consistently falls within the modern human distributions in all analyses. Stw 46 is attributed to *A. africanus,* which is often thought to have a more ape-like postcrania reflecting a retention of arboreal adaptations (McHenry and Berger, 1998; Haeusler, 2003) although these data disagree with that conclusion. Stw 46 has no appreciable differences from a modern human distal radius. There are no particular adaptations present for stability and thus it can be assumed that this individual's wrist could function in the same way as seen in modern humans.

Evidence from the distal radius has been used to argue that humans evolved from a knuckle-walking ancestor (Richmond and Strait, 2000; Richmond *et al.* 2001). These data lend weak support in that direction. In order to rule out any kind of suspensory, *Pongo*-like ancestor, the plotted distribution of *Pongo* and the knuckle-walking African apes should be separate and the oldest fossils should clearly fall within the African ape distribution. While the oldest fossils do fall within the African ape distribution becoming progressively more *Homo*-like through time,

Pongo is not sufficiently different to entirely rule out at least some degree of suspensory behavior in early hominins. In the PCA (fig 3.35), the distribution of *Pongo* entirely overlaps the distribution of *Pan* and *Gorilla.* Even in the CVA (fig 3.41)**,** *Pongo* and *Pan* overlap in their distributions, although the fossils do not fall in that area of overlap. From this, it is possible to conclude that the distal radius in isolation is not really that different between *Pongo* and the African apes despite the differences in locomotor patterns. What really seems to drive the differences between them is the angle of the distal surface in relation to the long axis of the bone (fig. 3.28)**.** Without information about the way that the proximal and distal end relate, it is impossible to entirely rule out a *Pongo*-like mode of locomotion for the last common ancestor of great apes and humans.

Ulna

Figure 3.43 shows the results of a PCA of the entire ulna for the extant individuals. While there is some overlap in the 95% equal frequency ellipses for each taxon, there is still very good separation.PC 1 separates *Gorilla* from *Pan* and *Homo.* There is substantial overlap between *Pan* and *Pongo* on PC 1 while PC 2 separates *Pongo* and *Homo* from the rest of the extant sample. PC 1 represents a change from a broad, semi-shallow trochlear notch in *Gorilla* to a narrow, more strongly keeled trochlear notch in *Homo* and *Pongo.* Additionally, the orientation of the olecranon process changes from being quite proximomedially projecting in *Gorilla* to being smaller and more proximally projecting without a medial or lateral bend. PC 2 is driven by the orientation of the trochlear notch; in *Pongo,* the entire notch is oriented more proximally. Both PC 1 and 2 are correlated with centroid size (figs 3.44 and 3.45). For PC 1,

Pongo falls off of the regression line and for PC 2, *Gorilla* falls off of the line. Figure 3.46 illustrates the wireframe transformation between all of the extant taxa for the entire ulna.

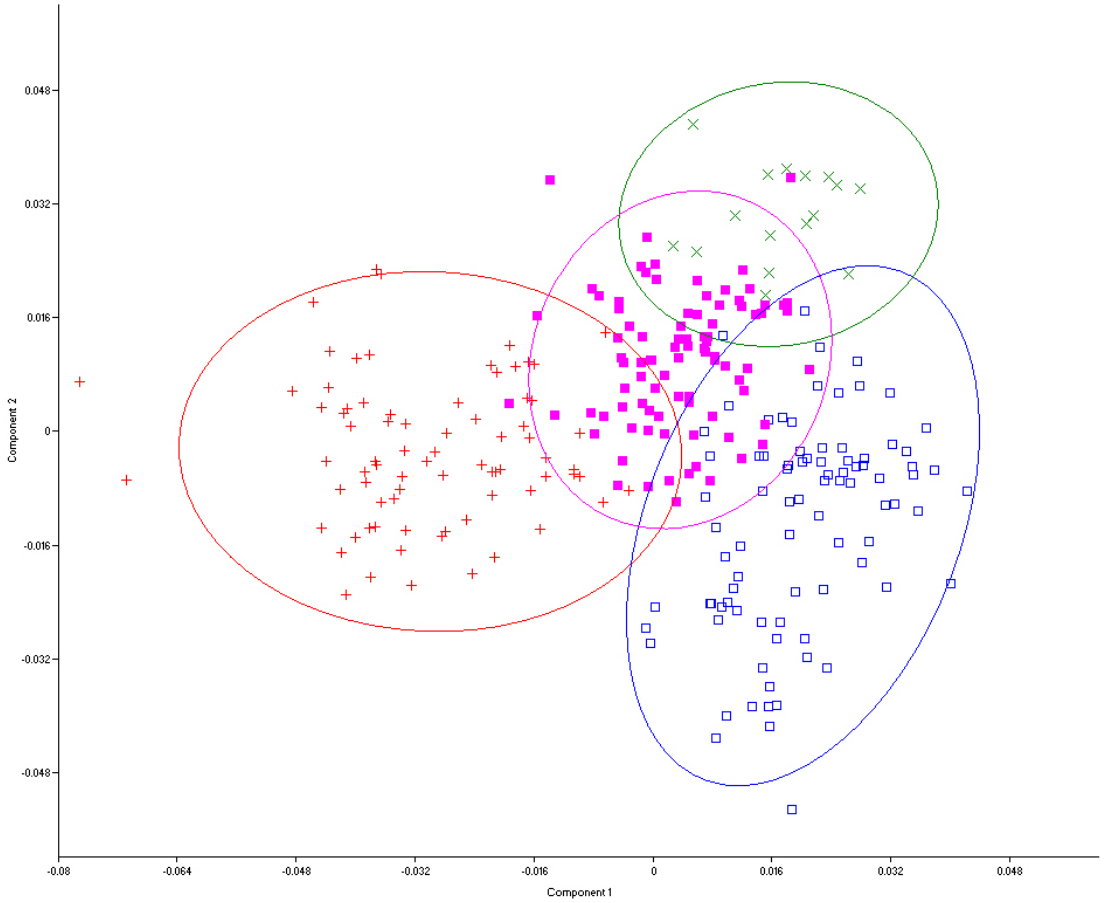

Fig. 3.43 Prinicpal components analysis of the entire ulna. *Homo* are blue squares, *Pan* are purple squares, *Pongo* are green Xs, and *Gorilla* are red pluses. Prinicpal component one represents 33% of the variance and principal component two represents 18% of the variance. Each group is surrounded by a 95% equal frequency ellipse.

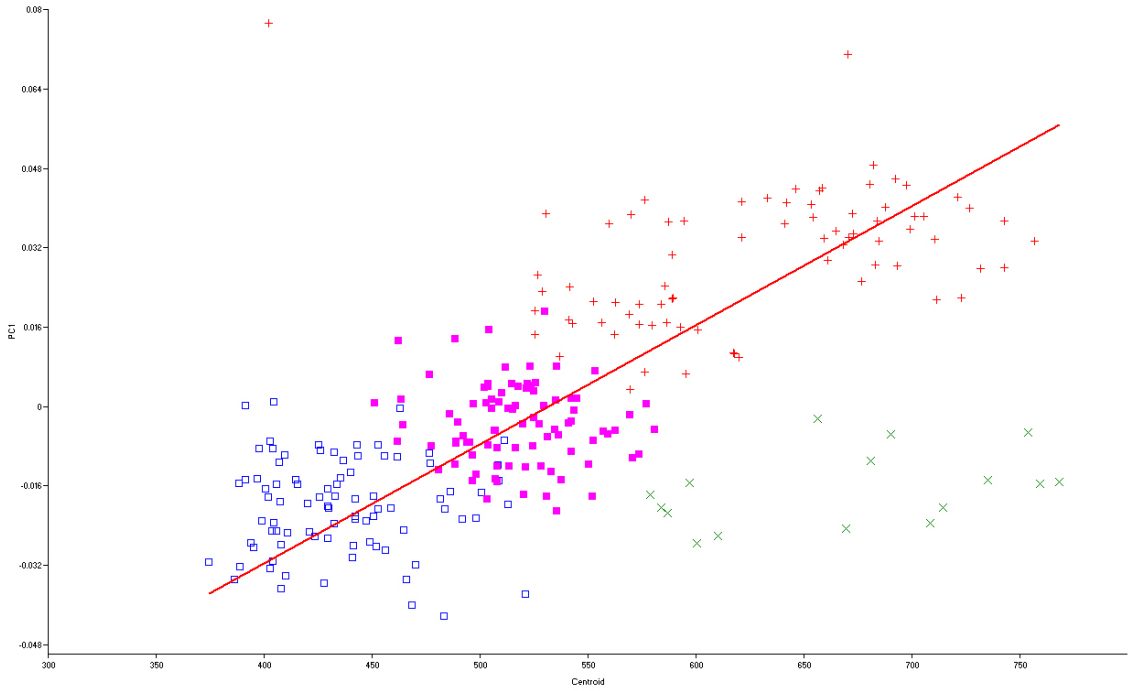

Fig. 3.44 Regression of principal component one on centroid size for the entire ulna. In this analysis r=0.649.

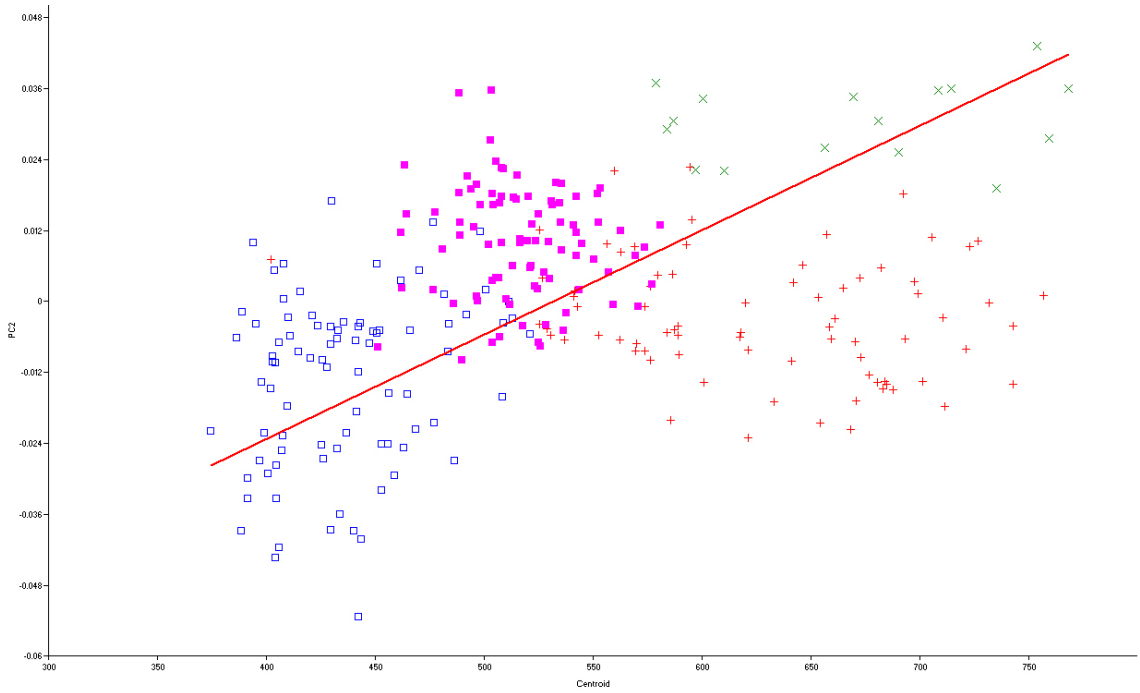

Fig. 3.45 Regression of principal component two on centroid size for the entire ulna. In this analysis r=0.338.

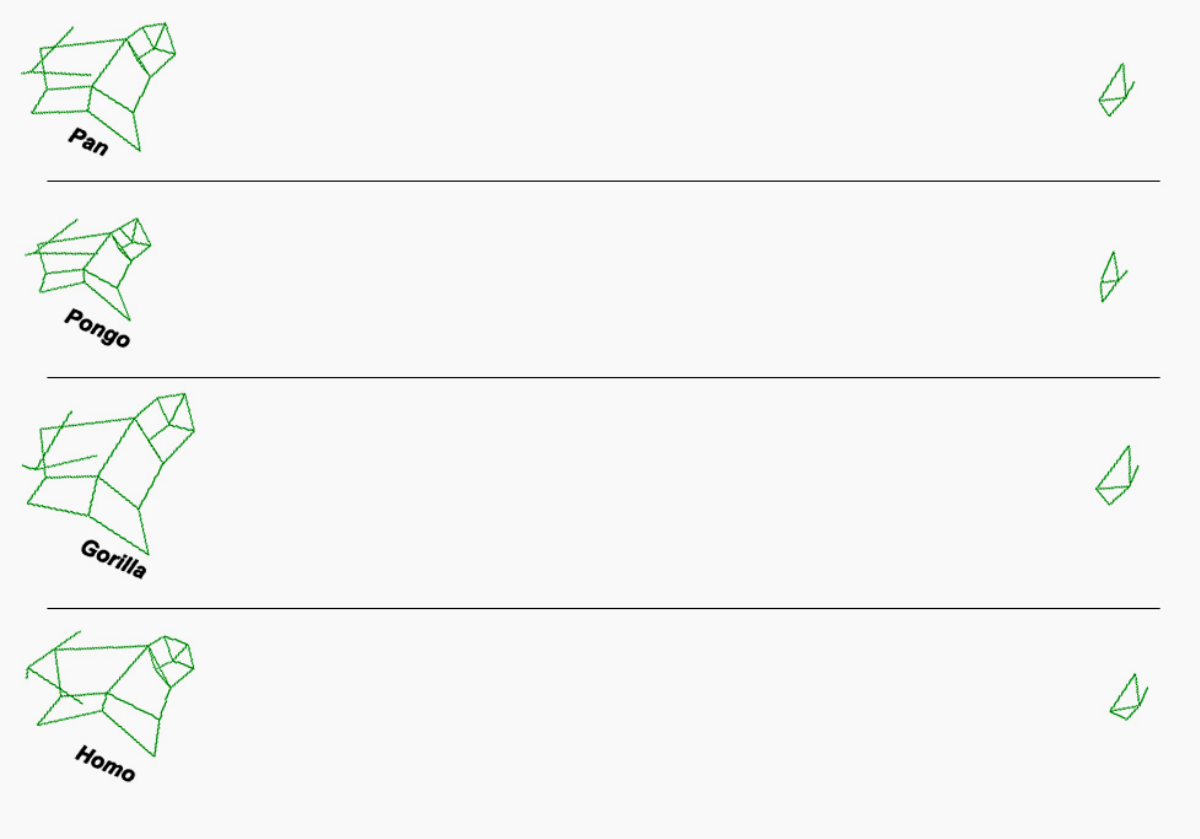

Fig. 3.46 Wireframe transformation between all extant taxa for the full ulna.

Full Ulna Discussion and Analysis

The differences between the extant specimens reproduced by the principal components graph correspond to known differences between the ulnae of extant species. These differences in turn correlate with known differences in the way that those ulnae function in different positional behaviors. The broad, shallow trochlear notch in *Gorilla* is likely an adaptation for supporting a heavy animal, while maintaining a high degree of mobility (Drapeau, 2008). Terrestrial cercopithecoids generally have narrower, smaller trochlear notches in a condition that runs parallel to more cursorial species, though this sacrifices the mobility at the joint which would be useful in more suspensory postures (Rose, 1993). The narrow, keeled notch in *Pan* and *Pongo* may be to resist the strong lateral forces exerted by the flexors of the finger during suspension

(Drapeau, 2008). The more proximally oriented trochlear notch in *Pongo* is an adaptation for quadrumanous climbing and habitual arm-overhead positions (Rose, 1993). No fossils preserve the entire ulna.

Proximal Ulna

The ulna was subdivided into proximal and distal regions, the proximal region consisting of landmarks 1 through 18 (see fig. 3.47). Figures 3.48 – 3.51 illustrate the results of several PCAs on the extant and fossil individuals for the proximal ulna for different landmark configurations. Most of the fossils were relatively complete; thus the alternate configurations are for only two other fossils (OH 62 and ER 1500) but they are particularly important fossils. Figure 3.48 shows the results for the full proximal ulna, utilizing all of the landmarks. PC 1 separates *Homo* and *Gorilla* from *Pongo* and *Pan* while PC 2 separates *Pongo* and *Pan.* The change along PC 1 is largely related to the olecranon process. In *Homo,* the olecranon process is more proximally oriented, whereas in *Gorilla,* it is more posteriomedially oriented. Also, PC 1 represents a widening of the trochlear notch with *Homo* having the narrowest notch and *Gorilla* having the widest notch. PC 2 separates *Pongo* and *Pan* on the basis of the short proximal projection of the olecranon in *Pongo*, and the more tightly curved trochlear notch in *Pan.* All of the fossils fall within the 95% equal frequency ellipses for modern humans, with the exception of Omo L40-19 which has a totally unique position.

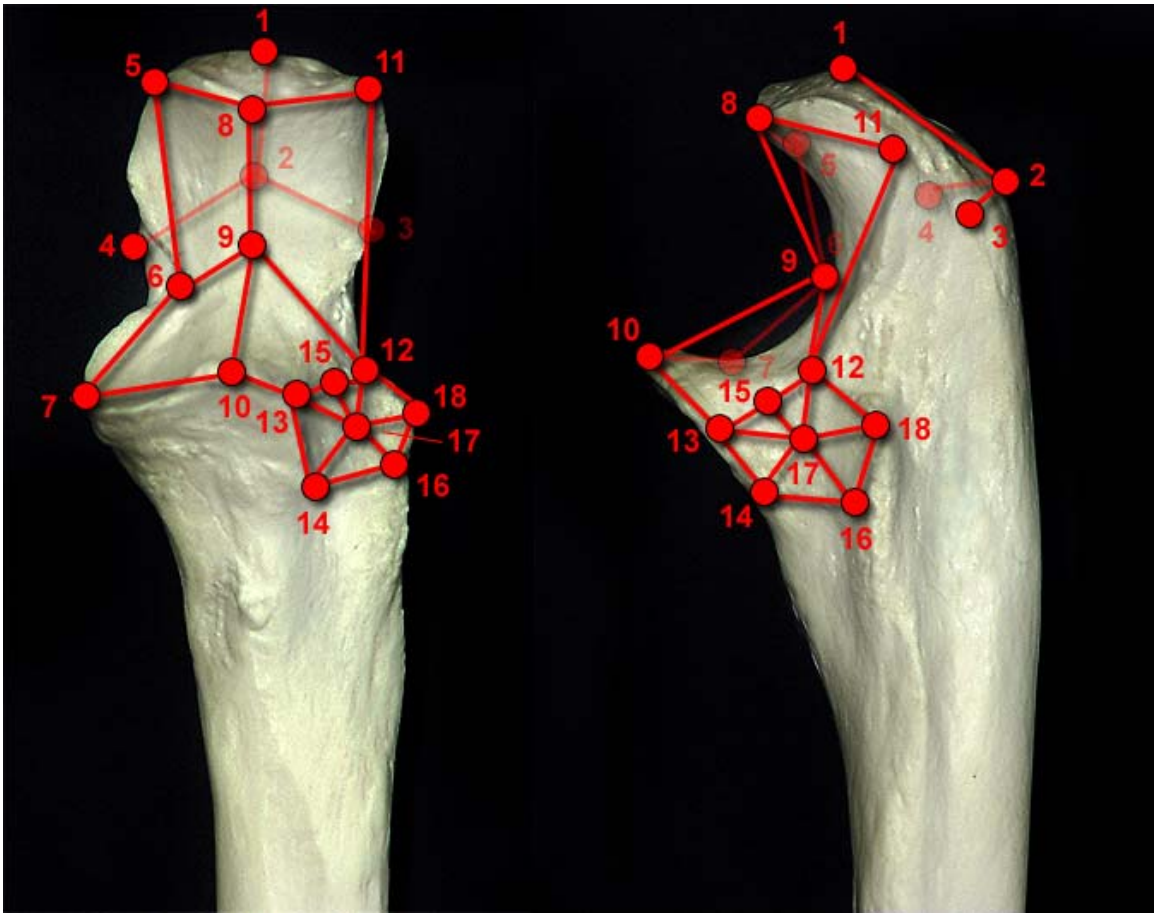

Fig. 3.47 Landmarks and wireframe for the full proximal ulna.

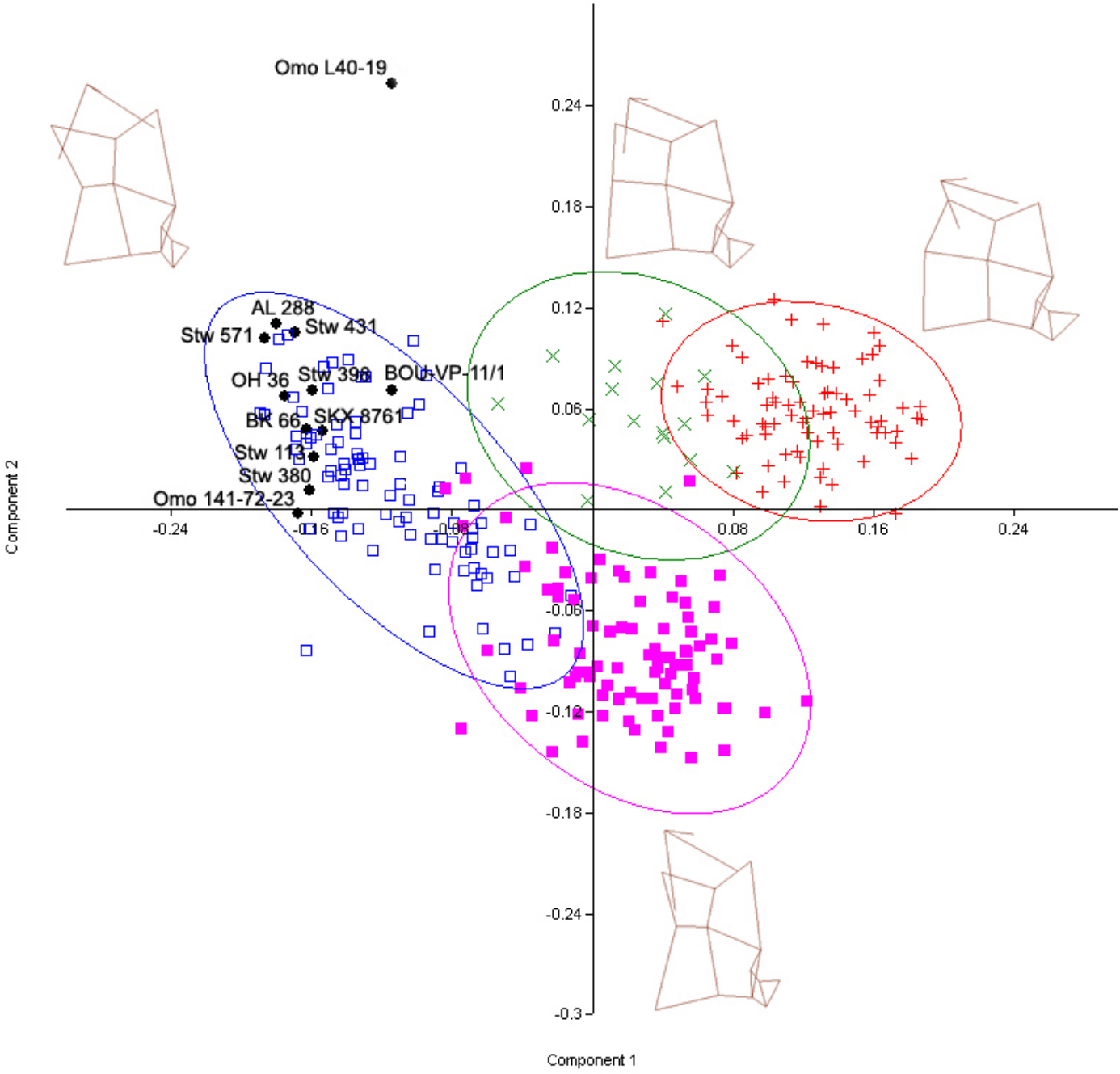

Fig 3.48 PCA of the full proximal ulna utilizing only fossils with a complete set of landmarks. Wireframe transformations are shown directly on the graph and are shown in anterior view. *Homo* is represented by blue squares, *Pan* by purple squares, *Pongo* by green Xs, and *Gorilla* by red pluses. PC 1 represents 27.1% of the variance and PC 2 represents 13.7% of the variance. Each group is surrounded by a 95% equal frequency ellipse. Fossils are in black and labeled.

Figure 3.49 is a PCA utilizing a slightly reduced landmark set where he points representing the proximal projection of the olecranon (landmarks 1 and 2) were removed in order

to allow for the inclusion of OH 62 in this analysis. OH 62 is an important fossils as many of the conculsions about the locomotor pattern of *Homo habilis sensu lato* rely upon this specimen (Johanson *et al* 1987; Hartwig-Sherer and Martin, 1991; Wood and Collard, 1999)**.** The removal of two points along the olecranon does not radically change the shape of the graph. Once again, PC 1 separates *Homo*, *Pan* and *Gorilla* while PC 2 separates *Pongo* and *Gorilla* from the rest of the sample. Most of the fossils fall within or extremely near to the 95% equal frequency ellipse for modern humans, with the exceptions of OH 62 which falls within the range of *Pongo* and Omo L40-19 which falls outside the 95% equal frequency ellipses of any of the extant taxa.

PC 1 is driven by the position of the most medial point on the olecranon process. In *Gorilla,* this point is located quite far distally and posteriorly. In *Homo* and the fossils, this point is more proximally located and does not project as far. Additionally, in *Gorilla* the trochlear notch is very wide and shallow whereas in *Homo* and the fossils, it is narrower. PC 2 is driven by the keeling in the trochlear notch. Individuals that fall towards the most positive values on PC 2 have the least waisted trochlear notches. Both PC 1 and 2 are correlated with centroid size (figures 3.52 and 3.53). Omo L40-19 falls well off of both regression lines as its size is comparable to male *Gorilla* but its morphology is more similar to much smaller individuals.

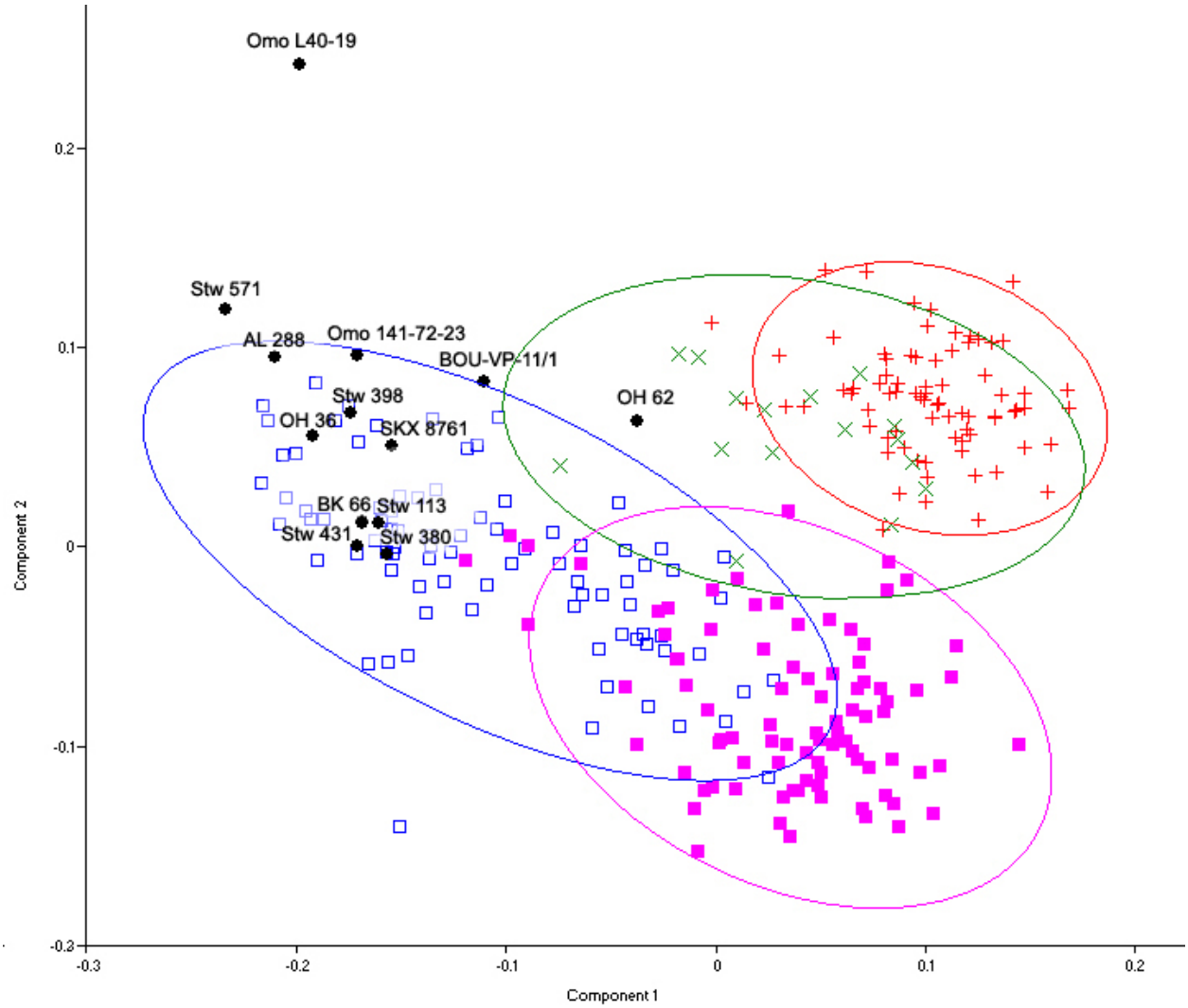

Fig. 3.49 PCA of the proximal ulna maximized for the greatest number of fossils to be included without losing resolution. PC 1 represents 29% of the total variance and PC 2 represents 14% of the total variance. *Homo* are represented by blue squares, *Pan* by purple squares, *Pongo* by green Xs, and *Gorilla* by red pluses. Each group is surrounded by a 95% equal frequency ellipse. Fossils are in black and labeled. No wireframes are presented here as the wireframes were not appreciably different from those presented in figure 3.48.

Figure 3.50 is a PCA without the landmarks that form the radial notch. This allowed for the inclusion of ER 1500, a fossil that is particularly important because it has multiple upper limb elements. There is excellent separation between all of the extant taxa, as in the previous two analyses. All of the fossils fall within the range of modern humans with the exception of Omo L40-19 and ER 1500. ER 1500 is not far from the human distribution and could be considered an outlier. It is certainly closer to the human distribution than and of the other taxa.

PC 1 and 2 are driven by the same factors that drove the axes in the first PCA (fig. 3.48a); PC 1 is driven by the orientation of the olecranon process with the most medial point located quite far distally and posteriorly in *Gorilla* and more proximally in *Homo* and the fossils as well as the width of the trochlear notch.. In *Gorilla* the trochlear notch is very wide and shallow whereas in *Homo* and the fossils, it is narrower. PC 2 is driven by the keeling in the trochlear notch. Individuals that fall towards the most positive values on PC 2 have the least waisted trochlear notches. PC 1 and PC 2 are correlated with centroid size.

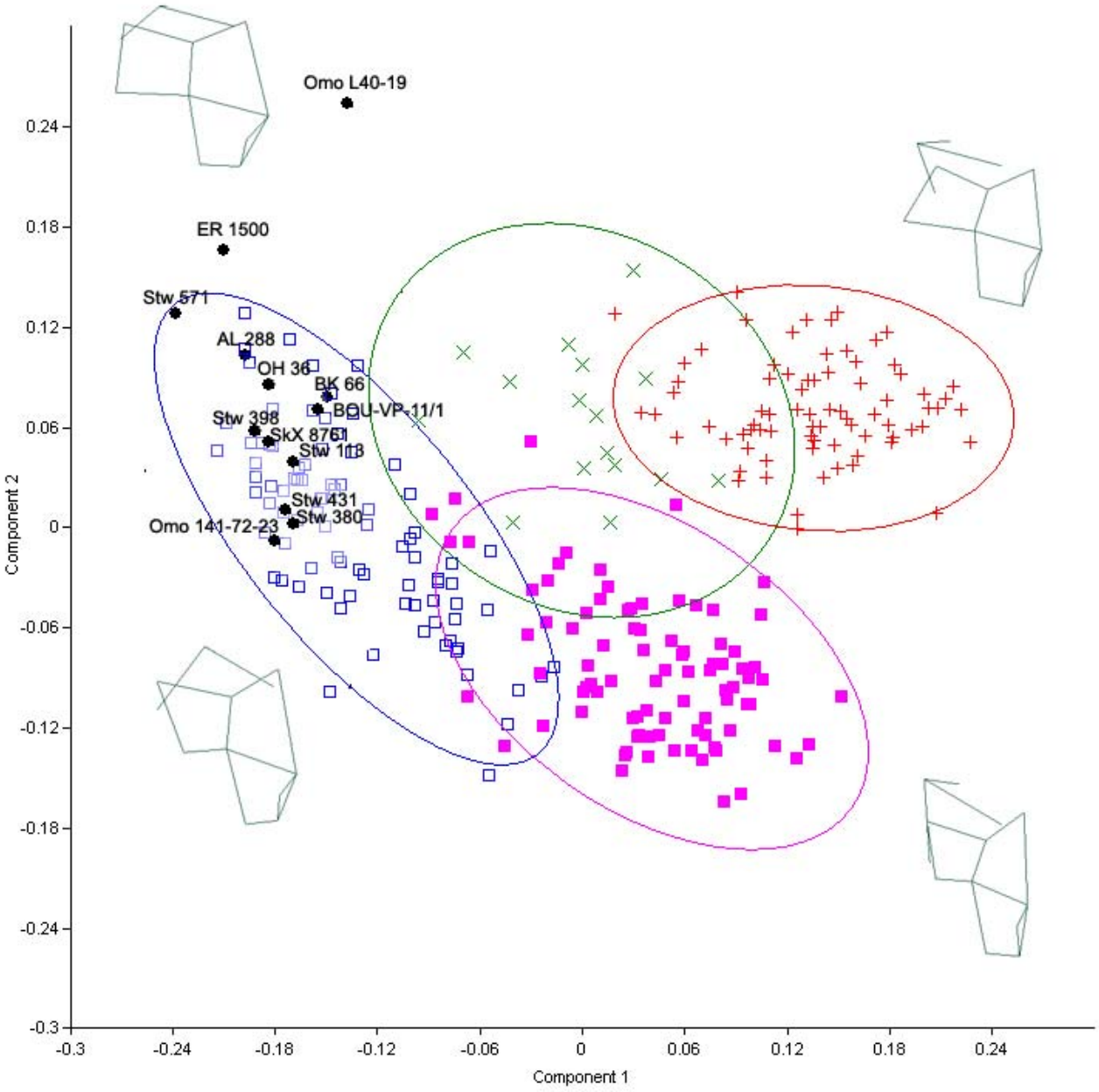

Fig. 3.50 PCA of the proximal ulna without the landmarks on the radial facet (landmarks 14 through 16) or landmark 13. PC 1 represents 32.6% of the total variance and PC 2 represents 13.9% of the total variance. *Homo* are represented by blue squares, *Pan* by purple squares, *Pongo* by green Xs, and *Gorilla* by red pluses. Each group is surrounded by a 95% equal frequency ellipse. Fossils are in black and labeled. Wireframes are from an anterior view.

Figure 3.51 is a PCA of just the trochlear notch. When the olecranon and radial facet points are removed, the separation between extant genera becomes less apparent. PC 1 separates *Homo* and *Pan* from *Pongo* and *Gorilla.* PC 1 is driven by the width of the trochlear notch through the horizontal midline. PC 2 slightly separates *Pan* from *Homo* and is driven by the depth of the trochlear notch relative to the proximal portion of the notch. Omo L40-19 has an almost symmetrical notch whereas particularly in *Homo* and *Pan,* the proximal portion of the notch is taller. Most of the fossils fall within the range of modern *Homo.* Omo L40-19 is most like *Gorilla* due to its extremely wide, flat trochlear notch. ER 1500, OH 62 Stw 571 and Omo 141-72-23 also fell outside the range of human variation. PC 1 is correlated with centroid size.

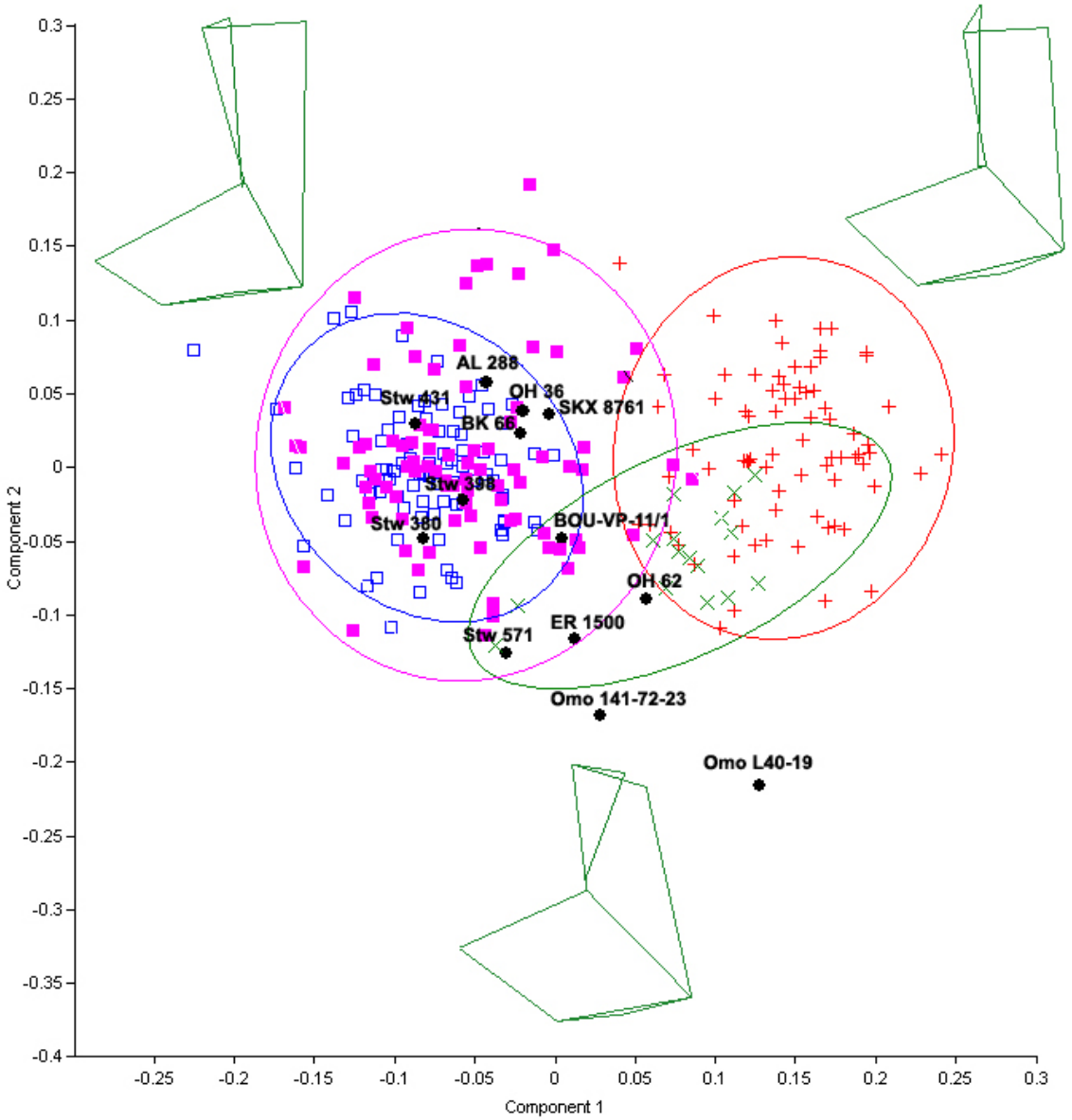

Fig. 3.51 PCA of the proximal ulna with just the trochlea. PC 1 represents 36.9% of the total variance and PC 2 represents 10.7% of the total variance. *Homo* are represented by blue squares, *Pan* by purple squares, *Pongo* by green Xs, and *Gorilla* by red pluses. Each group is surrounded by a 95% equal frequency ellipse. Fossils are in black and labeled. Wireframes are from a lateral view.

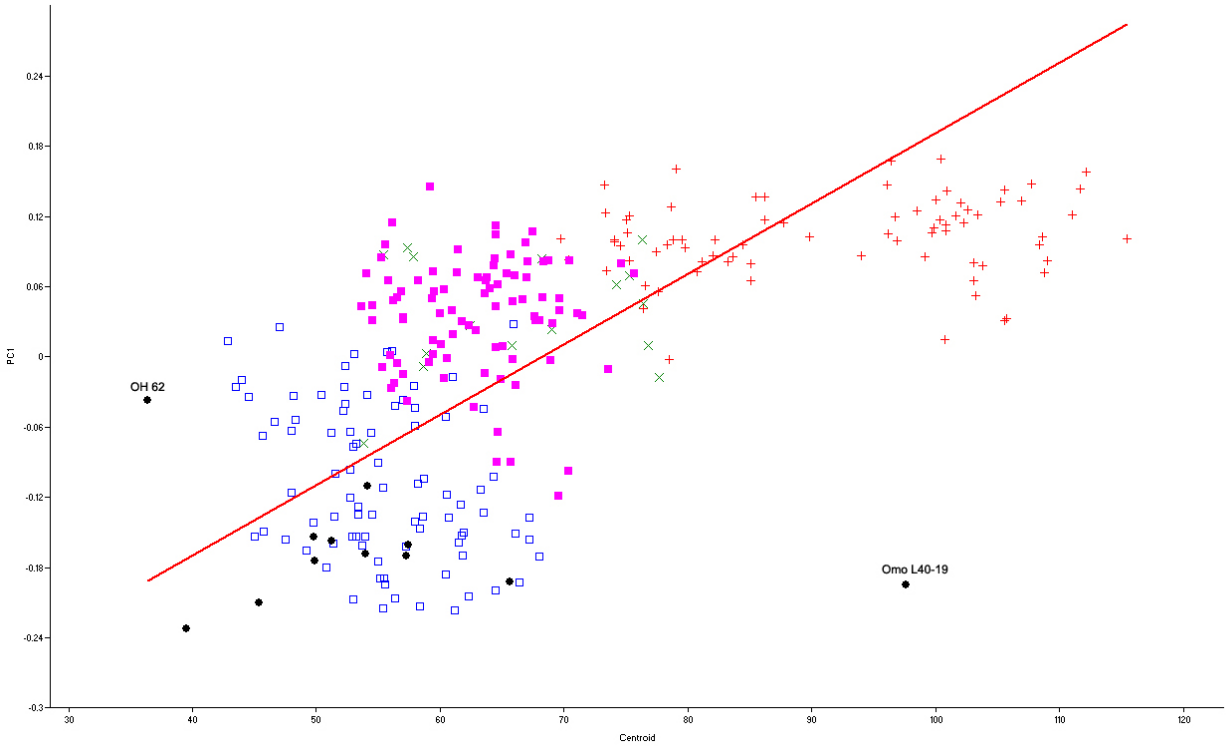

Fig. 3.52 Regression of PC 1 on centroid size for the proximal ulna (reduced landmark set).

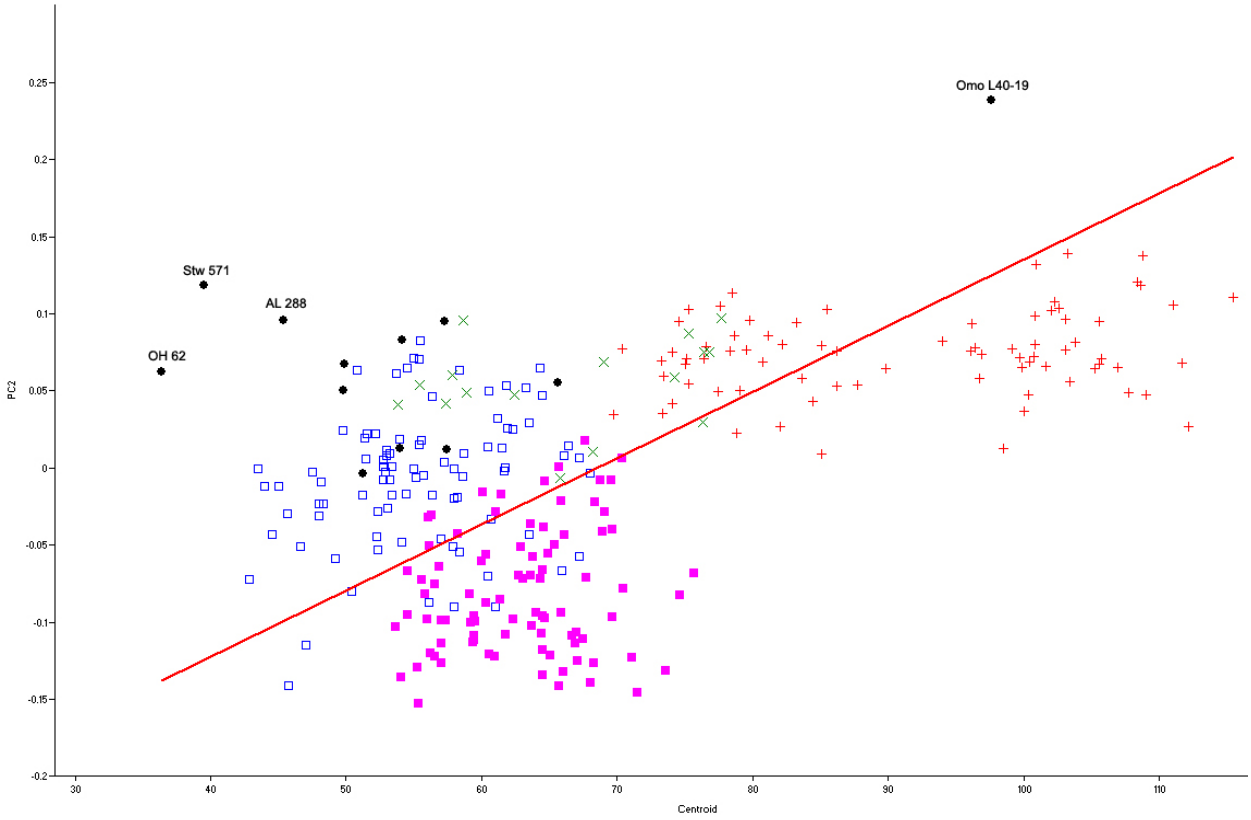

Fig. 3.53 Regression of PC 2 on centroid size for the proximal ulna (reduced landmark set).

Means were calculated for all of the extant species and a PCA was run using these values with the fossil individuals, using landmarks 3-12, 14-17 (the same configuration as fig. 3.49). The results of that analysis with a minimum spanning tree plotted on top and presented in figure 3.54. In this case, neither principal component one or two was correlated with centroid size. The results of this analysis lend further support to the idea that OH 62 has featurs that are *Pongo*-like, as it appears closes to *Pongo* in the graph and is *Pongo*'s nearest neighbor, according to the MST. All of the rest of the fossils fall in a cluster that is closest to *Homo.* The only exception is Omo L40-19 which is once again at an extreme, falling well away from all other individuals. PC 1 is mostly driven by the projection of the coronoid process and with width of the distal margin of the trochlear notch. The apes (and OH 62) have a large, projecting coronoid process whereas in humans and the other fossils, the coronoid is much smaller. In Omo L40-19, the proximal trochlear margin is very wide, and it gets progressively smaller in specimens moving towards the apes. PC 2 is driven by the width and depth of the trochlear notch across its midline. Omo L40-19 has a particularly shallow and wide trochlear notch. In general, the signal from the cluster analysis and the signal from the ordination analysis are the same with few instances where the individuals with the smallest procrustes distances are not nearest to one another in the ordination analysis.

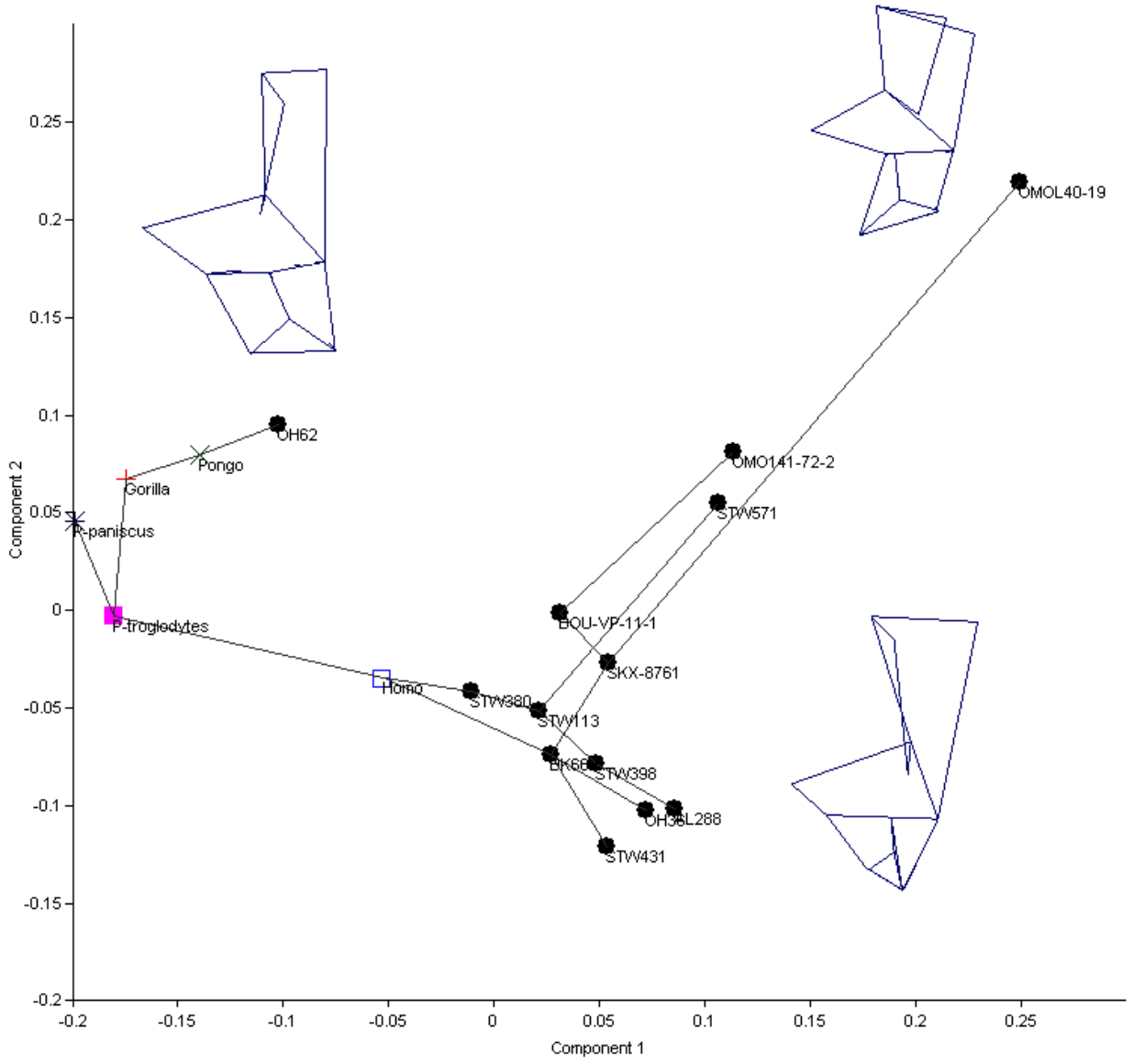

Fig. 3.54 Means were calculated for each species and a minimum spanning tree was plotted on top of the principal component graph for the reduced landmark set for the proximal ulna. PC1 accounts for 36% of the variance and PC2 accounts for 18% of the total variance. All individuals are labeled in the graph. The wireframes are in a lateral view

Means were calculated for the data on just the trochlear notch and a PCA and MST of this data are shown in Fig. 3.55. This is the only set of landmarks that contains all of the fossils. PC 1 separates Omo L40-19 and, to a lesser extent, ER 1500 and is driven by the width of the

trochlear notch. PC 2 separates OH 62, Stw 571 and Omo 141-72-23 and is driven by the keeling of the trochlear notch. OH 62 has the most keeled notch of all of the fossils in this sample. The rest of the fossils and the extant form a single cluster. Again, the signal from the cluster analysis and the signal from the ordination analysis are the same; the only fossil that is not linked to its nearest neighbor in the ordination analysis via the MST is BOU-VP-11/1.

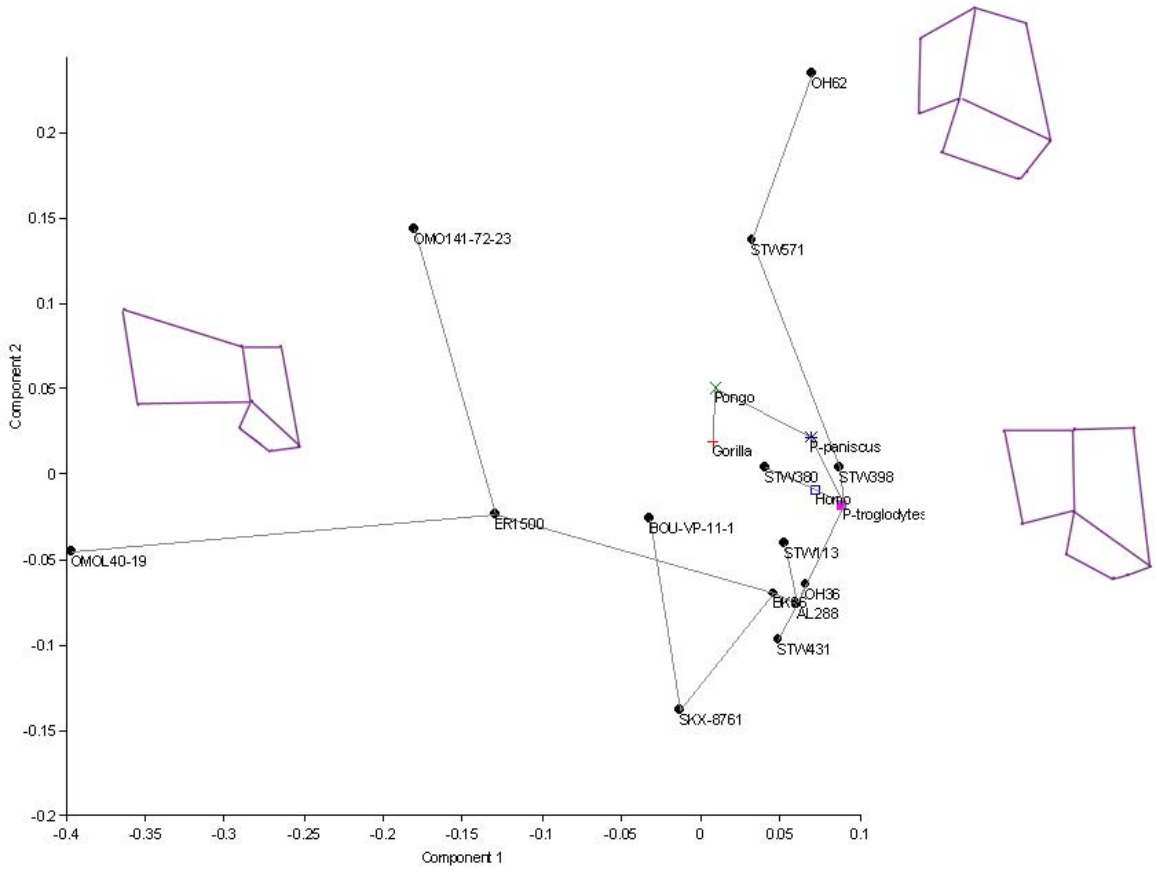

Fig. 3.55 MST and PCA for the trochlear notch. PC1 accounts for 36.6% of the variance and PC2 accounts for 20.9% of the total variance. All individuals are labeled in the graph. The wireframes are in an anterior view.

Four neighbor-joining trees were generated (fig. 3.56a-d) corresponding with the data for the four PCAs. Despite some relatively low bootstrap values, most of the clusters stay the same through all four of the landmark configurations. In general, there are three major clusters of fossils with all of the extants as the outgroup to those fossils. They are: 1) Stw 113 and Stw 380; 2) BOU-VP-11/1, Stw 571, Omo 141-72-32, Omo L40-19, ER 1500 and OH 62; and 3) Stw 398, AL 288, OH 36, BK 66, Stw 431 and SKX 8761. The only deviations from those major clusters are SKX 8761 shifting to the cluster with AL 288 in fig. 3.56a and Stw 113 shifting to the cluster with Stw 113 and 380 in fig. 3.56d.

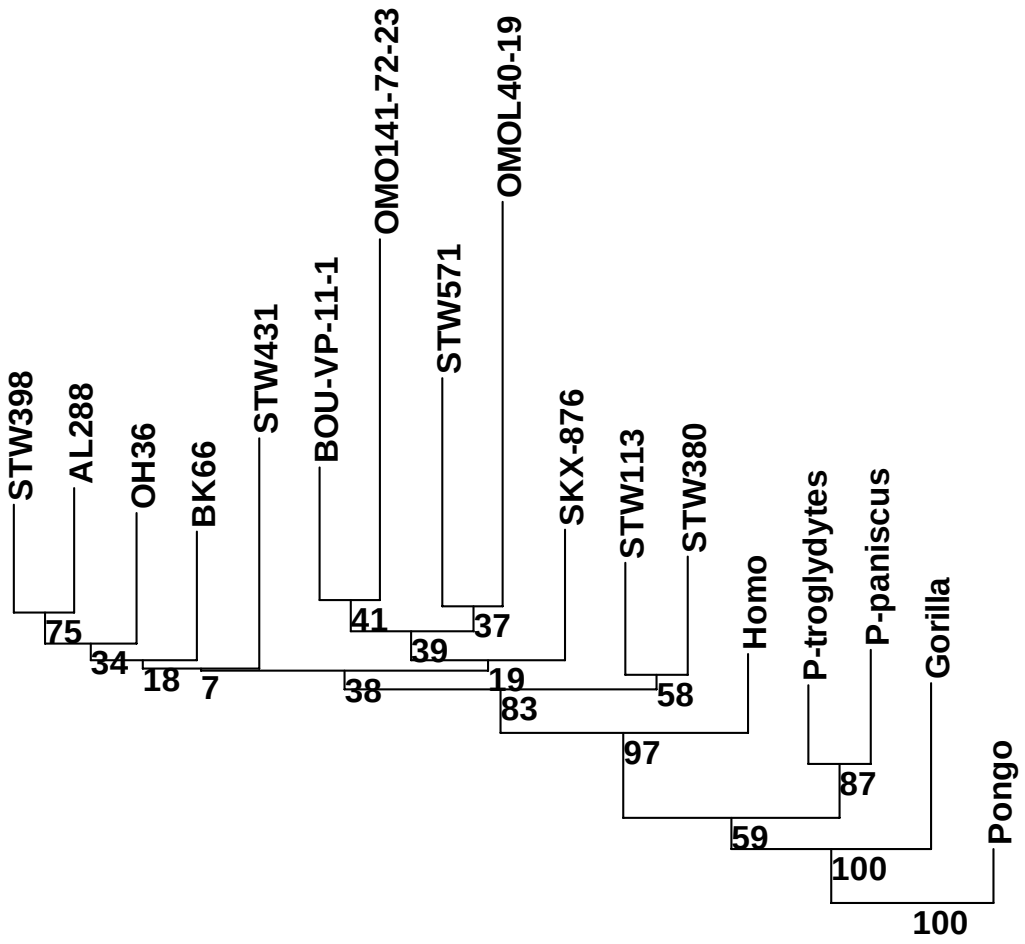

Fig. 3.56a Neighbor-joining tree for the proximal ulna, using the fossil data with the means for the extant taxa for the full landmark set. Procrustes chord distances were used to form this tree. Bootstrap values after 5000 replicates.

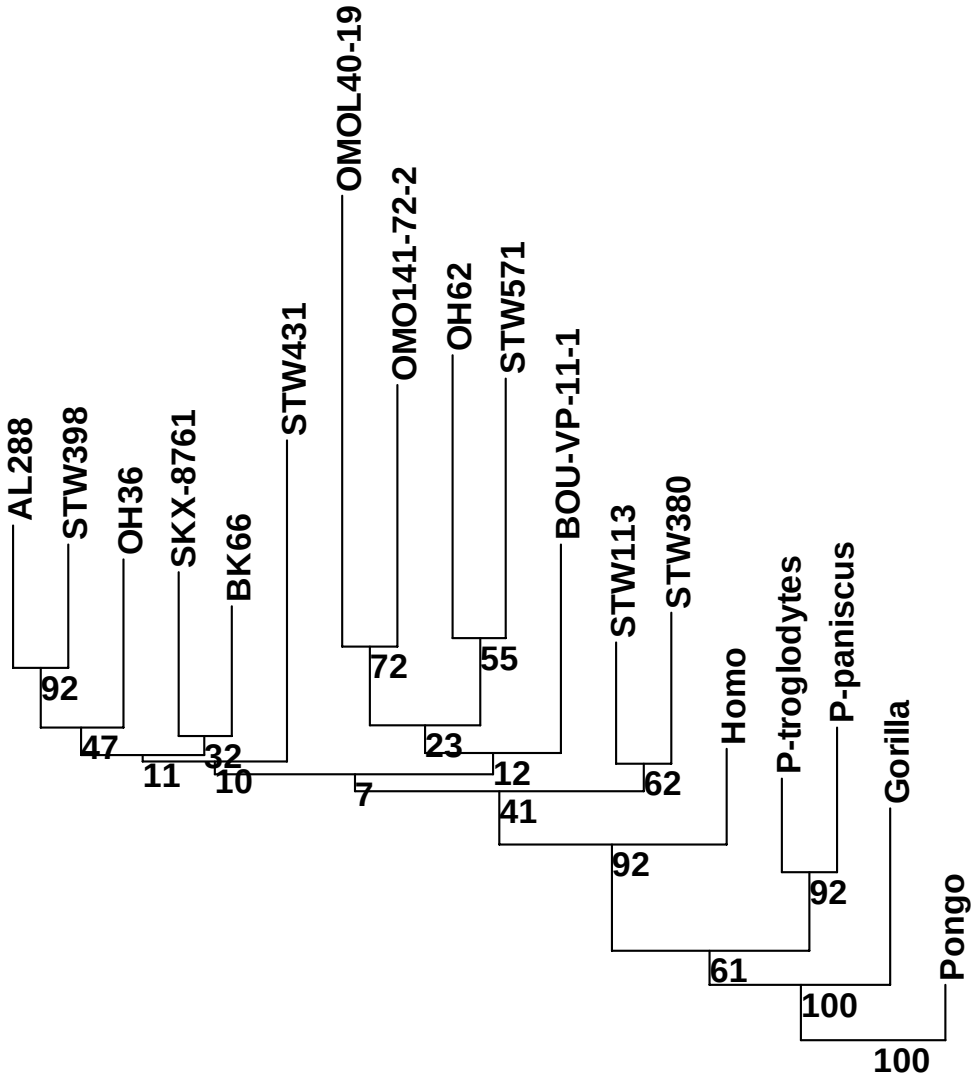

Fig. 3.56b Neighbor-joining tree for the proximal ulna, landmarks 3-12 and 14-17, using the fossil data with the means for the extant taxa for the reduced landmark set. Procrustes chord distances were used to form this tree. Bootstrap values after 5000 replicates.

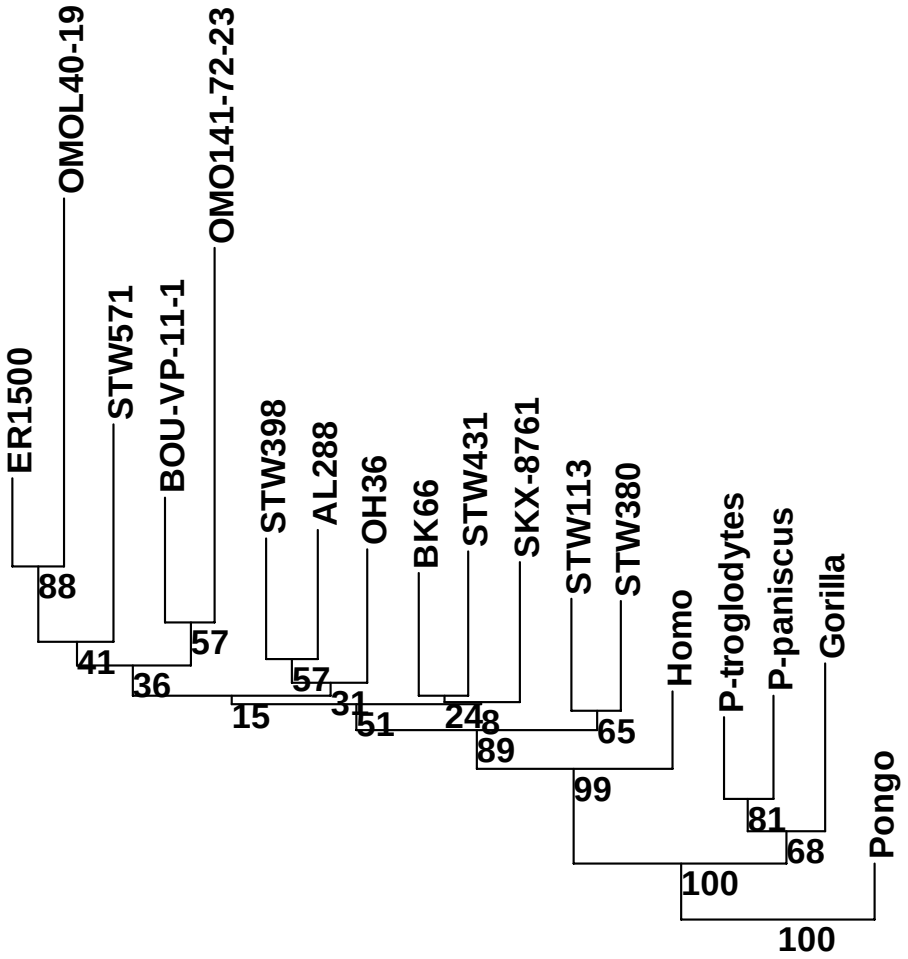

Fig. 3.56c Neighbor-joining tree for the proximal ulna without the radial facet. Procrustes chord distances were used to form this tree. Bootstrap values after 5000 replicates.

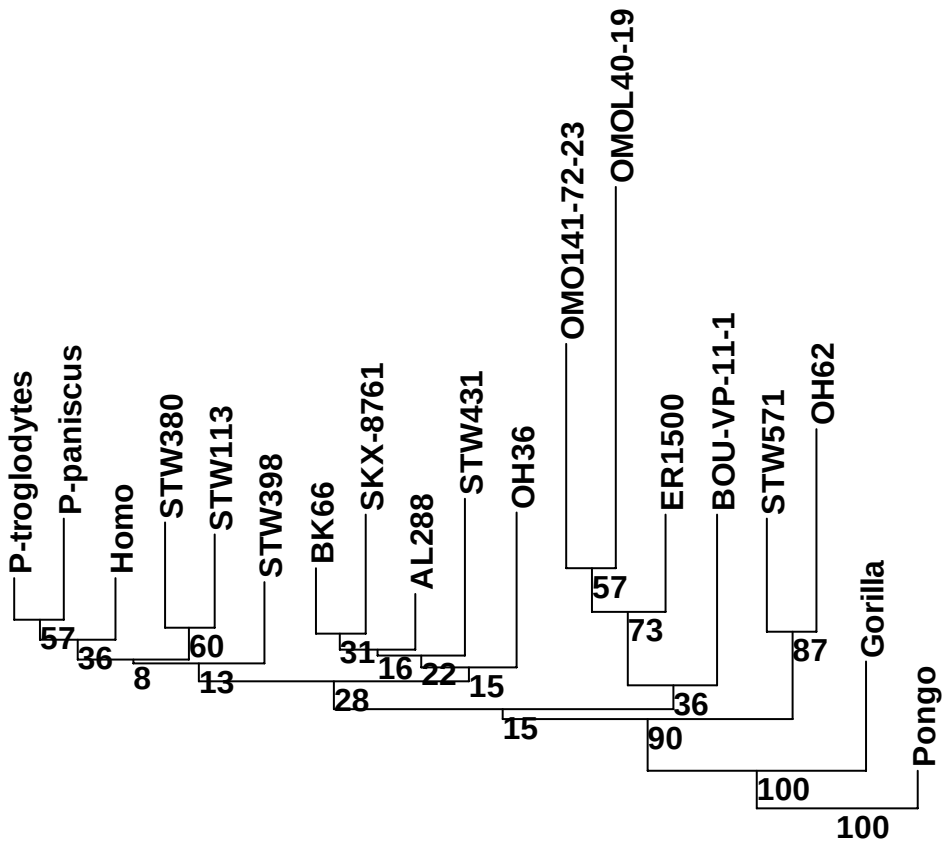

Fig. 3.56d Neighbor-joining tree for the proximal ulna, using the fossil data with the means for only the trochlear notch. Procrustes chord distances were used to form this tree. Bootstrap values after 5000 replicates.

Proximal Ulna Discussion and Analysis

In considering all of the forelimb elements, the proximal ulna has the most variation with in a single extant taxon (see fig 3.57), but has the least variation between fossil taxa. The variation in procrustes chord distance between the fossil proximal ulnae is greater than the variation within any single extant group, although it is very close to the average of the pair-wise distances between *Homo* and *Gorilla.* All of the fossil ulnae look relatively *Homo*-like and while there might be slight differences within the fossil sample, all the fossil ulnae clearly follow the human pattern for manipulation over stability at the elbow joint.

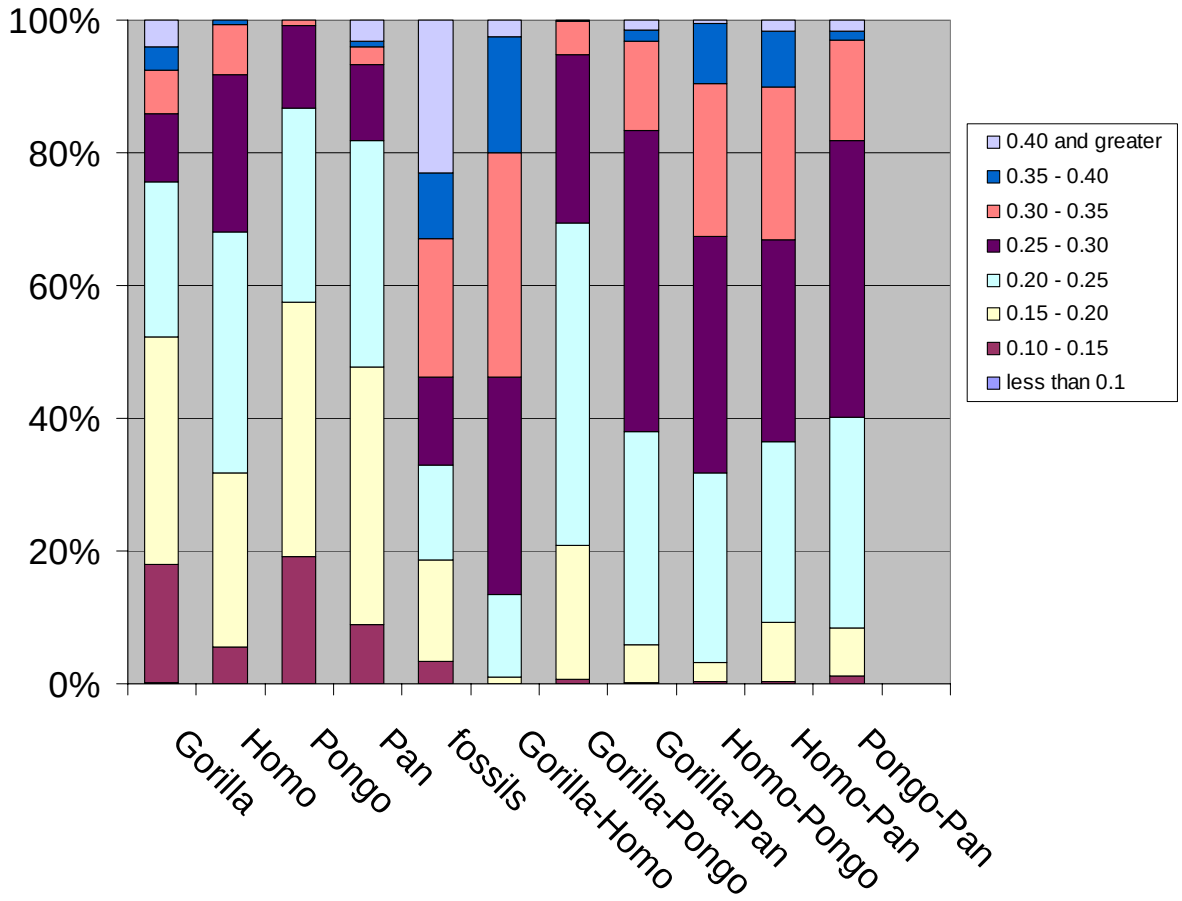

Fig. 3.57 This bar graph is a representation of the distribution of procrustes chord distances within and between the different genera in the sample of proximal ulnae. The array of procrustes distances were segmented into units of 0.05. The greatest average procrustes distance was found in the fossils, at 0.3087. This was very close to the average procrustes distance between *Homo* and *Gorilla* at 0.3057.

These data support the findings of Drapeau (2004). Drapeau examined the olecranon process of extant great apes and a small selection of fossil hominins. She found that in knuckle-walkers, the olecranon process projected more posteriorly, in order to maximize the strength of the triceps brachii muscle during extended forearm postures in quadrupedal locomotion. In *Pongo,* the olecranon process was fairly short, though it also projected posteriorly. The short olecranon would also function for maximum strength of the triceps brachii in multiple arm positions with the posterior projection increasing the strength during extension. Humans have a

more proximally oriented olecranon process, which increases the leverage of the triceps brachii during flexed forearm positions benefiting manipulative abilities.

These functional differences in the positioning of the olecranon correspond with the ways that these data are separated in figures 3.49 and 3.50. Drapeau (2004, 2005) found that all of the fossils in her study (AL 288, AL 428, L40-19 and OH 36) followed a *Homo*-like pattern for the olecranon. These data support her finding and add to it. Not only do AL 288, Omo L40-19 and OH 36 follow the *Homo* pattern, but nearly all proximal ulnae from the Plio-Pleistocene follow this pattern.

Omo L40-19 is the only fossil that repeatedly falls far outside the range of modern variation in this study. The large size of Omo L40-19 and the extreme shaft curvature have prompted many different researchers to categorize it as more ape-like and different from other ulnae from the Plio-Pleistocene (Feldesman, 1979; Drapeau, 2005; McHenry *et al* 2007). Omo L40-19 is so large that its size might be confounding the analyses. The proximal ulna is strongly influenced by size - perhaps as hominoids get larger, there have to be architectural changes in the ulna that represent a compromise between structural stability at the elbow joint and manipulation. However, in cluster analysis, Omo L40-19 is always in the same cluster with the much smaller Omo 141-72-73. The actual size corrected joint morphology is very *Homo*-like, a finding that has been supported by previous studies (Aiello *et al.* 1999; Drapeau, 2004 for the olecranon process; Drapeau, 2008 for the trochlear notch).

While it is impossible to know the morphology of the olecranon of OH 62, what morphology is preserved is consistently ape-like; specifically, it is *Pongo*-like, as evidenced by the PCA of the full sample and of the means (figs. 3.49, 3.51, 3.54). This is due to a relatively large coronoid process and keeled trochlear surface in this specimen, both traits that are more

ape-like. These are both adaptations for greater stability at the elbow (Knussman, 1967; Drapeau, 2008). However, in the neighbor-joining trees, it groups amid the rest of the fossil, although with low bootstrap values. OH 62 has been reconstructed to have more ape-like limb proportions (Johanson *et al* 1987; Hartwig-Sherer and Martin, 1991) as well as more ape-like limb strength proportions (Ruff, 2008) and has been used as example for why *H. habilis* should be sunk into the genus *Australopithecus* (Wood and Collard, 1999). Unfortunately, this fossil has not been used in other analyses of the ulna specifically, so there is nothing to directly compare these results to; however, these results do give weak support to the idea that *H. habilis sensu lato* had a more ape-like body plan.

In the forelimb, the most "ape-like" individuals have consistently come from Koobi Fora (see the portions on the humerus and radius in this chapter). At the time of data collection, ER 1500 was the only proximal ulna from Koobi Fora available. ER 1500 is part of an associated skeleton attributed to *Paranthropus boisei* (Grausz *et al.,* 1988). In analyses of the means where ER 1500 could be included, it was most similar to the large Omo ulna, despite the much smaller size (figs. 3.51, 3.55, 3.56c,d). ER 1500 has a more ape-like trochlear notch (fig. 3.51) coupled with a human-like olecranon process (fig. 3.50) which would indicate that the olecranon had already been selected for to maximize manipulative ability over stability (Drapeau, 2004) and the overall functional morphology of this ulna is *Homo*-like, opposed to this individual's position in previous analyses (see the radius portion of this chapter).

There have been many prior studies that have looked at variation in fossil proximal ulnae, searching for differences between individuals. Aiello *et al* (1999) described the nearly complete OH 36 fossil and compared it to BK 66 and Omo L40-19. These authors decided that OH 36 has a unique morphology which is like *Pan* in the way that the posterior portion of the trochlear

notch is heavily buttressed whereas it is unlike any African ape in that the olecranon process does not point medially. These authors suggested placing OH 36 in *Paranthropus boisei.* They found no compelling differences between Omo L40-19 and BK 66 despite Omo L40-19's large size. They placed BK 66 in *Homo erectus* and Omo L40-19 in either *Homo erectus* or *Homo habilis/rudolfensis.*

McHenry *et al.* (2007) re-examined Aiello *et al* (1999)'s previous study. In a discriminant function analysis where the fossils were not treated as their own group, these authors found that OH 36 was unique, Omo L40-19 was chimp-like in morphology and AL 438-1 human-like in its morphology. These authors also noted that if Omo L40-19, OH 36 and SKX 8761 are all considered as *Paranthropus*, then *Paranthropus* has an extremely heterogenous morphology for the proximal ulna, although these authors draw no functional conclusions about how that heterogeneity would have affected
locomotion.

Drapeau (2008) studied just the trochlear notch in extant apes and fossil homins. Like Aiello *et al* (1999) and McHenry *et al* (2007), she concluded that OH 36 had a unique morphology and that the more keeled trochlear notch indicated an arboreal component to its positional behavior. Unlike the previous authors, she found Omo L40-19 to have a flat trochlea, like *Homo.* And finally, she found that all specimens representing *A. africanus* and *A. afarensis* were intermediate between *Homo* and *Pan.*

Perhaps the results from this analysis differ from Aiello *et al* (1999) and McHenry *et al* (2007) because those studies relied on linear measurements and carefully parsing out where there were morphological differences between the fossils. When the shape is looked at as a whole there really is very little variation among individuals in the fossil group. Drapeau (2008) did use

landmark coordinate data to form her opinions on the importance of trochlear keeling to separate fossil taxa. The data presented here do not agree with her findings. Even when the olecranon points were removed, it was difficult to reproduce her results with this data (although she used many more points on the trochlear surface). Stw 571 and Stw 398 (possible *A. africanus)* fall most closely to the middle of the distribution of *Pan* in fig. 3.51, although they are still well within the range of modern human variation. Overall, many points had to be removed in order to make trochlear keeling the force driving shape variation in proximal ulnae. It seems like the most important shape differences are in the olecranon process, and in that way all of the fossils are most similar to *Homo*.

Overall, the seeming homogeneity in the fossil sample of proximal ulnae is evidence for very strong selection early on in the hominin lineage for maximizing manipulative ability in flexed forearm postures over stability in extended forearm postures. Given that the evolution of bipedalism as indicated by the hindlimb has been pushed back to *Orrorin* (Richmond and Jungers, 2008)**,** hominins would have had the ability to have their hands free from approximately 6 Ma. There is little evidence from the ulna for any kind of modification or retention of climbing or suspensory adaptations. These data could support the idea that having the hands free was a major advantage of bipedality.

Distal Ulna

A PCA was generated for the entire sample for the distal ulna, the results of which are presented in figure 3.58. Figure 3.59 is an illustration of the landmarks and wireframes on an actual ulna. For the PCA, the area of overlap between the extant species is tremendous. *Homo* tends to fall more to the right side of the graph and *Pan* tends to fall more towards the left side of the graph, but the overlap is so significant that few conclusions can be derived from that.

Because the separation is so poor, any conclusions made about the fossils should be very tentative. Of the five complete distal fossil ulnae, AL 333-12 falls outside of the range of all extant variation on both principal axes. Stw 326 falls within the overlap between *Homo*, *Pongo* and *Gorilla.* AL 288, AL 137-42 and Stw 328 all fall outside of the range of modern human variation, but within the overlap zone of *Pongo, Pan* and *Gorilla.* PC 1 is correlated with centroid size, although less strongly so than for other portions of the forelimb (see fig. 3.60). PC 1 is driven by the proximodistal height of the ulnar head and the projection of the styloid process with *Pan* having the shortest heads and most projecting styloid processes and *Homo* having the tallest heads and the least projecting styloids.

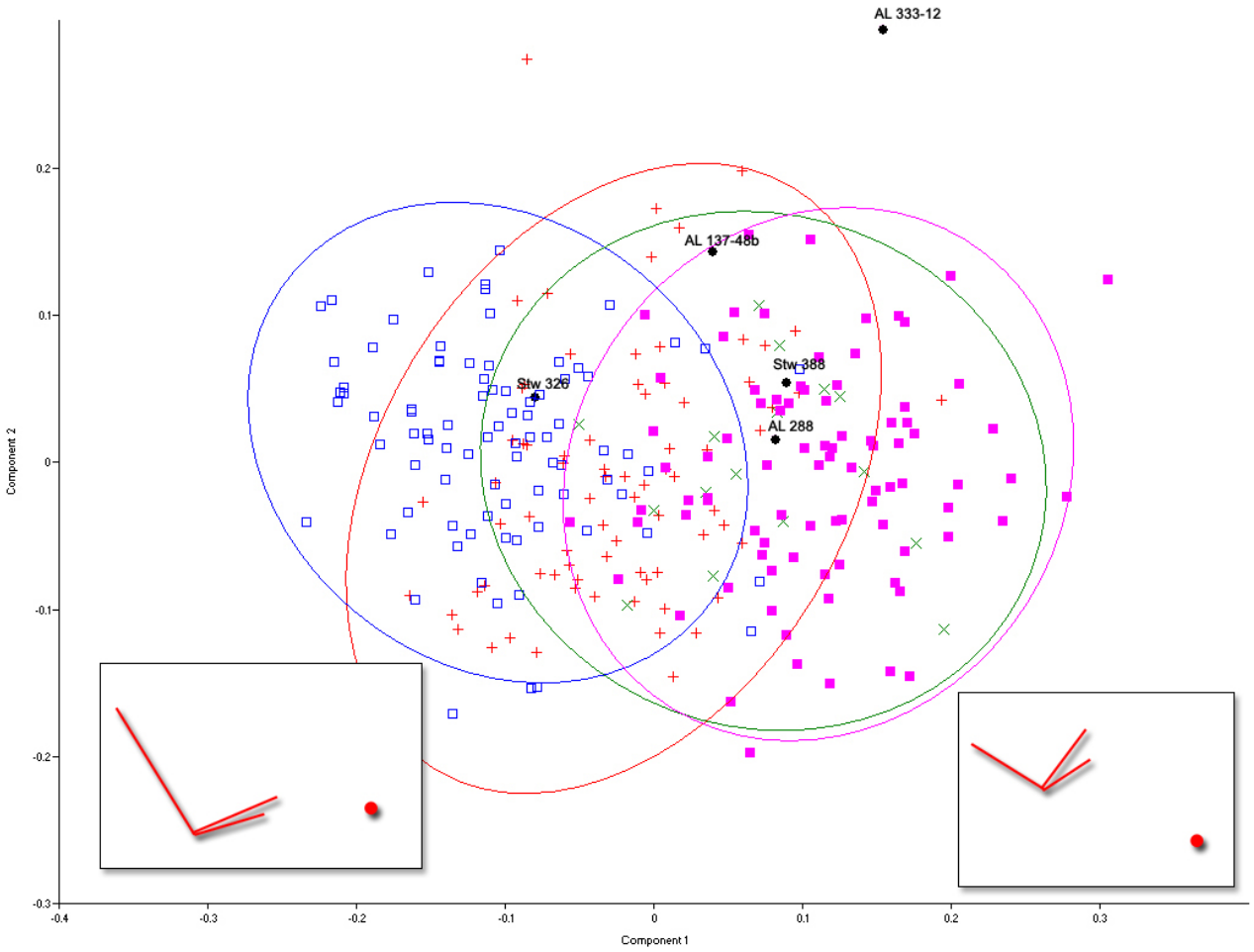

Fig. 3.58 Principal component analysis of the distal ulna. Prinicpal component one represents 38% of the total variance and principal component 2 represents 17% of the total variance. *Homo* is represented by blue squares, *Pan* by purple squares, *Pongo* by green Xs, and *Gorilla* by red pluses. Each group is surrounded by a 95% equal frequency ellipse. Fossils are in black and labeled. Wireframes are in a medial view.

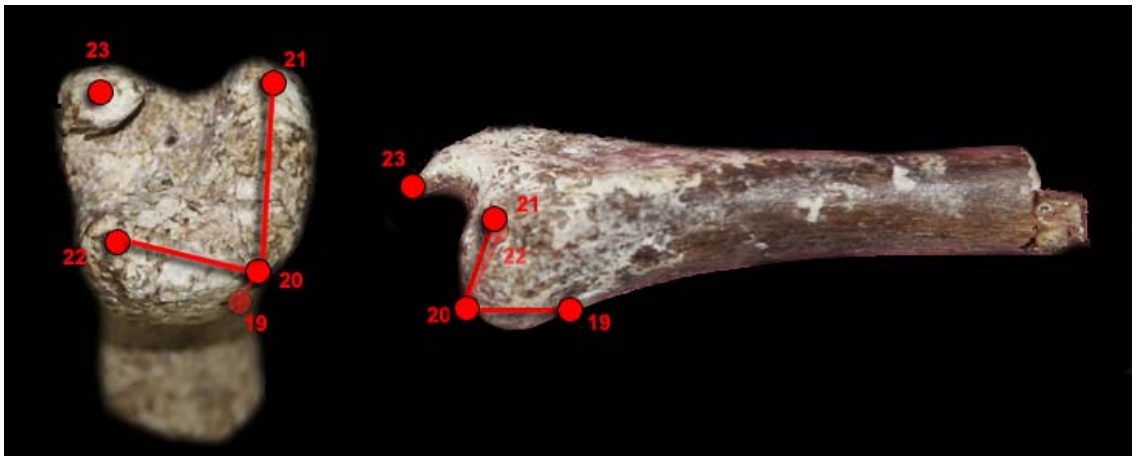

Fig. 3.59 Illustration of the landmarks and wireframe for the distal ulna. Faded landmarks and numbers indicate that those are on another side of the bone. These are shown on AL 137-48B.

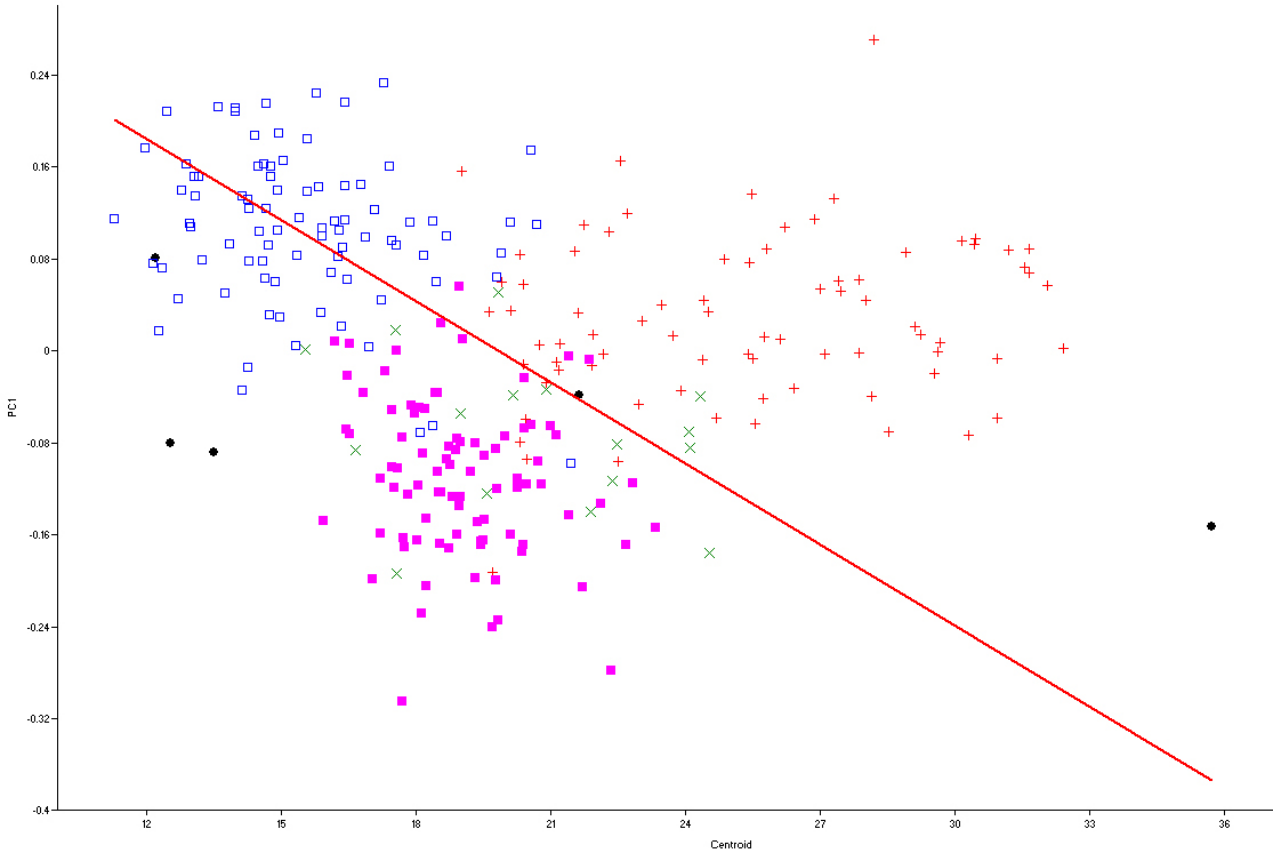

Fig. 3.60 Regression of principal component one on centroid size for the distal ulna. They are correlated with r =-0.17.

Means were calculated for all of the extant specimens and further analyses were running using these means with the fossil individuals. The results of a PCA with a MST are presented in

figure 3.61. In this case, PC 1 is not correlated with centroid size. PC 1 represents 71% of the total variance and the individuals seem to be distributed fairly randomly across it, with AL 333-12 at one extreme and *Homo* at the other. PC 1 is driven by the overall width of the ulnar head and the distal projection of the styloid process. AL 333-12 has a narrow head whereas the extant taxa and some of the other fossils have a wider head. *Pan*, AL 288 and Stw 388 have the most projecting styloid process, whereas AL 333-12 has the least projecting styloid. PC 2 is driven by the height of the ulnar head, with Stw 326 having the tallest head in the proximodistal direction.

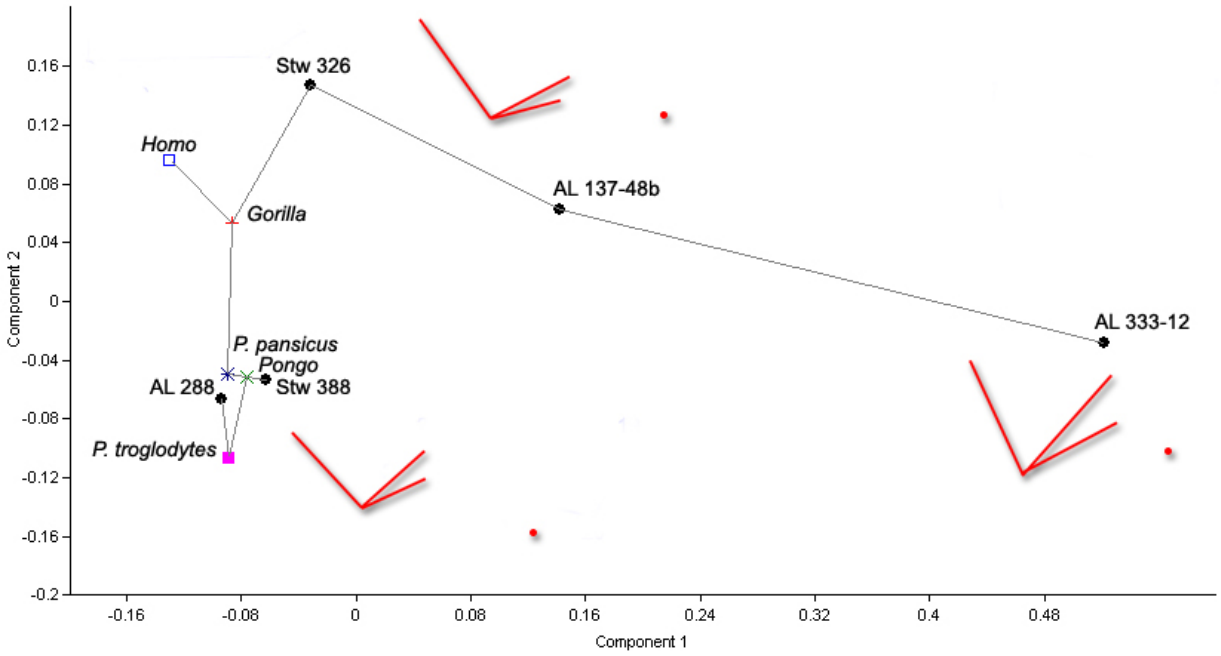

Fig. 3.61 Means were calculated for each species for the distal ulna and a minimum spanning tree was plotted on top of the principal component graph. PC1 accounts for 71% of the variance and PC2 accounts for 13% of the total variance. All individuals are labeled in the graph. Wireframes are in a medial view.

A neighbor-joining tree was also generated (figure 3.62) and the known relationships between extant individuals failed to be recreated properly. Nevertheless, it is interesting the AL 137-48B and AL 333-12 form a well supported cluster to the exclusion of AL 288. This is an instance where there seems to be a highly variable morpohological patterns within the Hadar sample (see chapter 4 for more).

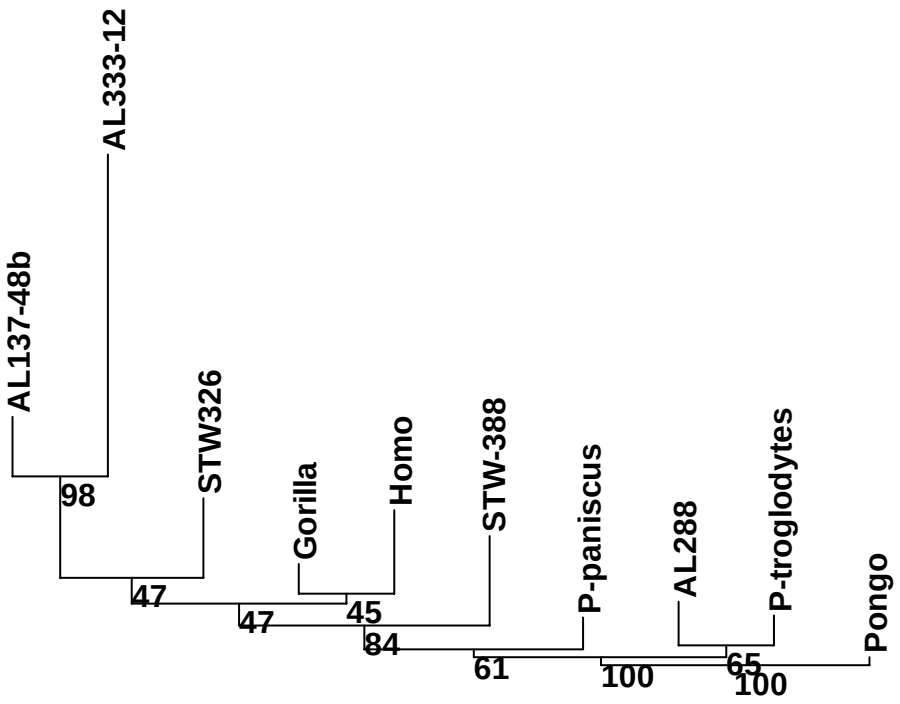

Fig. 3.62 Neighbor-joining tree for the distal ulna, using the fossil data with the means for the extant taxa. Procrustes chord distances were used to form this tree and it was rooted with *Pongo* as the outgroup.

Distal Ulna Analysis and Discussion

The distal ulna is not a functionally complicated joint. There are two portions to consider: the ulnar head and the styloid process. The styloid process is the original of the triangular articular disc that connects the distal radius and ulna (Lewis *et al.* 1970). In hominoids, the styloid process of the ulna does not directly interface with the proximal carpal row (Lewis *et al.* 1970; Rose, 1993); thus, it is less informative than it would be in monkeys or stepsirhines. In all of the apes, the styloid process is divided from the first carpal row by an intra-articular meniscus which isolates the styloid process in its own compartment. In *Gorilla* and *Homo*, the intra-articular meniscus is usually continuous with the triangular articular disc, thus fully excluding the ulna from participating in the wrist joint; in *Pan* the styloid process still participates in the carpal row through its interaction with the meniscus (Lewis, 1969; Lewis *et*

al., 1970). The separation of the distal radioulnar joint and proximal carpal row allows for independent movement in the hand and forearm (Lewis, 1969). The width of the articular surface on the ulnar head has also been linked to a wider range of motion for pronating and supinating. *Pongo* and *Pan* both have relatively large surfaces whereas *Gorilla* and *Homo* have smaller surfaces (Rose, 1993).

When considered in the context of the function of the radioulnar joint, the overlap between *Homo* and *Gorilla* in fig. 3.58 is not suprising. The fact that *Gorilla* and *Homo* have a similar pattern for the distal ulna is also what lessens the allometric effect along PC 1 as *Gorilla* has larger centroid sizes than most *Homo,* but similar values along PC 1 (fig. 3.60). AL 288 and Stw 388 are most similar to the *Pan* and *Pongo* condition of having a larger articular surface and a slightly longer styloid process (fig. 3.61) whereas Stw 326 is more like the *Homo/Gorilla* condition of having a smaller articular surface and shorter styloid process. This could indicate that the latter two fossils had a greater reliance on a wide range movement at the radioulnar join than Stw 326.

AL 333-12 is unique in having a relatively bulbous head with a large articular surface, but the styloid process is closer to the ulnar head. Functionally, the position of the styloid process shouldn't make much of a difference since it does not participate directly in the joint. Thus, AL 333-12 could be considered to have a joint that is functionally similar to *Pan* and *Pongo*. AL 333-37b has a slightly more intermediate morphology, but is most similar to AL 333-12 (fig. 3.62) and could therefore also be considered to have the same (or similar) morphology. While there is a lot of variation in the three *A. afarensis* distal ulnae, it has been noted that this joint is variable in general, particularly in humans (Lewis *et al.* 1970) and thus it should not be used as direct evidence for multiple species at Hadar.

In summary, the distal ulna provides weak evidence that some of the Plio-Pleistocene hominins (AL 288 and Stw 388) may have been using their wrists in ways similar to modern *Pongo* or *Pan,* emphasizing rotational ability. On the other hand, Stw. 326 has a distal ulna most like *Homo* and *Gorilla* and not built for extreme rotational ability. The two AL 333 specimens have a unique morphological pattern that is probably functionally more similar to the *Pan/Pongo* pattern than the *Homo/Gorilla* pattern.

Elbow Joint Complex

Humerus and Radius

Figure 3.63 – 3.65 illustrate the results of a two-block partial least squares (2BPLS) analysis of the radius and the humerus of all of the extant individuals and the hominins with associated elements. No landmarks had to be eliminated to include all four fossils in the analysis and there is strong covariation between the blocks. Based on the data from both the humerus and the radius, ER 3735 has a humerus most similar to *Gorilla,* Stw 431 and AL 288 have a humerus most similar to *Pan* and *Pongo* and SK24600/1 has a humerus most similar to modern humans. For the radius, all of the fossils fell within the 95% equal frequency ellipse for both *Homo* and *Pongo.* When taken together, it seems that ER 3735 has a unique morphology unlike any of the extant species. These findings further support the idea that the specimens from Koobi Fora have a unique, more primitive pattern in their forelimb despite being later in time than other taxa in this analysis. Stw 431 and AL 288 seem to have a pattern of covariance most similar to either *Pongo* or *Pan* in this analysis, as it fell within the 95% ellipse of those taxa in for both bones. SKX 24600/1 could be interpreted to have a human-like morphology, or a unique morphology.

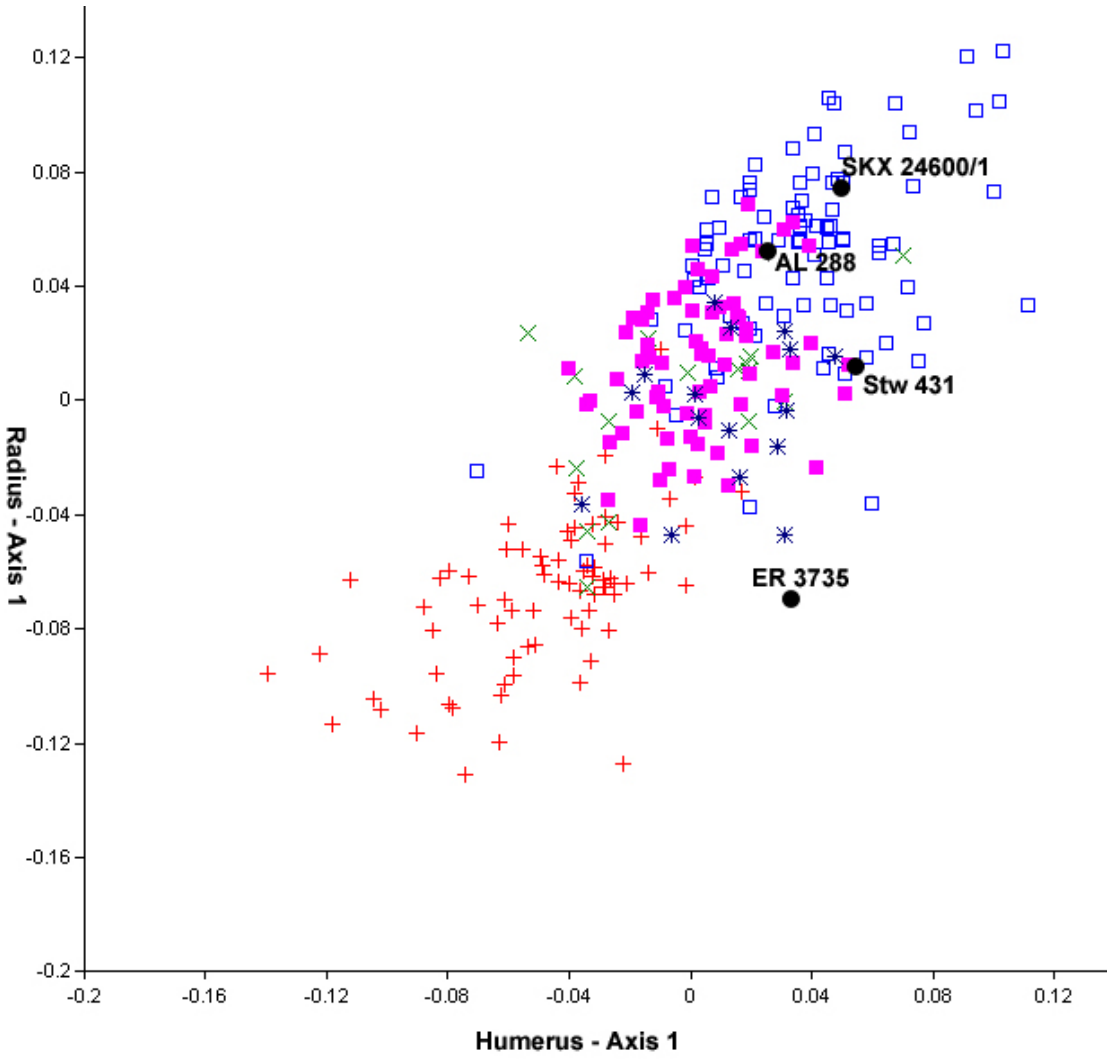

Fig. 3.63 2B-PLS analysis of the distal humerus and proximal radius. The first axis (presented here) accounts for 83.7% of the variation in the sample and has a correlation of 0.64. Axis 2 (not presented here) accounts for 7.7% of the variation and have a correlation of 0.39. The RV coefficient for the entire sample is 0.2014. *Homo* is represented by blue squares, *Pan troglodytes* by purple squares, *Pan paniscus* by blue stars, *Pongo* by green Xs, and *Gorilla* by red pluses. Fossils are labeled and in black.

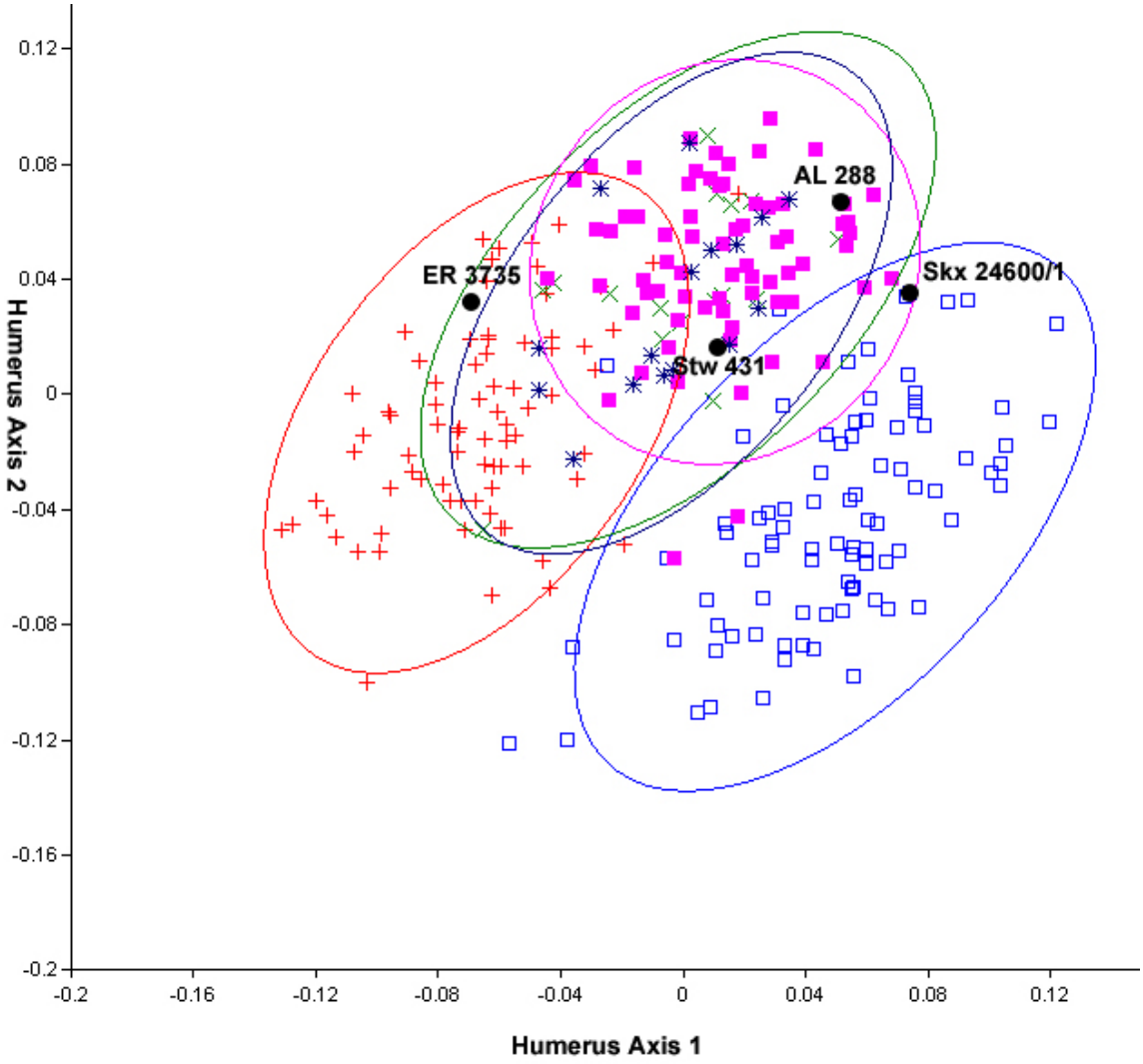

Fig. 3.64 2B-PLS analysis showing the relationship of the first and second humeral axes based on a cross-covariance matrix of the humerus and radius GPAed landmark coordinates. *Homo* is represented by blue squares, *Pan troglodytes* by purple squares, *Pan paniscus* by blue stars, *Pongo* by green Xs, and *Gorilla* by red pluses. Fossils are labeled and in black. Closed curves represent a 95% equal frequency ellipse.

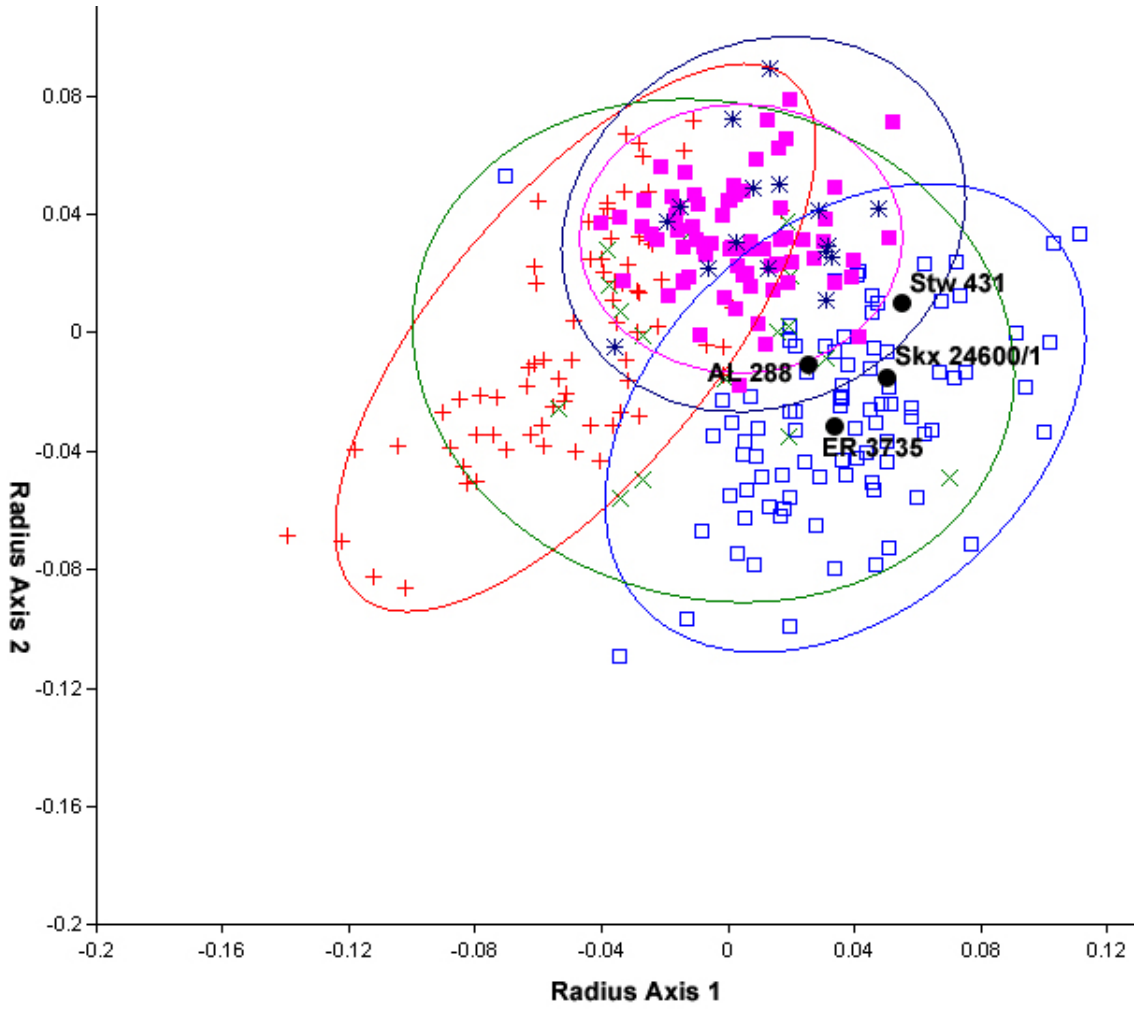

Fig. 3.65 2B-PLS analysis showing the relationship of the first and second radial axes based on a cross-covariance matrix of the humerus and radius GPAed landmark coordinates. *Homo* is represented by blue squares, *Pan troglodytes* by purple squares, *Pan paniscus* by blue stars, *Pongo* by green Xs, and *Gorilla* by red pluses. Fossils are labeled and in black. Closed curves represent a 95% equal frequency ellipse.

Humerus and Ulna

Figures 3.66-3.68 illustrate the results of a 2BPLS analysis of the humeroulnar joint. The landmark set for the ulna was reduced in order to include TM 1517. WT 15000 has been included despite being a juvenile simply because there are so few Plio-Pleistocene associated skeletons. There is excellent covariance between data blocks (fig. 3.66). All four fossils have a clear *Homo*-like ulnar morphology (fig. 3.67) and TM 1517 and AL 288 have a *Homo*-like humeral morphology as well (fig. 3.68). The position of AL 288 is particularly interesting as

when the humerus was combined with the radius in the previous analysis (fig. 3.64), the shape was most like either *Pan* or *Pongo.* Stw 431 falls in the zone of overlap between *Homo* and *Pongo* for the humerus (fig. 3.68), as opposed to the previous analysis where it was most similar to either *Pan* or *Pongo.* Finally, WT 15000 falls well outside the range of human variation for the humerus and within the zone of overlap between *Pongo* and *Gorilla* (fig. 3.68). It is possible that the fact that this specimen is a juvenile and has evidence of pathology has affected the data.

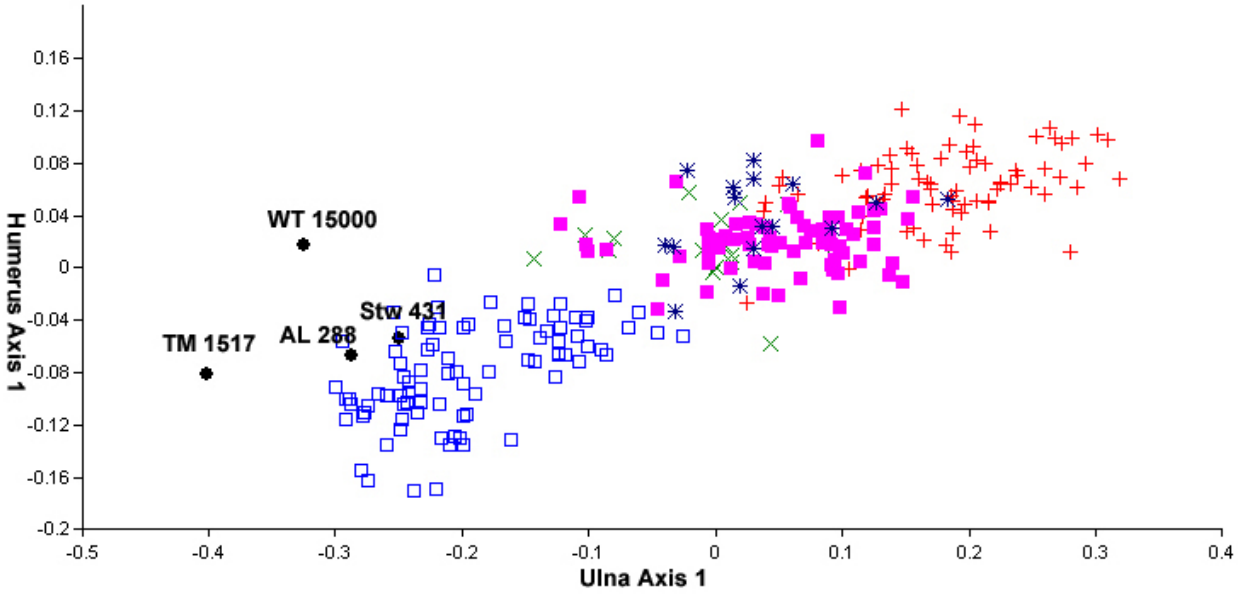

Fig 3.66 2B-PLS analysis of the distal humerus and proximal ulna. Only landmarks 1-5, 8-9, and 11-12 were used for the ulna so that TM 1517 could be included in the analysis. The first axis (presented here) accounts for 86% of the variation in the sample and has a correlation of 0.87. The second axis (not presented) accounts for 9% of the variation in this sample with a correlation of 0.65. *Homo* is represented by blue squares, *Pan troglodytes* by purple squares, *Pan paniscus* by blue stars, *Pongo* by green Xs, and *Gorilla* by red pluses. Fossils are labeled and in black. The RV coefficient for this data set is 0.5798.

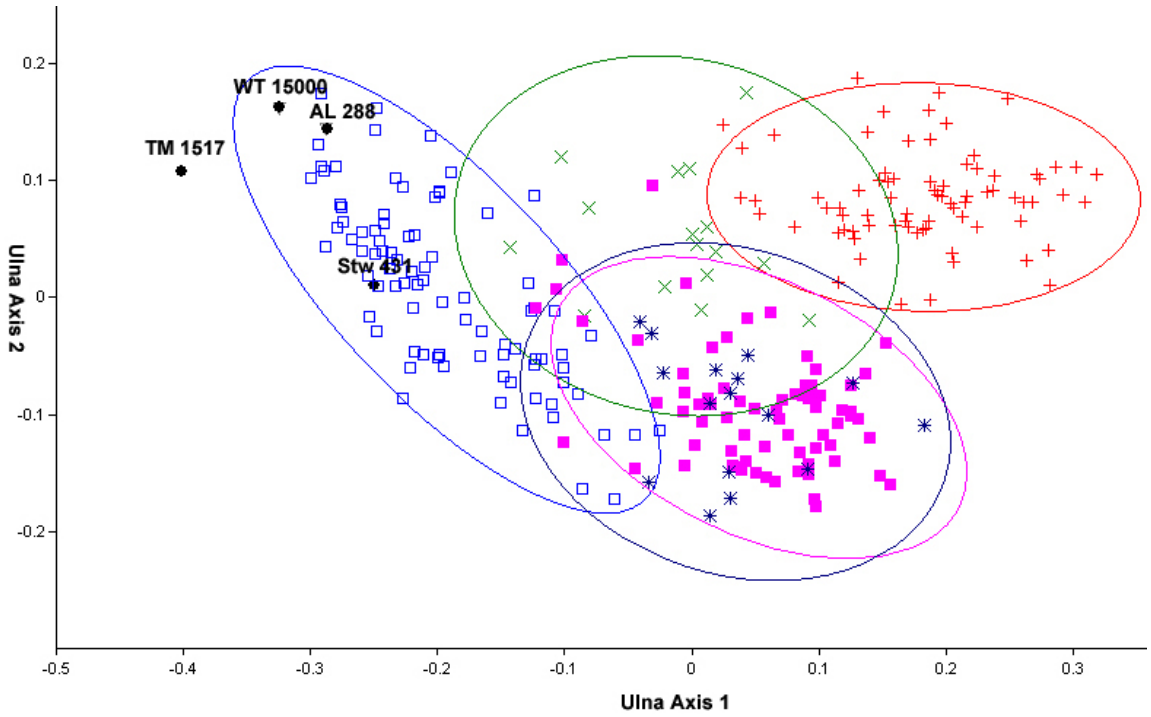

Fig. 3.67 2B-PLS analysis showing the relationship of the first and second ulnar axes based on a cross-covariance matrix of the humerus and ulna. GPAed landmark coordinates. *Homo* is represented by blue squares, *Pan troglodytes* by purple squares, *Pan paniscus* by blue stars, *Pongo* by green Xs, and *Gorilla* by red pluses. Fossils are labeled and in black. Closed curves represent a 95% equal frequency ellipse.

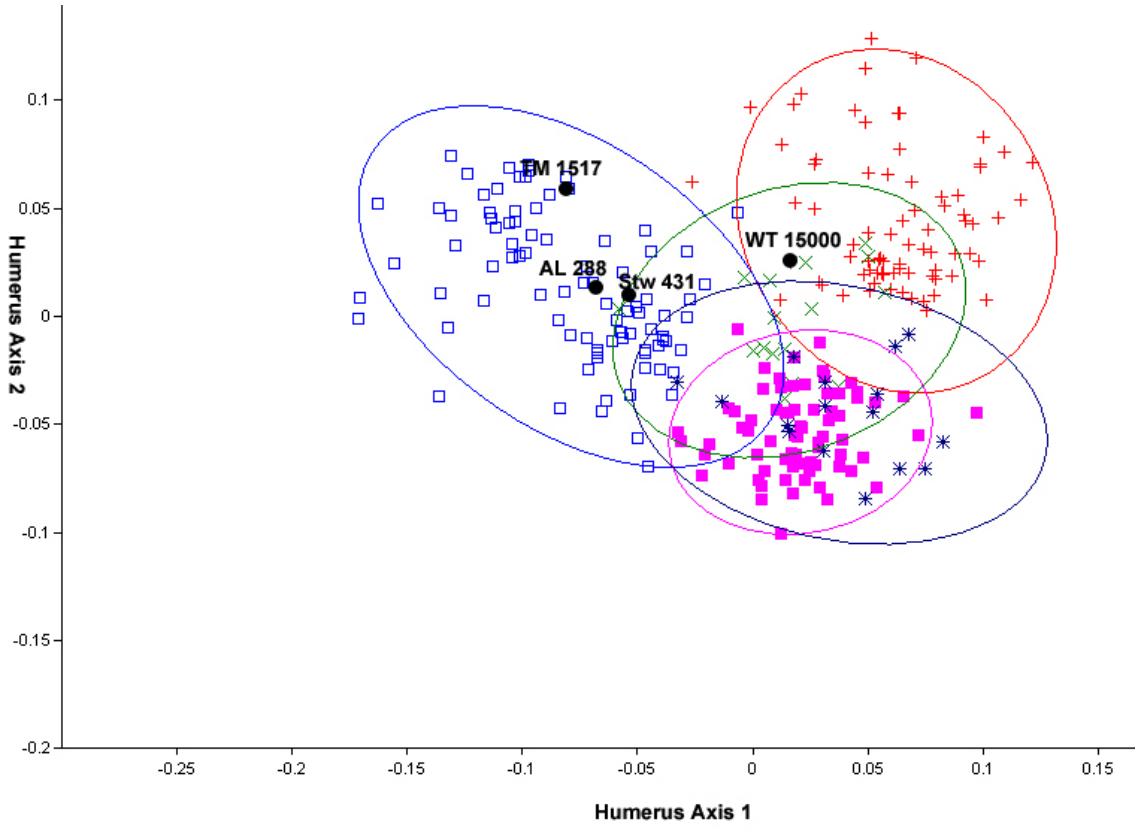

Fig. 3.68 2B-PLS analysis showing the relationship of the first and second humeral axes based on a cross-covariance matrix of the humerus and ulna GPAed landmark coordinates. *Homo* is represented by blue squares, *Pan troglodytes* by purple squares, *Pan paniscus* by blue stars, *Pongo* by green Xs, and *Gorilla* by red pluses. Fossils are labeled and in black. Closed curves represent a 95% equal frequency ellipse.

The data from these two analyses seem to reinforce the conclusion from the PCA analyses that a more modern looking humero-ulnar joint complex appeared before a more modern looking humero-radial joint complex. Perhaps this may indicate that selection was operating more strongly on the humero-ulnar joint, favoring morphology that allowed the muscles to be at their greatest advantage in flexed forelimb posture while retaining a more powerful, ape-like ability to pronate and supinate with the humero-radial joint.

Conclusions

- *Do different Plio-Pleistocene hominins have different patterns for the shoulder, elbow and wrist joints?*

There is a considerable amount of variation during the Plio-Pleistocene for the different elements. Of the elements sampled, the most informative parts were the distal humerus, the distal radius and the proximal ulna. The proximal radius and distal ulna also yielded interesting results, but results from those anatomical areas should be interpreted with caution due to the lack of separation extant between groups. The variation in the fossil sample was greatest in the distal humerus and the distal radius, whereas the proximal ulna was surprisingly homogenous within the fossil sample.

- *Do the changes in each of these joints follow a linear progression? If so, the most ape-like elbow joints would occur the earliest in time and the most human-like elbow joints would occur the latest in time. I hypothesized that there would be a considerable amount of variation, but that this variation would be largely uni-directional, leading from organisms with a clearly mosaic pattern to those which are obligate bipeds.*

In this case, the hypothesis was not supported by the data. The variation present in the elements of the forelimb does not appear to follow a pattern of increasing bipedalization. For the humerus, the most ape-like individuals were from Koobi Fora and occurred latest in time, whereas the most modern looking individuals were represented by *A. anamensis,* the earliest taxon sampled for the study. This pattern is also seen in the proximal radius, where individuals attributed to *A. afarensis* look more modern than those found at Koobi Fora. For the proximal ulna, almost all of the fossils looked like modern *Homo sapiens,* no matter how early or late in time they occurred. The only element that followed a somewhat linear pattern was the distal

radius, where individuals attributed to *A. anamensis* and *A. afarensis* were the most ape-like and earliest in time. However, in that analysis, *A. africanus* (Stw 46) was the most human-like.

- *For individuals that are either associated or have secure taxonomic attributions, is the taxonomic and functional signal the same across all bones? I hypothesized that it would be different, as different organisms could be practicing different locomotor repertoires, even if they are basically bipedal.*

Here, the hypothesis was supported by the data. If multiple segments of the postcranium are considered together, all of the different elements do not give the same signal. For *A. anamensis*, the distal humerus looks very modern whereas the distal and proximal radius look more pleisomorphic. For *A. afarensis,* the distal humerus and proximal ulna look very modern whereas the distal radius looks more pleisomorphic. *P. robustus* has an ape-like distal humerus and a more modern looking distal radius. Of all of the taxa sampled, only *A. garhi*, *H. habilis sensu lato* and *H. erectus* had the same affiliation for all segments analyzed (table 3.5).

Table 3.5 A list of fossil taxa and their affiliations in the various analyses. Multiple affiliations indicate that different individuals were similar to different extant groups. See each of the individual sections for more details.

	Humerus		**Radius**		**Ulna**	
	Proximal	Distal	Proximal	Distal	Proximal	Distal
A. .anamensis	Unique	Human	Ape	Ape	n/a	n/a
A. .afarensis	Unique	Human	Human	Ape	Human	Ape/Unique
A. africanus	Unique	Human	Human	Human	Human	Human/Ape
A. garhi	n/a	Human	Human	n/a	Human	n/a
P. boisei	n/a	n/a	Ape	n/a	Human	n/a
P. robustus	n/a	Unique	n/a	Human	Human	n/a
H. habilis sensu lato	n/a	Ape	Ape	n/a	Ape	n/a
H. erectus	n/a	n/a	Human	n/a	Human	n/a

It is possible that these different suites of traits are the result of phylogenetic lag (Vrba, 1980; Vrba and Gould, 1986)**,** and the most important joints are being selected for first and the rest of the more modern adaptations evolved later in time. However, since some of these individuals have unique patterns not seen anywhere else, it is also possible that the evolution of bipedalism was a far more diverse process than originally thought and these differences would have had an impact on the locomotor repertoire of these individuals. The distinct patterns of covariation at the elbow of TM 1517 (*P. robustus*) and ER 3735 (*H. habilis sensu lato*) would argue for novel locomotor patterns that were selected for. Regardless, this study illustrates why it is important to consider the multiple postcranial elements when making functional and phylogenetic conclusions about fossil taxa.

- *Are there any solid clues in the forelimb that indicate a particular mode of locomotion as the precursor to bipedalism?*

While there are adaptations present in some elements that indicate varying degrees of arboreality, there were no definitive markers for either knuckle-walking or suspensory behavior. If the data are taken as a whole, they would probably point to a more generalized quadruped with a flexible locomotor pattern that had the ability to change and adapt in many different ways.

CHAPTER 4: THE LOWER LIMB

Introduction

The adaptation for bipedal posture has long been thought to be one of the hallmarks of humanity. Charles Darwin wrote that:

> "Man alone has become a biped; and we can, I think, partly see how he has come to assume his erect attitude which forms one of his most conspicuous characters … If it be an advantage to have the hands and arms free, of which, from his preeminent success at life, there can be no doubt, then I can see no reason why it should not have been advantageous to the progenitors of man to become more and more erect or bipedal (1871: 76-77)."

However, the timing and pacing of the evolution of bipedal posture, as well as its selective advantage, has been the subject of many scientific debates. Some researchers have suggested that obligate bipedalism evolved very early and the locomotion we see in humans today differs very little from that of our earliest ancestors (*i.e.* Lovejoy, 1981 *et seq.*), whereas others have championed the idea that the earliest hominins retained adaptations for arboreal behavior until the emergence of *Homo erectus* (Stern and Susman, 1983 *et seq.*) and that the forms of locomotion in the Plio-Pleistocene were more diverse than the earlier researchers believed (McHenry and Brown, 2008).

Australopithecus afarensis is one of the most often studied species of early fossil hominins. This likely has to do with the abundance of both cranial and postcranial fossil material as well as the presence of a semi-complete skeleton, AL 288. These analyses have yielded largely contradictory results in terms of the locomotor function of this taxon. While some authors have concluded that the bipedal gait of *Australopithecus afarensis* was largely identical to that of modern humans (Lovejoy, 1988; Lovejoy *et al.*, 2002), other have postulated that *Australopithecus afarensis* represents a compromise morphology between increasing

terrestriality and continuing arboreality (Stern and Susman, 1983; Susman *et al.,* 1984, 1985; Rose, 1991; Hunt, 1994).

Researchers have found evidence throughout the postcranial skeleton that indicates *A. afarensis* still practiced some form of arboreality as part of its locomotor repertoire. The hindlimb of *A. afarensis* is absolutely shorter and the foot absolutely longer than the pattern seen in modern humans, which would have led to shorter, slower, less energetically efficient strides. The pedal phalanges are long and curved, and the overall pedal morphology points towards a more medio-laterally flexible foot than that seen in modern humans (Susman *et al.,* 1985). The scapular morphology of the new juvenile specimen from Dikika has a superiorly facing glenoid fossa and is phenetically most similar to modern *Gorilla.* This could indicate a more anteriorly placed shoulder girdle that is functionally linked to the head and neck as well as a greater reliance on postures where the arms are extended over the head (Alemseged *et al.,* 2006).

There are also contradictory findings for the number and composition of the species within the *A. afarensis* hypodigm represented by hindlimb material. Senut and Tardieu (1985) examined ER 1481, 1472, 1500 and AL 129-1a, 288, 333-4 and 333x-26 and found there to be two different groups of Plio-Pleistocene hominins based on the anatomy of the knee joint: These authors placed ER 1481, ER 1472, AL 333-4 and AL 333x-26 in a human-like group (genus *Homo)* and AL129-1a, AL288 and ER 1500 in an ape-like grouping (genus *Australopithecus*). They based these grouping on four different characters in the knee joint: the shape of the distal articular surface of the femur; the shape of the intercondylar notch; the degree of symmetry between the two femoral condyles; and the degree to which the tibial spine fit closely into the intercondylar notch on the femur. Their fourth trait relied upon the idea that the human meniscus has two points of attachment whereas the ape meniscus has only one; later studies have found

this trait to be quite variable in both human and ape populations (Dugan and Holliday, 2009). Conversely, Lague (2002) also examined the distal femora of AL 333-4 and AL 129-1a and concluded that they were not sufficiently different in size or shape to merit splitting them into different genera or species. He also concluded that the Hadar specimens are intermediate in shape between modern humans and apes.

Analyses of the locomotor repertoire of the taxa from Koobi Fora are problematic due to the presence of multiple sympatric hominins, disagreement about the number and patterning of taxa based on cranial remains and the scarcity of associated remains. Of particular difficulty is the differentiation between *H. habilis* and *H. rudolfensis.* Some researchers believe that *H. habilis* is a sexually dimorphic taxon represented at both Koobi Fora and Olduvai Gorge (Tobias, 1991; Miller, 1991) while others believe that the array of material first attributed to *Homo habilis* actually represents two taxa – *H. habilis* and *H. rudolfensis.* In this taxonomic scheme, the larger cranial material would belong in the taxon *H. rudolfensis* and the smaller cranial material – including the partial skeletons of OH 62 and ER 3735 – would belong in *H. habilis* (Wood, 1985; Wood and Chaberlain, 1987; Wood, 1991, 1992). The remains of OH 62 have been reconstructed to be relatively ape-like (Hartwig-Sherer and Martin, 1991) and to have ape-like limb strength proportions (Ruff, 2009). The ape-like reconstruction of the OH 62 skeleton has even prompted some researchers to move *Homo habilis* into the genus *Australopithecus* (Wood and Collard, 1999). ER 3735 has been seen as very similar to OH 62 (Leakey *et al.* 1989) and has been reconstructed to have ape-like limb proportions and a mosaic of ape-like and human-like traits (Hauesler and McHenry, 2007). Stern and Susman (1982) have suggested that *Homo habilis* had a human-like lower limb in combination with an ape-like upper limb based on their findings from the OH 35 tibia and assumptions that the OH 35 tibia, OH 8 foot and OH 7 hand

and mandible represent a single individual. However, there evidence that the OH 8 foot and the OH 7 hand and mandible are from at least two individuals, one being and adult and one being a subadult (DeSilva *et al.* in press).

There are no definitive hindlimb remains of *Homo rudolfensis*, although ER 1481 and ER 1472 have been sometimes referred to this taxon based on size and locality (*e.g.*, Wood, 1992). But because those two elements are not associated with any cranial remains, such attributions must be speculative – as are any reconstructions of the locomotor repertoire of *H. rudolfensis.* Occurring sympatrically with *H. habilis* and *H. rudolfensis* are *Homo erectus* and *Paranthropus boisei.* The *Homo erectus* postcranium in Africa is represented by the full skeleton of WT 15000. From this skeleton, *H. erectus* has been reconstructed to have modern human-like body plan and an efficient bipedal gait (Walker and Leakey, 1993). The known presence of a sympatric, fully bipedal hominin from East Africa futher clouds an assignation of a human-like unassociated postrcranial element (such as ER 1481) to *Homo rudolfensis* (Tobias, 1991).

ER 1500 is the only associated skeleton of *Paranthropus boisei* and consists of both forelimb and hindlimb elements and has been reconstructed to be *Australopithecus*-like in postcranial form and function (Grausz *et al.* 1988), although Wood (1991) suggested that it could be from *H. rudolfensis* based on the mandidule and DeSilva (2007) suggested that this specimen could belong to *H. habilis* based on phenetic similarity with the OH 35 tibia. McHenry (1991) has argued that all of the postcranial remains from Area 6A in Ileret could be referred to *P. boisei* as all of the cranial remains from that locality have been referred to *P. boisei.* It is from these remains (as well as those from South Africa) that he concluded that the bodies of all of the "robust australopithecines" were smaller than what would be expected based on their cranial remains (McHenry, 1991).

Various postcranial remains from the South African sites of Swartkrans and Sterkfontein have been attributed to *Australopithecus africanus*, *Paranthropus robustus, Homo habilis* and *Homo erectus.* Almost all of the postcranial remains from Swartkrans have been attributed to *P. robustus* based on the abundance of *P. robustus* cranial remains from that site. By this logic, the SK 82 and SK 97 proximal femora have been attributed to *P. robustus* and this taxon has been reconstructed to have ape-like locomotor pattern based on their cross-sectional geometry (Ruff *et al.* 1999) but a more human-like locomotor pattern based on their shape (Robinson,1972).

The *A. africanus* hypodigm from Sterkfontein has been considered one cohesive taxon (Robinson, 1972) or potentially multiple taxa (Harmon, 2009) based on the hindlimb remains. Functionally, they have been reconstructed to have a more ape-like mode of locomotion based on overall postcranial similarities to *A. afarensis* (McHenry, 1986) and similarities between their proximal tibiae and those of chimpanzees (Berger and Tobias, 1996). Conversely, they have also been reconstructed to have a very human-like form of bipedalism based on similarities to modern humans (Lovejoy and Heiple, 1970).

Considering all of these debates, this chapter aims to answer three basic research questions:

- *Do different Plio-Pleistocene hominins have distinct morphological patterns for the proximal and distal femur?* If there is more variation in the fossil sample for a limb segment than seen in any of the extant species, then it could be reasonably concluded that there are different patterns in various species of hominins. However, if there is less than or equal variation in the fossil sample as compared to the extant sample, then it could be concluded that there is no specific pattern that characterizes any of the different hominins

species for the bones of the hindlimb.

- *Do the changes in each of these joints follow a linear progression?* If changes in postcranial morphology follow a linear progression, then changes towards a human-like condition should roughly correlate with the age of the fossil, with the most ape-like individuals occurring the earliest in time and the most human-like individuals occurring the latest in time. If there is no temporal pattern to the postcranial affiliation, then it could be concluded that changes towards a human-like pattern occur randomly, as opposed to linearly.

- *For individuals that are either associated or have secure taxonomic attributions, is the taxonomic and functional signal the same across all segments, or is the pattern mosaic?* If a particular fossil taxon is always affiliated with the same extant taxon regardless of what segment is sampled, then it could be concluded that the functional and taxonomic signal is consistent across all the bones of the hindlimb. If a fossil taxon is affiliated with different extant taxa depending on the segment, then it would have a more mosaic morphological pattern.

Materials and Methods

Table 4.1 List of specimens used for the analyses of the femur. Please note that not all analyses used every specimen.

Proximal Femur	Distal Femur
AL 128	AL 129-1a
AL 129-1c	AL 333-4
AL 288	AL 333w-56
AL 333-3	BOU-VP-19/63
AL 333-123	ER 993
ER 738	ER 1472
ER 1472	ER 1481
ER 1481	ER 1500
ER 1503	ER 1592
MAK-VP-1/1	ER 3951
OH 20	Kibish 1 (Omo)
SK 87	SK 1896
SK 97	Sts 34
Sts 14	Stw 129
Stw 99	Stw 318
Stw 522	TM 1513
WT 15000	TM 3601
	WT 15000

Table 4.2 List of specimens used for the analyses of the tibia.

Proximal Tibia	Distal Tibia
AL 129-1b	AL 288
AL 288	AL 333-6
AL 333x-26	ER 1481
AL 333-42	ER 1500
BOU-VP-1/109	KP 29285
EP 1000/98	OH 35
ER 741	Stw 181
ER 1471	Stw 358
ER 1476	Stw 389
ER 1481	Stw 567
ER 1500	WT 15000
ER 1810	
ER 2594A	
KP 29285	
Stw 514	
WT 15000	
WT 19700	

The proximal and distal portions of the femur were analyzed separately. The proximal femur was further subdivided into two discrete anatomical areas: the femoral head/neck and the greater trochanter. Fossil preservation in the proximal femur is extremely variable, so multiple analyses using different landmark configurations were completed in order to include the greatest number of fossil specimens for each of these areas. The preservation of the distal femur was less variable, but still multiple analyses were run concentrating on the entire distal portion and then each condyle in order to include the greatest possible number of specimens.

Similarly, the proximal and distal portions of the tibia were also analyzed separately. Analyses were run on the full proximal tibia and landmarks 10-18 of the distal tibia. Landmarks 10-18 captured the full distal articular surface. Several fossils had broken or abraded medial malleoli; thus the points capturing that area were excluded.

Data were subjected to principal components and regression analyses using *PAST ver. 1.89* (Hammer *et al.,* 2009), and shape changes were visualized using *morphologika*^{2} (O'Higgins, 2006) and *Morpheus* (Slice, 1998). Shape changes were visualized as deformations between extant genera and fossil taxa along the major principal axes. A two-block partial least squares analysis (2B-PLS) was conducted using *PAST* on the elements comprising the knee joint. 2B-PLS is a way of assessing the covariance between two independent sets of data (Rohlf and Corti, 2000), and has been used successfully to look for covariance between shape data and geographical coordinates (Frost *et al.,* 2003) as well as patterns of covariance between dorsal and ventral views of mouse skulls (Corti and Fadda, 1996) and hominoid distal tibial and proximal astraglar articulations (Harcourt-Smith *et al.,* 2008).

Post-hoc analyses were run on specifically the proximal femur in order to assess the breadth of variation within *Australopithecus afarensis* by comparing pair-wise procrustes distances within the fossil sample to both intra- and interspecific pair-wise procrustes distances within each extant group (after Harmon, 2008). If the pairwise distance between the fossils exceeded 95% of the pairwise distances within the extant species, then this would support the hypothesis that there are multiple species within the *A. afarensis* hypodigm. If the pairwise distances between the fossils were less than 95% of the extant taxa, then I would reject that hypothesis. The proximal femur is the only segment where there is a larger number of *A. afarensis* individuals. No other groups approach the number of *A. afarensis* specimens in any segment sample, partially because of the problems with attribution at sites such as Koobi Fora.

A second post-hoc analysis was run on the distal femur to assess whether or not shape differences between the fossils in the distal femur are the result of heterochronic change. Two landmark configurations for distal fossil femora were subjected to a PCA and regression analysis

with separate ontogenetic samples of *Homo* from the Musée de L'Homme and *Pan troglodytes troglodytes* from the PCM. The first analysis used all of the landmarks in the distal femur; the second used only the landmarks describing the lateral condyle. The age of the *Homo* individuals was taken from the catalogues at the museum, and the age range spans from 2 to 20 years (n = 23). Sex was taken from the museum catalogue for younger individuals or assessed by pelvic morphology for the older individuals. For *Pan,* tooth eruption and epiphyseal closure were used as a proxy for age and were scored on a 1 to 7 scale (data from Gordon and Wood, humansoriginsdatabase.org, 2010**;** table 4.3). Sex was taken from the museum catalogue.

Table 4.3 A list of scores and the number of individuals for each taxa per score.

Score	Description	*Pan* n = 38
1	No epiphyses fused; M1 erupting	1
2	No epiphyses fused,; M1 erupted	10
3	No epiphyses fused; M2 erupting	7
4	No epiphyses fused; M2 erupting; P3-P4 erupted	2
5	Some epiphyses partially fused; M2 erupted	9
6	Some epiphyses partially fused; M3 erupting	5
7	Most epiphyses partially or fully fused; M3 erupted	2

Data and Analysis

Full Femur

Figure 4.1 is a PCA of the complete femur. For the entire sample, there is excellent separation between all of the extant genera. PC 1 is driven by the orientation of the femoral head and the presence of a bicondylar angle. In *Homo*, the femoral head is oriented the most proximally, whereas it is oriented most medially in *Gorilla,* and there is a bicondylar angle in *Homo* and not in the other taxa in this sample. PC 2 is driven by the depth of the trochanteric

fossa in the proximal femur and the intercondylar distance in the distal femur. *Pan* has an extremely deep trochanteric fossa with a narrow intercondylar distance whereas *Pongo* has a relatively shallow trochanteric fossa and a wider intercondylar distance. WT 15000 (*Homo erectus*) is the only fossil femur in this sample, and it falls squarely within the modern human distribution.

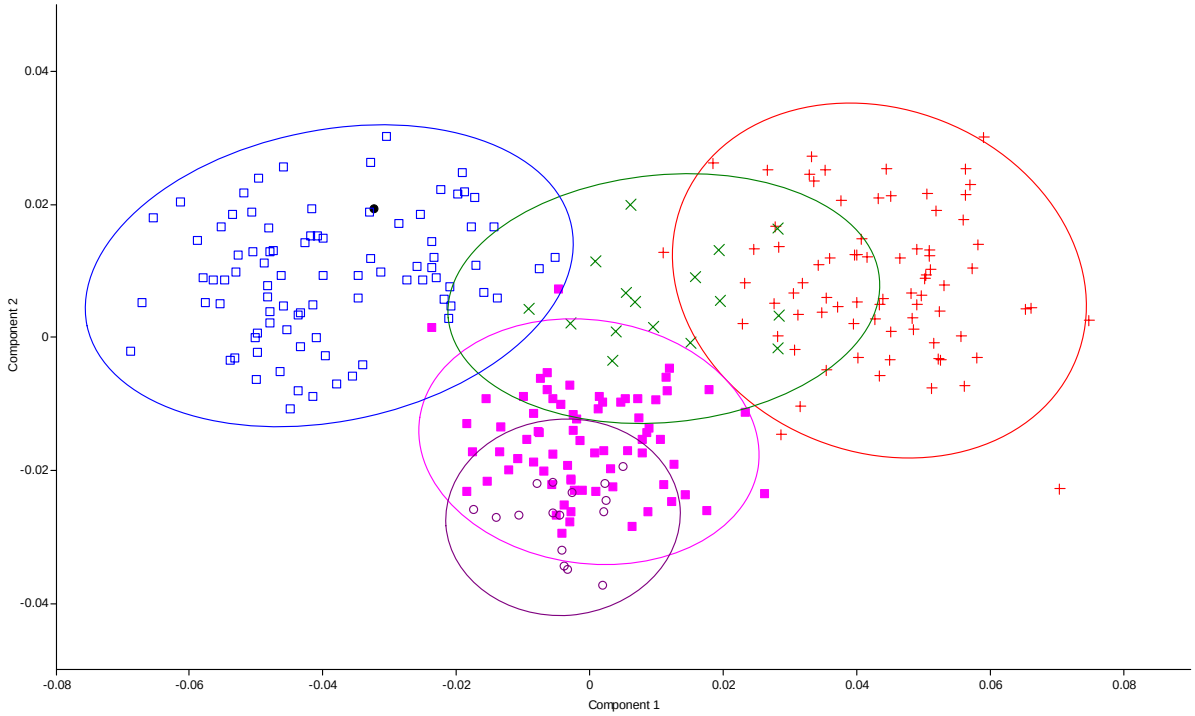

Fig. 4.1 Principal components analysis of the full femur. *Homo* is represented by blue open squares, *Pongo* by green Xes, *Gorilla* by red crosses, and *Pan troglodytes* by purple squares *with Pan paniscus* as purple open circles. The only fossil in this analysis is WT15000, and it is represented by the black circle. PC1 accounts for 48.79% of the total variance and PC2 accounts for 9% of the overall variance. Each closed curve represents a 95% equal frequency ellipse.

PC 1 is positively correlated with centroid size (fig 4.2), although the r-squared value of 0.41 indicates that it is not a perfect correlation with male and female *Gorilla* falling off of the

regression line. PC 2 is negatively correlated with centroid size (fig 4.3) and in this instance, *Pongo* falls off of the regression line.

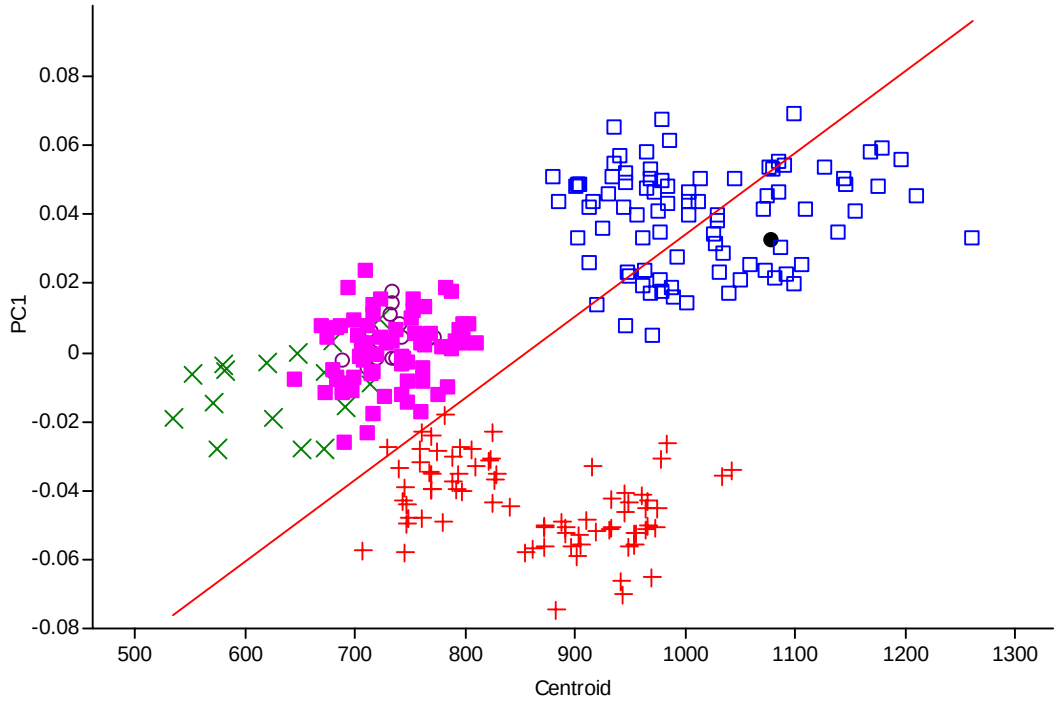

Fig 4.2 Regression of PC 1 against centroid size for the complete femur with r = 0.42.

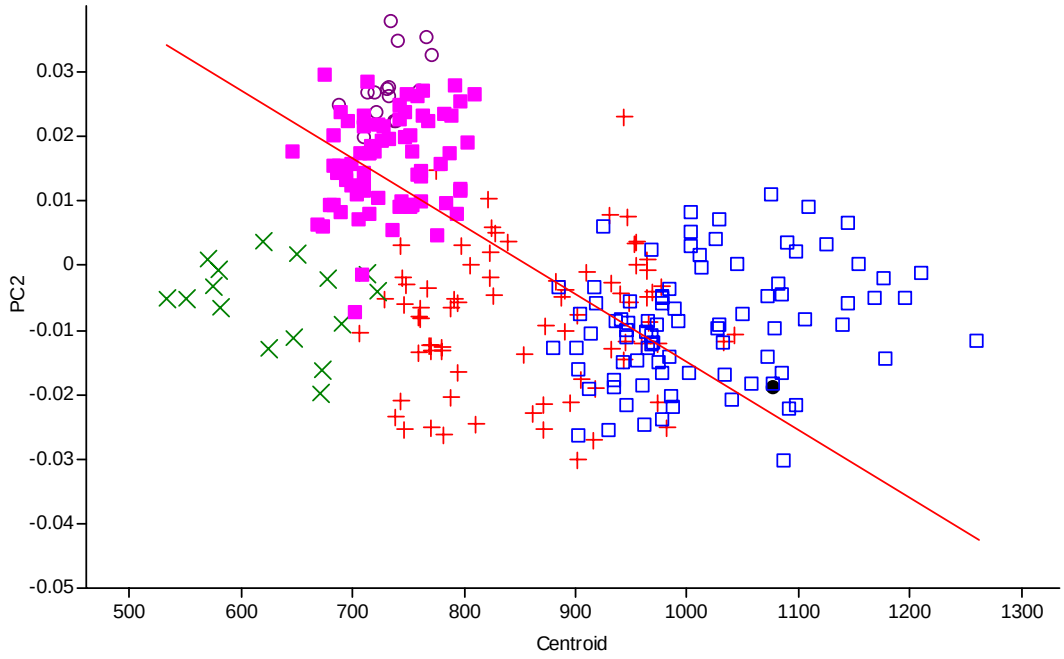

Fig 4.3 Regression of PC 2 against centroid size for the complete femur with r = -0.46.

Full Femur Discussion

The major anatomical differences between the extant genera are all related to the acquisition of upright posture in modern humans. A bicondylar angle places the knee directly below the body, allowing for economical weight transfer and full extension of the knee. A more proximally oriented femoral head and a long femoral neck allow for a greater range of motion in the hip joint (Aiello and Dean, 1990). Chimpanzees have a very distinct trochanteric fossa form, as it is deep and very vertically oriented. Although the trochanteric fossa is where the obturator externus and other lateral rotators of the hip insert (Aiello and Dean, 1990), the orientation and depth of this cavity in chimpanzees is not functionally related to this insertion (Gregory, 1950).

Proximal Femur Data

Figure 4.4 illustrates the positions of the landmarks and the wireframes for the proximal femur. A PCA for the full proximal femur is presented in figure 4.5. There is excellent separation among all of the extant genera, although *Pongo* overlaps with *Gorilla* and *Pan.* PC 1 separates *Homo* from *Pongo/Pan* and *Gorilla* and is driven by the lateral extension and height of the greater trochanter and the tilt of the femoral head. In *Homo*, the greater trochanter is relatively low, but it projects laterally, and the head is tilted more proximally. In the extant apes, the proximal extension of the femoral head and the greater trochanter are almost even. PC 2 separates *Gorilla* from all of the other taxa. It is driven largely by the depth of the trochanteric fossa which is extremely deep in *Pan.* In some *Pan* individuals, the trochanteric fossa is continuous with the medullary cavity (Gregory, 1950) whereas in *Gorilla,* the trochanteric fossa is extremely shallow. The majority of the fossils fall within the range of modern humans. SK 82 and SK 97 are just outside of the 95% equal frequency ellipses for modern humans, but not

inside the confidence interval of any of the other extant taxon. AL 333-3 is the only fossil that falls within the distribution of a different taxon; in this case, AL 333-3 falls in the area of overlap between *Pongo* and *Gorilla.* Figure 4.5 shows a side by side comparison of most of the complete fossil proximal femora. Both PC 1 and 2 are positively correlated with centroid size.

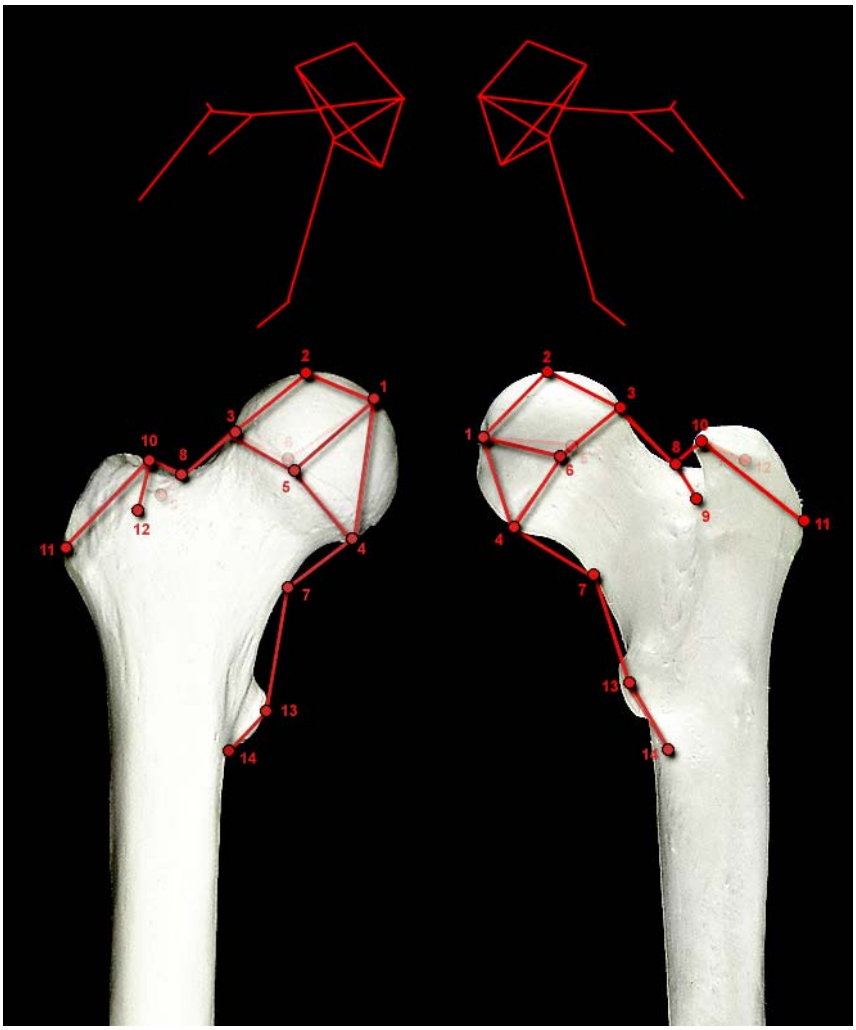

Fig. 4.4 This photo shows the positions of the landmarks on a human proximal femur, overlaid by a wireframe. The actual wireframes used in the analysis are shown above the anterior and posterior views for comparison.

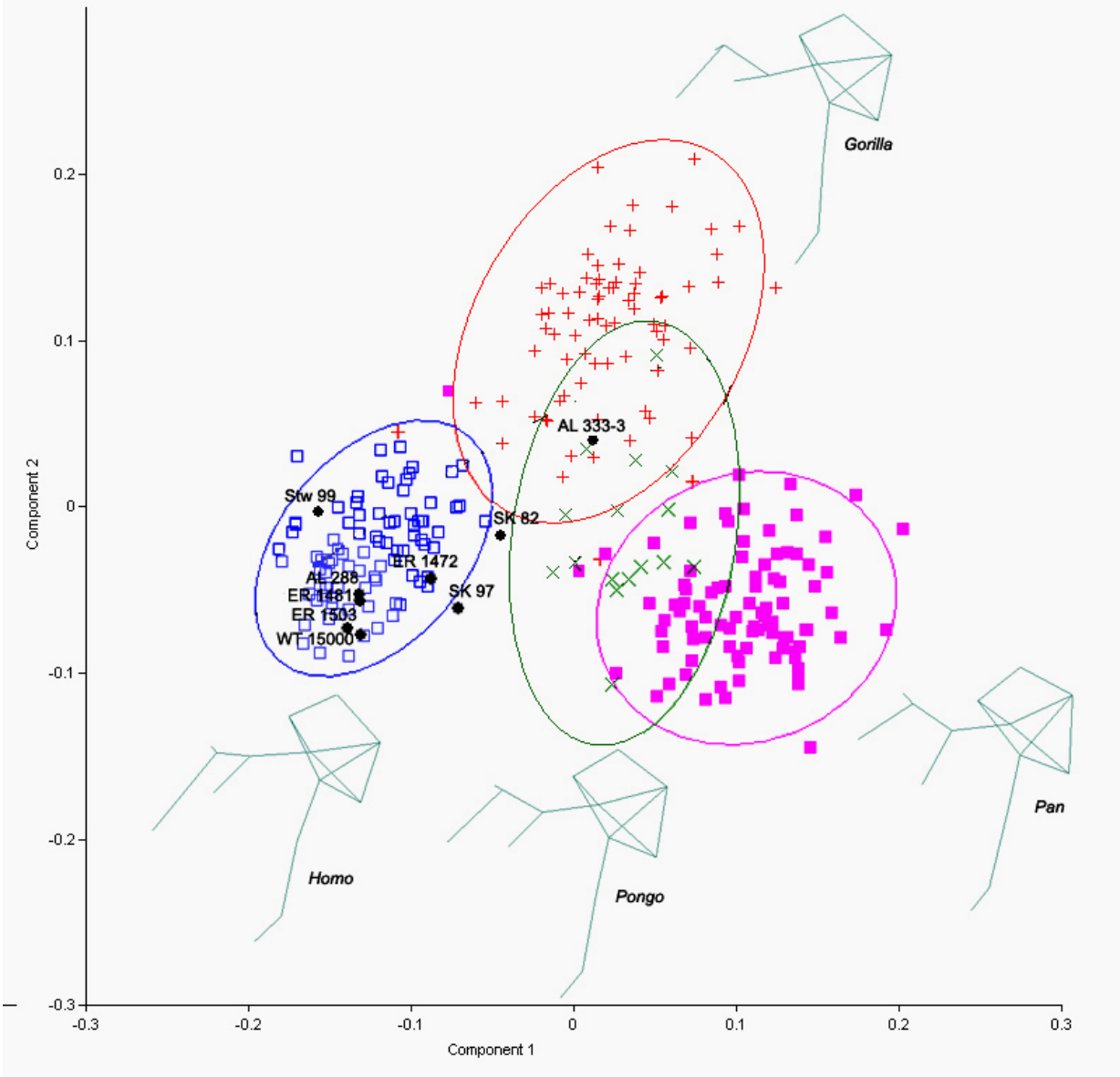

Fig. 4.5 Principal components analysis of the full proximal femur. *Homo* is represented by blue open squares, *Pongo* by green Xes, *Gorilla* by red crosses, and *Pan* by purple squares. The fossils are represented by black circles and are labeled in the graph. The wireframes are an anterior view of the proximal femur and they are taken from the middle of each extant grouping. PC1 accounts for 32% of the total variance and PC2 accounts for 19% of the overall variance. Each circle represents a 95% equal frequency ellipse.

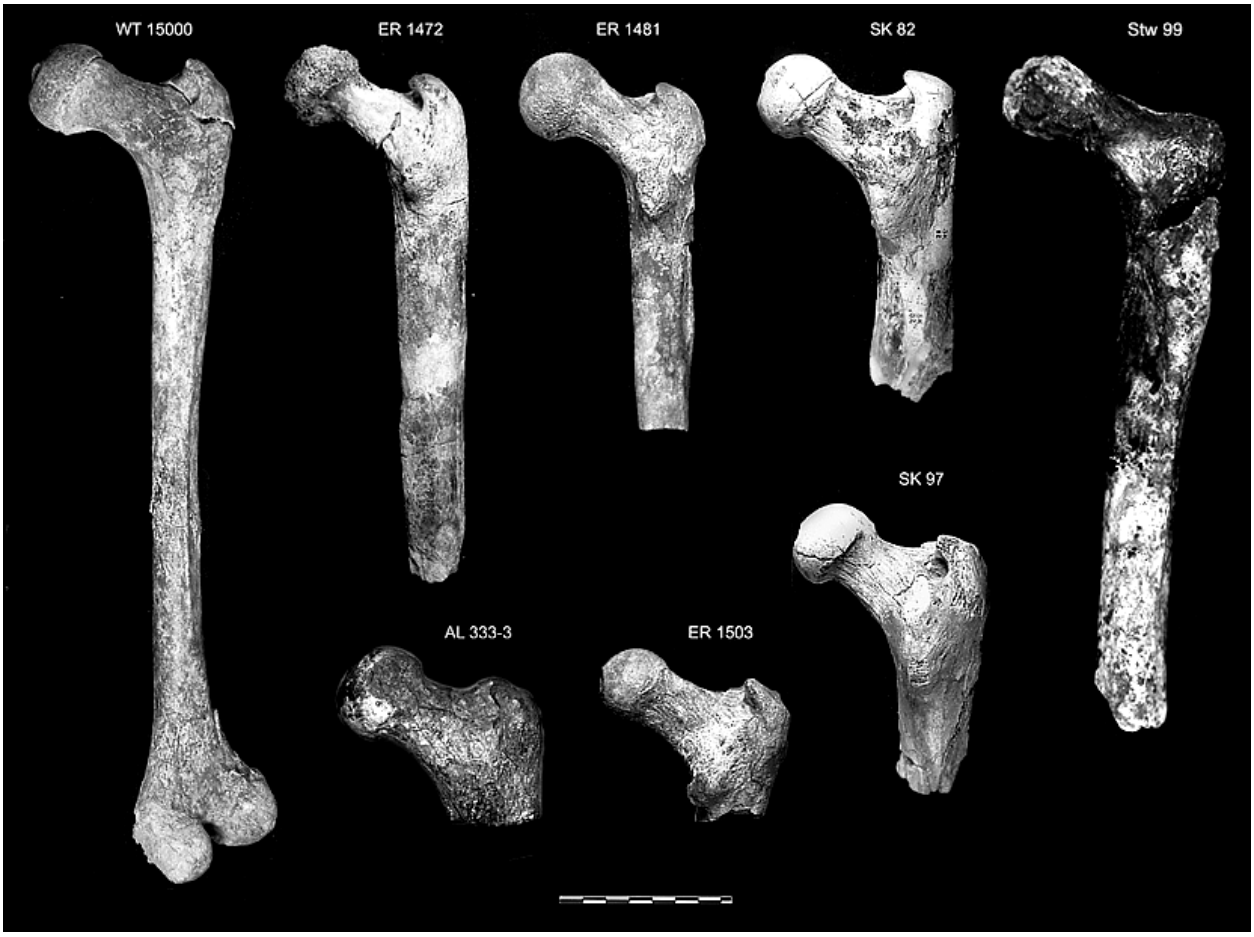

Fig. 4.6 Side by side comparison in posterior view of all of the full proximal femora from the Plio-Pleistocene, excluding AL 288 which wasn't photographed. All femora were placed in approximately the same position, mirrored (if necessary – ER 1481 and WT 15000) and scaled using Adobe Photoshop 7.0.

Means were calculated for all of the extant taxa and further analyses were performed using those means and the values for each fossil individual. Figure 4.7 is a PCA with a minimum spanning tree (MST). These results further confirm the results of the analysis of the full data set. PC 1 one separates *Homo* and almost all of the fossils from the extant great apes and AL 333-3 while PC 2 separates AL 333-3 from the rest of the sample. The MST indicates that all of the fossils' nearest neighbor relationships are with other fossils or *Homo*, with the exception of AL 333-3 which is closest to *Gorilla.* In this case, PC 1 and 2 are not correlated with size. PC 1 is driven by the low, laterally projecting greater trochanter in *Homo* and the relatively higher, less projecting one in the extant great apes. PC 2 is driven by the morphology

of AL 333-3, which is unique unique in that it combines a lower, slightly more projecting trochanter with a short femoral neck and a relatively large femoral head (see the analysis section for a discussion of this).

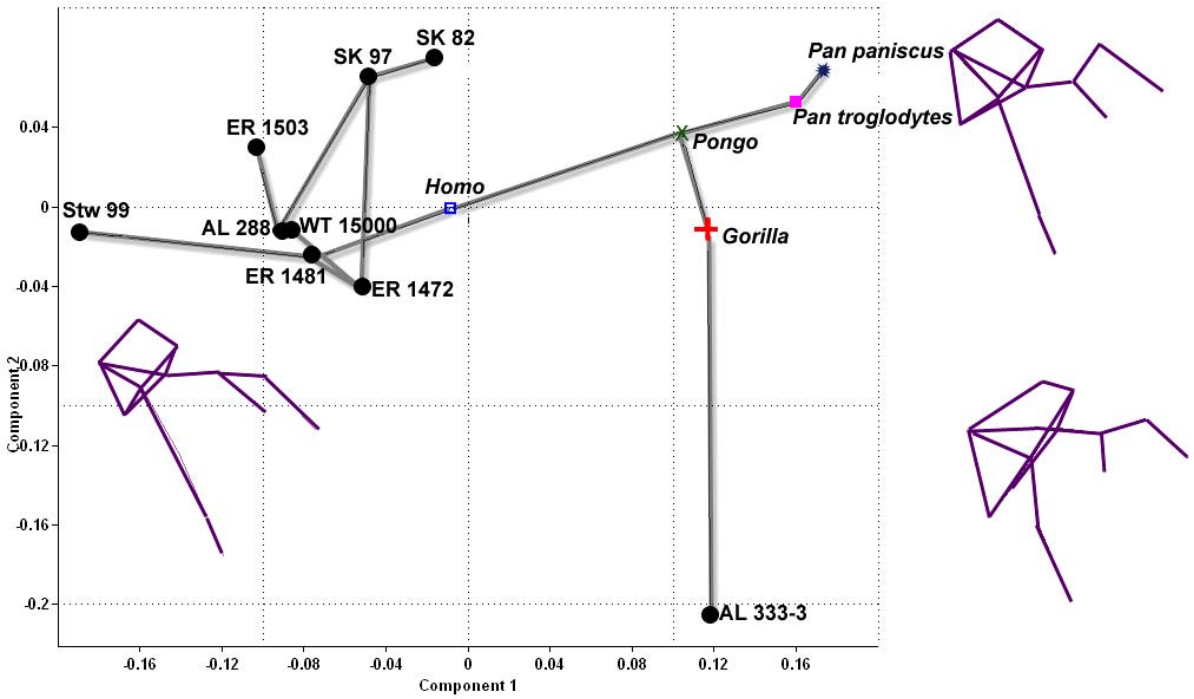

Fig. 4.7 Principal components analysis for the fossils plus means for the extant species for the full proximal femur. The lines represent a minimum spanning tree plotted on top of the principal components graph. PC1 accounts for 40.5% of the total variance and PC2 accounts for 19.1% of the overall variance.

A neighbor-joining tree using Procrustes chord distances was also generated (fig 4.8)**.** The phylogenetic relationships as indicated by molecular data are captured with regards to the extant individuals and all of the fossils form a cluster with *Homo*, with the exception of AL 333-3. Amongst the fossils, the only cluster with strong bootstrap values is SK 82 and SK 97. This is not necessarily surprising as these specimens occupy similar positions in the previous analyses and are both attributed to *Paranthropus robustus* (Robinson, 1972). This suggests that they have a distinct morphology relative to the other fossils that loosely cluster together.

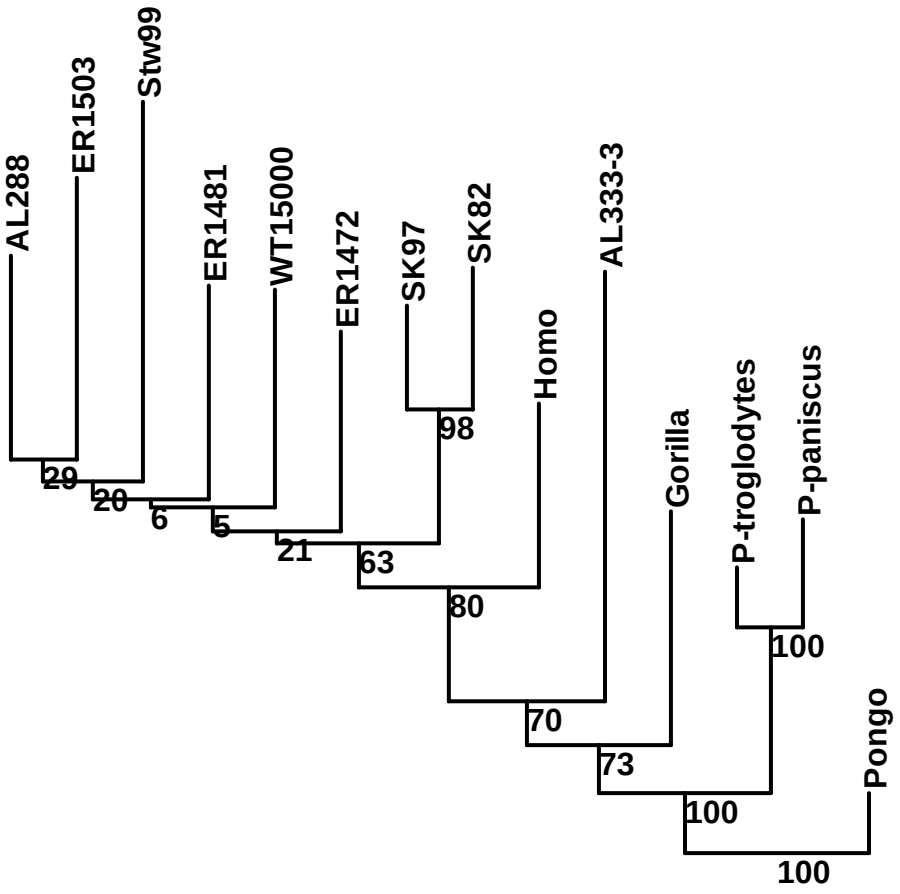

Fig. 4.8 Neighbor-joining tree using the procrustes chord distances for the means of the full proximal femur. The tree is rooted using *Pongo* as an outgroup. Bootstrapped values after 1000 replicates are given.

The proximal femur was then further segmented into anatomical areas to include more fossils in various analyses (Fig. 4.9). Landmarks 1 through 8 were utilized to represent the femoral head and figure 4.10 is a PCA of these landmarks. As can be expected, the separation between the extant taxa is not as good as it was for the entire proximal femur. PC 1 doesn't divide any of the extant taxa. It is driven by the height of the most anterior and posterior points on the femoral head. This accounts for the wide distributions of each extant taxon across PC1 as the analysis is certainly picking up slight differences in the way those type III landmarks were collected. PC 2 divides *Gorilla* from *Homo* with large areas of overlap and *Pongo* in between.

Fig. 4.9 Photographs of Stw 522 and ER 738, scaled mirrored (ER 738) and rotated to approximately the same orientation using Adobe Photoshop 7.0. These images are to the same scale as figure 4.6.

PC 2 is more biologically significant and is driven by the tilt of the femoral head and the depth of the femoral neck. Modern *Homo sapiens* have a deep femoral neck with a head that is tilted more proximally, whereas *Gorilla* has a much shallower femoral neck and a more medially facing femoral head. PC 1 is weakly correlated with size although PC 2 is not.

This analysis allowed for the inclusion of two additional fossils: Stw 522 and ER 738 (fig 4.9). All of the fossils used in the previous analysis grouped well within the 95% equal frequency ellipse for modern humans. ER 738 also fell within the distribution of modern humans, outside of any overlap zone. On the other hand, Stw 522 fell just inside the 95% equal frequency ellipse for modern humans and well within the 95% equal frequency ellipse for *Gorilla.* Once again, AL 333-3 grouped with *Gorilla.*

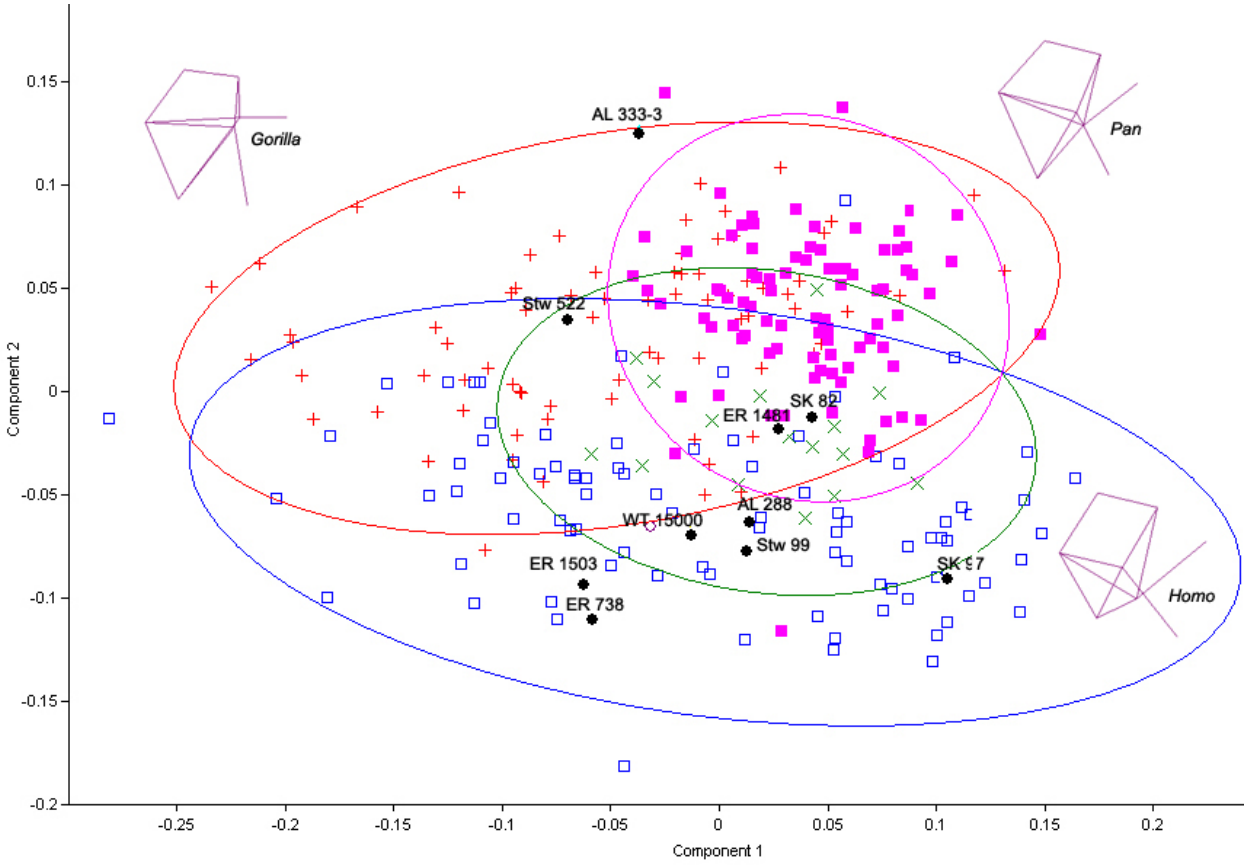

Fig. 4.10 PCA of the proximal femoral head using landmarks 1 through 8. In tests, removing landmarks 7 and 8 made it impossible to differentiate between any of the extant taxa. *Homo* is represented by blue open squares, *Pongo* by green Xes, *Gorilla* by red crosses, and *Pan* by purple squares. The fossils are represented by black circles and are labeled in the graph. PC 1 represents 26% of the variance within this dataset and PC 2 represents 14%. The wireframes represent a posterior view of the femoral head and are placed in the graph at approximately the same place the configuration was calculated.

Means were calculated for the extant taxa and a PCA with those values and those of the fossils was performed (fig 4.11)**.** The fossil individuals are distributed fairly evenly across PC 1, with ER 738 and AL 333-3 at either extreme. PC 2 separates AL 333-3 at one extreme and WT 15000 and ER 738 at the other extreme from the rest of the sample. PC 1 is driven by the overall length of the femoral neck and the tilt of the femoral head whereas PC 2 is driven by the medial protraction of the femoral head. AL 333-3 is from Hadar, usually considered *Australopithecus afarensis* and Stw 522 from Sterkfontein, usually considered *Australopithecus africanus* share a

near neighbor relationship with *Gorilla*, thus supporting the results from the PCA of the entire sample. The lack of differentiation between the fossils, *Homo* and the extant apes lends support to the idea that the points along the head and neck are not sufficient for capturing differences between bipeds and quadrupeds. PC 1 was not correlated with centroid size.

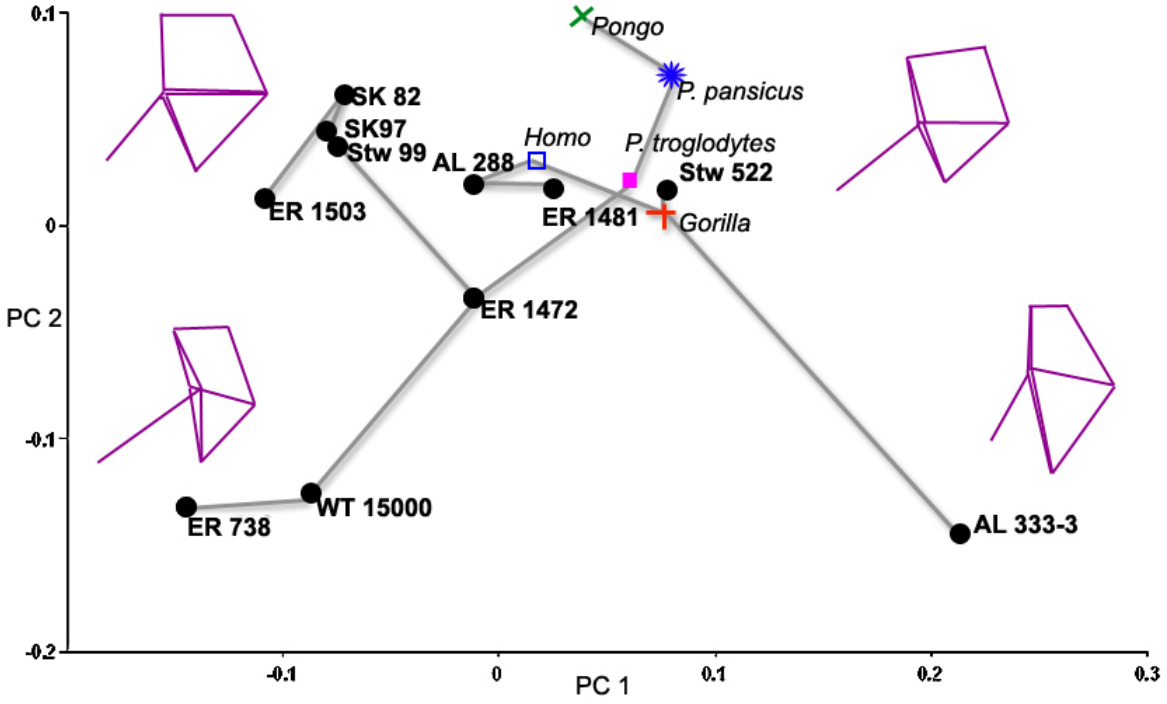

Fig. 4.11 Principal components analysis for the fossils plus means for the extant species for the femoral head. The lines represent a minimum spanning tree plotted on top of the principal components graph. PC1 accounts for 31% of the total variance and PC2 accounts for 20% of the overall variance. The wireframe is in a posterior view.

A neighbor-joining tree was also generated (fig 4.12) and the results of that analysis generally agree with the PCA. *Homo* is forms a cluster with AL 288 and together is outgroup to all of the other fossils. AL 333-3 and Stw 522 form a cluster with *Gorilla* instead of with the *Homo* and the other hominins. Bootstrap values are generally very low within the fossil clusters with the exception of SK 97 and SK 82 lending further support to their distinctness among the fossils, and WT 15000 and ER 738. WT 15000 is *Homo erectus* and ER 738 has no particular

attribution. Because the results of this analysis are not definitive, ER 738 should not be lumped into the same taxon with WT 15000, but the similarity should be noted.

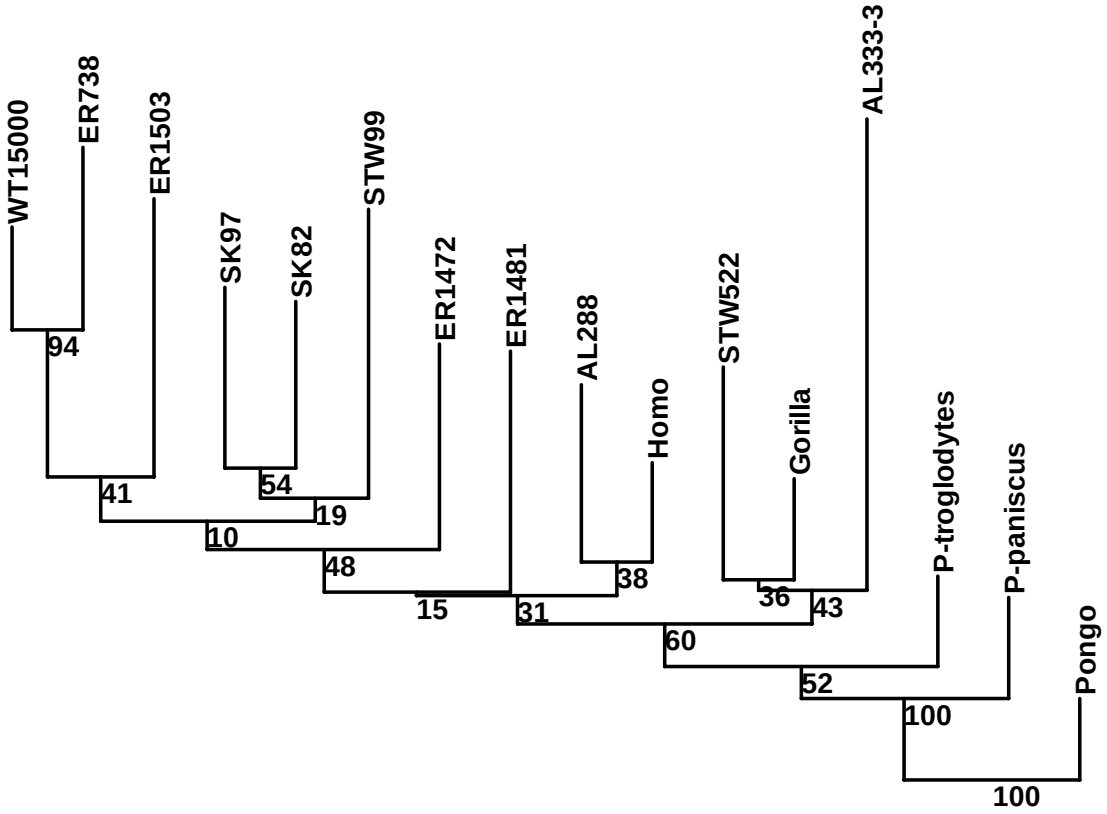

Fig. 4.12 Neighbor joining tree based on procrustes chord distances for the means for the femoral head. The tree is rooted with *Pongo* as an outgroup. Bootstrap values are given for 1000 replicates.

The landmark set for the proximal femur was further reduced to just the landmarks representing the shape of the proximal femur without the femoral head. A PCA (fig 4.13) was run using landmarks 7, 8, 9, 11 and 14 which allowed for the maximal inclusion of fossils while still retaining the differences between the extant taxa. These landmarks include the most medial point below the femoral head, the deepest point on the femoral neck, the deepest point in the trochanteric fossa, the most posterior point on the greater trochanter and the point just distal to the lesser trochanter. Point 10 is the height of the greater trochanter and was eliminated due to

breakage on some of the fossils. A second analysis was run (fig 4.16–18) which included this point and a slightly different set of fossils.

Despite reducing the landmark set to only five points, the differences between the extant taxa were largely still recovered. PC 1 separates *Gorilla, Pan* and *Homo* and PC 2 separates *Gorilla*, and to some degree *Pongo* from the rest of the extant taxa. PC1 is driven by the most lateral point on the greater trochanter and the overall orientation of the configuration of points. In *Homo,* the most lateral point on the greater trochanter is located more distally than in the other taxa and the configuration of points is oriented more proximally as a group. PC 2 is driven by the depth of the trochanteric fossa, with *Pan* having the deepest fossae and *Gorilla* the shallowest. The majority of the fossils fall well within the 95% equal frequency ellipse for modern humans. AL 333-3 falls within the distribution of *Pan* in this analysis. AL 333-123, and for the first time, SK 82 and SK 97 fall just outside the range of modern human variation within the range of *Pongo* variation. Both PC1 and PC2 are correlated with size.

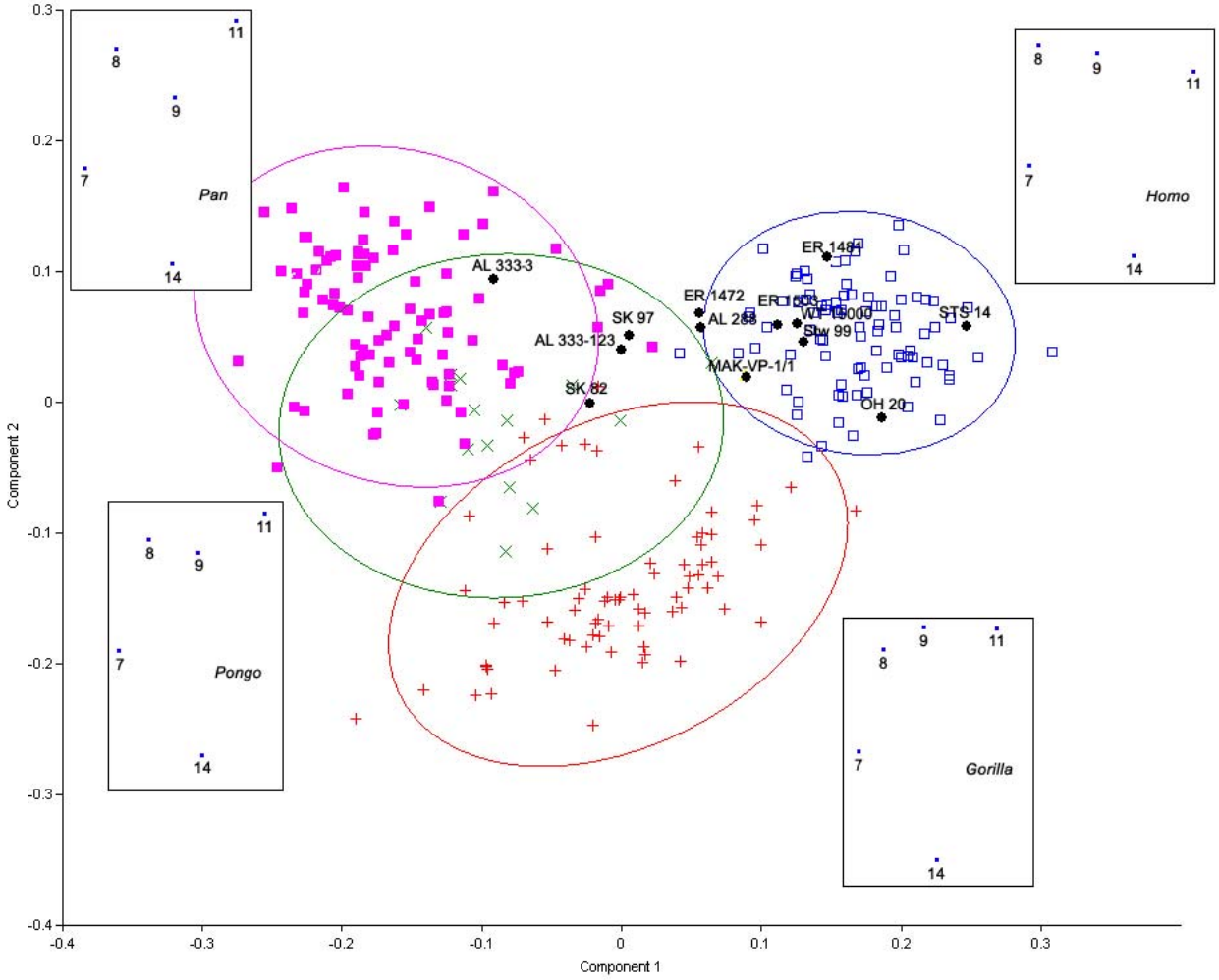

Fig. 4.13 Principal components analysis of the greater trochanter using landmarks 7-9,11 and 14. *Homo* is represented by blue open squares, *Pongo* by green Xes, *Gorilla* by red crosses, and *Pan* by purple squares. The fossils are represented by black circles and are labeled in the graph. PC 1 represents 53% of the variance within this dataset and PC 2 represents 25%. The boxes and numbered points represent a posterior view of the greater trochanter.

Means for the extant taxa were calculated and a PCA was generated with a MST (4.14). Neither PC was correlated with size. All of the data points are spread out fairly evenly across PC 1, with the extant apes and AL 333-3 at the far right side of the axis and OH 20 and STS 14 on the left. PC 2 separates AL 333-123 from the rest of the group. It is interesting that while AL 333-123 and AL 333-3 both cluster with the apes in the PCA of the larger sample (fig 4.13) but they do not cluster together here. So, while they are both large and broadly ape-like, they still

have divergent morphologies. PC 1 is driven by the height of the most lateral point on the greater trochanter with it being lowest in Sts 14 and highest in AL 333-3. PC 2 is driven by the mediolateral distance between the trochanteric fossa (point 9) and point 11 (the lateral extension of the greater trochanter). AL 333-123 has a deep trochanteric fossa with a larger distance between it and point 11.

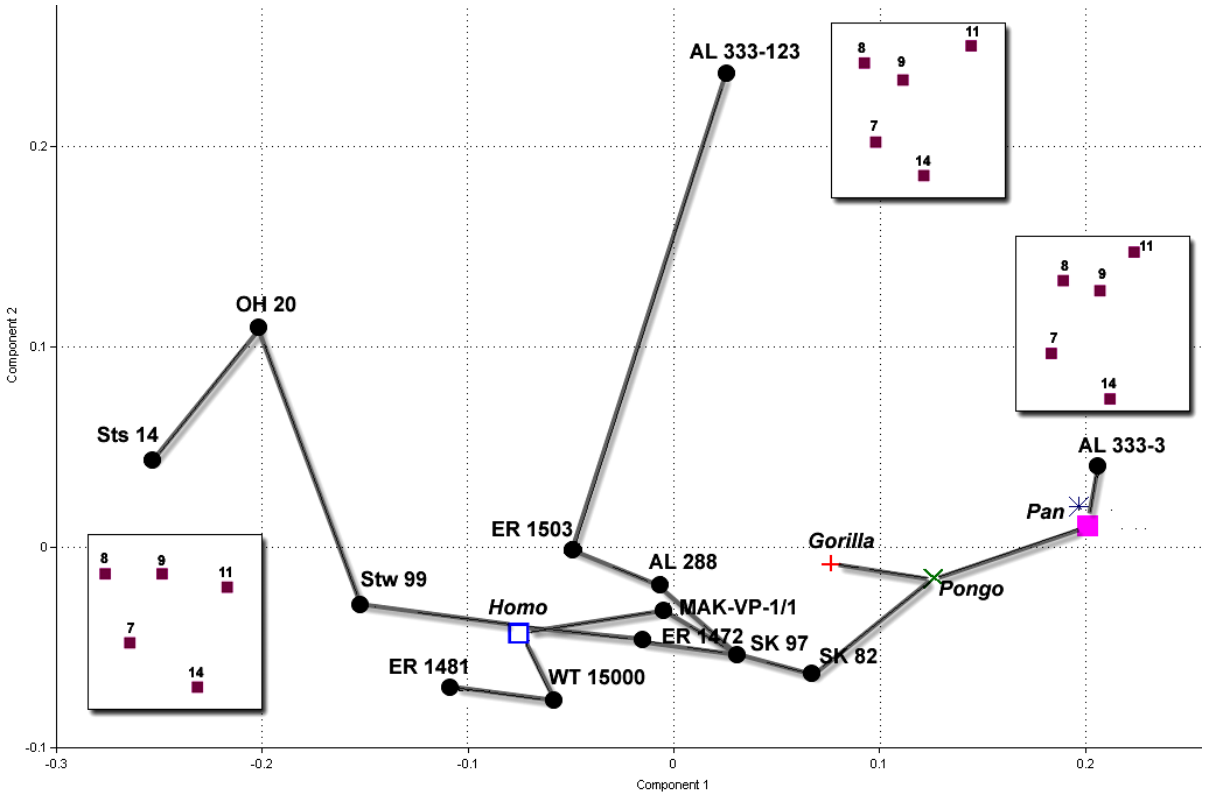

Fig 4.14 Principal components analysis for the fossils plus means for the extant species for the greater trochanter landmarks 7-9,11 and 14. *Homo* is represented by a blue open square, *Pongo* is represented by a green X, *Gorilla* is represented by a red cross, *and Pan* is represented by a purple square. The fossils are represented by black circles and are labeled in the graph. The lines represent a minimum spanning tree plotted on top of the principal components graph. PC1 accounts for 51% of the total variance and PC2 accounts for 16% of the overall variance.

A neighbor-joining tree (fig 4.15) further confirms these relationships. AL 333-3 forms a cluster with *Pan* and AL 333-123 is separate from them as the sister to the larger group of fossils and modern *Homo*. STS 14, OH 20 and MAK-VP-1/1, the other new fossils in these analyses, consistently group nearer to anatomically modern humans.

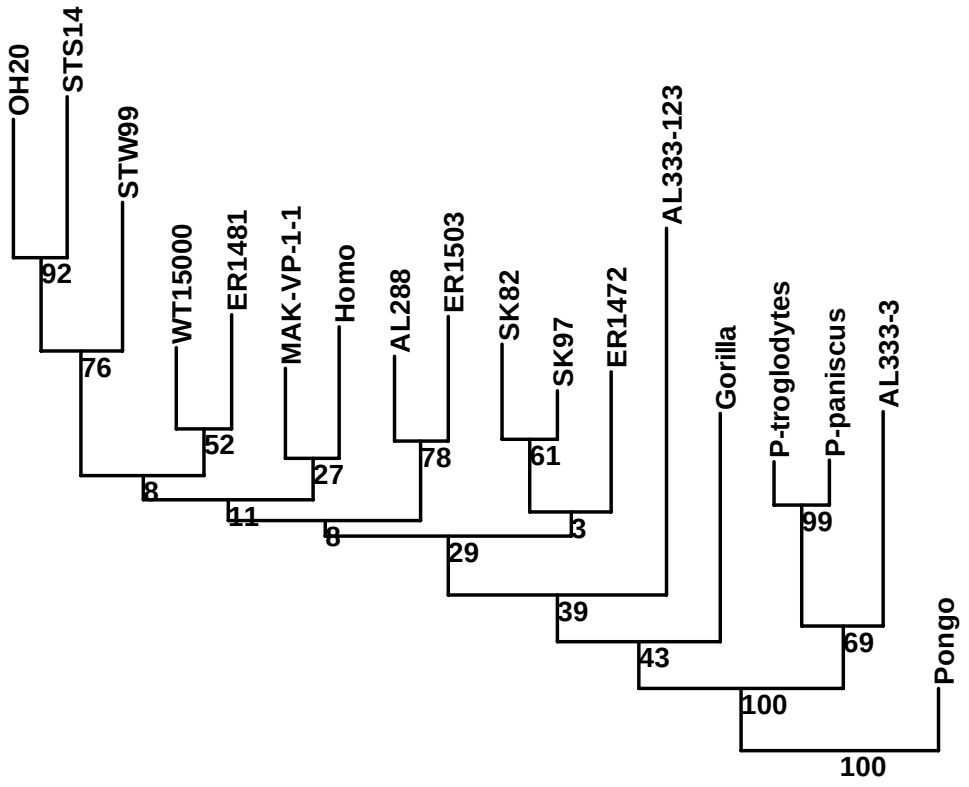

Fig. 4.15 Neighbor joining tree based on procrustes chord distances for the means for the greater trochanter landmarks 7-9,11 and 14 The tree is rooted with *Pongo* as an outgroup. Bootstrap values are given for 1000 replicates.

Due to the variation within the Hadar sample, one more analysis of the proximal femur was undertaken to include the maximum number of fossils from Hadar while still retaining the differences between extant specimens. In this case, landmarks 9, 10, 11 and 14 were used. Despite the fact that this is only four landmarks, the extant taxa were once again broadly separated in a PCA (fig 4.16). This landmark set captures the depth of the trochanteric fossa, the maximum proximo-anterior height of the greater trochanter, the maximum lateral extension of the greater trochanter and the point just distal to the lesser trochanter. This landmark configuration allowed for the inclusion of AL 128, AL 129-1c, AL 288, AL 333-3, AL 333-123, and MAK-VP-1/1 – the entire sample of *A. afarensis*. The orientation of the extant taxa is the same as in the previous analysis. PC 1 separates all of the extant taxa, while PC 2 separates

Gorilla and to a certain degree, *Pongo.* PC 1 is driven by the depth of the trochanteric fossa and the lateral extension of the greater trochanter. *Homo* has a strong lateral extension with a shallow trochanteric fossa whereas *Pan* is characterized by a deep trochanteric fossa with a less laterally projecting greater trochanter. PC 2 is driven by height of the greater trochanter; in *Gorilla,* it is very low.

The majority of the fossils fell within the distribution of modern humans. As in the previous analysis, SK 82 and SK 97 fell within the distribution of both *Gorilla* and *Pongo*, although unlike the last analysis, ER 1472 fell with them. AL 333-3 grouped with *Pan* again and AL 333-123 is outside the 95% equal frequency ellipses of all of the extant taxa, but closest to the distribution of *Pan*. AL 128, AL 129-1c and AL 288 all fell around the edge of the modern *Homo* distribution. For the first time, Stw 99 fell outside of the *Homo* distribution and with *Gorilla* instead. Both PC1 and PC2 are correlated with centroid size.

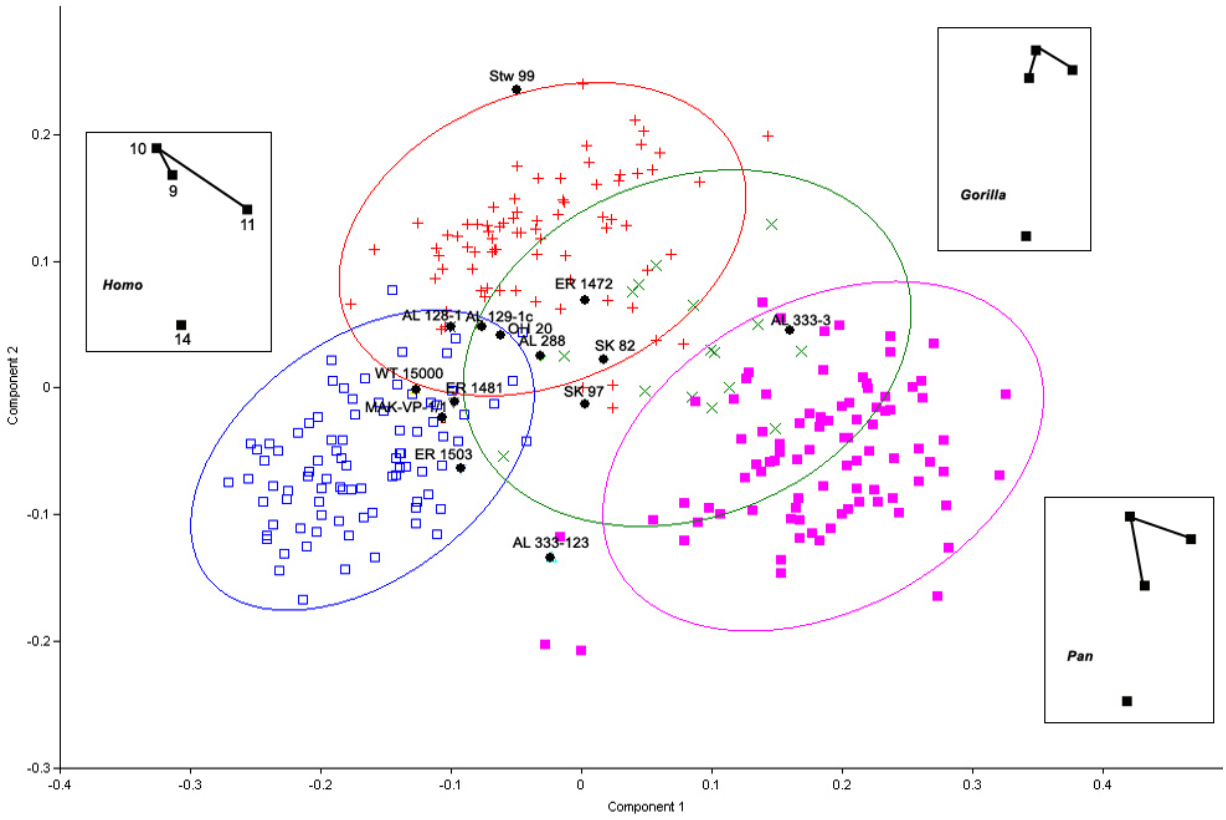

Fig. 4.16 Principal components analysis of the proximal femur, landmarks 9-11, and 14. *Homo* is represented by blue open squares, *Pongo* by green Xes, *Gorilla* by red crosses, and *Pan* by purple squares. The fossils are represented by black circles and are labeled in the graph. The mean shape of the extant specimens is represented by four black squares inside a rectangle. These are oriented in a posterior view. Circles represent the 95% equal frequency ellipses of each extant genus. PC1 accounts for 63%, of the total variance and PC2 accounts for 22%of the overall variance.

For the same landmark configuration, means were calculated for all of the extant taxon and additional analyses were performed using these values and those of the fossils. Fig 4.17 is a PCA with a MST. PC 1 separates *Pan* and AL 333-3 from the other individuals in this analysis and PC 2 separates *Homo* and many fossils from a cluster containing ER 1472, *Gorilla*, AL 128, AL 129-1c and at the extreme, Stw 99. Once again, AL 333-3 and AL 333-123 fall in completely different positions in this analysis, despite both being large and broadly ape-like. PC 1 seems to be driven by the depth of the trochanteric fossa (point 9) with the apes and AL 333-3 having the deepest fossae and the other fossils and *Homo* having the shallowest. PC 2 is driven by the position of the proximal extension of the greater trochanter; in *Homo* it occurs most

medially. It is the more lateral position of this point that drives Stw 99's unique position in both PCA graphs (fig. 4.16). It is possible that this could be due to its abraded condition (see fig. 4.6 for a photo.) Neither axis was correlated with centroid size.

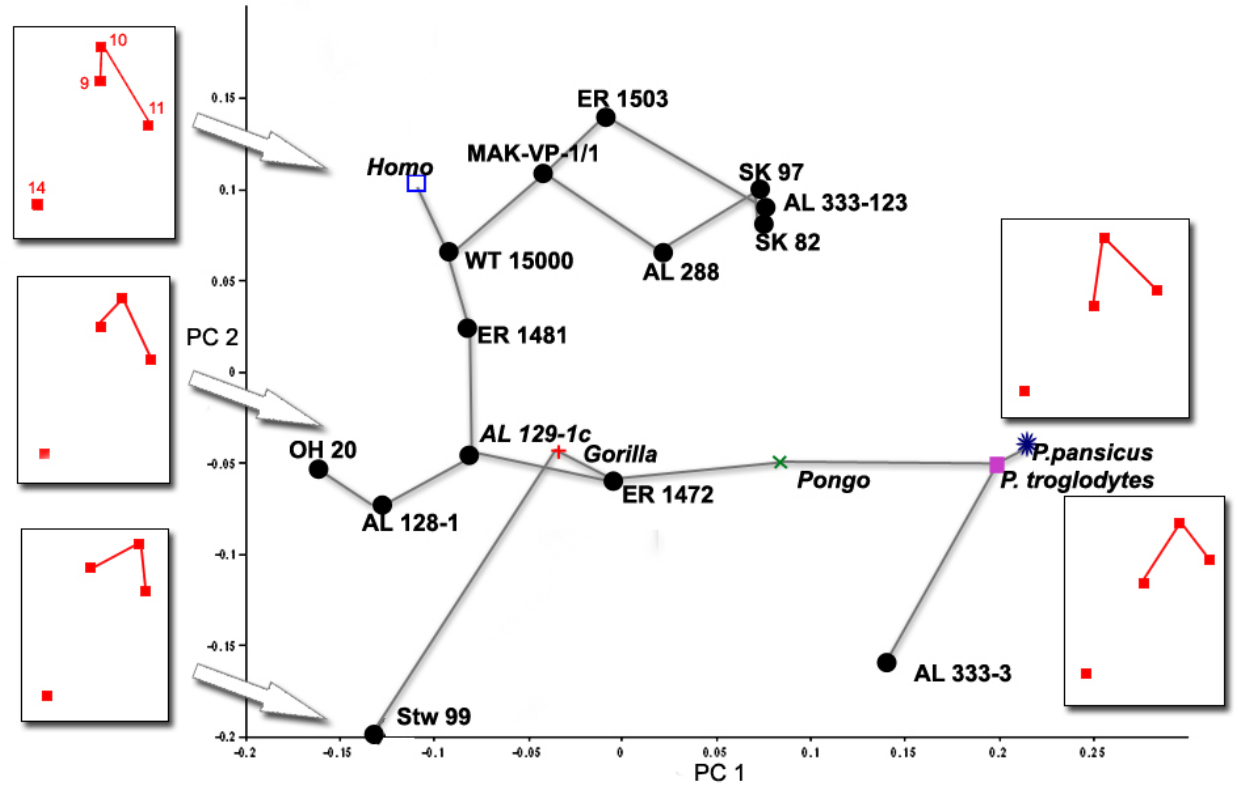

Fig. 4.17 Principal components analysis for the fossils plus means for the extant species for the proximal femur, landmarks 9-11, and 14. *Homo* is represented a blue open square, *Pongo* a green X, *Gorilla* by a red cross, and *Pan* by a purple square. The fossils are represented by black circles and are labeled in the graph. The lines represent a MST plotted on top of the PCA. PC1 accounts for 44.3% of the total variance and PC2 accounts for 32% of the overall variance. The wireframes are in a posterior view and the arrows on the left illustrate approximately where in the graph the wireframes represent.

A neighbor-joining tree was also created (figure 4.18) with these data. Once again, AL 333-3 clusters with *Pan.* In this analysis: Stw 99 and ER 1472 cluster with *Gorilla*; AL 288, SK 97 and SK 82 form a cluster with very high bootstrap values; AL 333-123 is in its own group; and all of the rest of the fossils fall within the larger cluster that also contains modern *Homo.* See figure 4.19 for photographs of the remaining proximal fossil femora.

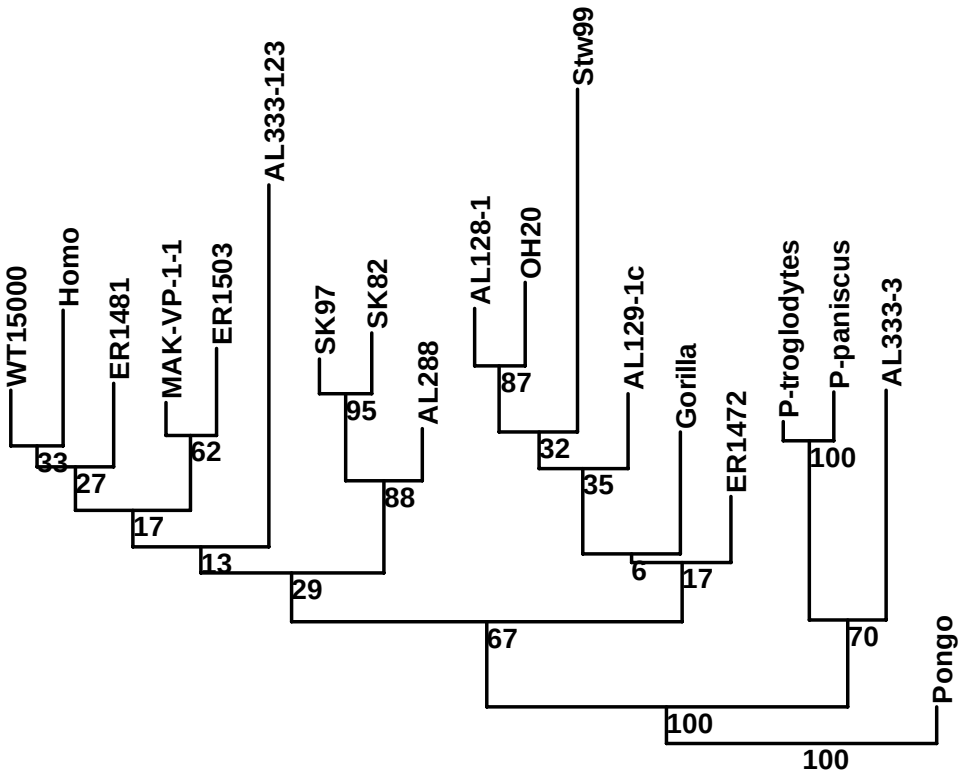

Fig. 4.18 Neighbor joining tree for the proximal femur, landmarks 9-11 and 14. This tree is based on procrustes chord distances and was rooted with *Pongo* as the outgroup. Bootstrap values are given for 1000 replicates.

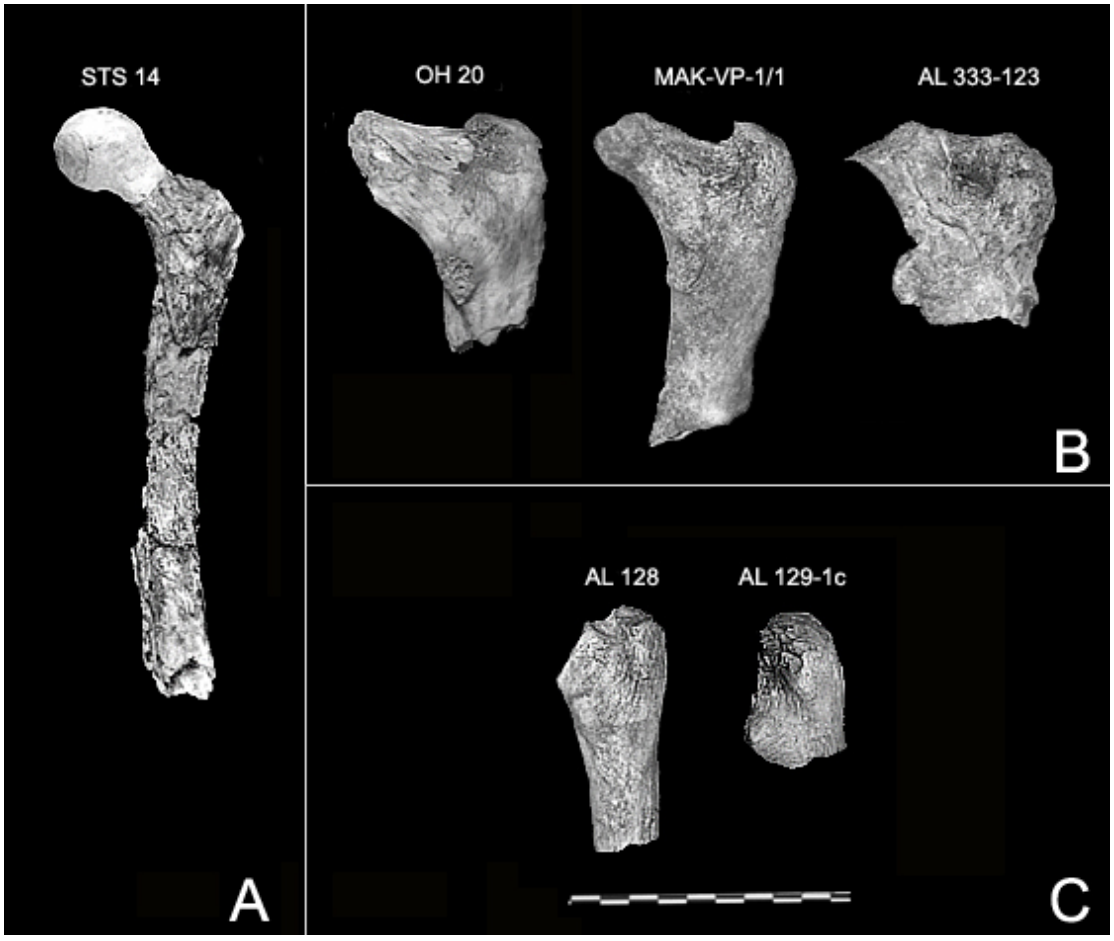

Fig4.19 Additional side-by-side comparisons of the femora added to the analysis for the proximal femur with the femoral head and the greater trochanter. The femur in box "A" was only in the first set of trochanter analyses (figs 4.13-4.15), the femora in box "B" were in both sets of analyses (figs 4.15-4.18) and the femora in "C" were only in the second set of analyses (figs 4.16-4.18). These were scaled, mirrored (STS 14, OH 20, MAK-VP-1/1, and AL 128-1)and positioned using Adobe Photoshop, and they are to the same scale as the previous two photographs. Note that the femoral "head" on STS 14 is largely composed of plaster and thus no points were collected on it.

Proximal Discussion and Analysis

In contrast to the upper limb, the overall variation within the fossils for both the entire proximal femur and the greater trochanter is greater than any single taxon, but less that the variation between almost any pair of extant taxa (see figs 4.20 and 4.21). This is likely because all of the fossils have morphological traits related to bipedality, although the greater range of shape variation in fossils as opposed to extant *Homo* could indicate that bipedalism was practiced in multiple ways by early hominins. This idea is supported by Harmon (2009) who found a large

amount of shape variation in the sample of *Australopithecus africanus* femora. There are fewer small procrustes distances for the full proximal femur than for the greater trochanter; this is likely due to the inclusion of the femoral head. The landmarks on the femoral head are all type III landmarks which are predisposed to be more variable than type I or type II landmarks (Bookstein, 1991).

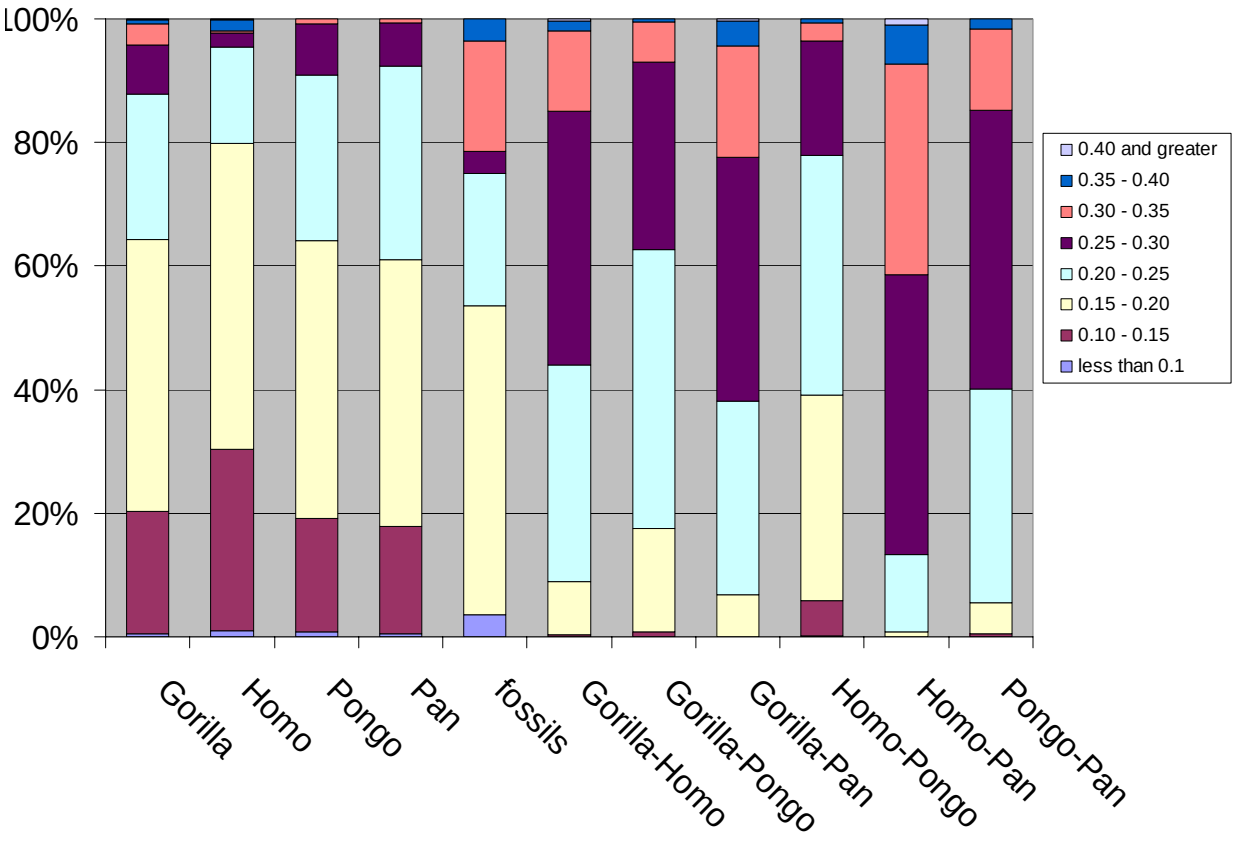

Fig. 4.20 This bar graph is a representation of the distribution of Procrustes chord distances within and between the different genera in the sample for the full proximal femur. The array of Procrustes distances was segmented into arbitrary units of 0.05. The average Procrustes distance between the fossils was higher than any of the single taxon samples, but lower than all of the between genera samples.

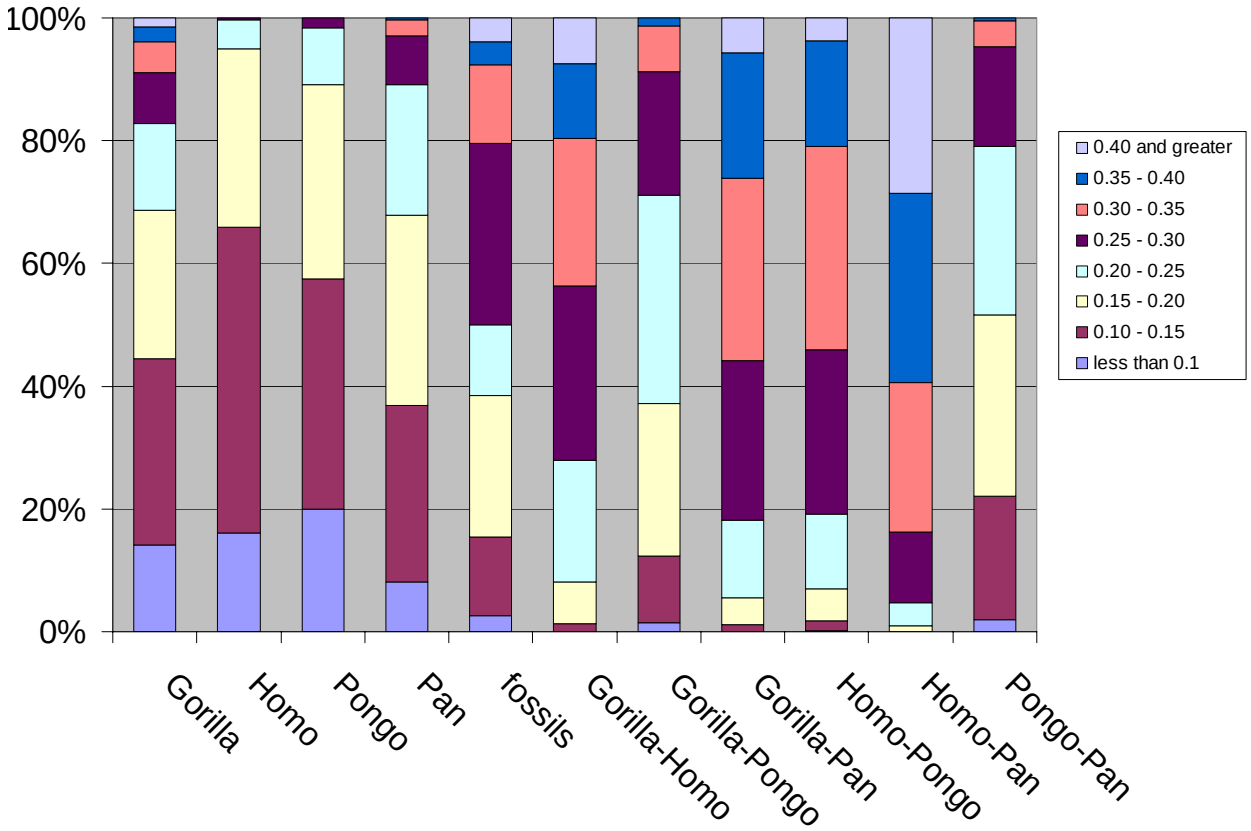

Fig. 4.21 This bar graph is a representation of the distribution of Procrustes chord distances within and between the different genera in the sample for the greater trochanter of the proximal femur. The same individuals used in the first greater trochanter analysis were used for the analysis. The array of Procrustes distances was segmented into arbitrary units of 0.05. The average Procrustes distance between the fossils was higher than any of the single taxon samples, but lower than all of the between genera samples with the exception of *Pongo/Pan.*

There are three patterns of variation present in the proximal femora of this sample: a completely human-like morphology; a mosaic where there is a mostly *Homo*-like morphology in the overall arrangement of the elements of the proximal femur but with a more ape-like greater trochanter; and a mostly ape-like morphology (see Table 4.4). The first group consists of ER 1481, ER 1503, MAK-VP-1/1, and WT 15000, while the second group consists of AL 128, AL 129-1c, AL 288, ER 1472, OH 20, SK 82, SK 97, and Stw 99. The only individual that has an ape-like morphology for the whole of the proximal femur is AL 333-3. The positions of Sts 14 and AL 333-123 are ambiguous as they could potentially fall into multiple groups due to missing data. Without the entire proximal femur, it is impossible to rule out the possibility that AL 333-

123 would have had a human-like pattern for the entire proximal femur, but an ape like morphology for the greater trochanter, as seen in SK 82 and 97. It is also possible for Sts 14 to have a pattern like Stw 99 and group with *Homo* or one of the apes. ER 738 and Stw 522 are excluded from any group as they could only be included in analyses utilizing the femoral head and neck which failed to reproduce the differences between the extant taxa.

Table 4.4 List of all fossil specimens included in analyses of the proximal femur and the taxa with which they ally grouped in each analysis. Fossils with an asterisk next to the attribution were technically outside the confidence interval of all extant taxa, but were closest to the starred taxon. Attributions with a multiple taxa fell into a zone of overlap, with the exception of femoral head. Zones of overlap were not indicated for the femoral head as there were very few areas in the graph where the extant taxa did not overlap. An x indicates that there were landmarks missing and that the fossil was not included in the analysis. The "variation pattern" is discussed in the text.

Fossil	Taxon (& ref.)	Complete Prox. Femur	Head	Greater trochanter I	Greater trochanter II	Variation Pattern
AL 128	*A. afarensis*[5]	x	x	x	*Homo/Gorilla*	2
AL129-1c	*A. afarensis*[5]	x	x	x	*Homo/Gorilla/Pongo*	2
AL 288	*A. afarensis*[5]	*Homo*	*Homo*	*Homo**	*Gorilla/Pongo*	2
AL 333-3	*A. afarensis*[5]	*Gorilla/Pongo*	*Gorilla*	*Pongo*	*Pan/Pongo*	3
AL333-123	*A. afarensis*[5]	x	x	*Pongo*	*Pan**	2 or 3
ER 738	*Homo?*	x	*Homo*	x	x	?
ER 1472	*Homo* sp.[4]	*Homo*	*Homo*	*Homo**	*Gorilla/Pongo*	2
ER 1481	*Homo* sp.[4]	*Homo*	*Homo*	*Homo*	*Homo*	1
ER 1503	*H. habilis?*	*Homo*	*Homo*	*Homo*	*Homo*	1
MAK-VP-1/1	*A. afarensis*[7]	x	x	*Homo*	*Homo*	1
OH 20	*P. boisei*[1]	x	x	*Homo*	*Homo/Gorilla*	2
SK 82	*P. robustus*[2]	*Homo**	*Homo*	*Pongo*	*Gorilla/Pongo*	2
SK 97	*P. robustus*[2]	*Homo**	*Homo*	*Pongo*	*Pongo*	2
Sts 14	*A. africanus*[2]	x	x	*Homo*	x	1 or 2
Stw 99	*A. africanus*[3]	*Homo*	*Homo*	*Homo*	*Gorilla*	2
Stw 522	*A. africanus?*	x	*Homo*	x	x	?
WT 15000	*H. erectus*[6]	*Homo*	*Homo*	*Homo*	*Homo*	1

[1] Day, 1969; [2] Robinson, 1972; [3] Clarke, 1985; [4] Leakey, 1973; [5] Johanson *et al.*, 1978; [6] Walker and Leakey, 1993; [7] Lovejoy *et al* 2002

Implications for Function of the Hip

Most of the individuals in the first group have been attributed to the genus *Homo* Leakey, 1973; Walker and Leakey, 1993), the only exception being MAK-VP-1/2 which has been attributed to *Australopithecus afarensis* (Lovejoy *et al.*, 2002). Functionally, these individuals

have a proximal femoral morphology that is indistinguishable from that of modern humans. They all have a large, globular femoral heads that are more proximally oriented, and a low and laterally projecting greater trochanter. The large femoral head in *Homo* functions to support the greater amount of weight passing vertically during bipedal locomotion compared to quadrupedal apes (Ruff, 1988), while the low and laterally projecting greater trochanter helps to put the gluteus minimus and medius in their most mechanically advantageous position while allowing for maximal mobility at the hip joint (Aiello and Dean, 1990).

The individuals in the second group are perhaps functionally more interesting than those in the first grouping. They have all been attributed to either *Australopithecus afarensis* or *Paranthropus* with the exception of ER 1472 (*Homo* sp.) (Day, 1969; Leakey, 1973; Johanson *et al.,* 1978). The individuals in the second group largely retain a modern human-like pattern for the arrangement of the different anatomical units of the proximal femur in that they have a relatively long femoral neck and globular head, yet retain a more ape-like morphology for the greater trochanter in that they lack both the pronounced lateral flare of the human greater trochanter and the medially oriented muscle attachment areas on the anterior aspect for the gluteus minimus and medius. This could indicate that these hominins used bipedalism as an important component of their locomotor repertoire, but had lesser gluteal muscles that lacked the same pelvic stabilization functions found in modern humans. Unfortunately, the function of the lateral projection of the greater trochanter still is poorly understood (Aiello and Dean, 1990). Of the fossils in this group, SK 82 and SK 97 have the greatest similarity with the extant apes and are supported as a cluster by large bootstrap values throughout the analyses of the proximal femur. Other studies have noted that they also have more cortical bone than modern humans and femoral strength proportions more like the extant apes (Ruff *et al.,* 1999). All of this together

indicates that of this grouping, SK 82 and SK 97 may have had the most conservative form of bipedality.

One interpretation of these results is that for hominins, the gross morphological arrangements of the parts of the proximal femur (*i.e.* neck orientation/thickness versus position of the greater trochanter) are integrated, but the smaller scale shape changes within the proximal femur are not. A similar result was found for the scapula of three closely related Sciuride in that during some evolutionary transitions the scapula changed as an integrated unit, but in other transitions singular parts changed (Swiderski, 1993). Questions of morphological integration in the femur are made difficult by its complicated ontogentic path. The tissue that eventually forms both femoral head and neck and the greater trochanter is derived from a single chondroepiphysis, from which two secondary ossification centers derive – one for the femoral head and neck and one for the greater trochanter. These ossification centers remain separate during growth and development for all primates (Ogden, 1981; Serrat *et al.,* 2007) and, in humans, appear after birth – this is in contrast to the distal femur which is formed from a single secondary ossification center whose ossification begins prior to birth (Moore and Persaud, 1998).

There are many epigenetic traits that are well documented for the human femur. Besides the bicondylar angle, the internal arrangement of the trabeculae, particularly in the femoral neck, is strongly influenced by the adoption of bipedal gait in the first and second year (Ryan and Krovitz, 2006) and the overall strength proportions of the femur are significantly affected by the biomechanical loading in bipedal gait (Ruff, 2003). In modern human populations, the neck/shaft angle has shown to be correlated with differences in lifestyle (sedentary vs. active) during ontogeny (Andersen and Trinkaus, 1998). This is in contrast to the distal femur where traits that are functionally linked to human bipedalism are already present in utero (Tardieu,

1999). It could be reasonably concluded that the external morphology of the proximal femur is likely more plastic than the distal femur and subject to greater epigenetic changes.

AL 333-3 was the only individual that consistently groups with the extant apes for all analysis. A wireframe transformation between AL 333-3 and ER 1481 is illustrated in figure 4.36. Like the extant apes and the hominins in group 2, AL 333-3 possesses a less laterally flaring greater trochanter than modern humans. Like only the extant apes, AL 333-3 has a femoral head that is lower and is similar in height to the greater trochanter. The lower femoral head would have resulted in a compromised mobility at the hip joint as compared to humans, although would have provided a greater lever advantage for vertical climbing as in the extant apes (Stern and Susman, 1981).

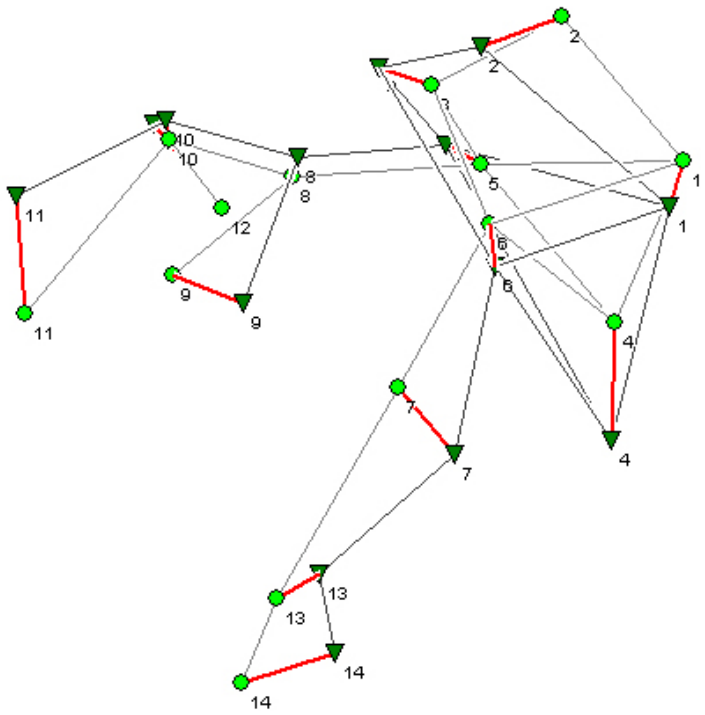

Fig. 4.22 Anterior view of the wireframe transformation of the proximal femur between AL 333-3 (green triangles) and ER 1481 (green circles). Point 11 illustrates the difference in the lateral flare of the greater trochanter while points 2 and 4 illustrate the differences in the proximal extension of the femoral head.

Taxonomic Case of Australopithecus afarensis

Questions about the taxonomic status of *Australopithecus afarensis* have yielded contradictory results. Some authors have argued that *Australopithecus afarensis* is a single, sexually-dimorphic species with little shape variation between large specimens and small specimens (White, 1985; McHenry, 1992; Richmond and Jungers, 1995; Lague, 2002; Harmon, 2006), while other have argued that there is biomechanically important shape variation between individuals (Stern and Susman, 1983; Stern *et al.,* 1984; Senut and Tardieu, 1985). These differences have been argued either to be sex based differences representing functionally different locomotor repertoires between males and females (Stern and Susman, 1983; Stern *et al.,* 1984; Senut *et al.,* 2001) or the presence of two taxa at Hadar (Senut and Tardieu, 1985; Hausler and Schmid, 1995).

Harmon (2006) compared all pairwise Euclidian distances between individuals in her fossil sample to pairwise Euclidian distances between extant individuals of the same species to assess the degree of shape variation in her *A. afarensis* sample. She concluded that it was not greater than that seen in any extant taxon, although she did note that AL 128-1 had a divergent morphology due to a shorter, more anteroposteriorly broad greater trochanter. When she compared the pairwise distances between all of the fossil taxa, there was only one pair where the distance was significantly greater than pairs of individuals seen in her extant sample: AL 128-1 and AL 827-1.

Following Harmon (2006), a similar procedure was undertaken for this data set. This study differs from Harmon's in two ways: here, landmark data were used as opposed to linear data; and MAK-VP-1/1 and AL 333-123 were included here while AL 827-1 was not. In all pairwise comparisons, the procrustes distance between AL 333-3 and the other fossil exceeded

95% or more of the pairwise comparisons in the extant taxa (subspecies were used if present). The distance between AL 288 and AL 128-1 also exceeded 95% of all extant pairings. AL 333-123 also significantly different from most of the other *A. afarensis* fossils, with the one exception of MAK-VP-1/1. The similarity between AL 129-1a and AL 128-1 gives some weak support to the idea that these fossils could have come from a single individual (Johanson and Taieb, 1976), although there are smaller pairwise distances in every extant group (Table 4.5).

Table 4.5 The pairwise procrustes chord distances are shown next to each pair of *A. afarensis* fossils for the greater trochanter (the only landmark set for which all specimens could be included). The percent pairwise procrustes distances of the total sample that are above that of *A. afarensis* are given for the other taxa. The last three columns give the percent pairwise procrustes distances that are above the *A. afarensis* value for a mixed subspecific and specific groups. Those that are significant (5% or less) are in bold and shaded. The minimum, maximum and average procrustes distances for each group are given at the bottom.

Fossil Pairwise Distances		*G. g. gor.*	*G. g. gra.*	*P. t. trog.*	*P. t. schwein.*	*P. paniscus*	*P. pygmaeus*	*H. sapiens*	*Gorilla* subsp.	*Pan* subsp.	*Pan* sp.
AL 333-3 & AL 333-123	0.28	**< 1**	**1**	**3**	**2**	**2**	**1**	**1**	**1**	6	6
AL 333-3 & MAK-VP-1/1	0.34	**< 1**	**0**	**1**	**0**	**1**	**0**	**0**	**< 1**	**1**	**2**
AL 333-3 & AL 128-1	0.30	**< 1**	**0**	**2**	**1**	**2**	**0**	**0**	**< 1**	**4**	**5**
AL 333-3 & AL 129-1c	0.26	**1**	**2**	**5**	**3**	**2**	**1**	**3**	**2**	7	7
AL 333-3 & AL 288	0.29	**0**	**0**	**3**	**1**	**2**	**0**	**0**	**0**	**5**	**5**
AL 333-123 & MAK-VP-1/1	0.22	**3**	8	11	10	**5**	**3**	8	**5**	13	9
AL 333-123 & AL 128-1	0.30	**< 1**	**0**	**2**	**1**	**2**	**0**	**0**	**0**	**4**	**5**
AL 333-123 & AL 129-1c	0.25	**1**	**3**	**5**	**4**	**2**	**2**	**4**	**2**	8	7
AL 333-123 & AL 288	0.24	**1**	**3**	6	6	**3**	**2**	**4**	**3**	9	7
AL 128-1 & MAK-VP-1/1	0.22	**3**	9	11	11	**5**	**4**	9	7	15	10
AL 128-1 & AL 129-1c	0.08	85	85	95	93	91	91	89	89	95	92
AL 128-1 & AL 288	0.26	**1**	**2**	**5**	**4**	**2**	**1**	**3**	**2**	7	7
AL 129-1c & MAK-VP-1/1	0.17	11	26	36	25	14	22	22	27	34	27
AL 129-1c & AL 288	0.20	**5**	12	18	15	**5**	11	13	12	18	14
AL 288 & MAK-VP-1/1	0.11	49	56	75	70	58	64	58	63	74	73
Min	0.08	0.02	0.03	0.03	0.02	0.04	0.04	0.02	0.02	0.02	0.03
Max	0.34	0.34	0.29	0.35	0.33	0.34	0.28	0.33	0.37	0.41	0.42
Average	0.23	0.11	0.13	0.15	0.14	0.12	0.13	0.13	0.13	0.15	0.15

The contradictory findings from previous studies are mirrored in the overall results of this analysis. In the principal components and cluster analyses, AL 333-3 was consistently most similar to the extant apes, and MAK-VP-1/1 was consistently the most similar to modern humans. AL 128-1, AL 129-1c, AL 288, and AL 333-123 all had varying degrees of intermediate morpohology, particularly with regard to the shape of the greater trochanter. The data from pairwise procrustes distances do not indicate a temporal, nor a size trend in the variation in *Australopithecus afarensis* proximal femora (Table 4.6).

Table 4.6 List of *A. afarensis* specimens with approximate dates and centroid sizes.

Fossil	Age	Centroid Size
AL 128-1[1]	3.4 Ma	41.0172
AL 129-1c[1]	3.4 Ma	41.6592
AL 288[1]	3.18 Ma	34.7769
AL 333-3[1]	3.2 Ma	69.0327
AL 333-123[1]	3.2 Ma	63.806
MAK-VP-1/1[2]	3.4 Ma	51.2163

[1]Walter, 1994; [2]Lovejoy *et al.*, 2002

AL 288 and AL 129-1c are of a similar size but have a large pairwise distance, as is true for AL 333-3 and AL 333-123. The Maka femur is the oldest fossil in this sample and AL 288 is the youngest, yet they have one of the smallest pairwise procrustes distance values. The pairwise distances do indicate that the variation in the fossil data is generally more consistent with that seen in the multi-subspecific and multi-specific samples of *Pan.*

Evidence for extensive variation within the Hadar sample is abundant. On the basis of pelvic morphology, Hausler and Schmid (1995) argued for two species at Hadar: a small, mostly monomorphic species represented by Lucy and one or more other species represented by the larger individuals. Senut and Tardieu (1985) have argued for a large species and a small species at Hadar on the basis of variation at the elbow and at the knee. Susman *et al.* (1984) also noted the large amount of variation in the Hadar sample, particularly between large and small individuals, in a variety of postcranial elements. These authors interpreted this variation as

indicating either extreme sexual differences in locomotor patterning or the presence of multiple species at Hadar.

The data presented here do not support hypotheses that posit a large species and a small species at Hadar: while the larger specimens are broadly different from the small specimens, they are also quite different from each other. However, the data do indicate that variation within *Australopithecus afarensis* proximal femora is greater than can be accommodated within a single extant taxon. Thus, there are three possible explanations:

(1) There are at least two species of Plio-Pleistocene hominins at Hadar, as suggested by Hausler and Schmid (1995) in their analysis of the pelvis. Perhaps there are multiple species at Hadar, but they cannot be sorted specifically into a small and a large morph. If this is the case, there could be one that is small and monomorphic as well as a second that is larger and potentially sexually dimorphic. This theory is contra studies conducted on the cranial data that indicate that *A. afarensis* is a single, cohesive species (Kimbel *et al.,*1984).

(2) The individuals from the Hadar assemblage are a single species, but practiced extremely diverse locomotor repertoires on an individual level that do not correlate perfectly with size or time. As previously discussed, the biomechanical stress of walking bipedally is the agent of many epigenetic changes in the femur (Shefelbine *et al.,* 2002; Ruff, 2003; Ryan and Krovitz, 2006); perhaps the variation seen in these proximal femora is correlated with individual activity pattern and the frequency and ontogenetic timing at which different individuals walked upright.

(3) These data do not exclude a single species hypothesis for this sample. While the procrustes distances between some of the specimens are large, they do not exceed the maximum procrustes distances in the extant sample of *Gorilla g. gorilla* or *Pan t. troglodytes,* and the high average procrustes distance could be an artifact of small sample size coupled with a larger time dimension than seen in the extant samples.

Considering the divergent morphology of AL 333-3 in all analyses, it seems likely that at least that individual could belong to a different taxon than the other individuals in the Hadar sample, despite being part of the AL 333 assemblage.

Other Taxonomic Implications from the Proximal Femur

Three of the specimens in this analysis have been attributed to the genus *Paranthropus:* SK 82, SK 97 and OH 20. Day (1969) likened OH 20 to SK 97 and SK 82 based on the position of the lesser trochanter (although later studies have cast doubt on the use of the position of the lesser trochanter as a functionally significant character [Aiello and Dean, 1990]). Day (1969) also claimed that the greater trochanter of OH 20 was not laterally expanded as in modern humans. He used these two traits to postulate that the center of gravity in OH 20 was located further forward than in modern *Homo*, which would have led to a less efficient form of bipedalism and he therefore attributed this specimen to *Australopithecus* (now *Paranthropus*) *boisei.* Subsequent studies have used Day's (1969) attribution (*i.e.* Steudel, 1980; Wood *et al.,* 1998), although McHenry (1994) classified OH 20 as Hominidae sp. indet. The classification of

this particular fossil has been made difficult due to the presence of three or four different taxa in Olduvai Bed I: *H. habilis, H. rudolfensis, H. erectus* and *P. boisei* (Wood *et al.,* 1998).

The results of this study disagree with those of Day (1969). While the aspects of the greater trochanter that Day observed were captured in this analysis, OH 20 was not most ally similar to SK 97 and SK 82 in any analysis. Instead, OH 20 was most ally similar to Sts 14 and Stw 99, attributed to *A. africanus* (Robinson, 1972) or AL 128-1 (*A. afarensis*). These clusters had well supported bootstrap values (see Figs. 4.25 and 4.31); thus this study lends support to the idea that OH 20 is not a member of *Paranthropus boisei*. If there are four taxa in Olduvai Bed I, the most logical conclusion is that OH 20 is a member of *Homo* cf. *habilis.* If OH 20 is truly a member of *Homo habilis*, this would present more evidence that *Homo habilis* had not developed a fully human bipedal gait (Hartwig-Sherer and Martin, 1991)**,** giving more credence to the idea that *Homo habilis* belongs in the genus *Australopithecus* as advocated by Wood and Collard (1999). However, as there is much disagreement about even which cranial specimens compose the *H. habilis* hypodigm (Wood, 1985, 1987; Chamberlain and Wood, 1986; Johansen *et al.* 1987; Miller, 1991; Tobias, 1991), more fossils need to be found to truly answer this question.

Harmon (2009) analyzed the size and shape variation within *Australopithecus africanus* and found that the shape variation in *A. africanus* exceeded that of all modern taxa in her study. She tentatively suggested that there could be two species within the hypodigm of what is considered to be *A. africanus* that differ in shape but not in size. Stw 99 and Stw 598 (not sampled here) contributed most to the shape variation in her study. The results of this study neither support nor contradict Harmon's findings. Stw 99 and Stw 14, both attributed to *A. africanus*, are part of the same well-supported cluster in the second analysis (see fig. 4.25),

although Stw 99 has more divergent morphology in the third analysis (see fig. 4.29 and 4.31). Stw 14 is broken and thus could not be included in the third analysis.

Distal Femur Data

Four separate analyses were run on the sample of Plio-Pleistocene distal femora in order to include the maximal number of fossils. Figure 4.23 illustrates the landmarks collected for the distal femur as well as the way that they are connected to form a wireframe. Figure 4.24 is a PCA for the landmarks representing the entire distal femur. As is to be expected, there is clear separation between *Homo* and the other apes along PC 1. PC 1 accounts for driven by three major factors: first, the asymmetry in the patellar articular surface, which is more asymmetrical in *Homo;* second, the width of the trochanteric notch, which is wider in *Pan* and *Gorilla*; and third, the flatness of the femoral condyles as in *Homo* they make a flat surface but in *Pan* and *Gorilla* they are flexed upwards. PC 2 partially separates *Gorilla* and *Pan* and is driven by the height of the patellar articular surface, which is higher in *Pan*, and the orientation of the trochlear notch, which is almost laterally flexed in *Gorilla.* The *Pongo* distribution entirely overlaps the distribution of *Pan* and *Gorilla.* Although PC 1 is not correlated with centroid size, there is a relationship between size and PC 2.

Many of the fossils fall within the distribution of modern humans. Those fossils are: WT 15000, ER 1481, ER 1592, TM 1513, Kibish 1, and SK 1896. ER 993, ER 1472, ER1500, AL 129-1a, AL 333-4, and STS 34 all fall outside of the range of modern humans. ER 1472 is barely outside the 95% equal frequency ellipses for modern humans, although it is worth noting that for this most complete landmark set, there is no overlap between *Homo* and any of the quadrupedal taxa.

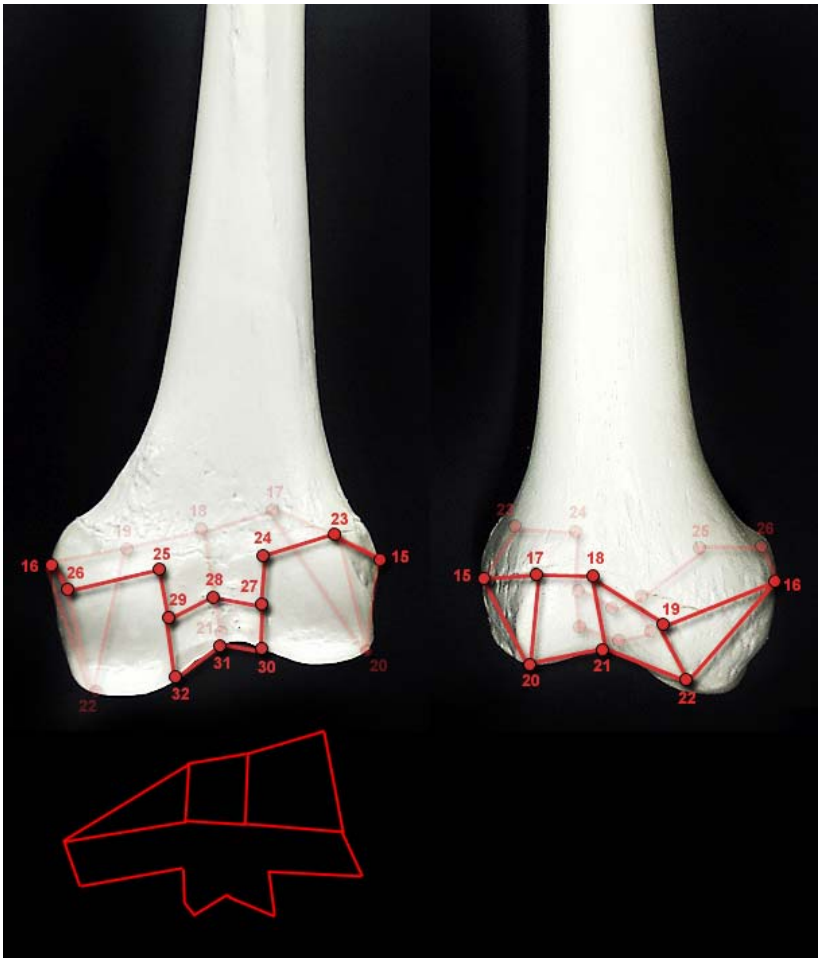

Fig. 4.23 This photo shows the landmark configuration for the distal femur in both anterior and posterior views. Below these, one of the actual wireframes generated from *morphologika* is illustrated for comparison.

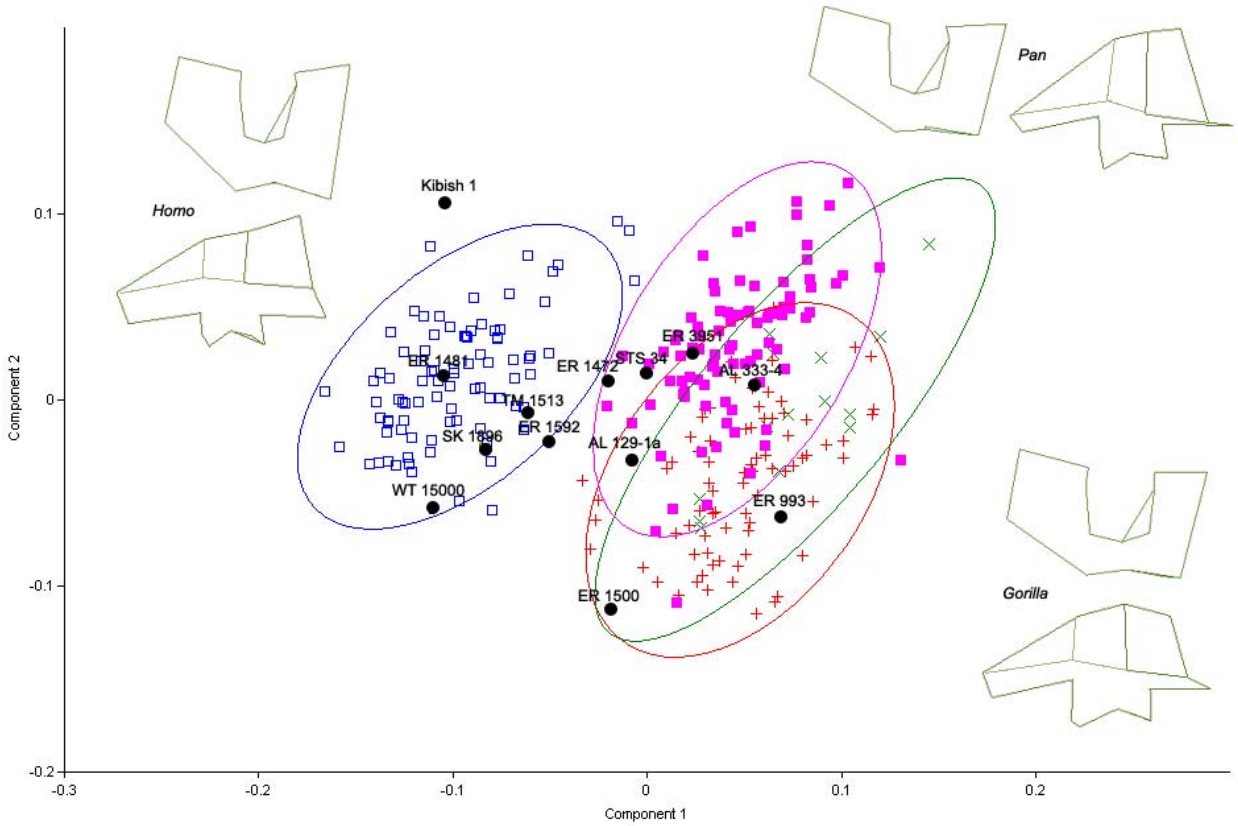

Fig. 4.24 PCA of the distal femur, landmarks 15, 17-19, 21-27 and 29-32. *Homo* is represented by blue open squares, *Pongo* by green Xes, *Gorilla* by red crosses, and *Pan* by purple squares. The fossils are represented by black circles and are labeled in the graph. Circles represent the 95% equal frequency ellipses of each extant genus. PC1 accounts for 25% of the total variance and PC2 accounts for 10% of the overall variance. The wireframes illustrate a distal view and a posterior view, looking towards the patellar articular surface for each of the three major clusters of extant genera.

Means were calculated for all of the extant taxa and additional analyses were run using these values and those of the fossil individuals. Fig 4.25 is a PCA with MST for these values. In this case, PC 1 separates SK 1896 from the rest of the sample and it is driven by the extreme asymmetry in the patellar articular surface and the extreme narrowness of the intercondylar notch. SK 1896 was broken at some time and glued back together, so it is possible that the reconstruction is slightly distorted and that is affecting these results (Fig. 4.26). PC 2 separates some of the *Homo*-like fossils (i.e. WT 15000 and TM 1513) from the other fossils and is driven by the relative height of the mid-point of the patellar articular surface. Again, in this analysis ER

1472 is between *Homo* and *Pan*, both in the principal component analysis and in the minimum spanning tree. Neither PC1 nor PC2 is related to centroid size.

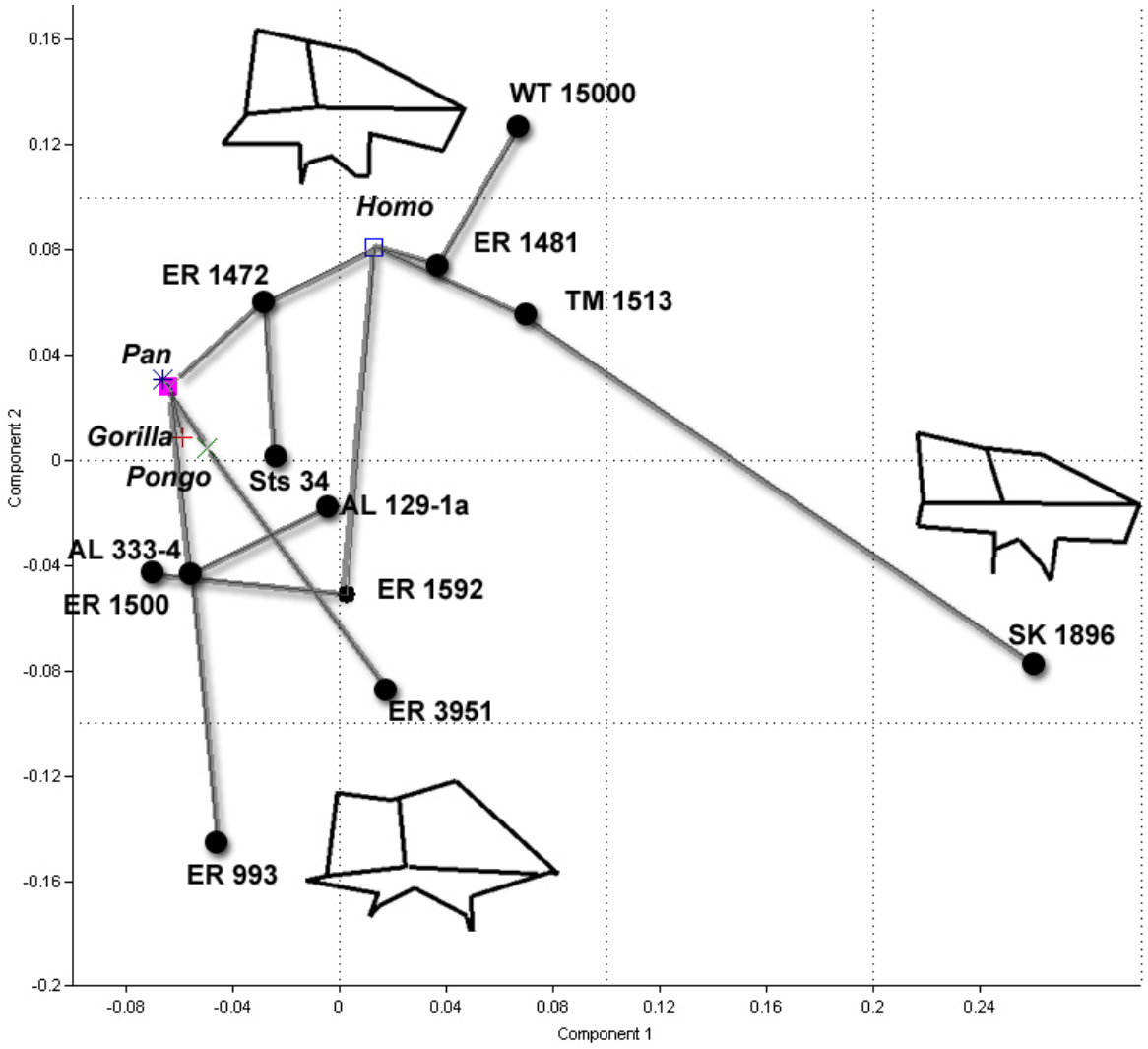

Fig. 4.25 PCA for the fossils plus means for the extant species for the distal femur, landmarks 15, 17-19, 21-27 and 29-32. *Homo* is represented by blue open squares, *Pongo* by a green X, *Gorilla* by a red cross, and *Pan* by a purple square and blue star. The fossils are represented by black circles and are labeled in the graph. The lines represent a minimum spanning tree plotted on top of the principal components graph. PC1 accounts for 25% of the total variance and PC2 accounts for 18%of the overall variance. The wireframes are in a posterior view, looking towards the patellar surface.

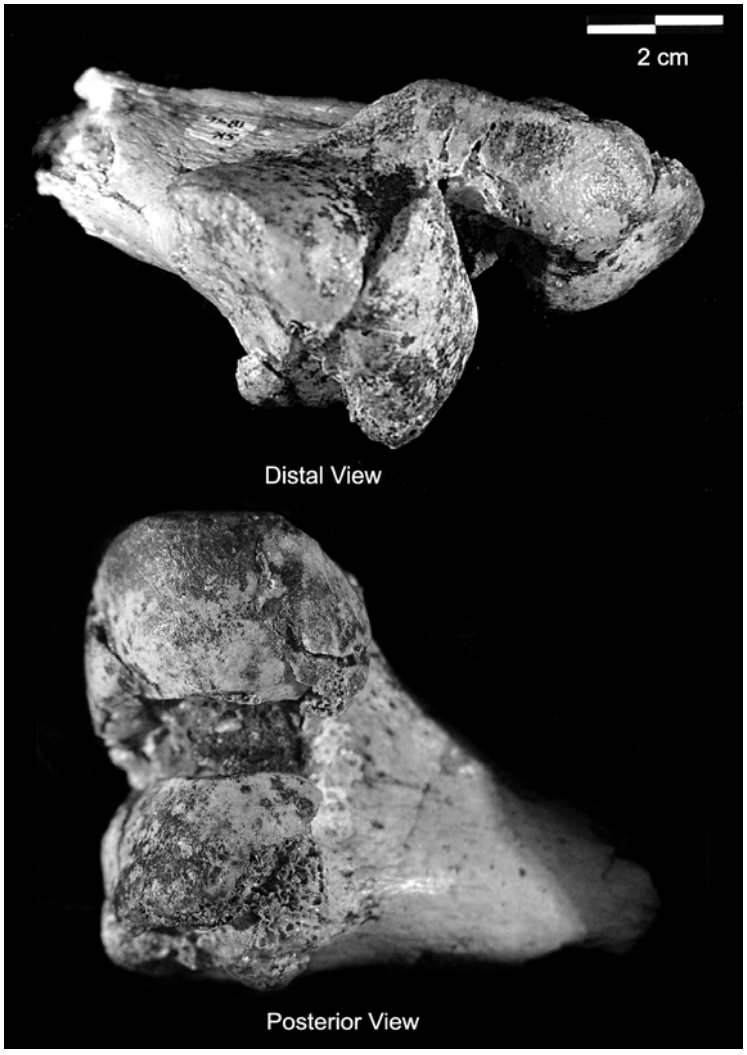

Fig. 4.26 Distal and proximal views of ER 1896. The breaks are obvious in the top photograph and the bottom photograph illustrates the extreme narrowness of the intercondylar notch.

A neighbor joining tree was also generated for these data, the results of which are presented in figure 4.27. Many of the fossil groupings from the previous analyses are recreated in this tree. The major differences are in the position of ER 3951 and ER 1472. ER 3951 groups firmly with *Pan* in the PCA of the entire sample (fig 4.24) and with the other *Pan*-like and *Gorilla*-like fossils in the PCA of the means (fig 4.25); however, in this analysis ER 3951 forms a cluster with SK 1896, a more *Homo*-like fossil. ER 1472 is on the edge of the *Homo* distribution in all other analyses, but it is the outgroup to the cluster which contains *Homo* and all

other fossils in this analysis. Despite the morphological affiliation with *Pan* and *Gorilla* in other analyses, none of the fossils cluster with the apes.

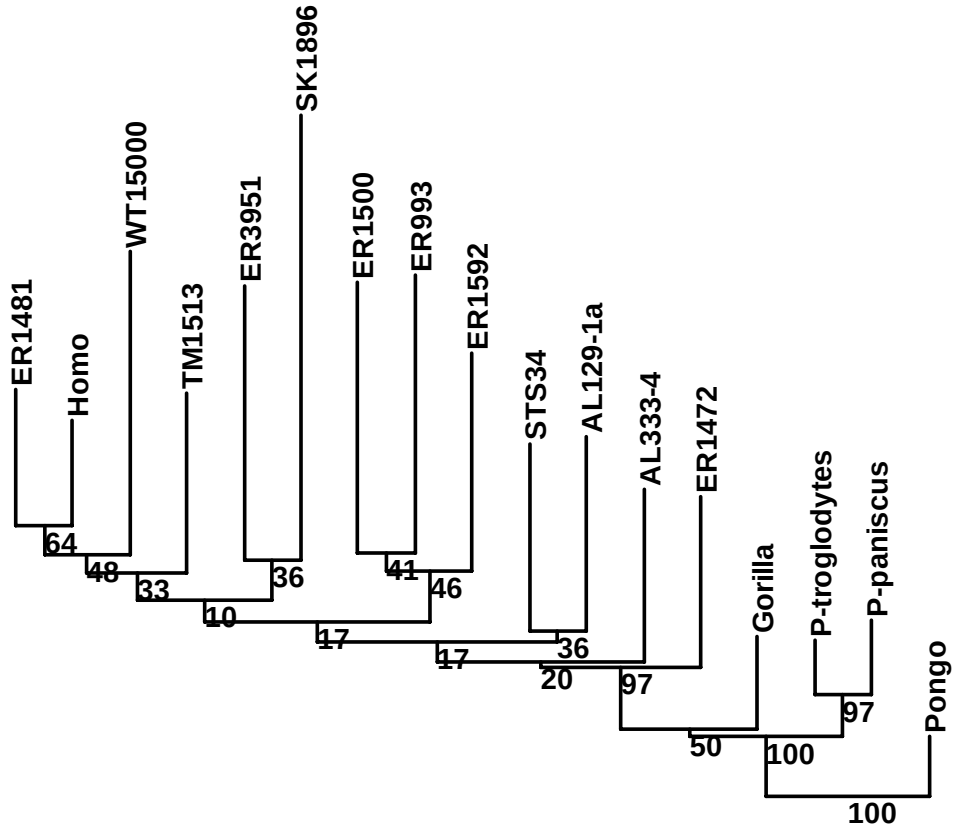

Fig. 4.27 Neighbor joining tree for the means for the distal femur, landmarks 15, 17-19, 21-27 and 29-32. This tree is based on procrustes chord distances and was rooted with *Pongo* as the outgroup. Bootstrap values are based on 1000 replicates.

In order to include more fossils in these analyses, the distal femur was subdivided into smaller subsets of landmark points. Figs 4.28 – 4.30 represent analyses using the landmarks for just the lateral femoral condyle. This allowed for the inclusion of three additional fossil individuals: AL 333w-56, BOU-VP-19/63 and Stw 318. Fig 4.45 is a principal components graph of the entire sample using these landmarks. Once again, there is excellent separation along PC 1 between *Homo* and the other genera, although there is a small area of overlap. Like the

first set of analyses, the longitudinal enlargement of the lateral condyle and the more acute angle between the patellar articular surface and the tibial articular surface are the driving factors for PC1. PC 2 partially separates *Pan* from *Gorilla* and is largely driven by the height of the patellar articular surface and the lateral flexion of the trochlear notch, also as in the previous analysis. Both PC 1 and PC 2 are negatively correlated with centroid size (Figs. 4.46 and 4.47).

For the fossils, WT 15000, ER 1481, Kibish 1, ER 1592 and TM 1513 fall well within the range of *Homo*. All of these fossils also grouped well within the range of variation of *Homo* in the previous analysis. BOU-VP-19/63 is the only fossil that falls within the small zone of overlap between *Pan* and *Homo*. All of the other fossils fall well within the range of the quadrupedal apes and outside of the 95% equal frequency ellipse for *Homo,* although Stw 318 falls very near to several *Homo* outliers.

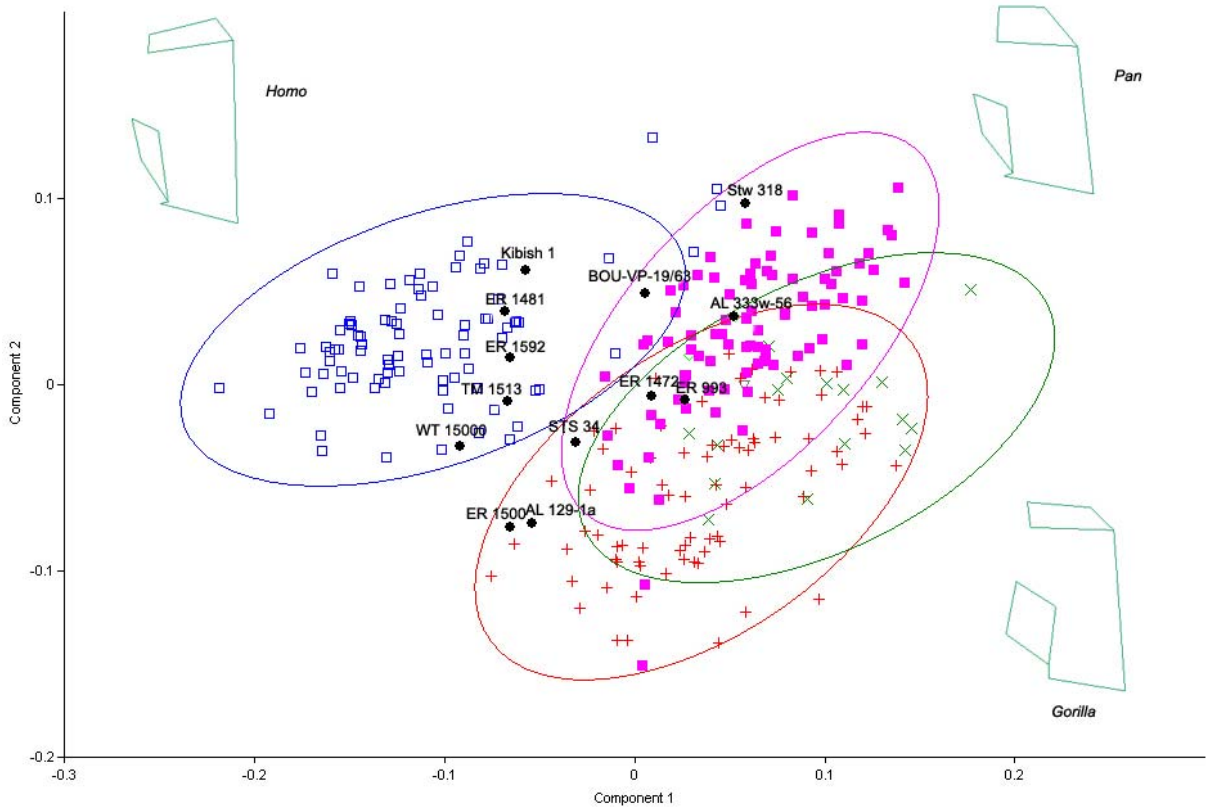

Fig. 4.28 PCA for the fossils plus means for the extant species for the distal femur, landmarks 18-19, 21-22, 25-26, 28-29, and 31-32.. *Homo* is represented by blue open squares, *Pongo* by green Xes, *Gorilla* by red crosses, and *Pan* by purple squares. The fossils are represented by black circles and are labeled in the graph. The lines represent a minimum spanning tree plotted on top of the principal components graph. PC1 accounts for 31%, of the total variance and PC2 accounts for 11%of the overall variance. The wireframe are a distal view of the lateral femoral condyle.

Means were calculated for each extant genus and further analyses were conducted. A PCA of this data was largely inconclusive as the fossils were evenly distributed across PC1 and PC2, although all of the extant apes fell towards the more positive values on PC 2 (fig 4.48). PC 1 is driven by the width of the lateral condyle and PC 2 is driven by the length of the lateral condyle and the acuteness of the angle between the distal articular surface and the patellar articular surface. Based on the MST, this distribution could possibly be broken into three groups. The first group is towards the more positive values on PC1 and contains WT 15000, TM 1513, STS 34, AL 129-1a, *Homo,* and ER 1481 while the second group contains all of the other

fossils and possibly *Gorilla.* The third contains only the extant apes: *Pan* and *Pongo.* These groupings are somewhat at odds with the previous analyses as AL 129-1a and STS 34 have been more ally more similar to the great apes, whereas WT 15000 has been consistently human-like. Neither PC 1 nor PC 2 was correlated with centroid size.

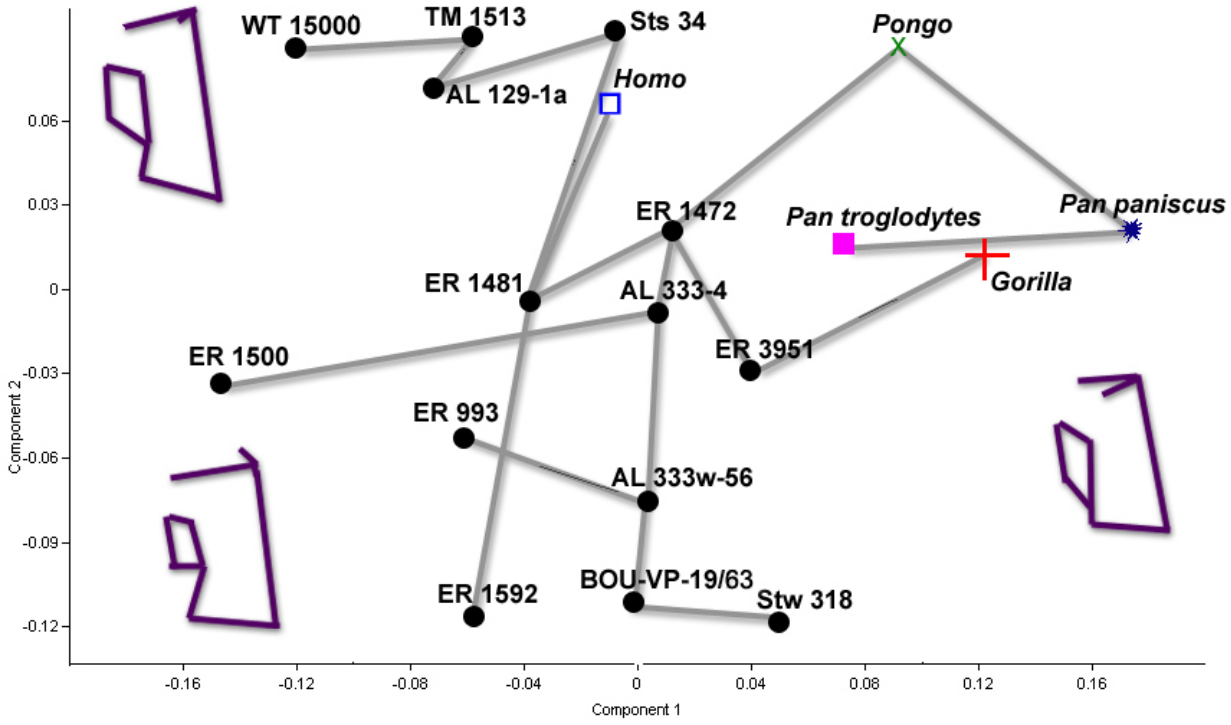

Fig. 4.29 PCA for the fossils plus means for the extant species for the distal femur, landmarks 18-19, 21-22, 25-26, 28-29, and 31-32. *Homo* is represented a blue open square, *Pongo* by a green X, *Gorilla* by a red crosse, and *Pan* by a purple square and blue star. The fossils are represented by black circles and are labeled in the graph. The lines represent a minimum spanning tree plotted on top of the principal components graph. PC1 accounts for 22%, of the total variance and PC2 accounts for 20%of the overall variance. The wireframes are in a distal view.

A neighbor-joining tree was also generated using these data. None of the fossils cluster within any of the apes. ER 1481 and ER 1592 are the only fossils in the direct cluster including *Homo.* The cluster created by the PCA containing WT 15000, TM 1513, STS 34 and AL 129-1a also appears in the neighbor-joining tree. None of the fossils cluster on the basis of site including the three fossils from Hadar, two of which are part of the AL 333 assemblage. In general, the bootstrap values are extremely low across all clusters (fig 4.30).

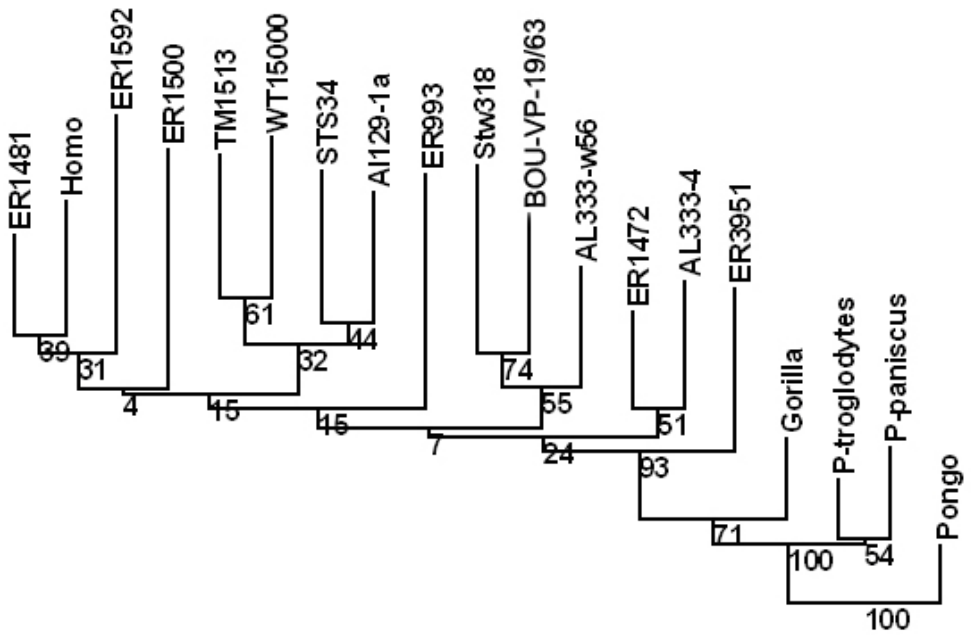

Fig. 4.30 Neighbor joining tree for the distal femur, landmarks 18-19, 21-22, 25-26, 28-29, and 31-32. This tree is based on procrustes chord distances and was rooted with *Pongo* as the outgroup. Bootstrap values are based on 1000 replicates.

Figs 4.31-4.33 are analyses performed using the only the landmarks that capture the shape of the medial condyle and patellar articular surface. This landmark subdivision allowed for the inclusion of Stw 129. This subset of landmarks also did not significantly change the shape of the graph in a principal components analysis (fig 4.31). PC 1 separates *Homo* from the rest of the sample and is driven by the keeled, assymetrical patellar articular surface present in *Homo.* PC 2 partially separates *Pan* and *Gorilla* and is largely driven by the height of the lateral corner of the patellar articular surface. In gorillas, is it generally lower than in *Pan* and *Homo.* To some degree, the condyle size is picked up in these principal axes, but to lesser degree than when the lateral condyle is present. PC1 accounts for negatively correlated with size and PC 2 is positively correlated with size.

The fossils occur in roughly the same places as they have in previous analyses. Stw 129, the only new fossil in this analysis, groups with the apes very near to ER 1592 and AL 129-1a. WT 15000, ER 1481 and Kibish 1 are the only fossils to fall solely within the distribution of *Homo* although ER 1472, TM 1513 and STS 34 fall within the overlap zone between *Homo* and the other taxa. The only fossil to significantly change positions is ER 1592; it grouped with *Homo* in the previous two analyses and groups with the other taxa in this analysis.

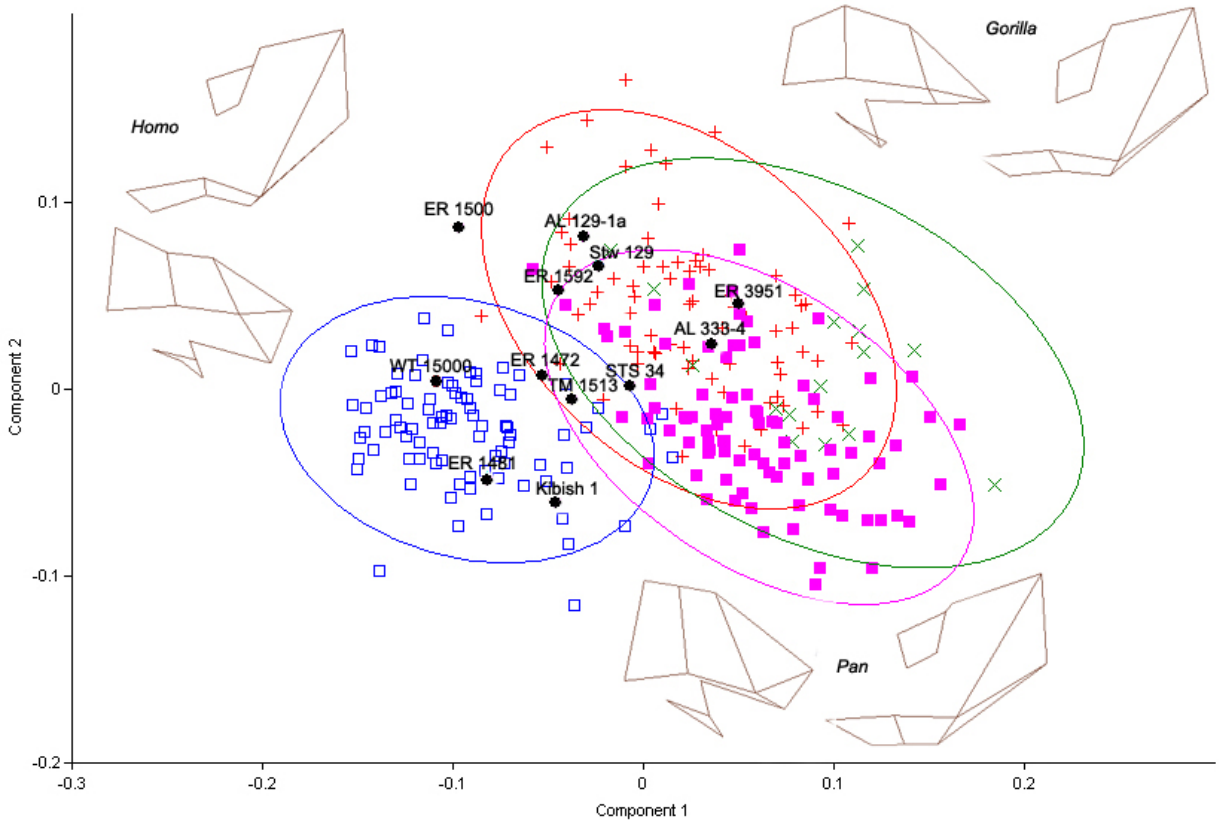

Fig. 4.31 PCA of the distal femur, landmarks 15, 17-24, 27-28, and 30-31. *Homo* is represented by blue open squares, *Pongo* by green Xes, *Gorilla* by red crosses, and *Pan* by purple squares. The fossils are represented by black circles and are labeled in the graph. Circles represent the 95% equal frequency ellipses of each extant genus. PC1 accounts for 24%, of the total variance and PC2 accounts for 9%of the overall variance. The wireframes are a distal view of the distal femur and a view towards the patellar articular surface from the posterior side of the femur.

The means for all of the extant taxa were calculated and additional analyses were performed and figure 4.32 is a PCA with an MST using these values. The fossils are fairly evenly distributed across PC 1, with WT 15000 having the least positive values and ER 3951 having the most positive values. The fossils are also evenly distributed across PC 2, with WT

15000 having the most positive values and Stw 129 having the moving negative values. In general, the extant taxa and the fossils that were more affliated with *Homo* in the previous analysis fall near the top of the graph and those fossils more affiliated with *Pan* and *Gorilla* fall in the lower parts of the graph. PC 1 is driven by the flatness of the patellar articular surface with the apes and some of the fossils having flat surfaces and *Homo*, WT 15000, and ER 1500 having deepest surfaces. PC 2 is driven by the shape of the most posterior portion of the medial condyle; in ER 1500, Stw 129 and ER 3951, it is angled differently than in the individuals towards the more positive values on the graph. Neither PC 1 nor PC 2 is correlated with size.

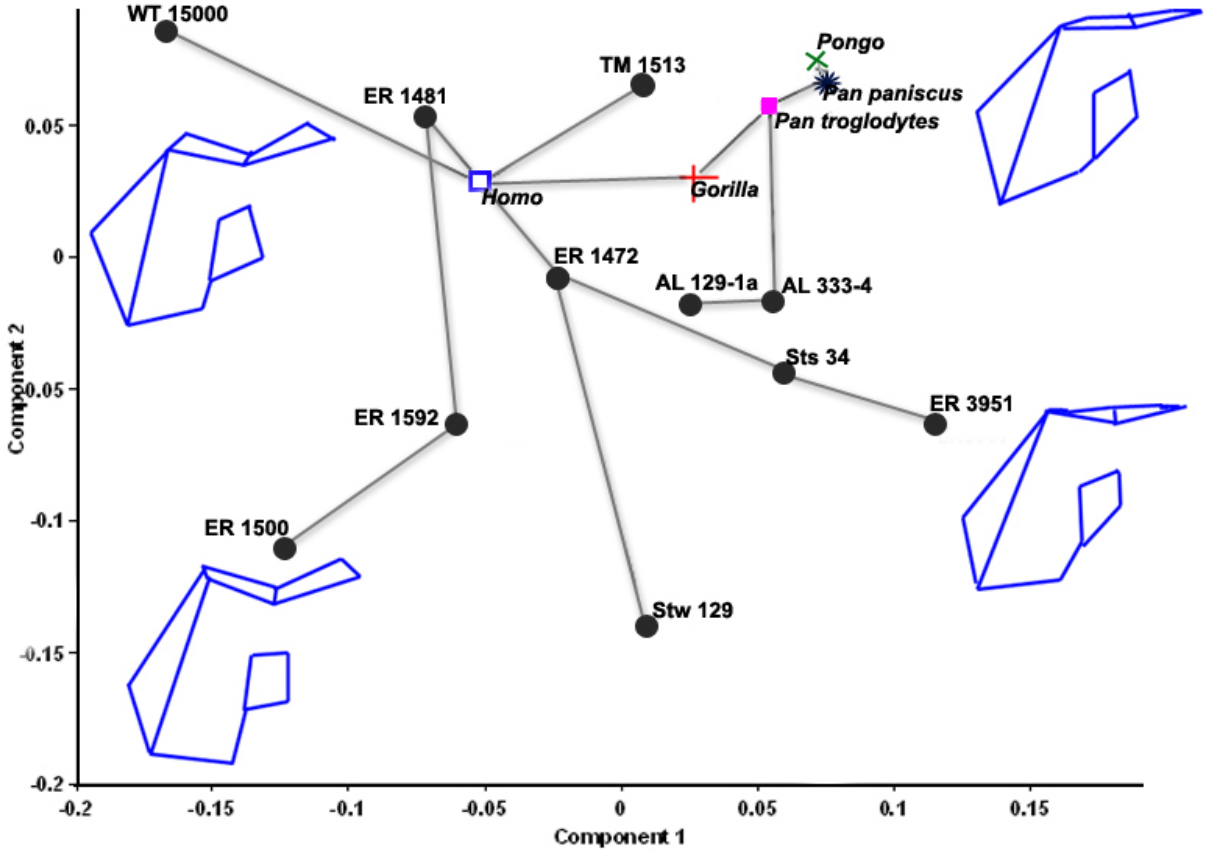

Fig. 4.32 PCA for the fossils plus means for the extant species for the distal femur, landmarks 15, 17-24, 27-28, and 30-31. *Homo* is represented by a blue open square, *Pongo* by a green X, *Gorilla* by a red cross, and *Pan* by a purple square and blue star. The fossils are represented by black circles and are labeled in the graph. The lines represent a MST plotted on top of the PCA. PC1 accounts for 24%, of the total variance and PC2 accounts for 20%of the overall variance. Wireframes are in a distal view.

A neighbor-joining tree was also created using these values (fig 4.58). ER 1481, WT 15000 and TM 1513 form a single cluster with *Homo* with a very high boostrap value, lending further support for the results from the other analyses. For the first time, both of the specimens from Hadar form a cluster separate from the other fossils, but there are low bootstrap values overall within the fossil grouping. None of the fossils fall within the cluster of quadrupedal apes.

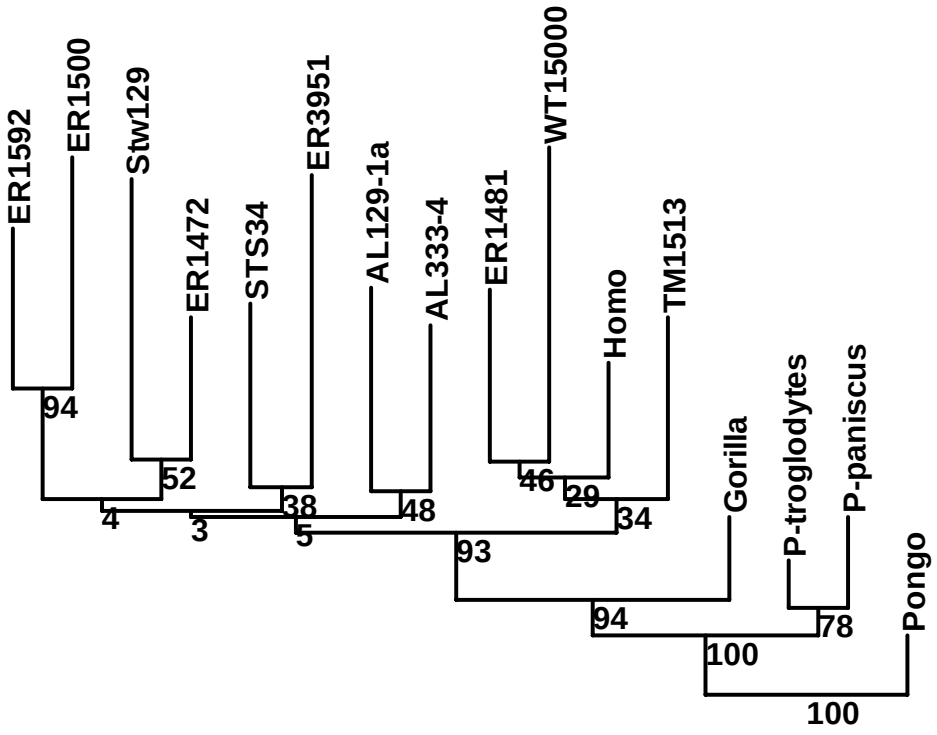

Fig. 4.33 Neighbor joining tree for the distal femur, landmarks 15, 17-24, 27-28, and 30-31. This tree is based on procrustes chord distances and was rooted with Pongo as the outgroup. Boot strap values are based on 1000 replicates.

Finally, the landmark set for the distal femur was segmented such that the majority of the utilized landmarks described the distal articular surface. This allowed for the inclusion of one additional fossil: TM 3601. A PCA for these values is shown in figure 4.59. There is still good separation between *Homo* and the quadrupedal apes along PC 1. PC1 accounts for driven by the

enlargement of the medial condyle in *Homo* with regards to the greater apes. PC2 does not split the sample in any meaningful way. For the fossils, ER 1481, STS 34, and WT 15000 fall in the range of solely modern humans. TM 1513 and ER 1472 fall within the range of overlap between *Homo* and the other taxa. Kibish 1 falls towards the *Homo* end of the graph, but outside the 95% equal frequency ellipses for modern humans. TM 3601 falls within the range of the apes for PC1, but outside of all 95% equal frequency ellipses on PC 2. All other fossils fall within the great ape distribution. PC 1 accounts for negatively correlated with size (fig 4.60).

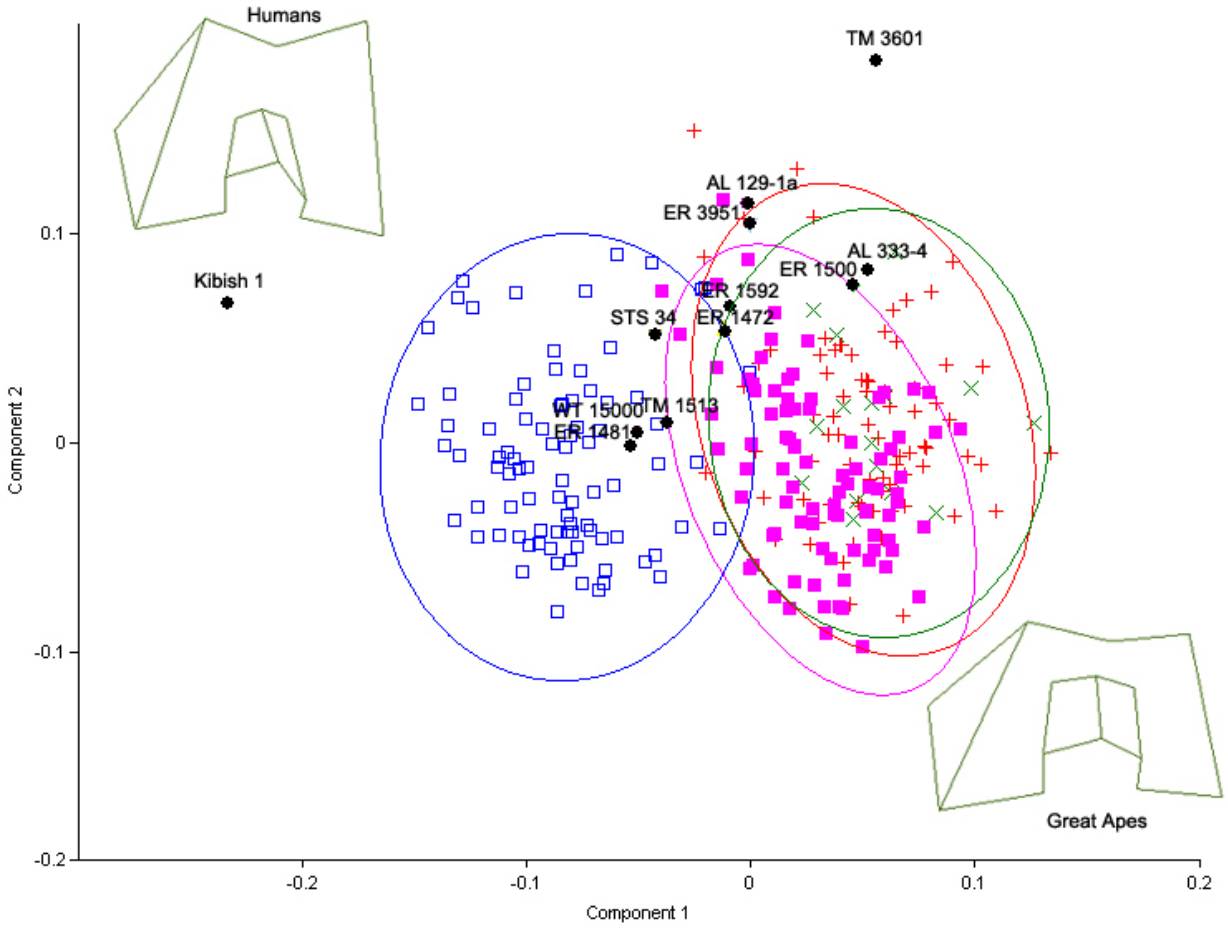

Fig. 4.34 Principal components analysis for the distal femur, landmarks 15, 20-32. Homo is represented by blue open squares, Pongo is represented by green Xes, Gorilla is represented by red crosses, Pan is represented by purple squares. The fossils are represented by black circles and are labeled in the graph. The closed curves are 95% equal frequency ellipses for the extant genera. PC1 accounts for 21%, of the total variance and PC2 accounts for 10%of the overall variance. The wireframes illustrate a distal view of the distal femur. Only a wireframe for the "ape" cluster is shown as there is complete overlap for all three taxa.

Means were calculated for the extant genera and further analyses were conducted. The results of a PCA with MST are shown in figure 4.35. The fossils are relatively evenly distributed across PC 1, although there are definite differences on PC 2. PC 1 is driven by the overall length of the two condyles with those individuals falling towards the negative values having longer condyles than those falling towards the positive values. On PC 2, TM 3601, ER 3951, TM 1513 and WT 15000 all have similar values, as well as ER 1500 and ER 1592 in the opposite direction. PC 2 is driven by the width of the intercondylar notch with ER 1500 and ER 1592 having especially wide notches. PC 1 is not correlated with centroid size.

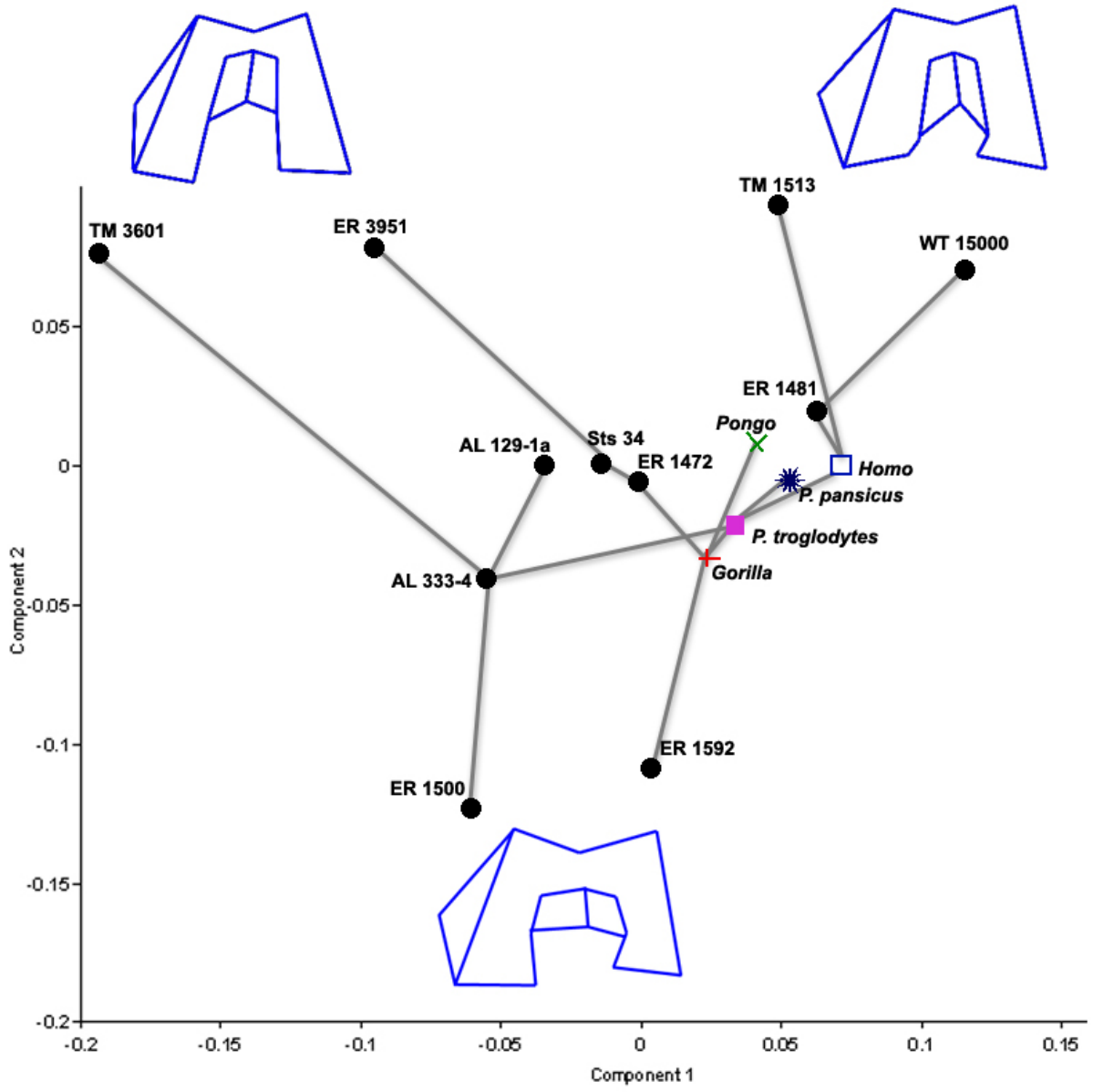

Fig. 4.35 Principal components analysis for the fossils plus means for the extant species for the distal femur, landmarks 15, 20-32. Homo is represented by blue open squares, Pongo by green Xes, Gorilla by red crosses, and Pan by purple squares. The fossils are represented by black circles and are labeled in the graph. The lines represent a minimum spanning tree plotted on top of the principal components graph. PC1 accounts for 25%, of the total variance and PC2 accounts for 20% of the overall variance. The wireframes are in a distal view.

A neighbor-joining tree was also generated with these data (fig 4.36). ER 1481, WT 15000, TM 1513 and *Homo* form their own cluster with a relatively high boostrap value as in the

previous analysis (fig. 4.33). The other fossils are distributed in different clusters that are sister to that containing *Homo.* No fossils group with the quadrupedal apes.

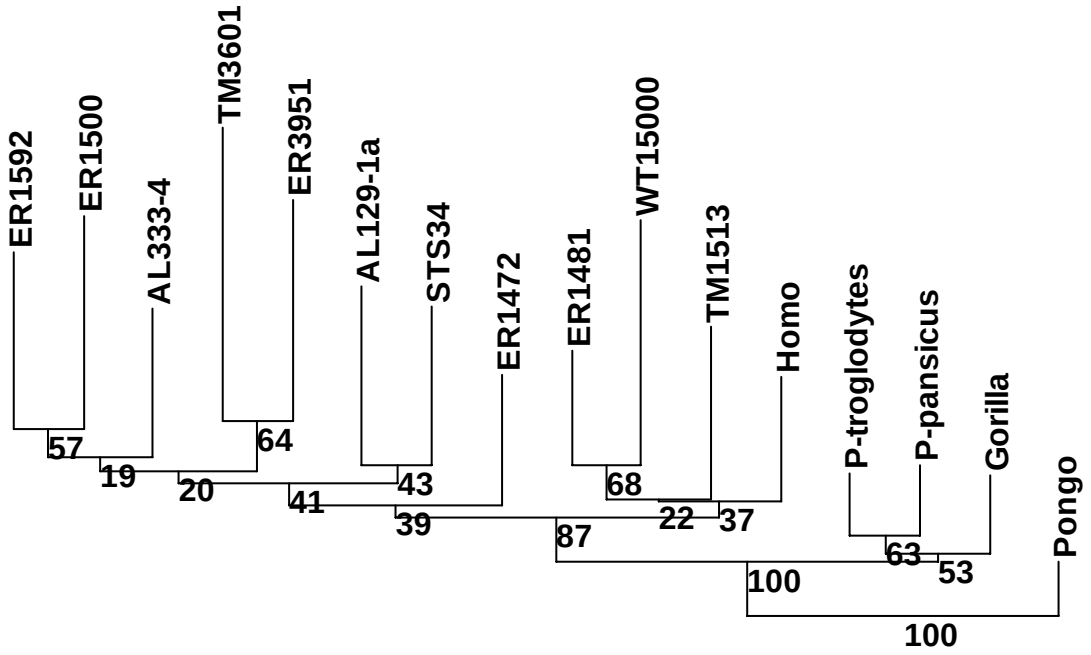

Fig. 4.36 Neighbor joining tree for the distal femur, landmarks 15, 20-32. This tree is based on procrustes chord distances and was rooted with Pongo as the outgroup. Boot strap values are after 1000 replicates.

Distal Femur Discussion and Analysis

There is a high degree of variation within the fossil sample. Figure 4.37 is a bar graph depicting the distribution of procrustes chord distances in the entire sample. The group of fossils has higher average pairwise procrustes distance than all other comparison groups, as well as has some of the highest single pairs of individuals. The maximum pairwise procrustes distance in the entire sample is between SK 1896 and ER 1500. Therefore, it is reasonable to assume that there are likely two or probably more taxa present within the fossil distribution.

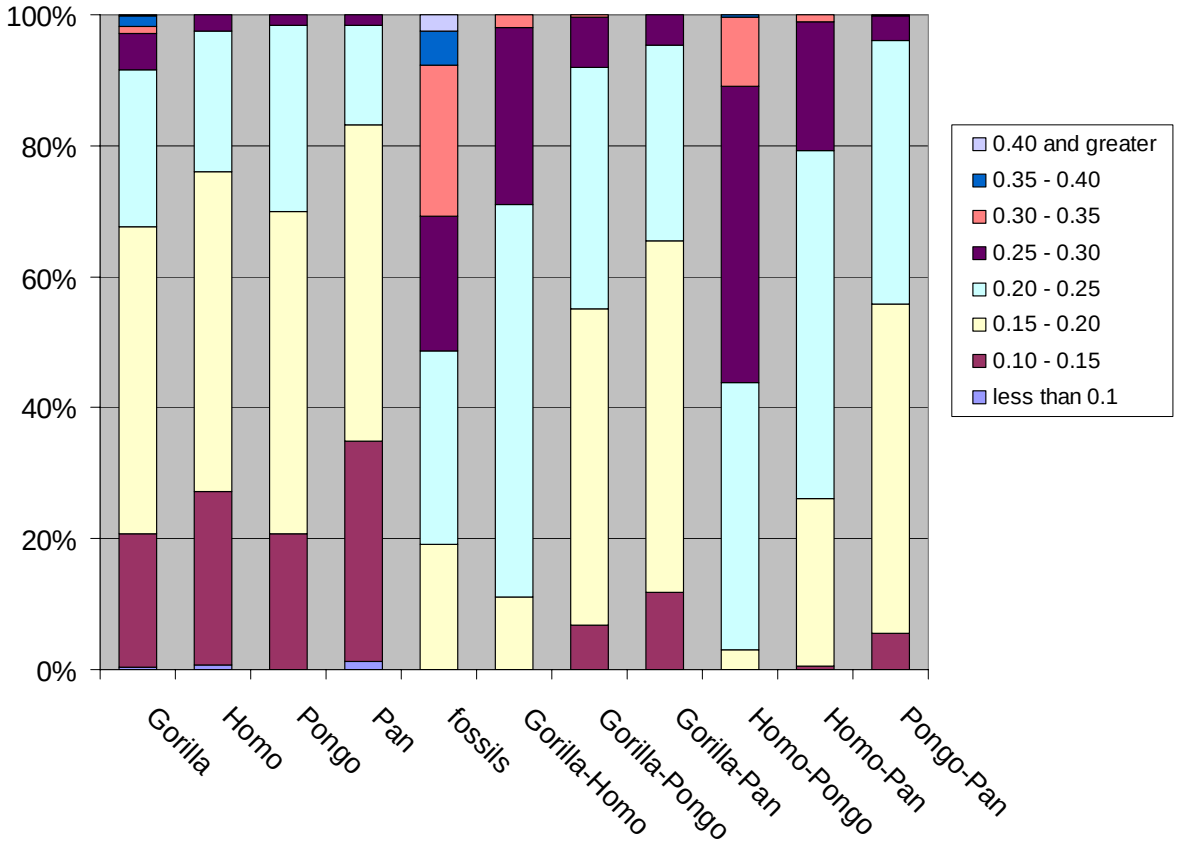

Fig. 4.37 This bar graph is a representation of the distribution of procrustes chord distances within and between the different genera in the most complete sample of the distal femur. The array of procrustes distances were segmented into arbitrary units of 0.05. The average procrustes distance between the fossils was higher than all other comparison groups. The maximum procrustes distance within the fossils was larger than any other pairwise distance in the entire sample.

The differences between the extant taxa for the distal femur are relatively consistent, regardless of landmark configuration. The same factors that drove PC 1 and PC 2 in the PCA of the largest set of landmarks also drove the smaller landmark subsets. Because of this, all of the fossils can be looked at as a group, despite not necessarily having been compared directly by using the more complete femora as a proxy for comparison. The most complete femora were relatively static in their position in the PCA of the entire sample, regardless of the landmark set. Those results are presented in table 4.7.

For the distal femur, all of the fossils fall in one of three broad groupings. The first group (ER 1481, Kibish 1, TM 1513, SK 1896 and WT 15000) has a distal femoral morphology that is

indistinguishable from that of modern humans. The second group (ER 1472, ER 1592, and BOU-VP-19/63) has a distal femoral morphology that is on the periphery of the modern human distribution. For the individuals in this group, there are aspects of the distal femur that are extremely human-like, and aspects that are not completely modern. The third group (AL 129-1a, AL 333-4, AL 333w-56, ER 993, ER 1500, ER 3951, STS 34, STS 129 and Stw 318) looks most like the extant great apes for the distal femur and these individuals retain characteristics that unite them with *Pan* and/or *Gorilla* and could indicate a proficiency at other positional behaviors besides bipedalism. TM 3601 has a unique morphology, but fell closest to the extant apes (Table 4.6).

Table 4.7 List of specimens used for the analysis of the distal femur and their affiliation with the extant taxa. Specimens with multiple attributions indicate that the fossil fell in an area of overlap. The "variation pattern" is discussed in the text.

Fossil	Previous Taxonomic Attribution (& refs.)	Taxon Affiliation(s)	Variation Pattern
AL 129-1a	*A. afarensis*[9]	*Pan/Gorilla*	3
AL 333-4	*A. afarensis*[9]	*Pan /Gorilla*	3
AL 333w-56	*A. afarensis*[9]	*Pan*	3
BOU-VP-19/63	*H. erectus?*[8]	*Pan/Homo*	2
ER 993	Hominidae *sp indet*[7], *P. boisei*[12]	*Pan/Gorilla*	3
ER 1472	*Homo sp*[4,5,7]	*Pan/Homo* or *Pan*	2
ER 1481	*Homo sp.* [4,5,7]	*Homo*	1
ER 1500	*P. boisei*[2,7]	*Pan/Gorilla*	3
ER 1592	Hominidae *sp indet*[7]	*Homo* or *Pan*	2
ER 3951	Hominidae *sp indet*[7], *Homo*[11]	*Pan/Gorilla*	3
Omo 1	*Homo sapiens*	*Homo*	1
SK 1896	*Homo* cf. *erectus* [6,7]	*Homo*	1
Sts 34	*A. africanus*[1,7]	*Pan* or *Pan/Homo*	3
Stw 129	*H. habilis*[7]	*Pan*	3
Stw 318	*A. africanus*[3,7]	*Pan*	3
TM 1513	*A. africanus*[1] , Hominidae *sp indet*[7]	*Homo* or *Pan/Homo*	1
TM 3601	???	none	3
WT 15000	*H. erectus*[10]	*Homo*	1

1 Robison, 1972; 2 Grausz, 1988; 3 McHenry and Berger, 1998; 4 Senut and Tardieu, 1985; 5 Leakey, 1973; 6 Susman *et al.,* 2001; 7 McHenry 1994; 8 Gilbert 2009; 9 Johanson *et al.,* 1978; 10 Walker and Leaky, 1993; 11 Tardieu, 1997, 12 Walker, 1972

Functional Implications for the Knee

All of the individuals in the first group have the full human pattern for the distal femur and would have been "good" bipeds. In humans, the lateral and medial condyles are of similar size because they equally important in transmitting downward forces during bipedal locomotion. In apes, the medial condyle is larger and is used more in load transmission. Also, humans have condyles that are more elliptical (particularly the lateral condyle) and more symmetrical in order to provide a larger surface for articulation with the tibia. The condyles also increase the lever arm for the quadriceps femoris (which is the main flexor of the knee) by making a flatter anterior surface; this then orients the patella more anteriorly than is seen in the apes. (Aiello and Dean, 1990) The deep, asymmetrical patellar groove in *Homo* is likely to prevent the patella from

being laterally dislocated during flexion of the knee. In *Homo,* the quadriceps femoris pulls up along the human bicondylar angle, pulling the patella in the lateral direction whereas in a quadruped, it is pulled proximally in a straight line (Heiple and Lovejoy, 1971; Stern and Susman, 1983).

Ontogenetically, the distal femur forms differently from the proximal femur. The distal femoral epiphysis begins its formation in utero (Moore and Persaud, 1998). The distinctive keel of the human femoral trochlea also begins to form in utero. Thus, the shape of the trochlea is the result of a change in the human genome and not an epigenetic trait (Tardieu, 1997, 1999; but see Fulkerson and Hungerford, 1990 for opposite view). During human puberty, the human femur elongates and there are further modifications to the distal epiphysis. The lateral condyle enlarges longitudinally and takes on its full elliptical form, the patellar groove deepens and the lateral edge becomes even more pronounced (Tardieu, 1997). Based on the femoral form, the individuals in the first group (of Table 4.6) both had all of the necessary genetic changes and a long enough adolescent growth period (not necessarily a "spurt") to see those changes phenotypically manifested.

Distal Femoral Shape Variation: The Result of Heterochronic Changes?

The second and third groups are potentially more interesting. Tardieu (1997) hypothesized that the cause of the distal femoral shape variation was a heterochronic difference between late *Homo,* early *Homo* and *Australopithecus.* Using radiographs, she compared the shape of the distal articular surface and the profile of the lateral condyle of AL 129-1a, ER 1472 and ER 1481 to a human growth series. She found that AL 129-1a looked most similar to a

human child, aged 10 yrs, whereas ER 1472 was most similar to a late adolescent aged 16 yrs and ER 1481 was most like the 17yr.

Figure 4.38 is a PCA of the full fossil distal femora (AL 333-4, AL 129-1a, ER 1472, ER 1481, ER 1592, WT 15000 and Sts 34) and the ontogenetic sample. PC 1 divides the ontogenetic sample into two significantly different ($p<0.0001$) groups with children ages 2 to 7 falling on the right side of the graph and those 10 to 20 on the left side of the graph. WT 15000, ER 1481 and ER 1472 all fall within the 95% equal frequency ellipse for the group of older children. The two specimens from Hadar, ER 1592 and STS 34 fall outside the 95% equal frequency ellipse for the older children. PC 1 is positively correlated with age (fig. 4.39), with the majority of the fossils falling well off of the line. When the fossils are removed from the analysis, the correlation between age and PC 1 for just the humans increases to an r value of 0.95 (fig. 4.40). PC 1 is also correlated with centroid size (fig. 4.41), but that is unsurprising because age and centroid size are also correlated (fig. 4.42). PC 1 is driven by the change in the angle between the patellar surface and the distal articular surface, as well as the longitudinal enlargement of the lateral condyle.

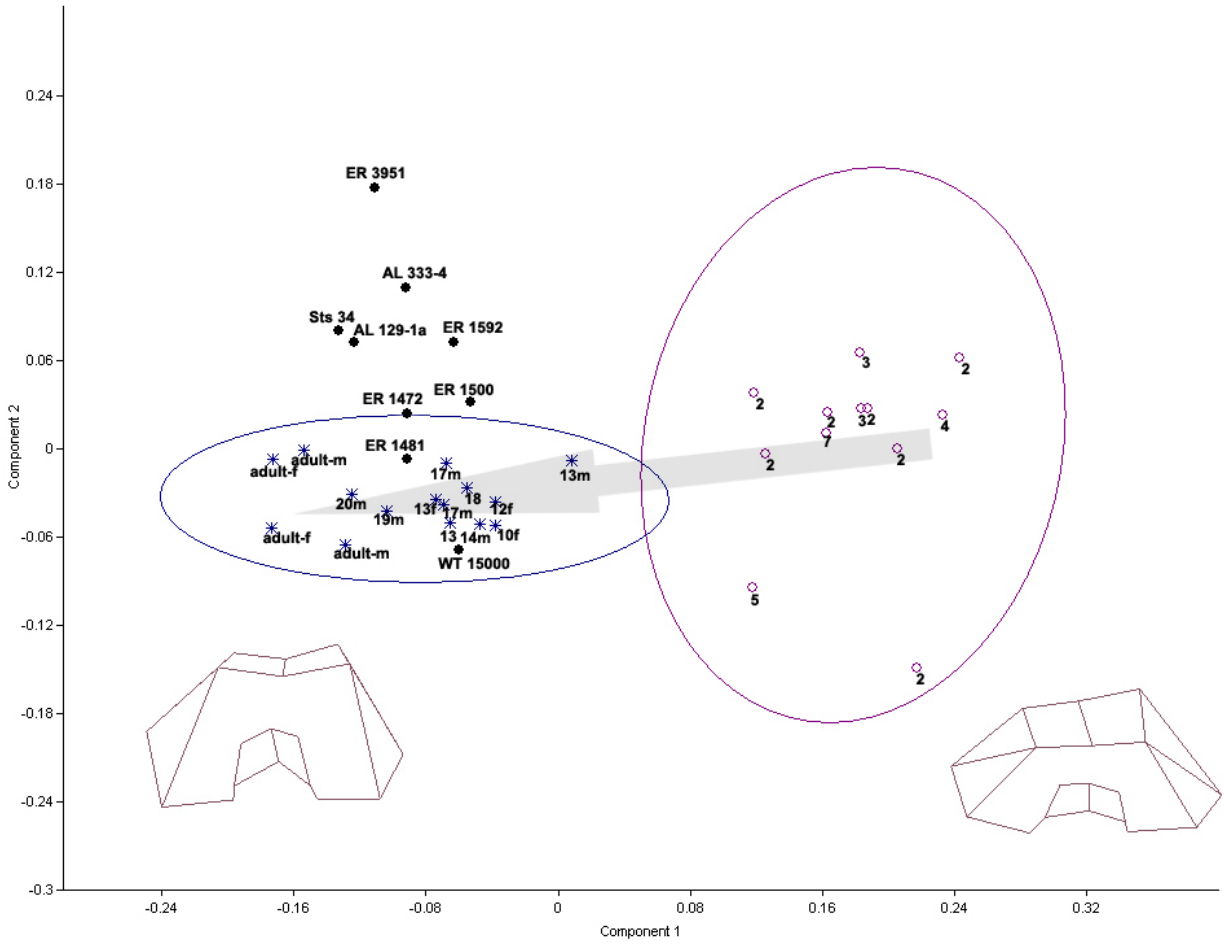

Fig. 4.38 A PCA of the ontogenetic sample of *H. sapiens* femora and the complete fossils. The wireframes are oriented towards the distal articular surface. All individuals are labeled with their age or accession number. There was a natural break along PC1 between the 2-7 year and 10-20 year samples, so two groups were assigned. The 2-7 year old individuals are represented by purple circles and the 10-20 year old individuals are represented by blue stars. PC1 represents 48% of the total variation in this sample and PC2 represents 8%. The arrow indicates the direction of ontogenetic change.

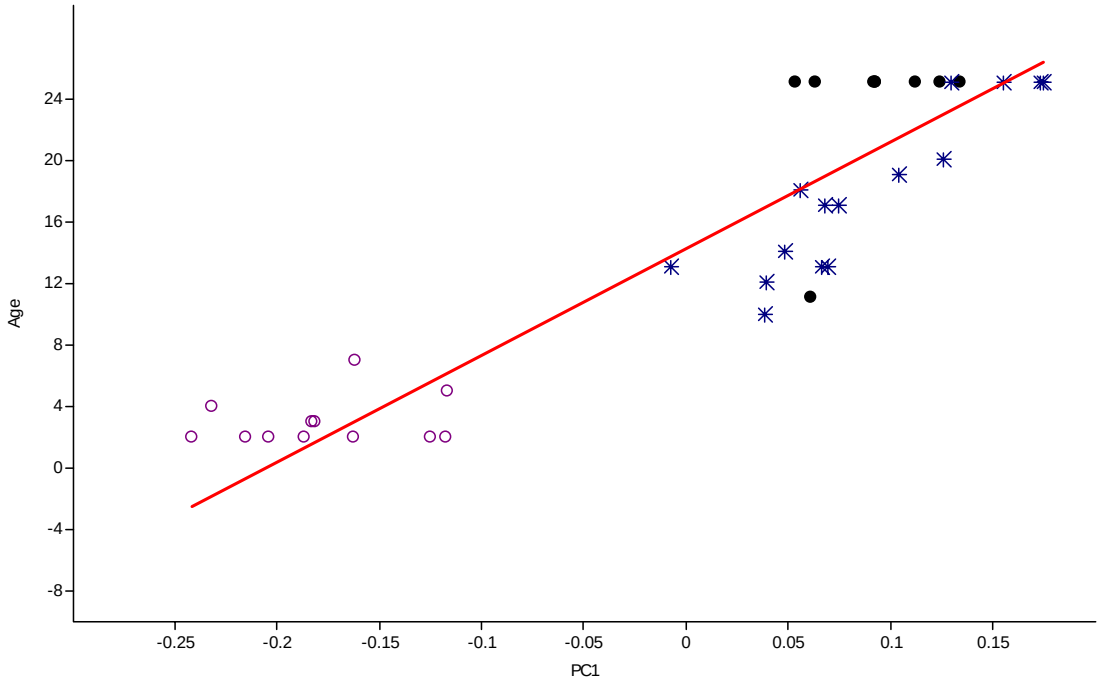

Fig 4.39 A linear regression of PC1 against age for the ontogenetic human sample. WT 15000 was assigned an age of 11 based on a human growth pattern for the dentition (Smith, 1993). The rest of the fossils and the adult humans were assigned the arbitrary age of 25. The result is significant with $p<0.0001$ and r=0.91.

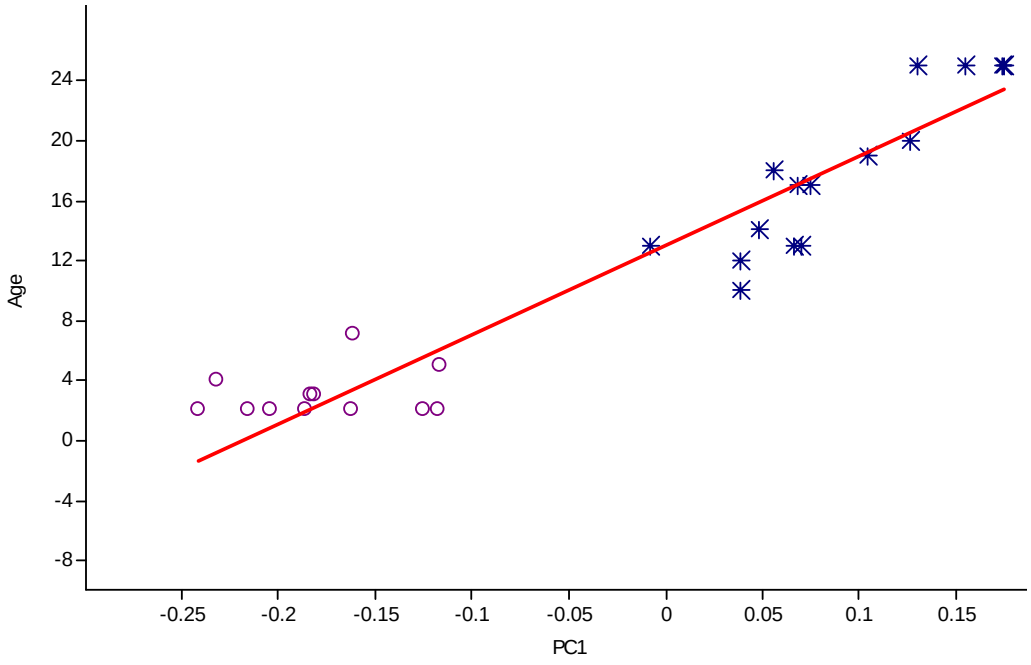

Fig. 4.40 A linear regression of PC1 against centroid size for only the ontogenetic human sample. The relationship is significant with $p<0.0001$ and r = 0.95.

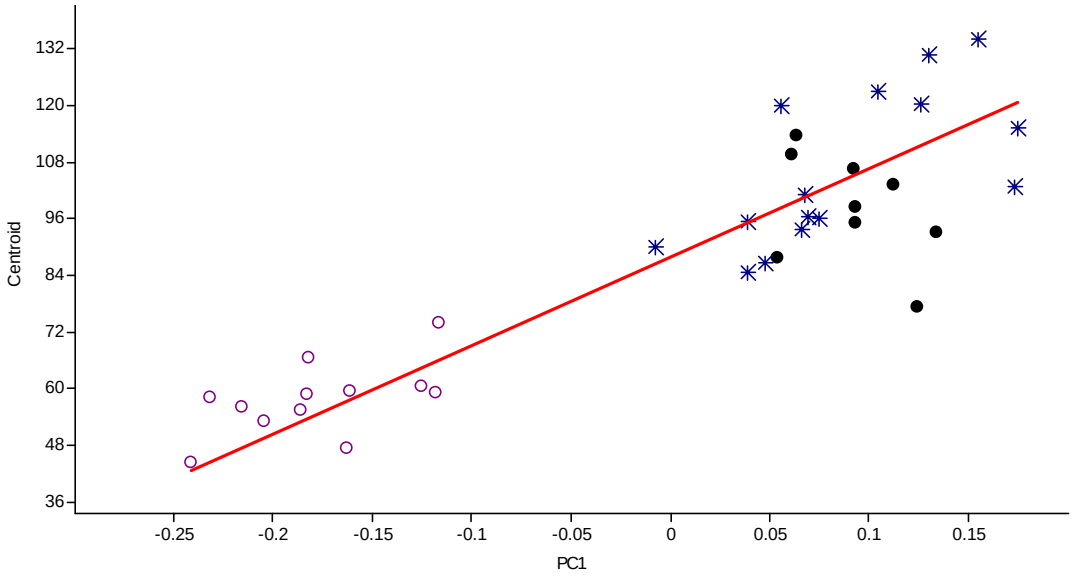

Fig. 4.41 A linear regression of PC1 against centroid size for the ontogenetic human sample and fossil. The relationship is significant with $p<0.0001$ and r = 0.89. AL 129-1a and Sts 34 fall well off of the regression line.

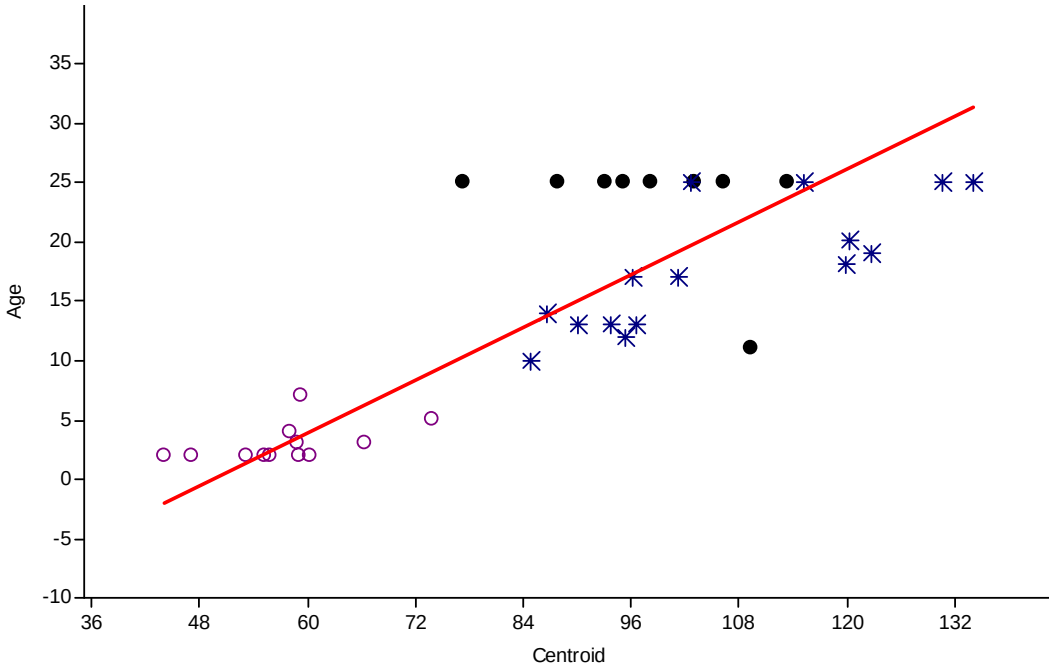

Fig. 4.42 Linear regression of age on centroid size for the human ontogenetic sample. The results are significant with p<0.0001 and r = 0.82.

The same analysis was completed using a comparable ontogenetic sample of *Pan troglodytes*. Figure 4.43 is the results of a PCA of this ontogenetic sample and the same relatively complete fossil femora. The ontogenetic trajectory of the *Pan* distal femur is not quite as simple as *Homo*, as it occupies part of both PC 1 and PC 2, as opposed to being almost entirely represented by PC 1 in the previous analysis. While the fossils certainly contribute to that distribution, analyses run without the fossils have a similar pattern. WT 15000 and ER 1481 both fall well outside the 95% equal frequency ellipse of all of the *Pan* individuals on PC 2 while ER 3951 falls well outside the 95% equal frequency ellipses on PC 1. Sts 34, ER 1472 and ER 1592 are all very close to the 95% confidence line for the older *Pan* individuals. On the other hand, AL 333-4 and AL 129-1a both fell well within the range of the adult *Pan* individuals inside the 95% equal frequency ellipse.

The shape change along the first two arrows noted in the PCA (fig. 4.43) involves the enlargement of the medial condyle and a shift in the position of the medial epicondyle from a more anterior position to a more posterior position. The second shape change along the third arrow involves a narrowing of the intercondylar notch and the distal articular surface taking on a more square shape. PC 1 is correlated with age and centroid size, as in the previous analysis (fig. 4.44- 4.45) and age and centroid size are also correlated (fig. 4.46). The correlations are not as high as for *Homo* because important age related shape change occupies more than one principal axis.

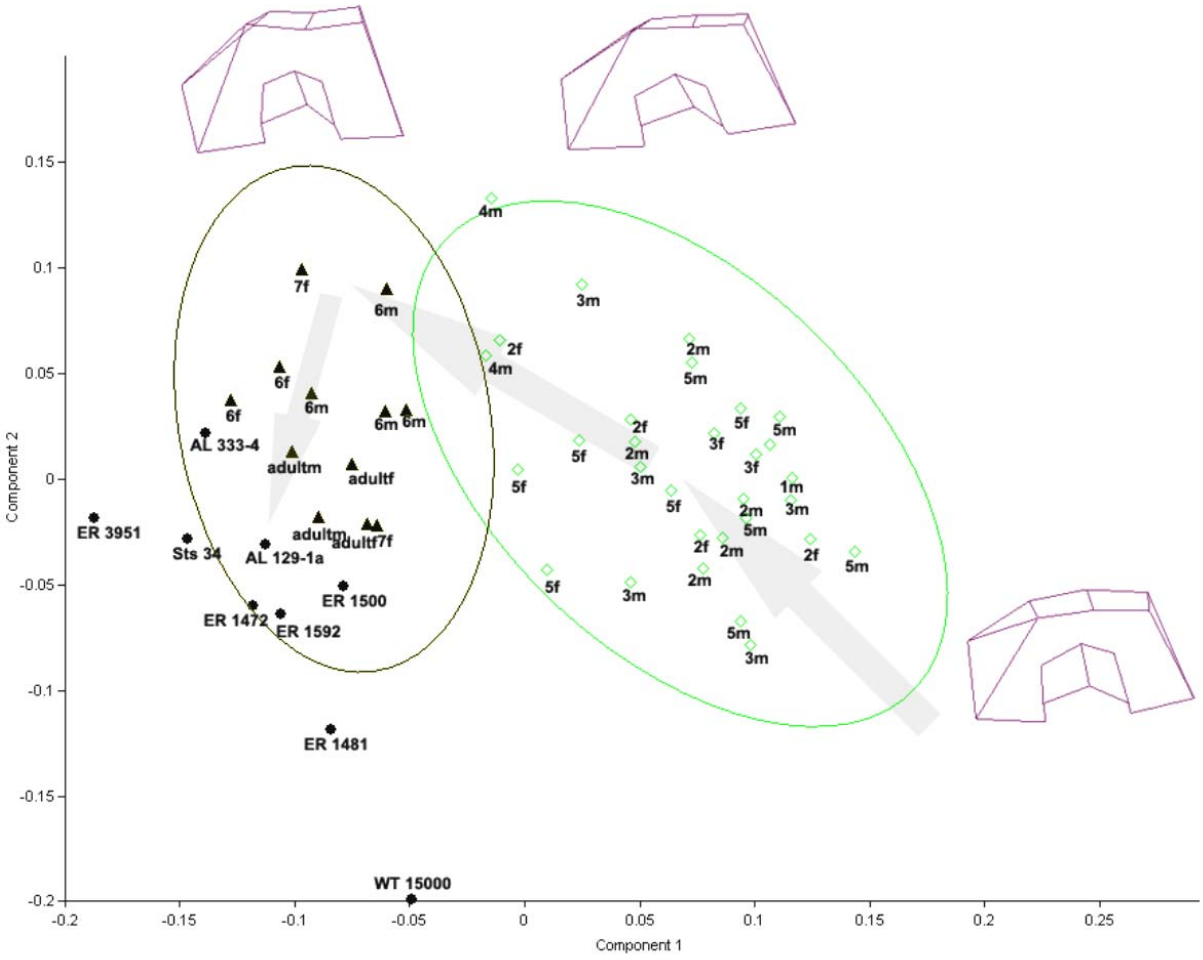

Fig. 4.43 A PCA of the ontogenetic sample of *P. troglodytes* femora and the complete fossils. The wireframes are oriented towards the distal articular surface. All individuals are labeled with their age class or accession number. There was a natural break between those 1 – 5 and those 6 – adult so two groups were assigned. The 1-5 age classed individuals are represented by green circles and the 6-adult age classed individuals are represented by black triangles. PC1 represents 27.9% of the total variation in this sample and PC2 represents 10.9%. The arrows indicats the direction of ontogenetic change.

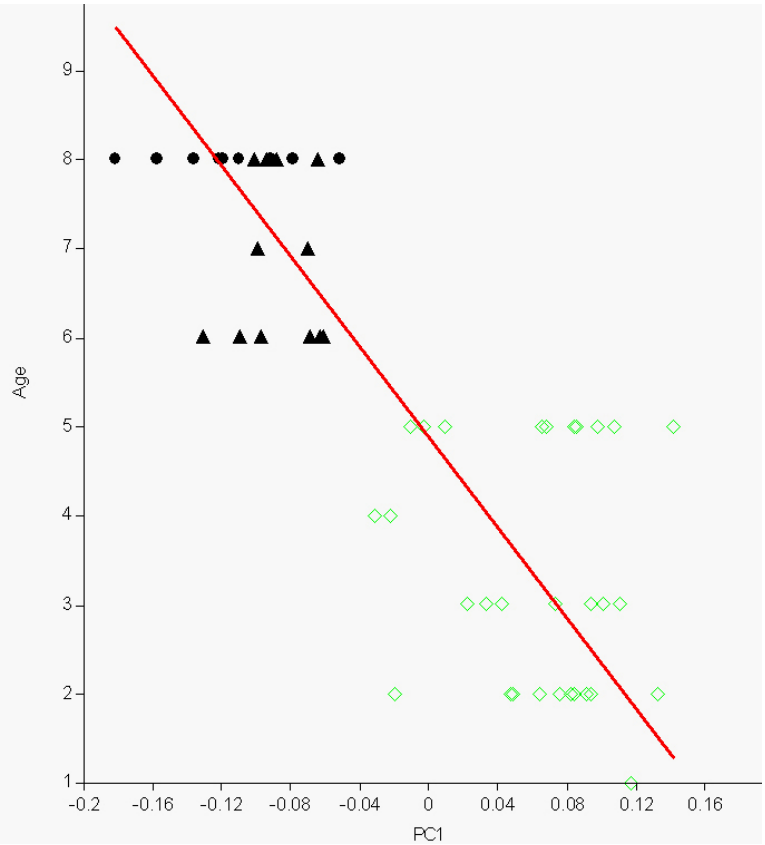

Fig. 4.44 A linear regression of age against PC 1 for the ontogenetic sample of *Pan* distal femora and the fossils. Adults and fossils were assigned an age class of "8". The results are significant with r = -0.81 and $p<0.0001$

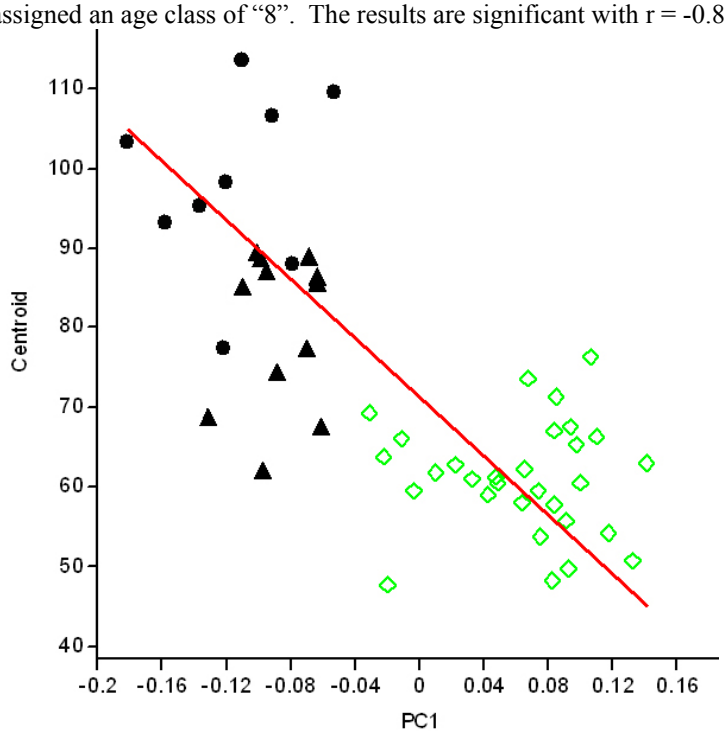

Fig. 4.45. A linear regression of centroid size against PC 1 for the ontogenetic sample of *Pan* distal femora and the fossils. Adults and fossils were assigned an age class of "8". The results are significant with r=-0.73 and $p<0.0001$

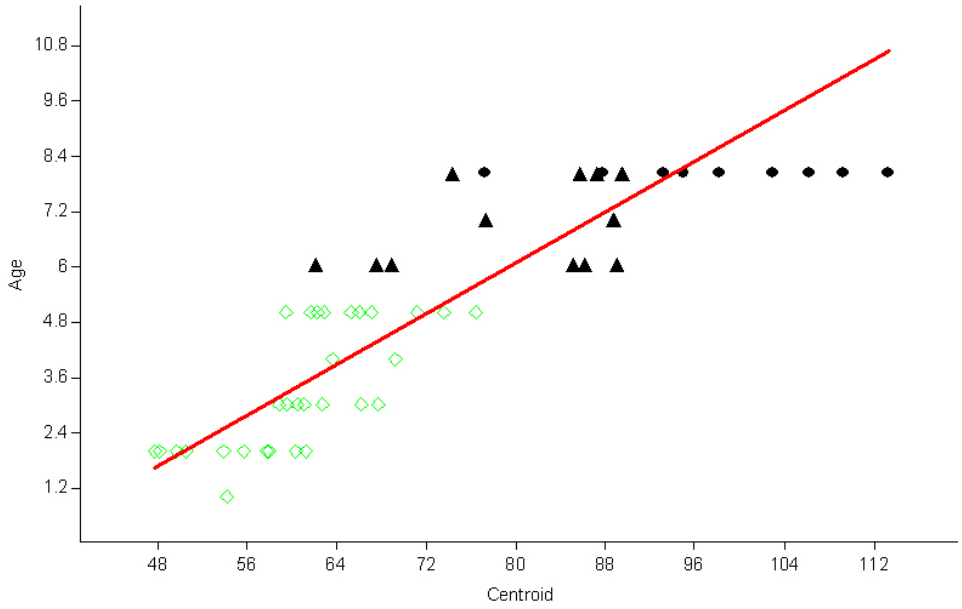

Fig. 4.46 A linear regression of age against centroid size for the ontogenetic sample of *Pan* distal femora and the fossils. Adults and fossils were assigned an age class of "8". The results are significant with, r=0.83 and $p<0.0001$.

These data do not support that idea that *all* distal femoral shape variation is the result of changes in growth patterning and speed. If the morphology of *Australopithecus afarensis* simply represented an early cessation of growth as compared to *Homo sapiens,* then AL 333-4 and AL 129-1a should have been most similar to the younger *Homo sapiens* specimens; instead, they were well outside the range of human variation for the entire distal femoral epiphysis. On the other hand, they were easily included in the 95% equal frequency ellipse for *Pan* indicating they are more like adult *Pan* in their overall morphological pattern. This same pattern is true for ER 1500 and ER 1592, but to a lesser degree. An opposite result was obtained for WT 15000 and ER 1481 which were well within the 95% equal frequency ellipse for adult *Homo,* but far outside all confidence intervals for *Pan.*

The other fossils occupy a murkier position. ER 3951 and Sts 34 were outside the confidence intervals for both *Pan* and *Homo.* Particularly, ER 3951 was far outside the confidence intervals in both instances. This is certainly evidence that these fossils don't fall on

the ontogenetic path of the extant species tested here and could be more evidence for a completely unique morphological pattern of which there is no extant analogue. ER 1472 falls just outside the 95% equal frequency ellipse for *Pan* and *Homo,* occupying a similar position both analyses. This is more evidence for its intermediate position between *Pan* and *Homo.*

While more data needs to be collected on a larger ontogenetic sample of modern humans (particularly in the time between 7 and 12 years), the overall results of these analyses indicate that morphological pattern of the fossils individuals cannot be explained by changes in heterochrony. If the morphological variation in Plio-Pleistocene hominin distal femora is not due to epigenetic changes or differences in growth patterning, then the next logical conclusion is that it represents a functional adaptation. The individuals in the third group have a morphology that is intermediate between the great apes and *Homo,* particularly in the size of the lateral condyle and the projection of the lateral patellar lip (see fig. 4.47 for a wireframe transformation between ER 1481 representing group 1 and Sts 34 representing group 3). The smaller size of the lateral condyle likely indicates that these individuals did not have a fully modern mechanism for load transmission in bipedal locomotion and that their patellae were not subjected to the same lateral forces by the quadriceps femoris muscle. The results presented here and in previous studies (*e.g.* Stern and Susman, 1983; Lague 2002) point towards a locomotor pattern that does not absolutely require a stable knee. Perhaps these individuals retained climbing and other arboreal positional behaviors as important components to their locomotor repertoire.

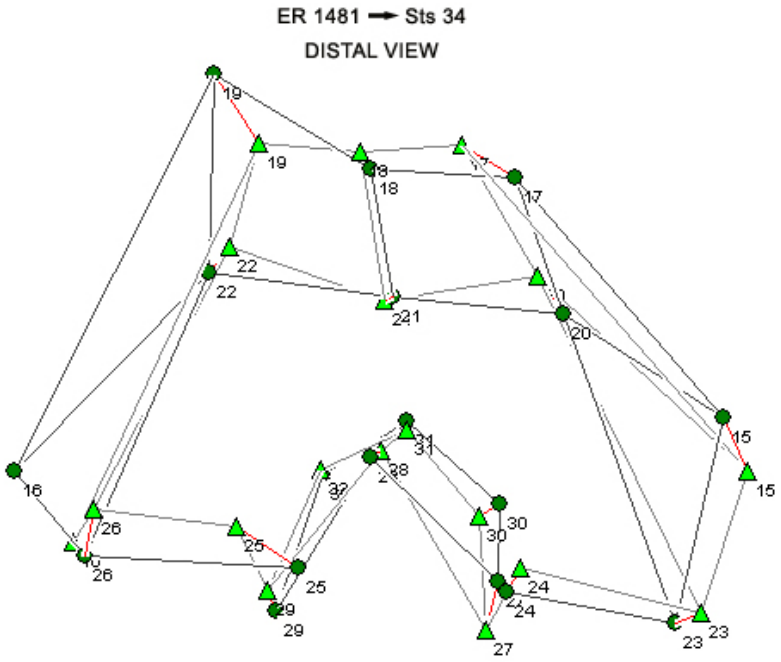

Fig. 4.47 Distal view of a wireframe transformation between ER 1481 represented by circles and Sts 34, represented by triangles. The red lines represent vectors of change. The two fossils differ most at points 19 and 17, which are along the proximal edge of the patellar articular surface, and points 25 and 26, which represent the posterior edge of the lateral condyle.

The individuals that fall in the second group have a morphology that is more difficult to interpret. The hypothesis that the morphology of ER 1472 is the result of a short growth period for a modern human pattern cannot necessarily be dismissed on the basis of the data presented here, although its similar position in the ontogenetic series of *Pan* would argue that is it equally likely that it represents a step in the *Pan* growth sequence.

ER 1592 does not fit quite the same pattern as it was quite far from the *Homo* distribution yet just inside the range of older *Pan* in the ontogenetic tests. ER 1592 seems to have a larger medial condyle than lateral condyle, although the preservation on ER 1592 is quite poor and the surface is highly abraded. It is possible that the landmark accuracy was affected by the preservation of the fossil (fig. 4.48)

Fig. 4.48 Posterior view of ER 1592

BOU-VP-19/63 is a partial femur from Daka, Ethiopia dated to ca 1.0 Ma. The preservation of the specimen is very good and while there is no cranial material associated with it, the only taxon found in those sediments thus far is *H. erectus* (Gilbert, 2009). There were two other less complete femora from the same site, and Gilbert (2009) compared them as a sample to modern *H. sapiens* and other early Pleistocene *Homo* specimens for a variety of non-metric traits. For most of the traits, BOU-VP-19/63 was very similar to modern *Homo sapiens,* with the exception of cortical bone thickness and position of minimum femoral breadth; the Daka specimen has thicker cortical bone overall and the minimum femoral breadth is distal to the midshaft (as opposed to at the midshaft). Gilbert (2009) further observed that the condyle shape looked similar to modern *H. sapiens,* although there no metric analyses were presented.

The length of BOU-VP-19/63 certainly points towards it being a biped, however, there are features of the trochlear surface the are less modern human-like. Figure 4.49 illustrates the wireframe transformation between ER 1481 and BOU-VP-19/63. BOU-VP-19/63 differs from the more human-like fossil in that it lacks the full elongation of the lateral condyle. Thus, this individual would have had less surface area coming into contact with the proximal tibia and possibly less stable movement at the knee joint.

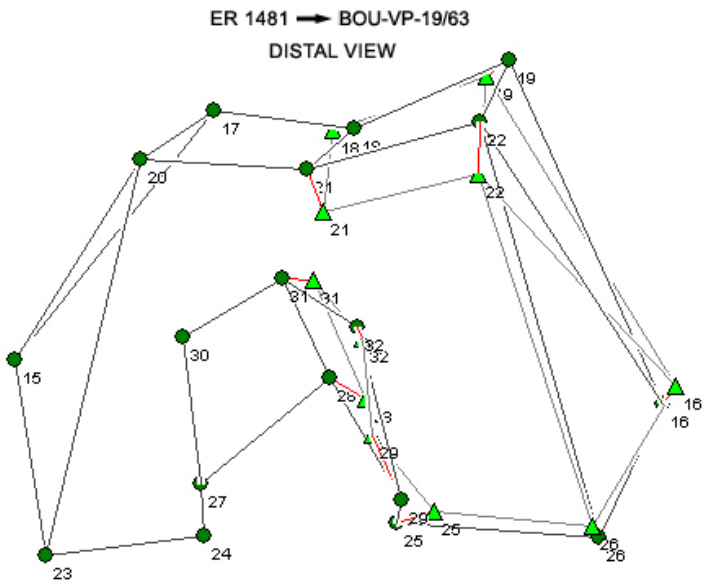

Fig. 4.49 Distal view of a wireframe transformation between ER 1481 represented by circles and BOU-VP-19/63, represented by triangles. The red lines represent vectors of change. Points 21 and 22 illustrate the shortness of lateral condyle.

Taxonomic Implications from the Distal Femur

If the shape of the distal femur is less a product of epigenetic changes caused by different activity patterns than the proximal femur, then it should provide a better taxonomic signal than the proximal femur. The results presented here indicate that individuals attributed to later members of the genus *Homo* (*H. erectus*, possible *H. rudolfensis*) had a more modern morphology than those attributed to *Australopithecus, Paranthropus* or potential *Homo habilis,* but there are no useful distinguishing features to differentiate between the latter three. These results are contra Senut and Tardieu (1985), who advocated for multiple species within the Hadar sample, and more in line with Lague (2002) who found the Hadar sample to be relatively homogenous for the distal femur. The modern human state is clearly derived away from the ancestral primate pattern.

If one were to assign a taxon to all of the fossils based on the results from the distal femur, SK 1896, ER 1481, WT 15000 and TM 1513 could all tentatively be assigned to *Homo* cf. *erectus* (or potentially *Homo rudolfensis*). The attribution of WT 15000 is not in question (Walker and Leakey, 1993) and Susman *et al.* (2001) already argued that SK 1896, found in Member 1 Hanging Remnant, represented a large male of *Homo* cf. *erectus* based on a large patellar groove and an increased area of articular surface in comparison to *Australopithecus.* ER 1481 is from the Upper Burgi Member at Koobi Fora and is broadly dated to 1.89 – 0.05 Ma (Feibel *et al.* 1989). There are definitive *Homo* cf. *erectus* fossils from this time period and the strong similarity between ER 1481 and WT 15000 would argue that ER 1481 belongs in this taxon. TM 1513 was originally attributed to *A. africanus* (Robinson, 1972) but later classified as Hominidae sp. indet by McHenry (1994). Grine *et al.* (1996) suggested that there was a form of *Homo* in South Africa not found in East Africa consisting of SK 847 and Stw 53. Perhaps TM 1513 belongs in the same category. It is more human like than some of the other East African material and yet not as perfectly human-like as ER 1481 and WT 15000, although TM 1513 is from Member 4 (McHenry, 1994a) whereas Stw 53 is from Member 5 (Tobias, 1978).

ER 1472, ER 3951, ER 1592 and ER 993, all currently assigned to Hominidae sp. indet. are likely either *Paranthropus* or early *Homo* cf. *habilis.* Additionally, if Stw 129 is truly *H. habilis* (and not *A. africanus*) (McHenry, 1994a), then that is further evidence that *H. habilis* had a much more conservative body plan than *H. rudolfensis* and other later *Homo.*

Overall Conclusions from the Femur

Figures 4.50-4.52 are the results of a two-block partial least squares analysis (2BPLS) of the proximal and distal femur for the entire sample and the fossils with associated proximal and

distal ends. Some researchers believe that AL 333-3 and AL 333-4 represent the same individual (Tardieu, 1997) so they were included in this analysis as a single individual. Modern *Homo sapiens* has a unique pattern of covariation by comparison to the extant apes, which all have overlapping patterns of distribution. WT 15000 and ER 1481 both have the human pattern for both the proximal and distal femur whereas AL 333-3/4 has an ape-like pattern of covariance for both. The position of the composite AL 333-3/4 supports the combination of these bones in a single taxon if not individual; had they been from widely different organisms, the plotted point would not fall near other points (Harcourt-Smith *et al.* 2008). ER 1472 has a unique pattern of covariance with a proximal femur that is most similar to modern humans and a distal femur that is more similar to modern apes.

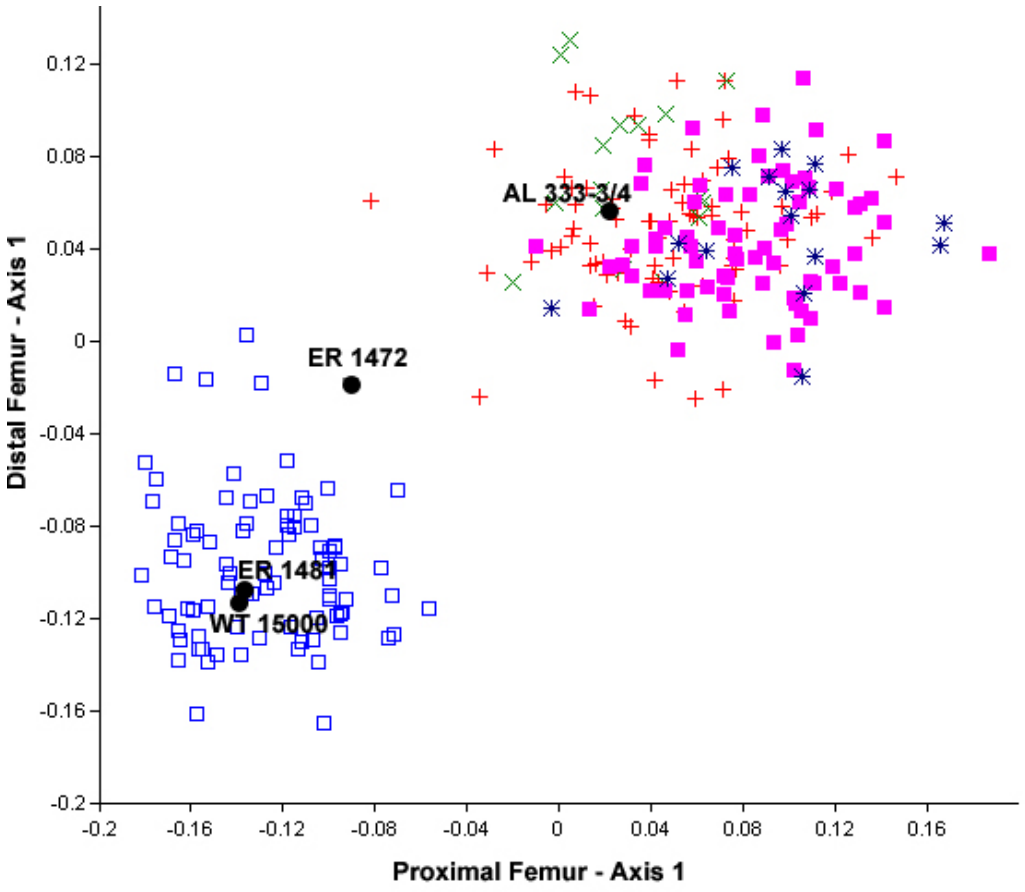

Fig. 4.50 Plot of the results of a two-block partial least squares analysis of the entire proximal and distal femur. These two axes comprise 85% of the variation within the sample and have a correlation coefficient of 0.83. The second axes (not pictured here) comprise 11% of the variation within the sample and have a correlation coefficient of 0.65. The entire data set has an RV coefficient of 0.51. *Homo* is represnted by blue open squares, *Pan troglodytes* is represented by pink closed squares, *Pan paniscus* is represented by blue stars, *Pongo* is represented by greens Xes, and *Gorilla* is represented by red crosses. Fossils are represented by black circles and are labeled in the graph.

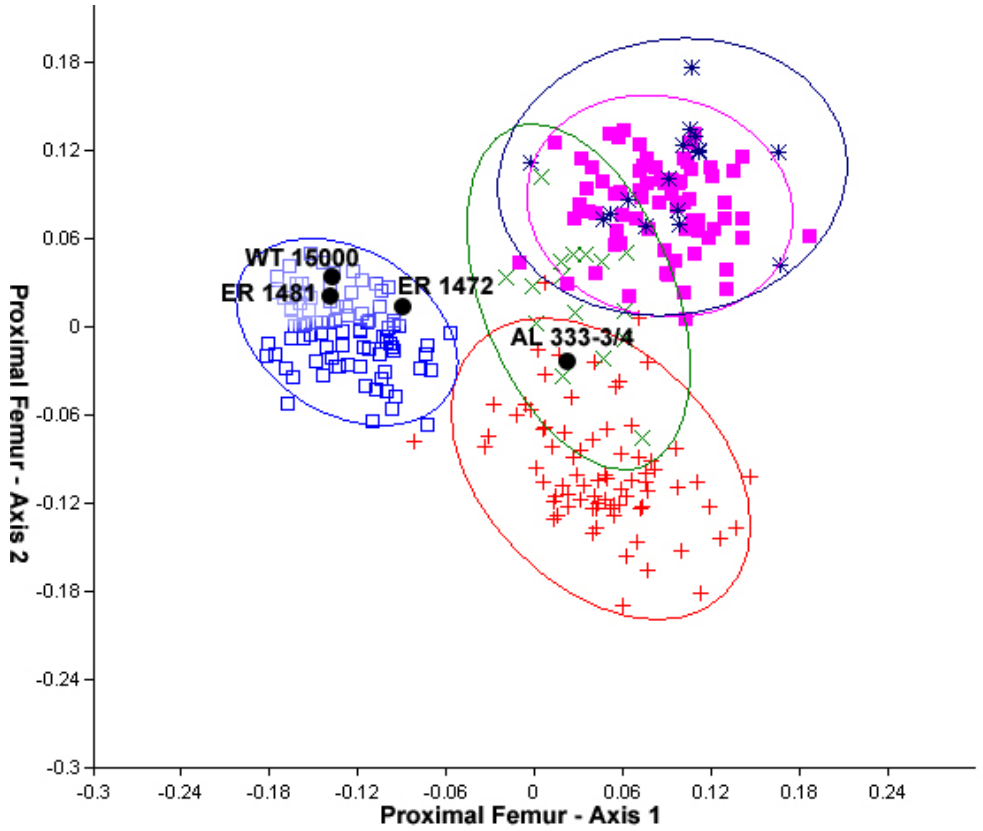

Fig. 4.51 2B-PLS analysis showing the relationship of the first and second proximal femoral axes based on a cross-covariance matrix of the proximal and distal femur GPAed landmark coordinates. *Homo* is represented by blue squares, *Pan troglodytes* by purple squares, *Pan paniscus* by blue stars, *Pongo* by green Xs, and *Gorilla* by red pluses. Fossils are labeled and in black. Closed curves represent a 95% equal frequency ellipse.

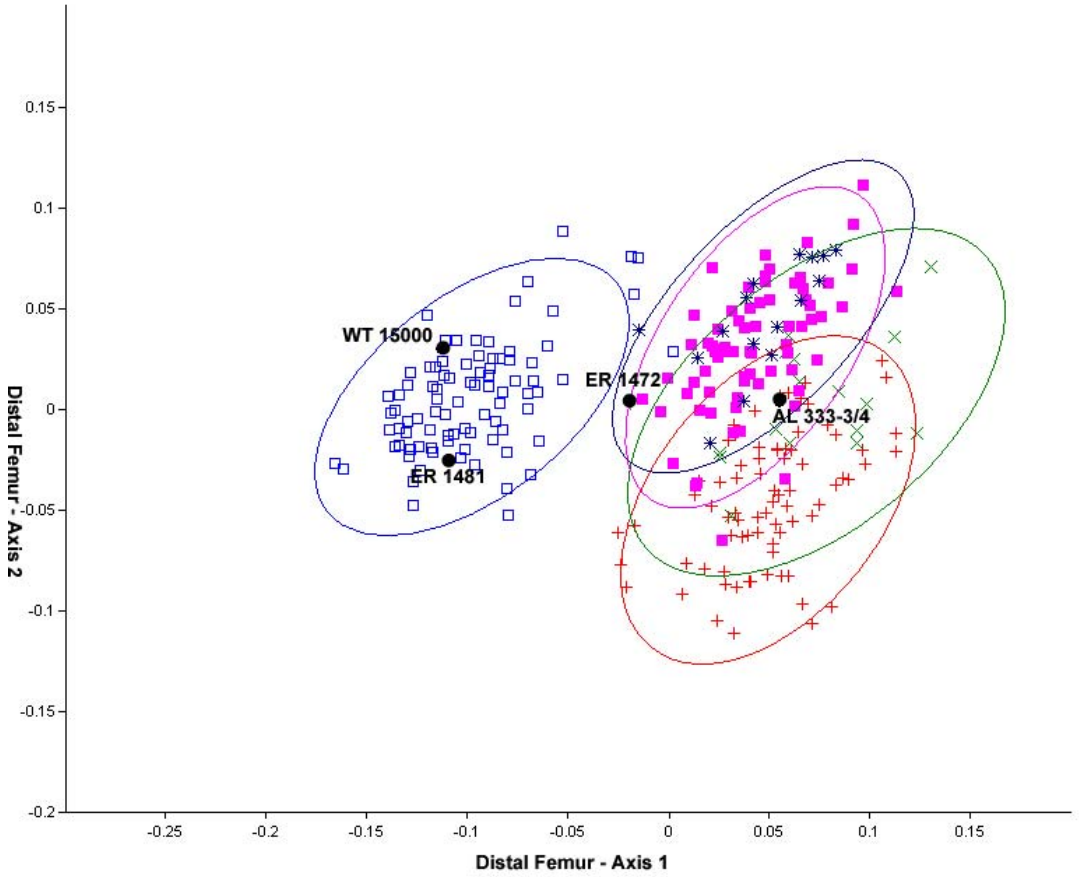

Fig. 4.52 2B-PLS analysis showing the relationship of the first and second distal femoral axes based on a cross-covariance matrix of the proximal and distal femur GPAed landmark coordinates. *Homo* is represented by blue squares, *Pan troglodytes* by purple squares, *Pan paniscus* by blue stars, *Pongo* by green Xs, and *Gorilla* by red pluses. Fossils are labeled and in black. Closed curves represent a 95% equal frequency ellipse.

Figures 4.53-4.55 illustrate the results of a second 2BPLS, this time utilizing only the landmarks on the greater trochanter for the proximal portion of the femur. This allowed for the inclusion of AL 129-1, the last specimen in this sample with both a proximal and distal end. ER 1481 and WT 15000 fell within the modern human distribution for both the greater trochanter and distal femur, whereas AL 333-3/4 and ER 1472 fell within the modern great ape distribution for both. AL 129 has a possible unique pattern of covariation with a distal femur firmly within the ape distribution, but a greater trochanter that falls within the small area of overlap between humans and apes.

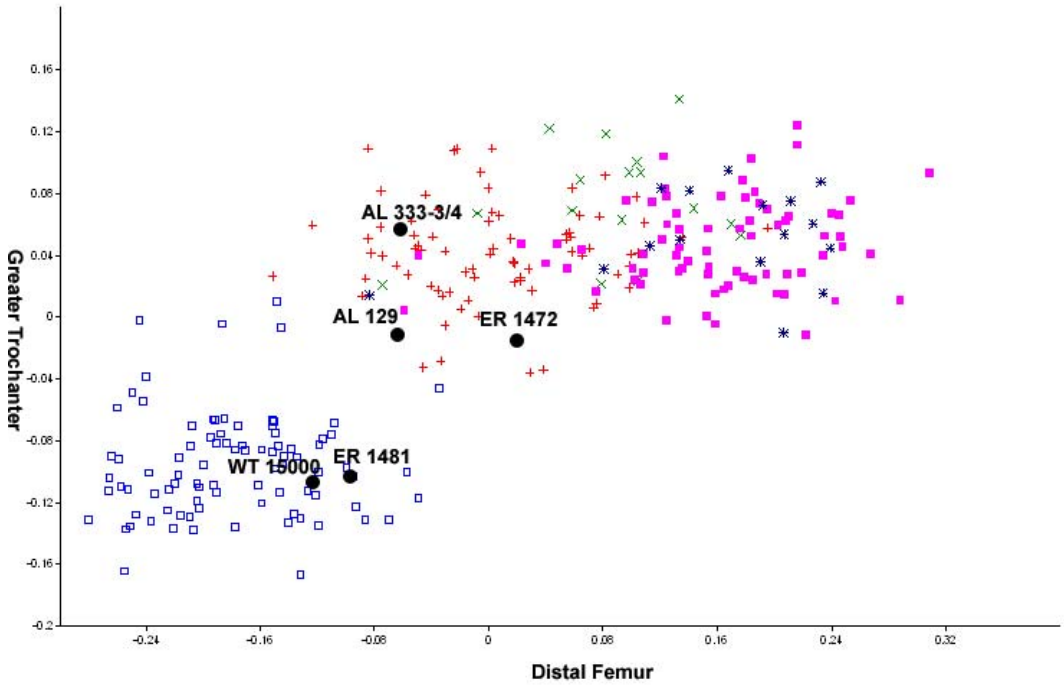

Fig. 4.53 The results of a two-block partial least squares analysis of the greater trochanter (landmarks 9-11, and 14) and distal femur. These two axes comprise 89.5% of the variation within the sample and have a correlation coefficient of 0.77. The second axes (not pictured here) comprise 9.8% of the variation within the sample and have a correlation coefficient of 0.65. The entire data set has an RV coefficient of 0.47. *Homo* is represnted by blue open squares, *Pan troglodytes* is represented by pink closed squares, *Pan paniscus* is represented by blue stars, *Pongo* is represented by greens Xes, and *Gorilla* is represented by red crosses. Fossils are represented by black circles and are labeled in the graph.

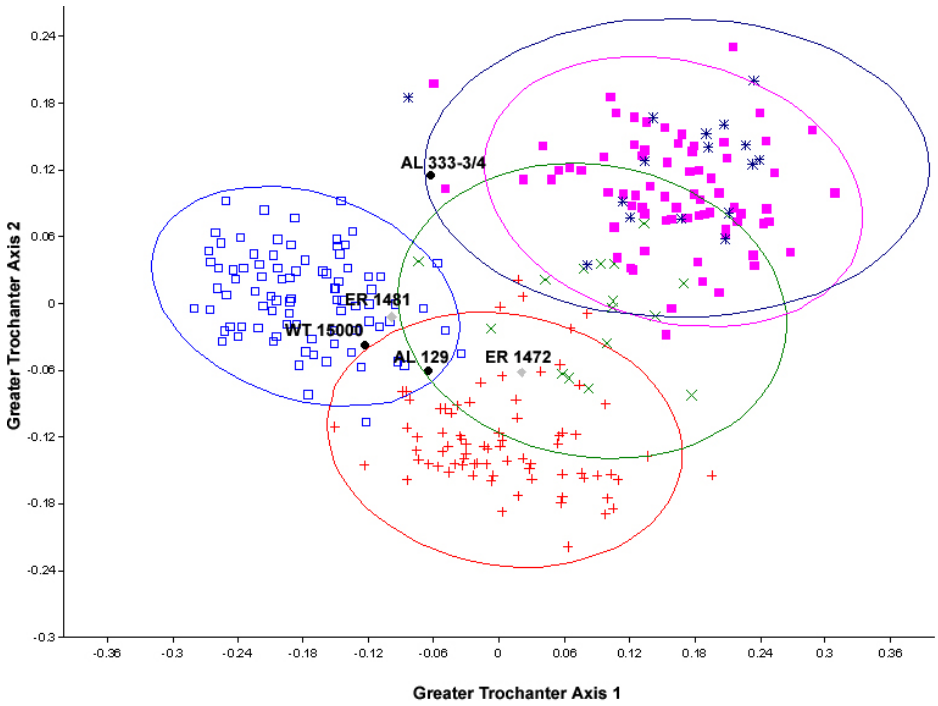

Fig. 4.54 2B-PLS analysis showing the relationship of the first and second greater trochanter axes based on a cross-covariance matrix of the greater trochanter and distal femur GPAed landmark coordinates. *Homo* is represented by blue squares, *Pan troglodytes* by purple squares, *Pan paniscus* by blue stars, *Pongo* by green Xs, and *Gorilla* by red pluses. Fossils are labeled and in black. Closed curves represent a 95% equal frequency ellipse.

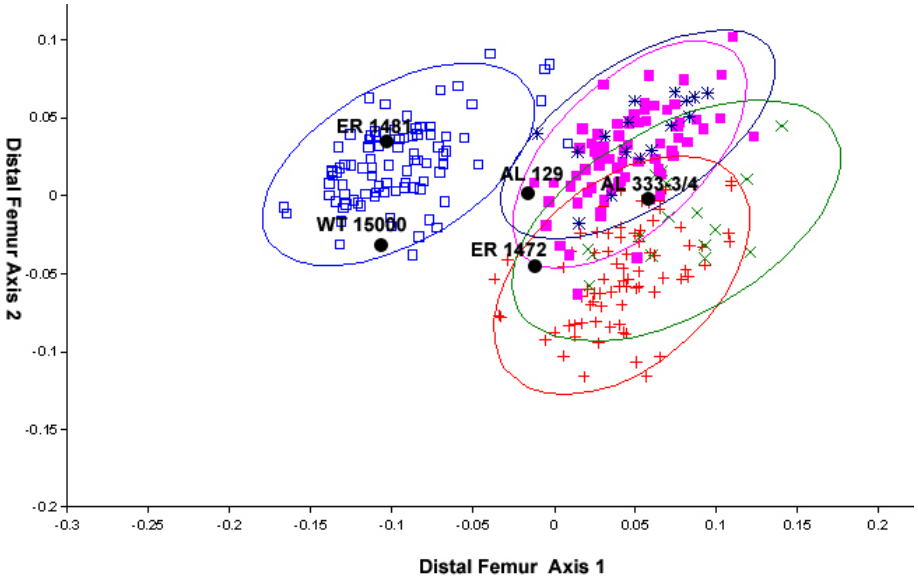

Fig. 4.55 2B-PLS analysis showing the relationship of the first and distal femur axes based on a cross-covariance matrix of the greater trochanter and distal femur GPAed landmark coordinates. *Homo* is represented by blue squares, *Pan troglodytes* by purple squares, *Pan paniscus* by blue stars, *Pongo* by green Xs, and *Gorilla* by red pluses. Fossils are labeled and in black. Closed curves represent a 95% equal frequency ellipse.

The results of the partial least squares analysis underscore the results of the single element analyses. WT 15000 and ER 1481 have a morpohological shape in both the proximal and distal femur that is indistinguishable from that of modern humans. The Hadar individuals are more ape-like, although they occur towards the edge of the ape distribution, particularly in the second analysis. ER 1472 has a unique pattern when the whole proximal femur is considered. It has a mostly human-like proximal femur, except for the greater trochanter with has a shape that is slightly more ape-like. The distal femur also shares an affinity with both humans and apes depending on the analysis. Whether the differences in the morphology of ER 1472 were caused by a difference in growth patterns or some other factor, it is clear that it would not have moved in the same way as a perfect biped, such as ER 1481 or WT 15000.

The femur participates in two joints that have been extensively modified in bipedal species: the knee and the hip. For most taxa, the signal was the same from the proximal and distal femur, the major exception being *Australopithecus afarensis.* In *Australopithecus afarensis*, there was a tremendous amount of variation in the proximal femur, whereas in the distal femur, the *A. afarensis* sample was consistently ape-like. This likely has to do with the different ontogenetic paths of the proximal and distal portions of the femur and the way that bone is deposited and remodeled due to activity patterning.

The change from a more ape-like shape to a more human-like shape does seem to roughly correlate with timing in the fossil record, with the more pleisiomorphic individuals (*i.e.* the *A. afarensis* sample) occurring earliest in time and the most derived individuals (*i.e.* WT 15000) occurring latest, although there are exceptions to this. The major one is BOU-VP-19/63, dated to ca. 1.0 Ma, which lacks some of the characteristics of a modern human femur. If this

femur belongs to *Homo erectus,* its bipedal gait was not as well perfected as that of WT 15000, which occurs earlier in time (Brown and McDougall, 1993). *Homo erectus* is a wide-spread taxon with a large amount of cranial variation between populations (Terhune *et al.* 2007; Baab, 2008). It seems likely that degree of cranial variation would be partially mirrored in some postcranial variation between populations. Even in modern humans there is evidence that some femoral characteristics vary predictably between populations, such as the shape of the intercondylar notch (Baker *et al.,* 1990), the degree of platymeria (Gill, 2001) and bone density (Bachrach *et al.,* 1999), so perhaps the Daka specimens represent an African subpopulation of *H. erecuts.*

Full Tibia Analysis and Discussion

Data were also collected on the proximal and distal tibia for analysis. Figure 4.56 is a PCA of the extant taxa for the full tibial landmark set. There is excellent separation between almost all of the extant taxa with the exception of *Pongo* which has a distribution that overlaps with that of *Pan.* Both PC1 and PC 2 are significantly correlated with centroid size, although the relationship is weak in both cases with *Gorilla* falling off of the regression line for PC 1 and *Homo* falling off of the regression line for PC 2. PC 1 is driven by the overall bone length versus joint size with *Gorilla* having relatively large joints on a shorter diaphysis and *Homo* having smaller joints on a longer diaphysis. Additionally, PC 1 is driven by the angle of inclination of the distal tibial surface with *Homo* having flat surfaces and the extant apes having more angled surfaces. PC 2 is specifically driven by the degree of torsion between the proximal and distal segments. In *Pongo,* the distal articular surface is medially turned in comparison to the proximal segment (fig. 4.56). There are no complete fossil tibiae.

The differences between the extant taxa can be related to functional differences in their locomotor repertoires. The more perpendicular orientation of the distal tibial surface in *Homo sapiens* has been hypothesized to be an adaptation to resisting shearing stresses during normal bipedal movement (Latimer *et al.* 1987). In *Pan* and *Gorilla,* it is likely that the joint sizes scale allometrically; they may appear relatively smaller in *Homo* due to the overall elongation of the hindlimb (Aiello and Dean, 1990).

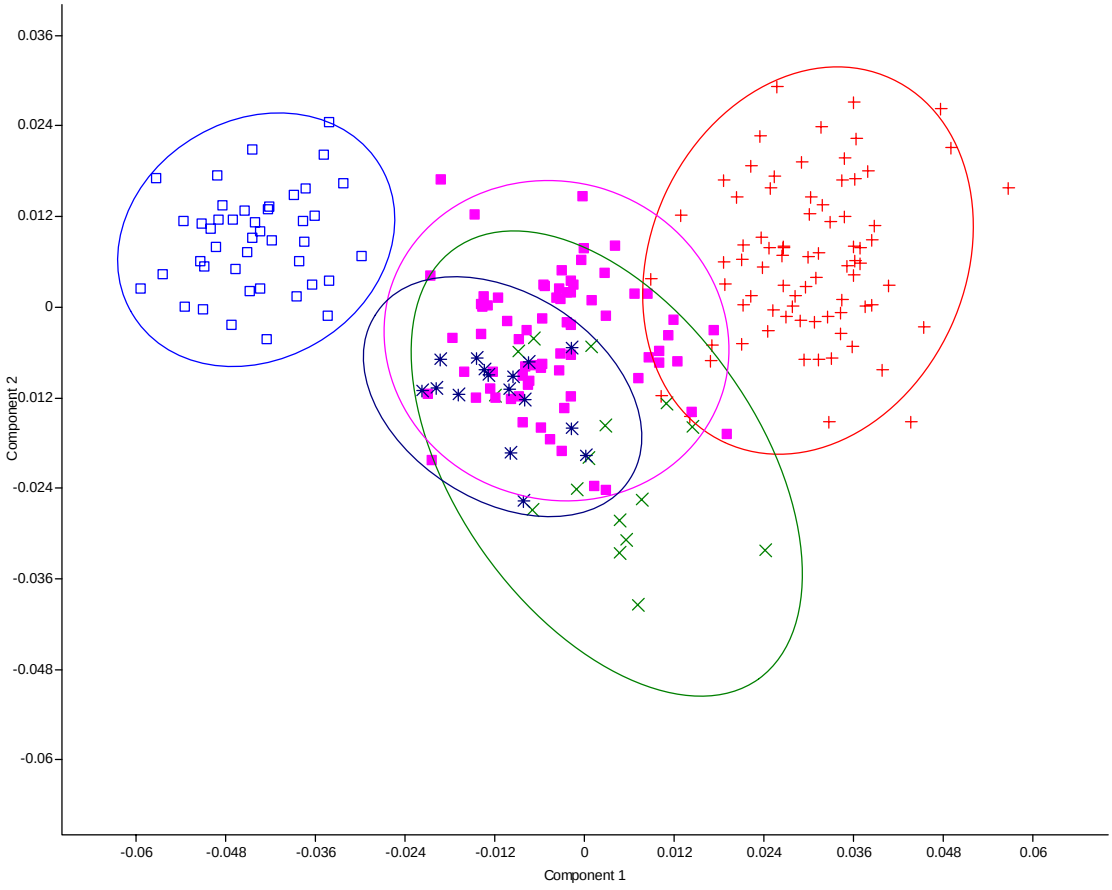

Fig. 4.56 PCA for the full tibia. *Homo* is represented by blue open squares, *Pongo* by green Xes, *Gorilla* by red crosses, *Pan troglodytes* by purple squares, and *Pan paniscus* by blue stars. The closed curves are 95% equal frequency ellipses for the extant genera. PC1 accounts for 54.5% of the total variance and PC2 accounts for 10.8% of the overall variance.

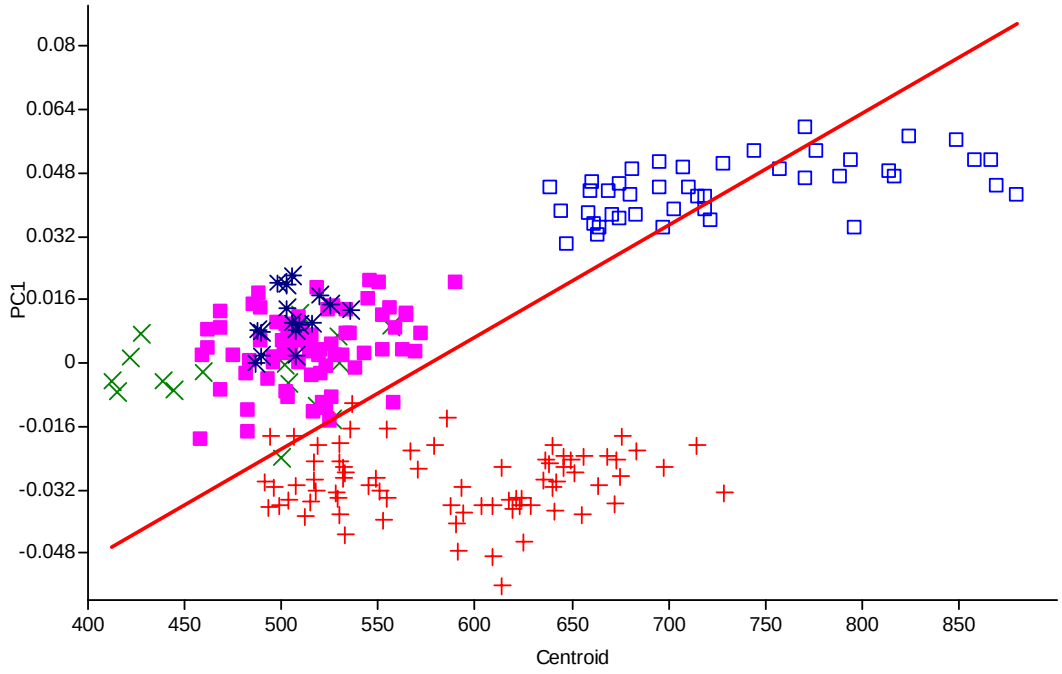

Fig 4.57 A linear regression of PC1 against centroid size for the for the full tibia with r = 0.43.

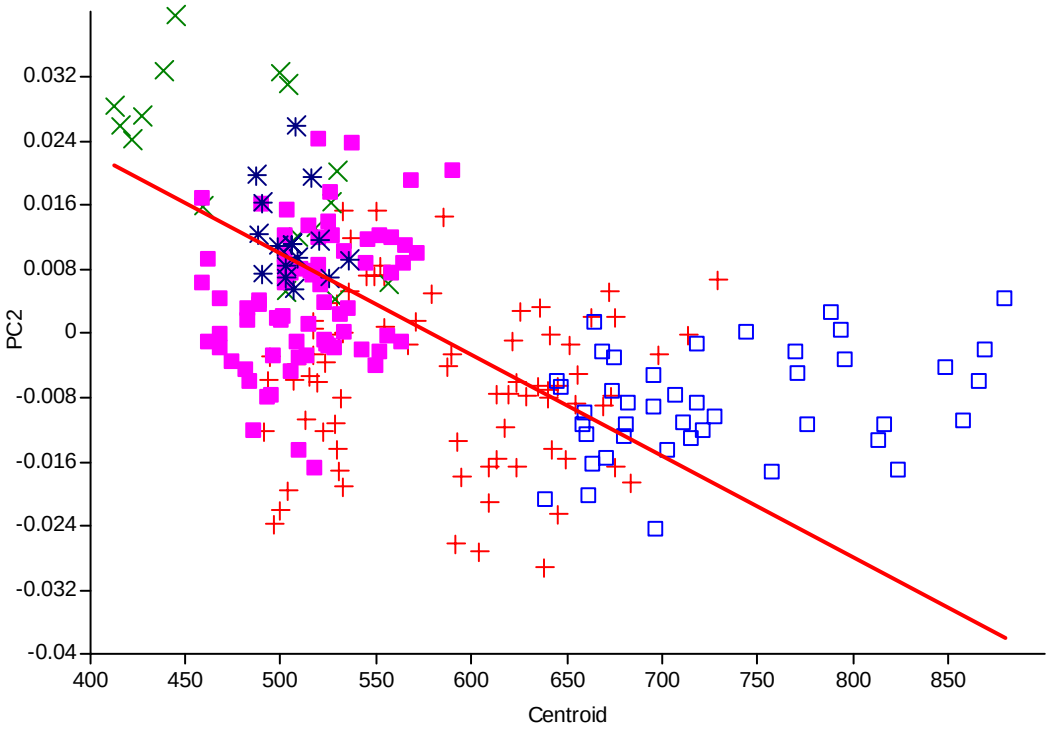

Fig 4.58 A linear regression of PC2 against centroid size for the for the full tibia with r = -0.47.

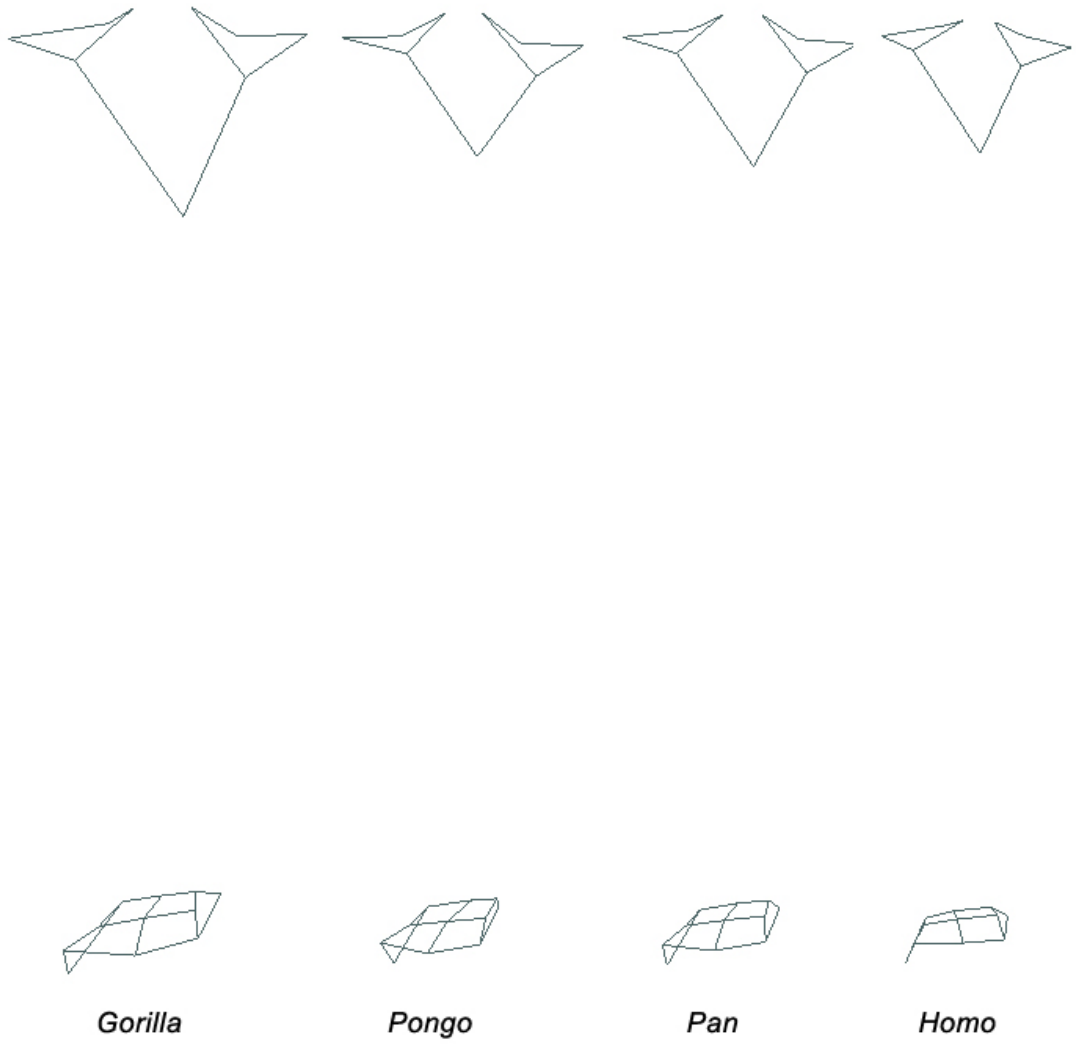

Fig 4.59 Wireframe transformation between the four extant genera for the full tibia. These wireframes are from a posterior view, tilted slightly backwards in order to visualize the change in the depth of the tibial condyles and the orientation of the distal articular surface.

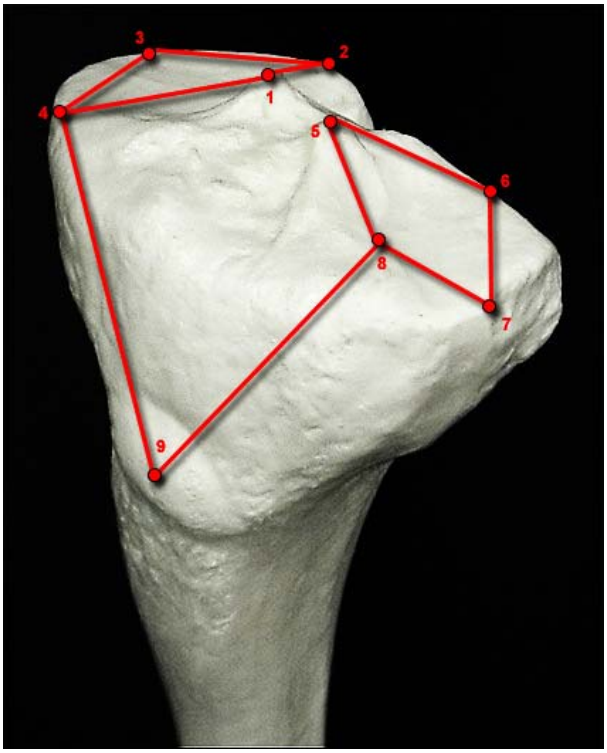

4.60 Landmarks and wireframe for the proximal tibia.

Proximal Tibia

The tibia was segmented into proximal and distal portions. Figure 4.60 illustrates the landmark configuration and wireframe for the proximal tibia. Figure 4.61 is a PCA of the full proximal tibia. There is no differentiation between the extant taxa. The fossils fall within the area of overlap with the exceptions of WT 15000 and WT 19700 which are outliers to the entire sample. Within the fossil distribution, there does not seem to be any patterning of fossils based on age or taxonomic attribution. PC 1 is driven by the proximodistal distance of the tibial tuberiosity from the proximal articular surface with individuals towards the negative values having it relatively closer than those at the positive values. PC 2 is driven by the mediolateral distance between the midpoints of the anterior margin of the tibial condyles. PC 1 is weakly correlated with centroid size with an r value of 0.21.

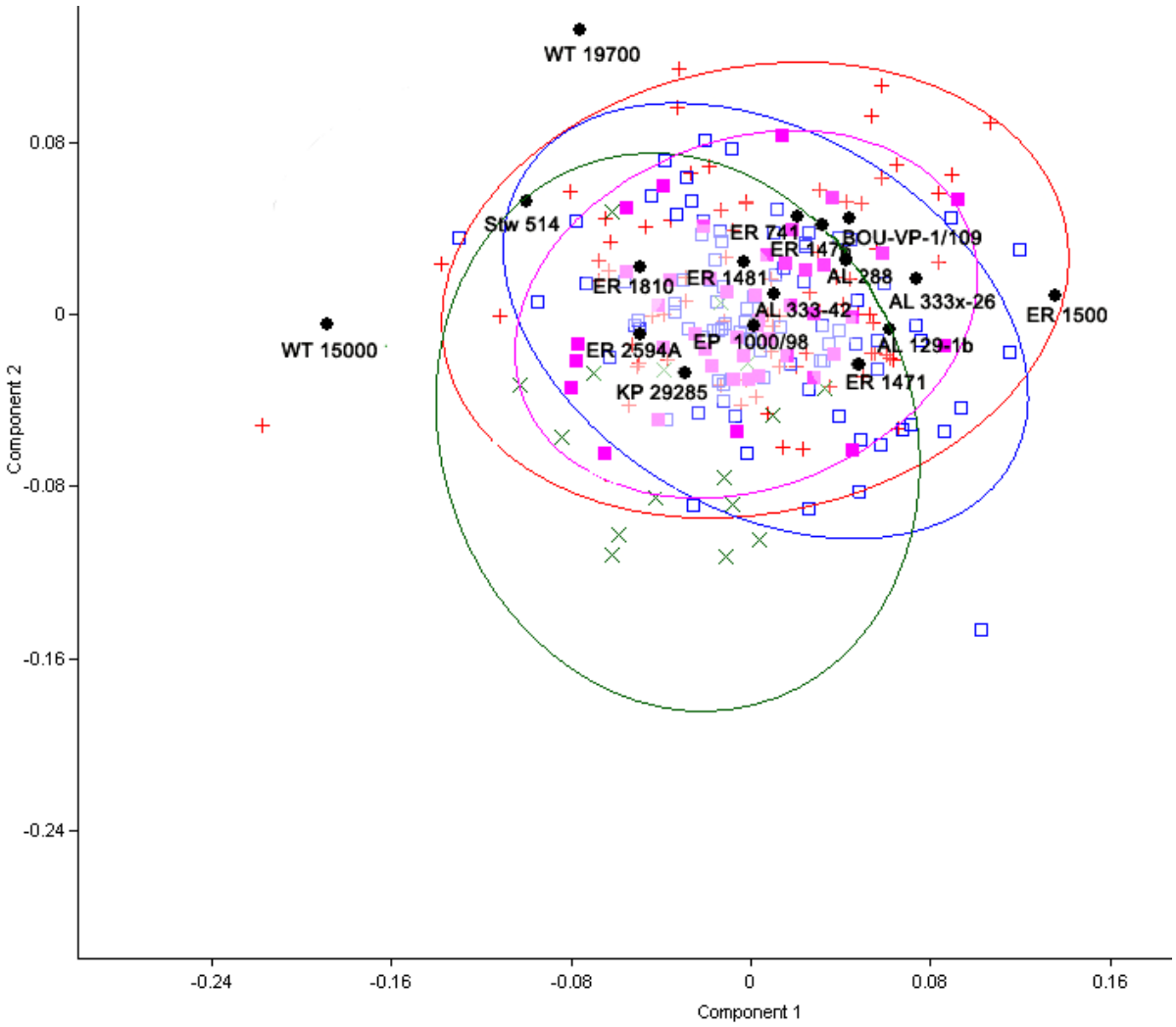

Fig. 4.61 Principal components analysis for the proximal tibia. *Homo* is represented by blue open squares, *Pongo* is represented by green Xes, *Gorilla* is represented by red crosses, *Pan troglodytes* is represented by purple squares, and the fossils are represented by black circles and are labeled in the graph. The closed curves are 95% equal frequency ellipses for the extant genera. PC1 accounts for 17.8% of the total variance and PC2 accounts for 12.6% of the overall variance.

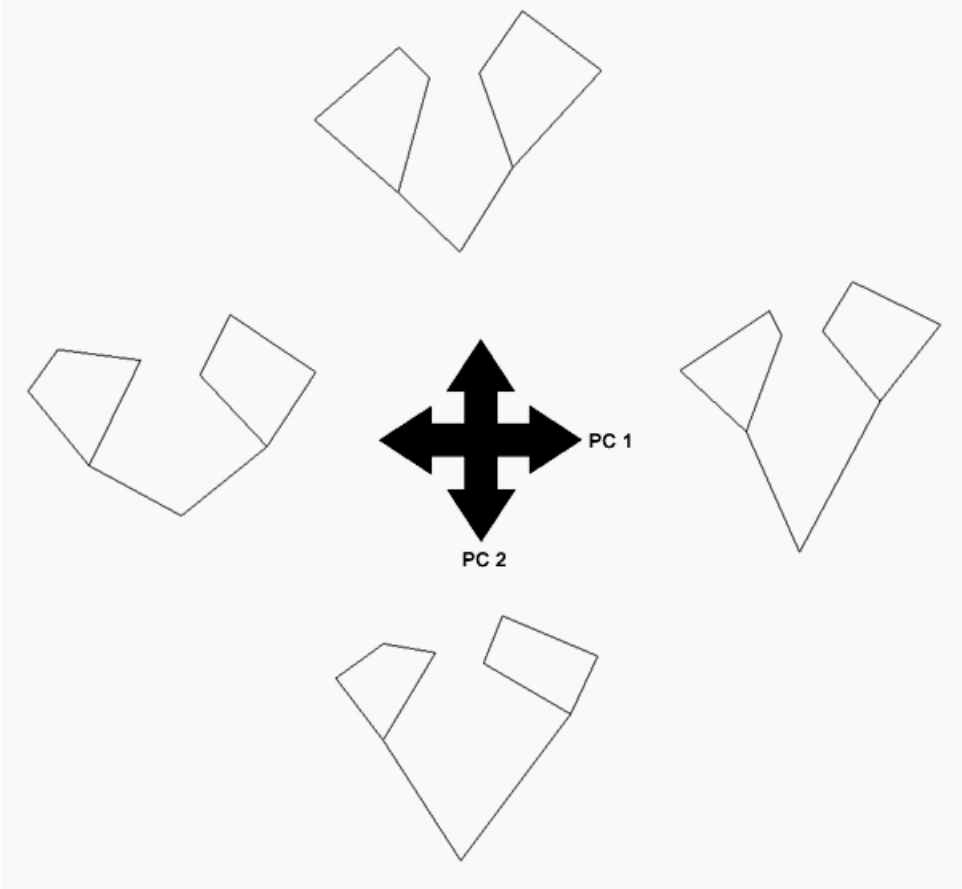

Fig. 4.62 Wireframe transformations along PC 1 and PC 2 for the proximal tibia.

Means were calculated for the proximal tibia of the extant taxa and additional analyses were completed using those values and the fossils. Figure 4.63 is a PCA of the fossils and the means. Most of the fossils and all of the extant means form a group that has little shape differentiation. AL 333-42, Stw 514, ER 2954A, WT 15000 and WT 197000 are not part of that group and are distributed evenly across PC 1. PC 2 separates WT 15000 and WT 19700 from the rest of the sample at opposite extremes. PC 1 is driven by the width of the intercondylar eminence and the extension of the medial condylar surface onto the anterior surface of the tibia. PC 2 is driven by the proximodistal location of the tibial tuberosity and the anterior-posterior position of the lateral intercondylar tubercle. WT 15000 is different in that is has a wider

intercondylar eminence with more widely spaced intercondylar tubercles than the rest of the sample. In addition, the medial condylar surface extends more anteriorly than most of the other fossils. WT 19700 has uniquely positioned medial and lateral condyles in that one is small and very flat whereas the other is much larger. PC 1 was not correlated with centroid size.

Because there was so little differentiation between the fossils, a non-metric MDS was also performed in order to look for patterns in the fossils (fig. 4.64). In the non-metric MDS analysis, the extreme differences between WT 15000, WT 19700 and the other outliers from the PCA were retained and the group of fossils and extant individuals were spread out more. Most of the proximal tibiae from Koobi Fora form a single cluster and three of the *A. afarensis* specimens form a second cluster. Aside from those, there are no other obvious patterns in the distribution of the fossil taxa.

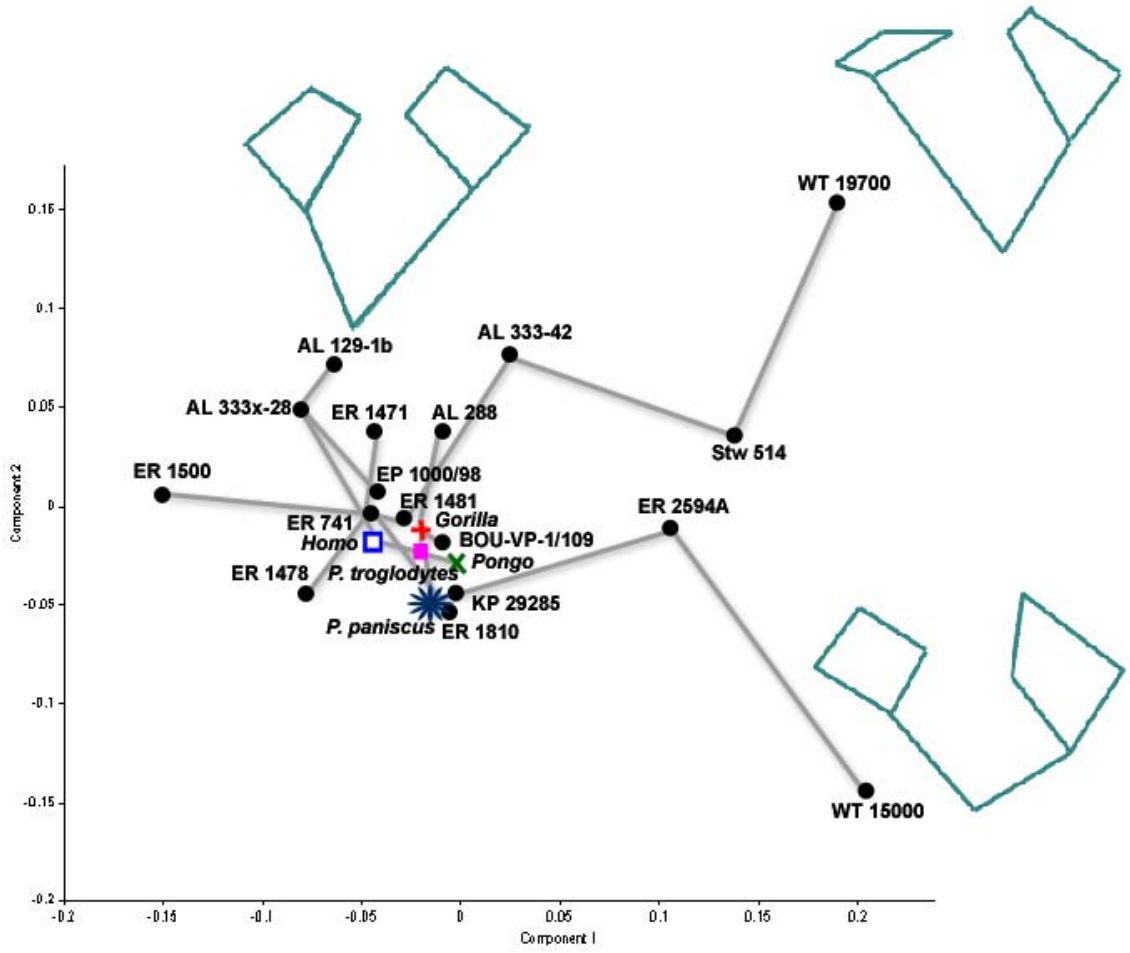

Fig. 4.63 PCA for the fossils plus means for the extant species for the proximal tibia. *Homo* is represented by a blue open square, *Pongo* by a green X, *Gorilla* by a red cross, and *Pan* by a purple square and blue star. The fossils are represented by black circles and are labeled in the graph. The lines represent an MST. PC1 accounts for 35.8%, of the total variance and PC2 accounts for 16.2% of the overall variance. Wireframes are in a proxmo-anterior view

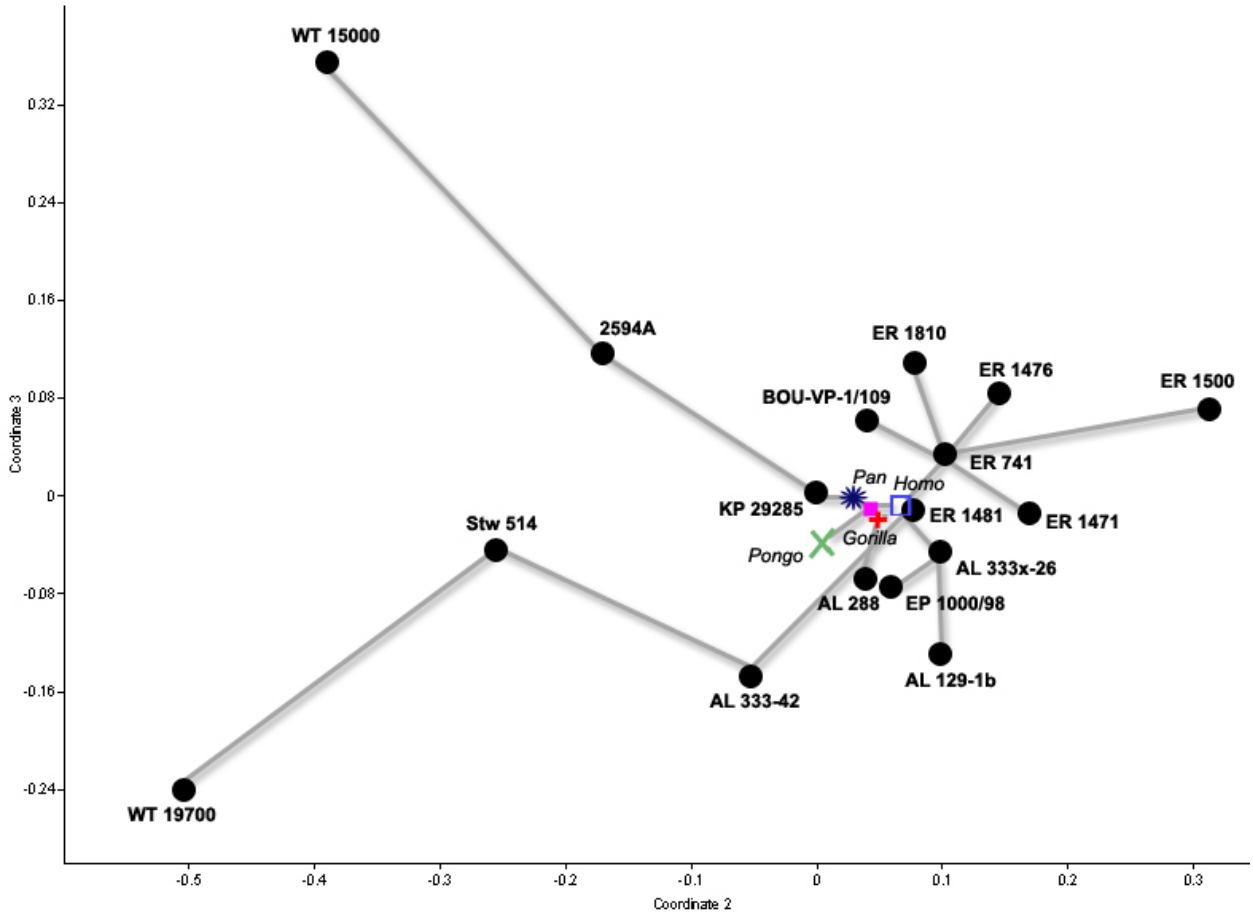

Fig. 4.64 Non-metric MDS of the proximal tibia for the fossils and extant means. Stress = 0.4301

Finally, a neighbor-joining tree was also generated with these data (fig. 4.65). The relationships between the extant taxa were not fully recovered, with *Pan troglodytes* as the sister to *Gorilla* and *Pan paniscus* as the sister to KP 29285. *Homo* is the outgroup to all of the fossils except for that *A. anamensis* individual. There are some interesting clusters that were formed including one of all *A. afarensis* (AL 333x-26, AL 129-1b, EP 1000/98 and AL 288) and one of most Koobi Fora specimens (ER 1476, 741, 1810, 1500 and 1471) with the Daka tibia as the sister, although bootstrap values for all of the larger clusters were very low.

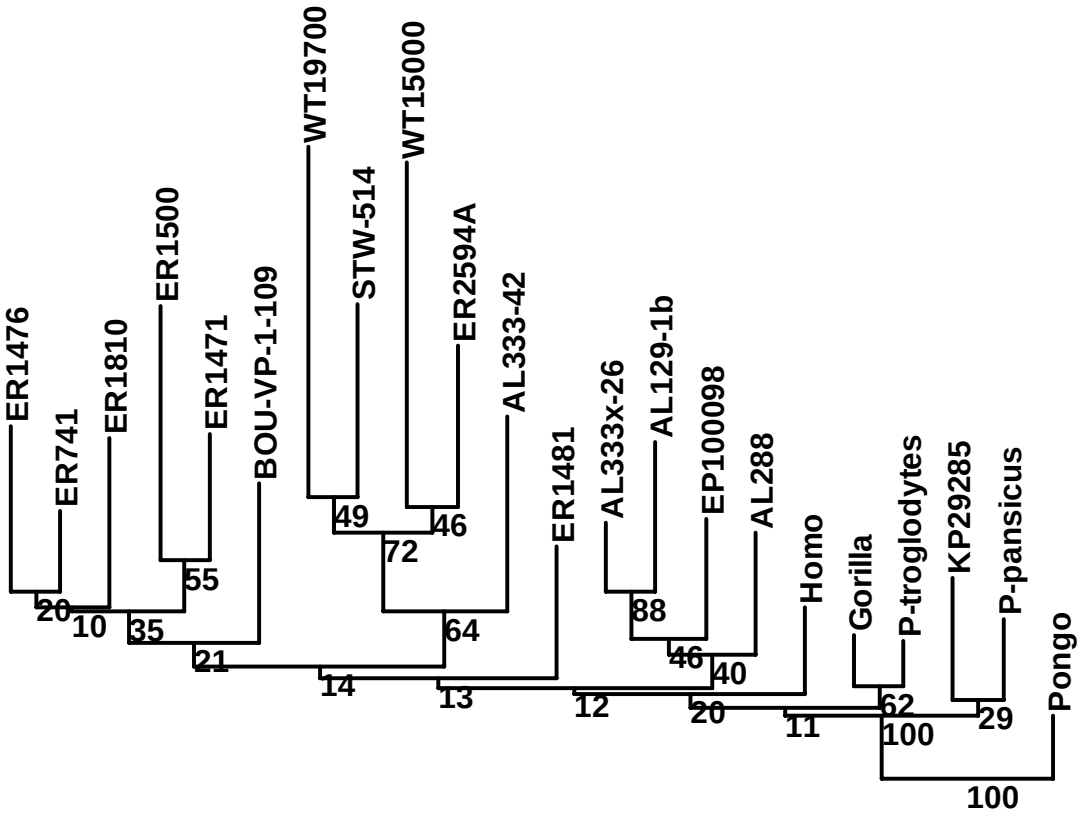

Fig 4.65 Neighbor joining tree for the proximal tibia. This tree is based on procrustes chord distances and was rooted with Pongo as the outgroup. Boot strap values are after 1000 replicates.

Proximal Tibia Discussion

Despite the wealth of proximal fossil tibiae, there has been very little work done on them, probably because it is so difficult to differentiate between taxa. The trait cited most frequently as the differentiating the modern taxa is whether there is a single or double insertion of the lateral meniscus, with apes and other mammals having only a single insertion and many hominins (including *Homo*) having a double insertion (Senut and Tardieu, 1985); however, the utility of the trait has been called into question by Dugan and Holliday (2009), who found that this trait was variable in modern human populations and not a particularly good marker for differentiating between taxa.

Organ and Ward (2006) analyzed the contour of the lateral condyle of the proximal tibia to assess whether there is a correlation between tibial "flatness" and increasing body size and to see whether there was a difference in curvature associated with different locomotor patterns. These authors found significant overlap between modern taxa and no particular correlation with size. Furthermore, there was no discernable difference in condylar morphology between *A. africanus* and *A. afarensis.*

While many authors have made arguments about the proximal tibial morphology of hominin being relatively more ape-like or human-like (*e.g.* Berger and Tobias, 1996 for Stw 514; Ward, 2002 for the entire sample of *A. afarensis*; Harrison, in press for EP 1000/98) these data do not support the idea that there is any ability to differentiate between extant individuals, much less fossils, based on the proximal tibia. Perhaps laser surface scanning or collecting a greater number of landmarks would yield better results.

Distal Tibia Data

The distal tibial segment was also analyzed separately. Figure 4.66 illustrates the landmarks and the wireframe on the distal tibia. A PCA of the entire sample was performed using landmarks 10 through 18 (fig.4.67). Landmark 19 was eliminated as many of the fossils have broken medial malleoli, and landmark 20 was eliminated as it seemed to vary greatly within each extant taxon, and many of the fossils were too abraded to pinpoint it accurately. There is reasonably good separation between *Homo*, *Gorilla* and *Pongo,* although *Pan* overlaps the distribution of all three of these taxa. Most of the fossils fall within the range of modern *Homo sapiens* or as outliers towards the human side of PC 1. Stw 181 was the exception and fell within the 95% equal frequency ellipse for *Pongo.* PC 1 is driven by the length of the mediolateral

border on the anterior surface of the bone with *Homo* having a short border and *Gorilla* having a long border. PC 2 is driven by overall width of the distal surface; in *Pongo,* it is narrower than in the rest of the sample. PC 1 is correlated with centroid size.

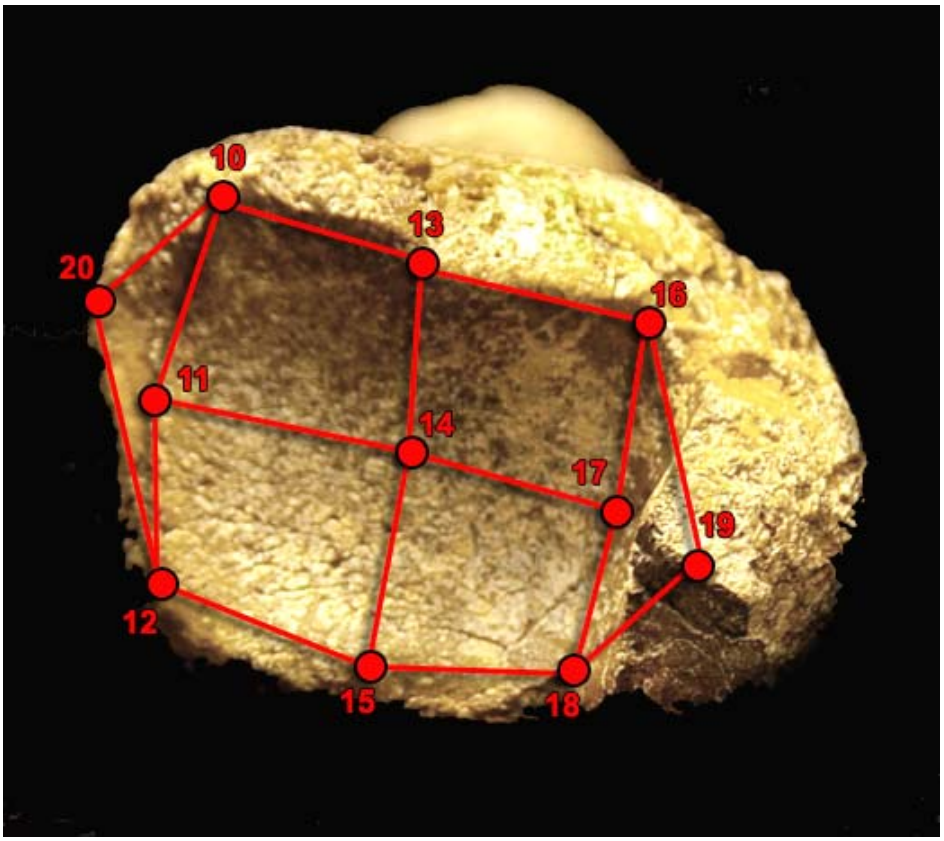

Fig. 4.66 Landmarks and wireframe on the distal tibia, illustrated using KP 29285. All analyses were performed without landmarks 19 and 20.

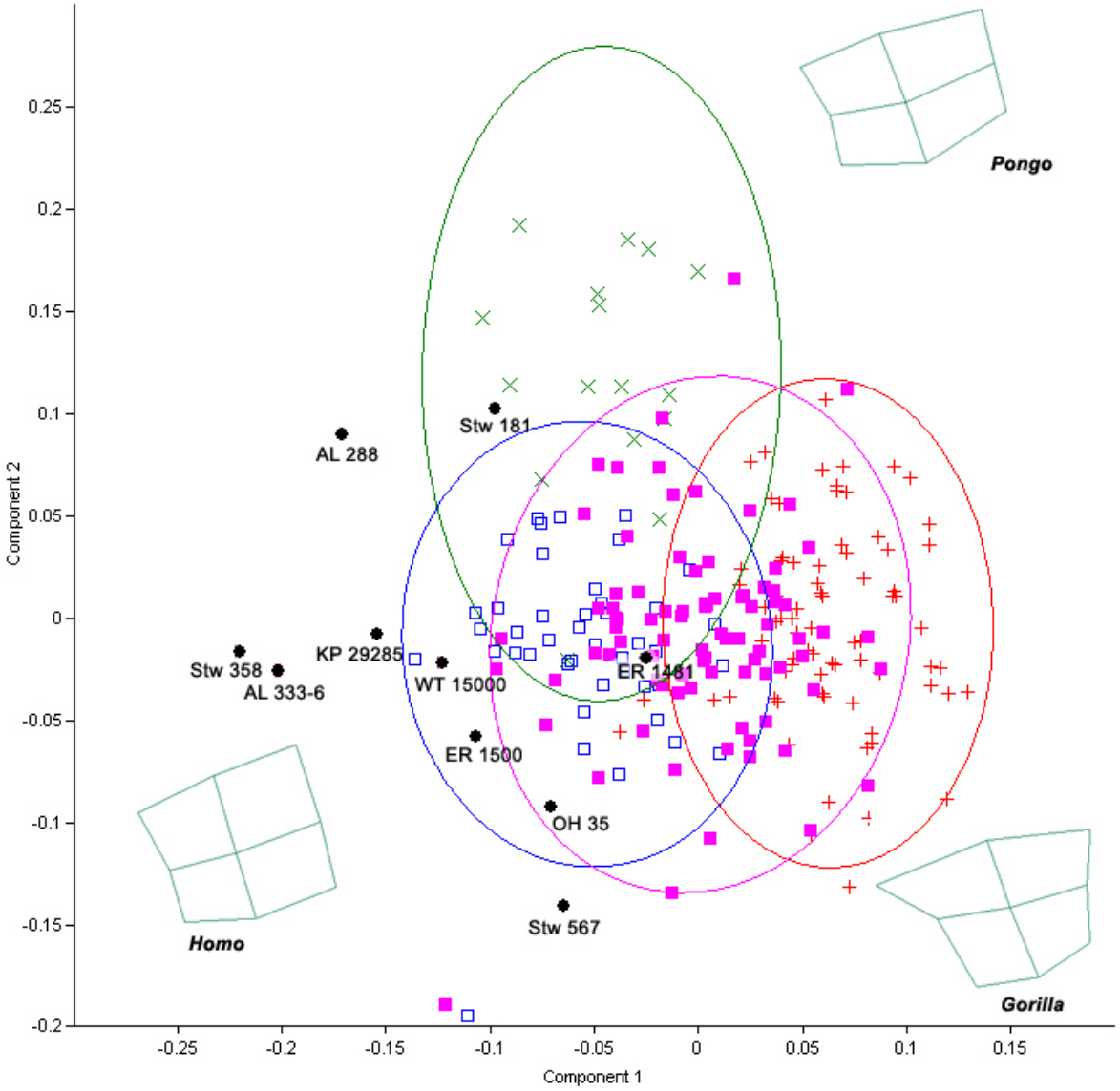

Fig. 4.67 PCA for the distal tibia, landmarks 10-18 (the full articular surface). *Homo* is represented by blue open squares, *Pongo* by green Xes, *Gorilla* by red crosses, *Pan* by purple squares, and the fossils are represented by black circles and are labeled in the graph. The closed curves are 95% equal frequency ellipses for the extant genera. PC1 accounts for 21.7%, of the total variance and PC2 accounts for 17.4%of the overall variance. The wireframes are from a distal view of the articular surface with the medial edge to the right.

Means were calculated for the extant taxa, and additional analyses were run. Figure 4.68 is a PCA and MST with these values. PC 1 separates the extant individuals and ER 1481, ER 1500, OH 35 and Stw 567 from *A. afarensis* (from Hadar), *A. africanus* (represented by all of the Stw tibiae save Stw 567) and *A. anamensis* (KP 29285). Stw 567 is from Sterkfontein Member 5

and considered to be *Homo* by some authors (Kuman and Clarke, 2000; Curnoe *et al.* 2007). WT 15000 has an intermediate position. PC 2 separates Stw 567 at one extreme and Stw 181 at the other. PC 1 is driven by the length of the anterior margin of the distal articular surface. In *Gorilla* there is a long anterior border leading into the medial malleolus and that border gets shorter towards the positive values on the graph. PC 2 is driven by the overall shape of the distal articular surface with *Pongo* and Stw 181 having a more rectangular surface and Stw 567 having the most square shaped surface.

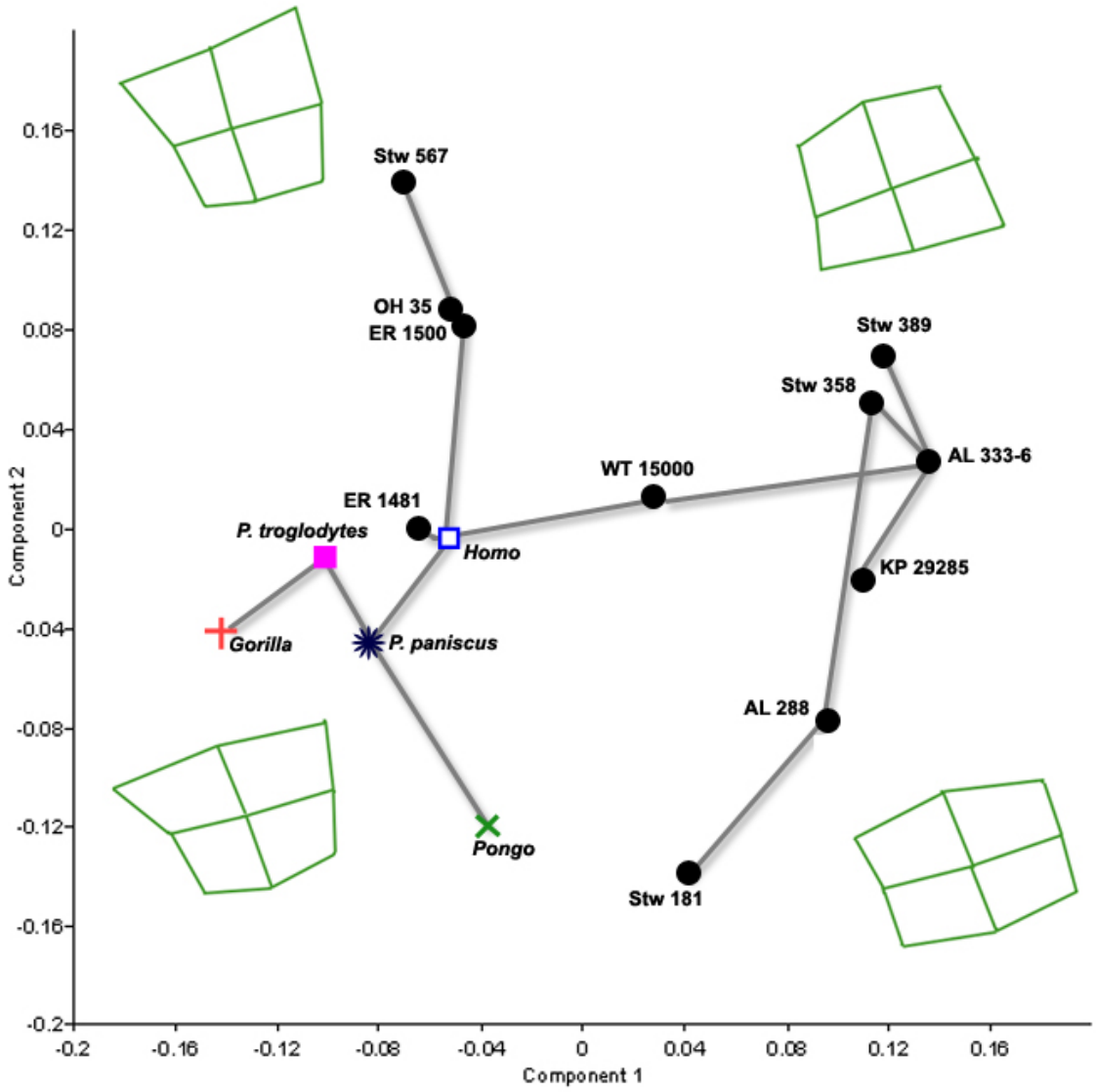

Fig. 4.68 PCA for the fossils plus means for the extant species for the distal tibia, landmarks 10-18. *Homo* is represented a blue open square, *Pongo* by a green X, *Gorilla* by a red cross, and *Pan* by a purple square. The fossils are represented by black circles and are labeled in the graph. The lines represent a minimum spanning tree plotted on top of the principal components graph. PC1 accounts for 36%, of the total variance and PC2 accounts for 25% of the overall variance. The wireframes are a distal view with the medial edge to the right.

Lastly, a neighbor-joining tree was generated for the same values as the previous analysis (fig. 4.69). Stw 181 is the outgroup to all of the other fossils with a bootstrap value of 100, underscoring the fact that it has a slightly different, more *Pongo*-like morphology. The cluster of OH 35, Stw 567 and ER 1500 from the PCA is also reproduced with a relatively high bootstrap

value of 86. The group of *A. anamensis, A. africanus* and *A. afarensis* is also partially recovered but with low bootstrap values and with AL 288 as an outgroup to it.

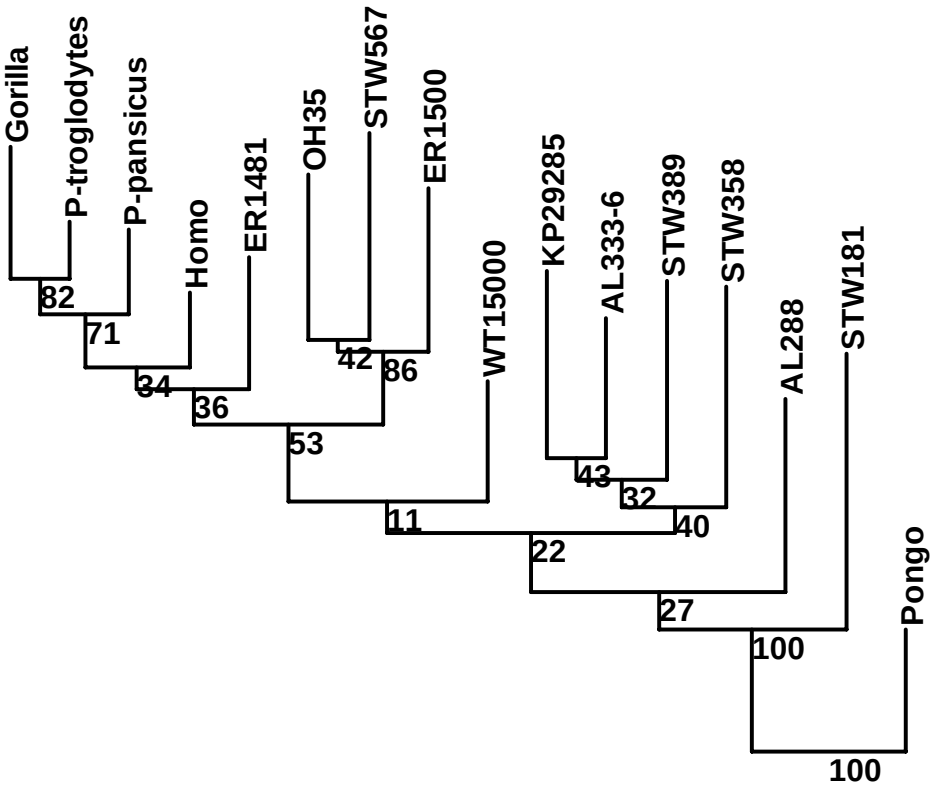

Fig 4.69 Neighbor joining tree for the distal tibia, landmarks 10-18. This tree is based on procrustes chord distances and was rooted with *Pongo* as the outgroup. Bootstrap values are after 1000 replicates.

Distal Tibia Discussion and Analysis

The major features that separate *Homo sapiens* from the extant apes for the tibia are the orientation of the distal articular surface perpendicularly to the long axis of the bone and the degree of lateral torsion in the distal surface in comparison to the proximal surface (Harrison, 1989; Rose, 1993; McHenry, 1994b; DeSilva, 2009). Because this landmark set only captured the distal articular surface without reference to the proximal surface or diaphysis, these features have been lost. Some authors have suggested that there is a posterior tilt to the distal articular surface in apes as compared to *Homo sapiens,* but that has been found to be inconsistent within

modern human populations (Latimer *et al.*, 1987). Thus, there is very little in this data set to separate the extant genera, and only a few inferences can be made about the fossils within this framework.

In general, most of the fossils follow a more human-like pattern with a shorter mediolateral border on the anterior aspect of the distal articular surface and would probably have been most functionally similar to *Homo*. These findings mirror those of DeSilva (2009) who also found the fossils to be mostly *Homo*-like in their form. He argued that the morphology of the distal tibia in early hominins would preclude the ability to engage in vertical climbing safely as it would have been impossible for them to strongly dorsiflex their feet.

Within the fossils, there does seem to be a morphological difference between *A. anamensis, A. afarensis* and *A. africanus* as one group and *P. boisei, H. habilis* and *H. erectus* as a second group. These two groups are separated based on the anterior-posterior width of the articular surface and the length of the anterior border of the articular surface; the differences between these groups seem to be broadly correlated with the relative age of the fossils (see Chapter 2, table 2.2). Whether these changes would translate into functional differences is unclear, as in the overall analysis they all are most similar to modern *Homo* (fig. 4.68).

The only possible functional exception to this is Stw 181, the somewhat *Pongo*-like distal tibia from Sterkfontein. It occupies a more unique position in most of the previous analyses and shares an especially narrow distal articular surface with *Pongo.* Orangutans have a highly flexible foot and ankle (Morbeck and Zilhman, 1988) and it is possible that this morphology is an indicator that the ankle of Stw 181 was equally mobile.

Conclusions

In the introduction to this chapter, three research questions were posed. The discussions and analyses here represent a major step in answering these questions.

- *Do different Plio-Pleistocene hominins have distinct morphological patterns for various limb lower limb segments?*

As a whole for the hindlimb, the fossil hominins are a fairly heterogenous group. If they were all perfectly human-like bipeds (as suggested by Lovejoy, 1988 *et seq.*), then they should all have been most similar in shape to modern humans regardless of how the data were segmented. This was not the case; for both the proximal and distal femur, the variation present in the fossil group exceeded that of the exant groups. In the proximal femur there were three clear patterns of variation: one that was human-like, one that was ape like and one that was a mosaic of human and ape-like traits. The sample of *A. afarensis* was particularly heterogenous, and the large procrustes distances between AL 333-3 and AL 333-123 and the rest of the fossils exceeded the variation in most extant groups, lending support to the idea that there could be multiple taxa represented in the *A. afarensis* hypodigm. For the distal femur, there were also three morphological patterns (human-like, ape-like and intermediate), and a greater number of fossils were more ally similar to the apes than for the proximal femur.

The data for the femur were generally more conclusive than those for the tibia. However, in the distal tibia there was evidence of a variable pattern of morphology particularly in regards to the *Pongo*-like features of Stw 181. This could potentially be a different taxon from the rest of the distal tibiae from Sterkfontein that differs in shape, but not in size from the rest of the

sample. While the rest of the fossils were broadly *Homo*-like, there did seem to be a difference in the morphological patterning of the earlier fossil hominins versus the later ones.

- *Do the changes in each of these joints follow a linear progression?*

For most of the segments, there is no clear linear pattern of change from an ape-like form to a human-like form. For each segment (proximal femur, greater trochanter, distal femur, proximal tibia and distal tibia), the ages of the fossils were plotted against their Procrustes distances from the human centroid (after McHenry and Brown, 2008; figs. 4.70-4.72). While these graphs don't show the direction of change, they do give a rough estimate of how different each of the fossils is from modern humans. The distal tibia is the only segment where there is a clear linear pattern of change (fig 4.70, bottom). For this segment, the oldest fossil in the analysis (KP 29285, *A. anamensis*) has the largest procrustes distance from the human centroid and the youngest fossils (either ER 1481 or WT 15000, *H. erectus*) have the smallest procrustes distances.

For the proximal femur, and particularly for the greater trochanter, there is almost a linear pattern of change (fig. 4.71). If AL 333-3 were the sole *A. afarensis* in the analysis, there would be a relationship between trochanter shape and the age of the fossil. The rest of the *A. afarensis* sample is far more human-like than would be expected for a group of fossils of that antiquity, particularly MAK-VP-1/1 which has one of the smallest procrustes distances in the analysis. Although, on the other hand if AL 333-3 and Stw 99 were removed, there would be no linear transformation at all and individuals the occurring earliest in time would have proximal femora as human-like as those that occur later in time.

There is no strong relationship between age of a fossil and procrustes distance for the proximal tibia (fig. 4.70, top) and the distal femur (fig. 4.72). Perhaps this indicates that there are more ways to modify a knee joint and have it be functionally stable than a hip or an ankle joint. This could be because the knee joint has more soft tissue components that influence its stability than the hip or the ankle (Moore and Dalley, 1999).

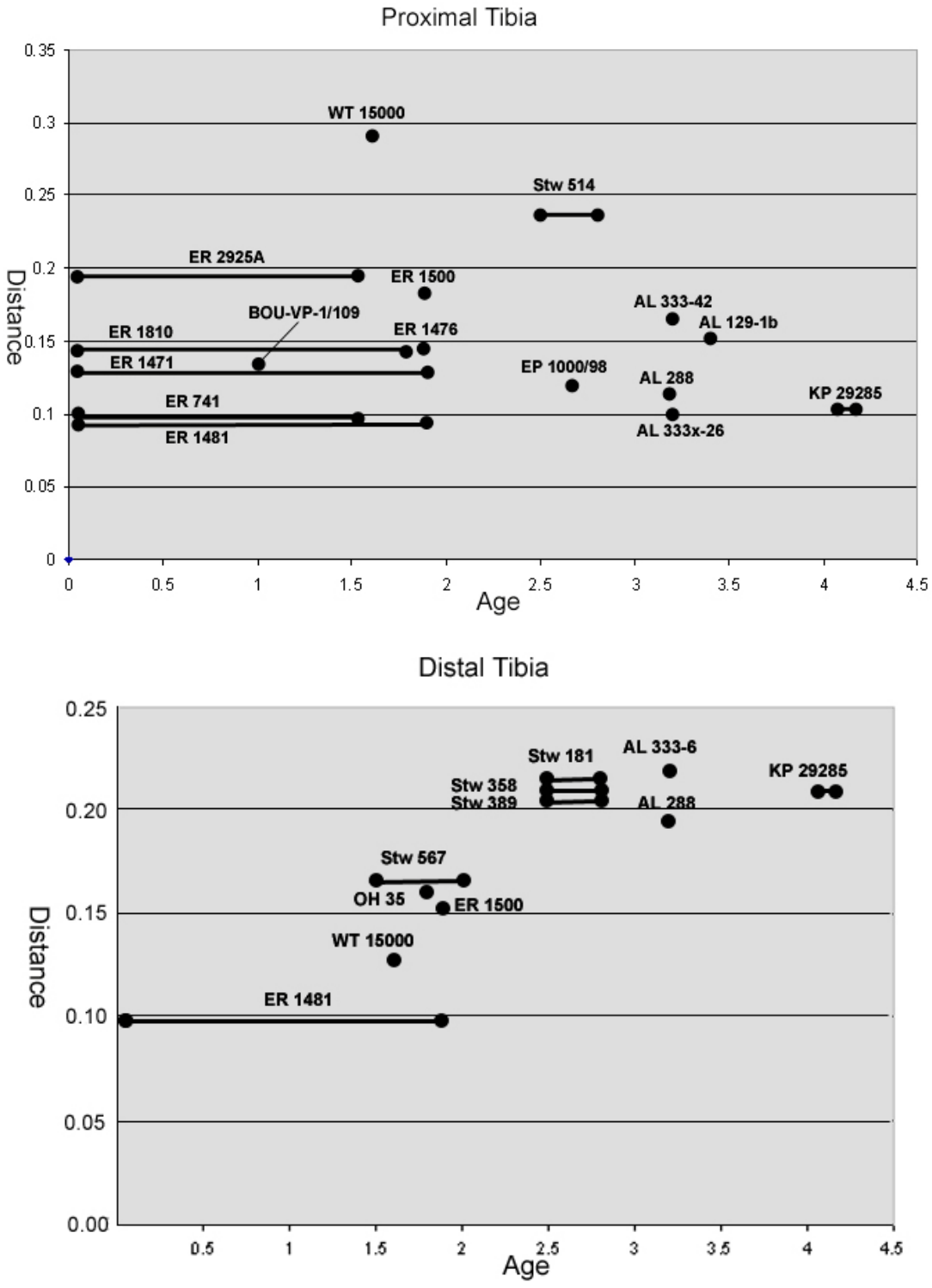

Fig. 4.70 X Y plot of each fossils age range against their procrustes chord distance from the *Homo sapiens* centroid for the proximal and distal tibia. Fossils without an age range are represented by a labeled dot; fossils with an age range are represented by two dots connected by a line.

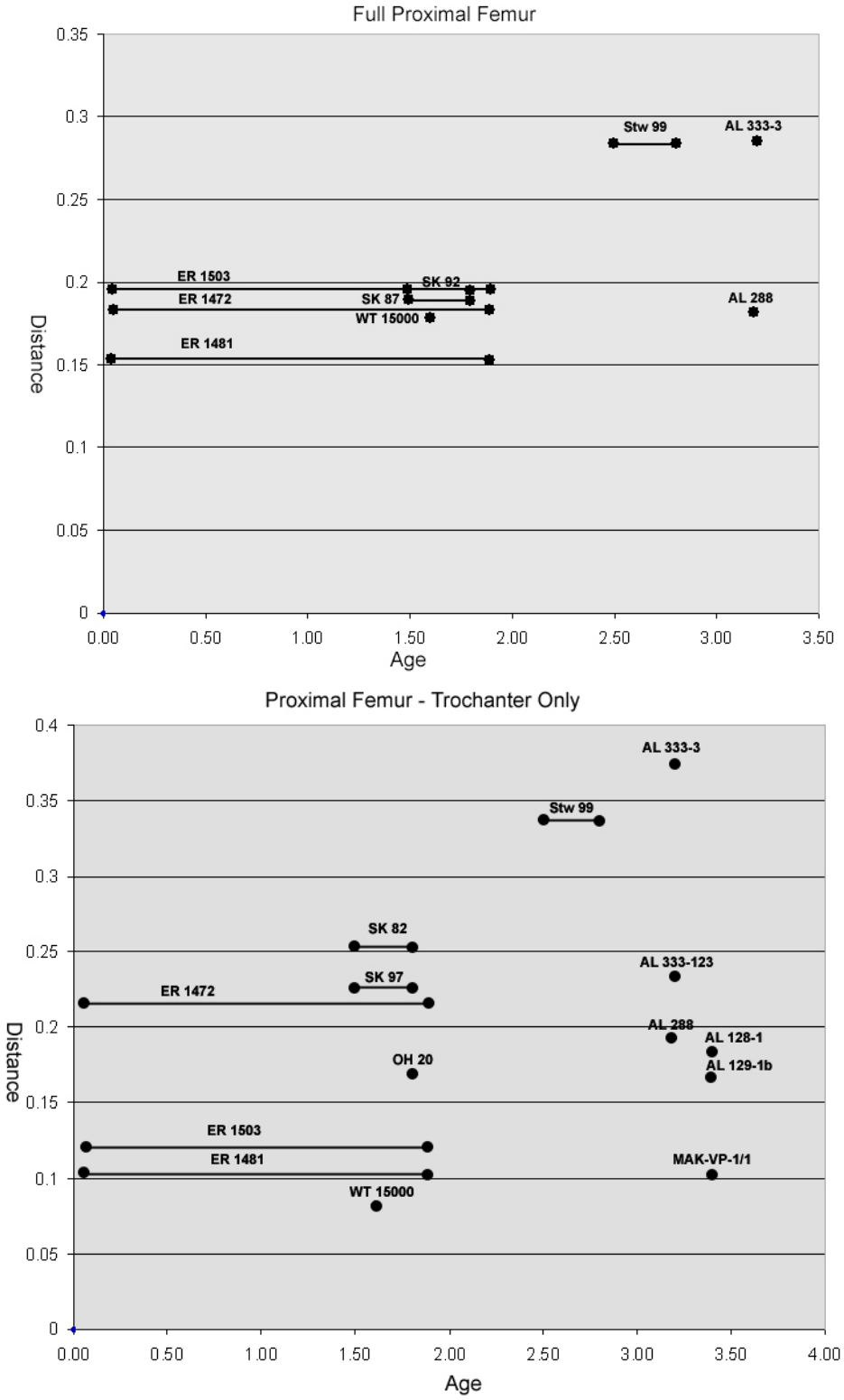

Fig. 4.71 X Y plot of each fossils age range against their procrustes chord distance from the *Homo sapiens* centroid for the proximal femur. Fossils without an age range are represented by a labeled dot; fossils with an age range are represented by two dots connected by a line. The top graph is for the full femur; the bottom for just the greater trochanter

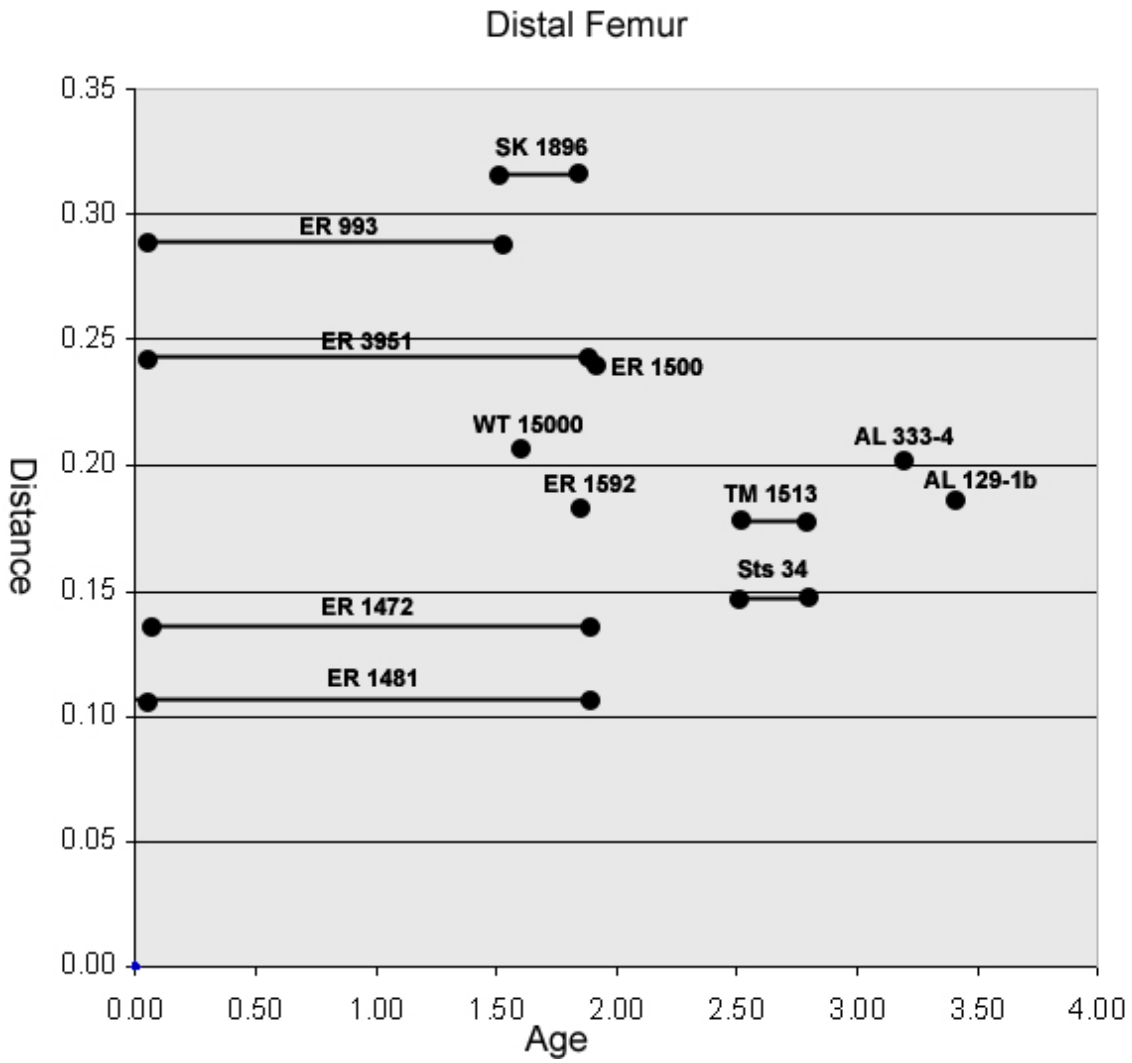

Fig. 4.72 X Y plots of each fossil's age range against their procrustes chord distance from the *Homo sapiens* centroid for the distal femur. Fossils without an age range are represented by a labeled dot; fossils with an age range are represented by two dots connected by a line.

- *For individuals that are either associated or have secure taxonomic attributions, is the taxonomic and functional signal the same across all segments, or is the pattern mosaic?*

The pattern seen in the hindlimb does seem to be a mosaic. The individuals from Hadar, for example, have very human-like proximal femora (with the major exception of AL 333-3) combined with much more ape-like distal femora and ape-like hip/knee covariance. On the other hand, fossils such as ER 1481 and WT 15000 appeared quite human- like regardless of which

limb segment was sampled. The position of ER 1472 is particularly enigmatic in that it has a mostly human-like proximal femur but a somewhat intermediately shaped distal femur, and its hip/knee covariance is like either a human or an ape, depending on whether the full proximal femur or just the greater trochanter was sampled. Thus, the overall pattern for the hindlimb is not one of simple obligate bipedalism for all of the fossils but one of variation.

CHAPTER 5: COVARIATION IN THE FORE- AND HINDLIMB

This chapter seeks to examine the postcranium as an integrative unit in a way that sidesteps the necessity of estimating limb proportions. Instead of using indices such as limb or joint proportions, shape covariation is used to answer questions about the way that multiple bones of the postcranium could function as a unit and to address questions about potential morphological shape integration.

This chapter will answer three broad research questions:

- Is there substantial shape integration between fore- and hindlimb serial homologues?
- Are all skeletal segments developmentally integrated equally? In other words, are some units (*e.g.*, the proximal femur and proximal humerus) more or less integrated than other units?
- Does the pattern of fore- and hindlimb covariance differ among associated skeletons of earlier hominins and is it limited by developmental integration?

Hominin Body Proportions

The most common way to examine the postcranium as a complex is to use body proportions. Numerous studies have been done on the partially complete skeletons of fossil hominins to quantify fore- to hind- limb length and joint proportions. Limb proportions are an important tool in determining possible locomotor repertoires in the fossil record as they are tightly correlated with positional behavior. Species that practice more suspensory, upper-limb dominated modes of locomotion tend to have longer forelimbs (both segment and total length) than hindlimbs. Species that practice hindlimb dominated locomotor patterns, such as vertical

clinging and leaping or bipedalism have longer hindlimbs in proportion to the forelimb. All of the extant apes have high intermembral indices with *Pongo* and *Hylobates* achieving the greatest forelimb to hindlimb lengths, whereas modern *Homo sapiens* has a quite low intermembral index reflecting the lengthening of the hindlimb as an adaptation to obligate bipedalism (Jungers, 1985; Fleagle, 1999).

Studies of fossil limb and joint proportions in the Plio-Pleistocene record have for the most part yielded contradictory results. Analyses on the two most complete specimens from the time period – AL 288 and WT 15000 – have yielded consistent results. AL 288 is said to have proportions which are intermediate between modern *Homo sapiens* and *Pan* (Jungers, 1982), whereas WT 15000 has proportions more like modern *Homo sapiens*, specifically tropically adapted populations (Ruff and Walker, 1993). Other less complete fossil skeletons such as OH 62, BOU-VP-12/1 and ER 3735 have also been used to estimate limb, joint and limb segment proportions with less consistent results.

OH 62 has been suggested to have more chimpanzee-like humerofemoral proportions than *A. afarensis* (Johanson *et al* 1987; Hartwig-Sherer and Martin, 1991), although that has been questioned (Korey, 1990; Asfaw *et al.* 1999). Korey argued that the error involved in estimating the humerus length for OH 62 precludes the ability to accurately measure humerofemoral proportions. Eckhardt (2000) claimed that the differences in the limb lengths between OH 62 and AL 288 could be encompassed by the variation present within a single modern human population, although Richmond *et al.* (2002) disagreed and found that the differences between OH 62 and AL 288 could not comfortably be found within modern extant ape variation; however, that result could change depending on the way that humeral and femoral lengths were estimated.

The BOU-VP-12/1 specimen has been reconstructed to have a humerofemoral index most like modern *Homo sapiens,* but an ape-like brachial index (Asfaw *et al.* 1999; DeGusta, 2004). Richmond *et al.* (2002) supported these conclusions and found that the differences between the humerofemoral index of BOU-VP-12/1 and ER 15000 were easily encompassed by the natural variation in extant populations, but that the brachial index more closely resembled that of *Pongo.* However, the margin of error in estimating the limb proportions of both this skeleton and OH 62 are high. Slight changes in the limb reconstruction could change the results of these limb proportion analyses substantially (Reno *et al.,* 2005).

More recently, KNM-ER 3735 was used to estimate body proportions. Hauesler and McHenry (2007) admitted freely that this skeleton is too fragmentary to actually reconstruct limb proportions; instead, these authors took various measurements all over the postcranium, computed ratios and compared the differences between ER 3735 and AL 288 to differences between pairs of extant specimens. These authored concluded that ER 3735 had a mosaic of traits in the postcraium, some ape-like and some human-like.

Studies that have attempted to quantify limb proportions in *Australopithecus africanus* are on even shakier ground. Researchers have tried to show that the joint proportions in *Australopithecus afarensis* are more human-like than those of *Australopithecus africanus.* However, there are no skeletons of *A. africanus* with both the fore- and the hind- limb to analyze. Analyses using Stw 431 require the least amount of extrapolation as it has a nearly complete forelimb. Stw 431 is said to have larger upper limb arm joints in comparison to lower limb arm joints, making it more ape-like than AL 288 (McHenry and Berger, 1998; Green *et al.* 2007), although these results have been questioned (Dobson, 2005). Stw 573 has a complete fore- and

hind- limb, although it has yet to be described (Clark, 1998; Partridge *et al.* 1999)**.** That fossil promises to yield more concrete data considering the limb proportions of *A. africanus.*

Instead of using limb proportions, Ruff (2008, 2009) used limb strength proportions to examine the postcranium as an integrative unit. He found that OH 62 had humeral/femoral strength proportions that are most similar to modern chimpanzees, indicating that OH 62 had greater upper limb strength and was perhaps subjected to greater mechanical loads on the arms. This indicated that *H. habilis* (*sensu stricto*) would have had a strong arboreal component to its locomotor behavior. On the other hand, WT 15000 and ER 1808 have femoral/humeral strength proportions most similar to modern *H. sapiens,* including sex based differences if ER 1808 is assumed to be female.

Limb Development

Another way to examine patterns of postcranial variation is through the lens of morphological integration and pattern of fore-/hindlimb covariation. The forelimb and hindlimb are serially homologous structures. Because of their common evolutionary history, quantitative genetic theory posits that the size and shape of the fore- and hindlimb should evolve in tandem as they rely upon the same genes and signaling cascades during development (Wagner and Altenberg, 1996). Among primates, humans particularly seem to challenge this idea as our hindlimb is elongated in comparison to our forelimb and our hands and feet have divergent functional roles (Young *et al.,* 2010).

The upper and lower limbs are both derived from lateral mesoderm of the developing embryo. The upper and lower limb buds appear during the fourth week of gestation with the upper limb buds appearing one or two days in advance of the lower limb buds. They are composed of mesenchyme, covered by ectoderm (O'Rahilly and Gardner, 1975). The apical

ectodermal ridge (AER) is a thick band of ectoderm at the end of each limb bud that promotes outgrowth of the limb buds and influences the development of the proximodistal limb dimension by keeping the distal-most cells in an undefined and proliferating state. This mechanism is driven by the fibroblast growth factor (*Fgf)* family of genes, particularly *Fgf4* and *Fgf8.* Once the cells are defined, the *HoxA* family of genes defines the particular features of the stylopod (most proximal), and zeugopod (mid-limb) (Zeller *et al.* 2009).

During the fifth week of development, chondrification centers appear and an entire cartilaginous skeleton is produced by the end of the sixth week (Moore and Persaud, 1998). Chondrocyte differentiation is driven by the *Sox9* gene and mediated by ectodermal WNT molecules which regulate cell to cell signaling (Zeller *et al.* 2009). Osteogensis begins during the seventh week from the primary centers of ossification and continues for the remainder of embryologic and fetal development (Moore and Persaud, 1998).

Hands and foot plates also appear by the sixth week and digits appear by the end of the eighth week. The hand and foot make up the autopod and the formation of digits is driven by signaling cascades that define the anterior-posterior axis of the limb. *HoxD* genes influence the secretion of the *Sonic Hedgehog (shh)* morphogen from the Zone of Polarizing Activity (ZPA), located posterior to the AER. The spatial and temporal gradient in the expression of *shh* leads to the differentiation between the anterior and posterior surfaces of the limb, with the posterior digits (part of 3, 4 and 5) deriving from cells with the highest and most prolonged exposure to *shh* (Zeller *et al.* 2009).

The previously mentioned *HoxA* and *HoxD* genes families affect both the fore- and hindlimb buds in the formation of the limb compartments (Shubin *et al.* 1997).

However, there are additional *T-box* gene families that are expressed differentially in the fore- and hindlimbs after bud formation and thus could be responsible for fore- and hindlimb differentiation. Mutations in the *Tx4* and *Tx5* genes have led to developmental abnormalities in the musculoskeletal system of the fore- and hindlimb respectively (Hasson *et al.* 2010).

There have been only a few studies that have examined covariation in serially homologous structures in adult primates. Rolian *et al.* (2009) compared the length and shape of manual and pedal phalanges in hominoids and found that they covaried strongly. These authors have suggested that manual phalanx morphology is a by-product of strong selection on the pedal morphology for efficient bipedality and not necessarily from selection for manual dexterity. Young *et al.* (2010) tested covariance in length in serially homologous (stylopod, zeugopod and autopod) modules in humans, great apes and some Old World monkeys. These authors found that fore- and hindlimb integration was more relaxed in apes than in quadrupedal monkeys due to the difference in functional roles of the fore- and hindlimb.

Materials and Methods

Table 5.1 List of fossil individuals and elements used

Accession #	Taxon	Elements
AL 288	*A. afarensis*	Humerus Ulna Femur
AL 129	*A. afarensis*	Femur
ER 1500	*P. boisei*	Ulna Femur
ER 1503/1504		Humerus Femur
Omo (Kibish) 1	*H. sapiens*	Humerus Ulna Femur
WT 15000	*H. erectus*	Humerus Ulna Femur

The full extant sample as described in Chapter 2 was utilized for these analyses, as well as the fossils listed in Table 5.1. ER 1503 and ER 1504 were combined as some researchers believe these represent a single individual (McHenry, 1978). The distal femur of AL 129 was analyzed with the forelimb elements of AL 288 as they are both from the same taxon (Johansen *et al.* 1978)

and are of a similar size (see Chapter 4). Previous studies have noted that covariation in elements of two different individuals within a single species do not differ greatly from matched elements (Harcourt-Smith *et al.,* 2008). Each postcranial landmark configuration was analyzed as a whole as well as subdivided into proximal and distal subsets. All of these data were subjected to a generalized procrustes analysis and used in multivariate analyses.

In order to assess the degree of morphological shape integration present in this data set, two-block partial least squares analyses were conducted using *MorphoJ v. 1.02* (Klingenberg, 2008). 2B-PLS is a way of assessing the covariance between two independent sets of data (Rohlf and Corti, 2000) and has been used successfully to look for covariance between shape data and geographical coordinates (Frost *et al.,* 2003) as well as patterns of covariance between dorsal and ventral views of mouse skulls (Corti and Fadda, 1996) and hominoid distal tibial and proximal astraglar articulations (Harcourt-Smith *et al.,* 2008). Computing a 2B-PLS of all extant hominoids emphasizes species-specific differences in order to make inferences about patterns of covariance among hominoids. Performing the same computations on adult, single-species samples can answer questions of developmental integration. The pattern of covariance among different species is different from developmental integration in that it takes into account both integrative developmental pathways and possible past selective events in each lineage (Mitteroecker and Bookstein, 2008). Multiple traits that are not developmentally integrated could be selected for together if they are part of a common functional complex (Cheverud, 1996).

Within each hominoid species, 2B-PLS analyses were run between all possible pairs of fore- and hindlimb segments and the degree of covariation on the first principal axes was recorded, as well as the RV coefficient. The RV coefficient is analogous to the Pearson's

correlation coefficient, but for high-dimensional data sets, and it can be interpreted in the same was as any coefficient of correlation (Escoufier, 1973). The degree of covaration should be stronger and the RV coefficients should be higher in developmental homologues than in those that are non-homologous if the shapes are strongly integrated.

Additionally, 2B-PLS analyses including the fossils and all extant individuals were run to examine patterns of evolutionary integration in the modern and fossil taxa. In some cases, landmark sets were further decimated to allow for the inclusion of the maximal number of fossils; this is noted throughout the text. These graphs were compared to principal components analyses of the individual segments in order to assess whether testing for patterns of covariance yields different interpretations of the data.

Data Analysis

Results: Developmental Integration

Two-block partial least squares analyses were run for all possible pairs of fore- and hindlimbs and the RV coefficients and percent covariance along the first axis were extracted, the results of which are presented in table 5.2. Permutation tests of ten thousand replicates were performed to test that the correlations between the blocks was greater than what would be expected in a random sample; in all pairs, all axes and the RV coefficients were significantly different from the null hypothesis. T-tests were performed to assess whether the serially homologous pairs were significantly different from the non-serially homogolous pairings. The only significant difference was between the humerus/femur and the humerus/tibia where the RV values were significantly greater in the serially homologous pairs (p=0.045).

Table 5.2 Percent covariance (%cov) and correlation (corr) of first common axes and RV coefficients in 2B-PLS analysis between Procrustes aligned shape data for serially and non-serially homologous bones. The non-homologous pairings are shaded gray.

	HUM/FEM			**RAD/TIB**			**HUM/TIB**			**RAD/FEM**		
	% cov	***corr***	***RV***	***% cov***	***corr***	***RV***	***% cov***	***corr***	***RV***	***% cov***	***corr***	***RV***
Gorilla gorilla	47.4	0.80	0.43	49.5	0.72	0.26	52.0	0.72	0.32	43.2	0.73	0.31
Homo sapiens	66.4	0.87	0.48	61.2	0.70	0.32	57.3	0.84	0.36	84.1	0.74	0.37
Pongo pygmaeus	40.5	0.77	0.55	51.5	0.79	0.44	25.6	0.77	0.37	49.6	0.91	0.56
Pan troglodytes	51.7	0.81	0.34	39.3	0.62	0.23	59.5	0.76	0.32	34.6	0.64	0.24
Pan paniscus	39.6	0.82	0.57	36.4	0.70	0.39	29.7	0.72	0.43	42.6	0.79	0.48

A Generalized Procrustes Analysis of an entire long bone tends to emphasize length and width dimensions and orientation of the proximal and distal ends with respect to each other over the details of shape (see Chapters 3, 4, and 5 for wireframe transformations that illustrate this). Thus, the previous analysis contained information about both shape and length which would

impact these results. It is expected that the length/width dimensions of serially homologous elements should be integrated due to both using the same regulatory pathways (Shubin *et al.,* 1997; Zeller *et al.,* 2010).

The data were further segmented into proximal and distal portions and a similar set of analyses were run in order to specifically assess shape integration. By analyzing the proximal and distal portions separately, we remove all length information as well as information about orientation, and shape is prioritized. The data for *Pongo* and *Pan paniscus* are not presented as all of the results were not significantly different from two independent data sets when tested by a permutation test of ten thousand replicates. This is likely because the number of variables was greater than the number of individuals in the sample (Rohlf and Corti, 2000). The covariance between the serially homologous pairs was so low that no non-serially homologous pairs were tested. The results of these analyses are presented in table 5.3.

Table 5.3 Percent covariance (%cov) and correlation (corr) on the first common axis and RV coefficients in 2B-PLS analysis between Procrustes aligned shape data for serially and non-serially homologous proximal and distal bone segments.

	Prox Hum/Prox Fem			**Dist Hum/Dist Fem**			**Prox Rad/Prox Tib**			**Dist Rad/Dist Tib**		
	%cov	***corr***	***RV***	***%cov***	***corr***	***RV***	***%cov***	***corr***	***RV***	***%cov***	***corr***	***RV***
Gorilla gorilla	61.4	0.65	0.22	60.4	0.75	0.22	45.7	0.42	0.11	66.3	0.73	0.31
Homo sapiens	69.8	0.53	0.18	49.6	0.60	0.18	34.4	0.64	0.22	37.0	0.52	0.19
Pan troglodytes	45.2	0.64	0.17	54.7	0.66	0.17	39.9	0.48	0.11	26.4	0.55	0.15

Considering both of these analyses, there is little support for the idea that there is strong shape integration in the stylopod and zeugopod in large hominoids. For the full stylopod, the RV coefficients were significantly higher than in the non-serially homologous pairings, but considering the results of the segmented bone analysis, integration is more likely to due to

length, robusticity and orientation of the proximal and distal ends with regard to each other than to shape.

Results: Interspecific Patterns of Covariance

As there is no strong evidence that serially homologous pairs are phenotypically constrained by developmental genes (*i.e.,* if postcranial shape were strongly developmentally integrated, natural selection could only select for genes that would not have a deleterious effect on the serially homologous element), all pairs of postcranial segments were tested in order to examine covariance of fore- and hindlimb elements. This has the added benefit of allowing for a greater number of fossil pairings to be analyzed.

The results of pairwise comparisons of the humerus, radius, ulna, femur and tibia using 2B-PLS are presented in table 5.4. The percent covariance along the first common axis and the RV coefficients were significantly higher in the multiple species analyses than within a single species indicating that for postcranial shape, evolutionary integration is stronger than developmental integration. There is no statistically significant difference between the homologous and non-homologous pairings.

Table 5.4 Percent covariance (%cov) and correlation (corr) along the first common axis and RV coefficients for pairs of fore-/hindlimb elements. In all cases, the %cov and RV were higher in the mixed species analysis. Non-serially homologous pairs are shaded grey.

	% cov	***corr***	***RV***
Full Humerus/Full Femur	89.366	0.85	0.5545
Full Radius/Full Tibia	96.517	0.78	0.5524
Full Humerus/Full Tibia	91.423	0.85	0.5234
Full Radius/Full Femur	93.771	0.80	0.5618
Full Ulna/Full Femur	90.521	0.88	0.6398
Full Ulna/Full Tibia	94.832	0.85	0.6152

Finally, 2B-PLS analyses for all possible pairs of fore- and hindlimb segments – including fossil individuals that preserved the relevant portions - were completed, the results of which are presented in table 5.5. Overall, the RV coefficients were much lower than for the full landmark set, indicating that length/breadth and proximodistal orientation of the articular surfaces are more integrated than shape of the articular surfaces. All pairings were significantly different from the null hypothesis of independence in permutation tests. There were four pairings with relatively high RV scores: proximal ulna/proximal femur; proximal ulna/distal femur; distal humerus/proximal femur; and distal humerus/distal femur. In analyses presented in chapters 3 and 4 the proximal ulna, distal humerus and femur were the best at discriminating between taxa, so this result is not surprising. 2B-PLS graphs were generated for these four pairings and are presented in figures 5.2 – 5.7.

Table 5.5 Percent covariance (% cov) and correlation (corr) along the first and second common axes and RV coefficients for pairs of fore-/hindlimb segments. Bolded entries indicate comparatively high RV values.

	% cov 1	**% cov 2**	**corr 1**	**corr 2**	***RV***
Prox Ulna/Prox Femur	**67.472**	**28.709**	**0.81**	**0.80**	**0.5183**
Prox Ulna/Dist Femur	**83.066**	**10.235**	**0.82**	**0.63**	**0.4842**
Prox Ulna/Prox Tibia	58.133	19.348	0.67	0.49	0.1645
Prox Ulna/Dist Tibia	68.797	17.944	0.77	0.56	0.304
Dist Radius/Prox Femur	74.627	20.603	0.78	0.53	0.3336
Dist Radius/Dist Femur	81.473	10.588	0.82	0.48	0.3118
Dist Radius/Prox Tibia	49.34	21.613	0.65	0.40	0.126
Dist Radius/Dist Tibia	43.259	27.763	0.63	0.56	0.209
Prox Radius/ Prox Femur	88.119	7.522	0.60	0.34	0.1983
Prox Radius/Dist Femur	89.63	3.623	0.62	0.31	0.2071
Prox Radius/Prox Tibia	57.497	16.478	0.50	0.30	0.0728
Prox Radius/Dist Tibia	57.143	15.199	0.48	0.37	0.0802
Dist Humerus/Prox Femur	**66.561**	**26.903**	**0.81**	**0.78**	**0.5293**
Dist Humerus/Dist Femur	**81.521**	**9.919**	**0.85**	**0.62**	**0.4932**
Dist Humerus/Prox Tibia	50.344	20.674	0.68	0.56	0.1653
Dist Humerus/Dist Tibia	61.952	15.33	0.75	0.56	0.2815
Prox Humerus/Prox Femur	69.713	24.187	0.66	0.54	0.2344
Prox Humerus/Dist Femur	61.952	15.338	0.68	0.52	0.2815
Prox Humerss/Prox Tibia	39.242	29.694	0.46	0.45	0.088
Prox Humerus/Dist Tibia	56.474	23.257	0.55	0.50	0.1487

For the distal humerus and proximal femur, there was strong covariance between the first axis of each dataset (fig. 5.1). AL 288 and ER 1503/1504 are both *Homo*-like in their pattern of covariance in both the proximal femur and distal humerus. WT 15000 seems to have a unique pattern of covariance with a human-like femur and a slightly more ape-like humerus (figs. 5.2 and 5.3). However, WT 15000 is very close to 95% equal frequency ellipse for modern humans; in addition, this specimen is both a juvenile and pathological. The first humeral axis is driven by the height of the lateral epicondyle with *Homo* having it more distally flexed and the apes having it more proximally flexed. It is also driven by the shape of the trochlea, particularly the proximal-anterior margin. In *Homo,* that margin is straight, while in apes it has a "V" shape. Additionally, *Homo* has a less symmetrical trochlea than do the apes (fig. 5.4). The first femoral axis is largely driven by the lateral extension of the greater trochanter and the height of the femoral head with *Homo* having laterally projecting trochanters and more proximally oriented femoral heads in comparison to the apes (fig. 5.5).

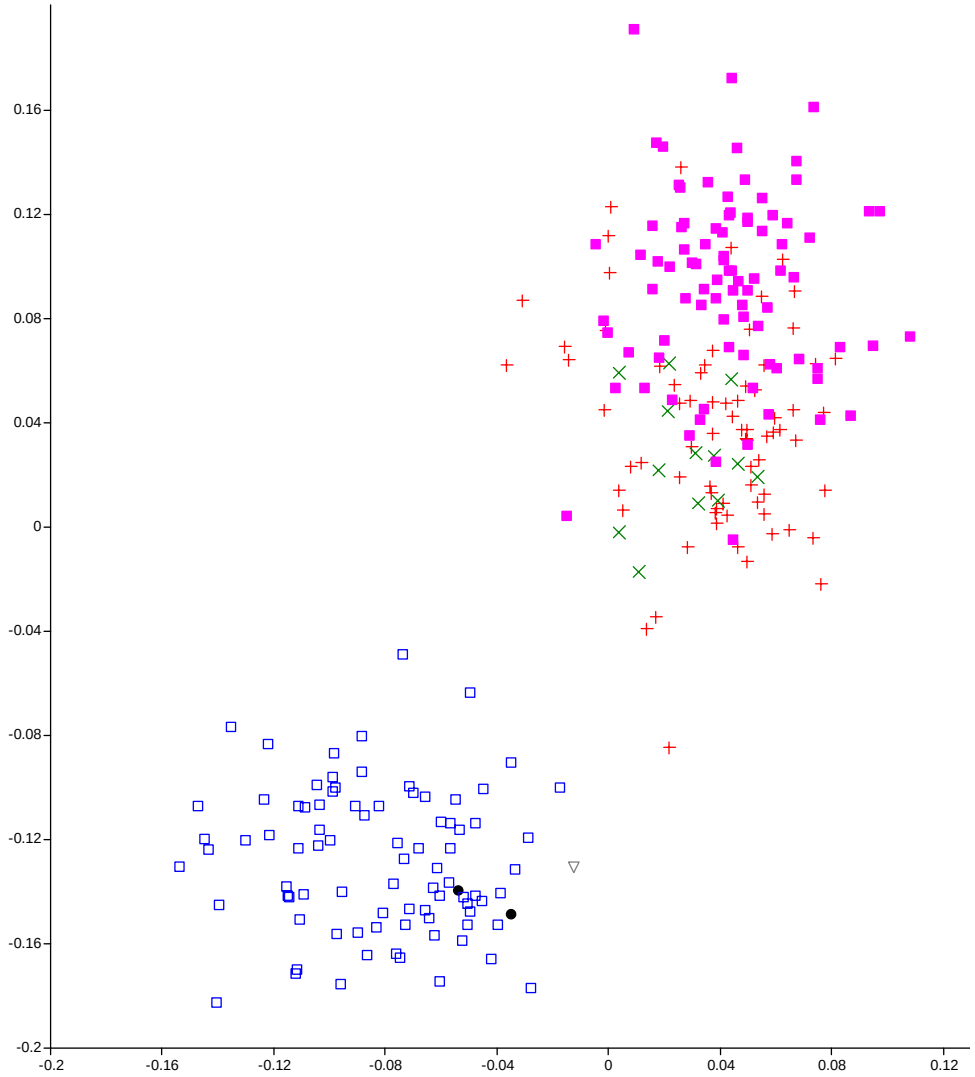

Fig. 5.1 2B-PLS plots of the first common factor for the Procrustes aligned coordinates for all pairwise fore-/hindlimb analyses using the full distal humerus and full proximal femur. *Gorilla* is represented by red crosses, *Pan troglodytes* by purple squares, *Pongo* by green Xes and *Homo* by blue open squares. Fossils are represented by black circles and grey triangles. The % covariance on the first common axis and the RV coefficients are presented in table 5.5.

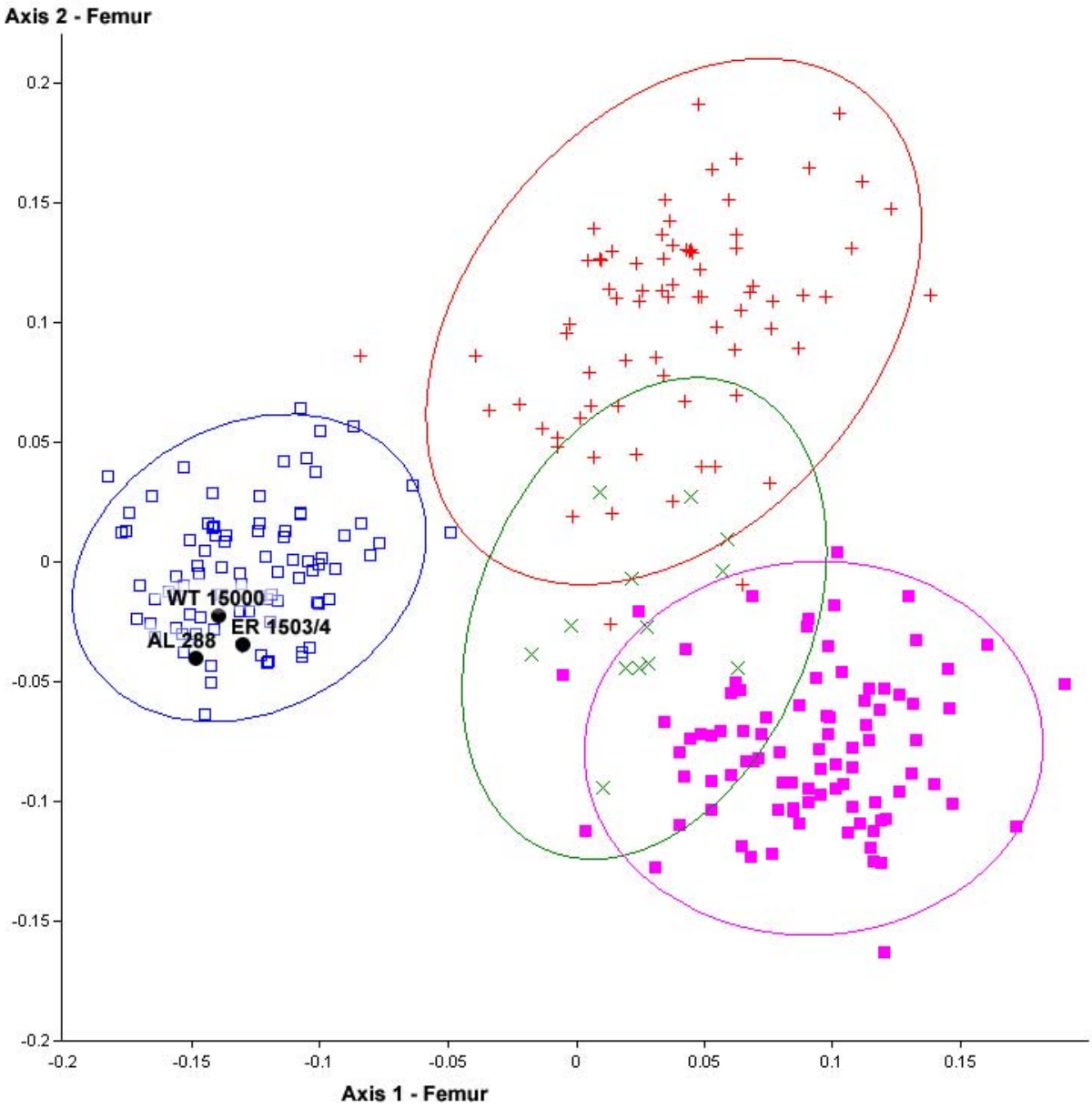

Fig. 5.2 Singular value decomposition of the first two proximal femoral axes based on a cross covariance matrix of data for the distal humerus and proximal femur as part of a partial least squares analysis. *Homo* is represented by blue open squares, *Pan* by purple squares, *Gorilla* by red crosses and *Pongo* by green Xes. Fossils are in black and labeled in the graph. The closed curves represent 95% equal frequency ellipses.

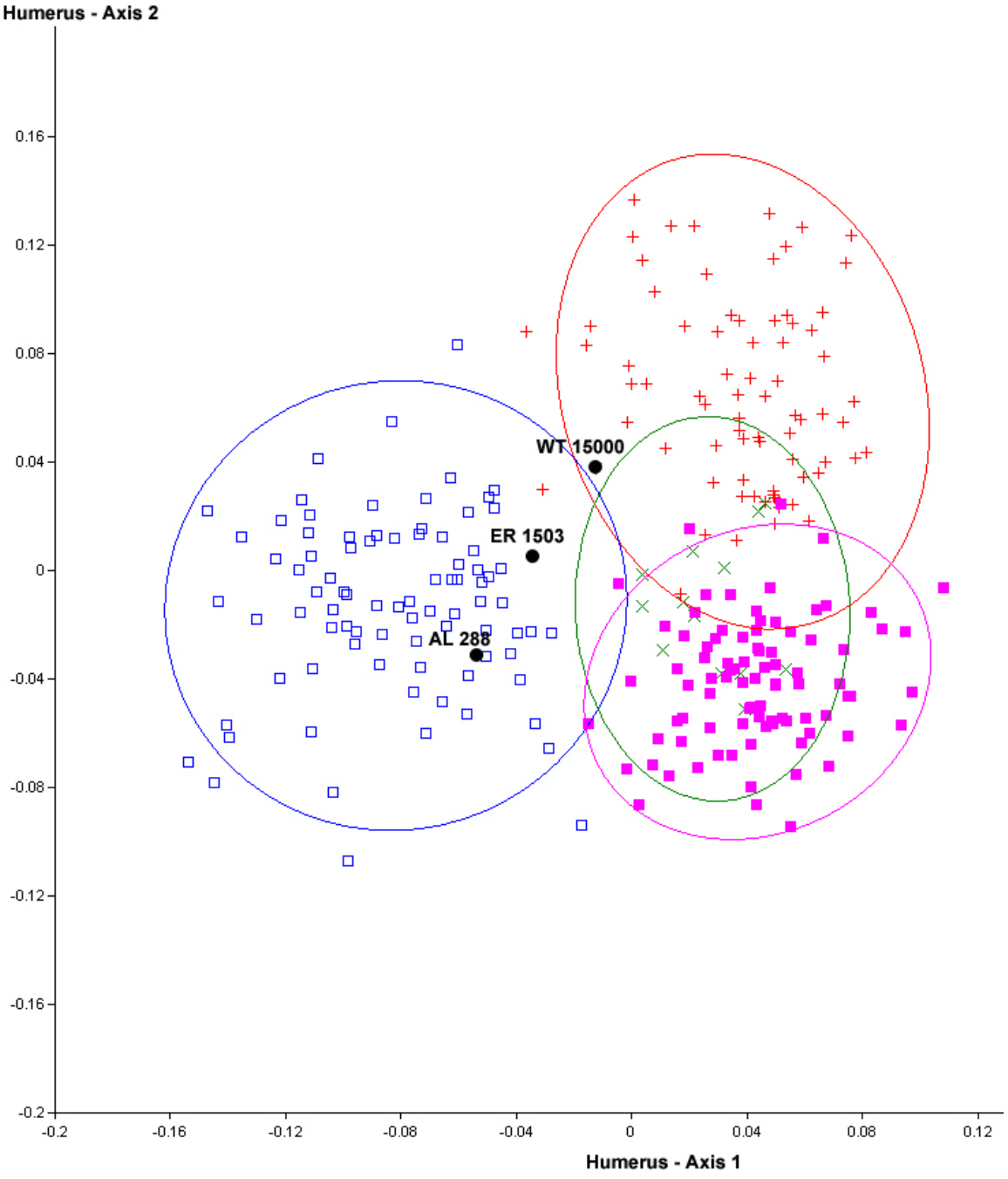

Fig. 5.3 Singular value decomposition of the first two distal humerus axes based on a cross covariance matrix of data for the distal humerus and proximal femur as part of a partial least squares analysis. *Homo* is represented by blue open squares, *Pan* by purple squares, *Gorilla* by red crosses and *Pongo* by green Xes. Fossils are in black and labeled in the graph. The closed curves represent 95% equal frequency ellipses.

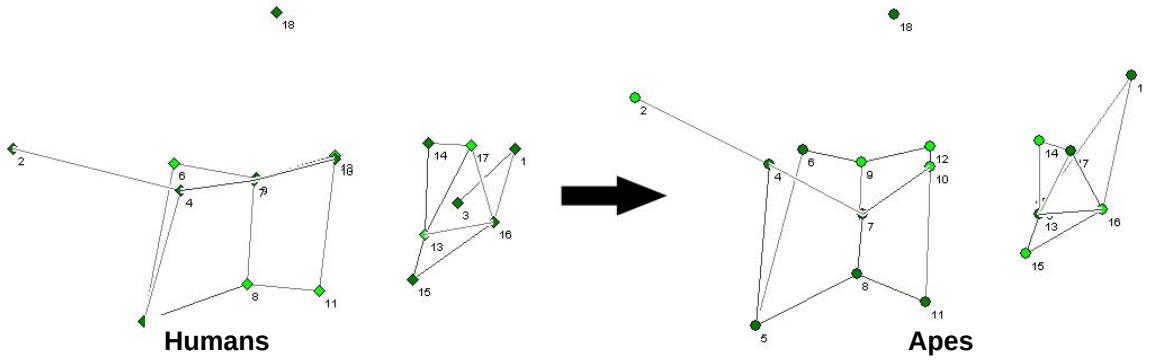

Fig. 5.4 Wireframe transformation between humans and the great apes along the first humeral axis for the 2B-PLS analysis of the distal humerus and proximal femur. Wireframes are in an anterior view.

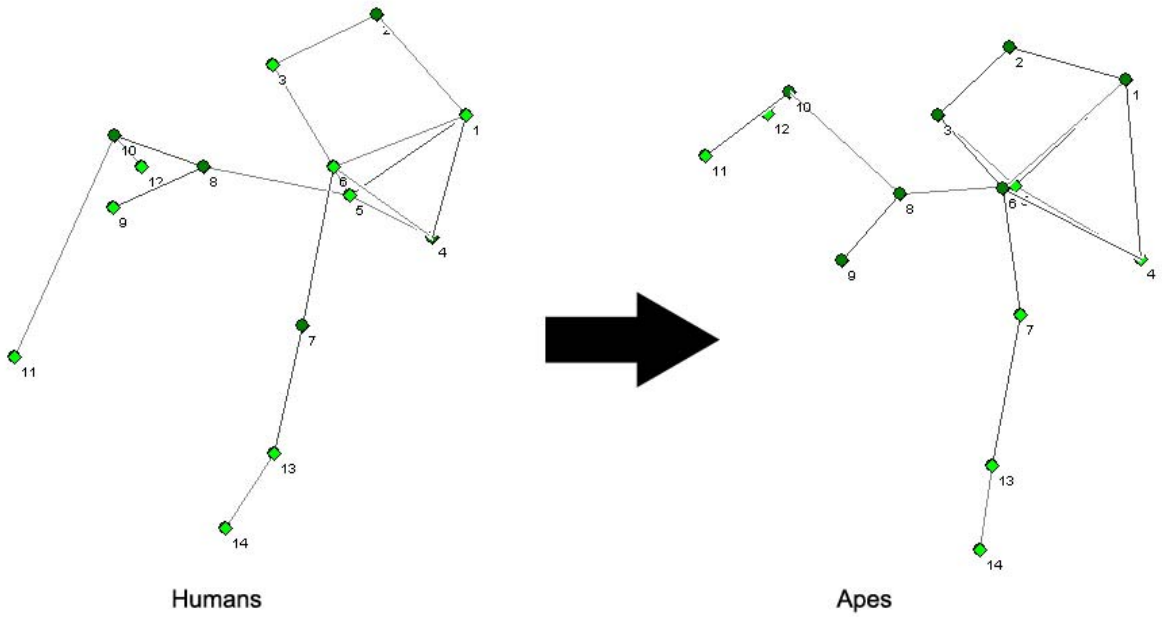

Fig. 5.5 Wireframe transformation between humans and the great apes along the first femoral axis for the 2B-PLS analysis of the distal humerus and proximal femur. Wireframes are in a posterior view.

There is excellent covariance for the distal humerus and the distal femur (fig. 5.6). Omo (Kibish) 1 has a pattern for forelimb/hindlimb covariance most similar to modern *Homo sapiens* whereas the other two fossils have a unique pattern of covariance. *A. afarensis* (represented by a composite AL 288 and AL 129) has a human-like humerus combined with a more ape-like distal femur while WT 15000 has a human-like distal femur combined with a more ape-like distal

humerus. Again, the fact that WT 15000 is a juvenile and has evidence of pathology cannot be discounted (figs. 5.7 – 5.8). The first humeral axis is driven by the position of both the medial and lateral epicondyles, which are relatively low in humans as opposed to the apes, as well as the proximal-anterior border and shape of the trochlea. In humans, the proximal-anterior border is straight and the medial corner projects somewhat anteriorly; the trochlea as a whole is less symmetrical than those of the apes (fig. 5.9). The first femoral axis is driven solely by the asymmetry of the patellar articular surface in *Homo sapiens* (fig. 5.10).

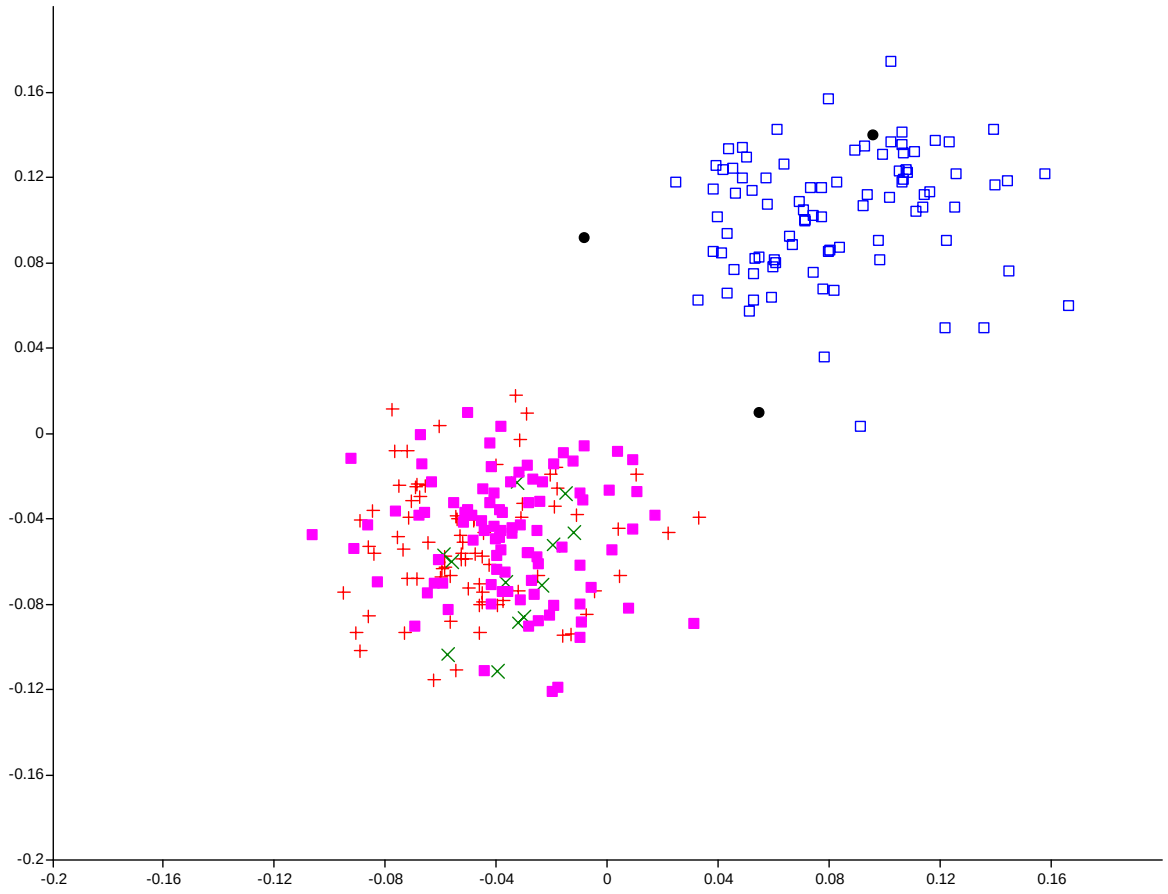

Fig. 5.6 2B-PLS plots of the first common factor for the Procrustes aligned coordinates for all pairwise fore-/hindlimb analyses using the full distal humerus and full distal femur. *Gorilla* is represented by red crosses, *Pan troglodytes* by purple squares, *Pongo* by green Xes and *Homo* by blue open squares. Fossils are represented by black circles. The % covariance on the first common axis and the RV coefficients are presented in table 5.5. The second and third common axes failed to separate any extant taxa.

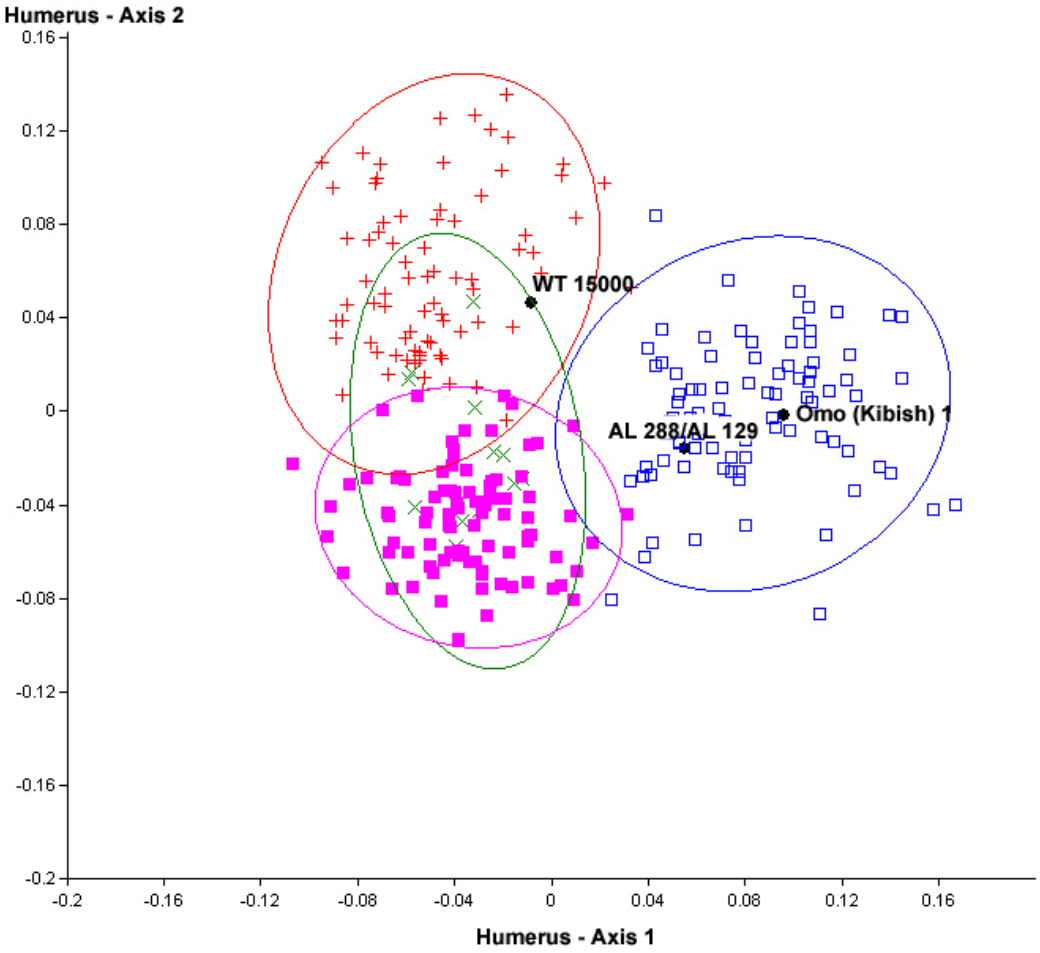

Fig. 5.7 Singular value decomposition of the first two distal humerus axes based on a cross covariance matrix of data for the distal humerus and distal femur as part of a partial least squares analysis. *Homo* is represented by blue open squares, *Pan* by purple squares, *Gorilla* by red crosses and *Pongo* by green Xes. Fossils are in black and labeled in the graph. The closed curves represent 95% equal frequency ellipses.

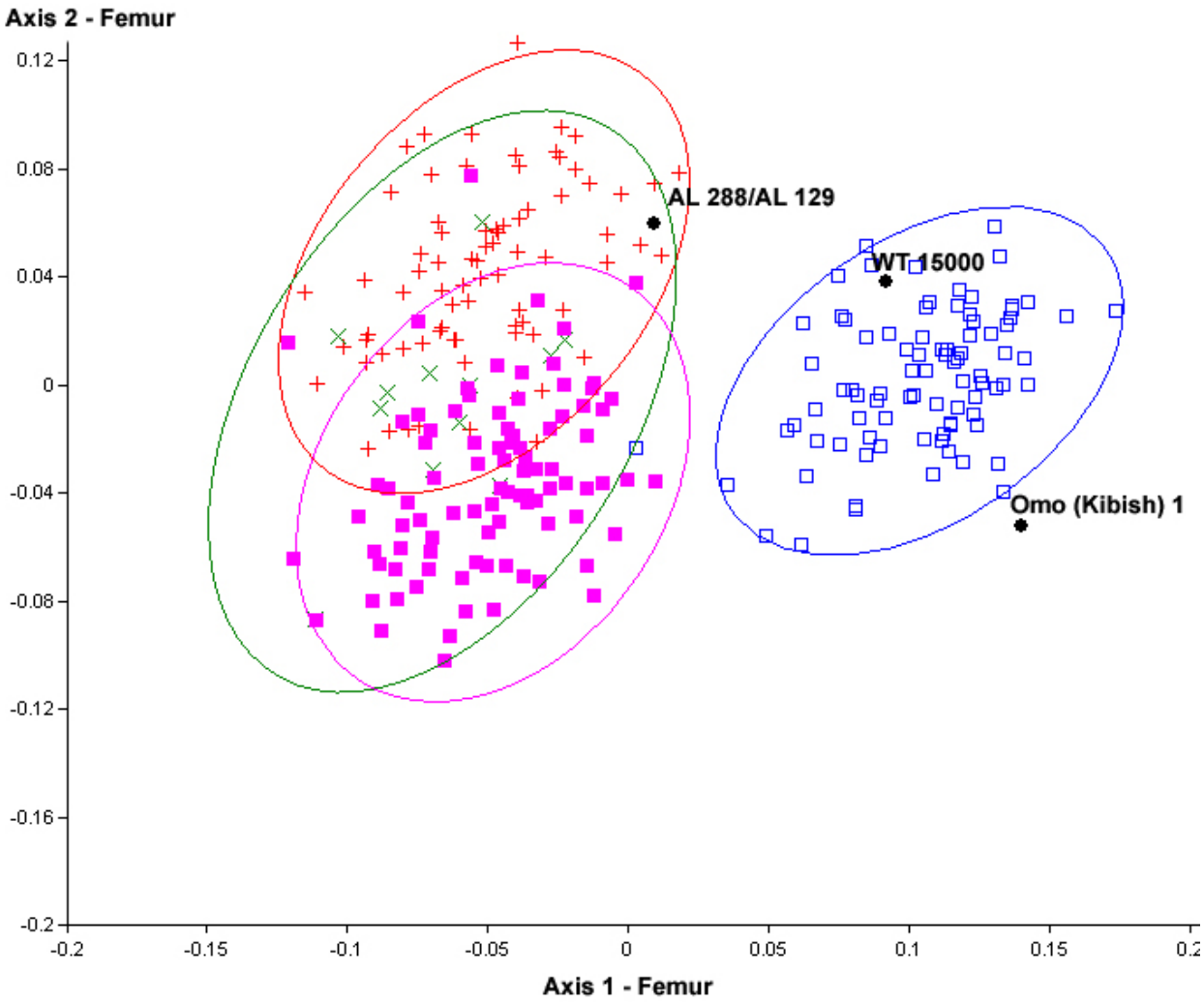

Fig. 5.8. Singular value decomposition of the first two distal femoral axes based on a cross covariance matrix of data for the distal humerus and distal femur as part of a partial least squares analysis. *Homo* is represented by blue open squares, *Pan* by purple squares, *Gorilla* by red crosses and *Pongo* by green Xes. Fossils are in black and labeled in the graph. The closed curves represent 95% equal frequency ellipses.

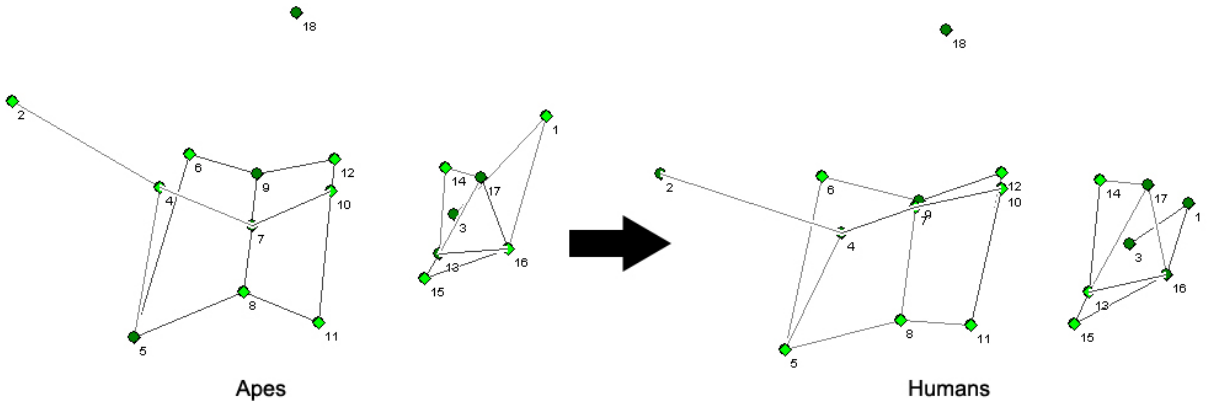

Fig. 5.9 Wireframe transformation between humans and the great apes along the humeral axis for the 2B-PLS analysis of the full landmark set for the distal humerus and distal femur. Wireframes are in an anterior view.

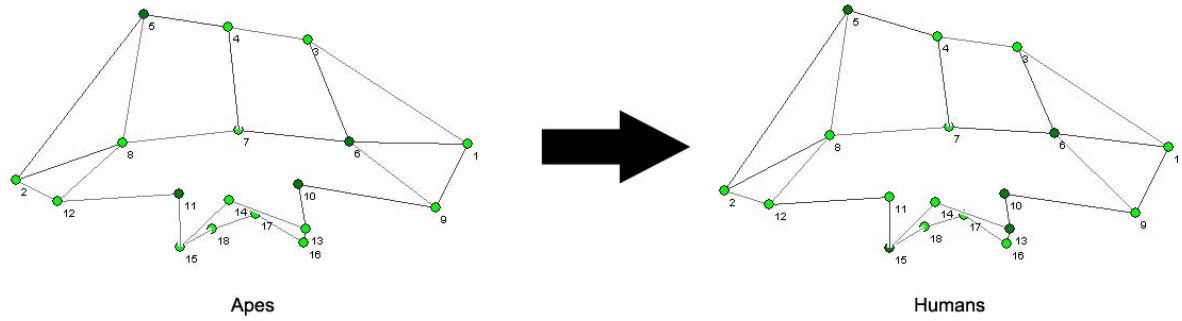

Fig. 5.10 Wireframe transformation between humans and the great apes along the femoral axis for the 2B-PLS analysis of the full landmark set for the distal humerus and distal femur. Wireframes are in an anterior view.

The proximal ulna was compared to the proximal femur. Once again, there was excellent covariance between the two elements (fig. 5.11). WT 15000 and AL 288 both have a modern human pattern of covariance for both the proximal ulna and proximal femur (figs. 5.12 and 5.13). The first ulnar axis was driven by the shape of the olecranon process and the depth and keeling of the trochlear notch. Modern humans have a relatively flat and shallow notch in comparison to the apes and an olecranon process that is smaller and does not have a strong posterior projection (fig. 5.14). The first femoral axis is driven by the low, laterally projecting greater trochanter in modern humans as opposed to the higher, less projecting trochanter of the apes. In addition, the

length of the femoral neck also seems to be contributing to this axis with modern humans having a longer neck than the apes (fig. 5. 15).

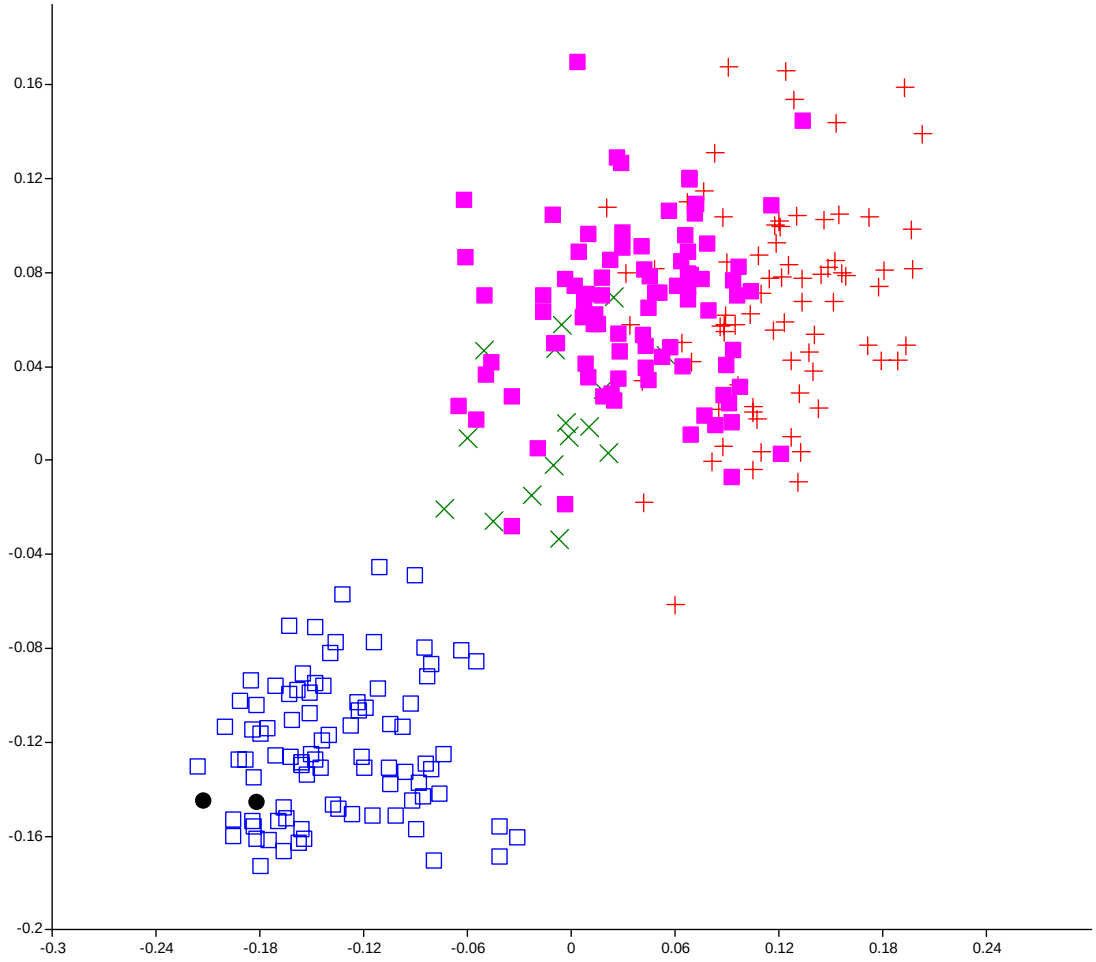

Fig. 5.11 2B-PLS plots of the first common factor for the Procrustes aligned coordinates for all pairwise fore-/hindlimb analyses using the full proximal ulna and full proximal femur. *Gorilla* is represented by red crosses, *Pan troglodytes* by purple squares, *Pongo* by green Xes and *Homo* by blue open squares. Fossils are represented by black circles. The % covariance on the first common axis and the RV coefficients are presented in table 5.5. The second and third common axes failed to separate any extant taxa.

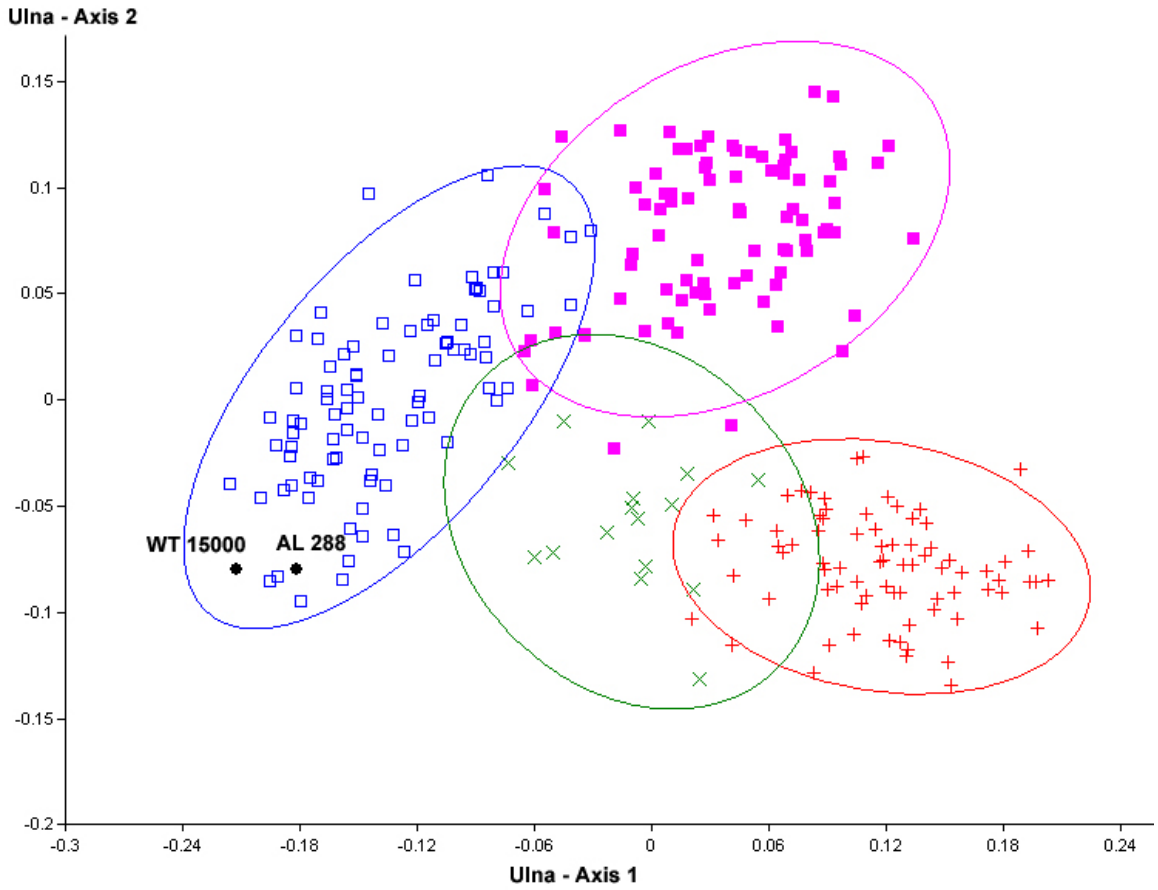

Fig. 5.12. Singular value decomposition of the first proximal ulnar axes based on a cross covariance matrix of data for the proximal ulna and proximal femur as part of a partial least squares analysis. *Homo* is represented by blue open squares, *Pan* by purple squares, *Gorilla* by red crosses and *Pongo* by green Xes. Fossils are in black and labeled in the graph. The closed curves represent 95% equal frequency ellipses.

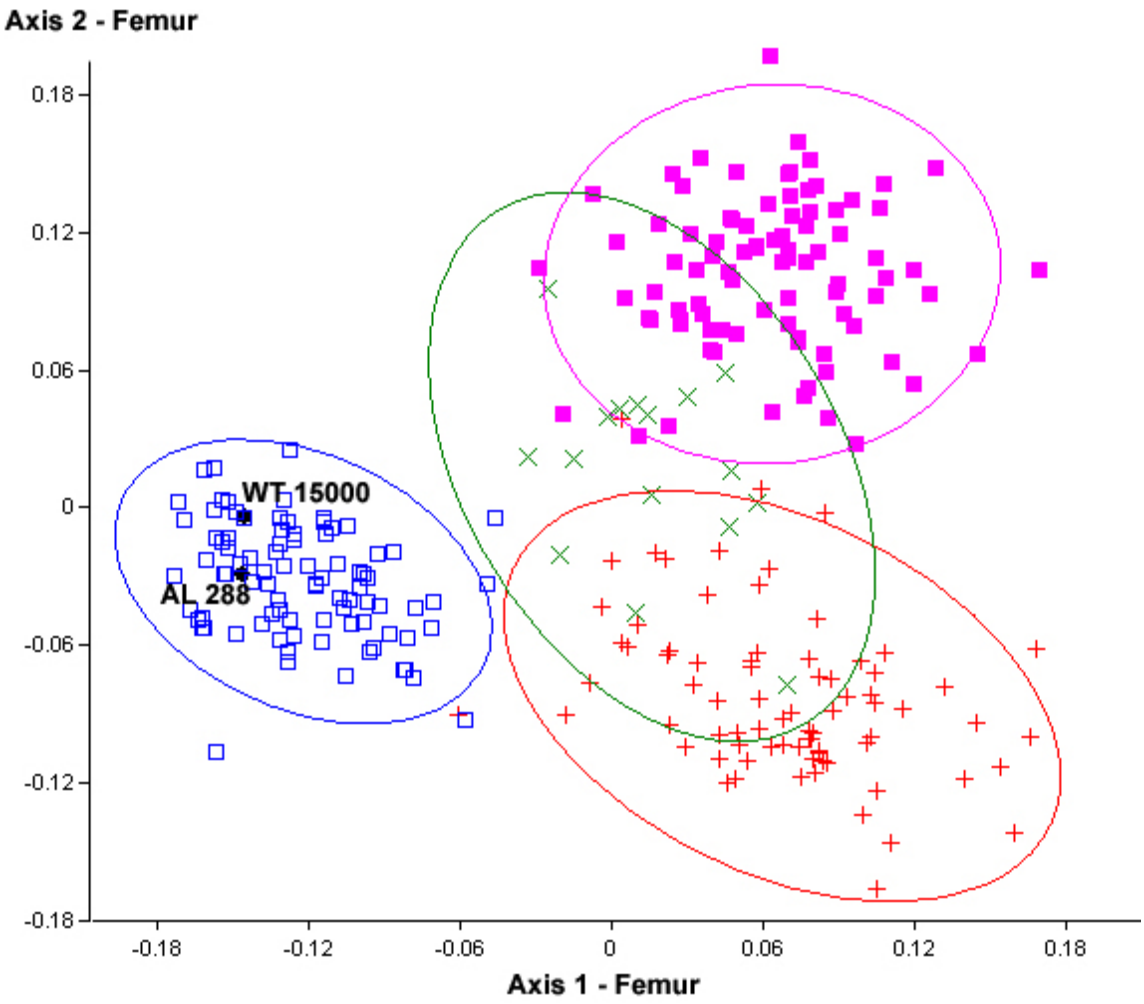

Fig. 5.13. Singular value decomposition of the first proximal femoral axes based on a cross covariance matrix of data for the proximal ulna and proximal femur as part of a partial least squares analysis. *Homo* is represented by blue open squares, *Pan* by purple squares, *Gorilla* by red crosses and *Pongo* by green Xes. Fossils are in black and labeled in the graph. The closed curves represent 95% equal frequency ellipses.

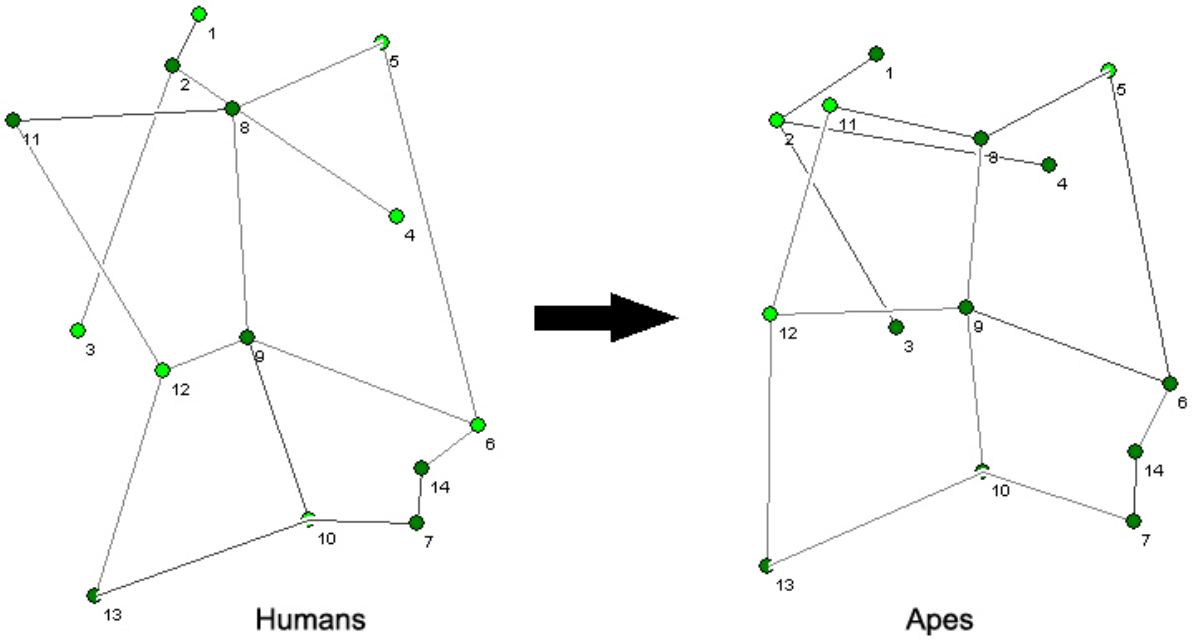

Fig. 5.14 Wireframe transformation between humans and the great apes along the ulnar axis for the 2B-PLS analysis of the full landmark set for the proximal ulna and proximal femur. Wireframes are in an anterior view.

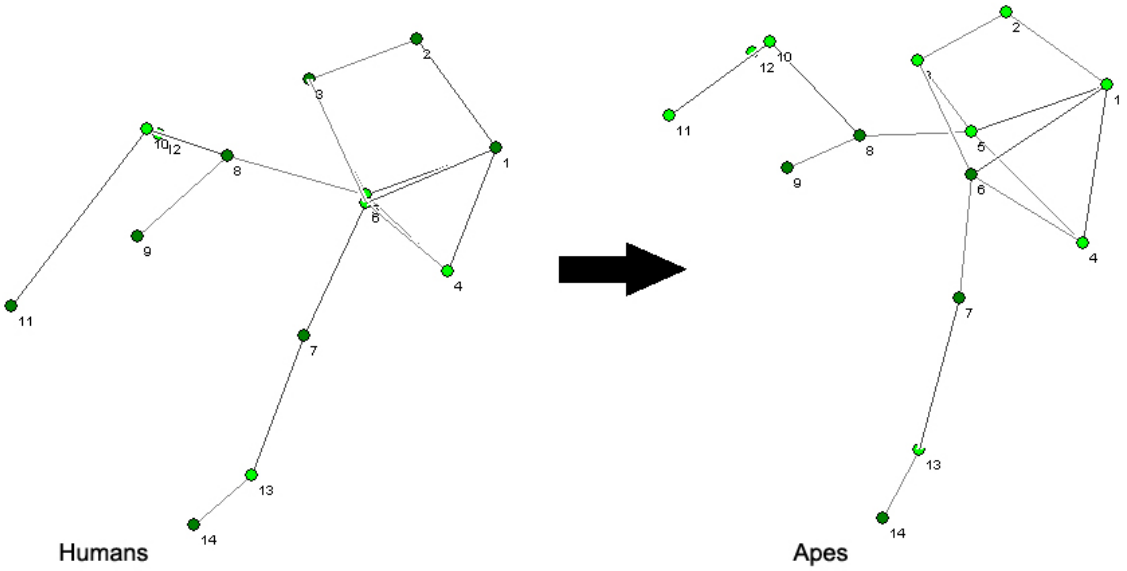

Fig. 5.15 Wireframe transformation between humans and the great apes along the femoral axis for the 2B-PLS analysis of the full landmark set for the proximal ulna and proximal femur. Wireframes are in an posterior view.

Finally, the proximal ulna and distal femur also covaried strongly along the first axis (fig. 5.16). In this analysis, WT 150000 has a pattern of covariance that most closely resembles that

of modern humans. Omo (Kibish) 1 also has a pattern that is similar to modern humans, although it falls outside the range of all extant taxa for the ulna. This may be an effect of allometry as Omo (Kibish) 1 has a centroid size that is most similar to extant male *Gorilla.* ER 1500 and AL 288/129 both have a unique pattern of covariation with a more human-like proximal ulna and an ape-like distal femur (figs. 5.17 and 5.18). The first ulnar axis was driven by the shape of the olecranon process and the depth and keeling of the trochlear notch. Modern humans have a relatively flat and shallow notch in comparison to the apes and an olecranon process that is smaller and does not have a strong posterior projection (fig. 5.19). The first femoral axis is driven by the asymmetry in the patellar articular surface with humans being very asymmetrical and apes being more symmetrical. Additionally, there is a tighter angle between the patellar and distal articular surfaces in the modern humans than in the other apes (fig. 5.20).

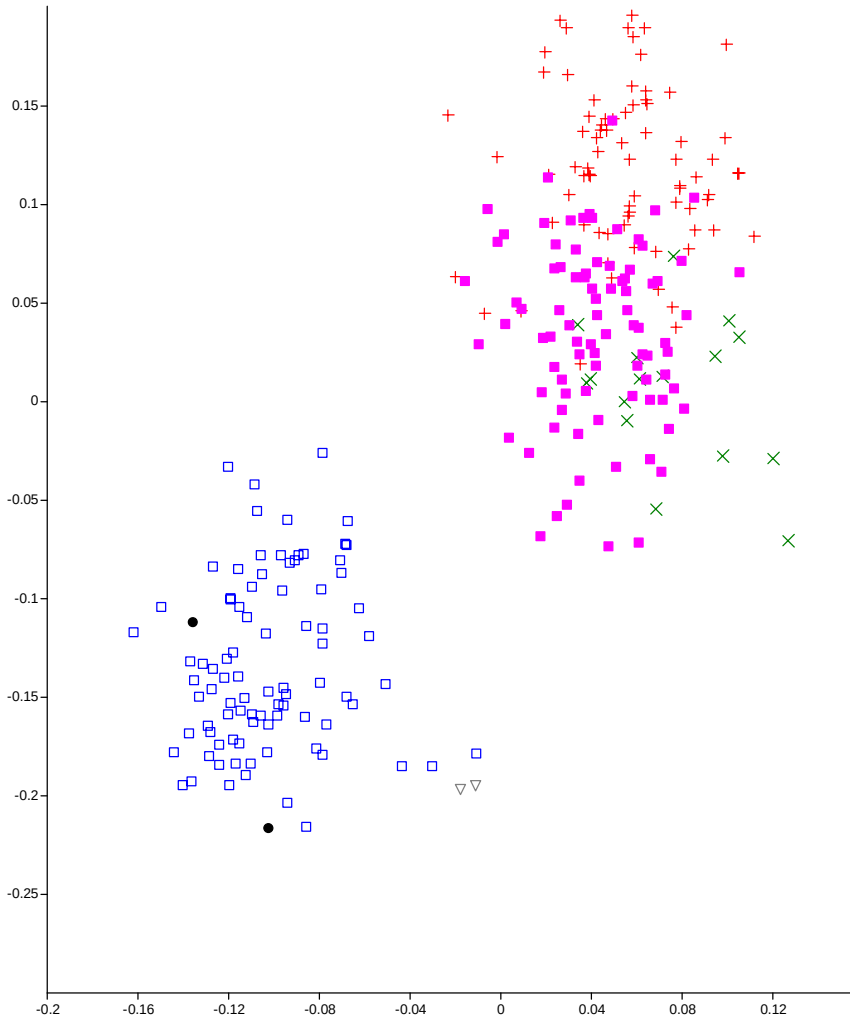

Fig. 5.16 2B-PLS plots of the first common factor for the Procrustes aligned coordinates for all pairwise fore-/hindlimb analyses using the full proximal ulna and full distal femur. *Gorilla* is represented by red crosses, *Pan troglodytes* by purple squares, *Pongo* by green Xes and *Homo* by blue open squares. Fossils are represented by black circles and are labeled in the graph. The % covariance on the first common axis and the RV coefficients are presented in table 5.5.

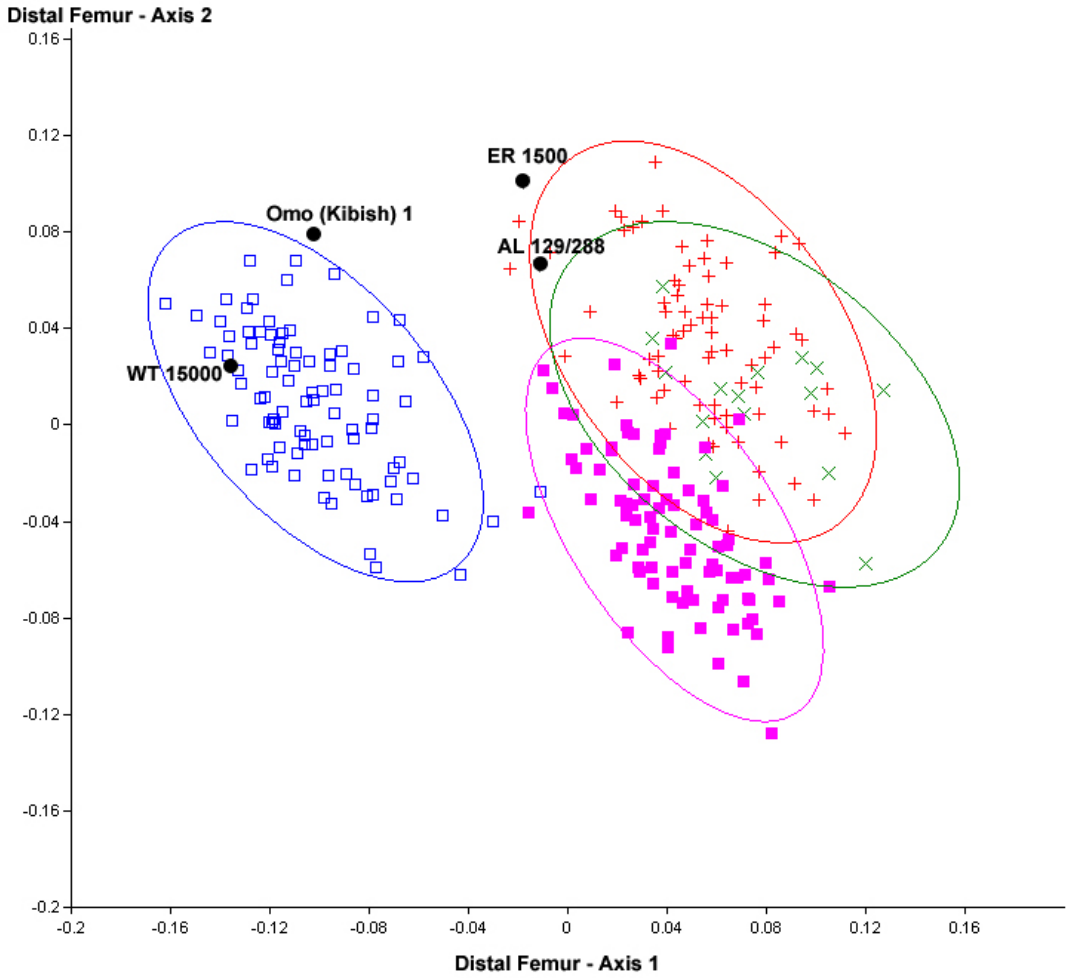

Fig. 5.17 Singular value decomposition of the first distal femoral axes based on a cross covariance matrix of data for the proximal ulna and distal femur as part of a partial least squares analysis. *Homo* is represented by blue open squares, *Pan* by purple squares, *Gorilla* by red crosses and *Pongo* by green Xes. Fossils are in black and labeled in the graph. The closed curves represent 95% equal frequency ellipses.

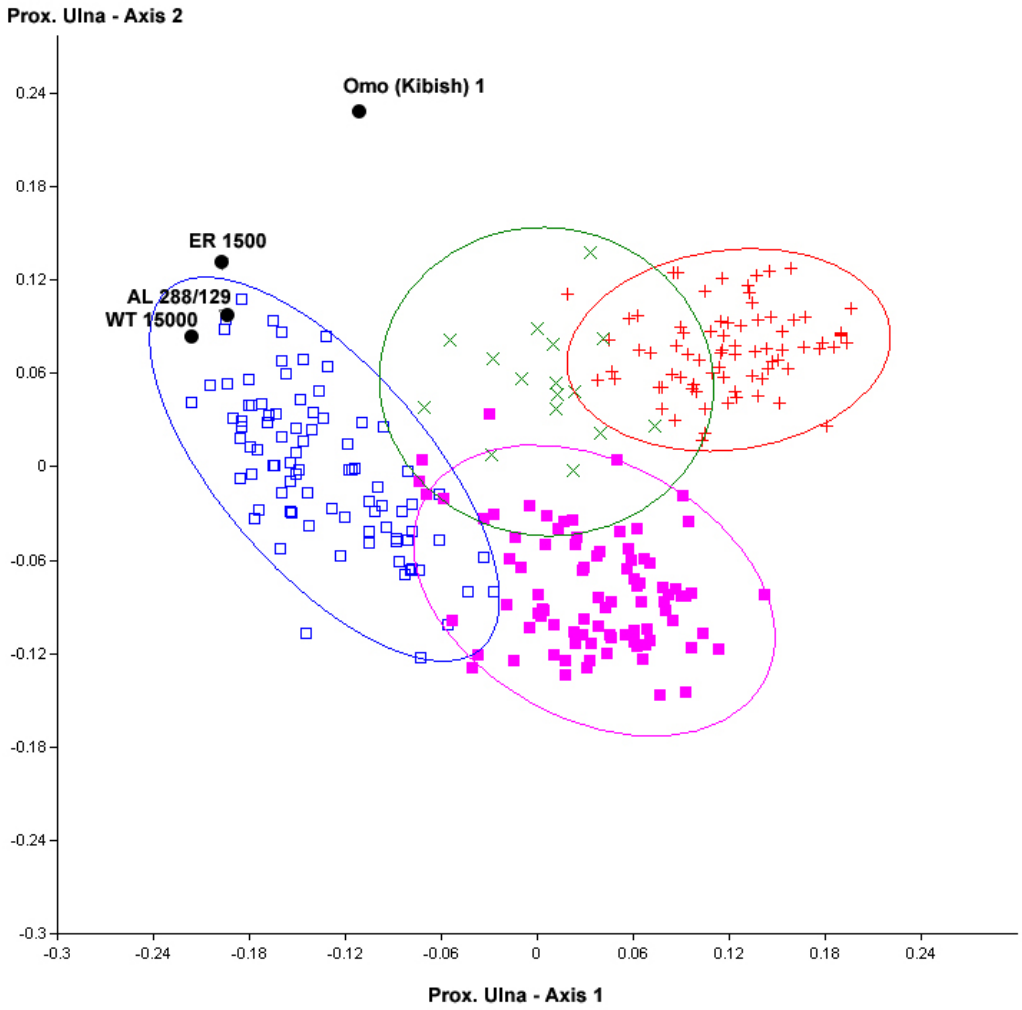

Fig. 5.18 Singular value decomposition of the first proximal ulnar axes based on a cross covariance matrix of data for the proximal ulna and distal femur as part of a partial least squares analysis. *Homo* is represented by blue open squares, *Pan* by purple squares, *Gorilla* by red crosses and *Pongo* by green Xes. Fossils are in black and labeled in the graph. The closed curves represent 95% equal frequency ellipses.

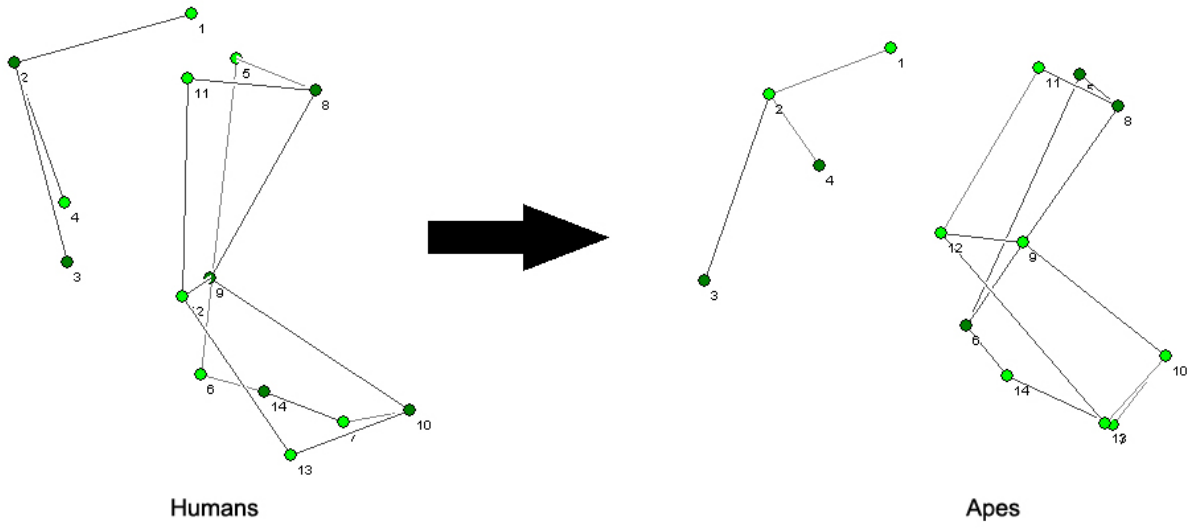

Fig. 5.19 Wireframe transformation between humans and the great apes along the ulnar axis for the 2B-PLS analysis of the full landmark set for the proximal ulna and distal femur. Wireframes are in a medial view.

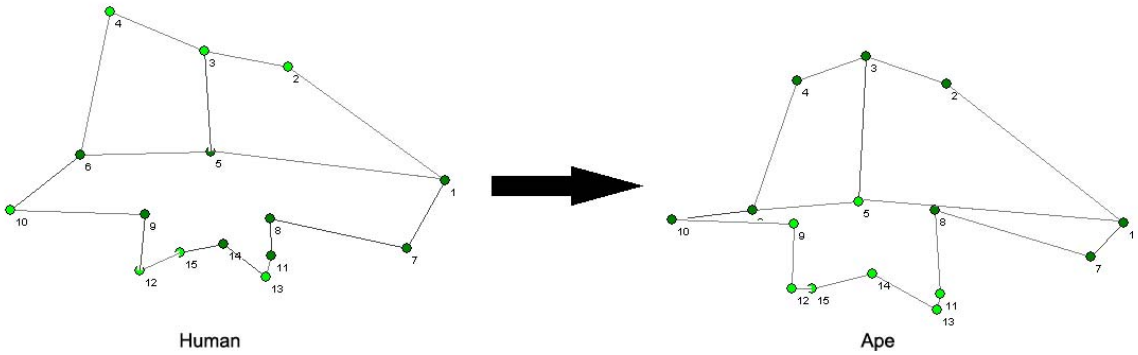

Fig. 5.20 Wireframe transformation between humans and the great apes along the femoral axis for the 2B-PLS analysis of the full landmark set for the proximal ulna and distal femur. Wireframes are in a posterior view.

In summary, for all of the full segment pairings, there is a clear difference in the pattern of covariation for *Homo* and that of the other large bodied hominoids. WT 15000 (*H. erectus*) was included in all analyses and was consistently human-like in the hindlimb and proximal ulna, and somewhat ape-like in the distal humerus regardless of the pairing. AL 288 (*A. afarensis*)

was also included in all analyses and had a consistently unique pattern of covariation with a human-like distal humerus, proximal ulna and proximal femur with an ape-like distal humerus. ER 1500, attributed to *Paranthropus boisei* (Grausz, 1988) was included only in the analyses including the proximal ulna and distal femur and it was found to have a human-like proximal ulna combined with an ape-like distal femur. All of these results largely mirror the findings from PCAs in previous analyses in this dissertation.

Omo (Kibish) 1 *(Homo sapiens;* McDougall and Brown, 2008) was excluded from the analyses using the proximal femur as that region is not preserved in the specimen. In the other analyses, it largely fell within the 95% confidence interval for modern humans, the exception being for the proximal ulna where it is unlike any extant taxa. This is likely an artifact of size. The Omo (Kibish) 1 skeleton was not used in any previous analyses as it is thought to be a modern *Homo sapiens (*McDougall and Brown, 2008). Finally, for the single analysis where ER 1503/1504 (*Homo* sp.) was used, it also had a human-like pattern of covariation. This is interesting as it is contra the findings in Chapters 3 and 4, where ER 1504 had an ape-like distal humerus and ER 1503 had an ape-like greater trochanter shape.

Discussion

While there are many genes that operate both in the forelimb and the hindlimb (*e.g. HoxA, HoxD;* Wagner and Altenberg, 1996), there are also genes that work to differentiate the hindlimb from the forelimb. Many researchers believe that the forelimb is the "default" pathway for limb development (Marcil *et al.,* 2003), and the hindlimb will resemble the forelimb if the hindlimb specific patterning genes are not activated correctly (Szeto *et al.* 1999).

The three genes that affect hindlimb morphogenesis are *Tbx4, Pitx1* and *Pitx2*. *Tbx5* is an analogous Tbox gene that operates in the forelimb but *Tbx4* and *Tbx5* have been shown to be mutually exclusive (Logan and Tabin, 1999). *Pitx1* and *Pitx2* both function upstream of *Tbx4*, the hindlimb specific t-box gene. Murine and chick models have shown that *Pitx1* genes affect only hindlimb development (Logan and Tabin, 1999; Marcil *et al.* 2003). In murine models, when the *Pitx1* gene was knocked out, the hindlimb started to resemble the forelimb in terms of shape, particularly in the zeugopod. They had a stylopod that was considerably shortened, but which retained its basic shape (Szeto *et al.,* 1999). *Pitx1* and *Pitx2* knockout mice failed to even generate a hindlimb bud. In knockout experiments with the *Tbx* genes using murine models, *Tbx5 -/-* resulted in no forelimb buds, whereas *Tbx4 -/-* mice retained their hindlimb buds. Thus, it has been hypothesized that *Pitx1* and *Pitx2* function in hindlimb outgrowth, whereas *Tbx4* functions more for hindlimb shape. On the other hand, in the forelimb *Tbx5* is necessarily for basic outgrowth (Marcil *et al.* 2003; Minguillon *et al.*, 2005).

Considering the number of integrated genes in the hindlimb, we might actually expect stronger integration *within* the hindlimb than between the forelimb and hindlimb since *Pitx1, Pitx2* and *Tbx4* function in the development of the entire limb. A rough analysis with this data on proximodistal femoral integration yielded higher RV coefficients than fore-/hindlimb pairs for all taxa, particularly in *Homo* (table 5.6). Perhaps fore-/hindlimb morpohological evolution is not necessarily constrained by their common developmental pathway, but shape within the hindlimb could be constrained by development. More research would need to be done to definitively support this hypothesis.

Table 5.6 Percent covariance on the first common axis and RV coefficient for the proximal and distal femur.

	Prox Femur/Distal Femur	
	%cov	***RV***
Gorilla gorilla	42.34%	0.2800
Homo sapiens	73.55%	0.3602
Pan troglodytes	40.70%	0.2011

Fore- and hindlimb shape are not strongly evolutionarily integrated either, but since there are different genes that pattern the shape of the hindlimb, it should be possible for selection to act separately on it. Young *et al.* (2010) found a similar result when they looked at developmental integration in catarrhine limb lengths. They found evidence of independent selection in the limbs with lengthening of the hindlimb being selected for before modifications to the structure of the forelimb.

As humans became bipedal, selection would have been acting more strongly to modify hindlimb shape than to modify forelimb shape. In fact, many researchers have noted that the human forelimb is not far derived from the other large-bodied hominoids, and the changes in the human forelimb would have been selected for more recently possible maximize forelimb use as the hands were liberated from locomotor uses (Aiello and Dean, 1990; Rose, 1993; Young *et al.* 2010). Much of the data presented in chapter three showed a high degree of overlap in the forelimb shape of the extant taxa, particularly in the proximal humerus, proximal radius and distal radius.

The forelimb areas that differ most in terms of shape for the extant hominoids are the proximal ulna and distal humerus (Chapter 3). Those areas, as well as the proximal and distal femur, had the highest degree of covariance and correlation along the first and second axes. This could be due to a bias in data collecting. The proximal and distal humerus, the proximal ulna and the proximal and distal femur are all relatively complex joints with many type II landmarks, as opposed to the proximal radius and humerus which are relatively simple joints. It is possible that laser surface scanning would result in better data for examining these joints as it would capture the shape of the entire surface with millions of triangles (Harcourt-Smith *et al.*, 2008) as opposed to four to six points. On the other hand, there are many functionally important traits in

these regions that relate directly to specific shapes (*e.g.,* the orientation of the capitulum in the humerus for stability in the great apes as opposed to for dexterity in humans or the positioning of the greater trochanter to maximize the efficiency of the gluteus medius in *Homo*; see Chapters 3 and 4 for more functional examples; Aiello and Dean, 1990). Perhaps selection is stronger on these regions because they are more complex and are formed for specific movements.

ER 1503/1504, Omo (Kibish) 1 and WT 15000 all had a basically human pattern for fore- and hindlimb co-variation. AL 288 was also human-like in all elements in all analyses except for the distal femur. ER 1500 had a human-like proximal ulna with an ape-like distal femur. Omo (Kibish) 1 is a modern *Homo sapiens* (Brown and Fuller, 2008) and WT 15000 is reconstructed to have modern human limb proportions (Ruff and Walker, 1993); and thus a modern human pattern of co-variation in the fore- and hindlimb is expected for both of these specimens. The other three specimens are more interesting to consider.

AL 288 has consistently been found to have more ape-like limb proportions than seen in later hominins (Jungers, 1982), and ER 1500 and ER 1503/1504 have been reconstructed to have intermediate body proportions similar to AL 288 (McHenry, 1978; Grausz *et al.* 1988). Typically, the more ape-like body proportions of these individuals have been interpreted to mean that they practiced a less efficient form of bipedal locomotion (Berge, 1994) and (when interpreted in the light of other characteristics) maintained other adaptations for arboreality (Stern and Susman, 1983, but see Lovejoy, 1988). The data presented in this chapter (and in previous chapters in this dissertation) generally support those conclusions. AL 288 had a largely human-like elbow paired with an ape-like wrist and knee and ER 1500 had a human-like proximal ulna with an ape-like distal femur. The similarity between the conclusions of limb proportion studies and conclusions here lend support to the idea that comparison of fore-

/hindlimb covariance could be used as a tool to bypass the necessity of estimating limb proportions in considering overall locomotor function.

ER 1503/1504 is of particular interest as in previous analyses (in Chapter 3) it grouped with the apes for some features of the distal humerus whereas in this analysis, it grouped with modern humans. The features of the distal humerus that were most important in separating *Homo* from *Pongo, Pan* and *Gorilla* in principal components analyses were the asymmetrical trochlea and the more anteriorly oriented capitulum. In the 2B-PLS analysis, the traits in the distal humerus that covaried most strongly with the proximal femur were height of the medial and lateral epicondyles, the symmetry of the trochlea and the shape of the anterior-proximal trochlear border. The forelimb and hindlimb were not found to be developmentally integrated in shape, so selection would not be constrained by any common developmental pathway.

All of the fossils tended towards having a human-like morphology overall. It is possible that earlier specimens, particularly the newly published skeleton of *Ardipithecus ramidus,* would yield more ape-like results especially if it truly was a more generalized quadruped (Lovejoy *et al.* 2009). We would expect overall integration to be higher in taxa where the forelimb and the hindlimbs are used equivalently (Young *et al.* 2010).

When taken as a whole, these results tentatively indicate that selection towards a human-like pattern for fore- and hindlimb co-variation (at least for these elements) had already taken place by the appearance of *Australopithecus afarensis,* with the distal femur lagging behind the other elements. This would mean selection away from the forelimb as a supporting limb and a more flexible, arboreal hindlimb towards a more stable hindlimb and a forelimb liberated from the constraints of locomotion. However, considering the proximodistal co-variation in the femur, this does not indicate that (contra Lovejoy, 1988) these individuals were all perfect,

human-like bipeds; just that the overall pattern of covariance was generally more human-like than ape-like when taken as a whole.

Conclusions

In summary, while there is very little evidence for developmental shape integration in the fore- and hindlimb, there is more evidence for shape covariation in mixed species samples of fore- and hindlimb elements. The lack of developmental integration could be the result of selection on the genes that specifically act to pattern hindlimb shape, like *Pitx1, Pitx2* and *Tbx4,* and it is possible that there is more developmental integration within the hindlimb than between the fore- and hindlimb. The more complex joints had a higher degree of covariation mixed species samples than the less complex joints, which could be an artifact of the way that the data were collected, but could also reflect real functional changes in these anatomical regions. Finally, the fossils all had patterns of co-variation that most closely matched *Homo*, tentatively indicating that by the appearance of *Australopithecus afarensis,* a more modern human-like division of use could already have been in place for the fore- and hindlimb.

CHAPTER 6: CONCLUSIONS

The data and analyses presented in chapters 3, 4 and 5 were aimed towards answering the three broad research goals stated in the introductory chapter. This chapter revisits the initial research questions and represents a synthesis of the information from the forelimb, the hindlimb, and covariation chapters in an attempt to answer those questions.

Are there postcranial traits that are characteristic of specific Plio-Pleistocene hominin groups?

Previous studies have indicated that there are quantifiable gross differences in postcranial morphology, at least between early specimens (*i.e., A. afarensis*) and late specimens (*i.e., H. erectus sensu lato*). The majority of these studies have been carried out using traditional linear methods to quantify morphology. This dissertation investigated the resolution at which differences could be detected within the fossil record by using three-dimensional geometric morphometrics to quantify overall shape of the humerus, radius, ulna, femur and tibia.

In considering this question, the first challenge is designating groups. In paleoanthropology, species are defined primarily on the basis of cranial morphology. One of the biggest difficulties in assigning Plio-Pleistocene postcrania to a particular taxon is the lack of agreement about the number of taxa present in the fossil record based on cranial remains. Currently there are four species widely recognized as members of the genus *Australopithecus: A. anamensis, A. afarensis, A. garhi* and *A. africanus,* but this is not without controversy. Some authors suggest that there are multiple species within the sample of *A. afarensis* from Hadar (Senut and Tardieu, 1985; Hausler and Schmid, 1995) whereas others see it as one sexually

dimorphic species (White, 1985; McHenry, 1992; Harmon, 2008). It has also been recently suggested that, based only on proximal femora, the sample of *A. africanus* from South Africa contains at least two species that differ in terms of shape but not size (Harmon, 2009). Grine *et al.* (1996) also argued, based on cranial remains, that there was an additional as yet unnamed species present in South Africa represented by Stw 53. The genus *Homo* is even more controversial with some people recognizing four taxa in the Plio-Pleistocene – *Homo habilis, Homo rudolfensis, Homo ergaster* and *Homo erectus* (*e.g.* Wood, 1992) – and some accepting only two – *Homo habilis* and *Homo erectus* (*e.g.* Tobias, 1991). Those who consider *Homo habilis* and *Homo rudolfensis* two separate taxa do so based on tooth size and endocranial volume with *H. rudolfensis* being the larger, more *Homo sapiens*-like species and *H. habilis* being the smaller species (Wood, 1985 *et seq.*).

New fossil finds continue to complicate matters of hominin taxonomy. The last ten years have added *Kenyanthropus platyops* (Leakey *et al.,* 2001), and *Australopithecus sediba* (Berger *et al.,* 2010) to the hominin tree, as well as the extensive analysis of *Ardipithecus ramidus* (Lovejoy *et al.,* 2009; White *et al.,* 2009) to our consideration of human evolution in Africa during the Plio-Pleistocene.

The second challenge is matching the postcranial fossils to their appropriate taxon. Of all the species that have been named from the Plio-Pleistocene, few include cranially-associated postcranial material within their hypodigm. For some taxa the lack of multiple sympatric species can allow us to associate postcranial remains with cranial remains to a reasonable degree of certainty. For *Australopithecus anamensis,* we can be relatively sure that the postcranial material from Kanapoi and Sibilot Hill belongs to the same taxon as the cranial material as that is the only taxon present (Ward *et al.* 2001). In South Africa, we assume that much of the postcranial

material from Swartkrans can be assigned to *Paranthropus robustus* because the overwhelming majority of cranial material is from that taxon and that most of the postcranial material from Sterkfontein Member 4 can be assigned to *A. africanus* for the same reason (Robinson, 1972).

For all other taxa, it is necessary to rely on similarity between associated and unassociated elements in order to make taxonomic conclusions. AL 288 (Johanson *et al.* 1978) was used as a model for *Australopithecus afarensis,* Stw 431 (Partridge *et al.* 2003) was used for *Australopithecus africanus,* TM 1517 (Thackeray *et al.* 2002) was used for *Paranthropus robustus,* OH 62 and ER 3735 (Feibel *et al.* 1989; Wood, 1991) were used for *Homo habilis,* ER 1500 (Grausz *et al,* 1988, but see Wood 1991) was used for *Paranthropus boisei* and WT 15000 (Walker and Leakey, 1993) was used as the model for *Homo erectus sensu lato*. Any conclusions about the postcrania of *Homo rudolfensis* are purely speculative as there are no postcranial remains for this taxon, and reconstructions of a more "advanced" body form for *Homo rudolfensis* are based on having a larger brain size. Thus, for the purposes of this analysis, all postcrania that could be either *H. habilis* or *H. rudolfensis* were treated as *Homo habilis sensu lato.*

Overall, there are few specific postcranial characters that can be definitively tied to one Plio-Pleistocene hominin group. *Paranthropus robustus* had a unique pattern for the distal humerus (TM 1517) and a distinct pattern for the proximal femur (SK 82 and SK 97). In the distal humerus, *Paranthropus robustus* was characterized by a flattened capitulum and a distally flexed medial epicondyle. For the proximal femur, it was characterized by an extremely ape-like greater trochanter paired with an overall femoral form that was broadly *Homo*-like. Their greater trochanter is less laterally projecting and has a more laterally placed maximum height than modern *Homo sapiens*. The distal radius (SKX 3602) is very similar to *Australopithecus*

afarensis (AL 288) except that it has a higher proximal-posterior corner of the ulnar facet than all of the other fossils. The proximal ulna of *P. robustus* (SKX 8761) is no different from the rest of the hominin fossil sample. These traits could be used to link new fossils to *P. robustus.*

Homo habilis sensu lato may also have some unique postcranial characters, although it is difficult to discern which bones should be attributed to this taxon. Using ER 3735 as the reference standard, the humeri ER 739, ER 1504 and possibly ER 6020 could tentatively be assigned to this taxon. *Homo habilis s. l.* would then be characterized by a very symmetrical trochlea and more distally oriented capitulum. OH 62, also attributed to *Homo habilis s. l.,* had the only non-*Homo* pattern for the proximal ulna in that it had a large coronoid process and keeled trochlear surface. These traits from the forelimb could be used to identify this taxon.

There were no hindlimb bones that could be definitively tied to *Homo habilis s. l.* that had a distinct morphological pattern. However, if ER 1500 were *Homo habilis s. l.* and not *Paranthropus boisei* (as proposed by Wood, 1991), then an argument could be made that *Homo habilis s. l.* also had a unique shape for the distal tibia in that it has square overall dimensions with a longer anterior border than that seen in modern *Homo sapiens* as well as a more distinct shape for the proximal radius that maximized flexion ability by having a distally placed radial tuberosity.

For the rest of the fossil taxa, while there didn't seem to be any unique characters, there could be unique patterns of variation when all of the postcranial elements are considered. BC 1745 (Wood, 1999), ER 20419, KP 271 and KP 29285 (Ward, 2001) are all assigned to *Australopithecus anamensis* and represent a proximal and distal humerus, radius and tibia. Based on these fossils, *A. anamensis* was characterized by a distal humerus with a human-like overall shape but with a slightly different trochlea in that the lateral side of it does not extend as

far distally as the medial side. The proximal humerus may have been adapted for more stability at the shoulder joint, but those data are somewhat suspect. It had an unremarkable proximal radius paired with an extremely ape-like distal radius in that it is narrow and mediolaterally flexed and has a more medially rotated ulnar facet. The proximal tibia was uninformative, but the distal tibia had a form that is more human-like than ape-like, although also most distant from the human centroid. Ultimately, all of this points to a taxon that was not very different from modern humans, except possibly in the wrist joint. This indicates that bipedalism was probably the most important positional behavior in its locomotor repertoire.

MAK-VP-1/1 and all of the material from Hadar save AL 333-3/AL 333-4 are assigned to the taxon *Australopithecus afarensis.* For the purposes of this analysis, AL 333-3/4 was tentatively removed from this taxon as it has a more ape-like shape in the proximal femur than the rest of the specimens in the sample. Based on these fossils, *A. afarensis* had a very human-like distal humerus and proximal ulna, combined with a more ape-like distal radius. The distal ulna was possibly also more ape-like, although in that analysis AL 288 and the other two *A. afarensis* did not form a cohesive group. In the hindlimb, it had a human-like proximal femur and distal tibia in combination with a more ape-like distal femur. This morphological pattern contrasts with *A. anamensis* in that it lacks most of the more pleisomorphic traits present in that taxon.

A. africanus was characterized by having a very human-like forelimb, with a distal humerus and proximal ulna that were more similar to modern *Homo sapiens* coupled with a more pleisomorphic distal femur. Assuming that both Stw 99 and Sts 14 are in this taxon, then it had a variable proximal femur, tending towards being more human-like than ape-like. If Stw 99 represents a different taxon (as suggested by Harmon, 2009) then *A. africanus* could be

interpreted to have had a very human-like proximal femur based on Sts 14. All but Stw 181 had a distal tibia with human-like morphology. Overall, this pattern of morphology is similar to very *A. afarensis,* especially if Stw 99 is omitted.

WT 15000 is an associated *H. erectus* skeleton. Other postcranial elements that are likely attributable to *Homo erectus* are: BOU-VP-19/63, ER 1481, SKX 2045, SKX 24600/24601, SK 18b, and SK 1896. It is possible that there are more *H. erectus* elements within the sample from Koobi Fora, but the data do not support any definitive taxonomic conclusions. Those postcranial elements that are likely *Homo erectus* indicate that it had a fully bipedal pattern, virtually indistinguishable from that of *Homo sapiens.* The distal femur of BOU-VP-19/63 is interesting as it could represent evidence of postcranial variation matching the cranial variation in the *H. erectus* hypodigm (see fig. 6.1 for a summary).

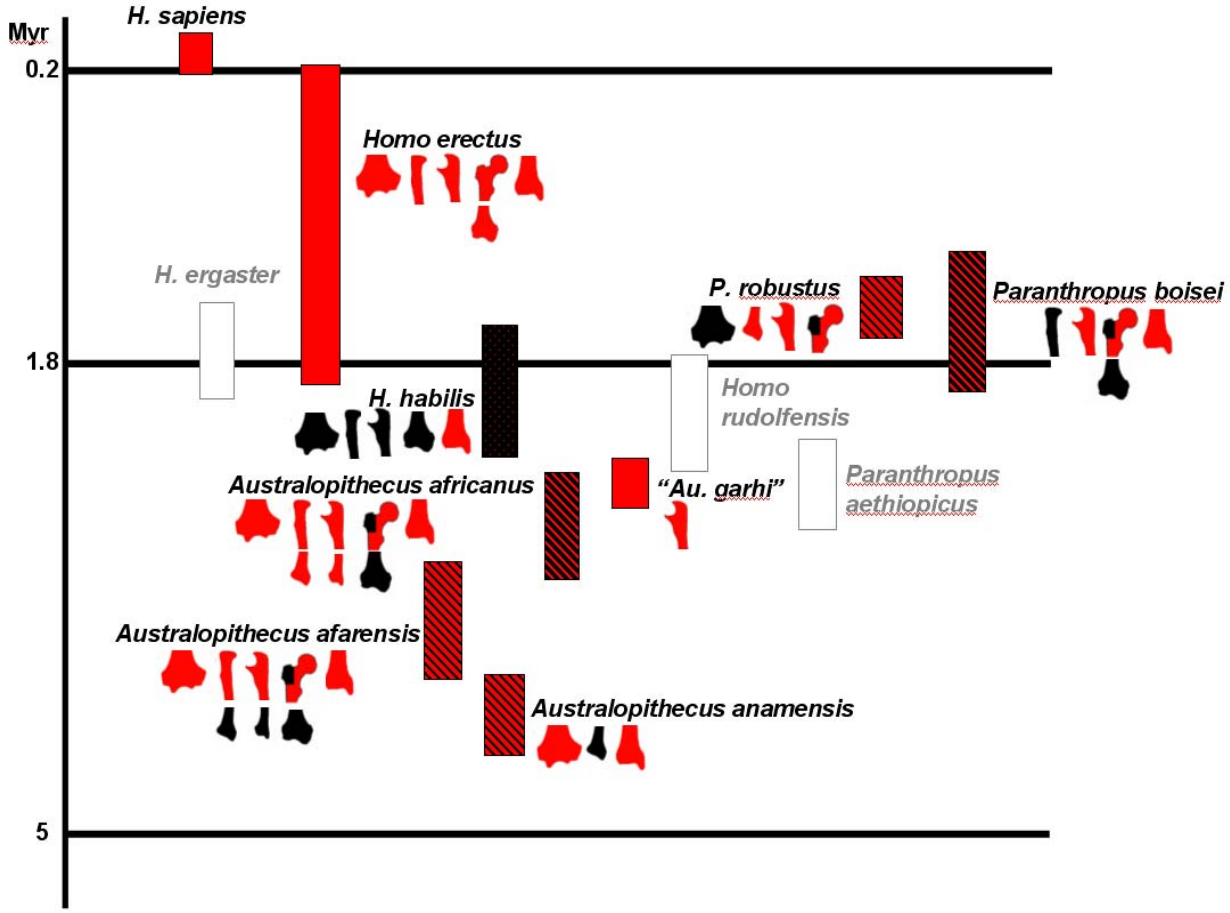

Fig. 6.1 Pictorial representation of hominin species ranges derived from Wood (1991). Bones and blocks shaded in red indicate that for that species, the majority of the fossils followed a human-like pattern and bones shaded in black indicate an ape-like pattern. Blocks with red and black diagonal lines indicate an overall mosaic morphological pattern. *H. ergaster* and *H. rudolfensis* are shown to indicate temporal ranges based on cranial elements, but postcranially they are not distinguished here from *H. erectus* and *H. habilis*. No postcrania can yet be associated with *P. aethiopicus.*

What do postcranial remains imply about the locomotor repertoires of Plio-Pleistocene hominins? Are there different locomotor types?

Many previous studies have concentrated on a careful analysis of single postcranial elements. The next step in considering postcrania was to incorporate these data into analyses that took into account the ways that the bones of the postcranium work together during locomotion. This dissertation examined patterns of covariation in fore- and hind-limb morphology and within joint complexes as a method for evaluating the degree of mosaicism

present in the hominin fossil record.

Overall, when multiple bones of the postcranium were included in a single analysis, a somewhat different picture emerged. In the humero-radial joint, none of the fossils had a clear *Homo*-like pattern for either the humerus or the radius with all individuals falling within the equal frequency ellipses of extant great apes and many falling outside the range of human variation all together. On the other hand, in the humero-ulnar joint, most of the fossils had a modern human like pattern of covariance. This may indicate that selection was operating more strongly on the humero-ulnar joint, favoring morphology that allowed the muscles to be at their greatest advantage in flexed forelimb posture while retaining a more ape-like ability to pronate and supinate with the humero-radial joint.

In the lower limb, *H. sapiens* had a distinct pattern of hip to knee joint covariation compared to the apes. The proximal and distal segments were GPAed separately so the unique pattern in *H. sapiens* is the result of shape differences in the proximal and distal ends and not the presence of the bicondylar angle. For the femur, *H. erectus* (WT 15000 and ER 1481) had a fully human-like pattern and *A. afarensis* had an ape-like pattern in all analyses. ER 1472 (possible *H. habilis s.l.*) had a pattern intermediate between modern humans and the apes, although it was more similar to the apes when just the greater trochanter was used to represent the proximal femur.

In examining forelimb to hindlimb covariation, most of the fossils had a human-like pattern of covariation, except in pairs that involved the distal femur. The features of the distal femur that were important in separating humans from the other apes were the shape of the patellar articular surface (particularly the symmetry – or asymmetry – of the proximal border and the strong lateral projection of the surface), the comparative size of the medial and lateral

condyles, the angle between the patellar surface and the distal surface, and the width of the intercondylar notch. Particularly, AL 288/129-1b and ER 1500 both had the ape-like pattern for the distal femur combined with the human-like pattern for the rest of the comparisons. This result indicates that selection for a modern human-like knee would have occurred after selection towards a human elbow and hip joint. These results also indicate that by the emergence of *Australopithecus afarensis*, there had already been a fundamental change in forelimb to hindlimb covariation in the hominin lineage from a pattern where the forelimbs were actively used in locomotion towards one where forelimb use was divorced from hindlimb use. This is not to say that all hominins had a perfectly human-like pattern of locomotion; the fossils that were sampled for those analyses did not encompass all Plio-Pleistocene taxa. In particular, there were no definitive *H. habilis s. l.* in the analysis (OH 62, ER 3735) and no *A. africanus.* The ape-like nature of the forelimb of OH 62, the ulna in particular, would suggest that it may have had a different pattern from the rest of the fossils.

What does the pattern of morphology in postcranial remains say about the patterning of the evolution of bipedality?

Modern bipedalism is ultimately derived from the locomotor pattern of the last common ancestor. Thus far, there are two fossils taxa with postcranial remains that have been purported to represent that locomotor pattern: *Orrorin tugenensis* and *Ardipithecus ramidus. Orrorin's* estimated age of 6 Ma places it close to the divergence of *Pan* and *Homo* (Pickford *et al.* 2002; Senut *et al.* 2002). The proximal femur from *Orrorin* has been found to look very similar to *Australopithecus* and *Paranthropus* proximal femora (Richmond and Jungers, 2008) and the distal pollical phalanx has recently been suggested to most closely resemble modern humans and

indicate precision grasping capability (Almécija *et al.*, 2010). On the other hand, *Ardipithecus ramidus* has been reconstructed to have a *Proconsul*-like body plan that is completely unlike any extant or known fossil hominin (Lovejoy *et al.* 2009).

Considering the relatively modern morphology present in the earliest fossil australopiths (see fig. 6.1), it is probably more likely that the last common ancestor had a more derived body plan than the quadrupedal *Ardipithecus ramidus,* more similar to *Orrorin* or some other as-yet undiscovered Miocene ape. I would propose that the locomotion of the last common ancestor could have been some kind of facultative biped that frequently used its arms in more flexed forearm positions. The more proximally located olecranon in all of the earliest hominins would have put the triceps brachii at is greatest mechanical advantage in flexed fore-arm positions (Drapeau, 2004). Having a strong mechanical advantage in flexed forearm postures could be advantageous for various forms of manipulative ability – perhaps manipulating natural resources and/or doing some kind of precise extractive feeding. The dominant mode of locomotion for such an organism could be vertical climbing as some studies have suggested that the musculature of the hip and thigh in vertically climbing primates could be transformed into bipedal musculature with minimal changes (Stern, 1975; Prout, 1980; Schmitt, 2003). Additionally, there are other Miocene apes, such as *Nacholapithecus* and *Pierolapithecus,* that have clear adaptations for orthograde posture necessary for vertical climbing without additional adaptations for suspension (Nakatsukasa *et al.,* 2003, Moyà-Solà *et al.* 2004, Almécija *et al.* 2009).

If the earliest fossil hominins were largely human-like, then *Paranthropus* and particularly *Homo habilis sensu lato* seem to represent morphological reversals in the fossil record. While *Paranthropus* had a more ape-like than human-like morphology, in many ways they are simply unique. Perhaps the unique nature of their cranial morphology is matched by

unique, derived characteristics present also in their postcranial morphology, particularly in the shape of the distal humerus and proximal femur. *Homo habilis sensu lato* (as represented by OH 62 and ER 3735) has overall the most ape-like morphology of all of the early hominins, which really does seem like a "reversal" when considering earlier fossil hominins. It is worth considering that in both cases, the "reversals" appear in places where there are a number of competing sympatric hominins – perhaps the "reversals" (or in the case of *Paranthropus,* unique adaptations) to a more ape-like form have to do with hominins trying to exploit different niches in the same environment.

Future Research

Shape covariation is an excellent tool for examining questions about locomotor repertoires. In the future, I plan to extend this methodology to primates with fore- and hindlimbs that have been shown to be functionally more integrated, such as Old World monkeys (Young *et al.* 2010) and very early hominoids. I suspect that there may be greater shape integration in taxa where the forelimbs and the hindlimbs are used in functionally similar ways. While in Nairobi, I have collected data on the nearly complete skeleton of *Proconsul africanus* (RU 2036) that could be included in such analyses. This type of data could inform us on trends in locomotor evolution from a more monkey-like pattern of locomotion to a hominoid pattern of locomotion.

Also, the phylogenetic position of many Plio-Pleistocene hominins is enigmatic, and there has been considerable debate in the literature about where to place certain taxa and/or specimens. In the future, these data could be used to try and reconstruct hominin trees that could be compared with the craniodental trees. Additionally, it could be combined with craniodental data, and "supertrees" based on characters across the entire skeleton could be built. This could

be advantageous as many phylogenetic studies based on skeletal materal rely on discrete anatomical areas. This is not directly comparable to large, genome-based studies that include genes that control many different functions. The present analysis is a step in this direction.

REFERENCES

Adams, D.C., F.J. Rohlf, and D.E. Slice. (2004). Geometric morphometrics: ten years following the "revolution". *Italian Journal of Zoology*, 71: 5-16.

Aiello, L. and C. Dean (1990) *An Introduction to Human Evolutionary Anatomy* London: Academic Press Ltd.

Aiello, L., B. Wood, C. Key and M. Lewis (1999) Morphological and taxonomic affinities of the Olduvai ulna (OH 36). *Am J Phys Anth* 109:89-110.

Almécija, S., D.M. Alba and S. Moyà-Solà (2009) Pierolapithecus and the functional morphology of Miocene ape hand phalanges: paleobiological and evolutionary implications. *J Hum Evol* 57: 284-297.

Almécija, S., S. Moyà-Solà and D. M. Alba (2010). Early origin for human-like precision grasping: a comparative study of pollical distal phalanges in fossil hominins *PLoS One* 5: 1-10.

Amaral, L. Q. (2008) Mechanical analysis of infant carrying in hominoids. *Naturwissenschaften* 95: 281-292.

Amaral, L.Q. (1989) Early hominid physical evolution. *Hum Evol* 4: 33-44.

Anderson, J. Y. and E. Trinkaus (1998) Patterns of sexual, bilateral and interpopulational variation in human femoral neck-shaft angles *J. Anat* 192: 279-285

Asfaw, B., W.H. Gilbert, Y. Beyene, W.K. Hart, P.R. Rennek, G. Wolde-Gabriel, W.S. Vrba, and T.D. White. (2002) Remains of *Homo erectus* from Bouri, Middle Awash, Ethiopia. *Nature* 416, 317-320

Asfaw, B., T. White, O. Lovejoy, B. Latimer, S. Simpson, and G. Suwa. (1999). *Australopithecus garhi:* a new species of early hominid from Ethiopia. *Science*, 284: 629-635.

Baab, K.L. (2008) The taxonomic implications of cranial shape variation in *Homo erectus. J Hum Evol.* 54: 827-847.

Bachrach L.K, T. Hastie, W. Wang, B. Narasimhan, R. Marcus.(1999). Bone mineral acquisition in healthy Asian, Hispanic, Black and Caucasian youth: a longitudinal study. *Journal of Clinical Endocrinology and Metabolism,* 84:4702-4712.

Baker SJ, Gill GW, Keiffer DA. 1990. Race and sex determination from the intercondylar notch of the distal femur. In: *Skeletal Attribution of Race*, ed. GW Gill and S Rhine. Albuquerque: Maxwell Museum of Anthropology. Pp 91-95.

Beard, K.C., M. Dagosto, D.L. Gebo, and M. Godinot. (1988). Interrelationships among higher primate taxa. *Nature*, 331: 712-714

Begun, DR (2003) Knuckle-walking and the original of human bipedalism. In *From Biped to Strider* eds. D.J. Meldrum and C.E. Hilton. New York: Kluwer.

Begun D.R., B.G. Richmond and D.S. Strait. (2007) Comment on "Origin of Human Bipedalism as an Adaptation for Locomotion on Flexible Branches. *Science* 318: 1066.

Berge, C. (1994) How did the australopithecines walk? A biomechanical study of the hip and thigh of *Australopithecus afarensis. J Hum Evol* 26: 259-273

Berger, L.R., D.J. de Ruiter, S.E. Churchill, P. Schmid, K.J. Carlson, P.G.H.M. Dirks, and J.M. Kibii (2010). *Australopithecus sediba*: a new species of *Homo*-like Australopith from South Africa. *Science,* 328:195–204.

Bingham, P.M. (1999) Human uniqueness: a general theory. *Quart Rev Biol* 74: 133-169.

Blumenschine R.J., C.R. Peters, F.T. Masao, R.J. Clarke, and A.L. Deino (2003) Late Pliocene Homo and hominid land use from western Olduvai Gorge, Tanzania. *Science* 299: 1217-1221

Bramble, D.M. and D. E. Lieberman. (2004) Endurance running and the evolution of *Homo. Nature* 432: 345-352

Brown, F.H. (2000) Turkana Basin. In *Encyclopedia of Human Evolution and Prehistory* (E. Delson, I. Tattersall, J.A. van Covering and A. Brooks, Eds.) New York: Garland Publishing Inc. pp711-714.

Brown, F.H., and C.R. Fuller (2008). Stratigraphy and tephra of the Kibish Formation, southwestern Ethiopia. *J. Hum. Evol.,*

Brown, F.H., J. Harris, R. Leakey and A. Walker. (1985) Early *Homo erectus* from west Lake Turkana. *Nature* 316: 788-792.

Cartmill, M. (1981). Hypothesis testing and phylogenetic reconstruction. *Zeitschrift für zoologische Systematik und Evolutionsforschung* 19: 73-96.

Cartmill, M. and K. Milton. (1977) The lorisiform wrist joint and the evolution of "brachiating" adaptation in the Hominoidea. *Am J Phys Anth* 47: 249-272

Cheverud, J.M. (1996) Developmental integration and the evolution of pliotropy. *Amer Zool.* 36:44-50.

Clarke, R.J. (1998). First ever discovery of a well-preserved skull and associated skeleton of *Australopithecus*. *South African Journal of Science*, 94:460-4.

Clark, R.J. and P.V. Tobias. (1995). Sterkfontein member 2 foot bones of the oldest South African hominid. *Science,* 269: 521-524.

Coppens, Y. (2004). The hominids of Melka Kunture. Some general reflections. In *Studies of the Early Paleolithic site of Melka Kunture, Ethiopia* eds. J. Chavaillon and M. Piperno. Florence: Istituto Italiano di Preistoria e Protostoria. pp 685-686

Corruccini, R.S. and H.M. McHenry (2001) Knuckle-walking hominid ancestors. *J Hum Evol* 40:507-511

Corti, M., and C. Fadda. (1996) Systematics of *Arvicanthis* (Rodentia, Muridae) from the Horn of Africa: a geometric morphometrics evaluation. *Ital. J. Zool.* 63:185–192.

Crompton, R.H. and S.K.S. Thorpe (2007) Response to Comment on "Origin of Human Bipedalism As an Adaption for Locomotion on Flexible Branches" *Science* 318: 1066

Crompton, R.H., L. Yu, W-J. Wang, M.M. Gunther and R. Savage (1998) The mechanical effectiveness of erect and "bent-hip, bent knee" bipedal walking in *Australopithecus afarensis. J. Hum Evol* 35: 55-74.

Dainton, M. and GA Macho (1999). Did knuckle-walking evolve twice? *J Hum Evol.* 36: 171-194

Darwin, C. (1871) *The Descent of Man and Selection in Relation to Sex.* London: John Murray, Albemarle Street.

Davis, P.R. (1965) Hominid Fossils from Bed I, Olduvai Gorge, Tanganyika. *Nature,* 201: 967-970

Day, M.H. and T. I. Molleson (1976) The Puzzle from JK2-A Femur and a Tibial Fragment (O.H. 34) from Olduvai Gorge, Tanzania *J Hum Evol* 5:455-465

Degusta D.A. (2004) *Pliocene Hominid Postcranial Fossils from the Middle Awash, Ethiopa*. University of California, Berkeley. Ph.D. Dissertation.

Deloison, Y. (2003). The origin of hominoid locomotion. In *From Biped to Strider* eds. D.J. Meldrum and C.E. Hilton. New York: Kluwer.

DeMenocal, P. (2004) African climate change and faunal evolution during the Pliocene–Pleistocene *Earth and Planetary Science* 220: 3-24.

de Ruiter, D.J. (2001). On the taxonomic status of the Swartkrans humerus, SK860. *Annals of the Transvaal Museum* 38: 71-72.

Delson, E., J.A. van Couvering, and A. Hill. (2000) Baringo Basin/Tugen Hills. In *Encyclopedia of Human Evolution and Prehistory* (E. Delson, I. Tattersall, J.A. van Covering and A. Brooks, Eds.) New York: Garland Publishing Inc. pp127-130.

Delson, E. (1988) Chronology of South African Australopiths site units. In: Grine FE, editor. *Evolutionary history of the robust Australopithecines.* New York: Aldine de Gruyter. pp 317–325.

DeSilva, J.M. (2008) *Vertical Climbing in Anthropoid Ankle and Midfoot: Implications for Locomotion in Miocene Catarrhines and Plio-Pleistocene Hominins*. University of Michigan. Ph.D. Dissertation.

DeSilva, J. (2009) Functional morphology of the ankle and the likelihood of climbing in early hominins. *Proc. Nat. Acad. Sci.* 106: 6567-6572

DeSilva, J.M., B. Zipfel, A. P. Van Arsdalec and M. W. Tocheri (in press) The Olduvai Hominid 8 foot: Adult or subadult? *J Hum Evol.*

Dobson, S.D. (2005) Are the differences between Stw 431 (*A. africanus*) and AL 288 (*A. afarensis*) significant? *J Hum Evol* 49: 143-154.

Drapeau, M.S.M. (2004) Functional anatomy of the olecranon process in Hominoids and Plio-Pleistocene Hominins. *Am J Phys Anth* 124: 297-314.

Drapeau, M.S.M. (2008) Articular morphology of the proximal ulna in extant and fossil hominoids and hominins. *J Hum Evol,* 55:86-102.

Drapeau, M.S.M., C.V. Ward, W.H. Kimbel, D.C. Johanson and Y. Rak (2005) Associated cranial and forelimb remains attributed to *Australopithecus afarensis* from Hadar, Ethiopia. *J. Hum Evol* 48: 593-642.

Dugan, J. and T.W. Holliday (2009) Utility of the lateral meniscal notch in distinguishing hominin taxa. *J Hum Evol.* 57:773-776.

Dunsworth, H., J. H. Challis and A. Walker. (2003) Throwing and bipedalism: a new look at an old idea. *Cour Forch Inst. Senckenberg.* 243: 105-110.

Eckhardt B.A. (2000) *Human Paleobiology.* Cambridge: Cambridge University Press.

Endicott, P., M. Thomas, P. Gilbert, C. String, C. Lalueza-Fox, E. Willerselv, A J. Hansen and A. Cooper. (2003) The Genetic Origins of the Andaman Islanders *Am J Hum Genet.* 72(1): 178–184.

Escoufier, Y. (1973). Le traitement des variables vectorielles. *Biometrics*, 29: 751–760.

Fajardo, R.J. and R. Muller. (2001). Three-dimensional analysis of nonhuman primate trabecular architecture usuing micro-computer tomography. *Am J Phys Anthropol.* 115, 827-836.

Feldesman, M.R. (1979). Further morphometric studies of the ulna from the Omo Basin, Ethiopia. *Am J Phys Anth* 51: 409-416.

Feibel, C.S., F.H. Brown and I. McDougall. (1989). Stratigraphic Context of Fossil Hominids From the Omo Group Deposits: Northern Turkana Basin, Kenya and Ethiopia *Am J Phys Anth* 78: 595-622

Fifer, F.C. (1987) The adoption of bipedalism by the hominids: a new hypothesis. *Hum Evol*, 2: 135-147.

Fleagle J.G. 1999. *Primate Adaptation and Evolution*. Academic Press: San Diego.

Frost S.R., L.F. Marcus, D. Reddy, F. Bookstein and E. Delson (2003). Cranial allometry, phylogeography and systematics of large bodied papionins (Primates: Cercopithecinae) inferred from geometric morphometric analysis of landmark data. *Anatomical Record* 275A: 1048-1072.

Gebo, D.L. (1996) Climbing, brachiation and terrestrial quadrupedalism: historical precursors of hominid bipedalism. *Am J Phys Anth* 101:55-92.

Gebo, D.L., Dagosto, M., Beard, K.C., Qi, T. (2001). Middle Eocene primate tarsals from China: implications for Haplorhine evolution. *Am. J. Phys Anthropol.* 116: 83-107

Gilbert, W.H. (2009) Daka member postcranial remains. In *Homo erectus Pleistocene Evidence from the Middle Awash, Ethiopia* (Eds. B. Asfaw and W.H. Gilbert). Berkeley: University of California Press. pp373-397.

Gill GW. (2001). Racial variation in the proximal and distal femur: heritability and forensic utility. *J. Forensic Sci.* 46:791-799.

Grausz, H.M., R.E.F.Leakey, A.C. Walker, and C.V. Ward. (1988). Associated cranial and postcranial bones of *Australopithecus boisei*. In *Evolutionary History of the Robust Australopithecines*, ed. F.E. Grine. New York: Aldine de Ruyter. Pp. 127-132.

Green D.J., A.D. Gordon and B.G. Richmond. (2007) Limb-size proportions in *Australopithecus afarensis* and *Australopithecus africanus. J Hum Evol* 52:187-200.

Grine, F.E. (2000) Sterkfonetin. In *Encyclopedia of Human Evolution and Prehistory* (E. Delson, I. Tattersall, J.A. van Covering and A. Brooks, Eds.) New York: Garland Publishing Inc. 665-666pp

Grine, F.E., W.L. Jungers and J. Schultz. (1996). Phenetic affinities among early *Homo* crania from East and South Africa. *J Hum Evol* 30: 189–225

Grine, FE and RL Susman (1991) Radius of *Paranthropus robustus* from Member 1, Swartkrans Formation, South Africa. *Am J Phys Anth* 84: 229-248.

Haeusler, M. (2003) New insights into the locomotion of *Australopithecus africanus. Evol Anth.* 11: 53-57

Haeusler, M. and H.M. McHenry (2007) Evolutionary reversals of limb proportions in early hominids? Evidence from KNM-ER 3735 (*Homo habilis*). *J Hum Evol* 53: 383-405.

Haile-Selassie, Y. and G. WoldeGabriel. (2009) Introduction. In Ardipithecus kadabba*: Late Miocene Evidence from the Middle Awash, Ethiopia* (Y. Haile-Selassie and G. WoldeGabriel Eds.) Berkley: University of California Press. 1-26pp.

Hammer, Ø., D.A.T. Harper, and P. D. Ryan, 2001. PAST: Paleontological Statistics Software Package for Education and Data Analysis. *Palaeontologia Electronica* 4: 9pp. http://palaeo-electronica.org/2001_1/past/issue1_01.htm

Harcourt-Smith W.E.H., M. Tallman, S. Frost, F.J. Rohlf, D.F.Wiley and E. Delson (2008) Analysis of selected hominoid joint surfaces using laser scanning and geometric morphometrics: a preliminary report. In Eric J. Sargis and Marian Dagosto, eds., *Mammalian Evolutionary Morphology: A Tribute to Frederick S. Szalay*; Springer, Dordrecht, pp. 401-411.

Hardy, A. (1960). Was man more aquatic in the past? *New Scientist,* 7, 642-645.

Hartwig-Sherer S. and R.D. Martin (1991). Was "Lucy" more human than her "child"? Observations on early homind postcranial skeletons. *J Hum Evol* 21:439-449.

Harrison, T. (1987). The phylogenetic relationships of the early catarrhine primates: A review of the current evidence. *J Hum Evol,* 16: 41–80

Harrison, T. (1989). New postcranial remains of *Victoriapithecus* from the Middle Miocene of Kenya. *J Hum Evol*. 18: 3-54.

Harrison, T. (in press) Hominins from the Upper Laetolil and Upper Ndolanya Beds, Laetoli. In *Paleontology and Geology of Laetoli: Human Evolution in Context. Vol. 2: Fossil Hominins and the Associated Fauna* (T. Harrison, Ed.). Springer.

Harmon, E. H. (2006) Size and shape variation in *Australopithecus afarensis* proximal femora. *J Hum Evol* 51:217-227.

Harmon, E.H. (2009) Size and shape variation in the proximal femur of *Australopithecus africanus*. *J Hum Evol* 551-559.

Hasson P., A. DeLaurier, M. Bennett, E. Grigorieva, L.A. Naiche, V. E. Papaioannou, T. J. Mohun, M. P.O. Logan (2010). Tbx4 and Tbx5 acting in connective tissue are required for limb muscle and tendon patterning *Developmental Cell*, 18(1):148-156.

Haeusler, M. and H.M. McHenry (2007). Evolutionary reversals of limb proportions in early hominids? evidence from KNM-ER 3735 (*Homo habilis*). *J Hum Evol.* 53:383-405

Hay, R.L. (1976) Geology of the Olduvai Gorge. *A study of Sedimentation in a Semiarid Basin.* Berkeley: University of California Press.

Heinrich, R.E., M.D. Rose, R.E. Leakey and A.C. Walker. (1993). Hominid radius from the middle Pliocene of Lake Turkana, Kenya. *Am J Phys Anth* 92: 139-148.

Heiple, K.G. and C.O. Lovejoy. (1971) The distal femoral anatomy of Australopithecus. *Am J Phys Anth*, 35:75-84

Holt, B.M. (2003). Mobility in upper Paleolithic and Mesolithic Europe: Evidence from the lower limb. *Am J Phys Anthropol* 122, 200-215

Horovitz, I. and M.R. Sánchez-Villagra. (2003). A morphological analysis of marsupial mammal higher-level phylogenetic relationships. *Cladistics*, 19: 181-212.

Howell, F.C. (1978) Hominidae. In VJ Maglio and HBS Cooke (eds.): T*he Evolution of African Mammals*. Cambridge: Harvard University Press, pp. 154-248.

Hunt, K.D. (1994) The evolution of human bipedality: ecology and functional morphology. *J Hum Evol* 26: 183-202.

Inouye, S.E., (1992) Ontogeny and allometry of African ape manual rays. *J. Hum. Evol.* 23: 107–138.

Isaac, B. (1987) Throwing and human evolution. *The African Anthropological Review* 5:3-17

Isbell, L.A. and T. P. Young (1996) The evolution of bipedalism in hominids and reduced group size in chimpanzees: alternative responses to decreasing resources. *J Hum Evol* 30:389-397.

Jablonski, N. and G. Chaplin. (1993) Origin of habitual bipedalism in the ancestor of the Hominidae. *J Hum Evol* 24:259-280.

Johanson D.C, F.T. Massao, G.G. Eck, T.D. White, and R.C.Walter. (1987). New partial skeleton of *Homo habilis* from Olduvai Gorge, Tanzania. *Nature* 327:205–9

Johanson, D. C. and M. Taieb. (1976) Plio-Pleistocene hominid discoveries in Hadar, Ethiopia. *Nature* 260: 293-297.

Johanson, D. C., White, T. D., & Coppens, Y. (1978). *A new species of the genus Australopithecus (primates: Hominidae) from the Pliocene of eastern Africa.* Kirtlandia, no. 28. Cleveland, Ohio: The Cleveland Museum of Natural History.

Jolly, C.J. (1970) The seed-eaters: a new model of hominid differentiation based on a baboon analogy. *Man* 5:5-26.

Jungers, W. L., D. J. Meldrum and J.T. Stern Jr. (1993) The functional and evolutionary significance of the human peroneus tertius muscle. *J Hum Evol* 25: 377-386.

Jungers, W.L. (1982) Lucy's limbs: Skeletal allometry and locomotion in *Australopithecus afarensis* (A.L. 288-1). *Nature* 297:676-678

Jungers W.L. (1985) Body size and scaling of limb proportions in primates. In *Size and Scaling in Primate Biology (*ed. W. Jungers). New York: Plenum. pp345-381.

Jungers, W.L. and J.T. Stern, Jr. (1983) Body proportions, skeletal allometry and locomotion in the Hadar hominids: a reply to Wolpoff. *J Hum Evol* 12:673-684.

Kay, R. (1973) Humerus of robust Austrapolithcus. *Science* 182: 396

Kepple, T.M., H.J. Sommer, K. Lohmann-Siegel, and S.J. Stanhope. (1998) A Three-Dimensional Musculoskeletal Database for the Lower Extremities. J*ournal of Biomechanics* 31:77-80.

Keith, A. (1903) The extent to which the posterior segments of the body have been transmuted and suppressed in the evolution of man and allied primates. *J. Anat. and Physiol*., 37: 18-40.

Kelley, R.E. (2001) Tripedal knuckle-walking: A proposal for the evolution of human locomotion and handedness. *J. theor. Biol.* 213: 333-358.

Kidd R.S., P.O. O'Higgins and C.E. Oxnard (1996) The OH8 foot: a reappraisal of the functional morphology of the hindfoot utilizing a multivariate analysis. *J Hum Evol* 31:269–291.

Kimbel, W., D.C. Johansen, T.D. White (1984) Cranial morphology of *Australopithecus afarensis*: a comparative study based on a composite reconstruction of the adult skull *Am J Phys Anthro* 64:337-338.

Kimbel, W.H. and R. Walters (2000) Hadar. In *Encyclopedia of Human Evolution and Prehistory* (E. Delson, I. Tattersall, J.A. van Covering and A. Brooks, Eds.) New York: Garland Publishing Inc. 299-302pp.

Kimbel, W.H. and T.D. White. (1988) Variation, sexual dimophism, and the taxonomy of Australopithecus. In: Grine, F.E. (Ed.), *Evolutionary History of the ''Robust'' Australopithecines*. Aldine de Gruyter, New York, pp. 175–192.

Kleindienst, M. R. (1973) Excavations at site JK 2, Olduvai Gorge Tanzania 1961–1962: the geological setting. *Quaternaria* 17:145–208

Klingenberg C.P.. (2008). MorphoJ. Faculty of Life Sciences, University of Manchester, UK. http://www.flywings.org.uk/MorphoJ_page.htm

Köhler, M. and S. Moyà-Solà (1997) Ape-like or hominid-like? The positional behavior of *Oreopithecus bambolii* reconstructed. *Proc Natl Acad Sci USA* 94: 11747-11750

Korey K.A. (1990) Deconstructing reconstruction: the OH 62 humerofemoral index. *Am J Phys Anth* 83: 25-33.

Kortlandt, A. (1980) How might early hominids have defended themselves against large predators and food competitors? *J Hum Evol* 9:79-112.

Kramer, P. A. (1999) Modelling the locomotor energetics of extinct hominids. *J Exper Biol* 202:2807-2818

Kramer, P.A. and G.G. Eck (2000) Locomotor energetics and leg length in hominid bipedality. *J Hum Evol* 38: 651-666.

Kuman, K. and R. J. Clarke (2000). Stratigraphy, artifact industries and hominin associations for Sterkfontein, Member 5. *J Hum Evol*. 38: 827-847.

Langdon, J.H. (1997) Umbrella hypotheses and parsimony in human evolution: a critique of the aquatic ape hypothesis. *J Hum Evol* 33: 479-494.

Lague M.R. (2002): Another look at shape variation in the distal femur of *Australopithecus afarensis*: implications for taxonomic and functional diversity at Hadar. *J Hum Evol*, 42:609-26.

Lague, M.R. and W.L. Jungers. (1996). Morphometric variation in Plio-Pleistocene hominid distal humeri. *American Journal of Physical Anthropology,* 101: 401-427.

Latimer, B., J.C. Ohman, and C.O. Lovejoy (1987). Talocrural joint in African hominoids:implications for *Australopithecus afarensis*. *Am J Phys Anthropol.*. 74: 155-175.

Leakey, L.S.B., P.V.Tobias, and J.R. Napier. (1964). A new species of the genus *Homo* from Olduvai Gorge. *Nature*, 202:7-9.

Leakey M.G., Feibel C.S., McDougall I., and Walker A.C. (1995): New four-million-year old hominid species from Kanapoi and Allia bay, Kenya. *Nature*, 376:565-71.

Leakey, M.G., F. Spoor, F.H. Brown, P.N. Gathogo, C. Kiarie, L.N. Leakey and I. McDougall (2001) New hominin genus from eastern Africa shows diverse middle Pliocene lineages. *Nature* 410:433-440

Leakey R.E. (1973): Evidence for an advanced Plio-Pleistocene hominid from east Rudolf, Kenya. *Nature*, 242:447-50.

Leakey, R.E., M.G. Leakey and A.K. Behrensmeyer. (1991) The Hominid Catalogue. In *The Koobi Fora Research Project Volume IV* (Ed. B. Wood) Oxford University Press.

Leakey, R.E., A. Walker, C.V. Ward and H.M. Grausz (1989). A partial skeleton of a gracile hominid from the Upper Burgi Member of the Koobi Fora Formation, East Lake Turkana, Kenya *Proc. 2nd Int Congress Human Paleontology* (ed. G. Giacobini) Jaca: Milan, pp167-173.

Leonard, W.R. and M.L. Robertson (1997) Rethinking the energetics of bipedality. *Current Anthropology* 38: 304-309.

Leutenegger, W. and J.T. Kelley. (1977) Relationships of sexual dimorphism in canine size and body size to social, behavioural, and ecological correlates in anthropoid primates. *Primates* 18, 177–186.

Lewis, O.J., R. J. Hamshere and T. M. Bucknill (1970) The anatomy of the wrist joint *J. Anat.* 106:539-552

Lieberman, D.E., D. M. Bramble, D.A. Rachlan and J.J. Shea. (2007) The evolution of endurance running and the tyranny of ethnography: a reply to Pickering and Bunn (2007). *J Hum Evol* 53: 434-437.

Lieberman, D.E., M.J. Devlin, and O.M. Pearson (2001). Articular area responses to mechanical loading: effects of exercise, age, and skeletal location. *Am J Phys Anthropol*, 16: 266-277.

Lieberman, D.E., B.A. Wood, and D.R. Pilbeam. (1996). Homoplasy and early Homo: An analysis of the evolutionary relationships of *Homo habilis sensu stricto* and *H. rudolfensis J Hum Evol*, 30:97-120

Logan M. and C.J. Tabin (1999) Role of Pitx1 upstream of Tbx4 in specifcation of hindlimb identity *Science* 283: 1736-1739.

Lovejoy, C. O. (1988). The evolution of human walking. *Sci. Am.* 259: 118-125.

Lovejoy, C. O. (2009) Reexamining human origins in light of *Ardipithecus ramidus. Science* 326: 742-748

Lovejoy, C.O. and K. Heiple. (1970) A reconstruction of the femur of *Australopithecus africanus. Am J Phys Anth.* 32: 33-40.

Lovejoy, C.O., R. S. Meindl, J.C. Ohman, K. G. Heiple, T.D. White(2002) The Maka femur and its bearing on the antiquity of human walking: Applying contemporary concepts of morphogenesis to the human fossil record. *Am J Phys Anth* 119:7 – 133

Lovejoy, C.O., G. Suwa, S.W. Simpson, J.H. Matthernes, and T.D. White. (2009a) The great divides: *Ardipithecus ramidus* reveals the postcrania of our last common ancestors with African apes. *Science* 326:100-106

Marcil A., É. Dumontier, M. Chamberland, S. A. Camper and J. Drouin (2003) Pitx1 and Pitx2 are required for development of hindlimb buds *Development* 130: 45-55.

Mason, O.K. (1998) The contest between the Ipiutak, Old Bering Sea, and Birnirk Polities and the origin of whaling during the first millennium A.D along Bering Strait. *Journal of Anthropological Archaeology* 17:240-325

McDougall, I., F.H. Brown and J.G. Fleagle (2005) Stratigraphic placement and age of modern humans from Kibish, Ethiopia. *Nature* 433: 733-736.

McHenry, H.M. (1978) Fore- and hindlimb proportions in Plio-Pleistocene hominids. *Am J Phys Anth* 49: 15-22.

McHenry, H.M. (1986). The first bipeds: a comparison of the *A. afarensis* and *A. africanus* postcranium and implications for the evolution of bipedalism. *J Hum Evol* 15: 177-191.

McHenry, H.M. (1991). The petite bodies of the ‘‘robust’’ australopithecines. A*m J Phys Anthropol.* 86:445–454.

McHenry, H.M. (1991). Sexual dimorphism in *Australopithecus afarensis*. *Journal of Human Evolution*, 20:21-32.

McHenry, H.M. (1994a). Early hominid postcrania: phylogeny and function. In: *Integrative Pathways to the Past: Paleoanthropological Papers in Honor of F. Clark Howell,* eds. R. S. Corruccini and R. Ciochon. Inglewood Cliffs: Prentice-Hall. pp. 251-261.

McHenry, H.M. (1994b) Tempo and mode in human evolution. *Proc. Nat. Acad. Sci.* 91:6780-6786

McHenry H.M., and L.R. Berger (1998) Body proportions in *Australopithecus afarensis* and *A. africanus* and the origin of the genus *Homo. J Hum Evol* 35:1-22.

McHenry, H.M. and C.C. Brown. (2008) Side steps: the erratic pattern of hominin postcranial change through time. *J Hum Evol* 55: 639-651.

McHenry, H.M., C.C. Brown and L. J. McHenry (2007) Fossil hominin ulnae and the forelimb of *Paranthropus. Am J Phys Anth* 134:209-218

McHenry, H.M., R.S. Corruccini and F.C. Howell. (1976) Analysis of an Early Hominid Ulna from the Omo Basin, Ethiopia *Am J Phys Anth*, 44: 295-404

Menter, C.M. (2002) *Hominid Distal Humeri, Proximal Radius and Proximal Ulnae from Sterkfontein, in Comparison with the Elbow Bones of Other Plio-Pleistocene Fossil Hominids.* University of Witswaterstrand, South Africa.

Miller, J. A. (1991). Does brain size variability provide evidence of multiple species in *Homo habilis? Am. J. Phys. Anthropol.* 84, 385–398.

Minguillon C., J. Del Buono, M. Logan. (2005) Tbx5 and Tbx4 Are Not Sufficient to Determine Limb-Specific Morphologies but Have Common Roles in Initiating Limb Outgrowth *Developmental Cell*, 8: 75-84

Mitteroecker P. and F. Bookstein (2008). The evolutionary role of modularity and integration in the hominoid cranium. *Evolution*. 62:943-958

Moore K.L. and T.V.N. Persaud. (1998) *The Developing Human: Clinically Oriented Embryology.* Philadelphia: W.B. Saunders and Co.

Morbeck, M.E. and A.L. Zihlman. (1988) Body composition and limb proportions. In *Orangutan Biology*, ed. J. Schwartz. New York: Oxford pp285-297

Morgan, E. (1972) *The Descent of Woman.* London:Souvenir Press.

Morris, A. (1992). *A Master Catalogue: Holocene Human Skeletons from South Africa* Witwaterstrand University Press.

Morton, DJ. (1927) Human Origins: Correlations of previous studies of primate feet and posture with other morphologic evidence. *Am J Phys Anth* 10(2): 173-201.

Moyà-Solà, S., M. Kőhler I. Casanovas-Vilar, and J. Galindo. (2004) *Pierolapithecus catalaunicus*, a New Middle Miocene Great Ape from Spain. *Science*, 306: 1339-1344.

Nakatsukasa, M., Y. Kunimatsu, Y. Nakano, T. Takano and H. Ishida. (2003) Comparative and functional anatomy of phalanges in *Nacholapithecus kerioi*, a Middle Miocene hominoid from northern Kenya. *Primates*, 44:371-412.

Napier, J.R. (1964). The evolution of bipedal walking in the hominids. *Arch. Biol. (Leige)* 75:673-708.

Napier, J. R. (1997) The antiquity of human walking. *Sci Amer.* 216: 56-66.

O'Higgins, P. and N Jones (2006) Tools for statistical shape analysis. Hull York Medical School. http://sites.google.com/site/hymsfme/resources

O'Rahilly R. and E. Gardner (1975). The timing and sequencing of events in the development of the limbs in the human embryo. *Anat Embryol* 148:1-23.

Ogden, J.A. (1981). Hip development and vascularity: the relationship to chondro-osseous trauma in the growing child. In *The Hip, Proceedings of the Ninth Open Scientific Meeting of the Hip Society.* St. Louis: CV Mosby, pp. 139-187.

Otis, J.C., J.T. Deland, S. Lee and J. Gordon. (2004) The peroneus brevis is a more effective everter of the foot than peroneus longus. *Foot and Ankle,* 25: 242-246.

Oxnard, C.E. (1975) The place of the australopithecines in human evolution: grounds for doubt? *Nature* 258: 389-393

Parker, S.T. (1987) A sexual selection model for Hominid evolution. *Human Evoution* 2: 235-253.

Partridge, T.C., D.E. Granger, M.W. Caffee, and R.J. Clarke (2003) Lower Pliocene hominid remains from Sterkfontein.. *Science* 300: 607-612.

Partridge T.C., J. Shaw, T. Heslop and RJ Clark. (1999) The new hominid skeleton from Sterkfontein, South Africa: age and preliminary assessment. *J Quaternary Sci* 14:293-298.

Patel, B. (2005). The hominoid proximal radius: re-interpreting locomotor behaviors in early hominins. *J Hum Evol* 48: 415-432.

Patterson, B and WW Howells. (1967) Hominid humeral fragment from Early Pleistocene of northwestern Kenya. *Science* 156: 64-66.

Plavcan J.M., C.A. Lockwood, W.H. Kimbel, M.R. Lague and E.H. Harmon (2005). Sexual dimorphism in Australopithecus afarensis revisited: How strong is the case for a human-like pattern of dimorphism? J Hum Evol 48:313-320.

Pickering, T.R. and H.T. Bunn (2007) The endurance running hypothesis and hunting and scavenging in savanna-woodlands. *J. Hum. Evol.* 53:438-442.

Pickering, T.R., R.J. Clarke and J. Moggi-Cecchi (2004) Role of carnivores in the accumulation of the Sterkfontein Member 4 hominid assemblage: a taphonomic reassessment of the complete hominid fossil sample (1936–1999), *Am. J. Phys. Anthropol*. 125: 1–15.

Pickford, M. (2006) Palaeoenvironments, palaeoecology, adaptations and the origins of bipedalism in Hominidae. In: H. Ishida, R. Tuttle, M. Pickford, *et al.* (Eds). *Human Origins and Environmental Backgrounds,* Chicago: Springer pp. 175-198,

Pickford, M. and B. Senut. (2001) The geological and faunal context of Late Miocene hominid remains from Lukeino, Kenya. In Comptes Rendus de l'Académie de Sciences, vol. 332, pp. 145-152.

Pontzer, H., D.A. Rachlan and M.D. Sockol (2009) The metabolic cost of walking in humans, chimpanzees, and early hominins. *J Hum Evol* 56: 43-54.

Potts, R. (1998) Environmental hypotheses of human evolution. *Yrbk Phys Anth* 41:93-136.

Prost, JH. (1980). Origin of Bipedalism. *Am J Phys Anth* 52: 175-189

Preuschoft, H (2004) Mechanisms for the acquisition of habitual bipedality: are there biomechanical reasons for the acquisition of upright bipedal posture? *J Anat* 204: 363-384.

Rainey, F. (1941) The Ipiutak Culture at Point Hope, Alaska. *American Anthropologist*, 43:364-375.

Rak, Y. (1991) Lucy's pelvic anatomy: its role in bipedal gait. *J Hum Evol* 20: 283-290.

Reed, K.W., J.W. Kitching, F.E. Grine, W.L. Jungers, and L. Sokoloff. (1993) Proximal femur of Australopithecus africanus from member 4, Makapansgat, South Africa *Am J Phys Anth* 92:1-15

Reno P.L., D.A. DeGusta, M.A. Serrat, R.S. Meindl, T.D. White, R.B. Eckhardt, A.J. Kuperavage, K. Galik, and C.O. Lovejoy (2005). Plio-Pleistocene hominid limb proportions: evolutionary reversals or estimation errors? *Current Anthropology* 46: 575-588

Richmond, B.G., L.C. Aiello, and B.A. Wood (2002) Early hominin limb proportions. *J Hum Evol* 43: 529-548.

Richmond, B.G., J.G. Fleagle, J. Kappleman and C.C. Swisher, III (1998) First hominoid from the Miocene of Ethiopia and the evolution of the catarrhine elbow. *Am J Phys Anth* 105: 257-277.

Richmond, B.G. and W.L. Jungers (2008) *Orrorin tugenensis* femoral morphology and the evolution of hominin bipedalism. *Science* 319:1662-1665

Richmond, BG. and DS Strait (2000) Evidence that humans evolved from a knuckle-walking ancestor. *Nature*

Robinson, J. (1972) *Early Hominid Posture and Locomotion.* Chicago: University of Chicago Press.

Rodman, P.S. and H.M. McHenry (1980). Bioenergetics and the origin of hominid bipedalism. *Am J Phys Anth* 52:103-106. .

Rohlf, F.J. and M. Corti. (2000). Use of two-block partial least squares to study covariance in shape. *Syst. Biol.* 49:740-753.

Rohlf, F.J. and L.F. Marcus. (1993). A revolution in morphometrics. *Trends in Ecology and Evolution*. 8: 129-132.

Rohlf, F. J., and D.E. Slice (1990). Extensions of the Procrustes method for the optimal superimposition of landmarks. *Systematic Zoology*, 39: 40-59.

Roilan C., D.E. Lieberman, and B. Hallgrímsson (2010) The coevolution of human hands and feet. *Evolution.* Accepted article.

Rook, L., L. Bondioli, M. Kohler, S. Moya-Sola, and R. Macchiarelli. (1999) *Oreopithecus* was a bipedal ape after all: evidence from the iliac cancellous architecture. *Proc Nat Acad Sci USA* 96: 8795-8799

Rose, M.D. (1991) The process of bipedalization in hominids. *Origine(s) de la Bipédie chez les Hominides,* Eds Y. Coppens and B. Senut, Paris: CNRS. 38-48pp

Rose, M. (1993) Functional anatomy of the elbow and forearm in primates. In *Postcranial Adaptations of Nonhuman Primates* (Ed. D. L. Gebo). DeKalb: Northern Illinois University Press. 70-95pp

Rosenberg, K. and W. Trevathan. (1996) Bipedalism and human birth: the obstetrical dilemma revisited. *Evol Anth* 4: 161-168

Ruff, C.B. (1988) Hindlimb articular surface allometry in Hominoidea and *Macaca*, with comparisons to diaphyseal scaling. *J. Hum. Evol*., 17: 687-714.

Ruff, C.B. (2002). Long bone articular and diaphyseal structure in old world monkeys and apes. I: Locomotor effects. *Am J Phys Anthropol* 119: 305-342

Ruff C.B. (2008) Femoral/humeral strength in early African *Homo erectus. J Hum Evol.,* 54:383-390

Ruff C.B. (2009) Relative limb strength and locomotion in *Homo habilis. Am J Phys Anth,* 138: 90-100

Ruff, C.B., H.M. McHenry, and J.F. Thackeray (1999). Cross-sectional morphology of the SK 82 and 97 proximal femora. *American Journal of Physical Anthropology*, 109: 509-521.

Ruff, C.B. and A.C. Walker. (1993). Body size and body shape. In *The Nariokotome* Homo Erectus *Skeleton*. Eds. A.C. Walker and R.E. Leakey. Cambridge: Harvard Press. Pp. 234-265.

Ruff C.B., A.Walker, and E. Trinkaus. (1994). Postcranial robusticity in *Homo.* III: ontogeny. *Am J Phys Anthropol* 93:35–54.

Sánchez-Villagra, M.R. and B.A. Williams. (1998). Levels of homoplasy in the evolution of the mammalian skeleton. *Journal of Mammalian Evolution*, 5: 113-126.

Sargis, E.J. (2002) The postcranial morphology of *Ptilocercus lowii* (Scandentia, Tupaiidae): an analysis of Primatomorpha and Volitantian characters. *Journal of Mammalian Evolution,* 9, 137-160

Schmitt, D. (2003) Insights into the evolution of human bipedalism from experimental studies of humans and other primate. *J Exper Biol* 206: 1437-1448.

Senut, B. (1981) Humeral outlines in some hominoid primates and in Plio-Pleistocene hominids. *Am J Phys Anth* 56:275-283.

Senut, B. (1992). French Contribution to the study of Human Origins: The case of *Australopithecus afarensis* . *Human Evolution,* 7: 15-24.

Senut, B., M. Pickford, D. Gommery, P. Mein, K. Cheboi, and Y. Coppens. 2001. First hominid from the Miocene (Lukeino Formation, Kenya). In *Comptes Rendus de l'Académie de Sciences*, vol. 332, pp. 137-144.

Senut, B. and C. Tardieu (1985). Functional aspects of Plio-Pleistocene hominid limb bones: implications for taxonomy and phylogeny. In *Ancestors: the Hard Evidence*, ed. E. Delson. New York: Alan R. Liss, Inc. pp. 193-201.

Shefelbine, S.J., C. Tardieu, and D.R. Carter. (2002). Development of the femoral bicondylar angle in hominid bipedalism. *Bone*, 30:765-660.

Shubin N., C. Tabin and S. Caroll. (1997). Fossils, genes and the evolution of animal limbs. *Nature,* 388: 639-648.

Singleton, M. (2002) Patterns of cranial shape variation in the Papionini (Primates: Cercopithecinae). *J Hum Evol* 42:547–578.

Slice, D.E. (1998). Morpheus et al.: software for morphometric research. Revision 01-30-98. Department of Ecology and Evolution, State University of New York, Stony Brook, New York.

Stanford, C.B. (2006) Arboreal bipedalism in wild chimpanzees: implications for the evolution of hominid posture and locomotion. *Am J Phys Anth* 129: 225-231.

Stern, J.T. (1975) Before Bipedality. *Yrbk Phys Anth* 19: 59-68

Stern. J.T. (1999). The cost of bent-knee, bent-hip bipedal gait. A reply to Crompton, et al. *Journal of Human Evolution*, 36: 567-570.

Stern, J.T. and R.L. Susman. (1983). The locomotor anatomy of *Australopithecus afarensis. American Journal of Physical Anthropology*, 60: 279-317.

Stern, J.T. and R.L. Susman. (1991). 'Total morphological pattern' versus 'the magic trait': conflicting approaches to the study of early hominid bipedalism. In *Origine(s) de la Bipédie Chez les Hominidés*. Eds. Y. Coppens and B. Senut. Paris: Editions du CNRS. Pp. 99-111.

Stock, J. and Pfeiffer, S. (2001). Linking structural variability in long bone diaphyses to habitual behaviours: foragers from the southern African late stone age and the Andaman Islands. *Am J Phys Anthropol.* 115: 337-348.

Strier, K.B. (2000) *Primate Behavioral Ecology.* Boston: Allyn and Bacon.

Swiderski, D.L. (1993). Morphological evolution of the scapula in tree squirrels, chipmunks and ground squirrels (Sciuridae): an analysis using thin-plate splines. *Evolution,* 47: 1854-1873.

Susman R.L. (1989) New Hominid fossils from the Swartkrans Formation (1979-1986 excavations): postcranial specimens. *Am. J. Phys. Anthropol*. 79: 409-449

Susman, R.L. (2004) *Oreopithecus bambolii:* an unlikely case of hominidlike grip capability in a Miocene ape, *J. Hum. Evol.* 46:105–117

Susman, R.L., D. de Ruiter, and C.K. Brain. (2001). Recently identified postcranial remains of *Paranthropus* and Early *Homo* from Swartkrans Cave, South Africa *J Hum Evol* 41: 607–629

Susman, R.L. and Stern, J. T., Jr (1982). Functional morphology of *Homo habilis. Science* 217: 931 -934.

Szeto D.P, C. Rodriguez-Esteban, A. K. Ryan, S. M. O'Connell, F. Liu, C. Kioussi, A. S. Gleiberman, J. C. Izpisúa-Belmonte, and M. G. Rosenfeld (1999) Role of the Bicoid-related homeodomain factor Pitx1 in specifying hindlimb morphogenesis and pituitary development. *Genes & Dev*. 13: 484-494

Tardieu, C. (1999) Ontogeny and phylogeny of femoro-tibial characters in humans and hominid fossils: functional influence and genetic determinism. *Am J Phys Anth* 110:365-377

Taylor, A. (1997) Scapula form and biomechanics in gorillas *J Hum Evol* 33: 529-553

Terhune, C., W.H. Kimbel and C.A. Lockwood (2007). Variation and diversity in *Homo erectus*: a 3D geometric morphometric analysis of the temporal bone. *J Hum Evol.* 53: 41-60.

Thackeray, J. F., D.J. de Ruiter, L.R. Berger and N.J. van der Merve (2002). *Hominid fossils from Kromdraai: a revised list of specimens discovered since 1938*. Annals of the Transvaal Museum 38, 43-56

Thorpe, S.K.S, R.L. Holder and R.H. Crompton (2007) Origin of bipedalism as an adaptation for locomotion on flexible branches. *Science* 316: 1328-1331.

Tobias, P. V. (1978). The earliest Transvaal members of the genus Homo with another look at some problems of hominid taxonomy and systematics. *Z. Morph. Anthropol.* 69: 225–265.

Tobias, P. V. (1991). *Olduvai Gorge, Vol. 4*. Cambridge: Cambridge University Press.

Tuttle, R.H. (1969). Knuckle-walking and the problem of human origins. *Science* 166: 953-961

Tuttle, R.H. and G.W. Cortright (1988) Positional behavior, adaptive complexes and evolution. In *Orangutan Biology*, ed. J. Schwartz. New York: Oxford pp 311-330

Verhaegen, M. P-F. Puech and S. Munro. (2002) Aquarboreal ancestors? *Trends in Ecology and Evolution* 17: 212-217

Vidian, E.N. and W.C. McGrew (2001) Bipedality in chimpanzee (Pan troglodytes) and bonobo (Pan paniscus): Testing hypotheses on the evolution of bipedalism. *Am J Phy Anth* 118: 184-190.

Vrba, E. S. (1980). Evolution, species, and fossils: how does life evolve? *South African Journal of Science*, 76: 61–84.

Vrba, E. S.and Gould, S. J. (1986). The hierarchical expansion of sorting and selection: sorting and selection cannot be equated. *Paleobiology*, 12: 217–228.

Wagner G.P. and L. Altenberg. (1996). Perspective: Complex adaptations and the evolution of evolvability. *Evolution.* 50:967-976.

Walker, A. and R.E. Leakey (1993) The Skull. In *The Nariokotome* Homo erectus *Skeleton* (A. Walker and R.E. Leakey, Eds). Cambridge: Harvard University Press. 63-94pp

Walter, R.C. (1994). Age of Lucy and the First Family: single-crystal $^{40}Ar/^{39}Ar$ dating of the Denen Dora and lower Kada Hadar members of the Hadar Formation, Ethiopia. *Geology.* 22: 6-10.

Walter, R.C., P.C. Manega and R.L. Hay (1992) Tephrochronology of Bed I, Olduvai Gorge: an application of laser-fusion 40Ar/39Ar dating to calibrating biological and climatic change, *Quatern. Int.* 13/14:pp. 37–46.

Wang, W-J. , R.H. Crompton, Y. Li and M.M. Gunther (2003) Energy transformations during erect and 'bent-hip, bent-knee' walking by humans with implications for the evolution of bipedalism. *J Hum Evol.* 44: 563-579.

Wang, W-J. and R. H. Crompton (2004) The role of load-carrying in the evolution of modern body proportions. *J Anat.* 204:417-430

Wang, W-J., R. H. Crompton, T.S. Carey, M. M. Gunther, Y. Li, R. Savage, W. I. Sellers (2004) Comparison of inverse-dynamics musculo-skeletal models of AL 288-1 *Australopithecus afarensis* and KNM-WT 15000 *Homo ergaster* to modern humans, with implications for the evolution of bipedalism. *J Hum Evol* 453-478.

Ward, C.V. (2002). Interpreting the posture and locomotion of *Australopithecus afarensis*: where do we stand? *Yrbk Phys Anth* 45:185–215

Ward, C.V., M.G. Leakey, and A. Walker (2001). Morphology of *Australopithecus anamensis* from Kanapoi and Allia Bay, Kenya. *J Hum Evol* 41: 255-368.

Washburn, S.E. (1967). Behaviour and the Origin of Man. *Proc. Reg Anth. Inst. Of Great Britian and Ireland.* 1967: 21-27

Westergaard, G.C., C. Liv, M.. Haynie, and S. J. Suomi. (2000) A comparative study of aimed throwing by monkeys and humans. *Neuropsychologica* 38: 1511-1517

Wheeler, P.E. (1991) The influence of bipedalism on the energy and water budgets of early hominids. *J Hum Evol* 20: 107-115.

Wheeler, P.E. (1992) The thermoregulatory advantages of large body size for hominids foraging in savannah environments. *J Hum Evol* 23: 351-362.

Wheeler, P.E. (1993) The influence of stature and body form on hominid energy and water budgets: a comparison of *Australopithecus* and early *Homo* physiques. *J Hum Evol.* 24: 13-28.

White, T.D. (2000a) Melka Kontoure. In *Encyclopedia of Human Evolution and Prehistory* (E. Delson, I. Tattersall, J.A. van Covering and A. Brooks, Eds.) New York: Garland Publishing Inc. 406 pp.

White, T.D. (2000b) The Middle Awash. In *Encyclopedia of Human Evolution and Prehistory* (E. Delson, I. Tattersall, J.A. van Covering and A. Brooks, Eds.) New York: Garland Publishing Inc. pp 411-413.

White, T.D. (2000c) Olduvai Gorge. In *Encyclopedia of Human Evolution and Prehistory* (E. Delson, I. Tattersall, J.A. van Covering and A. Brooks, Eds.) New York: Garland Publishing Inc. pp. 486-489

White, T.D., B. Asfaw, Y. Beyene, Y. Haile-Selassie, C. O. Lovejoy, G. Suwa, G. WoldeGabriel (2009). *Ardipithecus ramidus* and the paleobiology of early hominids. *Science* 326: 75–86.

White, T.D., G. WoldeGabriel, B. Asfaw, S. Ambrose, Y. Beyene, R. L. Bernor, J.-R. Boisserie, B. Currie, H. Gilbert, Y. Haile-Selassie, W. K. Hart, L. J. Hlusko, F. C. Howell, R. T. Kono, T. Lehmann, A. Louchart, C. O. Lovejoy, P. R. Renne, H. Saegusa, E. S. Vrba, H. Wesselman and G. Suwa (2006) Asa Issie, Aramis and the origin of Australopithecus. *Nature* 440: 883-889

Wood, B. A. (1985). Early Homo in Kenya, and its systematic relationships. In (E. Delson, Ed.) *Ancestors: The Hard Evidence*, pp. 206–214. New York: Alan R. Liss.

Wood, B.A. (1987). Who is the 'real' Homo habilis? *Nature* 327, 187–188.

Wood B.A. (1991). *Koobi Fora research project. Hominid cranial remains*, Vol. 4. Oxford: Clarendon Press.

Wood, B.A. (1992) Origin and evolution of the genus *Homo*. *Nature,* 355: 783 – 790

Wood, B. (1999) Plio-Pleistocene hominins from the Baringo Region, Kenya. In *Late cenozoic environments and hominid evolution: a tribute to the late Bill Bishop* (P. Andrews and P. Banham Eds.). London: Geological Society. pp 113-122.

Wood, B.A., L. Aiello, C. Wood and C. Key. (1998) A technique for establishing the identity of "isolated" fossil hominin limb bones. *J Anat* 193:61-72.

Wood, B. A. and A. T. Chamberlain (1986). Australopithecus: grade or clade? In (B. A. Wood) *Primate and Human Evolution*, pp. 220–248. Cambridge: Cambridge University Press.

Wood, B. and M. Collard. (1999). The human genus. *Science*, 284: 65-71

Young, N.M. (2003). A reassessment of living hominoid postcranial variability: implications for ape evolution. *Journal of Human Evolution*, 45: 441-464.

Young, N.M., G.P. Wagner, and B. Hallgrimsson. (2010). Development and the evolvability of the human limbs. *Proc Nat Acad Sci* 107: 3400-3405.

Zeller R., J. Lopez-Rios and A. Zuniga. (2009). Vertebrate limb bud development: moving towards integrative analysis of organogenesis. *Nature Reviews Genetics,* 10: 845-858

Zihlman, A. (1985) *Australopithecus afarensis*: two sexes or two species? IN: *Hominid Evolution, Past, Present, and Future,* P.V. Tobias (ed.) Alan R. Liss, New York, pp. 213-220.